Metal Complexes with Tripodal and Chelating Thiourea Ligands towards Nuclear Medical Imaging

Inaugural-Dissertation

to obtain the academic degree

Doctor rerum naturalium (Dr. rer. nat.)

submitted to the Department of Biology, Chemistry, Pharmacy

of Freie Universität Berlin

by

Anna Charlott Grunwald

Berlin, December 2020

This thesis was done in the period between April 2017 and December 2020 in the research group of Prof. Dr. Ulrich Abram at the Institute of Chemistry and Biochemistry. Hereby, I confirm that I wrote the thesis independently. It was independently done without the help of other sources than the ones cited and acknowledged and it was not submitted to any prior doctoral procedure.

1. Supervisor: Prof. Dr. Ulrich Abram

2. Supervisor: Dr. Leif Schröder

Date of defence: 31.03.2021

Acknowledgements

First, I would like to thank my doctoral supervisor Prof. Dr. Ulrich Abram for his great support during the development of my research projects. He gave me his valuable advice on many occasions and therefore, I am deeply grateful.

My special thanks go to Dr. Leif Schröder for the willingness to be the second reviewer of my thesis.

I very appreciate the great patience of Dr. Adelheid Hagenbach for the measurement and refinement of my crystals and her steady helpfulness throughout these years.

I am particularly grateful for the friendly assistance of Prof. Dr. Roger Alberto and Dr. Henrik Braband who hosted me during my stays at the University of Zurich and who gave me scientific advices for the research with ^{99m}Tc.

I would like to show my gratitude to Prof. Dr. Winfried Brenner and Dr. Nicola Beindorff from the Charité Berlin who gave me the chance to realise *in vivo* experiments. A special thanks goes to Dr. Sarah Spreckelmeyer for her support during the whole extensive preparations and all her effort she put in this project. Matthias Balzer and Fabian Schmitz-Peiffer, I thank you for the implementation of the experiments.

Dr. Dorian Mikolajczak is thanked for introducing me into the interesting field of peptide chemistry on a resin. The synthesis of the small bioconjugate has been made possible with your support.

I also want to thank Dr. Lukas Greifenstein for the synthesis of the bisphosphonate bioconjugate and Dipl. Ing. Chem. Stephan Maus for the help with the ^{99m}Tc reactions at the Universitätsklinikum Mainz.

I appreciate the very warmly welcome of Prof. Ernesto Schulz-Lang from the Universidade Federal de Santa Maria. For me, this research stay in Brasil was a genuinely nice experience. I thank Dr. Camila Nunes Cechin for hosting me during this time and her friendship. I won´t forget you, don´t worry.

I thank the former and current group members of the AG Abram for the amazing time. You helped me a lot in the lab, with technical problems and answering all my questions concerning chemistry. It has been a cooperative and friendly working atmosphere.

I thank my students Alexandra Tsouka, Selina Heß, Yifu Wang and Sinem Özcirpan for their interest and support to my research.

This work could not have been possible without the financial support of the Graduate School “BIOQIC”.

Finally, I really appreciate the everlasting support of my family and friends. You give me the needed power of endurance, happiness and love to my life.

Table of Contents

List of Abbreviations

3,4,7,8-Me_4-phen	3,4,7,8-Tetramethyl-1,10-phenanthroline
5-NO_2-phen	5-Nitro-1,10-phenanthroline
Boc	*tert*-Butoxycarbonyl
bpy	2,2'-Bipyridine
Cp	Cyclopentadienyl
CV	Cyclic voltammetry
d	doublet
DCFPyL	2-(3-{1-carboxy-5-[(6-[^{18}F]fluoro-pyridine-3-carbonyl)-amino]-pentyl}-ureido)-pentanedioic acid
DIPEA	Diisopropylethylamine
DOTA	Dodecane tetraacetic acid
ESI	Electron spray ionisation
fac	Facial
Fmoc	Fluorenylmethoxycarbonyl
Gly	Glycine
HBED-CC	*N*,*N*-bis[2-hydroxy-5-(carboxyethyl)benzyl]ethylenediamine-*N*,*N*-diacetic acid
HBTU	2-(1H-Benzotriazol-1-yl)-1,1,3,3-tetramethyluronium-hexafluorophosphat
HMBC	Heteronuclear Multiple Bond Coherence
HMPAO	Hexamethylpropyleneamine oxime
HMQC	Heteronuclear multiple quantum correlation
HOBt	1-Hydroxybenzotriazol
HPLC	High Performance Liquid Chromatography
IR	Infrared
IDA	Iminodiacetic acid

L	Ligand
Lys	Lysin
m	medium (IR), multiplet (NMR)
m/z	Mass per charge
MAG3	Mercaptoacetyltriglycine
MIP	Maximum intensity projection
MS	Mass spectrometry
N-Fmoc-traneamix	*trans*-4-(Fmoc-aminomethyl)cyclohexanecarboxylic acid
NMR	Nuclear magnetic resonance
PBS	Phosphate buffered saline
PET	Positron Emission Tomography
Ph	Phenyl
phen	Phenanthroline
PSMA	Prostate-specific membrane antigen
q	Quartet
RT	Room temperature
s	Strong (IR), singlet (NMR)
SPECT	Single Photon Emission Computed Tomography
t	Triplet
tacn-ba	*N*-benzyl-2-(1,4,7-triazonan-1-yl)acetamide
TFA	Trifluoroacetic acid
TIPS	Triisopropylsilane
UPLC	Ultra performance liquid chromatography
UV	Ultraviolet
w	Weak (IR)
x	

1 Introduction

1.1 Recent Development of Radioactive Tracers in Nuclear Medicine

In spite of the considerable progress in the improvement of existing tracers and the development of novel tracers for positron emission tomography (PET),[1-5] the single-photon emission computed tomography (SPECT) with its workhorse ^{99m}Tc (E_γ = 141 keV, $t_{1/2}$= 6 h) remains the dominating technique in diagnostic nuclear medicine.[4-7] About 80 % of all nuclear medicine procedures are currently done with this metastable nuclear isomer of the artificial element technetium. This comprises approximately 40 million annual studies per year.[8] In particular, solutions are required, which allow the coupling of radioactive metal ions *via* a bifunctional chelator to a biologically active molecule like a peptide or antibody, which is targeting the tracer to the desired region in the body of the patient. Kinetically inert and/or thermodynamically stable complexes are required in order to avoid ligand-exchange reactions *in vivo* with plasma components. An impressive example of kinetic stabilization is the myocardial imaging agent ^{99m}Tc-sestamibi, in which the coordination of six monodentate isocyanide ligands is stabilized by the d^6 electronic configuration of Tc(I).[6-7] However, commonly stabilization is achieved by means of ligand systems with a high denticity. This means that chelators with a denticity of three or larger provide the required stabilization in SPECT radiopharmaceuticals such as ^{99m}Tc-MAG3,[9] ^{99m}Tc-HMPAO,[10] and the members of the ^{99m}Tc-IDA family.[11]

Prostate cancer is one of the most widespread types of cancer in men and at the forth position of common cancer types in 2018 according to the World Health Organization report of 2020.[12] The prostate-specific membrane antigen (PSMA) is highly expressed on prostate cancer cells and it is the important target for imaging and therapy of prostate cancer. Thereby, the pharmacophore 'Glu-urea-Lys' shows a high affinity to PSMA and therefore it is present in most of the related radiotracers (Figure 1.1). A good overview about the current status of targeting PSMA radiotracers in diagnostics and therapy is the data analysis of clinical studies done by Klaus Kopka.[13] In this analysis, 104 clinical studies were systematically selected from the registered prospective trails with PSMA-ligands on ClinicalTrials.gov between 2014 and 2019. In these 104 studies, 25 different radiotracers were used: 32 % [^{68}Ga]Ga-PSMA-11, 24 % [^{18}F]DCFPyL and 10 % [^{177}Lu]Lu-PSMA-617.[13] Only one ^{99m}Tc radiotracer is named in this study: [^{99m}Tc]Tc-MIP-1404. It shows that more research is needed in this field of Tc radiotracers.

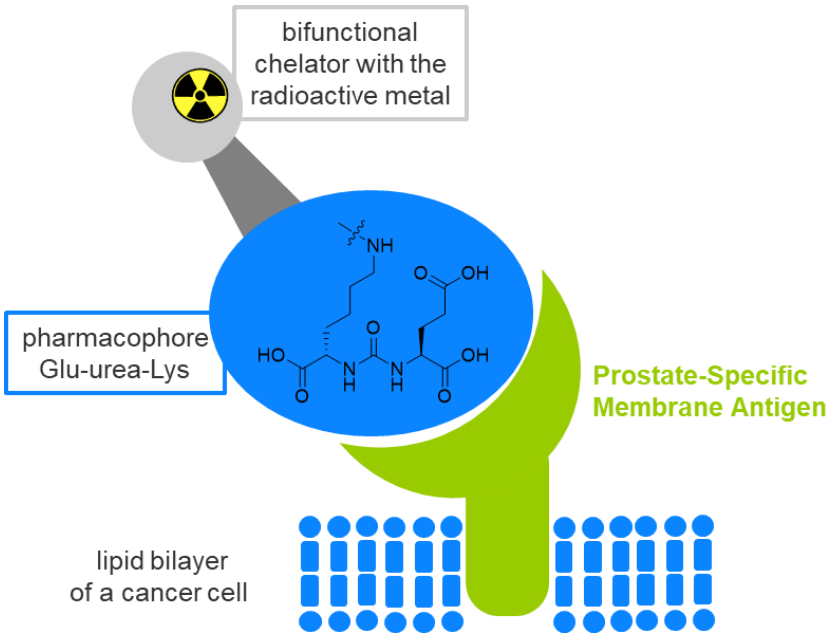

Figure 1.1. The pharmacophore 'Gly-urea-Lys' shows high affinity to prostate cancer cells

The hitherto most successful and commonly used radiotracer for the detection of prostate cancer is Ga-PSMA-11 based on the PET isotope ^{68}Ga coordinated by the HBED-CC chelator.[13] However, this chelator (Figure 1.2) cannot coordinate many other relevant isotopes for imaging or therapy. Trials to change the chelator from HBED-CC to DOTA, which coordinates more isotopes, resulted in a drastic decrease of tumor uptake.[14] Keeping DOTA due to the ability of coordinating e.g. ^{177}Lu, ^{111}In or ^{90}Y, different linkers between the pharmacophore 'Gly-Urea-Lys' and the chelator DOTA were screened because with the choice of the improved linker, tumor uptake could also be increased.[15] The result was PSMA-617 (Figure 1.2), which is also clinically established.[16] The presence of the naphthylic linker at PSMA-617 has a high impact on pharmacokinetics, tumor-targeting and biological activity.[17]

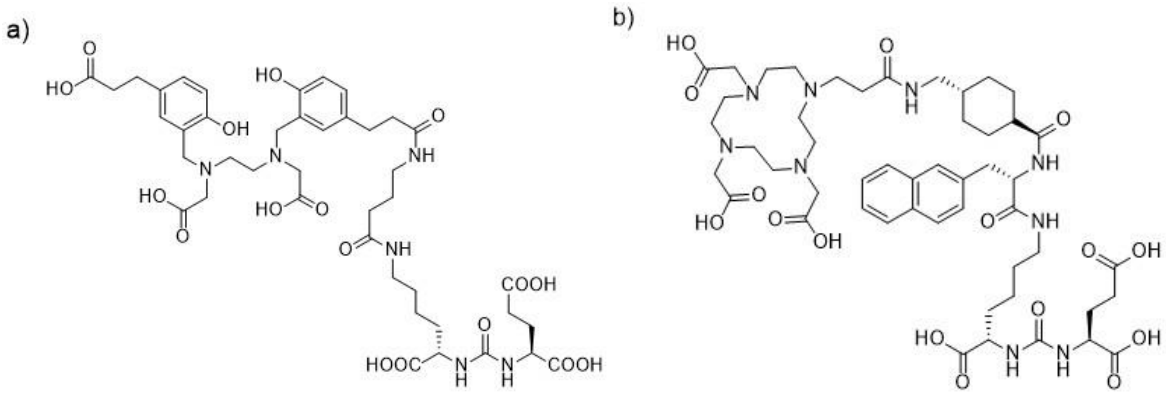

Figure 1.2. a) PSMA-11 with the HBED-CC chelator and b) PSMA-617 with the DOTA chelator.

The fundament for labelling reactions with ^{99m}Tc is an exact knowledge of the coordination chemistry of the radioactive transition metal. The related structural studies are commonly done with the long-lived isotope ^{99}Tc, a weak β^- emitter (E_{max}= 0.294 MeV) with a half-life of 211,100 years since there is no stable isotope of technetium. Thereby, rhenium as the heavier homologue of technetium and non-radioactive metal can serve as a model due to a similar chemical behavior and coordination chemistry. Other metals with nuclides of importance for nuclear medical imaging or therapy such as ^{68}Ga, ^{111}In or ^{177}Lu have stable isotopes, which can be used for fundamental chemical research.

1.2 Multidentate Ligands used for the Designing of new Tracers

A relatively new approach is the exploration of the chances given with the use of organotechnetium compounds and a number of promising studies with arene and cyclopentadienyl species of technetium in its low oxidation states have been brought to our attention.[18-32] The stability of such products with pseudo-tridentate ligands also makes it interesting to study related products with isolobal ligand systems such as scorpionates and similar systems. Some work has been done with tris(pyrazoyl)borate and related systems,[33-35] as well as with cyclic thioethers such as 1,4,7-trithiacyclononane (9-ane-S3) and corresponding cyclic amines such as triazacyclononane.[33-34, 36-40] Another interesting ligand system of this family is the so-called "Kläui ligand" η^5-cyclopentadienyltris(dialkylphosphito-P)cobaltate(III). Although already in the early days of the "Kläui ligand" chemistry there were considerations concerning the application of such systems for nuclear medical procedures and some related rhenium complexes have been prepared,[41] this idea has not been pursued further. Thus, there have been only a few reports about technetium complexes[42-43] and only a few more about rhenium compounds.[41, 43-47]

η^5-Cyclopentadienyltris(dialkylphosphito-P)cobaltates(III), $\{L^{OR}\}^-$, are a yellow, air- and water stable metalorganic compounds (Scheme 1.1).

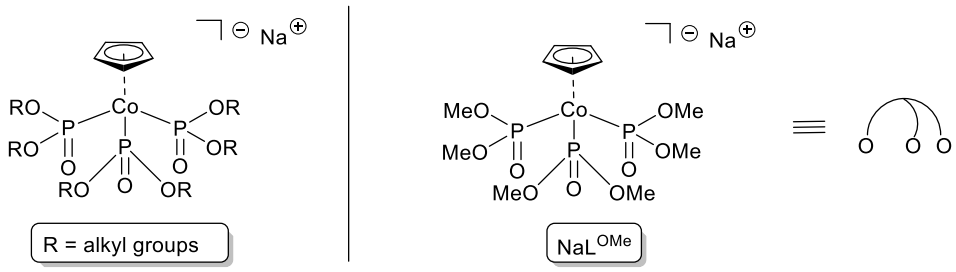

Scheme 1.1. The "Kläui ligands" NaL^{OR} and NaL^{OMe}, which was used in this work.

They are negatively charged and coordinate to many different metal ions. Remarkably, the ligands can stabilize “hard” and “soft” metal ions, as well as metal ions in high and low oxidation states. In this work, NaL^{OMe} η^5-cyclopentadienyl)tris(dimethylphosphito-P)cobaltate(III), is used. The coordination of $\{L^{OMe}\}^-$ occurs tripodal *via* three oxygen atoms in a facial coordination mode. The $^1H\{^{31}P\}$ NMR spectrum in $CDCl_3$ shows two signals for the protons of the methoxy groups and one for the aromatic protons. In the $^{31}P\{^1H\}$ NMR spectrum, a singlet is visible at 109 ppm with a half-line width of 49 Hz. A ^{59}Co NMR spectrum could not be detected. This is in agreement with literature reports.[48] The solid structure of NaL^{OMe} is not known. But, it is highly probable that it has a similar structure like the sodium salt of the ligand with ethoxy groups $\{L^{OEt}\}^-$, where a trimeric structure with $[(NaL^{OEt})_3(H_2O)_2]$ subunits has been found.[49] The arrangement of the polar, water-coordinated Na^+ ions in the center of the trimeric units and the formation of an outer sphere consisting of the {Co(Cp)} units explains the ready solubility of this sodium salt even in nonpolar solvents. Such a behavior is favorable for reactions with a number of neutral metal complexes, which are only soluble in nonpolar solvents and finally offers the opportunity to perform the reactions introduced in the present work. Complexes with rhenium, technetium, gallium, indium and lutetium were synthesized and fully characterized (Chapter 2). Furthermore, a functional group for possible bioconjugation was introduced. The synthesis of this modified “Kläui ligand” is described in Chapter 2.4.

The second class of used ligands in this work are potentially tetra- or pentadentate thiourea ligands with *S*, *N* and *O* donor atoms (Scheme 1.2). They have a benzoylthiourea unit with different alkyl substituents on the secondary amine, giving the opportunity to tune the chemical properties of these compounds. Starting from the corresponding benzimidoyl chlorides, the chloride can be replaced by different organic building blocks including a functional group for possible bioconjugation. Suitable, functional groups are –COOH or $–NH_2$ substituents as potential linkers for peptides.

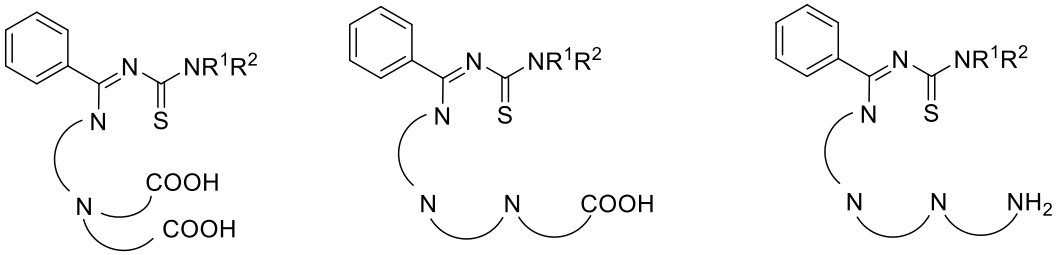

Scheme 1.2. Potentially tetra- or pentadentate thiourea ligands (R^1 and R^2 are alkyl or aryl substituents).

The thiourea ligands of Scheme 1.2 can be designed with a varying number of carboxylic groups. Three positions for deprotonation are contained in the ligands used in this thesis. Thus, they perfectly fit to the $\{Re^{V}O\}^{3+}$, $\{Re^{V}NPh\}^{3+}$, $\{Re^{V}NPhF\}^{3+}$ and $\{Tc^{V}O\}^{3+}$ cores.

2 Metal Complexes with the "Kläui Ligand" NaL^{OMe}

2.1 Technetium Complexes

Relatively little is known about technetium complexes with η^5-cyclopentadienyltris(alkylphosphito-P)cobaltates(III), the so-called "Kläui ligands". This is surprising, since such potentially tripodal ligands are extremely versatile donors, which form stable complexes with almost all metal ions and found consideration in various fields of coordination chemistry.[41, 43, 50-53] A survey of the coordination capabilities of η^5-cyclopentadienyltris(dimethylphosphito-P)cobaltate(III), $\{L^{OMe}\}^-$, to technetium with consideration of all common oxidation states of this transition metal is reported here. Reactions were performed with a series of technetium complexes covering all oxidation states of this metal from +I to +VII: $[Tc^{I}(NO)Cl_2(PPh_3)_2(MeCN)]$, $(NBu_4)[Tc^{II}(NO)Cl_4(MeOH)]$, $[Tc^{III}Cl_3(PPh_3)_2(MeCN)]$, $[Tc^{IV}Cl_4(PPh_3)_2]$, $[Tc^{V}NCl_2(PPh_3)_2]$, $(NBu_4)[Tc^{V}OCl_4]$, $(NBu_4)[Tc^{VI}NCl_4]$ and $(NH_4)[Tc^{VII}O_4]$.[54] Finally, all reactions proceeded without redox processes on the metal and the isolation of technetium complexes with $\{L^{OMe}\}^-$ ligands containing the metal in seven different oxidation states was possible. A summary of the obtained products is given in Scheme 2.1.

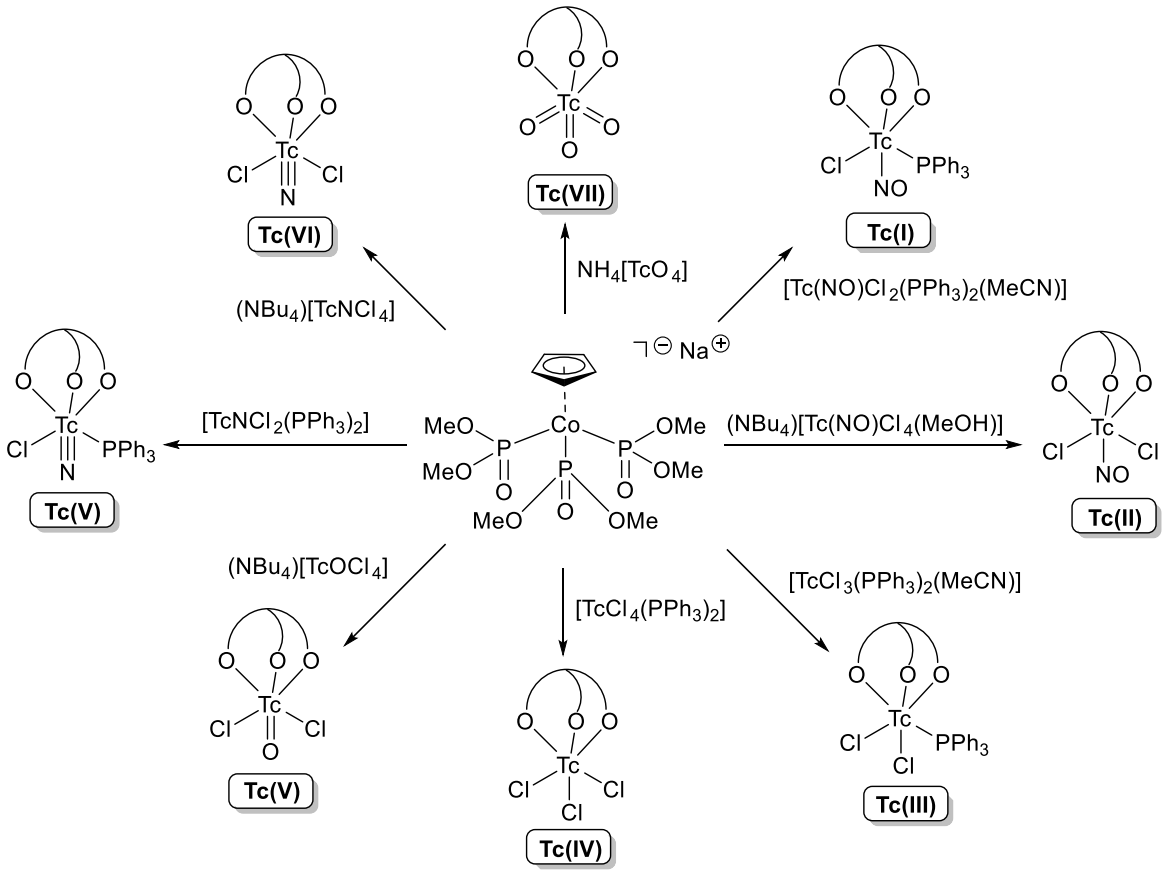

Scheme 2.1. Overview about the reactions of different technetium starting materials with NaL^{OMe}.[54]

2.1.1 $[Tc^{I}(NO)Cl(PPh_3)(L^{OMe})]$

The sparingly soluble Tc(I) complex $[Tc^{I}(NO)Cl_2(PPh_3)_2(MeCN)]$ dissolved during heating in a toluene solution of NaL^{OMe}, and the colour of the solution changed from green to red. Upon cooling, a red solid of $[Tc^{I}(NO)Cl(PPh_3)(L^{OMe})]$ deposited. The product is readily soluble in polar solvents such as $CHCl_3$, CH_2Cl_2 and acetonitrile, but is almost insoluble in hydrocarbons. Six different ^{1}H NMR signals between 2.89 and 3.90 ppm are observed for the methoxy protons of the chiral complex, while the ^{13}C signals of the methyl groups give three resonances at 51.5, 52.5, and 53.9 ppm. The ^{99}Tc NMR signal of $[Tc^{I}(NO)Cl(PPh_3)(L^{OMe})]$ appears at 1475 ppm (Figure 2.1b), which is at surprisingly low field in comparison with the signals of the related complexes $[Tc^{I}(NO)Cl(PPh_3)(Cp)]$ and $[Tc^{I}(NO)Cl(PPh_3)(HBpz_3)]$ ($HBpz_3^-$ = hydrotris(pyrazolyl)borate).[55] More comments about the ^{99}Tc NMR spectra of the diamagnetic complexes of the present study can be found below. The cyclic voltammogram of the compound shows a quasi-reversible one-electron oxidation with a half-wave potential of −0.16 V.

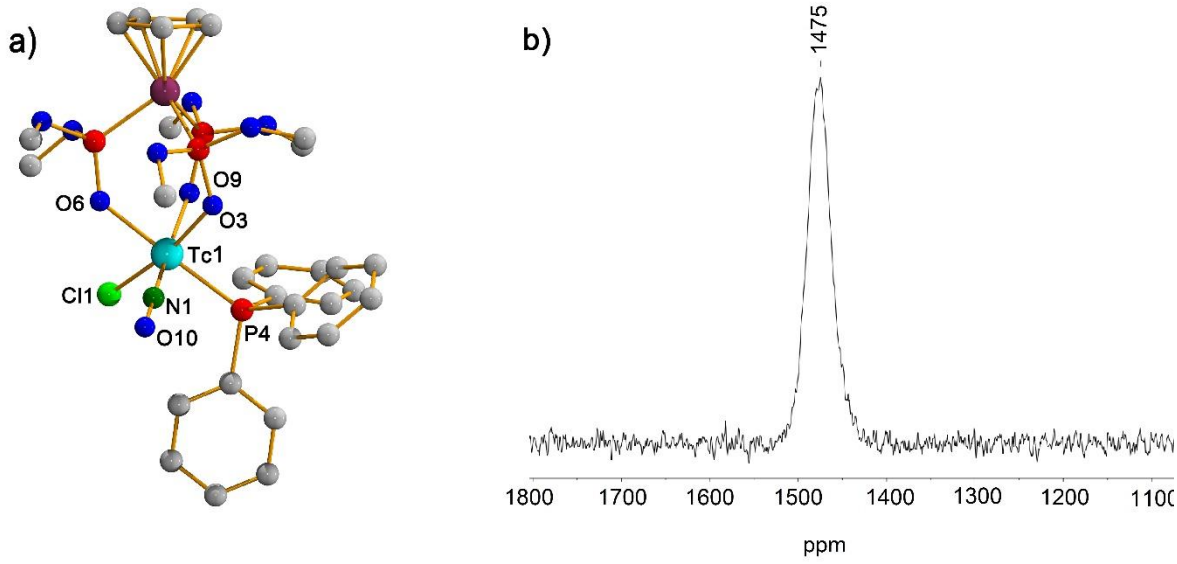

Figure 2.1. a) Molecular structure of $[Tc^{I}(NO)Cl(PPh_3)(L^{OMe})]$. The hydrogen atoms have been omitted for clarity. b) ^{99}Tc NMR spectrum of $[Tc^{I}(NO)Cl(PPh_3)(L^{OMe})]$ in $CDCl_3$.

The molecular structure of $[Tc^{I}(NO)Cl(PPh_3)(L^{OMe})]$ shows a distorted-octahedral coordination environment for the technetium atom (Figure 2.1a). As expected, $\{L^{OMe}\}^-$ binds in a tripodal arrangement via its three oxygen atoms. The Tc–O bond lengths slightly differ with values between 2.124(1) and 2.166(1) Å depending on their *trans* ligands, indicating that the strongest *trans* influence is due to the NO^+ ligand. Unfortunately, the values are somewhat disturbed by a NO^+/Cl^- structural disorder with occupational factors of 0.57/0.43. The nitrosyl ligand is linearly coordinated as in all

hitherto structurally characterized nitrosyl complexes of technetium and should consequently be regarded as a formal NO^+ unit.[56] The IR spectrum of $[Tc^{I}(NO)Cl(PPh_3)(L^{OMe})]$ shows the characteristic *v*(NO) band at 1692 cm^{-1}. This is in the typical range for technetium(I) complexes and reflects a considerable degree of back-donation of the d^6 systems into anti-bonding orbitals of the NO ligand.[31-32, 56-61]

2.1.2 $[Tc^{II}(NO)Cl_2(L^{OMe})]$

A *v*(NO) frequency at higher wavenumbers (1743 cm^{-1}) is found for the technetium(II) complex $[Tc^{II}(NO)Cl_2(L^{OMe})]$. This compound is formed during the reaction of $(NBu_4)[Tc^{II}(NO)Cl_4(MeOH)]$ with NaL^{OMe}. Both complexes are d^5 systems with one unpaired electron, which allows an EPR detection of the course of the reaction and shows a maximum formation of the red $[Tc^{II}(NO)Cl_2(L^{OMe})]$ after 1 h in refluxing methanol, while paramagnetic side products appear on prolonged heating. Pure $[Tc^{II}(NO)Cl_2(L^{OMe})]$ is obtained after column chromatography on silica. Figure 2.2 depicts the molecular structure of the compound with a linearly bonded nitrosyl ligand, which exerts a slight *trans* influence also via the Tc(II) ion and stretches the Tc−O6 bond to a value of 2.075(3) Å, while the Tc−O3 and Tc−O9 bonds have values of 2.053(3) and 2.054(3) Å, respectively.

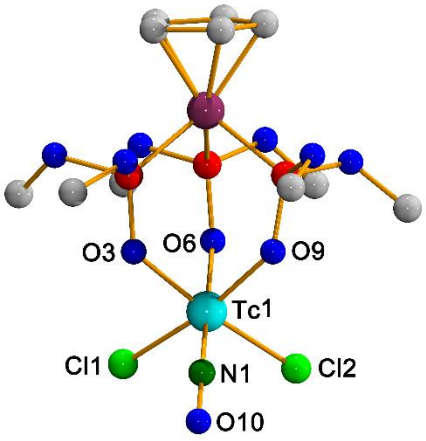

Figure 2.2. Molecular structure of $[Tc^{II}(NO)Cl_2(L^{OMe})]$. The hydrogen atoms have been omitted for clarity.

Solutions of $[Tc(NO)Cl_2(L^{OMe})]$ give well-resolved X-band EPR spectra (Figure 2.3). At room temperature, the typical 10-line pattern is visible, which is due to the coupling of the unpaired electron with the nuclear spin of ^{99}Tc of I = 9/2 (g_0 = 2.002, $a_0^{Tc} = 168 \cdot 10^{-4}\ cm^{-1}$). The frozen-solution spectrum shows a typical axially symmetric coupling pattern with 10 well-resolved hyperfine lines in the parallel and perpendicular parts ($g_\parallel$ = 1.930, $g_\perp$ = 2.010, $A_\parallel^{Tc} = 280 \cdot 10^{-4}\ cm^{-1}$, $A_\perp^{Tc} = 120 \cdot 10^{-4}\ cm^{-1}$). Couplings due to the ^{14}N nucleus of the axial NO ligand are not resolved. This is not unexpected with regard to the

MO of the unpaired electron, which has mainly “xy character” in this type of compounds. Similar findings have been reported before for other nitrosyl- and thionitrosyltechnetium(II) compounds.[31, 56, 58-62]

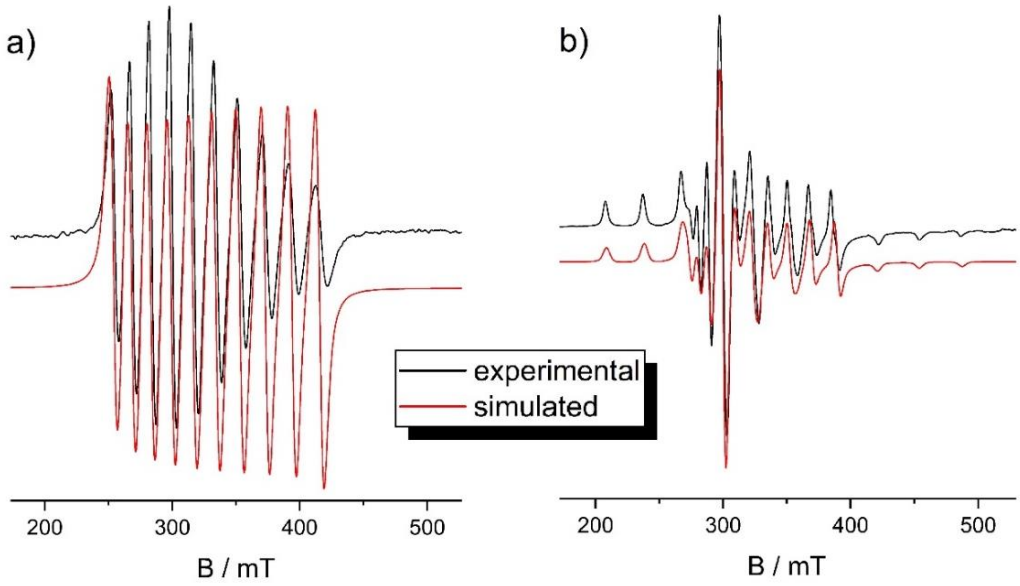

Figure 2.3. X-Band EPR spectra of $[Tc^{II}(NO)Cl_2(L^{OMe})]$ in CH_2Cl_2 at room temperature (a) and 77 K (b).

2.1.3 $[Tc^{III}Cl_2(PPh_3)(L^{OMe})]$

A technetium(III) complex with the “Kläui ligand” was prepared by a reaction starting from $[Tc^{III}Cl_3(PPh_3)_2(MeCN)]$. The sparingly soluble starting material slowly dissolves after treatment with 1 equiv. of NaL^{OMe} in refluxing CH_2Cl_2. A clear brown solution is formed after 2 h. Addition of MeOH and slow evaporation of the solvents gave brown single crystals of the paramagnetic complex $[Tc^{III}Cl_2(PPh_3)(L^{OMe})]$. The compound is readily soluble in CH_2Cl_2 or $CHCl_3$. The molecular structure of the complex is shown in Figure 2.4a. The coordination environment of the technetium atom in $[Tc^{III}Cl_2(PPh_3)(L^{OMe})]$ is distorted octahedral, and the bond lengths and angles are unexceptional. Three slightly different Tc−O bond lengths are found (2.104(3), 2.119(3) and 2.133(3) Å). The lengthening of the Tc−O6 bond is due to the structural *trans* influence of the PPh_3 ligand. Slight differences are also found for the Tc−Cl bonds (Tc−Cl1 2.342(1) Å and Tc−Cl2 2.339(1) Å). Cyclic voltammetry shows a quasi-reversible one-electron oxidation with a half-wave potential of −0.304 V (Figure 2.4b).

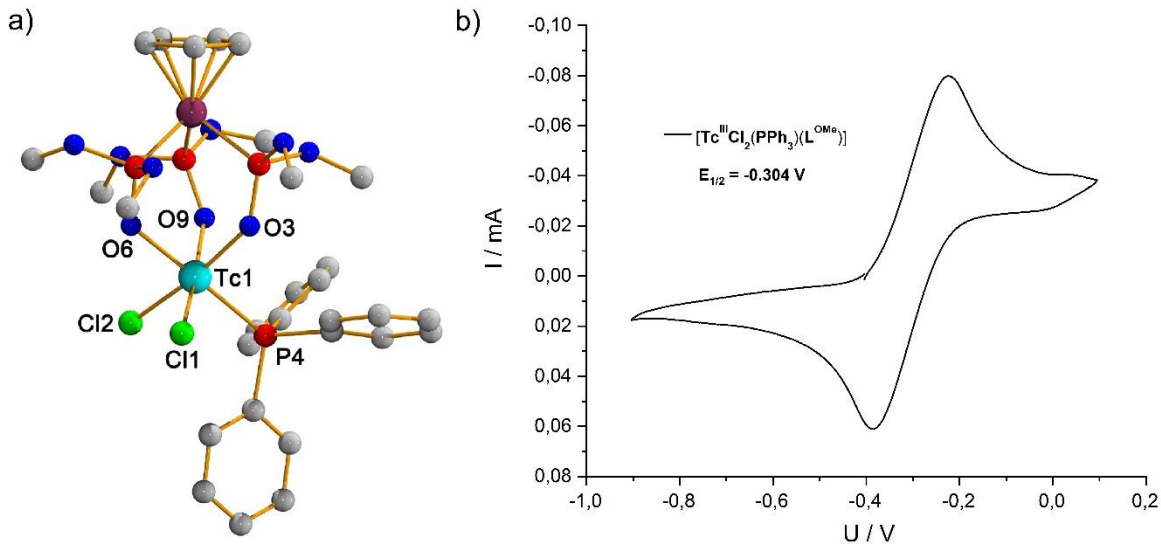

Figure 2.4. a) Molecular structure of $[Tc^{III}Cl_2(PPh_3)(L^{OMe})]$. The hydrogen atoms have been omitted for clarity. b) Cyclic voltammogram of $[Tc^{III}Cl_2(PPh_3)(L^{OMe})]$ in CH_2Cl_2.

2.1.4 $[Tc^{IV}Cl_3(L^{OMe})]$

A stable technetium(IV) complex with $\{L^{OMe}\}^-$ was obtained from a reaction of NaL^{OMe} with the sparingly soluble complex $[Tc^{IV}Cl_4(PPh_3)_2]$. The green starting material rapidly dissolves in boiling CH_2Cl_2 and a yellow crystalline solid could be isolated from the resulting brown solution. An X-ray diffraction study proves the formation of $[Tc^{IV}Cl_3(L^{OMe})]$. The technetium atom has a distorted octahedral coordination sphere. The molecular structure is depicted in Figure 2.5a. Although the molecule contains three virtually identical Cl^- ligands, three slightly different Tc−Cl bond lengths (2.3036(7), 2.3098(7), and 2.3136(7) Å) have been found. Also the Tc-O bond lengths are slightly different: 2.035(2), 2.027(2) and 2.026(2) Å. However, this differences are small and also occur in the $[Tc^{VII}O_3(L^{OMe})]$ with the virtually identical oxido ligands. Two molecules of $[Tc^{IV}Cl_3(L^{OMe})]$ are in the asymmetric unit. Each chlorido ligand has a slightly different chemical environment, which explains the small differences in the bond lengths. The unit cell of $[Tc^{IV}Cl_3(L^{OMe})]$ is shown in Figure 1.7b.

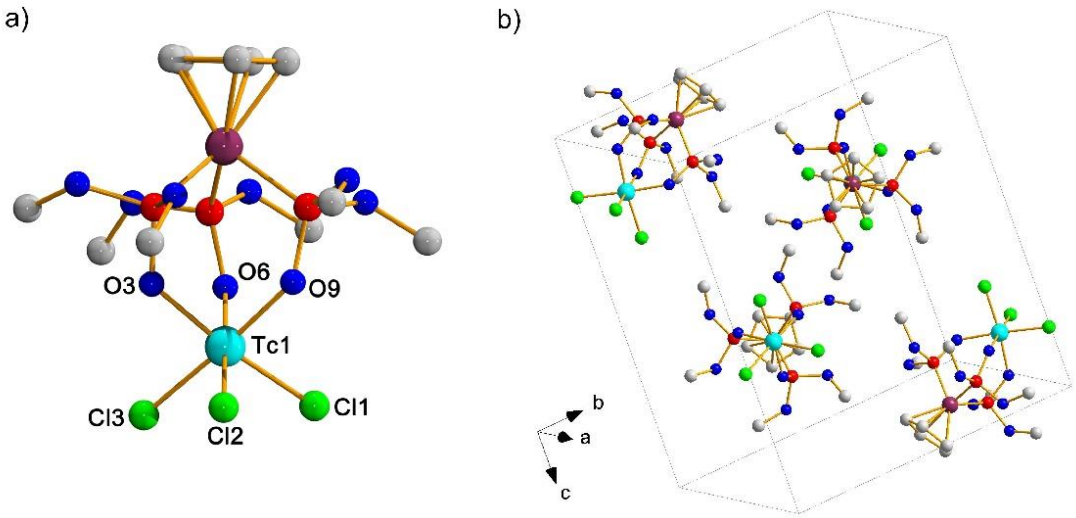

Figure 2.5. a) Molecular structure of $[Tc^{IV}Cl_3(L^{OMe})]$. b) Crystal packing of $[Tc^{IV}Cl_3(L^{OMe})]$. The hydrogen atoms have been omitted for clarity.

2.1.5 $[Tc^{V}OCl_2(L^{OMe})]$ and $[Tc^{V}NCl(PPh_3)(L^{OMe})]$

Technetium complexes in the oxidation state +V frequently show a core structure, which means that the stability of complexes with such electron-poor metal ions is supported by the presence of multiply bonded strong donors such as O^{2-}, N^{3-} or $\{NPh\}^{2-}$.[7, 33] This results in the formation of $\{TcO\}^{3+}$, $\{TcN\}^{2+}$, $\{trans\text{-}TcO_2\}^{+}$ or $\{Tc(NPh)\}^{3+}$ cores, in which the coordination positions of incoming ligands are frequently predefined by the core and/or the structural *trans* influence caused by the multiply bonded ligands. Here, some oxido- and nitridotechnetium(V) complexes with NaL^{OMe} are included.

$[Tc^{V}OCl_2(L^{OMe})]$ was isolated from a reaction of $(NBu_4)[TcOCl_4]$ with NaL^{OMe} in analogy to the synthesis of the corresponding diethyl derivative $[Tc^{V}OCl_2(L^{OEt})]$.[42] The IR spectrum of the resulting yellow-green crystals shows the ν(Tc=O) band at 959 cm^{-1}. Three singlets for the methyl groups and one singlet for the Cp^{-} protons are observed in the ^{1}H NMR spectrum of the diamagnetic d^2 complex. In addition, the ^{13}C NMR spectrum shows signals for three methyl groups, which is in agreement with the suggested bonding situation. In contrast to the situation in the uncoordinated $\{L^{OMe}\}^{-}$ ligand, for which the ^{31}P resonance is observed as a sharp singlet at 109 ppm in $CDCl_3$, the ^{31}P signals of the chelating ligand in all diamagnetic Tc complexes of this study are shifted downfield and split as a consequence of their inequivalence. For $[Tc^{V}OCl_2(L^{OMe})]$, a broad multiplet is observed between 121 and 126 ppm. A notable line broadening of ^{31}P signals is frequently observed for diamagnetic technetium complexes and explained by scalar couplings between ^{31}P and the large quadrupole moment of ^{99}Tc.[31-32, 63-64] In many cases (as in $[Tc^{I}(NO)Cl(PPh_3)(L^{OMe})]$ and $[Tc^{V}NCl(PPh_3)(L^{OMe})]$ of the present thesis), such broadenings make the related ^{31}P phosphine NMR signals practically invisible. The molecular structure of

[$Tc^{V}OCl_2(L^{OMe})$] (Figure 2.6) confirms the expected distorted-octahedral coordination sphere of the metal atom. [$TcOCl_2(L^{OMe})$] was refined as a two-component inversion twin. Main distortions from an ideal octahedron are caused by the presence of the double-bonded oxido ligand, which increases the O10−Tc−Cl1 and O10−Tc−O3 angles to values between 99.84(8)° and 91.71(1)°. Remarkably, no lengthening of the Tc−O6 bond (2.078(2) Å) as a consequence of the structural *trans* influence of the oxido ligand is observed in [$Tc^{V}OCl_2(L^{OMe})$]. It is found in the same range as the Tc−O3 (2.079(2) Å) and Tc−O9 (2.065(2) Å) bonds.

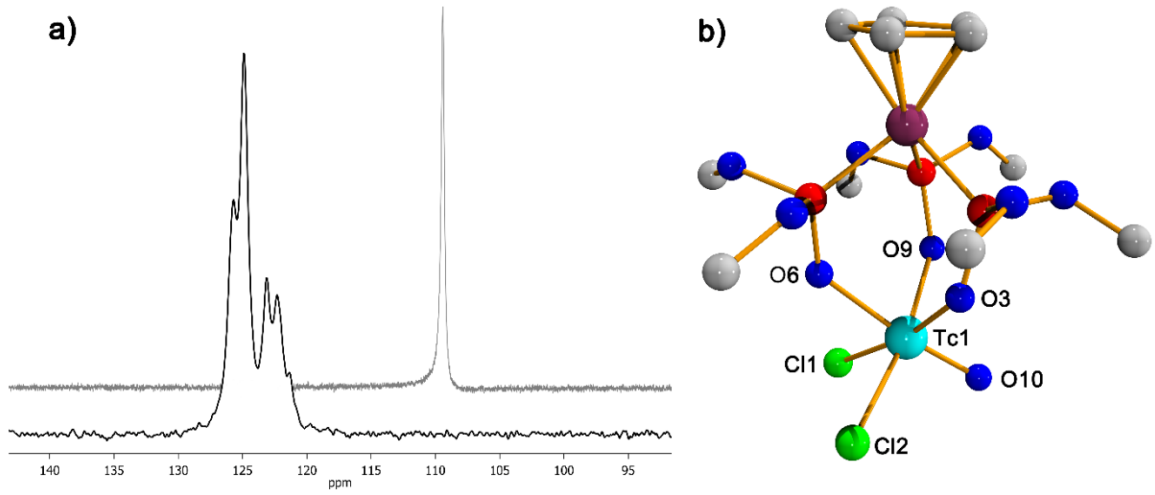

Figure 2.6. a) ^{31}P NMR spectrum of [$Tc^{V}OCl_2(L^{OMe})$] (front) and of NaL^{OMe} (back) in $CDCl_3$.
b) Molecular structure of [$Tc^{V}OCl_2(L^{OMe})$]. The hydrogen atoms have been omitted for clarity.

This is unlike the situation in [$Tc^{V}NCl(PPh_3)(L^{OMe})$], the second technetium(V) complex, which has been studied by X-ray diffraction. It is known that N^{3-} ligands exert a strong *trans* labilisation of ligands. The nitrido and one chlorido ligand are disordered. Also the Tc atom was refined at two positions. The ratio between the both structures is nearly 1:1. In both structure parts, the strong *trans* labilisation of N^{3-} is visible. The Tc1−O6 bond *trans* to the nitrido ligand (2.363(2) Å) is clearly longer than the other two Tc1−O bonds (2.058(2) and 2.129(2) Å) (Figure 2.7a). The Tc-N triple bond length is in the expected region (1.635(5), 1.632(6) Å).

The technetium-nitrido stretch of [$Tc^{V}NCl(PPh_3)(L^{OMe})$] is found in the IR spectrum at 997 cm^{-1} as a strong and sharp band. Tc(V) can be oxidized electrochemically to Tc(VI). The cyclic voltammogram is shown in Figure 2.7b.

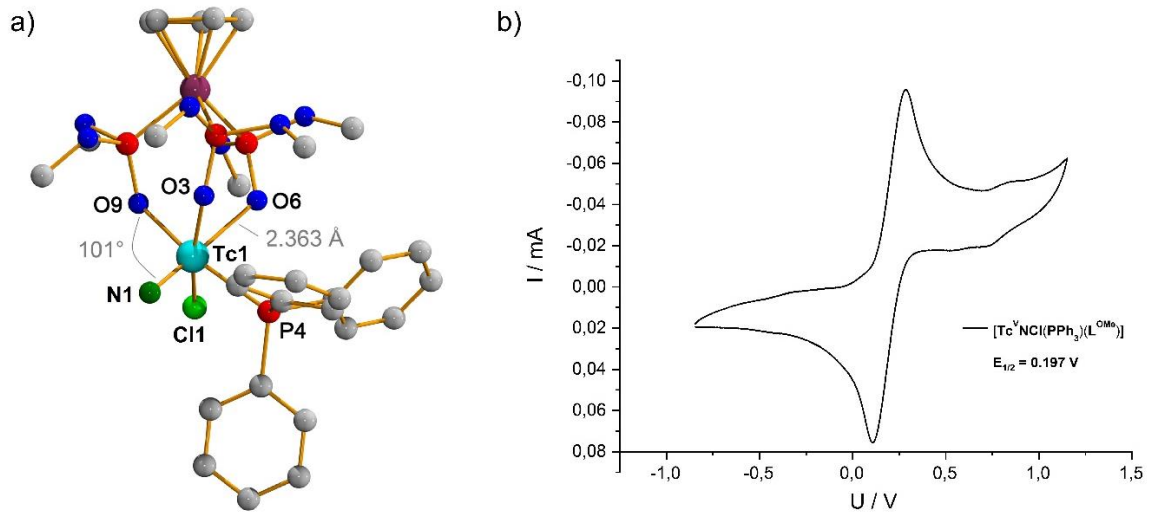

Figure 2.7. a) Molecular structure of $[Tc^{V}NCl(PPh_3)(L^{OMe})]$. The hydrogen atoms have been omitted for clarity. b) Cyclic voltammogram of $[Tc^{V}NCl(PPh_3)(L^{OMe})]$ in CH_2Cl_2.

2.1.6 $[Tc^{VI}NCl_2(L^{OMe})]$

A considerable structural *trans* influence is also observed in the nitridotechnetium(VI) complex, which was obtained from the reaction of $(NBu_4)[Tc^{VI}NCl_4]$ with NaL^{OMe} in boiling CH_2Cl_2. Although the colour of the reaction mixture did not change, the consumption of the d^1 starting material could be readily followed by EPR spectroscopy. The signals of $[TcNCl_4]^-$ almost completely disappeared within 1 h and another paramagnetic complex, $[Tc^{VI}NCl_2(L^{OMe})]$, was formed (Figure 2.8).

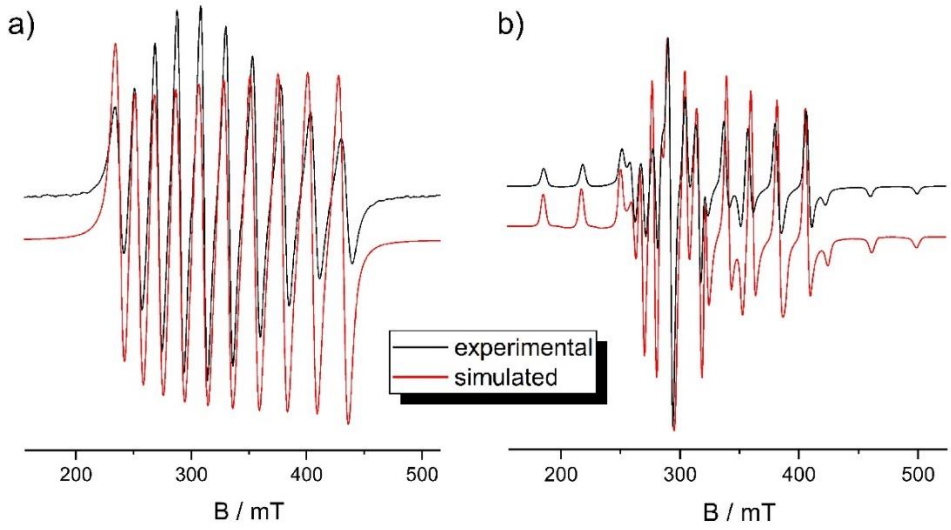

Figure 2.8. X-Band EPR spectrum of $[Tc^{VI}NCl_2(L^{OMe})]$ in CH_2Cl_2 at a) room temperature and b) 77 K.

A partial exchange of the donor atoms in the equatorial coordination sphere can clearly be concluded from the decrease of the g_0 ($[TcNCl_4]^-$, 2.003;[65] $[TcNCl_2(L^{OMe}]$, 1.991) and $g_\parallel$ values ($[TcNCl_4]^-$, 2.008;[66] $[TcNCl_2(L^{OMe})]$, 1.952) and the increase in the ^{99}Tc hyperfine coupling constants a_0^{Tc} ($[TcNCl_4]^-$, $187 \cdot 10^{-4}\,cm^{-1}$;[65] $[TcNCl_2(L^{OMe})]$, $199 \cdot 10^{-4}\,cm^{-1}$) and $A_\parallel^{Tc}$ ($[TcNCl_4]^-$, $293 \cdot 10^{-4}\,cm^{-1}$;[66] $[TcNCl_2(L^{OMe})]$, $319 \cdot 10^{-4}\,cm^{-1}$). Both the g values and the coupling constants in such axially symmetric complexes are roughly correlated to the spin–orbit coupling constants of the donor atoms, as has been shown by a number of previous studies.[66-70]

Red single crystals were obtained from a CH_2Cl_2/Et_2O mixture. The molecular structure of $[Tc^{VI}NCl_2(L^{OMe})]$ is depicted in Figure 2.9. The influence of the steric bulk of the short technetium–nitrogen triple bond (1.64(2) Å) on the coordination sphere of the metal is documented by N–Tc–O and N–Tc–Cl angles ranging between 94.89(9) and 97.53(7)°. The Tc–O6 bond of 2.284(2) Å is clearly longer than the other two Tc–O bonds.

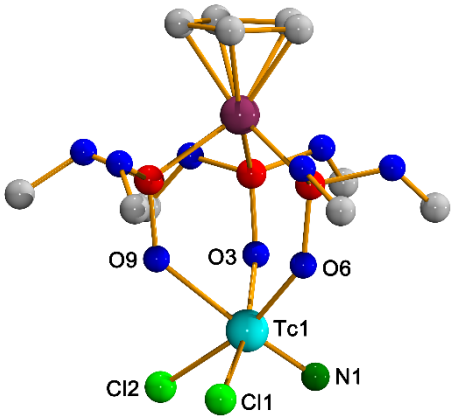

Figure 2.9. Molecular structure of $[Tc^{VI}NCl_2(L^{OMe})]$. The hydrogen atoms have been omitted for clarity.

It should be mentioned that a number of Re(V) and Re(VI) complexes with the related "Kläui ligand" $\{L^{OEt}\}^-$ have been synthesized, among them the nitrido complexes $[Re^{V}NCl(PPh_3)(L^{OEt})]$ and $[Re^{VI}NCl_2(L^{OEt})]$.[46-47] Unlike the technetium complexes of the present study, they readily react with Lewis bases such as electron-poor metal complexes or carbenium salts with formation of heterobimetallic complexes or imido compounds, which could not be observed for the technetium complexes of this study. Such different behaviour of structurally identical rhenium and technetium complexes, however, is not completely surprising and has been observed before on a series of nitrido complexes of these two transition metals.[71] Technetium complexes with nitrido bridges have only been isolated in exceptional cases and are frequently not stable in solutions at ambient temperature.[72-74]

2.1.7 $[Tc^{VII}O_3(L^{OMe})]$ and $[Tc^{V}O(glycolate)(L^{OMe})]$

Technetium(VII) compounds with "Kläui-type" and related ligands attracted some attention as potential tracers in nuclear medical procedures in the 1990s, and a number of related rhenium complexes of the composition $[ReO_3(L^{OR})]$ have been synthesized and structurally characterized.[41-44, 75] In this context, also the synthesis and some spectroscopic data of the corresponding technetium complexes with $\{L^{OMe}\}^-$, $\{L^{OEt}\}^-$, and $\{L^{OBu}\}^-$ have been reported.[42, 44] In the present study, $[Tc^{VII}O_3(L^{OMe})]$ was prepared by a slight modification of the reported synthesis. The diamagnetic compound were obtained as a yellow solid in an almost quantitative yield. Single crystals for X-ray diffraction were grown from CH_2Cl_2/MeOH. Figure 2.10a illustrates the molecular structure of the compound. The coordination sphere of technetium is distorted octahedral with some deviations from the ideal geometry due to the restrictions given by the geometry of the tripodal ligand. The diamagnetic $[Tc^{VII}O_3(L^{OMe})]$ gives a ^{99}Tc NMR signal at +343 ppm in $CDCl_3$ with a half-line width $\Delta\nu$ of 680 Hz, which is in the range of the corresponding signals for other trioxidotechnetium(VII) complexes (Figure 2.10b).[42, 75-77]

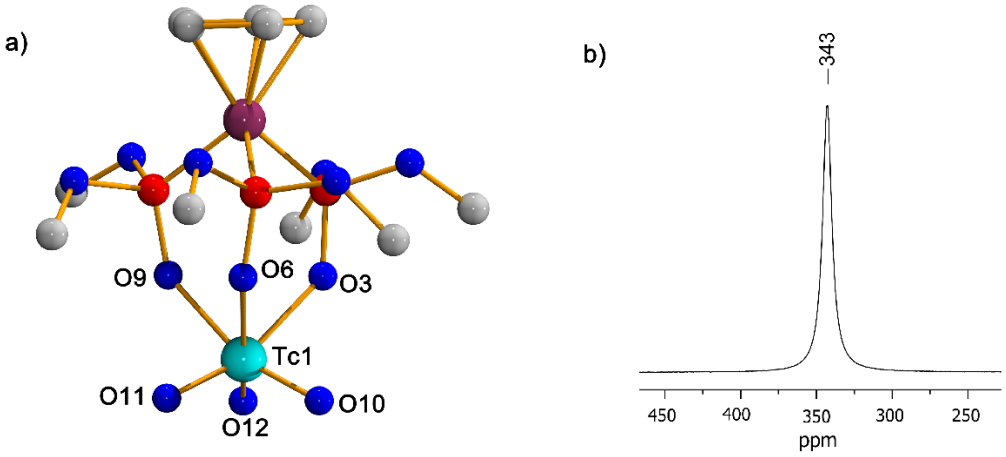

Figure 2.10. a) Molecular structure of $[Tc^{VII}O_3(L^{OMe})]$. The hydrogen atoms have been omitted for clarity. b) ^{99}Tc NMR spectrum of $[Tc^{VII}O_3(L^{OMe})]$ in $CDCl_3$.

$[Tc^{VII}O_3(L^{OMe})]$ reacts with ethene in chloroform under formation of $[Tc^{V}O(glycolate)(L^{OMe})]$ (Scheme 2.2). The $\{L^{OMe}\}^-$ ligand and one Tc=O bond remain untouched. The colour of the reaction solution turned from yellow to green after 30 min. Green single crystals were obtained from a CH_2Cl_2/Et_2O solution in the refrigerator after slow evaporation. Tc was reduced from the oxidation state +VII to +V under formation of ethylene glycol by consumption of two oxido ligands.

The coordination sphere of the technetium atom is distorted octahedral. The Tc-O11 and Tc-O12 bonds are clearly single bonds with lengths of 1.859(6) Å and 1.891(8) Å. One Tc=O double bond was retained

(Tc-O10: 1.625(8) Å). The phosphorus and oxygen atoms of the $\{L^{OMe}\}^-$ ligand are disordered in a ratio of 60:40. The Tc=O stretch is found in the IR spectrum at 952 cm^{-1}. The protons of the ethylene glycol appear in the $^1H\{^{31}P\}$ NMR spectrum at 4.81 and 5.64 ppm as multiplets. The analogous reaction with $[Re^{VII}O_3(L^{OMe})]$ and ethene does not occur. Only the starting material was obtained. This is due to the different reduction potentials between technetium and rhenium.

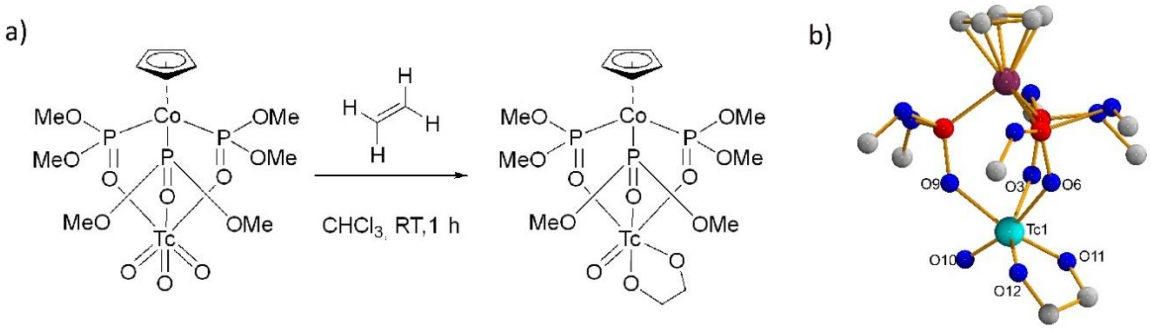

Scheme 2.2. a) Reaction of $[Tc^{VII}O_3(L^{OMe})]$ with ethene in $CHCl_3$. b) The molecular structure of $[Tc^{V}O(glycolate)(L^{OMe})]$. The hydrogen atoms have been omitted for clarity.

The [3+2] cycloaddition of an ethene derivative with a trioxo core of technetium complexes was already published with different bidentate or tridentate ligands. Different substituted olefins with functionalised side chains were oxidized by $[Tc^{VII}O_3Cl(AA)]$ (AA = phen, bpy, 5-NO_2-phen, 3,4,7,8-Me_4-phen) under formation of ethylene glycol derivatives using two oxido ligands.[78] The varity of chelating aromatic diamine ligands change the inductive effects on the reduction potential of the metal ion. However, all Tc complexes show similar reactivity. The corresponding rhenium complex $[Re^{V}OCl(glycol)(phen)]$ decomposed while heating to the starting materials $[Re^{VII}O_3Cl(phen)]$ and ethene.[78] Also the substituted, tridentate tacn-ba ligand was used for such approaches.[39] $[Tc^{VII}O_3(tacn\text{-}ba)]$ oxidised substituted alkene derivatives like 4-vinylbenzenesulfonate. This concept could be used to introduce a specific functionality like a fluorescence marker or a targeting moiety for nuclear medical imaging. Also the $[Tc^{VII}O_3(L^{OMe})]$ complex with the $\{L^{OMe}\}^-$ ligand is a potentially candidate for this approach (Scheme 2.3).

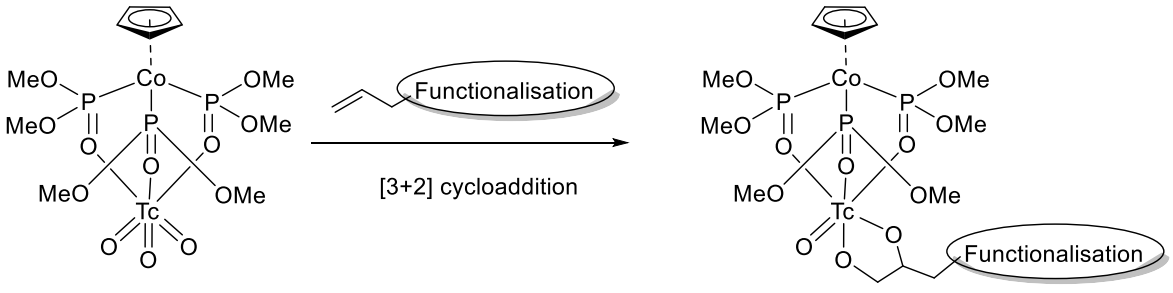

Scheme 2.3. Possible strategy to introduce a functionalization *via* alkenes.

2.1.8 Summary of the Tc Chemistry with the "Kläui-type" Ligands

The tripodal η^5-cyclopentadienyltris(dialkylphosphito-P)-cobaltates(III), the "Kläui ligands" $\{L^{OR}\}^-$, are perfectly suitable for the stabilization of technetium complexes with the metal in various oxidation states. Irrespective of the oxidation state and the metal core, the ligands coordinate in a tripodal arrangement and the bonding situation inside the ligand is almost uninfluenced by the technetium site, as can be concluded by almost unchanged bond lengths and angles and ^{1}H and ^{31}P NMR signals. Table 2.1 summarizes selected bond lengths and angles of the studied Tc "Kläui-type" complexes. The values confirm that marked bond length modifications in the coordination sphere are only observed for the nitrido complexes. Surprisingly, a similar *trans* influence was not observed for the oxido technetium(V) complex $[Tc^{V}OCl_2(L^{OMe})]$, despite the fact that the corresponding Tc-O bond of 1.643(2) Å has a usual value. The O11-Tc1-O6 angle in $[Tc^{VII}O_3(L^{OMe})]$ is with 85.24(8)° the smallest angle found in the coordination sphere of the obtained Tc complexes with $\{L^{OMe}\}^-$. The largest angle was obtained in $[Tc^{V}NCl(PPh_3)(L^{OMe})]$ (N1-Tc1-O9 angle of 101.37(2)°).

Table 2.1. Selected bond lengths [Å] and angles [°] in the coordination sphere of the Tc complexes with $\{L^{OMe}\}^-$. Grey-marked: *Trans* influence of the nitrido ligand.

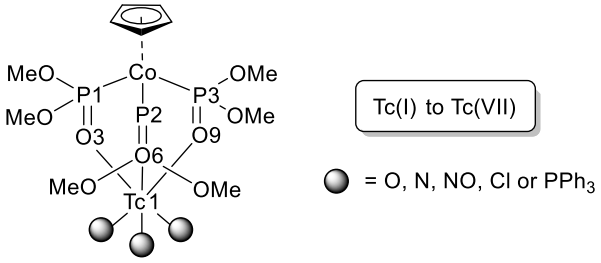

	[Tc(NO)Cl-(PPh$_3$)(L^{OMe})]	[Tc(NO)Cl$_2$–(L^{OMe})]	[TcCl$_2$(PPh$_3$)–(L^{OMe})]	[TcCl$_3$–(L^{OMe})]	[TcOCl$_2$–(L^{OMe})]	[TcNCl(PPh$_3$)–(L^{OMe})]	[TcNCl$_2$–(L^{OMe})]	[TcO$_3$–(L^{OMe})]
Tc1-O3	2.124(1)	2.054(3)	2.104(3)	2.035(2)	2.079(2)	2.058(2)	2.034(2)	2.144(2)
Tc1-O6	2.166(1)	2.075(3)	2.133(3)	2.027(2)	2.078(2)	2.363(2)	2.284(2)	2.176(2)
Tc1-O9	2.134(1)	2.053(3)	2.119(3)	2.026(2)	2.065(2)	2.129(2)	2.027(2)	2.141(2)
P1-O3	1.519(1)	1.527(3)	1.527(3)	1.538(2)	1.533(2)	1.508(2)	1.531(2)	1.521(2)
P2-O6	1.510(1)	1.516(3)	1.518(3)	1.531(2)	1.535(2)	1.510(2)	1.532(2)	1.516(2)
P3-O9	1.518(1)	1.532(3)	1.513(3)	1.535(2)	1.534(2)	1.515(2)	1.505(2)	1.519(2)
Tc1-O3-P1	127.29(7)	132.7(2)	129.1(2)	129.8(1)	128.2(1)	135.1(1)	136.9(1)	138.0(1)
Tc1-O6-P2	128.13(7)	134.4(2)	128.0(2)	131.5(1)	133.7(1)	125.39(9)	136.4(1)	137.4(1)
Tc1-O9-P3	129.85(7)	131.3(2)	126.3(2)	130.2(1)	131.0(1)	127.03(9)	133.7(1)	138.5(1)

The observed ^{99}Tc NMR signal for $[Tc^{VII}O_3(L^{OMe})]$ at +343 ppm is in the range of the corresponding signals for $[Tc^{VII}O_3(L^{OEt})]$ and $[Tc^{VII}O_3(L^{OBu})]$ (Figure 2.11).[42] Although these NMR signals are clearly broad in comparison with those of highly symmetric species such as TcO_4^- ($\Delta\nu \approx 3$ Hz) or the hexakis(isocyanide)technetium(I) cations $[Tc(CNR)_6]^+$ ($\Delta\nu \approx 70$ Hz),[79] the signals can readily be detected due to the high NMR sensitivity of the nucleus ^{99}Tc, which is approximately 25 % of that of the proton.[80] The strong line broadening by the influence of the large quadrupole moment of ^{99}Tc is slightly weakened by the high nuclear spin (I= 9/2) of this nucleus.[79] Much broader than the ^{99}Tc NMR signal of $[Tc^{VII}O_3(L^{OMe})]$ is that of the technetium(I) complex $[Tc(NO)Cl(PPh_3)(L^{OMe})]$ ($\Delta\nu \approx 2700$ Hz). The line width is in the range of those observed for the related complexes $[Tc(NO)Cl(PPh_3)(HBpz_3)]$ and $[Tc(NO)Cl(PPh_3)(Cp)]$.[31, 55] The strong broadening of the signals is adequately explained with the lower local symmetry of the Tc atoms in these complexes. Remarkably, the chemical shifts for the three structurally strongly related nitrosyltechnetium(I) complexes are very different. The signals of $[Tc(NO)Cl(PPh_3)(L^{OMe})]$ and $[Tc(NO)Cl(PPh_3)(HBpz_3)]$ appear in the downfield region of the chemical shift range, which is typical for Tc(I) complexes and only very few other Tc(I) compounds have been observed in this range, such as $[Tc(NO)(py)_4]^+$, $[Tc(NO)(NH_3)_4F]^+$ and $[Tc(NO)(NH_3)_4(CF_3COO)]^+$.[58] The observed difference in the chemical shift of the corresponding cyclopentadienyl complex $[Tc^{I}(NO)Cl(PPh_3)(Cp)]$ (−231 ppm) is surprising in the light of the fact that the isolobal $\{L^{OR}\}^-$ and $\{HBpz_3\}^-$ ligands are frequently discussed as synthetic and electronic surrogates for Cp^-, and at least a strong electronic similarity among these three tripodal ligands should be reconsidered.

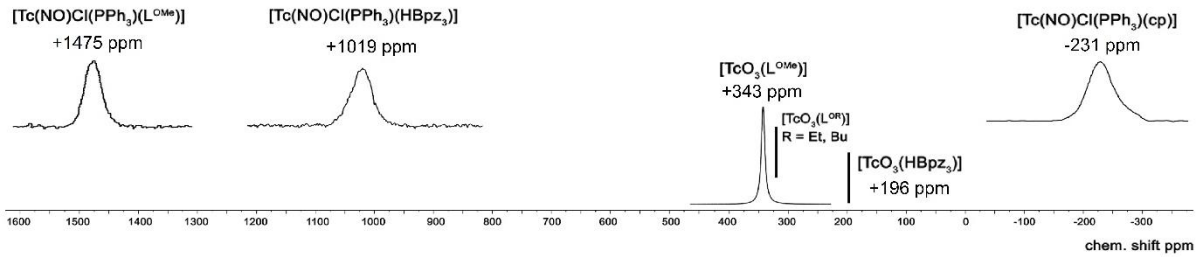

Figure 2.11. ^{99}Tc NMR spectra of $[Tc^{I}(NO)Cl(PPh_3)(L^{OMe})]$ in $CDCl_3$, $[Tc^{I}(NO)Cl(PPh_3)(HBpz_3)]$ in $CDCl_3$, $[Tc^{I}(NO)Cl(PPh_3)(Cp)]$ in $CDCl_3$, $[Tc^{VII}O_3(L^{OMe})]$ in $CDCl_3$, $[Tc^{VII}O_3(L^{OEt})]$ (+320 ppm) in CD_2Cl_2, $[Tc^{VII}O_3(L^{OBu})]$ (+320 ppm) in CD_2Cl_2 and $[Tc^{VII}O_3(HBpz_3)]$ in CD_2Cl_2.

The isolated complexes are air- and water-stable, which recommends them for nuclear medical applications. Modifications in the side chains of the phosphites or at the Cp ring of the $\{L^{OR}\}^-$ ligands should provide suitable compounds for bioconjugation. Possible candidates are discussed in Chapter 2.4. With the information that “Kläui-type” ligands form stable, neutral technetium complexes

with all oxidation states of the metal, restrictions for the synthesis of a defined technetium oxidation state or core structure do no longer play a crucial role in the preparation of suitable bioconjugates.

2.2 Rhenium Complexes

In comparison to the limited number of technetium complexes with the "Kläui-type" ligands, there are more examples of corresponding rhenium compounds for example the carbonyl compound $[Re^{I}(CO)_3(L^{OMe})]$,[43] the nitrido complexes $[Re^{VI}NCl(MeOH)(L^{OEt})]$[47] and $[Re^{V}NCl(PPh_3)(L^{OEt})]$[46] or the oxido complex $[Re^{V}OBr_2(L^{OMe})]$.[41] In order to compare the related coordination chemistry of Re and Tc, some more rhenium complexes with $\{L^{OMe}\}^-$ have been synthesised and their structures and spectroscopic properties have been studied. Common ligand exchange procedures have been applied in most of the cases. A summary is shown in Scheme 2.4.

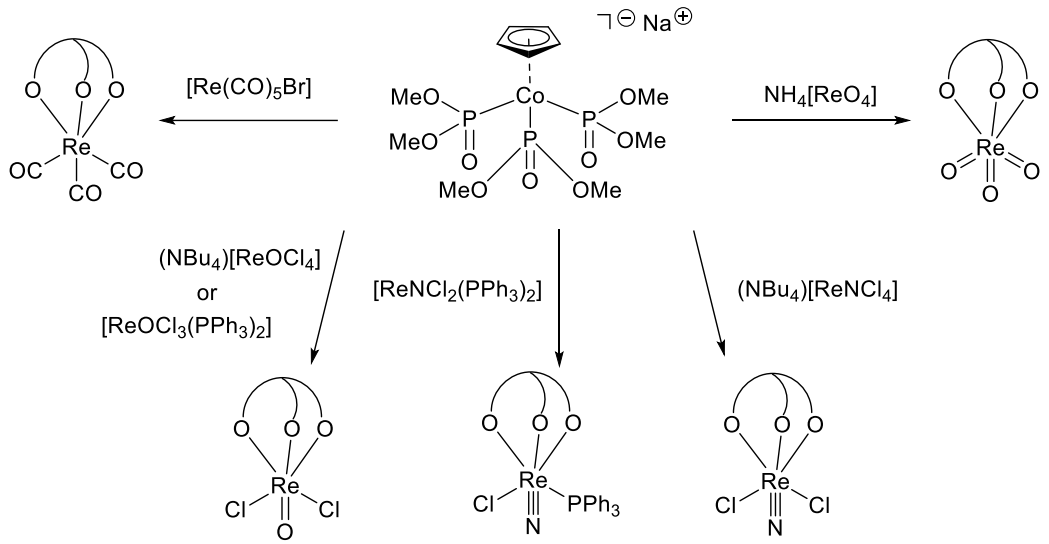

Scheme 2.4. Overview about the synthesis of rhenium complexes with NaL^{OMe}.

2.2.1 $[Re^{I}(CO)_3(L^{OMe})]$

$[Re^{I}(CO)_3(L^{OMe})]$ was synthesised from $[Re(CO)_5Br]$ with NaL^{OMe} in boiling toluene (Scheme 2.5). This synthesis is straightforward giving the product in very good yields after 4 h reaction time. The reaction in toluene is faster and more efficient than the previous procedures starting from $(NEt_4)_2[Re^{I}(CO)_3Br_3]$ or using THF as a solvent.[43, 81] Here, the reaction time could be reduced to a few hours and not dried toluene was used. A colourless precipitate (NaBr) was filtered off from the crude reaction mixture.

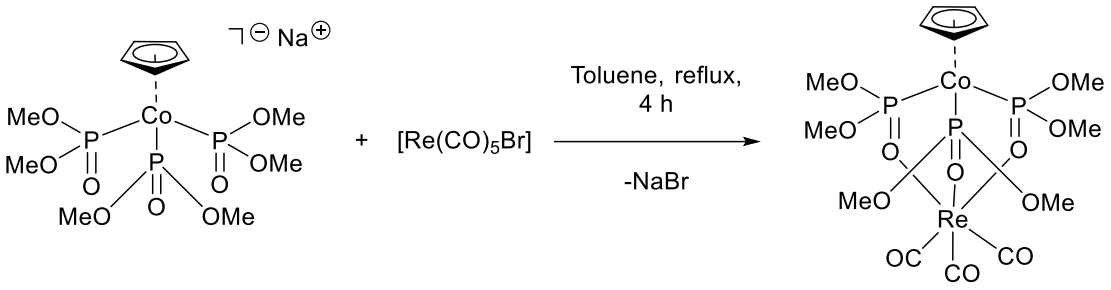

Scheme 2.5. Synthesis of $[Re^{I}(CO)_3(L^{OMe})]$ from $[Re(CO)_5Br]$ and NaL^{OMe}.

Pale-yellow single crystals were obtained directly from the filtered reaction mixture by slow evaporation at room temperature. The obtained single crystals were not of sufficient quality for a complete structure evaluation, but the preliminary results clearly confirm the composition of the compound. Additionally, the product was analysed by NMR, ESI MS and IR methods. The IR spectrum of $[Re^{I}(CO)_3(L^{OMe})]$ shows the expected *fac*-$\{Re(CO)_3\}^+$ A_1 + E pattern. The band at 2010 cm^{-1} was assigned to the carbonyl ligand. The band at 1876 and 1859 cm^{-1} are splitted due to the loss of symmetry by a slight distortion from the idealized C_{3v} symmetry because of the Cp ring as it was previously described.[43] Also the other bands are in agreement with the literature values.[43] The $^{1}H\{^{31}P\}$ NMR spectrum shows two singlets of the protons at the methoxy groups and the aromatic protons. In the ^{13}C NMR spectrum, the C-P coupling is visible, which is discussed in detail for the complex $[Re^{VII}O_3(L^{OMe})]$. Two doublets appear at 52.5 and 52.5 ppm with a coupling constant of 3.25 Hz for the carbon atoms at the methoxy groups. At 89.0 ppm appears a quartet for the carbon atoms at the Cp ring with a coupling constant of 1.5 Hz.

2.2.2 $[Re^{V}OCl_2(L^{OMe})]$

$[Re^{V}OCl_2(L^{OMe})]$ was synthesised starting from two different Re(V) compounds: $(NBu_4)[ReOCl_4]$ and $[ReOCl_3(PPh_3)_2]$ (Scheme 2.6). In the first method, the reaction mixture was heated on reflux in MeOH. Due to low solubility of $[ReOCl_3(PPh_3)_2]$, the reaction mixture with NaL^{OMe} was heated on reflux in toluene. In both cases, crystals could be obtained from a CH_2Cl_2/MeOH mixture. The yields are similar in the range around 45 %.

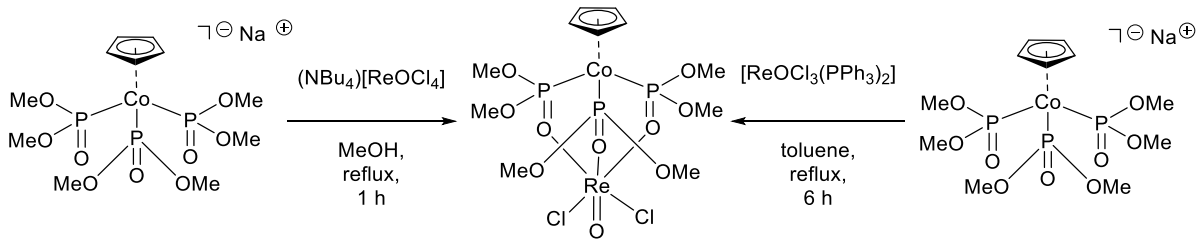

Scheme 2.6. Synthesis of $[Re^{V}OCl_2(L^{OMe})]$ from $(NBu_4)[ReOCl_4]$ or $[ReOCl_3(PPh_3)_2]$.

In the $^{1}H\{^{31}P\}$ NMR spectrum of $[Re^{V}OCl_2(L^{OMe})]$, there are three singlets for the three methoxy groups at 3.70, 3.77 and 3.83 ppm. Due to the rhenium oxido core, the three-fold symmetry is lowered and three different signals for the protons at the methoxy groups appear. The aromatic protons form one unique signal at 5.16 ppm. In the $^{13}C\{^{1}H\}$ NMR spectrum, for the methoxy groups there are two triplets and one doublet due to higher-order coupling to ^{31}P. The $^{31}P\{^{1}H\}$ spectrum shows a broad multiplet between 123.7 and 128.4 ppm. In the positive mode ESI MS spectrum, the molecular ion is found at m/z = 746.866, which belongs to the Re(V) complex with one sodium cation. The Re=O double bond gives in the IR spectrum a sharp, strong band at 957 cm^{-1}. The Re=O bond lengths in the crystal structure is in the expected region at 1.672(5) Å. The *trans* influence of the oxo core is weak. The Re-O3 bond *trans* to Re=O is by 0.021 Å longer than the Re-O6 and only by 0.012 Å longer than the Re-O9 bonds. The molecular structure of $[Re^{V}OCl_2(L^{OMe})]$ is shown in Figure 2.12.

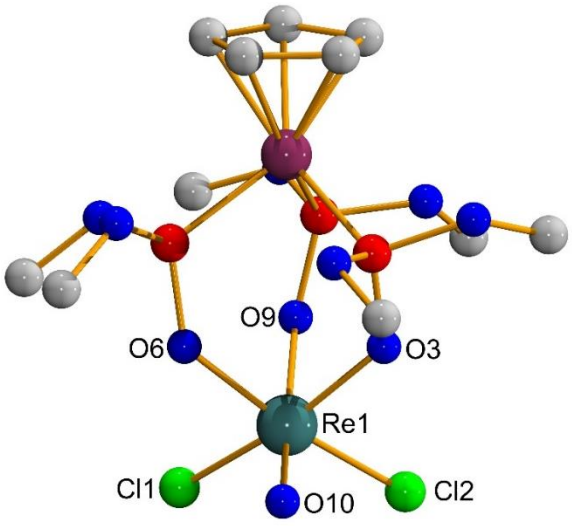

Figure 2.12. The molecular structure of $[Re^{V}OCl_2(L^{OMe})]$. The hydrogen atoms have been omitted for clarity.

2.2.3 $[Re^{V}NCl(PPh_3)(L^{OMe})]$

The nitrido complex $[Re^{V}NCl(PPh_3)(L^{OMe})]$ was obtained from a reaction of $[Re^{V}NCl_2(PPh_3)_2]$ and NaL^{OMe} in refluxing CH_2Cl_2. Orange-red single crystals of $[Re^{V}NCl(PPh_3)(L^{OMe})]$ were grown from a CH_2Cl_2/MeOH solution at room temperature. The crystals were filtered off and dried under vacuum. The $^{1}H\{^{31}P\}$ NMR spectrum of the complex in $CDCl_3$ shows five singlets for the 18 protons of the methoxy groups, whereas one singlet at 3.91 ppm has an integral for six protons indicating the overlap of two signals (Figure 2.13). The protons of the Cp ring appear as one singlet at 5.00 ppm. The protons of the PPh_3 ligand form two multiplets at 7.32 and 7.81 ppm. The $^{31}P\{^{1}H\}$ NMR spectrum shows a singlet at 11.6 ppm for the PPh_3 ligand and two broad multiplets at 113.8 ppm and 102.9 ppm for the $\{L^{OMe}\}^{-}$ ligand. The ReN stretch in the IR spectrum appears as a strong band at 989 cm^{-1}.

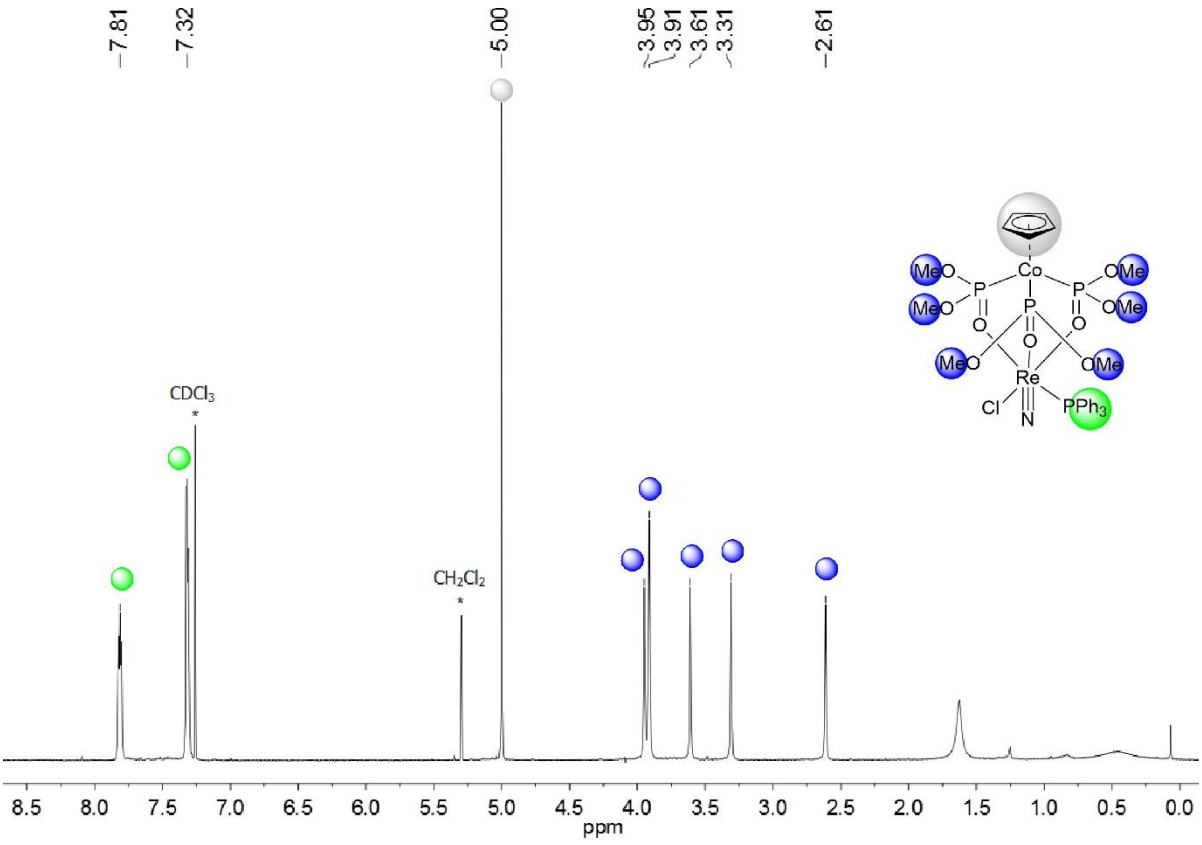

Figure 2.13. $^{1}H\{^{31}P\}$ NMR spectrum of $[Re^{V}NCl(PPh_3)(L^{OMe})]$ in $CDCl_3$.

Like in all other discussed complexes, $\{L^{OMe}\}^{-}$ coordinates with its three oxygen atoms to the metal ion (Figure 2.14). The nitrido, chlorido and triphenylphosphine ligands form a slightly distorted octahedral coordination sphere of rhenium. The nitrido and chlorido ligands are disordered with occupational

factors of 0.80/0.20. The same type of disorder was also found in the complex [$Re^{V}NCl(PPh_3)(L^{OEt})$].[46] The bond lengths in the related compounds are similar (Table 2.2). The ReN triple bond in the L^{OMe} complex is with 1.647 Å slightly shorter than in [$Re^{V}NCl(PPh_3)(L^{OEt})$] (1.795 Å). The *trans* influence of the nitrido ligand is in the L^{OMe} complex slightly stronger (Re-O6 2.334 Å vs. 2.251 Å). Generally, the substituents at the phosphorus atoms have an only marginal influence on the bond lengths.

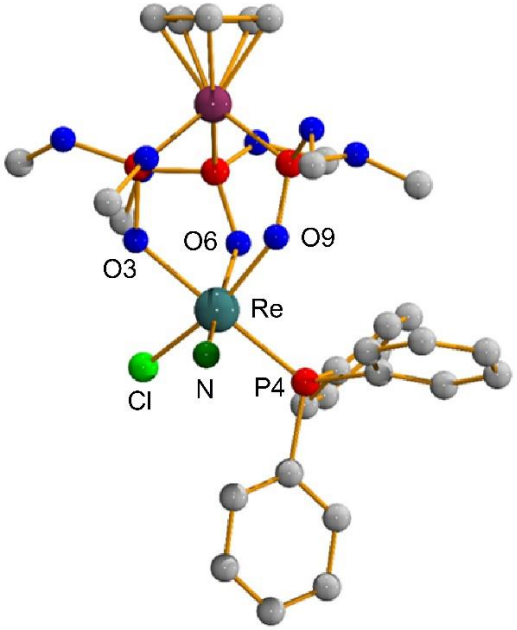

Figure 2.14. Molecular structure of [$Re^{V}NCl(PPh_3)(L^{OMe})$]. The hydrogen atoms have been omitted for clarity.

Table 2.2. Comparison of selected bond lengths (Å) of [$Re^{V}NCl(PPh_3)(L^{OMe})$] and [$Re^{V}NCl(PPh_3)(L^{OEt})$].[46] The naming of the {L^{OEt}} complex was modified accordingly.

	[$Re^{V}NCl(PPh_3)(L^{OMe})$]	[$Re^{V}NCl(PPh_3)(L^{OEt})$]
Re-N [Å]	1.647(1)	1.795(8)
Re-O3 [Å]	2.138(3)	2.179(4)
Re-O6 [Å]	2.334(3)	2.251(3)
Re-O9 [Å]	2.040(4)	2.115(3)

2.2.4 $[Re^{VI}NCl_2(L^{OMe})]$

$[Re^{VI}NCl_2(L^{OMe})]$ was synthesised from $(NBu_4)[Re^{VI}NCl_4]$ and NaL^{OMe} in refluxing CH_2Cl_2. The colour of the reaction mixture turned immediately from yellow *via* orange-red to dark red. The product was purified by column chromatography on silica with CH_2Cl_2 as the mobile phase and could be obtained as a bright yellow band. Crystallisation from a $MeCN/Et_2O$ mixture in the refrigerator gave yellow crystals suitable for X-ray crystallography. In the molecular structure, the typical tripodal coordination of the "Kläui ligand" is visible (Figure 2.15). The rhenium atom is coordinated in a distorted octahedral environment. The nitrogen and one chlorine atoms are disordered in a ratio of around 9:1. Also the rhenium atom was refined at two positions. The bond length of the Re nitrido triple bond is 1.625(5) Å. The *trans* influence of the nitrido ligand is visible in the elongated Re-O3 bond of 2.289(3) Å, which is longer by 0.261 Å than the Re-O6 bond and by 0.272 Å than the Re-O9 bond.

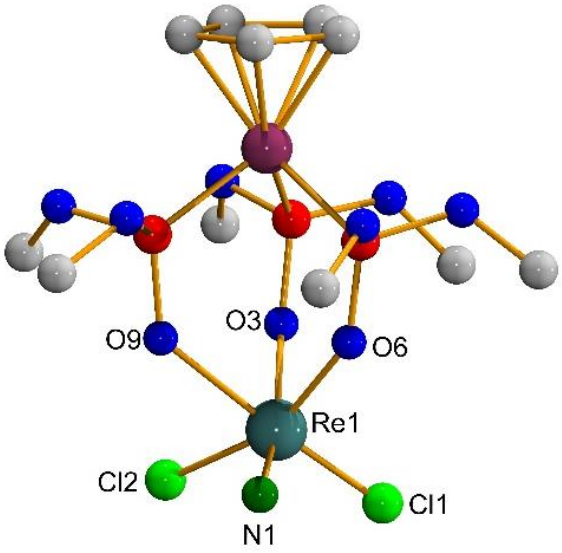

Figure 2.15. Molecular structure of $[Re^{VI}NCl_2(L^{OMe})]$. The hydrogen atoms have been omitted for clarity.

$[Re^{VI}NCl_2(L^{OMe})]$ is a d^1 system and hence paramagnetic. The EPR spectra shown in Figure 2.16 were taken in chloroform. The spectrum at room temperature shows six lines due to the coupling of the unpaired electron with the nuclear spin of $^{185,187}Re$, which is 5/2. The isotropic coupling constant a_0^{Re} is $650 \cdot 10^{-4}$ cm^{-1} and the g_0 value is 1.930. The spectrum at 77 K shows axial symmetry with resolved six-line patterns in the parallel and perpendicular parts. The coupling constants are $A_\perp^{Re} = 437 \cdot 10^{-4}$ cm^{-1} and $A_\parallel^{Re} = 859 \cdot 10^{-4}$ cm^{-1}. The g values are $g_\perp = 1.911$ and $g_\parallel = 1.802$.

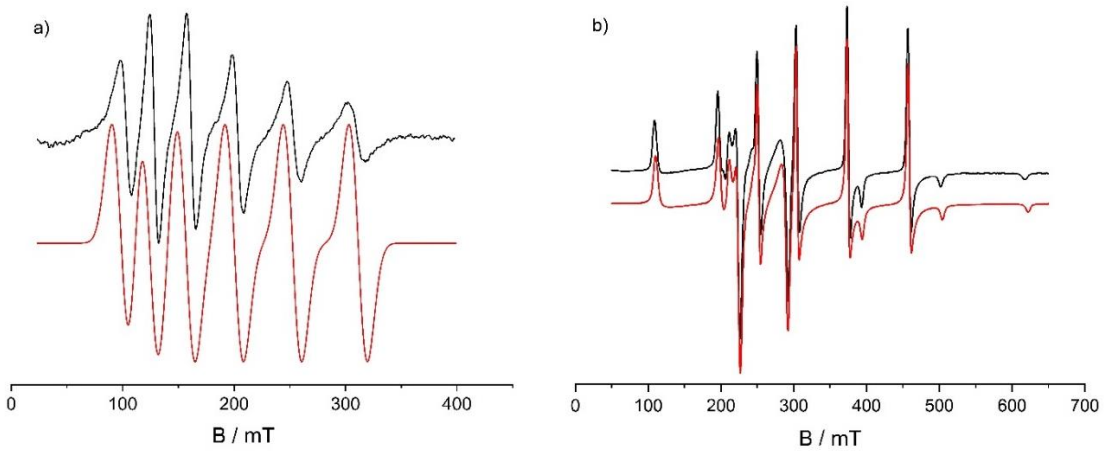

Figure 2.16. X-Band EPR spectra of [$Re^{VI}NCl_2(L^{OMe})$] in $CDCl_3$ a) at room temperature and b) at 77 K. Black: experimental spectrum. Red: simulated spectrum.

2.2.5 [$Re^{VII}O_3(L^{OMe})$]

[$Re^{VII}O_3(L^{OMe})$] was obtained from $NH_4[ReO_4]$ and NaL^{OMe} in MeOH after addition of three drops of concentrated sulfuric acid. The product precipitated directly from the reaction mixture as a yellow solid in good yields. It was analysed by $^1H\{^{31}P\}$, $^{31}P\{^1H\}$ and ^{13}C NMR spectroscopy, IR spectroscopy and mass spectrometry. The protons of the methoxy groups appear in the $^1H\{^{31}P\}$ spectrum at 3.74 ppm as one singlet with an integral of 18 protons. The five aromatic protons of the Cp ring result in another singlet at 5.11 ppm. In the $^{31}P\{^1H\}$ NMR spectrum, a broad singlet at 122.7 ppm is visible with a half-line width of 86 Hz. The P-C couplings are resolved in the ^{13}C NMR spectra of [$Re^{VII}O_3(L^{OMe})$]. Two doublets with a coupling constant of 3.35 Hz are shown at 53.69 and 53.76 ppm. The aromatic carbon atoms couple with the three phosphorus atoms and give a quartet at 89.30 ppm with a coupling constant of 1.62 Hz (Figure 2.17).

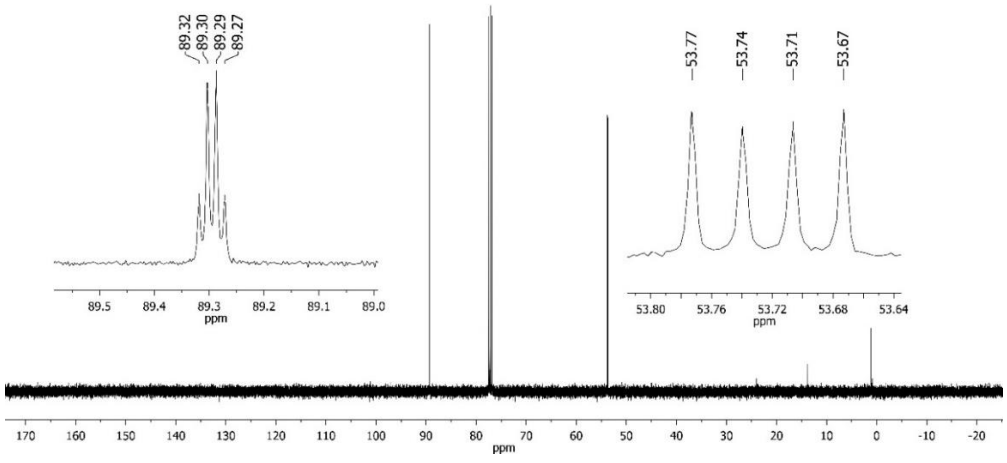

Figure 2.17. Phosphorus-carbon couplings in the ^{13}C NMR spectrum of [$Re^{VII}O_3(L^{OMe})$] in $CDCl_3$.

The strong bands at 908 and 941 cm^{-1} in the IR spectrum belong to the Re=O absorptions (Lit.: 910 and 940 cm^{-1}).[44]

Selected bond lengths of rhenium and technetium complexes with the $\{L^{OMe}\}^-$ ligand are compared in Table 2.3. The Re-O bonds of the shown complexes are in most of the cases marginally longer than the Tc-O bonds. The *trans* influence is visible in all four nitrido complexes.

Table 2.3. Comparison of selected bond lengths (Å) in oxido and nitrido complexes of rhenium and technetium with the $\{L^{OMe}\}^-$ ligand.

	[**M=O**$Cl_2(L^{OMe})$]		[**M≡N**$Cl(PPh_3)(L^{OMe})$]		[**M≡N**$Cl_2(L^{OMe})$]	
	M = Re	M = Tc	M = Re	M = Tc	M = Re	M = Tc
M=O/M≡N [Å]	1.672(5)	1.643(2)	1.647(1)	1.635(5)	1.65(2)	1.640(2)
M-O3 [Å]	2.092(6)	2.079(2)	2.138(3)	2.058(2)	2.067(5)	2.034(2)
M-O6 [Å]	2.071(5)	2.078(2)	2.334(3)	2.363(2)	2.062(6)	2.027(2)
M-O9 [Å]	2.080(5)	2.065(2)	2.040(4)	2.129(2)	2.290(6)	2.284(2)
IR (M=O/M≡N) [cm^{-1}]	957	959	989	997	986	1033

2.3 Gallium, Indium and Lutetium Complexes

Although some chemistry of gallium(III), indium(III) and lanthanide(III) complexes with "Kläui-type" ligands has been done,[82-84] some additional structural studies on such complexes with $\{L^{OMe}\}^-$ have been performed. Background for such studies is the use of ^{68}Ga, ^{111}In and ^{177}Lu complexes in nuclear medical diagnostics and therapy. Hence, it is important to have more information about the coordination modes of the tripodal ligand to metal ions of various size (ionic radii: Ga^{3+} 62 pm, In^{3+} 81 pm and Lu^{3+} 97 pm).[85-86]

One equivalent of the corresponding metal nitrates was added to two equivalents of NaL^{OMe} (Scheme 2.7). The reaction mixtures were stirred at room temperature or shortly heated on reflux. For the reaction with lutetium, a colourless precipitate ($NaNO_3$) was filtered off.

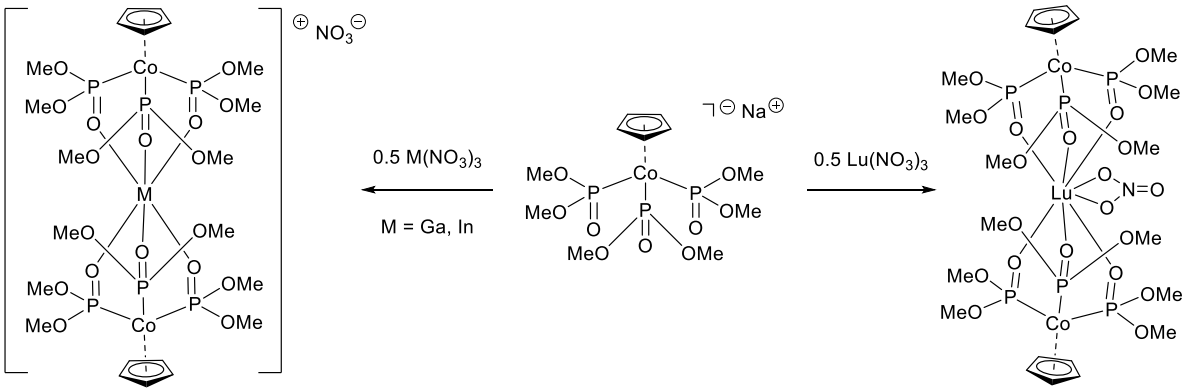

Scheme 2.7. Synthesis of $[Ga(L^{OMe})_2]NO_3$, $[In(L^{OMe})_2]NO_3$ and $[Lu(L^{OMe})_2(NO_3)]$.

Yellow single crystals of $[Ga(L^{OMe})_2]NO_3$ were obtained from the THF/H_2O reaction mixture after slow evaporation of the solvents. Both $\{L^{OMe}\}^-$ ligands coordinate *via* their three oxygen atoms to the Ga^{3+} ion. The Ga-O bond lengths are between 1.955(2) and 1.968(2) Å. Two of the three methoxy groups of the asymmetric unit are slightly disordered. The complex is positively charged, NO_3^- acts as a counter ion. The molecular structure is shown in Figure 2.18.

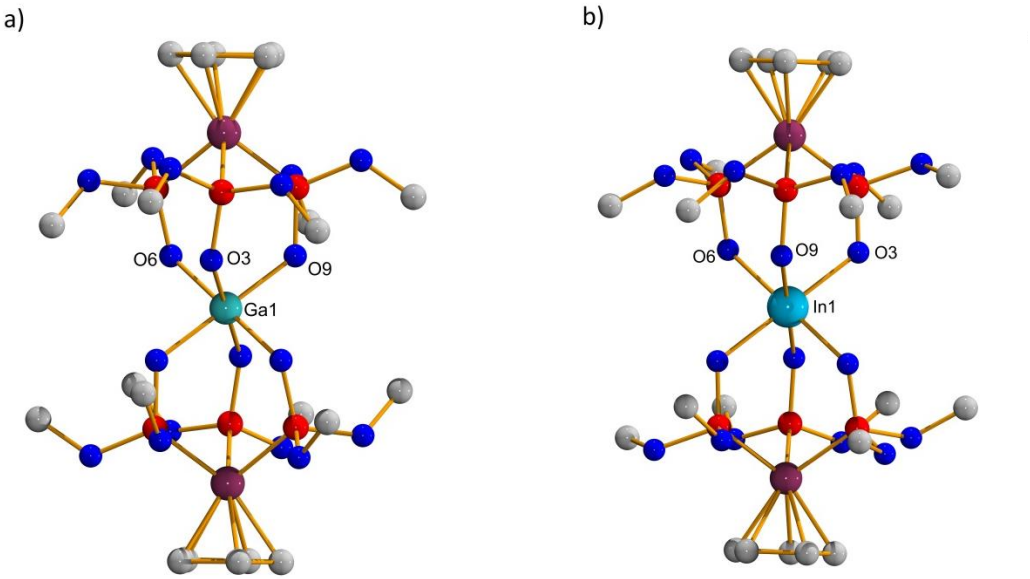

Figure 2.18. Molecular structures of the cations of a) $[Ga(L^{OMe})_2]NO_3$ and b) $[In(L^{OMe})_2]NO_3$. Hydrogen atoms are omitted for clarity.

Single crystals of $[In(L^{OMe})_2]NO_3$ were obtained after several days from a H_2O/MeCN solution at room temperature in a yield of 85 %. The compound was studied by NMR spectroscopy, IR spectroscopy and ESI mass spectrometry. The Indium(III) ion is coordinated by two “Kläui-type” ligands. The In-O bonds

are between 2.120(1) and 2.140(1) Å. The complex crystallised in the triclinic space group $P\bar{1}$ with two indium atoms being located on inversion centers. The asymmetric unit contains two half molecules, the counter ion and 1.5 molecules of solvent water.

$[Lu(L^{OMe})_2(NO_3)]$ crystallised from the filtered reaction mixture when left overnight at room temperature as bright-yellow, big hexagons. The molecular structure (Figure 2.19) shows two "Kläui-type" ligands being coordinated by the Lu^{3+} ion. In contrast to the complexes with gallium and indium, the NO_3^- ion is coordinated *via* two oxygen atoms to the Lu^{3+} ion. The angle Co-Lu-Co is 150.594(1)°. A comparison of the ionic radii of the three metal ions, confirms that Lu^{3+} has the largest ionic radius (97 pm)[86] followed by In^{3+} (81 pm)[85] and Ga^{3+} (62 pm).[85] Thus, the formation of an 8-coordinate Lu^{3+} ion is not unsual. In the gallium and indium complexes, the M-O bonds are similar. The complexes form slightly distorted octahedra (Table 2.4). Obviously, the M-O bonds of the three complexes are strictly correlated with the increasing ionic radii.

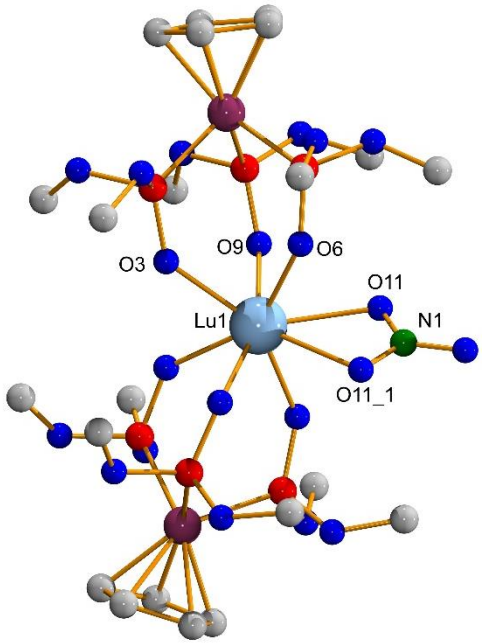

Figure 2.19. Molecular structure of $[Lu(L^{OMe})_2(NO_3)]$. Hydrogen atoms are omitted for clarity.

Table 2.4. Comparison of some structural details of $[Ga(L^{OMe})_2]NO_3$, $[In(L^{OMe})_2]NO_3$ and $[Lu(L^{OMe})_2NO_3]$.

	$[Ga(L^{OMe})_2]NO_3$	$[In(L^{OMe})_2]NO_3$	$[Lu(L^{OMe})_2(NO_3)]$
Ionic radius of M^{3+} [pm]	62	81	97
M-O3 [Å]	1.968(2)	2.127(1)	2.317(5)
M-O6 [Å]	1.955(2)	2.120(1)	2.274(5)
M-O9 [Å]	1.959(2)	2.140(1)	2.223(5)
Lu-O(nitrate) [Å]			2.485(1)
Co-M-Co [°]	180	180	150.59(1)

Phosphorus-carbon couplings are visible in the ^{13}C NMR spectra of the $[Ga(L^{OMe})_2]NO_3$, $[In(L^{OMe})_2]NO_3$ and $[Lu(L^{OMe})_2(NO_3)]$ complexes (Figure 2.20). Analogous features are found in the spectra of the Ga^{3+}, In^{3+} and Lu^{3+} complexes. Five chemically equivalent aromatic carbon atoms of the Cp ring couple with three phosphorus atoms splitting the signal at 89.96 ppm into a quartet with a coupling constant of 1.4 Hz (for the indium and lutetium complexes) and 1.5 Hz for the gallium complex. At around 52 ppm, two doublets appear with coupling constants of 3.4 Hz (In^{3+}), 3.1 Hz (Lu^{3+}) and 3.28 Hz (Ga^{3+}) between the carbon atoms of the methoxy groups with the respective phosphorus atoms. This shows that the methoxy groups are chemically different. They split into two groups. In the $^1H\{^{31}P\}$ NMR spectrum, the protons of all methoxy groups appear as one singlet at 3.62 ppm as well as the protons at the Cp ring give only one signal at 5.05 ppm. $^{31}P\{^1H\}$ NMR spectrum shows a broad singlet at 118.2 ppm.

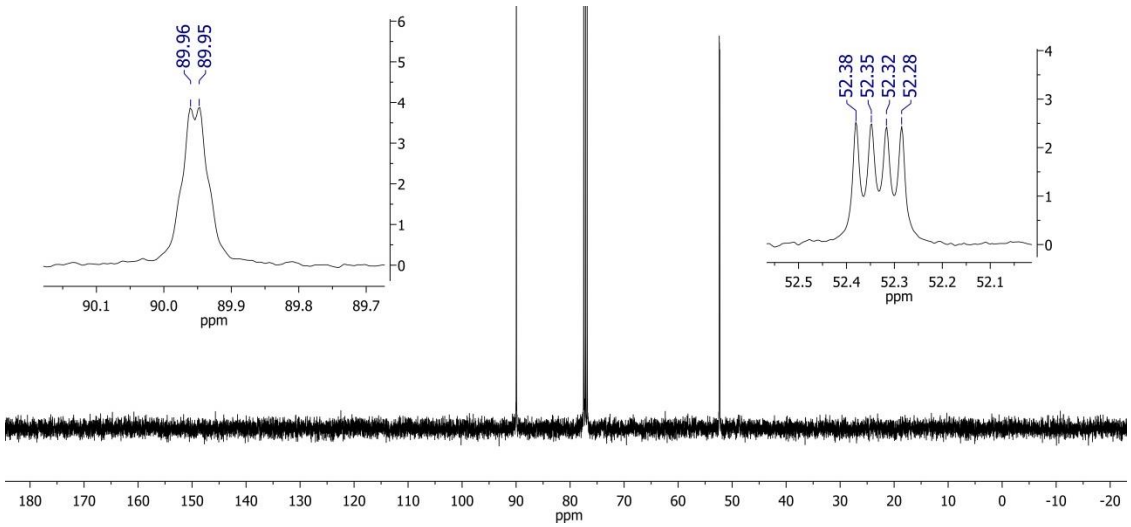

Figure 2.20. Phosphorus-carbon couplings in the ^{13}C NMR spectrum of $[In(L^{OMe})_2]NO_3$.

2.4 Synthesis of a "Kläui Ligand" with an Ester Group

The ability to coordinate to many metals in their low and high oxidation states makes the "Kläui-type" ligands suitable as a potential multi-metal tracers for diagnostics using ^{99m}Tc or ^{68}Ga and therapy using ^{111}In or ^{177}Lu. Such complexes are usually stable on air, in aqueous solutions and are obtained in good yields. Of particular interest for pharmaceutical applications might be the opportunity to use a stable ^{99m}Tc(VII) complex, such as [$^{99m}TcO_3(L^{OR})$], which needs no reducing agent during the preparation. The "Kläui-type" ligand can coordinate directly to a Tc(VII) ion.

However, a functional group for bioconjugation is needed to bind biomolecules targeting the tracer to the desired region in the body. There are two possibilities to integrate a functional group to the "Kläui ligand": at the side chain at the phosphorus atom or at the Cp ring. Here, the latter method is followed. The functionalization of a "Kläui-type" ligand with an ester group was performed as shown in Scheme 2.8. In the first step, NaCp was reacted with dimethyl carbonate in refluxing THF under argon. The resulting sodium carbomethoxy cyclopentadienide was further reacted with dicobaltoctacarbonyl and iodine. Subsequent oxidation of the Co(I) product was done with iodine to produce a Co(III) complex coordinating two iodido ligands together with one carbonyl ligand and the functionalised Cp ring. After slow addition of trimethyl phosphite, a Co(II) sandwich complex was obtained. This resulting complex was further reacted with sodium iodide to form the ester-substituted NaL^{OMeCOOMe}.

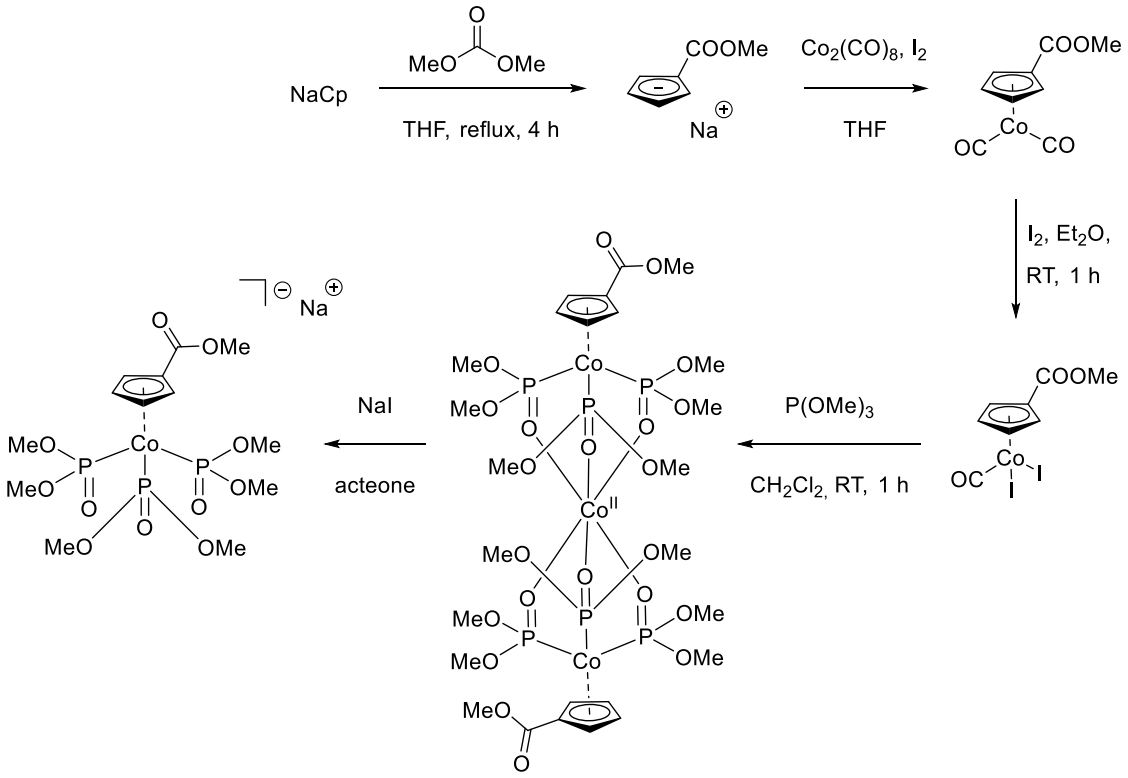

Scheme 2.8. Synthesis of the ester-substituted NaL^{OMeCOOMe}.

Single crystals of the [Co($L^{OMeCOOMe}$)$_2$] complex were obtained from a CH_2Cl_2/MeOH mixture by slow evaporation of the solvents. Figure 2.21 illustrates the molecular structure of the complex. The central Co(II) ion is located on a center of inversion. The Co2-O bonds lengths are between 2.076(1) and 2.095(1) Å. The methylester groups point in opposite directions to get a closer packing.

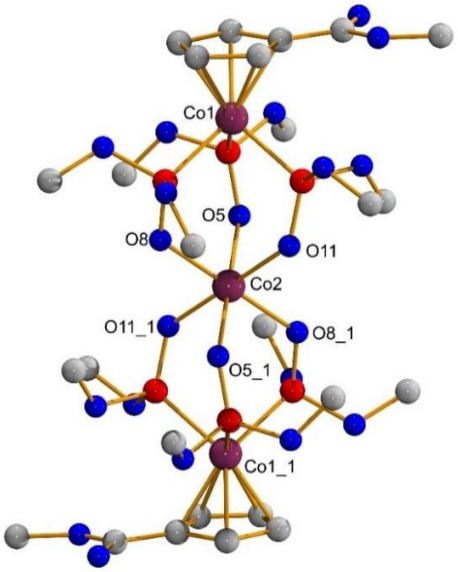

Figure 2.21. Molecular structure of [Co($L^{OMeCOOMe}$)$_2$].

Na$L^{OMeCOOMe}$ was taken as starting material for a reaction with (NBu_4)[$^{99}TcO_4$] (Scheme 2.9). The reaction proceeds immediately after the addition of two drops of concentrated H_2SO_4 in MeOH at room temperature. It delivers the corresponding trioxidotechnetium(VII) complex in a quantitative yield. The ^{99}Tc NMR spectrum of the product shows a singlet at 331 ppm. This chemical shift is very close to that of the [$^{99}TcO_3$(L^{OMe})] complex at 343 ppm. The ^{31}P NMR spectrum shows a broad signal between 111.7 and 121.5 ppm. The solution was stepwise neutralised with NaOAc dissolved in water. At a pH of around 6 the ^{99}Tc NMR signal at 331 ppm disappeared and a signal at 0 ppm was detected. The Tc complex is obviously not stable at this pH and TcO_4^- is re-formed. Especially, regarding the related ^{99m}Tc chemistry this could cause a problem because the injected solution to the patient has to be around a pH of 7 to 8. More experiments have to be done to solve this problem.

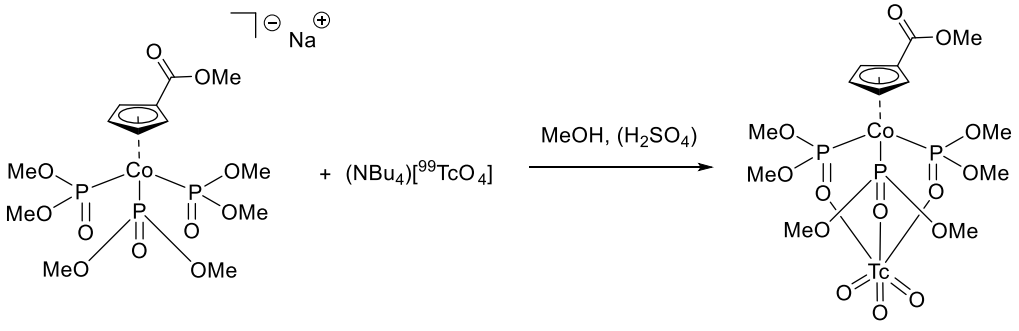

Scheme 2.9. Synthesis of [$^{99}Tc^{VII}O_3$($L^{OMeCOOMe}$)] starting from (NBu_4)[$^{99}TcO_4$] and Na$L^{OMeCOOMe}$.

3 Synthesis and Reactions with the Pentadentate Thiourea Ligand H_3L^{1EtEt}

3.1 Synthesis of H_3L^{1EtEt}

A multi-step synthesis of the pentadentate ligand H_3L^{1EtEt} was previously published.[87] However, the procedure contains some difficulties regarding the purification of the ligand at the end of the synthesis. Here, the sequence of the reactions was changed in order to purify already the intermediate products by column chromatography having a pure product at the end. By keeping the carboxylic acid groups protected as diethyl esters until the last reaction step, a purification of the intermediate product **5** on a silica column became possible (Scheme 3.1).

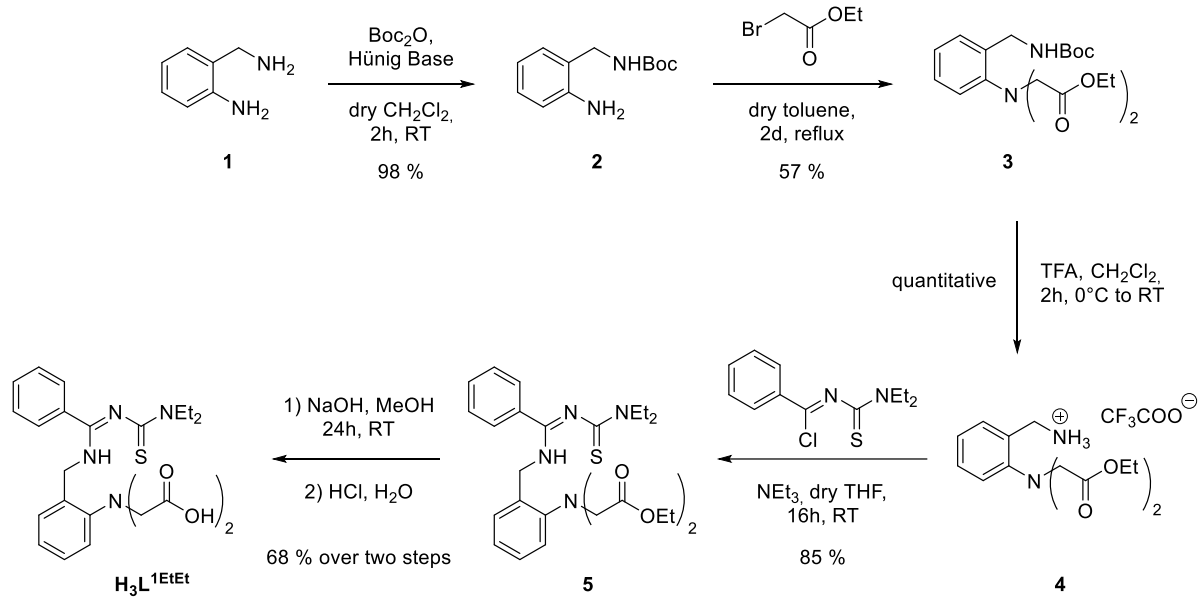

Scheme 3.1. Synthesis of the pentadentate ligand H_3L^{1EtEt}.

The selectively Boc protected 2-amino benzylamine **2** was heated on reflux in toluene with an excess of ethyl bromoacetate for two days. Potassium iodide was added as a catalyst for the activation of the ethyl bromoacetate.[88] The product **3** was extracted in a water/toluene mixture, purified by column chromatography and recrystallized from an EtOAc/hexane mixture giving colourless crystals in a good yield. The Boc group was cleaved by TFA quantitatively. Here, no further work-up was needed. The intermediate product **4** was dried under reduced pressure. Under basic conditions, the free amine reacted with the benzimidoyl chloride to **5**. This product was purified by column chromatography. As the last step, the ethyl ester groups were cleaved under basic conditions. By acidification, the carboxylic groups were protonated and the product precipitated in water. It was filtered off and dried under reduced pressure.

The product H_3L^{1EtEt} was analysed by IR and NMR spectroscopy. The strong band in the IR spectrum at 1488 cm^{-1} was assigned to the carbonyl moiety. The ^1H NMR spectrum in d_6-DMSO shows two triplets for the methyl groups at 1.02 and 1.08 ppm (Figure 3.1). The protons of the methylene groups of the ethyl substituents appear as two quartets at 3.47 and 3.73 ppm. The protons of the methylene groups of the N-C*H*$_2$-COOH arms form one singlet at 3.95 with an integral of four protons. The protons of the methylene group next to the NH group couples with the proton at the nitrogen atom and gives a doublet at 4.59 ppm. The proton at the nitrogen atom is visible as a broad singlet at 8.27 ppm. The aromatic protons appear as multiplets between 7.06 and 7.39 ppm. The signal at 12.52 ppm with an integral of two protons belongs to the COO*H* groups.

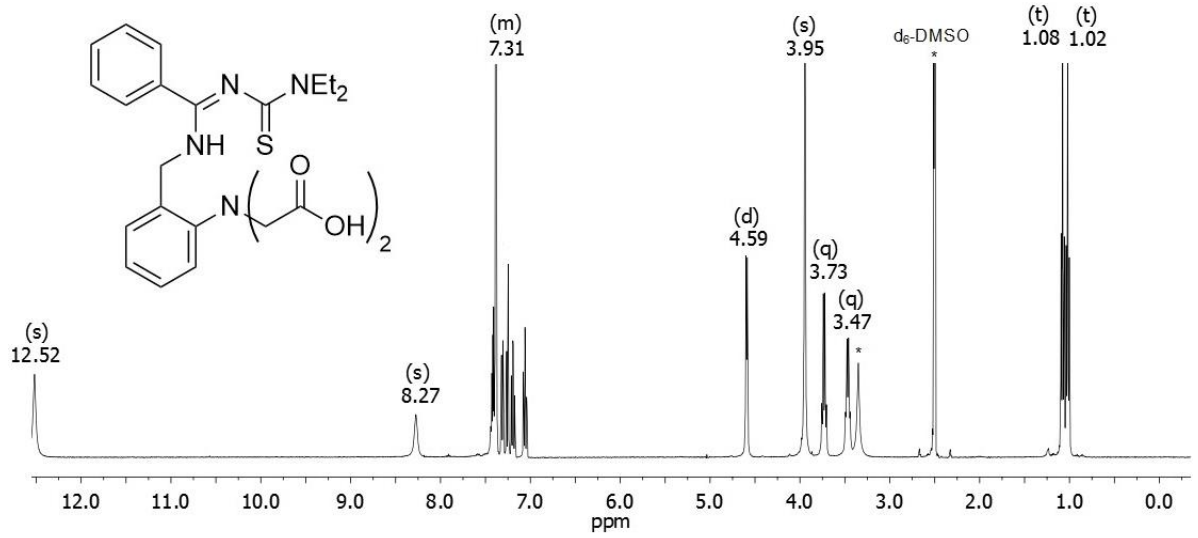

Figure 3.1. ^1H NMR spectrum of the pentadentate ligand H_3L^{1EtEt} in d_6-DMSO.

3.2 Synthesis of Re(V) and Tc(V) Oxido Complexes with H_3L^{1EtEt}

The pentadentate ligand H_3L^{1EtEt} forms stable oxidorhenium(V) and -technetium(V) complexes. Suitable starting materials are the $(NBu_4)[MOCl_4]$ complexes (M = Re, Tc). The reactions were done in the presence of NEt_3 in refluxing MeOH. The Re and Tc atoms coordinate in the same way to the *S*, *N*, *O* donor atoms of the ligand in a distorted octahedral fashion. Thereby, one of the carboxylic groups is directed to the position *trans* to the oxido ligand.[87-88]

For a potential use in nuclear medicine, it is favourable to start the sysnthesis from $Na[^{99m}Tc^{VII}O_4]$, which is obtained from commercial $^{99}Mo/^{99m}Tc$ generators. Reduction with a suitable reducing agent gives the $^{99m}Tc(V)O$ core. For a proof-of-principle reaction, first $Na[ReO_4]$ was used as the starting

material and $SnCl_2 \cdot 2\ H_2O$ as reducing agent (Scheme 3.2). $Na[ReO_4]$ was dissolved in a hot EtOH/acetone mixture under vigorous stirring. The pentadentate ligand H_3L^{1EtEt} dissolved in the same solvents was added. Afterwards, solid $SnCl_2 \cdot 2\ H_2O$ was added. The colour of the solution turned from slightly yellow to brown. Purple single crystals were grown from a $MeCN/CHCl_3/CH_2Cl_2$ (2:1:1) mixture. The measured unit cell and the spectroscopic data are identical with published values.[87]

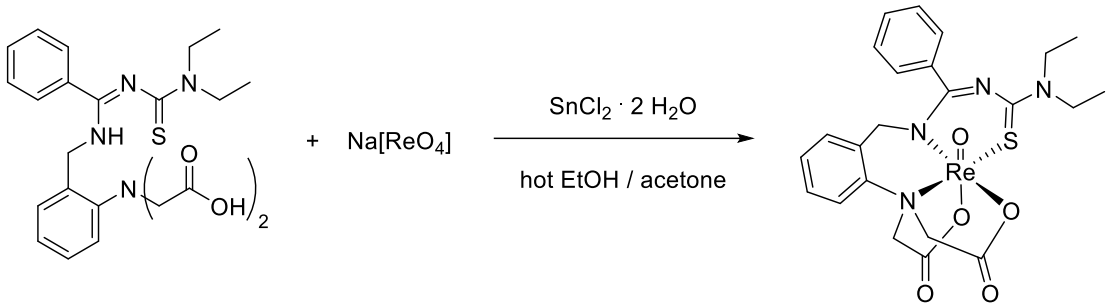

Scheme 3.2. Reaction of $Na[Re^{VII}O_4]$ with the pentadentate ligand H_3L^{1EtEt}.

Unfortunately, it was not possible to transfer the same reaction conditions to a reaction with $Na[TcO_4]$. The addition of the reducing agent $SnCl_2 \cdot 2\ H_2O$ to the mixture of $Na[TcO_4]$ and H_3L^{1EtEt} in hot EtOH gave a black-brown precipitate of $Tc(IV)O_2$. So here, the reduction to the Tc(IV) species is faster than the coordination of the pentadentate ligand H_3L^{1EtEt}. Also an attempt with sodium dithionite ($Na_2S_2O_4$) as reductant was not successful.

3.3 Synthesis of Re(V) Phenylimido Complexes with H_3L^{1EtEt}

In addition to the oxidorhenium(V) complex $[ReO(L^{1EtEt})]$,[89] an analogous phenylimido complex has been synthesised and characterised by spectroscopic methods and X-ray crystallography. Here, also a complex with a fluorinated phenylimido ligand is presented. The fluorination of ligands frequently increases the solubility of the products, which may have an impact on biological distribution patters. A reaction between H_3L^{1EtEt} and $[Re(NPhR)Cl_3(PPh_3)_2]$ (R = H, F) in boiling chloroform gives $[Re(NPhR)(L^{1EtEt})]$ complexes (Scheme 3.3). The presence of a base (NEt_3) decreased the reaction time from 10 h to 30 min. The product was purified by column chromatography and crystallised from a $MeOH/CHCl_3$ mixture by slow evaporation of the solvents.

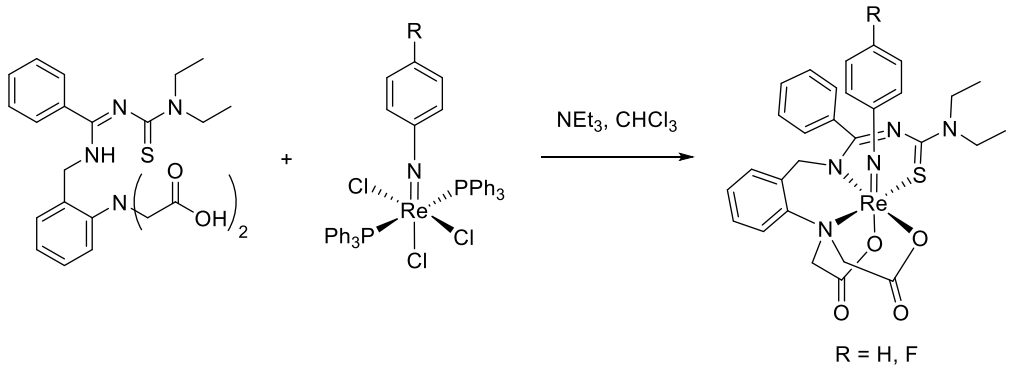

Scheme 3.3. Reaction of H_3L^{1EtEt} with $[Re(NPh)Cl_3(PPh_3)_2]$ and $[Re(NPhF)Cl_3(PPh_3)_2]$.

$[Re(NPhF)(L^{1EtEt})]$ was studied by NMR spectroscopy in $CDCl_3$ (Figure 3.2). In contrast to the complex with a Re(V) oxido core, here the triplets of the protons of the CH_3 groups are well resolved at 1.25 and 1.33 ppm. The protons of the CH_2 groups from the carboxylic arms are splitted into doublets at 4.35, 4.55, 5.11 and 5.55 ppm (labelled in blue). It means that the protons of the two carboxylic arms are magnetically not equivalent. The other methylene protons appear between 3.60 and 4.20 ppm as overlapping multiplets. The signals of the methylene groups are high-field shifted compared with their counter parts in the spectrum of $[ReO(L^{1EtEt})]$.[89] The aromatic protons appear between 6.36 and 7.47 ppm.

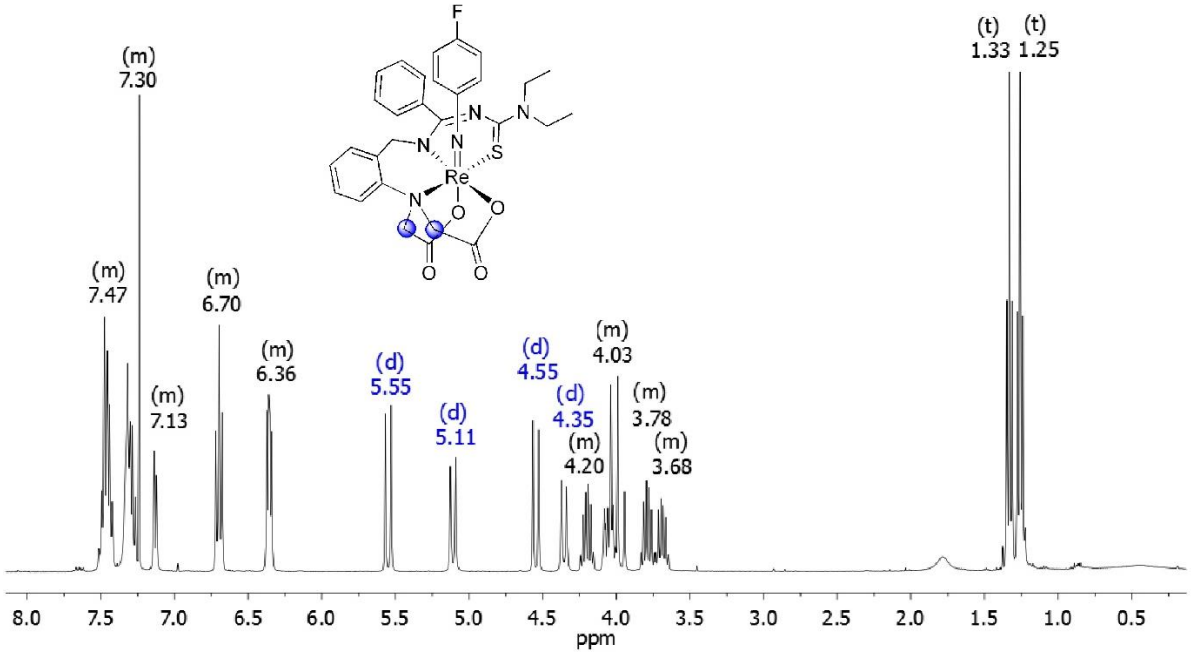

Figure 3.2. ^1H NMR spectrum of $[Re(NPhF)(L^{1EtEt})]$ in $CDCl_3$.

The ^{19}F NMR spectrum shows an overlapping triplet of triplets caused by couplings of the ^{19}F atom with the protons of the adjacent atoms of the phenyl ring. The 2D {^{19}F, ^{1}H} spectrum shows two cross peaks indicating that the signals at 6.36 and 6.70 ppm in the ^{1}H NMR spectrum belong to the fluorinated phenylimido ring. Couplings between fluorine and carbon are also visible. In the $^{13}C\{^{1}H\}$ NMR spectrum of [Re(NPhF)(L^{1EtEt})], two doublets are visible at 116.76 ppm and 122.56 ppm. They belong to the fluorinated phenylimido ring. The couplings disappear in the $^{13}C\{^{1}H,^{19}F\}$ NMR spectrum (Figure 3.3).

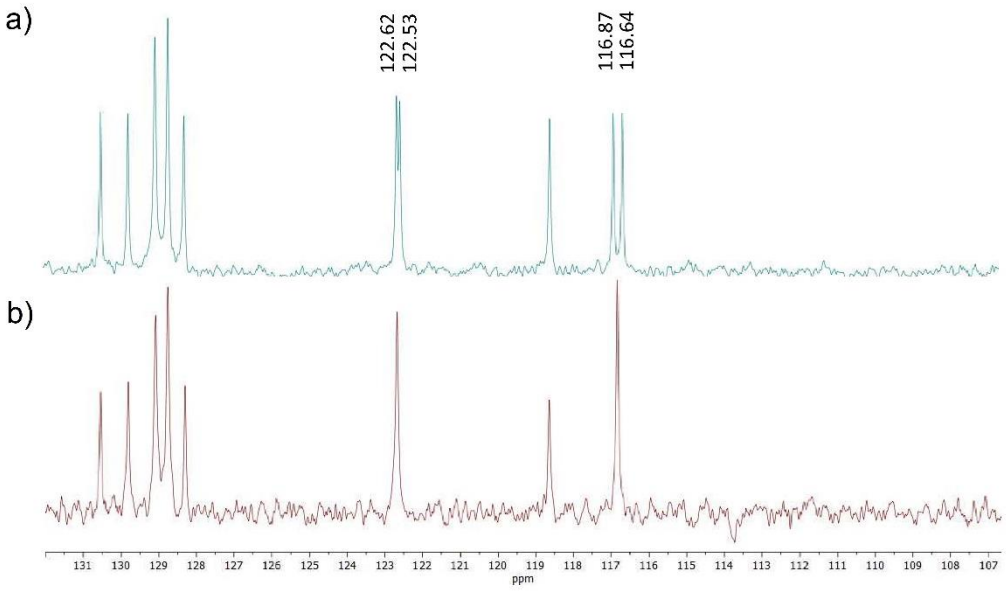

Figure 3.3. a) $^{13}C\{^{1}H\}$ NMR spectrum of [Re(NPhF)(L^{1EtEt})] with couplings between carbon and fluorine. b) $^{13}C\{^{1}H,^{19}F\}$ NMR spectrum of [Re(NPhF)(L^{1EtEt})] without such couplings.

A single-crystal X-ray structure analysis of [Re(NPhF)(L^{1EtEt})] exhibits a high symmetric space group (R3c) with 18 molecules in the unit cell (Figure 3.4b). MeOH molecules are co-crystallised. The rhenium atom is in a distorted octahedral environment with *S*, *N*, *N* and two oxygen atoms in its coordination sphere. One of the carboxylate groups is found *trans* to the phenylimido core. The two Re-O single bond lengths are equivalent with values of 2.057(9) and 2.057(7) Å. The N1-Re-O1 angle is 168.914(2)°. The Re1-N1 double bond length is 1.720(1) Å, which is in the common region for such bonds.[90] The bond length between the rhenium atom and the tertiary nitrogen atom N2 is 0.18 Å longer than the other Re-N single bonds. This was also observed in previous complexes with this pentadentate ligand.[89] An interesting aspect of the crystals packing of [Re(NPhF)(L^{1EtEt})] is the fact that the fluorine atoms of the complexes point into the center of large voids with a diameter of around 16 Å. In these voids, no electron density (e. g. of solvents molecules) was found. This kind of unusual crystal packing

was not observed in previous complexes with the $[Re(NPhF)]^{3+}$ core.[89, 91] This unusual crystal packing is not observed for the corresponding unfluorinated complex with the same ligand (Figure 3.4d).

Single crystals of [Re(NPh)(L^{1EtEt})] were obtained from a MeOH/$CHCl_3$ mixture by slow evaporation of the solvent in the refrigerator. [Re(NPh)(L^{1EtEt})] crystallises in the space group $P2_1$. The Re1-N1 double bond is again in the common region (1.712(7) Å) and slightly shorter than in the fluorinated compound. The N1-Re1-O1 angle is almost the same (168.275(9)°) and the same trend in the bond lengths of the tertiary nitrogen atom N2 is also visible (Re1-N2 2.241(8) Å vs. Re1-N3 2.063(7) Å).

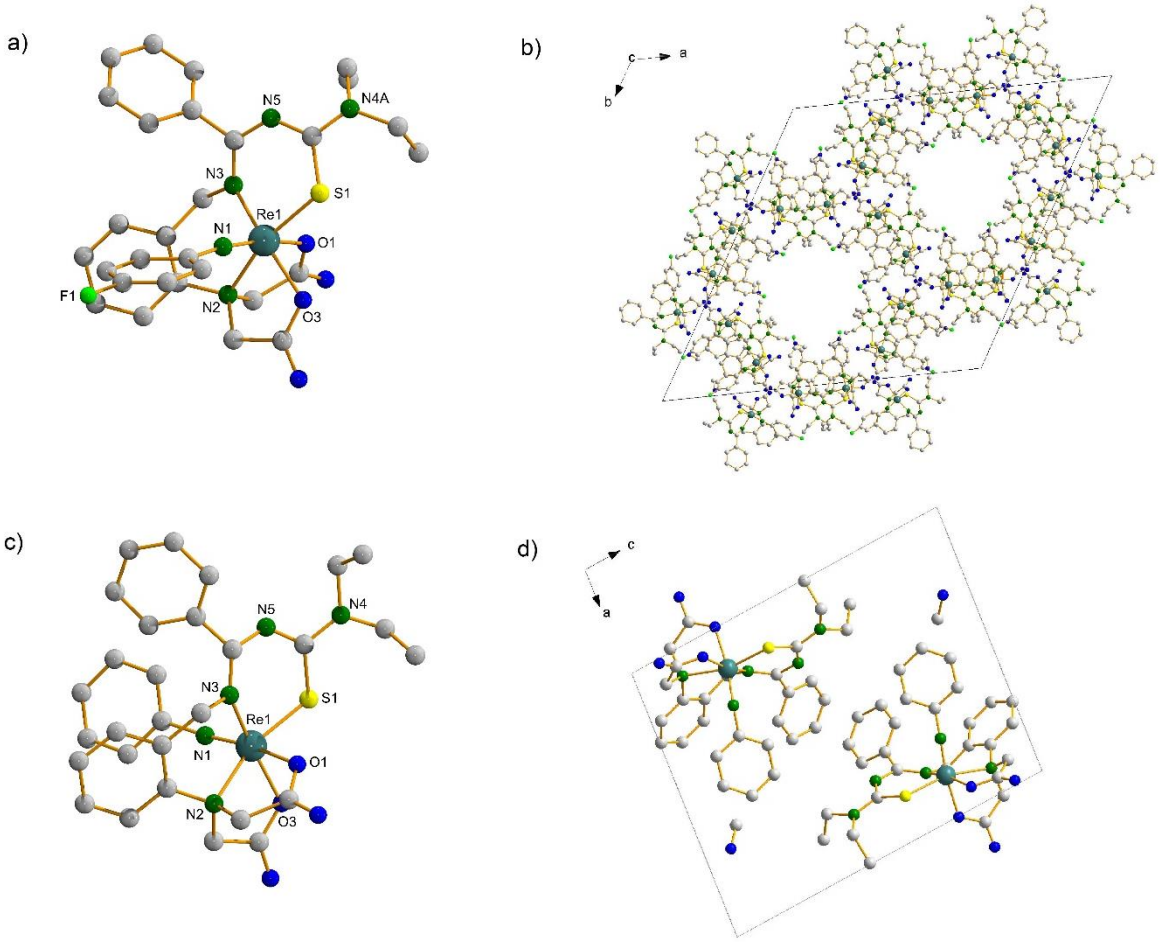

Figure 3.4. a) Molecular structure of [Re(NPhF)(L^{1EtEt})]. b) crystal packing of [Re(NPhF)L^{1EtEt}] c) molecular structure of [Re(NPh)(L^{1EtEt})] d) crystal packing of [Re(NPh)L^{1EtEt}]. Hydrogen atoms are omitted for clarity.

4 Potentially Tetradentate Thiourea Ligands for Bioconjugation

The previously discussed pentadentate thiourea ligand $\{L^{1EtEt}\}^{3-}$ can coordinate to different Re(V) cores such as $\{ReO\}^{3+}$ or $\{Re(NPhR\}^{3+}$ (R = H, F) and also to the Tc(V) oxido core as has been shown in a previous work.[89] For the development of new radiotracers for diagnostics or therapy, it is required to include a bioconjugation. This can be done in two different ways (Figure 4.1). Starting from the basic building blocks for the synthesis of the thiourea ligands, it is either possible to change the organic substituents at the nitrogen atom or to vary the side chain, which replaces the chloride atom of the benzimidoyl chloride. The focus in the present thesis is directed to a variation of the side chain by the addition of a functional group for bioconjugation. Two different ligands were synthesised providing a carboxylic or an amine substituent for coupling to peptides. The modified ligands mimic the N-terminus or C-terminus of a peptide molecule. The coordination to rhenium and technetium takes place *via* the sulfur atom and three nitrogen atoms of the triglycine substituents. The -COOH or $-NH_2$ groups remain available for bioconjugation. The synthesis of such ligands, a proof-of-principle reaction with rhenium, the labelling with ^{99m}Tc and also the bioconjugation to prototype biomolecules are described in the next subchapters.

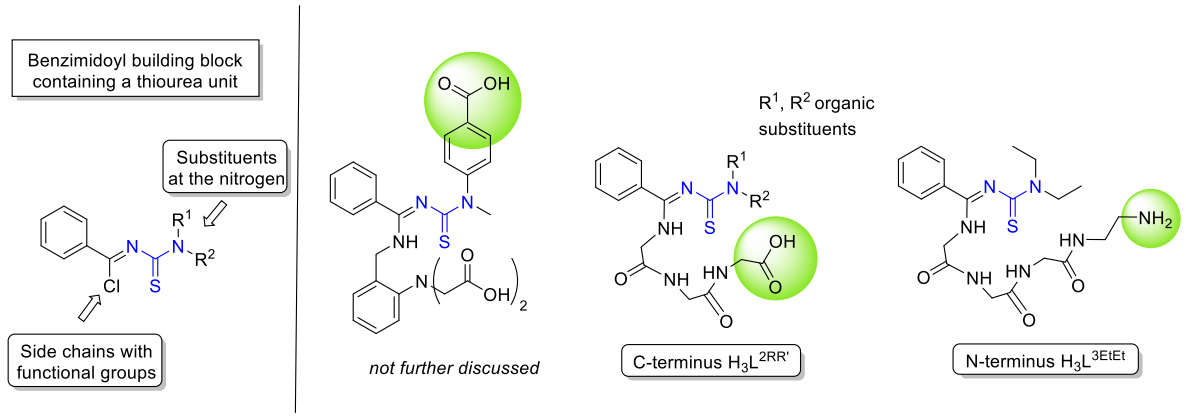

Figure 4.1. Possible positions for bioconjugation at the thiourea derivatives under study by changing the substituents of the nitrogen atoms or the addition of a side chain with a functional group replacing the chloride.

4.1 Synthesis of the "C-Terminus Ligands" $KH_3L^{2RR'}$

The tetradentate thiocarbamoylbenzamidine ligands were synthesized from triglycine and benzimidoyl chlorides with three different substituents (KH_3L^{2EtEt}, KH_3L^{2MePh}, KH_3L^{2PhPh}) under basic conditions at room temperature (Scheme 4.1). The addition of KOH was required for the deprotonation of triglycine. In the dry ethanol, KCl precipitated and could be removed. The products were isolated as potassium salts by the addition of potassium ethanolate to a vigorously stirred diethyl ether solution of the

reaction product between the benzimidoyl chloride and triglycine.[92] After filtration, the products were quickly transferred into a tared vial and dried in vacuum. Otherwise, they converted into sticky oils, which were hard to handle. The compounds were analysed by elemental analysis, NMR and IR spectroscopy and ESI mass spectrometry.

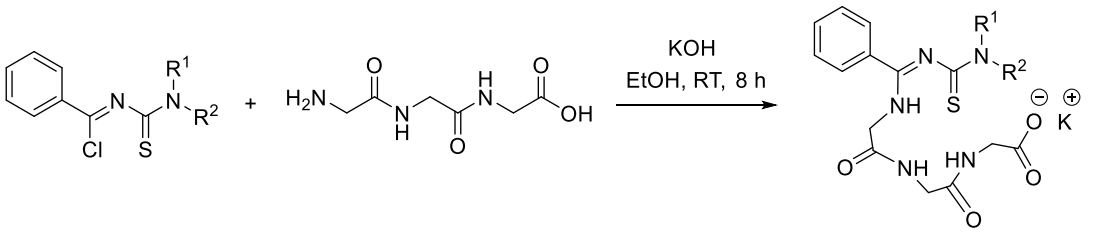

KH_3L^{2EtEt}: $R^1 = R^2 = Et$
KH_3L^{2MePh}: $R^1 = Me$, $R^2 = Ph$
KH_3L^{2PhPh}: $R^1 = R^2 = Ph$

Scheme 4.1. Syntheses of the ligands KH_3L^{2EtEt}, KH_3L^{2MePh} and KH_3L^{2PhPh}.

In the ^{1}H NMR spectrum of KH_3L^{2EtEt} in d_6-DMSO, the hydrogen atoms for both CH_3 groups overlap in a multiplet around 1.07 ppm. One of the CH_2 groups of the ethyl substituents appear as a quartet at 3.51 ppm and one CH_2 group of the triglycine chain as a doublet at 3.90 ppm. The other methylene protons form multiplets at 3.39 and 3.73 ppm. The N*H* protons appear as three triplets at 7.63, 8.37 and 8.48 ppm.

In the ^{1}H NMR spectrum of KH_3L^{2MePh} in d_6-DMSO, the signal for the methyl group overlaps with a broad water signal at 3.71 ppm. The methylene protons appear at 3.44, 3.48 and 3.87 ppm. Two of the N*H* signals show a broad singlet at 8.38 ppm, the third N*H* a triplet at 7.63 ppm. The aromatic protons appear between 7.2 and 7.55 ppm.

In the ^{1}H NMR spectrum of KH_3L^{2PhPh} in d_6-DMSO, the signals of the methylene groups are found between 3.67 and 3.88 ppm. The aromatic protons of the two phenyl groups form multiplets around 7.3 ppm. The N*H* protons appear at 8.44 and 8.54 ppm with the same splitting pattern found in KH_3L^{2MePh}, but are slightly downfield shifted.

The carbonyl absorptions in the IR spectrum of KH_3L^{2EtEt} give broad bands at 1648, 1594 and 1526 cm^{-1}. For the ligand KH_3L^{2MePh}, these strong bands appear at 1650, 1593 and 1529 cm^{-1}. For KH_3L^{2PhPh} the positions of the bands are similar to the previous ligands (1650, 1589 and 1528 cm^{-1}). The broad N-H frequencies are found in all three ligands around 3270 cm^{-1}.

In the ESI(-) MS spectra, the anionic species of the three ligands are visible. The calculated and observed value are in agreement for all three ligands ($\{H_3L^{2EtEt}\}^-$ calc.: 406.1554, found: 406.1473; $\{H_3L^{2MePh}\}^-$ calc.: 440.1398, found: 440.1351 and $\{H_3L^{2PhPh}\}^-$ calc.: 502.1554, found: 502.1553).

4.2 Synthesis of Re(V) Oxido Complexes with $\{HL^{2RR'}\}^{3-}$ Ligands

From reactions of KH_3L^{2EtEt}, KH_3L^{2MePh} and KH_3L^{2PhPh} with $(NBu_4)[ReOCl_4]$ in boiling $CHCl_3$, three Re(V) oxido complexes $[ReO(HL^{2EtEt})]$, $[ReO(HL^{2MePh})]$ and $[ReO(HL^{2PhPh})]$ were obtained. They are stable, neutral compounds and are formed with yields between 10 and 37 %. Single crystals suitable for X-ray analysis were obtained from acetone or methanol. The carboxylic group of $[ReO(HL^{2MePh})]$ was methylated during the crystallisation process. Trials to crystallise the complex $[ReO(HL^{2MePh})]$ from other solvents were not successful. However, the coordination mode in the three complexes is the same (Scheme 4.2).

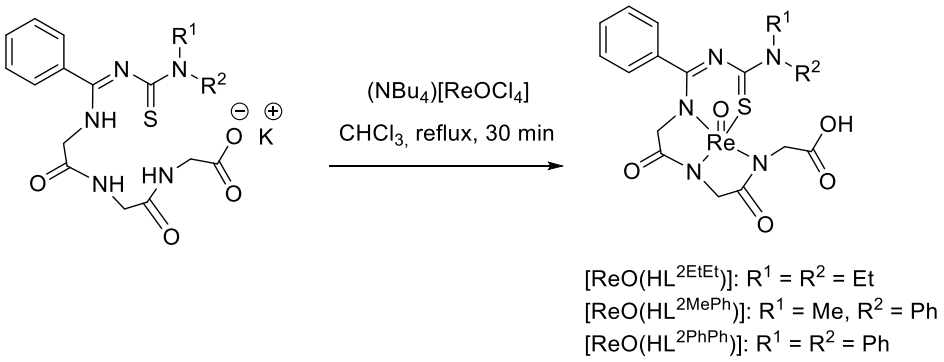

Scheme 4.2. Synthesis of the oxidorhenium(V) complexes $[ReO(HL^{2EtEt})]$, $[ReO(HL^{2MePh})]$ and $[ReO(HL^{2MePh})]$.

The CH_3 hydrogen atoms appear as two triplets at 1.21 and 1.32 ppm in the ^1H NMR spectrum of $[ReO(HL^{2EtEt})]$. This is due to hindered rotation of the diethylamino group. The signals of the CH_2 groups show resonances between 4.08 and 4.93 ppm. The hydrogen atom of the carboxylic group is visible as a broad singlet at 12.94 ppm.

In the ^1H NMR spectrum of $[ReO(HL^{2MePh})]$, the CH_3 protons show a singlet at 3.72 pm. The protons of the methylene groups appear between 4.21 and 4.91 ppm. The protons are diastereotopic due to the loss of the free rotation after the coordination to rhenium and the slightly different chemical environment due to the distorted square-pyramid. For this reason, the protons for each methylene group are splitted into six doublets. The doublets at 4.33 and 4.37 ppm overlap. Similar splittings are observed for the other two complexes.

In the ^{1}H NMR spectrum of the crystalline [ReO(HL^{2PhPh})] (Figure 4.2), the signals are well resolved and also the COO*H* proton is visible at 12.32 ppm. Again, the protons of the methylene groups are diastereotopic appearing in six doublets between 4.16 and 5.10 ppm with coupling constants between 18.5 and 17.3 Hz. They are slightly downfield shifted in comparison to [ReO(HL^{2EtEt})] and [ReO(HL^{2MePh})].

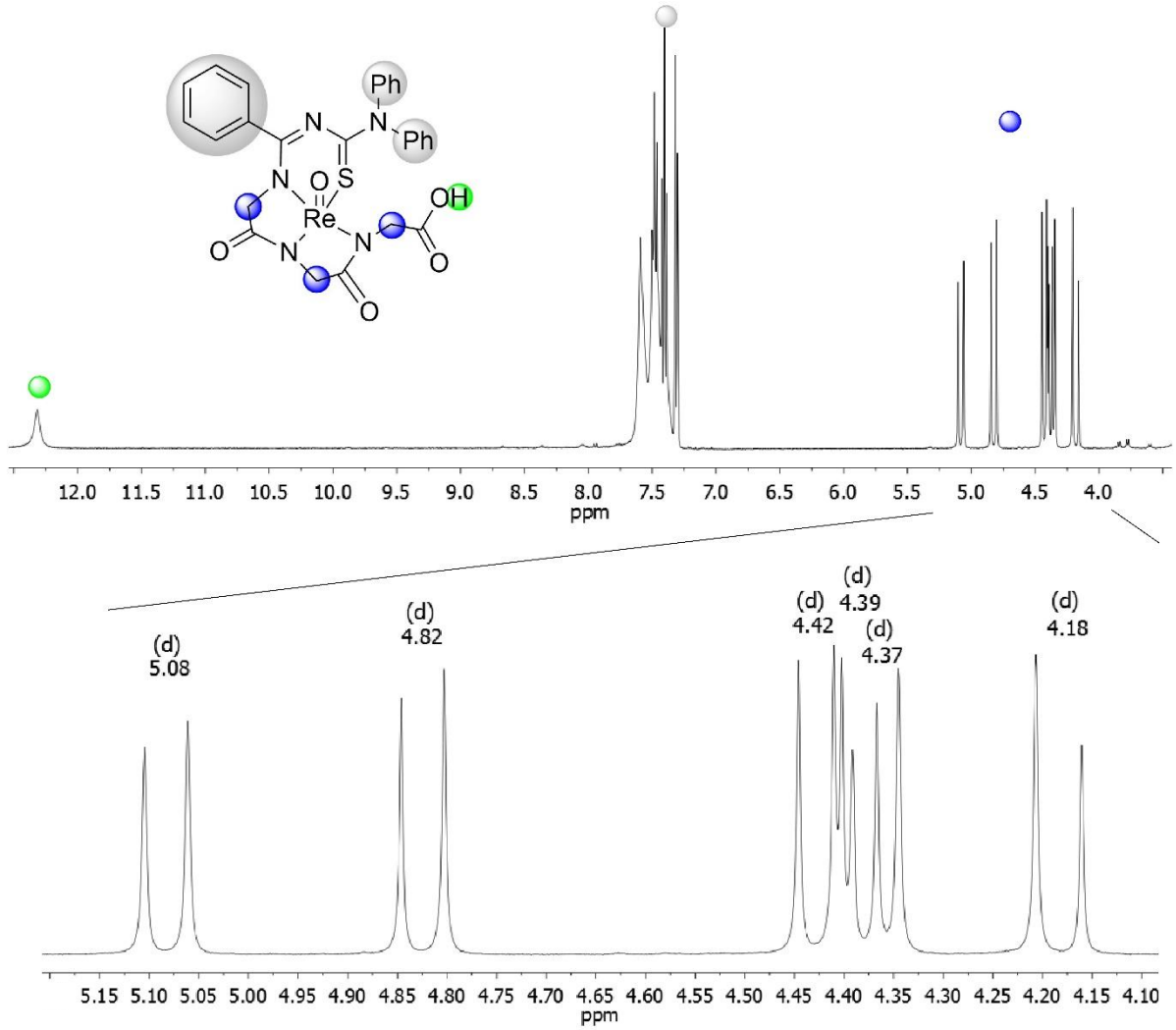

Figure 4.2. ^{1}H NMR spectrum of [ReO(HL^{2PhPh})] in d_6-DMSO. The protons of the methylene groups are diastereotopic and appear as doublets in the region between 4.1 and 5.1 ppm.

The IR spectra of the complexes are similar. The Re=O bands are in the expected region: for [ReO(HL^{2EtEt})][92] at 991 cm^{-1}, [ReO(HL^{2MePh})] at 984 cm^{-1} and for [ReO(HL^{2PhPh})] at 991 cm^{-1}. The carbonyl bands for [ReO(HL^{2EtEt})][92] are at 1739, 1672 and 1521 cm^{-1}, for [ReO(HL^{2MePh})] are at 1739, 1667 and 1612 cm^{-1} and for [ReO(HL^{2PhPh})] at 1714, 1666 and 1634 cm^{-1}. The ESI(-) MS spectra show the negatively charged ions for [ReO(L^{2EtEt})]$^{-}$ at 606.0800 (calc. 606.0826), for [ReO(L^{2MePh})]$^{-}$ at 640.0623

(calc. 640.0670) and for for [ReO(L^{2PhPh})]$^-$ at 702.0825 (calc. 702.0826). The isotopic ratio of rhenium (^{185}Re:^{187}Re around 2:3) also fits.

The substituents R^1 and R^2 at the nitrogen atom N1 have no influence on the coordination mode of the ligands (Figure 4.3). The rhenium atoms are coordinated in a distorted square-pyramidal environment. The rhenium atoms are found slightly above the basal plane formed by the four donor atoms of the organic ligands. The oxido ligands form the apexes of the pyramids. The Re1-O1 bond lengths are between 1.674(3) [ReO(L^{2PhPh})] and 1.681(2) [ReO(L^{2MePh})] Å. This is in the typical range of Re=O double bonds.[87, 93] More bond lengths and angles are given in Table 4.1. The carboxylic groups are not involved in the coordination of the transition metal. Therefore, they can be used for bioconjugation approaches.[92] During the purification process of [ReO(HL^{2MePh})], a methyl ester was formed because MeOH which was used as the solvent. Trials to crystallise this compound from other solvents failed. Single crystals of [ReO(HL^{2EtEt})] and [ReO(HL^{2PhPh})] were obtained from acetone.

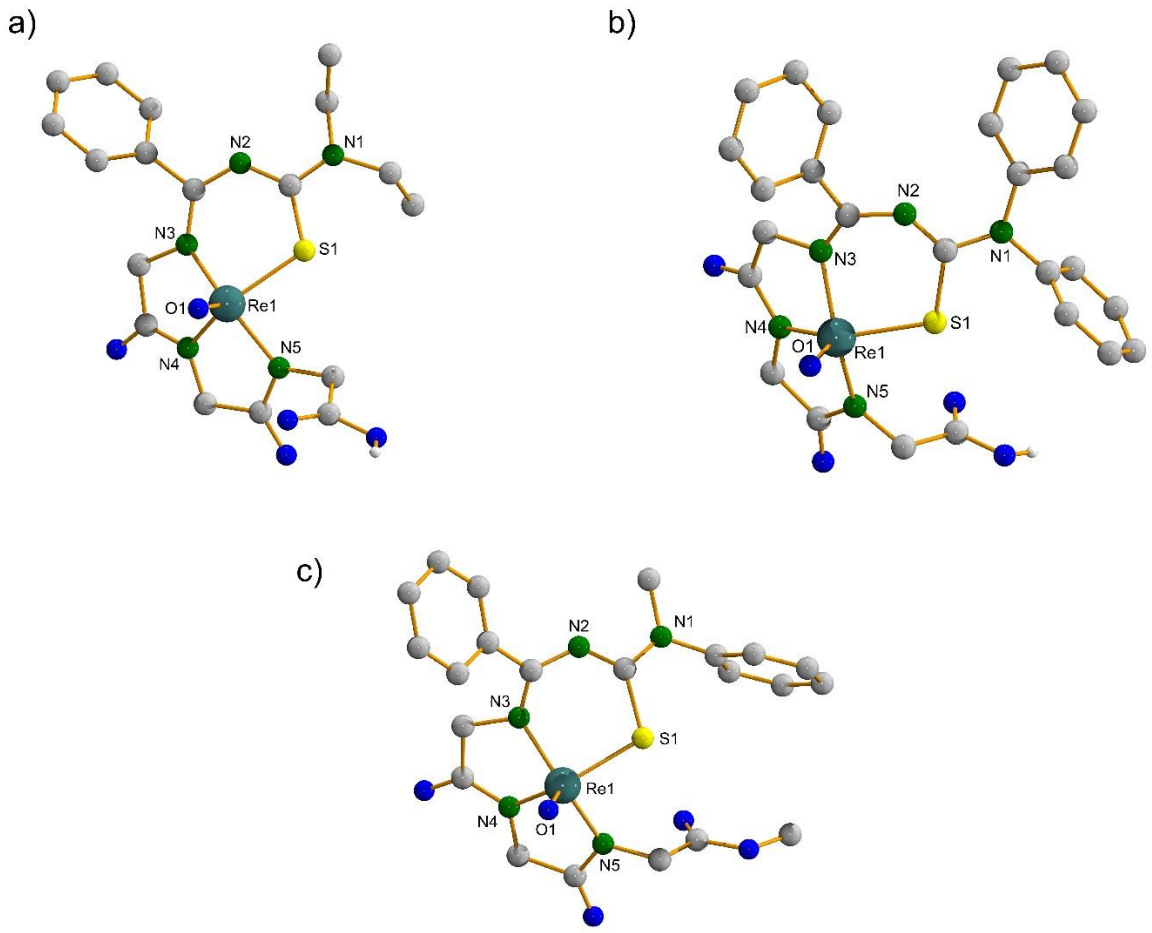

Figure 4.3. Molecular structures of a) [ReO(HL^{2EtEt})], b) [ReO(HL^{2PhPh})] and c) [ReO($L^{2MePh\text{-}ester}$)]. The hydrogen atoms are omitted for clarity except those of the carboxylic groups.

Table 4.1. Selected bond lengths [Å] and angles [°] of [ReO(HL^{2EtEt})], [ReO($L^{2MePh\text{-}ester}$)] and [ReO(HL^{2PhPh})].

	[ReO(HL^{2EtEt})]	[ReO($L^{2MePh\text{-}ester}$)]	[ReO(HL^{2PhPh})]
Re1-O1	1.679(2)	1.681(2)	1.674(3)
Re1-S1	2.299(8)	2.290(9)	2.286(9)
Re1-N3	2.005(3)	2.001(3)	2.015(3)
Re1-N4	1.972(3)	1.977(3)	1.966(3)
Re1-N5	2.022(3)	2.018(3)	2.014(3)
O1-Re1-S1	109.39(8)	109.39(9)	109.74(1)
O1-Re1-N3	107.26(11)	106.43(1)	105.40(1)
O1-Re1-N4	113.33(11)	113.41(1)	116.43(1)
O1-Re1-N5	108.27(12)	107.98(1)	106.16(1)
S1-Re1-N3	91.66(8)	92.24(8)	91.13(9)
N3-Re1-N4	78.07(11)	78.02(1)	78.84(1)
N4-Re1-N5	77.83(11)	77.81(1)	78.08(1)
N5-Re1-S1	87.08(8)	87.34(8)	87.87(9)

4.3 Synthesis of ^{99m}Tc(V) Oxido Complexes with $\{HL^{2EtEt}\}^{3-}$ and $\{HL^{2MePh}\}^{3-}$ Ligands

$Na[^{99m}TcO_4]$ was obtained from a commercial $^{99}Mo/^{99m}Tc$ generator in nanomolar concentrations. This low concentration frequently causes problems in the transfer of the chemistry of ^{99}Tc or Re, since the kinetics of the reactions will be influenced. Due to the short half-life of 6 h, the labelling should be as quick as possible. A so-called “kit”, containing a reducing agent and a supporting ligand usually helps to control the pH value and stabilizes the oxidation state of technetium. The products were analysed by an analytical HPLC with a radio detector (γ–scintillator).

$SnCl_2 \cdot 2\ H_2O$ was used for the reduction of pertechnetate. A solution of 5 mg $SnCl_2 \cdot 2\ H_2O$ in 5 mL H_2O was prepared as stock from which aliquots were taken. EtOH (100 µL) was added to increase the solubility. Optimal temperatures, reaction times and added amounts of the ligands KH_3L^{2EtEt}, KH_3L^{2MePh} and of $SnCl_2 \cdot 2\ H_2O$ were screened to find the best reaction conditions. Figure 4.4 shows a chromatogram with the most promising reaction conditions: 240 µg of the ligand KH_3L^{2EtEt}, 100 µg $SnCl_2 \cdot 2\ H_2O$ (100 µL of the prepared solution), 50 MBq of $Na[^{99m}TcO_4]$ (0.5 mL), 45 °C for 30 min plus additional 10 min cooling period. The reaction mixture was neutralized with a PBS buffer. A radiochemical purity of 91 % was reached. The retention time of 21.75 min is close to the UV trace of the rhenium compound (21.39 min).

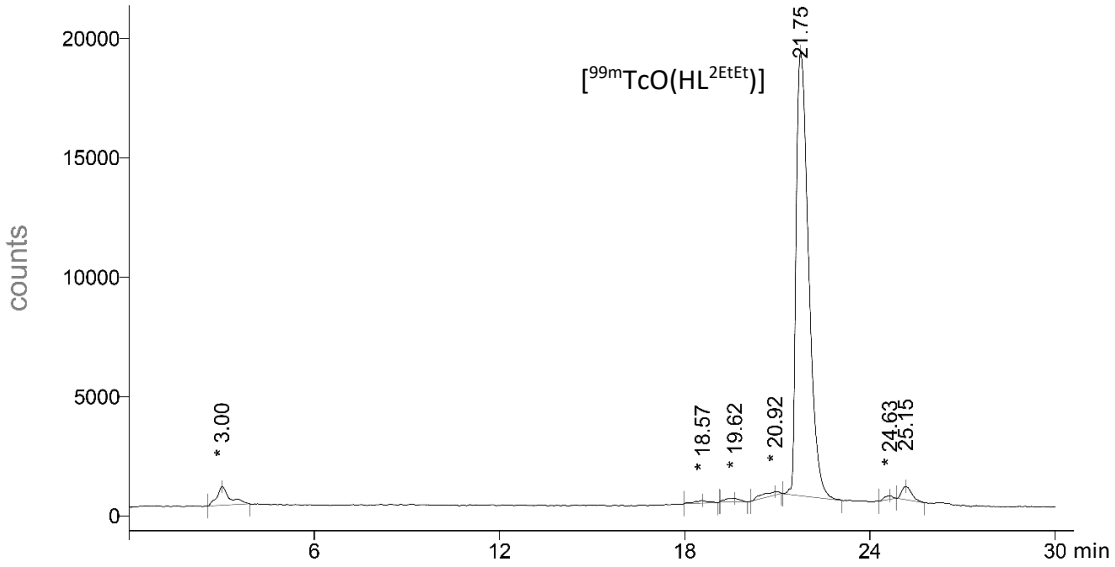

Figure 4.4. Radio trace of [^{99m}TcO(HL^{2EtEt})] under optimized conditions. Radiochemical purity: 91 %.

The optimized reactions conditions were transferred to the thiourea ligand KH_3L^{2MePh}. However, lower radiochemical yields were obtained in this case (63 % instead of 91 %). The best obtained radiochemical yield with the methyl/phenyl derivative was at higher temperature under following reaction conditions: 230 µg of the KH_3L^{2MePh} ligand, 100 µg $SnCl_2 \cdot 2\ H_2O$ (100 µL of the prepared solution), 50 MBq of Na[$^{99m}TcO_4$] (1.7 mL), 80 °C for 15 min plus additional 10 min during cooling to room temperature. The reaction mixture was neutralized with a PBS buffer. A radiochemical yield of 67 % was reached. The retention time of 21.95 min is close to the UV trace of the rhenium compound (21.56 min) (Figure 4.5). The formation of side products with retention times of 21.30 and 25.10 min was observed. The third ligand, KH_3L^{2PhPh}, was not regarded with ^{99m}Tc experiments since an extremely high lipohilicity is expected due to the phenyl groups.

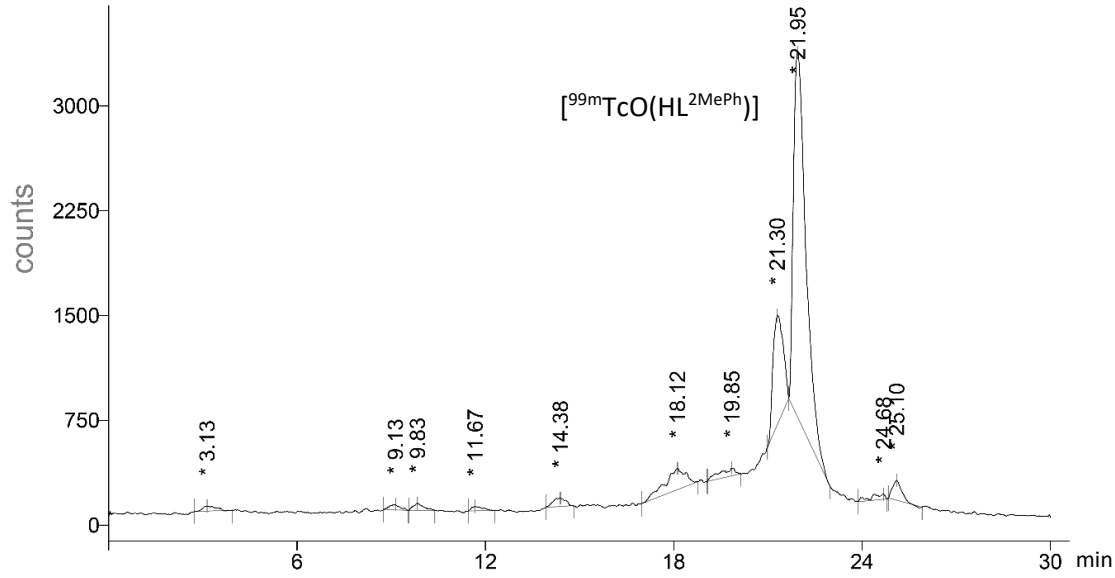

Figure 4.5. Radio trace of [^{99m}TcO(HL^{2MePh})]. Radiochemical purity: 67 %.

4.4 Synthesis of the Potential Prostate Tracers H_3P^{EtEt} and H_3P^{MePh}

It has been previously shown that the KH_3L^{2EtEt} ligand readily binds via a peptide bond to a biomolecule (e. g. Angiotensin II).[92] Here, the same ligand is connected to another biomolecule targeting the prostate-specific membrane-antigen (PSMA). The idea for such a potential ^{99m}Tc-based tracer is taken from an already established ^{68}Ga-PSMA-617 tracer, which shows good results in *in vivo* experiments.[16] The potential "^{99m}Tc-PSMA-617" tracer should be as similar as possible to achieve also similar results *in vivo* experiments. For this reason, also the linker between the bifunctional chelator and the pharmacophore 'Glu-urea-Lys' was kept identical (Figure 4.6). The chosen tetradentate thiourea chelator is well established in our group and was already used in an *in vivo* study with mice in similar experiments.[92] The bioconjugate of the previous study was stable under physiological conditions over a period of 1 h after injection.[92] These promising results were a good fundament for the experiment with PSMA-617.

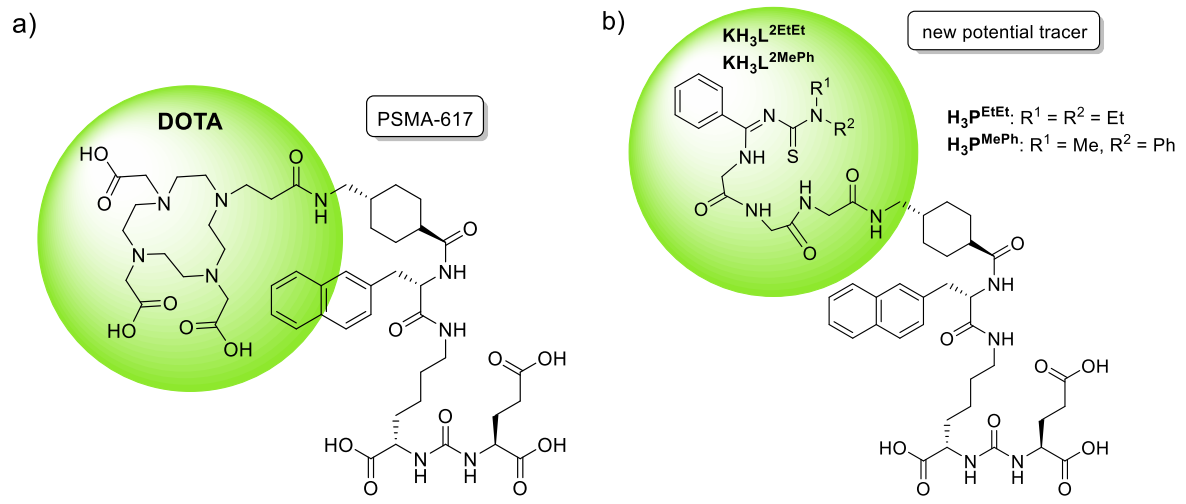

Figure 4.6. a) PSMA-617 with DOTA as a bifunctional chelator. b) The bioconjugates H_3P^{EtEt} and H_3P^{MePh} with the thiourea ligands KH_3L^{2EtEt} and KH_3L^{2MePh} as chelators.

The conjugates H_3P^{EtEt} and H_3P^{MePh}, consisting of a tetradentate thiourea-based chelator and PSMA-617, were synthesised on a Fmoc-Lys(Mtt)-Wang resin. After fmoc deprotection, the resin was stirred overnight at room temperature with the *in situ* generated isocyanate (di-tert-butyl (R)-2-isocyanatopentanedioate). The obtained resin-immobilised Glu-urea-Lys(Mtt) was filtered. The subsequent steps of the synthesis are illustrated in Scheme 4.3. In the last reaction steps, the *N,N,N,S*-thiourea chelators (KH_3L^{2EtEt} and KH_3L^{2MePh}) were coupled. Both conjugates were purified by preparative HPLC and analysed by ESI MS.

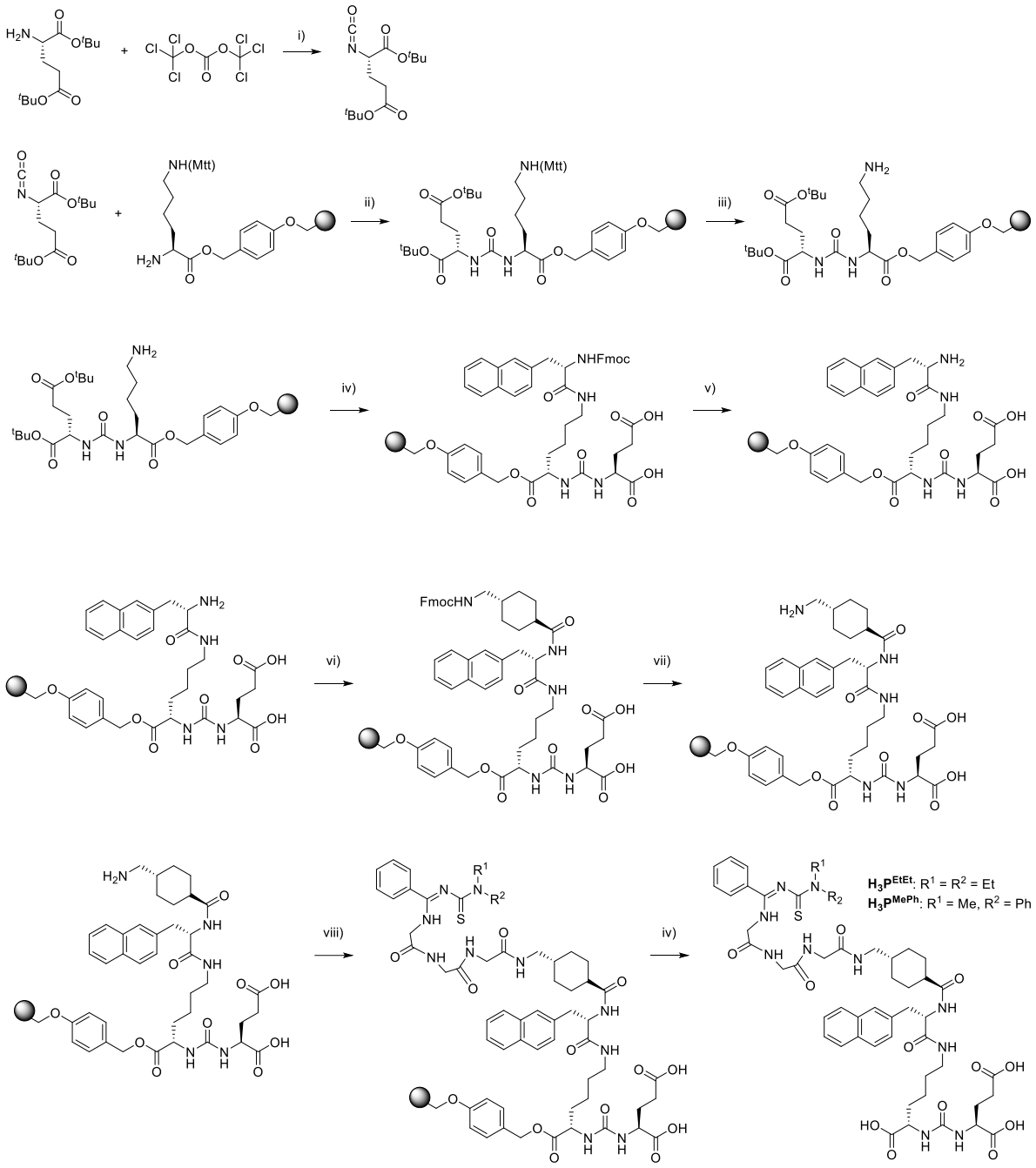

Scheme 4.3. Synthesis of H_3P^{EtEt} and H_3P^{MePh}. (i) DIPEA, CH_2Cl_2, 0 °C for 2 h, rt for 1 h. ii) rt, overnight. iii) 1 % TFA in MeOH/CH_2Cl_2, overnight. iv) Fmoc-L-2NaI-OH, HBTU, DIPEA, DMF. v) 20 % piperidine in DMF. vi) *N*-Fmoc-traneamix, HBTU, DIPEA, DMF. vii) 20 % piperidine in DMF. viii) L^{2EtEt} or L^{2MePh}, HBTU, DIPEA, DMF. iv) TFA, H_2O, TIPS.)

4.5 Synthesis of Re(V) and ^{99m}Tc(V) Oxido Complexes with H_3P^{EtEt} and H_3P^{MePh}

In a proof-of-principle reaction, the new conjugates H_3P^{EtEt} and H_3P^{MePh} were coordinated to the oxidorhenium(V) core starting from $(NBu_4)[ReOCl_4]$. The reaction was done in a refluxing EtOH/$CHCl_3$ mixture for 30 min (Scheme 4.4). The products were analysed by mass spectrometry (UPLC MS) showing the masses of 1245.46 (calc. 1245.41) for $[ReO(P^{EtEt})]$ and 1279.46 (calc. 1279.39) for $[ReO(P^{MePh})]$. Retention times of 22.06 and 22.28 min for $[ReO(P^{EtEt})]$ and 22.08 and 22.52 min for $[ReO(P^{MePh})]$ were obtained. The HPLC analysis shows the formation of two products for both chelates with just a few seconds difference in their retention time (13 and 26 s). Interestingly, this was not observed for $[ReO(HL^{2EtEt})]$ and $[ReO(HL^{2MePh})]$). Hitherto, there is no satisfactory explanation for this finding.

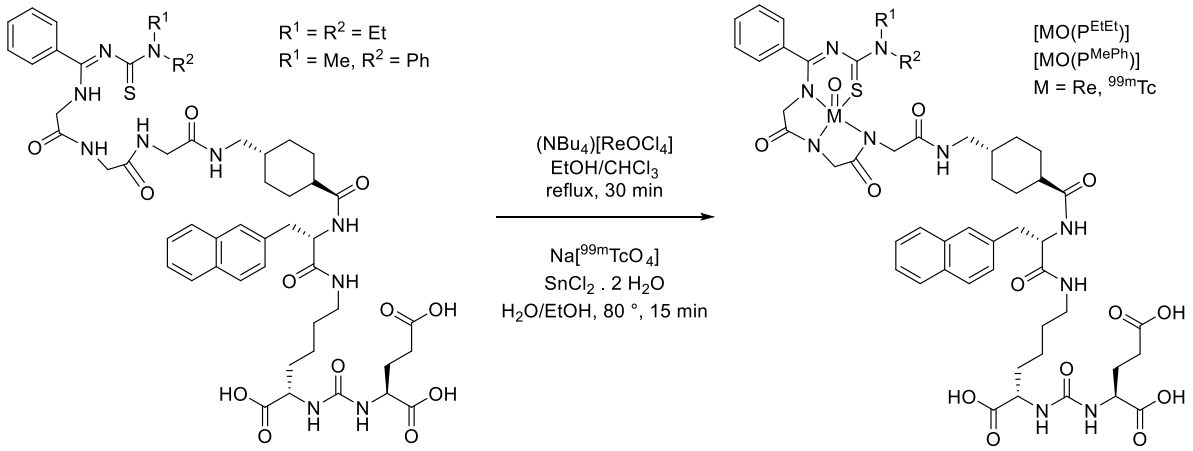

Scheme 4.4. Synthesis of $[MO(P^{EtEt})]$ and $[MO(P^{MePh})]$ (M = Re, ^{99m}T).

$[^{99m}TcO(P^{EtEt})]$ and $[^{99m}TcO(P^{MePh})]$ were synthesised from $Na[^{99m}TcO_4]$ and H_3P^{EtEt} or H_3P^{MePh} (Scheme 4.4). Different reaction conditions were screened for the optimization of product yield and purity changing the amounts of $SnCl_2 \cdot 2\ H_2O$ and the peptides, the reaction time, the temperature and solvent ratio H_2O/EtOH. The final, optimized reaction conditions are: 123 µg of H_3P^{EtEt}, 100 µg $SnCl_2 \cdot 2\ H_2O$, 50 MBq $Na[^{99m}TcO_4]$ in 1.7 mL and 100 µL EtOH kept at 80 °C for 15 min. The reaction product was purified using a C18 column (Chromafix). Under these conditions, a radiochemical purity of 98 % was achieved. The retention time of 22.43 min is similar to the retention time of the rhenium analogue $[ReO(P^{EtEt})]$. $[^{99m}TcO(P^{EtEt})]$ was stable in PBS buffer at room temperature under air over 3 h according to a HPLC analysis (Figure 4.7). No pertechnetate was reformed or side products were obtained.

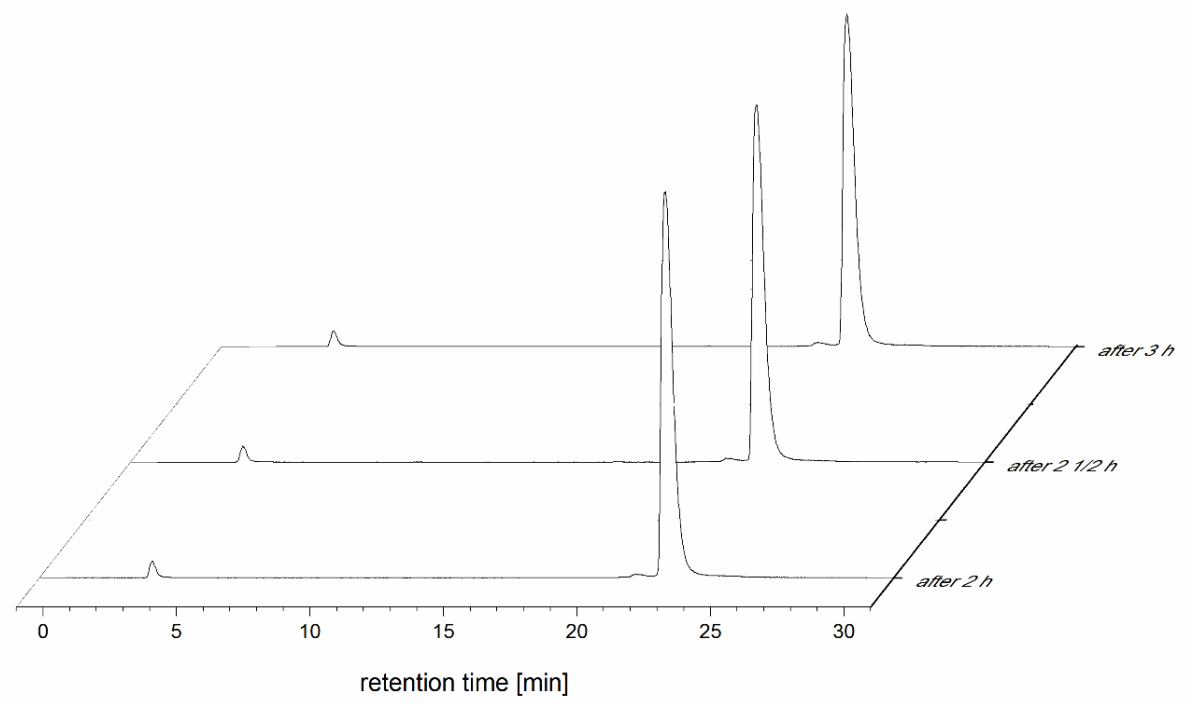

Figure 4.7. Radio traces of [^{99m}TcO(P^{EtEt})] after 2, 2 ½ and 3 h in PBS buffer solution.

The reaction conditions optimized for [^{99m}TcO(P^{EtEt})] were also applied for the analogue peptide H_3P^{MePh}. The HPLC trace of this product shows a similar retention time: 22.45 instead of 22.43 min. The radiochemical purity was 83 % and the radiochemical yield was 9 %. After purification with a C18 column, the radiochemical yield was 4 %. This might be due to the lower solubility of the more lipophilic compound. More experiments should be done to get a better yield and purity.

4.6 *In Vivo* Experiments with [^{99m}TcO(P^{EtEt})]

Two male mice with a subcutaneously growing human prostate-specific membrane-antigen (PSMA)-positive prostate cancer tumor were taken for the *in vivo* experiments with [^{99m}TcO(P^{EtEt})].

[^{68}Ga]Ga-PSMA-11, a specific PSMA ligand, was used as the clinical standard tracer for prostate cancer PET imaging to verify PSMA expression of the prostate tumor xenograft as depicted in Figure 4.8. Either [^{68}Ga]Ga-PSMA-11 (35 MBq) or [^{99m}TcO(P^{EtEt})] (31 MBq) were injected intravenously into the tail vein of the mouse. The scan range was chosen so that all relevant organs from the head to the bladder were included in the image.

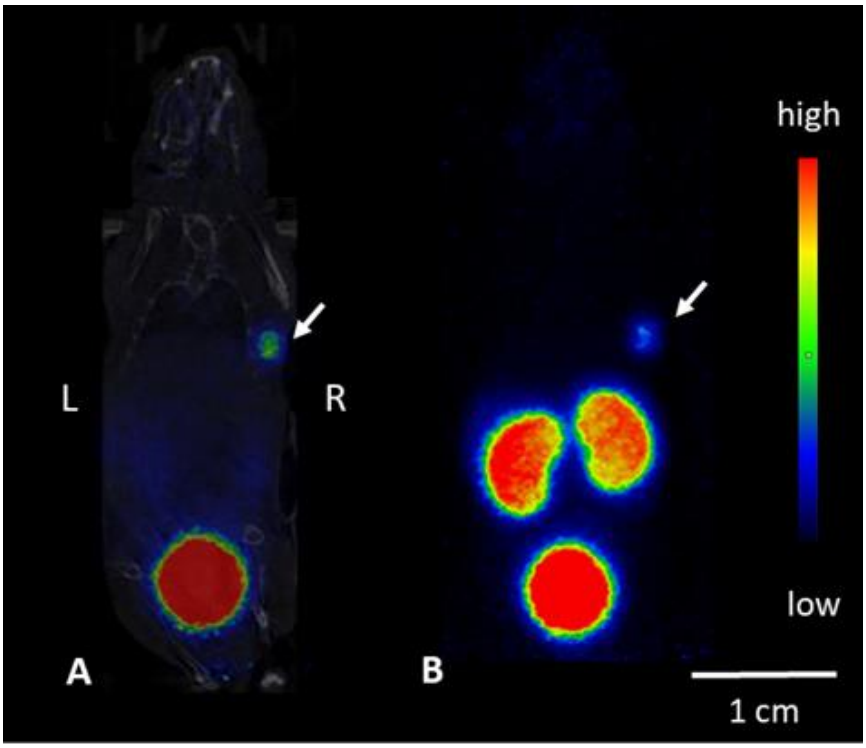

Figure 4.8. PET/CT scan after 50 min of intravenous injection of 35 MBq [^{68}Ga]Ga-PSMA-11. A: Coronal slice of the mouse with the tumor on the right side (white arrow). B: PET maximum intensity projection (MIP) with the white arrow indicating the PSMA-positive tumor xenograft. The scale bar is representative for all images.

[^{99m}TcO(P^{EtEt})] was injected to the second mouse (Figure 4.9). Most of the compound was rapidly excreted through the liver (pink arrow) into the intestines (yellow arrow) as shown on the MIPs (Figure 4.9A) at 10, 25, 40 and 55 min after injection. No uptake was observed in the tumor xenograft (white arrow, (Figure 4.9B)) while in another coronal slice of the mouse at the same time a high uptake in the gastrointestinal tract and the gall bladder was detected (Figure 4.9C). No specific activity accumulation in the thyroid was observed for [^{99m}TcO(P^{EtEt})] indicating that no pertechnetate is released from the chelator which would rapidly accumulate in the thyroid reaching a maximum uptake within 20-30 min.[94-95] These findings demonstrate the *in vivo* stability of the thiourea chelator $\{L^{2EtEt}\}^{3-}$ and confirm the results from previous experiments.[92] The SPECT/CT scans of [^{99m}TcO(P^{EtEt})] are different from the chelate $\{L^{2EtEt}\}^{3-}$.[92] Hence, the stability of the peptide bond between the chelate and the biomolecule (PSMA) is proofed.

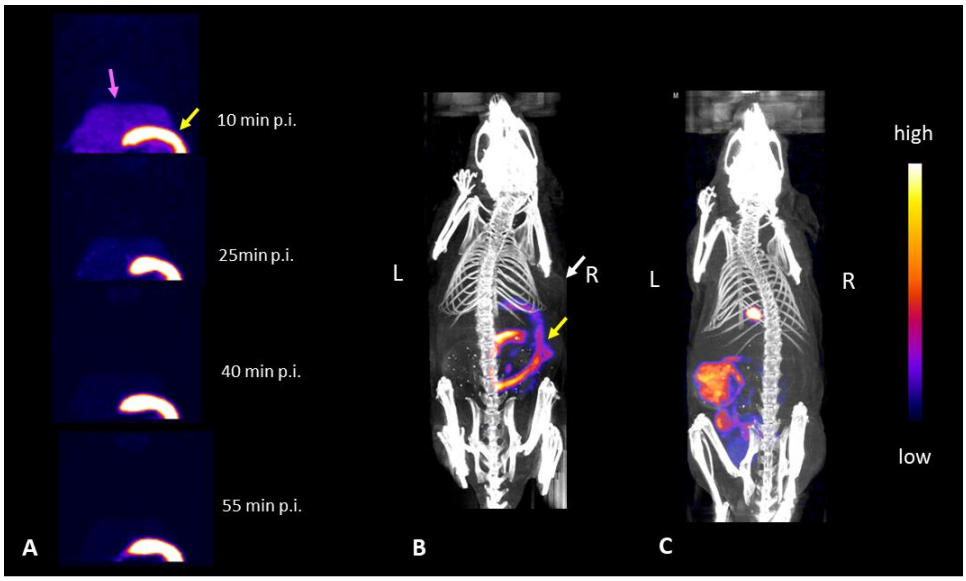

Figure 4.9. SPECT/CT scan of [^{99m}TcO(P^{EtEt})]. A: MIPs of the abdomen at 10, 25, 40 and 55 min p.i. depicting the liver and the intestines. B: Coronal slice of the tumor at 75 min after injection. C: Coronal slice showing the gall bladder and gastrointestinal tract at 75 min after injection. The scale bar is representative for all images.

The biodistribution of [^{99m}TcO(P^{EtEt})] shows the highest uptake in the kidney followed by the liver which is typical for lipophilic compounds (Figure 4.10). In the prostate tumor only 0.0676 %IA/g are accumulated. Also an uptake in the spleen, lung and heart is visible.

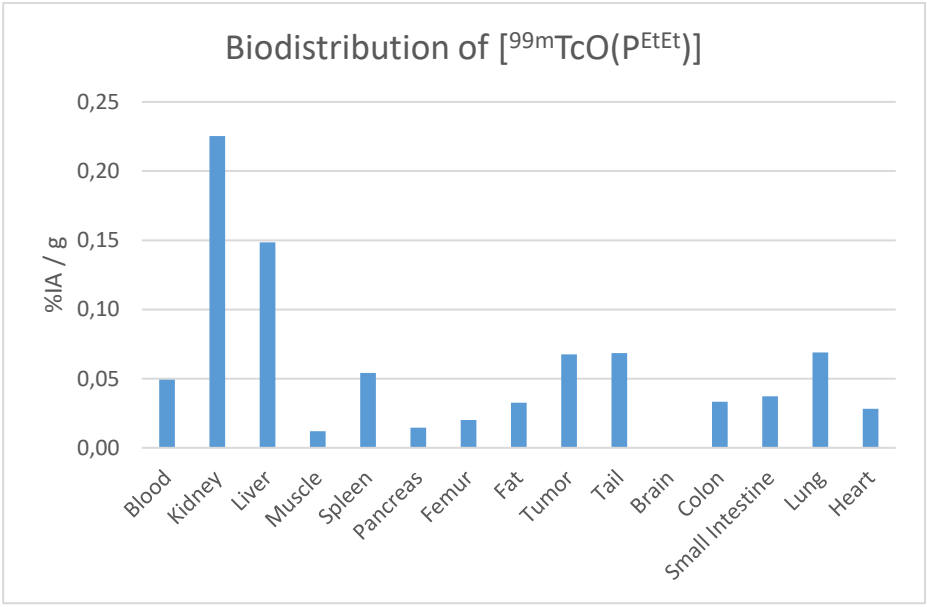

Figure 4.10. Biodistribution of [^{99m}TcO(P^{EtEt})] in injected activity per gramme of tissue (%IA/g).

Interestingly, similar results were recently obtained with [^{99m}TcO-Angiotensin(II)].[92] The highest uptake of [^{99m}TcO-Angiotensin(II)] with the same chelator $\{L^{2EtEt}\}^{3-}$ was observed in the gall bladder of healthy mice after 10 min. Angiotensin(II) is an eight amino acids long peptide and structurally a completely different biomolecule compared to the pharmacophore taken from PSMA-617. Both bioconjugates are lipophilic compounds, which is shown by the retention times on the HPLC on a reversed phase (C18). Two options are possible for the explanation of the similar behaviour of the two compounds: glucuronidation or the metabolisation of the lipophilic bioconjugate. In both cases, the liver, gall bladder and the intestine are visible during the scans. The fact that the SPECT/CT scan are similar indicates that the compounds have similar biokinetics.

4.7 Synthesis of the "N-Terminus Ligand" H_3L^{3EtEt}

For the synthesis of the "N-terminus ligand" H_3L^{3EtEt}, the backbone of the tetradentate ligands of the previous subchapter was elongated with a Boc-protected ethylene diamine unit. This means, a new peptide bond was established between the terminal -COOH group of KH_3L^{2EtEt} and the unprotected $–NH_2$ group of the single Boc-protected ethylene diamine (Scheme 4.5). The coupling product was purified by column chromatography and the Boc group was cleaved with TFA. Alternatively, this step can be done with HCl at 0 °C. No work-up was needed. The product was obtained as triflate or chloride salt depending on the deprotection of the Boc group.

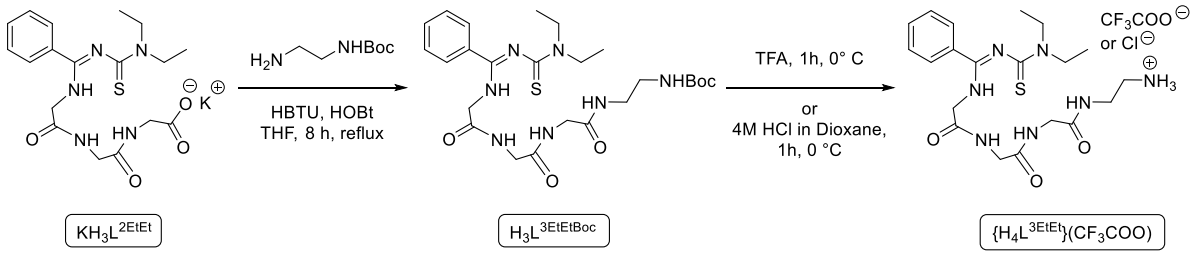

Scheme 4.5. Synthesis of the "N-terminus ligand" $\{H_4L^{3EtEt}\}(CF_3COO)$.

The product $\{H_4L^{3EtEt}\}(CF_3COO)$ was characterized by NMR spectroscopy. The ^{1}H NMR spectrum in d_4-MeOD shows a multiplet for the two CH_3 groups. The signal for the fourteen protons of the methylene groups form signals between 2.93 and 3.97 ppm appearing as a singlet, triplet or quartet depending on the surrounding coupling partners. The aromatic protons form a multiplet at 7.35 ppm (Figure 4.11). The protons at the free ammonium group are not visible because they exchanged with

the deuterium of the used deuterated solvent d_4-MeOD. The obtained ^{19}F NMR spectrum of the trifluoroacetate salt shows a singlet at -77.43 ppm for the triflate anion.

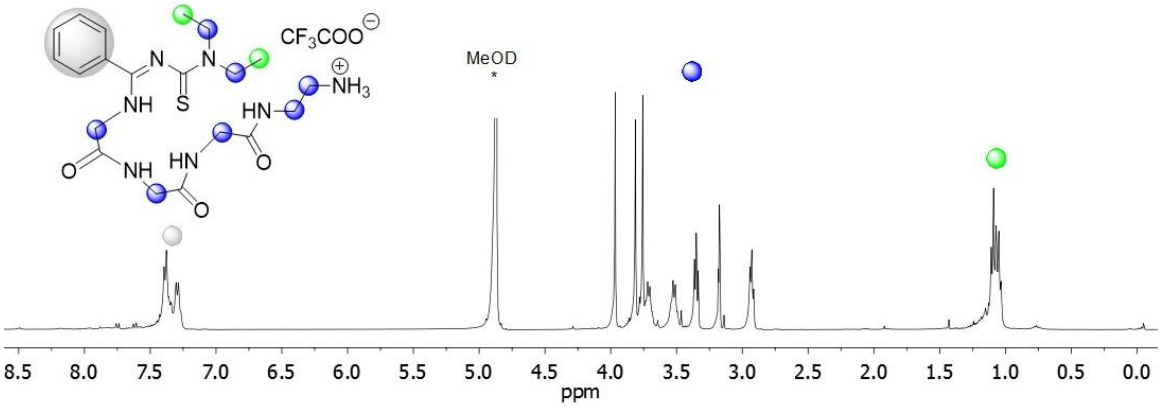

Figure 4.11. ^1H NMR spectrum of $\{H_4L^{3EtEt}\}(CF_3COO)$ in d_4-MeOD.

4.8 Synthesis of Re(V) and ^{99m}Tc(V) Oxido Complexes with H_3L^{3EtEt}

Before attempts with ^{99m}Tc were undertaken, the complex formation of the "N-terminus ligand" with rhenium(V) was studied. A reaction with $(NBu_4)[ReOCl_4]$ and the $H_3L^{3EtEtBoc}$ ligand was performed. The reaction was directed *via* an intermediate ethylene glycol complex of rhenium(V) (Scheme 4.6). Such a procedure allows to work at higher pH values. $(NBu_4)[ReOCl_4]$ and ethylene glycol were stirred in MeOH and 1 M NaOH solution was added until a pH of 9 was reached. The colour of the reaction mixture turned blue to dark violet. After the addition of the Boc-protected thiourea ligand $H_3L^{3EtEtBoc}$ dissolved in MeOH, the reaction mixture was stirred 4 h at room temperature. The product was separated by column chromatography obtaining an orange oil soluble in common organic solvents. The Boc group was cleaved with TFA at 0 °C giving a pale-orange product as a triflate salt.

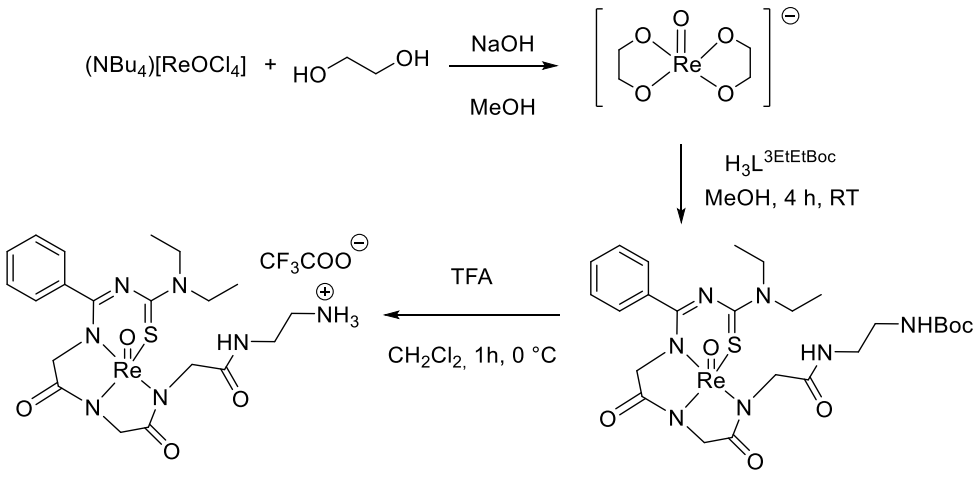

Scheme 4.6. Synthesis of $[ReO(HL^{3EtEt})](CF_3COO)$.

The complex was analysed by ^{1}H NMR spectroscopy, where the signals of the CH_3 groups appear as two triplets at 1.25 and 1.35 ppm. The methylene protons form broad multiplets between 3 and 5 ppm, which is slightly downfield shifted compared with the non-coordinated ligand. Only one of these signals at 5.01 ppm is well resolved as a doublet with an integral of one proton showing that the protons are diastereotopic. The signals for the aromatic protons form a multiplet at 7.46 ppm. In the ^{19}F NMR spectrum the signal of triflate anion appears at -75.8 ppm. The retention time of the rhenium complex with the Boc group on a C18 HPLC column is at 22.2 min and after deprotection at 20.45 min. This retention times can be used for comparison with the ^{99m}Tc products.

The ^{99m}Tc complex formation of $H_3L^{EtEtBoc}$ was done starting from $Na[^{99m}TcO_4]$ (Scheme 4.7). Different parameters were screened to find suitable reaction conditions. The reaction time, the temperature, the amount of $H_3L^{EtEtBoc}$ and supporting ligands were changed. The final, optimized reaction conditions are: 2 mg of $H_3L^{EtEtBoc}$ with 35 MBq $Na[^{99m}TcO_4]$ in 0.7 mL saline and 280 µg $SnCl_2 \cdot 2\ H_2O$ kept at 75 °C for 30 min. The pH of the reaction was 3. The retention time of the $[^{99m}TcO(L^{3EtEtBoc})]$ complex is 21.10 min.

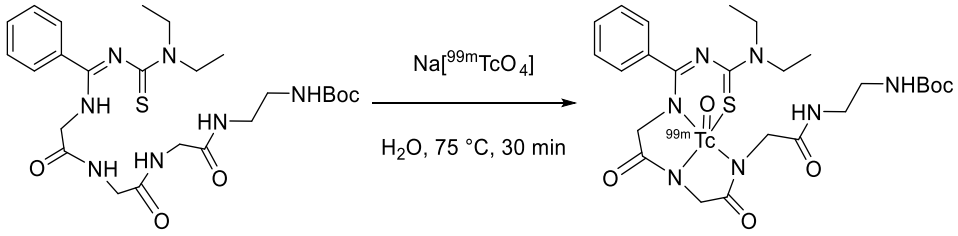

Scheme 4.7. Synthesis of $[^{99m}TcO(L^{3EtEtBoc})]$.

4.9 Synthesis of a $^{99m}Tc(V)$ Oxido Complex with a "Bisphosphonate Ligand"

H_3L^{3EtEt}-bisphosphonate was synthesised from H_3L^{3EtEt} and a squaric acid derivative, which contains a bisphosphonate unit, under basic, aqueous conditions (Scheme 4.8). The terminal amino group of H_3L^{3EtEt} attacks the squaric acid and forms a new C-N bond. The product was separated by preparative HPLC and analysed by mass spectrometry. Generally, bisphosphonates target hydroxyapatite in bones, which can be used for diagnosis of bone metastases.

$[^{99m}TcO(L^{3EtEt}$-bisphosphonate$)]$ was synthesised from $Na[^{99m}TcO_4]$ and H_3L^{3EtEt}-Bisphosphonate (Scheme 4.8). Different reaction conditions were screened for the optimization of product yield and purity changing the reaction time and the temperature. A kit containing 34 mg tartaric acid, 48 mg sodium tartrate dihydrate, 80 mg $SnCl_2 \cdot 2\ H_2O$ and 1684 mg lactose monohydrate was used. It helps to control the pH value and oxidation state +V of ^{99m}Tc.

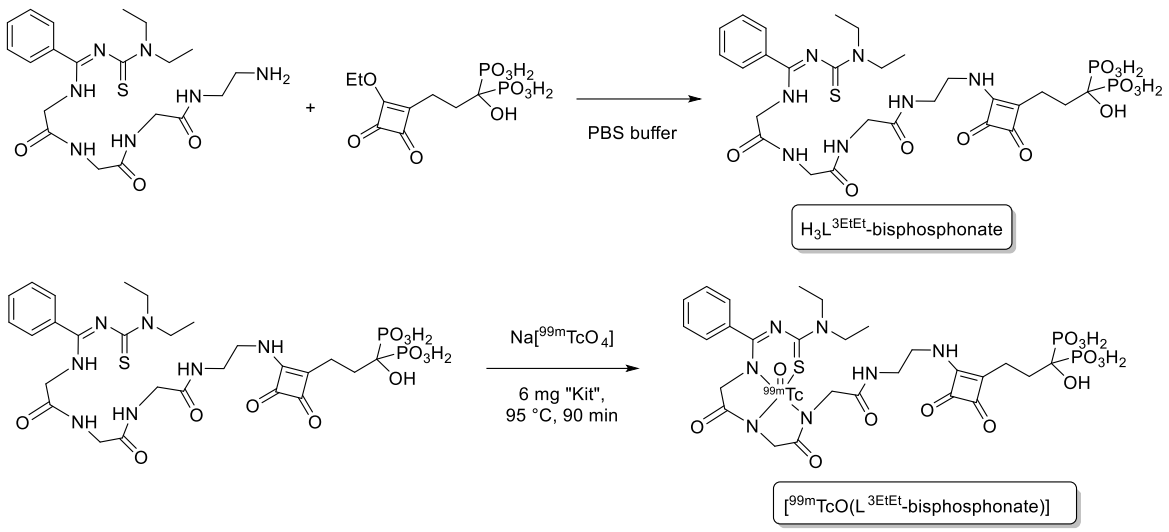

Scheme 4.8. Synthesis of H_3L^{3EtEt}-bisphosphonate and [^{99m}TcO(L^{3EtEt}-Bisphosphonate)].

The final, optimized reaction conditions are: 250 µg of H_3L^{3EtEt}-bisphosphonate, 95 °C, 90 min, 256 MBq Na[$^{99m}TcO_4$] in 1 mL saline solution and 6 mg of the kit. The pH was adjusted to 7 with NaOH and HCl. The reaction was analysed by TLC in H_2O and a Mini GITA (TLC reading-device with a bismuth germanate γ-szintillator). During this reaction, aliquots after 1, 5, 18, 30 and 90 min were taken and the radiochemical purity was determined by TLC in H_2O. The radiochemical purity increased over 90 min up to 64 % (not decay-corrected) (Figure 4.12).

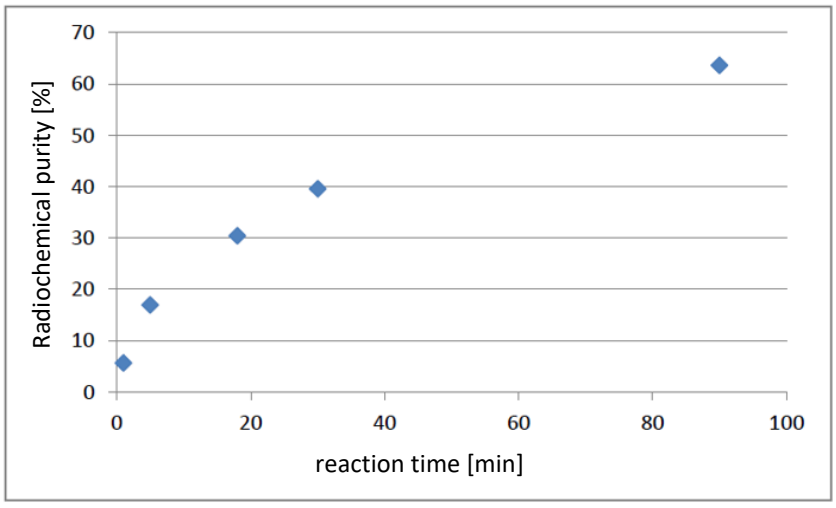

Figure 4.12. Radiochemical purity of [^{99m}TcO(L^{3EtEt}-Bisphosphonate)] following the reaction.

The final reaction conditions are relatively harsh. Besides the high temperature of 95 °C, the main challenge is the long reaction time of 90 min and the low radiochemical purity. A peak with a small R_f value on the TLC is the complex of tartaric acid and ^{99m}Tc. It reacted further slowly to the desired bisphosphonate tracer, which explains the long reaction times. More experiments should be done in order to find better reaction conditions.

5 Experimental Section

5.1 Analytical Methods

Infrared spectra were taken on a Shimadzu FTIR 8300 spectrometer between 400 and 4000 cm^{-1} from KBr pellets or on a Thermo Scientific Nicolet iS10 ATR spectrometer.

NMR spectra were recorded at 300 K on JEOL ECS and ECZ 400 MHz multinuclear spectrometers.

The X-band EPR spectra were recorded on a Miniscope MS400 Magnettech spectrometer with a rectangular TE102 microwave generator at 300 K and 77 K. The program WinEPR SimFonia was used for the simulations.[96]

ESI mass spectra were measured with an Agilent 6210 ESI-TOF mass spectrometer (Agilent Technologies, Santa Clara, CA, USA). The spray voltage was set to 4 kV and the drying gas flow rate to 15 psi (1 bar). All other parameters were adjusted for a maximum abundance of the relative $[M+H]^+$ or $[M]^-$ ions. All MS results are given in the form: m/z, assignment. Because of radiation safety reasons, the radioactive compounds were not measured. The masses of the molecular ion peaks were calculated with ChemDraw.[97]

Elemental analyses of carbon, hydrogen, nitrogen and sulfur were determined using a Heraeus vario EL elemental analyzer.

Technetium contents were measured by a HIDEX 300 SL liquid scintillation counter. An aliquot (0.2 mL) of each sample was added to 10 mL of a scintillation cocktail (Rotiszint ecoplus, Carl Roth) and the net count rates were measured over 1024 channels with a counting time of 120 s. Technetium values were calculated from the counting rate using the specific activity of ^{99}Tc ($6.3 \cdot 10^5$ Bq/mg).

The intensities for the X–ray determinations were collected on STOE IPDS 2T or Bruker D8 Venture instruments with Mo Kα or Cu Kα radiation. The space groups were determined by the detection of systematically absences. Absorption corrections were carried out by SADABS[98] or integration methods.[99] Structure solutions and refinements were performed with the SHELXT, SHELXS-97, SHELXS-86 and SHELXL-2014 programs included in the WinGX program package.[100-102] The representation of molecular structures was done using the programs DIAMOND 4.2.2[103] and POV-Ray.[104] Tables containing more information about crystal data, refinement, positional parameter and ORTEP[105] ellipsoid drawings are given in the crystallographic appendix. Some of the obtained molecular structures were disordered. All disorders were modelled with two parts and their contributing fractions were determined by free variables. In $[Tc(NO)Cl(PPh_3)(L^{OMe})]$ the positions of the NO and Cl ligands have been refined with occupational factors of 0.57/0.43 and their

thermal parameters were modelled with constraints (EADP). In [TcNCl(PPh_3)(L^{OMe})] the positions of the N and Cl ligands and also the Tc atom have been refined with occupational factors of 0.51/0.49 and their thermal parameters were modelled with constraints (EADP). In [TcO(glycolate)(L^{OMe})], P1, P2, P3 and all oxygen atoms of the $\{L^{OMe}\}^-$ ligand (O1 - O9) are disordered with occupational factors of 0.60/0.40. The thermal parameters were modelled with restraints (SADI, RIGU, DELU, ISOR). In [ReNCl(PPh_3)(L^{OMe})], the positions of the N^{3-} and Cl^- ligands and also the Re atom are disordered and have been refined with occupational factors of 0.80/0.20. The thermal parameters of the named atoms were modelled with constraints (EADP). In [$ReNCl_2$(L^{OMe})], the positions of the N^{3-} and Cl^- ligands and also the Re atom are disordered and have been refined with occupational factors of 0.89/0.11. The thermal parameters were modelled with constraints (EADP) and restrains (SADI). In [Ga(L^{OMe})$_2$]NO_3 the positions of O4, C8, O5, C9, O7, C10, O8 and C11 of the $\{L^{OMe}\}^-$ ligand are disordered. The thermal parameters of the atoms were modelled with restraints (SADI, RIGU, DELU). In the molecular structure of [Lu(L^{OMe})$_2$(NO_3)], the entire $\{L^{OMe}\}^-$ ligand is disordered along the Co-Lu axis. Additionally, the oxygen atom O10 of the NO_3^- ligand is disordered and named O11. The disorders were modelled with constraints (EADP) and restraints (SADI, DELU, RIGU) including the disordered solvent THF molecule. In [Re(NPhF)(L^{1EtEt})], the positions of N4, C36 and C37 are disordered with occupational factors of 0.54/0.46 and were modelled with constraints (EADP) and restraints (SADI). [$TcOCl_2$(L^{OMe})] was refined as a two-component inversion twin.

Purification of the peptide H_3P^{EtEt} was performed in two different ways. The first procedure was done on a Knauer low-pressure HPLC system (Knauer GmbH, Berlin, Germany). A Kinetex RPC18 endcapped (5 µM, 100 Å, 250 x 21.2 mm, Phenomenex®) HPLC-column was used with a Security GuardTM PREP Cartridge Holder Kit (21.20 mm, ID, Phenomenex®, USA) as a pre-column. Water and MeCN, both containing 0.1 % (v/v) TFA were applied as eluents. HPLC runs were performed with a flow rate of 10 or 20.0 mL/min. An isocratic gradient of 5 % MeCN + 0.1 % TFA of 5 min with a flow rate of 10.0 mL/min and then a linear gradient of 5–70 % MeCN + 0.1 % TFA from 5-15 min with a flow rate of 20.0 mL/min were applied. Another possible way of purification of H_3P^{EtEt} is a preparative HPLC performed using a Kinetix Evo 250 x 21.2 mm (reversed phase C18) including a pre-column. The run was isocratic. 30 % MeCN in water containing 0.5 M AcOH (eff. conc.) was used as eluent. HPLC runs were performed with a flow rate of 20.0 mL/min. The EZChrom Elite-Software was used for data analysis.[106] The purity of the collected fractions was determined by analytical HPLC.

Analytical HPLC of the fractions for H_3P^{EtEt} was carried out on a Chromaster 600 bar DAD-System with the EZChrom Elite-Software.[106] The system works with a low-pressure gradient containing a HPLC-

pump (5160) with a 6-channel solvent degaser, an organizer, an autosampler (5260) with a 20 µL sample loop, a column oven (5310) and a diode array flow detector (5430) with a high pressure semi-micro flow cell. A Purospher®STAR RP−C18 end-capped (2 µM, 50 x 2.1 mm, Merk, Deutschland) UHPLC column was used. Water and MeCN, both containing 0.1 % (v/v) TFA, were applied as eluents. A flow rate of 0.6 mL/min was used and the column was heated to 24 °C. A linear gradient of 5–70 % MeCN + 0.1 % TFA within 10 min or 5–100 % MeCN + 0.1 % TFA within 18 min was applied for all NFGAIL variants. Fractions with sufficient purity were combined. The solvent was removed by rotary evaporation. Lyophilization of the remaining aqueous solution yielded the pure product.

Preparative HPLC of H_3P^{MePh} was performed on a Varian ProStar 320 system using a Dr Maisch Reprosil C18 100–7 (40 × 250 mm) column (flow rate: 40.0 ml/min). HPLC solvents were H_2O + 0.1 % TFA and MeCN (HPLC grade). Analytical UPLC of H_3P^{MePh} was performed on a VWR Hitachi Chrommaster Ultra, using an Acquity UPLC BEH C18 1.7 µm (2.1 × 50 mm) column. UPLC solvents were H_2O + 0.1 % TFA and MeCN (UPLC grade).

Analytical HPLC analyses of the ^{99m}Tc complexes with KH_3L^{2EtEt}, KH_3L^{2MePh}, $H_3L^{3EtEtBoc}$, H_3P^{EtEt} and H_3P^{MePh} were performed on a Merck Hitachi LaChrom L 7100 pump coupled to a Merck Hitachi LaChrom L7200 tunable UV detector (Hitachi, Tokyo, Japan) and a radio detector Berthold LB508 (Berthold Technologies, Bad Wildbad, Germany) equipped with a bismuth germanium oxid (BGO) cell. Separations were achieved on a Macherey–Nagel C18 reversed-phase column (nucleosil 10 ml, 250/3 mm) using a gradient methanol (solvent A) and H_2O + 0.1% TFA (solvent B). Applied HPLC gradient: 0–3 min: 0% A, 100% B; 3–3.1 min: 0–25 % A, 100–75 % B; 3.1–9 min: 25 % A, 75 % B; 9–9.1 min: 25–34 % A, 75–66 % B; 9.1–18 min: 34–100 % A, 66–0 % B; 18–25 min: 100 % A, 0 % B; 25–25.1 min: 100–0 % A, 0–100 % B; 25.1–30 min: 0 % A, 100 % B. The flow rate was 0.5 mL/min.

Analytical measurements for the complex formation of the bisphosphonate-substituted ligand with ^{99m}Tc were performed using a Dionex P680 HPLC system with a UV-Vis variable wavelength detector (Idstein, Germany) and a NaI solid scintillation radio detector. A PerfectBond™ ODS-H column (150 x 4.0 mm, 5 µm, Art. No 150.4,0.1195.N) from MZ-Analysetechnik GmbH was used. Different gradients were performed with a flow rate of 2.6 mL/min starting with 100 % H_2O + 0.1 % TFA to 100 % MeCN in 6.5 min or 100 % MeCN to 100 % H_2O + 0.1 % TFA in 6.5 min. The pressure on the column was 240 bar. Analytical evaluations were also done by TLC in H_2O. The activity was recorded by a Gina Star TLC (bismuth germanate γ-szintillator) detector and analysed by the Raytest miniGita software.[107]

5.2 *In Vivo* Experiments

In vivo experiments were carried out with two male mice with a subcutaneously growing human prostate-specific membrane-antigen (PSMA)-positive prostate cancer tumor xenograft (swiss nude mice, approximately 4 months old). The mice were kept at the animal husbandry at the Berlin Radionuclide Imaging Center (BERIC), a core facility of the Charité for experimental small animal imaging. The animals were fed with water and food *ad libitum* and kept under standard conditions (20 ± 2 °C, 50 ± 10 % relative humidity, 12 h day-night-rhythm). All experiments were performed in compliance with the German animal protection law (Tierschutzgesetz). The *in vivo* PET/CT scans were performed on a dedicated small animal PET/CT scanner (nanoScan PET/CT, Mediso). The scanner provides a spatial resolution of approximately 0.8 mm for the radionuclide ^{68}Ga. *In vivo* SPECT/CT imaging was performed with a small animal SPECT/CT system (nanoSPECT/CTplus, Bioscan/Mediso) with a spatial resolution of approximately 0.5 mm. The mice were anesthetized by inhalation anesthesia (1.4 % isoflurane) before the injection of the tracer and during the measurement in the scanner. The breathing of the mice was controlled, and the amount of isoflurane was adjusted accordingly.

5.3 Starting Materials

All chemicals were reagent grade and used without further purification unless otherwise stated. Solvents were dried over molecular sieve (3 Å, Typ 564, Roth) when it is stated. Solvents were degassed three times following the freeze-pump-thaw method. All reactions with air- and moisture-sensitive compounds were performed under an argon atmosphere using standard Schlenk techniques.

Starting materials were purchased commercially or synthesised following literature procedures: $[Tc(NO)Cl_2(PPh_3)_2(MeCN)]$,[31] $(NBu_4)[Tc(NO)Cl_4(MeOH)]$,[60] $[TcCl_3(PPh_3)_2(MeCN)]$,[108] $[TcCl_4(PPh_3)_2]$,[109] $(NBu_4)[TcOCl_4]$,[110] $[TcNCl_2(PPh_3)_2]$,[111] $(NBu_4)[TcNCl_4]$,[66] $[Re(CO)_5Br]$,[112] $(NBu_4)[ReOCl_4]$,[110] $[ReNCl_2(PPh_3)_2]$,[113] $(NBu_4)[ReNCl_4]$,[114] $[ReOCl_3(PPh_3)_2]$,[115] $[Re(NPh)Cl_3(PPh_3)_2]$,[116] $[Re(NPhF)Cl_3(PPh_3)_2]$,[117] $(NBu_4)[ReO_4]$,[114] diethylcarbamothioylbenzimidoyl chloride,[118] methyl-phenylcarbamothioylbenzimidoyl chloride,[118] diphenylcarbamothioylbenzimidoyl chloride.[118]

5.4 Radiation Precautions

^{99}Tc is a long-lived β^- emitter (E_{max} = 0.292 MeV). Normal glassware provides adequate protection against the weak β^- radiation when milligram amounts are used. Secondary X-rays (bremsstrahlung) play a significant role only when larger amounts of ^{99}Tc are handled. ^{99m}Tc is a γ emitter (E = 140 keV)

with a half-life of 6 h. Na[$^{99m}TcO_4$] was eluted in a 0.9 % saline solution from a $^{99}Mo/^{99m}Tc$ generator. All experiments were done in a laboratory, which is approved for handling radioactive materials.

5.5 Metal Complexes with the "Kläui Ligand" NaL^{OMe}

[$Tc^{I}(NO)Cl(PPh_3)(L^{OMe})$]

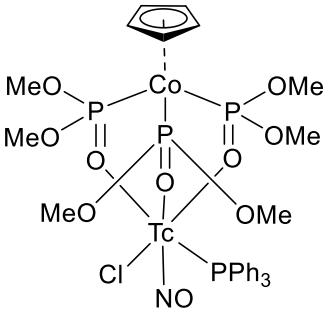

$[Tc(NO)Cl_2(PPh_3)_2(MeCN)]$ (71 mg, 0.1 mmol) and NaL^{OMe} (47 mg, 0.1 mmol) were suspended in 5 mL of toluene and heated on reflux for 1 h. During this time, the suspension changed its colour from green/yellow to red. After cooling to room temperature, the red precipitate was filtered off and recrystallized from CH_2Cl_2/Et_2O. Yield: 40 mg (47 %).

Anal. Calcd for $C_{29}H_{38}ClCoNO_{10}P_4Tc$: Tc, 11.5 %. Found: Tc, 11.1 %.

IR: 3055 (w), 2989 (w), 2943 (w), 2839 (w), ν(NO) 1692 (s), 1479 (w), 1433 (w), 1179 (w), 1117 (s), 1034 (s), 999 (s), 839 (w), 779 (m), 731 (m), 696 (w), 596 (m), 522 (w) cm^{-1}.

$^1H\{^{31}P\}$ NMR ($CDCl_3$): δ = 2.90 (s, 3H, CH_3), 3.04 (s, 3H, CH_3), 3.74 (s, 3H, CH_3), 3.77 (s, 3H, CH_3), 3.82 (s, 3H, CH_3), 3.90 (s, 3H, CH_3), 4.98 (s, 5H, Cp) 7.36 – 7.24 (m, 9H, PPh_3), 7.68 – 7.60 (m, 6H, PPh_3) ppm.

$^{13}C\{^1H\}$ NMR ($CDCl_3$): δ = 51.51 (CH_3), 52.51 (CH_3), 53.88 (CH_3), 89.97 (C_{Cp}), 127.66 (C_{Ph}), 129.54 (C_{Ph}), 134.47 (C_{Ph}) ppm.

$^{31}P\{^1H\}$ NMR ($CDCl_3$): δ = 111.2 (m_{broad}), 121.1 (m_{broad}) ppm.

^{99}Tc NMR ($CDCl_3$): δ = 1475 ppm, $\Delta\nu_{1/2}$ = 2716 Hz.

[$Tc^{II}(NO)Cl_2(L^{OMe})$]

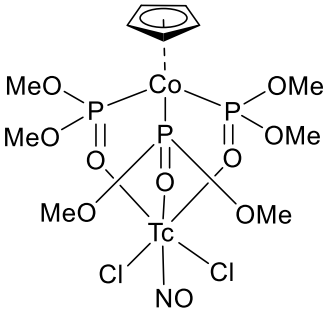

$(NBu_4)[Tc(NO)Cl_4(MeOH)]$ (52 mg, 0.1 mmol) was dissolved in 1 mL MeOH and NaL^{OMe} (47 mg, 0.1 mmol) in 1 mL MeOH was added. The mixture was heated on reflux for 1 h. After cooling to room temperature and concentration to about 0.5 mL, column chromatography on silica (CH_2Cl_2 → CH_2Cl_2/EtOAc → CH_2Cl_2/acetone → CH_2Cl_2/MeOH) was performed, from which a deep red fraction could be isolated. Crystals of the product were obtained by slow evaporation of a CH_2Cl_2/MeOH mixture in a refrigerator. Yield: 9 mg (12 %).

Anal. Calcd for $C_{11}H_{23}Cl_2CoNO_{10}P_3Tc$: Tc, 13.4 %. Found: Tc, 14.7 %.

IR: 2949 (w), 2922 (w), 2848 (w), 2789 (w), ν(NO) 1743 (s), 1458 (w), 1427 (w), 1174 (w), 1103 (s), 1049 (s), 1029 (s), 991 (s), 837 (w), 788 (m), 740 (m), 613 (m), 586 (w), 555 (w) cm^{-1}.

EPR (77 K, CH_2Cl_2): $A_{\perp}^{Tc}$ = 120 · 10^{-4} cm^{-1}, $A_{\parallel}^{Tc}$ = 280 · 10^{-4} cm^{-1}, $g_{\perp}$ = 2.010, $g_{\parallel}$ = 1.930.

EPR (RT, CH_2Cl_2): a_0^{Tc} = 168 · 10^{-4} cm^{-1}, g_0 = 2.002.

[$Tc^{III}Cl_2(PPh_3)(L^{OMe})$]

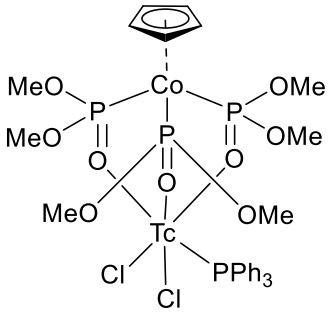

[$TcCl_3(PPh_3)_2$(MeCN)] (77 mg, 0.1 mmol) was suspended in 2 mL of CH_2Cl_2 and NaL^{OMe} (47 mg, 0.1 mmol) in CH_2Cl_2 (2 mL) was added. The mixture was heated on reflux for 2 h. Addition of MeOH (2 mL) and slow evaporation at 4°C gave brown single crystals suitable for X-Ray analysis. Yield: 38 mg (43 %).

Anal. Calcd for $C_{29}H_{38}Cl_2CoO_9P_4Tc$: Tc, 10.2 %. Found: Tc, 11.1 %.

IR: 3057 (w), 2987 (w), 2945 (m), 2839 (w), 1849 (w), 1481 (w), 1462 (w), 1435 (m), 1178 (m), 1103 (s), 1031 (s), 999 (s), 839 (m), 785 (s), 734 (s), 696 (s), 628 (w), 597 (s), 528 (m), 511 (w), 491 (w) cm^{-1}.

[$Tc^{IV}Cl_3(L^{OMe})$]

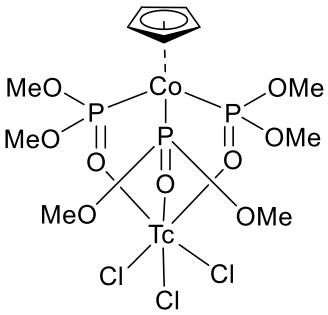

[$TcCl_4(PPh_3)_2$] (76 mg, 0.1 mmol) was suspended in 2 mL of CH_2Cl_2 and NaL^{OMe} (47 mg, 0.1 mmol) in 2 mL CH_2Cl_2 was added. The mixture was heated on reflux for 45 min and the solvent was removed in vacuum. The resulting brown oil was treated subsequently with hexane, water and MeOH, which gave finally a brown-beige solid. This solid was recrystallised from a CH_2Cl_2/MeOH mixture giving yellow single crystals suitable for X-ray analysis. Yield: 18 mg (25%).

Anal. Calcd for $C_{11}H_{23}Cl_3CoO_9P_3Tc$: Tc 13.3 %. Found: Tc 14.4 %.

IR: 3091 (w), 2951 (w), 2922 (w), 2846 (w), 1458 (w), 1421 (w), 1261 (w), 1180 (w), 1060 (s), 1029 (s), 833 (w), 850 (w), 800 (m), 750 (m), 613 (m), 482 (w) cm^{-1}.

[$Tc^{V}OCl_2(L^{OMe})$]

$(NBu_4)[TcOCl_4]$ (49 mg, 0.1 mmol) was dissolved in 1 mL of MeOH and NaL^{OMe} (47 mg, 0.1 mmol) in 1 mL MeOH was added. The mixture was heated under reflux for 2 h. Slow evaporation in a refrigerator gave green-yellow crystals suitable for X-ray analysis. Yield: 41 mg (64 %).

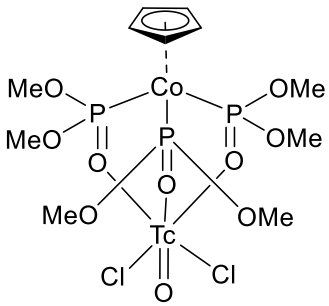

Anal. Calcd for $C_{11}H_{23}CoO_{12}P_3Tc$: Tc, 15.9 %. Found: Tc, 15.1 %.

IR: 3113 (w), 3091 (w), 2995 (w), 2947 (m), 2897 (w), 2841 (w), 1460 (w), 1425 (w), 1178 (m), 1074 (s), 1039 (s), 1028 (s), 997 (s), ν(TcO) 959 (s), 878 (w), 845 (w), 795 (m), 745 (m), 637 (m), 594 (m), 484 (w), 468 (w) cm^{-1}.

$^{1}H\{^{31}P\}$ NMR ($CDCl_3$): δ = 3.55 (s, 6H, CH_3), 3.87 (s, 6H, CH_3), 3.91 (s, 6H, CH_3), 5.13 (s, 5H, Cp) ppm.

$^{13}C\{^{1}H\}$ NMR ($CDCl_3$): δ = 53.60 (CH_3), 53.96 (CH_3), 54.06 (CH_3), 89.62 (C_{Cp}) ppm.

$^{31}P\{^{1}H\}$ NMR ($CDCl_3$): δ = 124.9 (m) ppm.

[$Tc^{V}O$(glycolate)(L^{OMe})]

$[Tc^{VII}O_3(L^{OMe})]$ (76 mg, 0.13 mmol) was dissolved in $CHCl_3$ (10 mL) and ethene was bubbled through the solution for 1 h. The clear yellow solution turned green after 30 min. The solvent was evaporated and the residue was washed with a small amount of cold MeCN. The remaining green solid was redissolved in CH_2Cl_2. Crystals suitable for X-ray analysis were obtained from a CH_2Cl_2/Et_2O solution by slow evaporation of the solvents in the refrigerator. Yield 33 % (25 mg).

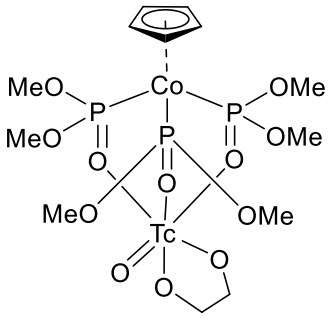

Anal. Calcd for $C_{11}H_{23}CoO_{12}P_3Tc$: Tc, 15.8 %. Found: Tc, 14.0 %.

$^{1}H\{^{31}P\}$ NMR ($CDCl_3$): δ = 3.28 – 4.10 (m, 18H, CH_3), 4.75 – 4.87 (m, 2H, OCH_2CH_2O), 5.04 (s, 5H, Cp), 5.58 – 5.69 (m, 2H, OCH_2CH_2O) ppm.

$^{13}C\{^{1}H\}$ NMR ($CDCl_3$): δ = 52.78 (CH_3), 87.31 (OCH_2CH_2O), 89.20 (C_{Cp}) ppm.

$^{31}P\{^{1}H\}$ NMR ($CDCl_3$): δ = 127.9 (m), 116.6 (m), 113.6 (m) ppm.

IR: 3446 (m), 3076 (w), 2985 (w), 2945 (m), 2841 (m), 1460 (m), 1423 (m), 1261 (w), 1176 (m), 1143 (s), 1101 (S), 1037 (s), 1004 (s), *ν*(TcO) 952 (s), 898 (m), 869 (w), 824 (w), 785 (s), 734 (s), 653 (s), 623 (s), 597 (s), 538 (w), 476 (w), 418 (w) cm^{-1}.

[$Tc^{V}NCl(PPh_3)(L^{OMe})$]

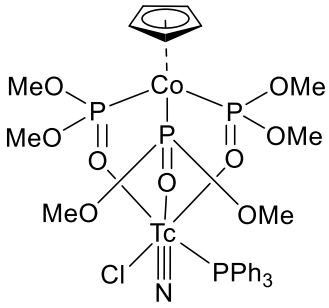

$[TcNCl_2(PPh_3)_2]$ (69 mg, 0.1 mmol) was suspended in 1 mL of CH_2Cl_2 and NaL^{OMe} (47 mg, 0.1 mmol) was added in 1 mL of MeOH/CH_2Cl_2. The mixture was heated under reflux for 2 h. The CH_2Cl_2 was distilled off and the resulting red precipitate was filtered off and washed with MeOH. Single crystals suitable for X-ray diffraction were obtained from slow evaporation of a CH_2Cl_2/MeOH solution of the product in a refrigerator. Yield: 45 mg (53 %).

Anal. Calcd for $C_{29}H_{38}ClCoNO_9P_4Tc$: Tc, 11.5 %. Found: Tc, 11.2 %.

IR: 3055 (w), 2988 (w), 2943 (m), 2837 (w), 1481 (w), 1458 (w), 1433 (w), 1176 (w), 1132 (s), 1090 (s), 1057 (s), 1034 (s), ν(TcN) 997 (s), 837 (w), 779 (m), 727 (m), 694 (m), 621 (w), 584 (m), 524 (w), 494 (w) cm^{-1}.

$^{1}H\{^{31}P\}$ NMR ($CDCl_3$): δ = 3.56 – 3.98 (m, 18H, CH_3), 4.98 (s, 5H, Cp), 7.39 – 7.27 (m, 9H, PPh_3), 7.83 – 7.74 (m, 6H, PPh_3) ppm.

$^{13}C\{^{1}H\}$ NMR ($CDCl_3$): δ = 52.83 (CH_3), 88.92 (C_{Cp}), 127.79 (d, J = 10 Hz, C_{Ph}), 129.93 (C_{Ph}), 133.15 (d, J = 46 Hz, C_{Ph}), 134.79 (d, J = 10 Hz, C_{Ph}) ppm.

$^{31}P\{^{1}H\}$ NMR ($CDCl_3$): δ = 111.9 (broad), 116.9 (broad), 124.1 (broad) ppm.

[$Tc^{VI}NCl_2(L^{OMe})$]

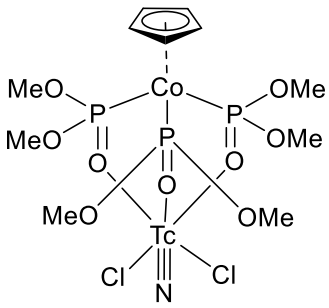

$(NBu_4)[TcNCl_4]$ (49 mg, 0.1 mmol) was dissolved in 1 mL of CH_2Cl_2 and NaL^{OMe} (47 mg, 0.1 mmol) in 1 mL of CH_2Cl_2 was added. The mixture was heated under reflux for 1 h and the solvent was removed in vacuum. The precipitate was extracted with CH_2Cl_2 and diethyl ether was added. Crystals suitable for X-ray analysis were obtained by slow evaporation of this CH_2Cl_2/Et_2O solution in a refrigerator. Yield: 19 mg (31 %).

Anal. Calcd for $C_{11}H_{23}Cl_2CoNO_9P_3Tc$: Tc, 15.6 %. Found: Tc, 15.3 %.

IR: 2949 (w), 2848 (w), 1458 (w), 1429 (w), 1174 (w), 1125 (s), ν(TcN) 1033 (s), 837 (w), 791 (m), 737 (m), 638 (w), 598 (m) cm^{-1}.

EPR: (77 K, CH_2Cl_2) $A_{\perp}^{Tc}$ = 152 · 10^{-4} cm^{-1}, $A_{\parallel}^{Tc}$ = 319 · 10^{-4} cm^{-1}, $g_{\perp}$ 1.981, $g_{\parallel}$ = 1.952.

EPR (RT, CH_2Cl_2): a_0^{Tc} = 199 · 10^{-4} cm^{-1}, $g_0 = 1.991$.

[$Tc^{VII}O_3(L^{OMe})$]

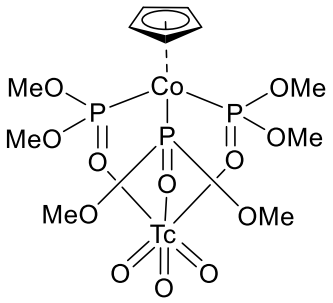

$(NH_4)[TcO_4]$ (36 mg, 0.2 mmol) was dissolved in 1 mL of water and NaL^{OMe} (97 mg, 0.2 mmol) in 1 mL H_2O was added. One drop of H_2SO_4 (conc.) was added under vigorous stirring. A yellow solid precipitated immediately. The mixture was stirred for 5 min at room temperature. The precipitate was filtered off, washed with water and dried under vacuum. Extraction of the aqueous phase with CH_2Cl_2 and evaporation of the dried organic phases gave more product. For crystallization, the solid was dissolved in 2 mL of a CH_2Cl_2/MeOH mixture (1:1, v:v). Yield: 112 mg (97 %).

Anal. Calcd for $C_{11}H_{23}CoO_{12}P_3Tc$: Tc, 16.6 %. Found: Tc, 16.1 %.

IR: 2951 (w), 2845 (w), 1458 (w), 1429 (w), 1177 (w), 1113 (s), 1036 (s), 1009 (s), ν(Tc=O) 897 (s), 843 (w), 789 (m), 737 (m), 629 (w), 590 (m) cm^{-1}.

$^1H\{^{31}P\}$ NMR ($CDCl_3$): δ = 3.73 (s, 18H, CH_3), 5.09 (s, 5H, Cp) ppm.

$^{13}C\{^1H\}$ NMR ($CDCl_3$): δ = 53.02 (CH_3), 88.96 (C_{Cp}) ppm.

$^{31}P\{^1H\}$ NMR ($CDCl_3$): δ = 120.4 ppm.

^{99}Tc NMR ($CDCl_3$): δ = 343 ppm, $\Delta\nu_{1/2}$ = 600 Hz.

[$Re^{I}(CO)_3(L^{OMe})$]

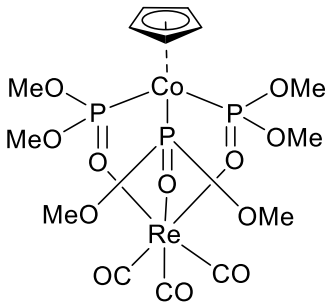

$[Re(CO)_5Br]$ (0.1 mmol, 41 mg) and NaL^{OMe} (0.1 mmol, 47 mg) were suspended in 3 mL of toluene and heated on reflux for 4 h. The reaction mixture was filtered hot to remove NaBr. Yellow crystals deposited directly from the reaction mixture at room temperature overnight. The crystals were washed with H_2O and toluene and dried under vacuum. Yield 89 % (64 mg).

$^1H\{^{31}P\}$ NMR ($CDCl_3$): δ = 3.71 (s, 18H, CH_3), 5.04 (s, 5H, H_{Ar}) ppm.

$^{13}C\{^1H\}$ NMR ($CDCl_3$): δ = 52.45 (d, J = 3.25 Hz, CH_3), 52.51 (d, J = 3.25 Hz, CH_3), 89.03 (q, J = 1.50 Hz, C_{Cp}) ppm.

$^{31}P\{^1H\}$ NMR ($CDCl_3$): δ = 113.0 (s) ppm.

ESI+ MS (m/z): 744.9269 (calc. 744.9292) $[M+Na]^+$.

IR: 2949 (w), 2843 (w), ν(CO) 2010 (m), ν(CO) 1876 (s), ν(CO) 1859 (s), 1458 (w), 1426 (w), 1261 (w), 1176 (w), 1108 (m), 1075 (m), 1061 (m), 1031 (s), 995 (s), 834 (m), 778 (s), 732 (s), 669 (w), 655 (w), 631 (w), 590 (s), 529 (w) cm^{-1}.

Anal. Calcd for $C_{14}H_{23}CoO_{12}P_3Re$: C, 23.31; H, 3.21 %. Found: C, 23.15; H, 3.18 %.

[$Re^{V}OCl_2(L^{OMe})$]

Method A: $(NBu_4)[ReOCl_4]$ (0.1 mmol, 58 mg) and NaL^{OMe} (0.1 mmol, 47 mg) were heated on reflux in 5 mL MeOH for 1 h. The reaction mixture was allowed to cool to room temperature and filtered. Recrystallisation was done from a CH_2Cl_2/MeOH mixture in the refrigerator. After a few days, bright yellow crystals were obtained. Yield 42 % (30 mg).

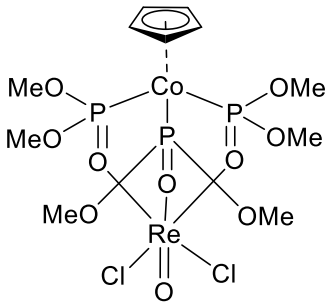

Method B: $[ReOCl_3(PPh_3)_2]$ (0.1 mmol, 58 mg) and NaL^{OMe} (0.1 mmol, 47 mg) were heated on reflux in 5 mL toluene for 6 h. The solvent was evaporated and the residue was dissolved in CH_2Cl_2. After filtration, the product was crystallised from a CH_2Cl_2/MeOH mixture in the refrigerator. After a few days, bright yellow crystals were obtained. Yield 47 % (34 mg).

$^{1}H\{^{31}P\}$ NMR ($CDCl_3$): δ = 3.70 (s, 6H, CH_3), 3.77 (s, 6H, CH_3), 3.83 (s, 6H, CH_3), 5.16 (s, 5H, H_{Ar}) ppm.

$^{13}C\{^{1}H\}$ NMR ($CDCl_3$): δ = 53.89 (t, J = 4.8 Hz, CH_3), 54.49 (d, J = 9.7 Hz, CH_3), 54.76 (t, J = 4.8 Hz, CH_3), 89.62 (q, J = 1.45 Hz, C_{Cp}) ppm.

$^{31}P\{^{1}H\}$ NMR ($CDCl_3$): δ = 123.7 – 128.4 (m) ppm.

ESI+ MS (m/z): 746.866 (calc. 746.8771) $[M+Na]^+$.

IR: 2950 (w), 1455 (w), 1423 (w), 1176 (w), 1018 (s), 991 (s), ν(Re=O) 957 (s), 879 (m), 846 (m), 794 (s), 741 (s), 639 (m), 592 (s), 526 (m) cm^{-1}.

Anal. Calcd for $C_{11}H_{23}Cl_2CoO_{10}P_3Re$: C, 18.24; H, 3.00 %. Found: C, 18.24; H, 3.20 %.

[$Re^{V}NCl(PPh_3)(L^{OMe})$]

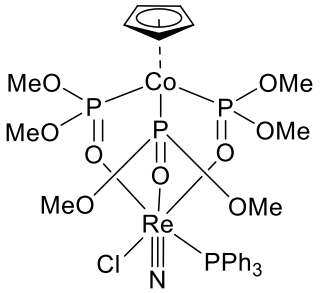

$[ReNCl_2(PPh_3)_2]$ (0.1 mmol, 80 mg) and NaL^{OMe} (0.1 mmol, 47 mg) were heated on reflux in 10 mL CH_2Cl_2 for 2 h. Brown-orange crystals were obtained from CH_2Cl_2/MeOH after a few days by slow evaporation of the solvent in the refrigerator. Yield: 10 % (10 mg).

$^{1}H\{^{31}P\}$ NMR ($CDCl_3$): δ = 2.61 (s, 3H, CH_3), 3.31 (s, 3H, CH_3), 3.61 (s, 3H, CH_3), 3.91 (s, 6H, CH_3), 3.95 (s, 3H, CH_3), 5.00 (s, 5H, H_{Ar}), 7.36 – 7.27 (m, 9H, PPh_3), 7.84 – 7.77 (m, 5H, PPh_3) ppm.

$^{31}P\{^{1}H\}$ NMR ($CDCl_3$): δ = 11.6 (s), 114.9 – 112.6 (m), 122.3 – 119.4 (m) ppm.

$^{13}C\{^{1}H\}$ NMR ($CDCl_3$): δ = 50.94 (s, CH_3), 52.28 (s, CH_3), 52.37 (s, CH_3), 53.19 (s, CH_3), 53.27 (s, CH_3), 53.79 (s, CH_3), 88.99 (s, C_{Cp}), 127.74 (d, J = 9.6 Hz, C_{Ph}), 129.79 (s, C_{Ph}), 132.17 (d, J = 9.6 Hz, C_{Ph}), 134.86 (d, J = 9.6 Hz, C_{Ph}) ppm.

IR: 2945 (w), 2839 (w), 1482 (w), 1435 (w), 1175 (w), 1122 (w), 1082 (s), 1059 (s), 1025 (s), ν(Re≡N) 989 (s), 833 (m), 780 (m), 761 (w), 751 (w), 725 (s), 692 (s), 623 (m), 583 (s), 533 (s) cm^{-1}.

ESI+ MS (m/z): 971.9969 (calc. 971.9967) $[M+Na]^+$.

Anal. Calcd for $C_{29}H_{38}ClCoNO_9P_4Re$: C, 36.70; H, 4.04; N, 1.48 %. Found: C, 36.65; H, 4.06; N, 1.47 %.

[$Re^{VI}NCl_2(L^{OMe})$]

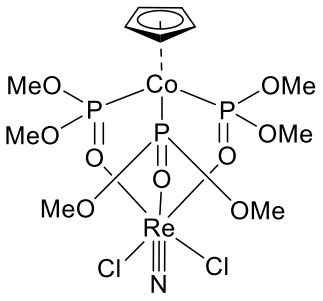

$(NBu_4)[ReNCl_4]$ (0.2 mmol, 116 mg) and NaL^{OMe} (0.2 mmol, 94 mg) were dissolved in 15 mL MeCN and heated on reflux for 30 min. The colour turned immediately from yellow to dark-red. The reaction was allowed to cool to room temperature. A colourless solid was filtered off. The product was separated by column chromatography (alumina, MeCN) as the first, bright yellow fraction. The product was crystallised from a MeCN/Et_2O mixture by slow evaporation in the refrigerator. Yield 14 % (20 mg).

IR: 2951 (w), 2844 (w), 1728 (w), 1456 (w), 1426 (w), 1172 (w), 1112 (m), 1057 (m), ν(Re≡N) 986 (s), 913 (m), 835 (w), 790 (s), 771 (m), 732 (s), 642 (m), 591 (s) cm^{-1}.

EPR (77 K, $CDCl_3$): $A_{\perp}^{Re}$ = 437· 10^{-4} cm^{-1}, $A_{\parallel}^{Re}$ = 859 · 10^{-4} cm^{-1}, $g_{\perp}$ = 1.911, $g_{\parallel}$ = 1.802.

EPR (RT, $CDCl_3$): a_0^{Re} = 650 · 10^{-4} cm^{-1}, g_0 = 1.9300.

ESI+ MS (m/z): 744.8783 (calc. 744.8744) $[M+Na]^+$.

Anal. Calcd for $C_{11}H_{23}Cl_2CoNO_9P_3Re$: C, 18.29; H, 3.21; N, 1.94 %. Found: C, 19.17; H, 3.34; N, 1.73 %.

$[Re^{VII}O_3(L^{OMe})]$

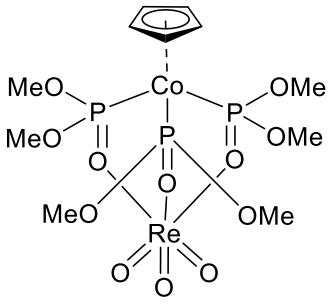

$(NBu_4)[ReO_4]$ (0.1 mmol, 49 mg) and NaL^{OMe} (0.1 mmol, 47 mg) were dissolved in 5 mL MeOH and 1 drop of conc. H_2SO_4 was added. The mixture was heated on reflux for 1 h. The product precipitated from the reaction mixture. The precipitate was filtered off and washed with MeOH and water. After drying under vacuum, a pale yellow solid (yield 70 %, 48 mg) was obtained.

$^1H\{^{31}P\}$ NMR ($CDCl_3$): δ = 3.74 (s, 18H, CH_3), 5.11 (s, 5H, H_{Ar}) ppm.

$^{13}C\{^1H\}$ NMR ($CDCl_3$): δ = 53.69 (d, J = 3.35 Hz, CH_3), 53.76 (d, J = 3.35, CH_3), 89.30 (q, J = 1.62 Hz, C_{Cp}) ppm.

$^{31}P\{^1H\}$ NMR ($CDCl_3$): δ = 122.7 (s) ppm.

IR: 3111 (w), 2952 (w), 2848 (w), 1459 (w), 1423 (w), 1261 (w), 1171 (w), 1097 (s), 1035 (s), 988 (s), ν(ReO) 941 (s), 908 (s), 852 (m), 789 (s), 733 (s), 630 (m), 583 (s) cm^{-1}.

ESI+ MS (m/z): 686.9333 (calc. 686.9365) $[M+H]^+$.

Anal. Calcd for $C_{11}H_{23}CoO_{12}P_3Re$: C, 19.28; H, 3.38 %. Found: C, 20.30; H, 3.62 %.

$[Ga(L^{OMe})_2]NO_3$

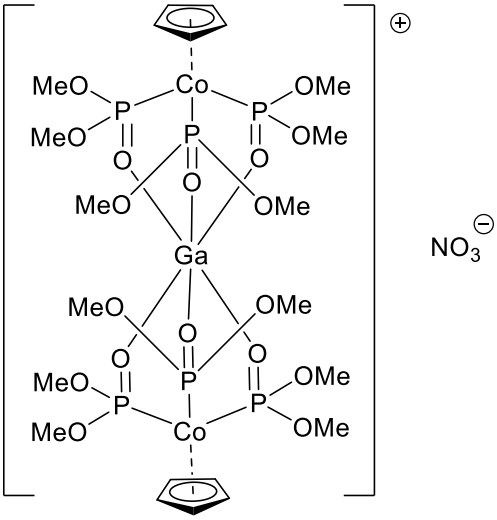

$Ga(NO_3)_3$ (25 mg, 0.1 mmol) dissolved in 5 mL THF/H_2O (1:1) was added dropwise to NaL^{OMe} (94.8 mg, 0.2 mmol) in 5 mL THF/H_2O (1:1). The reaction mixture was heated on reflux for 10 min. Single crystals were obtained directly from the reaction mixture by standing at room temperature. The yellow crystals were filtered off and dried. Yield 58 % (60 mg).

$^1H\{^{31}P\}$ NMR (d_4-MeOD): δ = 3.74 (s, 36H, CH_3), 5.22 (s, 10H, H_{Ar}) ppm.

^{13}C NMR (d_4-MeOD): δ = 53.18 (d, J = 3.28 Hz, CH_3), 53.24 (d, J = 3.28 Hz, CH_3), 90.57 (q, J = 1.51 Hz, C_{Cp}) ppm.

$^{31}P\{^{1}H\}$ NMR (d_4-MeOD): δ = 119.0 ppm.

IR: 2996; 2949 (w), 2843 (w), 1458 (w), 1425 (w), 1368 (w), 1342 (m), 1173 (w), 1121 (w), 1067 (s), 992 (s), 846 (m), 829 (m), 783 (s), 734 (s), 614 (s) cm^{-1}.

ESI+ MS (m/z): 970.8965 (calc. 970.9024) $[M]^+$.

Anal. Calcd for $C_{22}H_{46}Co_2GaNO_{21}P_6$: C, 25.55; H, 4.48; N, 1.35 %. Found: C, 25.22; H, 4.56; N, 1.27 %.

$[In(L^{OMe})_2]NO_3$

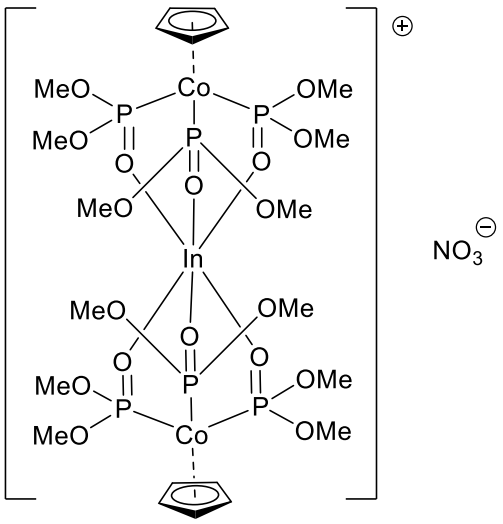

$In(NO_3)_3$ (30 mg, 0.1 mmol) dissolved in 3 mL MeOH was added dropwise to NaL^{OMe} (94.8 mg, 0.2 mmol) dissolved in 3 mL MeOH. The reaction mixture was stirred at room temperature for 30 min. The solvent was evaporated and the residue was redissolved in a MeCN/H_2O mixture (5:1). Single crystals were obtained after several days by slow evaporation of this solution at room temperature. The yellow crystals were filtered off and dried. Yield 85 % (90 mg).

$^{1}H\{^{31}P\}$ NMR ($CDCl_3$): *δ* = 3.66 (s, 36H, CH_3), 5.14 (s, 10H, H_{Ar}) ppm.

^{13}C NMR ($CDCl_3$): δ = 52.30 (d, *J* = 3.27 Hz, CH_3), 52.37 (d, *J* = 3.27 Hz, CH_3), 89.95 (q, *J* = 1.43 Hz, C_{Cp}) ppm.

$^{31}P\{^{1}H\}$ NMR ($CDCl_3$): δ = 117.7 ppm.

IR: 2958 (w), 2927 (w), 2873 (w), 2817 (w), 1621 (w), 1511 (s), 1469 (s), 1445 (s), 1381 (m), 1318 (w), 1098 (w), 1067 (m), 1024 (s), 958 (s), 885 (m), 800 (w), 738 (w), 683 (w), 560 (s) cm^{-1}.

ESI+ MS (m/z): 1016.8773 (calc. 1016.8807) $[M]^+$.

Anal. Calcd for $C_{22}H_{46}Co_2InNO_{21}P_6$: C, 24.49; H, 4.30; N, 1.30 %. Found: C, 24.13; H, 4.44; N, 1.25 %.

[Lu(L^{OMe})$_2$(NO$_3$)]

NaL^{OMe} (94 mg, 0.2 mmol) dissolved in warm THF (2 mL) was added dropwise to a solution of Lu(NO$_3$)$_3$ hydrate (36 mg, 0.1 mmol) in THF (1 mL). The mixture was stirred for 4 h at room temperature. A colourless precipitate (NaNO$_3$) was filtered off and the solution was evaporated slowly to obtain yellow crystals suitable for X-ray analysis. Yield 86 % (98 mg).

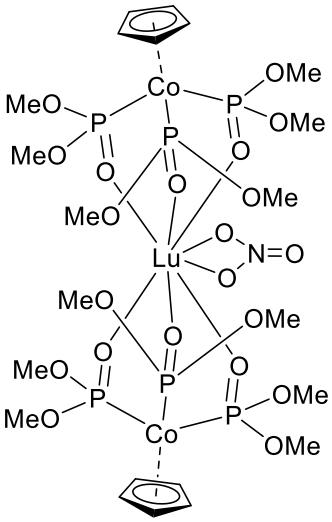

^{1}H{^{31}P} NMR (CDCl$_3$): δ = 3.62 (s, 36H, CH$_3$), 5.05 (s, 10H, H$_{Ar}$) ppm.

^{13}C NMR (CDCl$_3$): δ = 51.80 (d, *J* = 3.05 Hz, CH$_3$), 51.87 (d, *J* = 3.09 Hz, CH$_3$), 89.28 (q, *J* = 1.41 Hz, C$_{Cp}$) ppm.

^{31}P{^{1}H} NMR (CDCl$_3$): δ = 118.3 ppm.

IR: 2943 (w), 1456 (w), 1430 (w), *ν*(NO) 1316 (w), 1172 (w), 1124 (m), 1105 (m), 1094 (m), 1011 (s), 859 (w), 834 (m), 818 (w), 773 (s), 753 (s), 718 (s), 626 (m), 599 (s), 579 (s), 526 (w) cm^{-1}.

ESI+ MS (m/z): 1076.9456 (calc. 1076.9182) [Lu(L^{OMe})$_2$]$^+$.

Anal. Calcd for for $C_{22}H_{46}Co_2LuNO_{21}P_6$: C, 23.19; H, 4.07; N, 1.23 %. Found: C, 24.33; H, 4.28; N, 0.93 %.

5.6 Synthesis of an Ester-substituted "Kläui Ligand"

NaCp (2M in THF, 10 mmol, 5 mL) and dimethyl carbonate (50 mmol, 4.2 mL) were heated on reflux for 4 h in 5 mL of dry, degassed THF under an argon atmosphere. The THF was evaporated and the remaining beige solid was washed with dry and degassed Et$_2$O. The product was dried giving a slightly air sensitive, light beige solid. Yield 92 % (1.34 g). The crude product was used for the next reaction without purification.

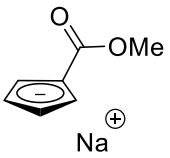

^{1}H NMR (d$_6$-DMSO): δ = 3.44 (s, 3H, CH$_3$), 5.48 (m, 2H, H$_{Ar}$), 6.06 (m, 2H, H$_{Ar}$) ppm. The proton NMR spectrum is in agreement with the literature.[119]

[Co$_2$(CO)$_8$] (0.51 mmol, 175 mg) was dissolved in dry, degassed THF (8 mL) under argon. Solid iodine (0.51 mmol, 129 mg) was slowly added. The colour of the red solution turned immediately green while CO was evolved. The reaction mixture was stirred at room temperature for 2 h. Sodium carbomethoxycyclopentadienide (1 mmol, 146 mg) was added as a solid and the colour of the reaction mixture turned red again. The

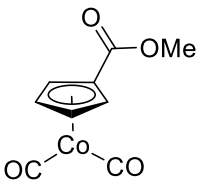

mixture was stirred at room temperature for additional 24 h. Half of the solvent was evaporated under reduced pressure and dry, degassed Et_2O was added. The reaction mixture was filtered over alumina in a reverse frit and washed with more Et_2O giving a red oil. The solvents were evaporated and an aliquot was taken for IR analysis. At this point, no yield was determined due to the air sensitivity of the oil. A yield of 40 % was assumed with respect to previous literature reports.[119] The product was taken for the next reaction.

IR: 2923 (w), 2851 (w), ν(C≡O) 2025 (s), ν(C≡O) 1961 (s), ν(C=O) 1718 (s), 1484 (m), 1434 (m), 1386 (m), 1273 (s), 1193 (m), 1141 (s), 1067 (w), 1018 (w), 974 (w), 901 (w), 820 (w), 787 (w), 772 (m), 615 (m), 558 (m), 537 (m) cm^{-1}. The IR spectrum is in agreement with the literature.[119]

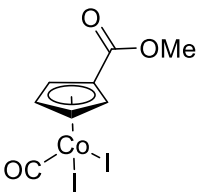

The red oil (0.4 mmol) from the previous reaction was dissolved in dry, degassed Et_2O. Iodine (0.43 mmol, 109 mg) dissolved in 5 mL Et_2O was added slowly. The colour of the reaction mixture turned immediately from red to dark red. The solution was stirred at room temperature for 2 h and filtered over cotton. The black precipitate on the cotton was dissolved in CH_2Cl_2 giving a dark purple, almost black solution. Evaporation of the solvent gave a black, microcrystalline solid. Yield over two steps: 24 % (110 mg).

^1H NMR ($CDCl_3$): δ = 3.89 (s_{br}, 3H, CH_3), 5.65 (s_{br}, 2H, CH_2), 6.14 (s_{br}, 2H, CH_2) ppm. The proton NMR spectrum is in agreement with the literature.[120]

^{13}C NMR ($CDCl_3$): δ = 53.65, 90.71, 92.78, 162.31 ppm. The quaternary carbon atom is not visible.

IR: 3104 (w), 3080 (w), 2957 (w), ν(C≡O) 2069 (s), ν(C=O) 1730(s), 1470 (s), 1422 (m), 1409 (m), 1367 (m), 1349 (w), 1278 (s), 1194 (s), 1142 (s), 1037 (m), 1026 (m), 960 (s), 888 (m), 851 (s), 787 (w), 767 (s), 575 (m), 541 (m) cm^{-1}.

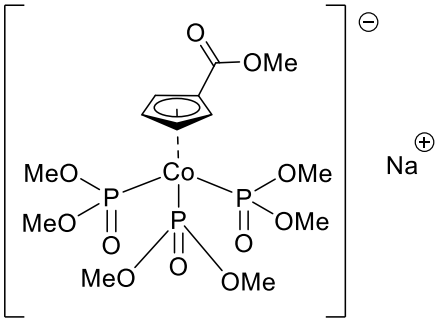

$P(OMe)_3$ (81 µL, 0.69 mmol) dissolved in 5 mL dry CH_2Cl_2 was slowly added to an ice-cold solution of $[Co(CO)I_2(CpCOOMe)]$ (0.24 mmol, 110 mg) in dry CH_2Cl_2. The reaction mixture was stirred for 2 h at 0°C and then for 30 min at room temperature. The colour of the solution turned brown-yellow. The solvent was evaporated and the residue was dissolved in 5 mL of dry acetone. Solid NaI (36 mg, 0.24 mmol) was added to the reaction mixture. The colour of the solution turned yellow-orange. The reaction mixture was stirred at room temperature for 1 h. The solvent was evaporated and the product was separated by column

chromatography (silica, CH_2Cl_2 → CH_2Cl_2/MeOH 3:1). It was obtained as a bright yellow fraction from the column. Yield: 4 % (10 mg).

^{1}H NMR ($CDCl_3$): δ = 3.58 (s, 18H, $POCH_3$), 3.76 (s, 3H, CH_3), 5.02 (s, 2H, H_{Ar}), 5.67 (s, 2H, H_{Ar}) ppm.

^{13}C NMR ($CDCl_3$): δ = 51.86 (CH_3), 51.86 (CH_3), 88.61 (C_{Ar}), 93.12 (C_{Ar}), 143.74 (CC=O), 165.49 (C=O) ppm.

^{31}P NMR ($CDCl_3$): δ = 103.6 ppm.

IR: 2944 (w), 2839 (w), ν(CO) 1731 (m), 1478 (m), 1432 (w), 1415 (w), 1373 (w), 1285 (m), 1176 (m), 1139 (s), 1127 (s), 1021 (s), 995 (s), 898 (m), 831 (m), 791 (m), 762 (s), 718 (s), 581 (s) cm^{-1}.

[$Tc^{VII}O_3(L^{OMeCOOMe})$]

The complex was synthesised by a similar procedure as described before for [$TcO_3(L^{OMe})$]. $NaL^{OMeCOOMe}$ (4 mg, 0.007 mmol) dissolved in 1 mL MeOH was added to (NBu_4)[TcO_4] (2.84 mg, 0.007 mmol) in 1 mL MeOH. One drop of conc. H_2SO_4 was added under vigorous stirring. The pale-yellow reaction mixture was stirred at room temperature for 5 min and analysed by NMR. The product was obtained in almost quantitative yield.

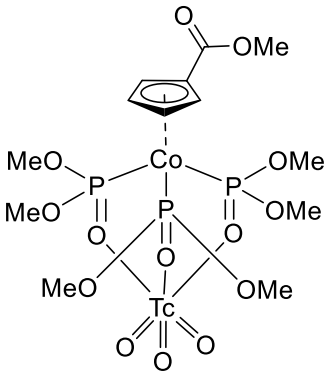

^{99}Tc NMR (MeOH): δ = 331 ppm, $\Delta\nu_{1/2}$ = 956 Hz.

^{31}P NMR (MeOH): δ = 111.7 – 121.5 (m) ppm.

5.7 Synthesis and Reactions of H_3L^{1EtEt}

The compound was synthesised by a slightly changed literature procedure.[87]

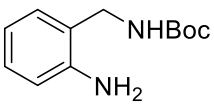

2-Aminobenzylamine (5.0 g, 40.9 mmol) was dissolved in 80 mL of dry CH_2Cl_2. DIPEA (7.84 mL, 45 mmol) and Boc_2O (9.8 g, 45 mmol) were added. The pale yellow solution was stirred at room temperature for 2 h. The solution was poured into a solution of 5 g citric acid in 50 mL of H_2O. The product was extracted with an EtOAc/brine solution. The organic phases were combined, dried over $MgSO_4$ and filtered. The solvent was evaporated. The obtained slightly yellow solid was dried. Yield 98 % (8.88 g).

^{1}H NMR ($CDCl_3$): δ = 1.43 (s, 9H, CH_3), 4.22 (d, J = 7.7 Hz, 2H, CH_2), 4.81 (s_{br}, 1H, NH), 6.64 – 6.69 (m, 2H, H_{Ar}), 6.99 – 7.02 (m, 1H, H_{Ar}), 7.06 – 7.11 (m, 1H, H_{Ar}) ppm.

The Boc-protected 2-aminobenzylamine (5 g, 22.4 mmol) was added to ethyl bromoacetate (7.8 mL, 70 mmol) in 100 mL of boiling toluene. Potassium iodide (500 mg) and DIPEA (15.6 mL, 89.6 mmol) were added. The reaction was heated on reflux for 2 days giving a dark brown-orange solution. The reaction mixture was cooled to room temperature and extracted with water. The combined organic phases were dried over $MgSO_4$, filtered and the volume was reduced to 2 mL. The product was separated by column chromatography (hexane/EtOAc 8:1 → 6:1 → 4:1 → 2:1) giving an orange-red solution. This solution was placed in a refrigerator for slow evaporation. After a few days, colourless crystals were obtained. Yield 57 % (5 g).

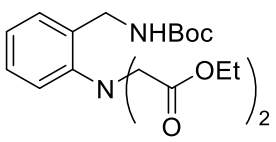

^{1}H NMR ($CDCl_3$): δ = 1.20 (t, *J* = 7.1 Hz, 6H, $CH_2C\underline{H}_3$), 1.42 (s, 9H, CCH_3), 3.96 (s, 4H, CH_2CO), 4.12 (q, *J* = 7.2 Hz, 4H, $C\underline{H}_2CH_3$), 4.36 (s, 2H, CH_2N), 7.04 – 7.10 (m, 1H, H_{Ar}), 7.17 – 7.22 (m, 1H, H_{Ar}), 7.26 – 7.33 (m, 2H, H_{Ar}) ppm.

The colourless crystals obtained from the previous step (986 mg, 2.5 mmol) were dissolved in CH_2Cl_2 (10 mL) and placed in an ice bath. TFA (5 mL) was added dropwise. The ice bath was removed and the reaction mixture was stirred at room temperature for 1 h. The progress of the Boc deprotection was checked by TLC (CH_2Cl_2/MeOH). The solvent was evaporated giving a slightly yellow oil in quantitative yield. This compound was directly used for the next reaction.

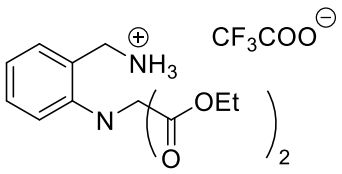

^{1}H NMR ($CDCl_3$): δ = 1.19 (t, *J* = 14.3 Hz, 6H, CH_3), 3.92 (s, 4H, CH_2CO), 4.10 (q, *J* = 7.1 Hz, 4H, $C\underline{H}_2CH_3$), 4.26 (q, *J* = 5.5 Hz, 2H, CH_2N), 7.15 – 7.22 (m, 1H, H_{Ar}), 7.26 – 7.30 (m, 1H, H_{Ar}), 7.36 – 7.40 (m, 2H, H_{Ar}), 7.9 (s_{br}, 3H, NH_3) ppm.

The product of the previous step (1.02 g mg, 2.5 mmol) was dissolved in dry THF. NEt_3 (0.3 mL) was added slowly under vigorous stirring to the slightly yellow solution. Solid diethylcarbamothioylbenzimidoyl chloride (610 mg, 0.96 mmol) was added. The mixture was stirred at room temperature for 16 h. The formed colourless precipitate ($HNEt_3Cl$) was filtered off. The solvents were evaporated and the resulting residue was dissolved in a minimum of EtOAc and loaded on silica. The product was purified by column chromatography (hexane/EtOAc 6:1). After drying the product for several days in vacuum, a pale-orange solid was obtained. Yield 85 % (1 g).

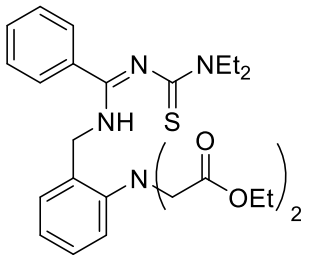

^{1}H NMR ($CDCl_3$): δ = 1.10 (t, *J* = 7.0 Hz, 6H, CH_3), 1.13 – 1.23 (m, 6H, CH_3), 3.54 – 3.66 (m, 2H, CH_2), 3.84 – 4.00 (m, 10H, CH_2), 4.65 (m, 2H, CH_2N), 7.05 – 7.11 (m, 1H, H_{Ar}), 7.17 – 7.23 (m, 1H, H_{Ar}), 7.25 – 7.42 (m, 7H, H_{Ar}) ppm.

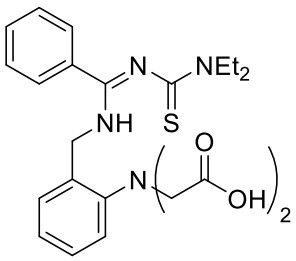

The ester coming from the previous step (379 mg, 0.74 mmol) was dissolved in MeOH (10 mL). Solid NaOH (88 mg, 2.22 mmol) was added. The colour of the reaction mixture turned slowly from yellow to colourless. The mixture was stirred for 16 h at room temperature. MeOH was evaporated and the residue was dissolved in a small amount of ice-cold brine and placed in an ice bath. Cold HCl (37 %) was added dropwise under stirring until a pH of around 1 was obtained and a colourless solid precipitated. The solvent was decanted and the remaining solid was washed with cold water. The product was dried giving a colourless product. Yield 68 % (182 mg).

^{1}H NMR (d_6-DMSO): δ = 1.02 (t, *J* = 7.0 Hz, 3H, CH_3), 1.08 (t, *J* = 7.0 Hz, 3H, CH_3), 3.47 (q, *J* = 7.0 Hz, 2H, CH_2CH_3), 3.73 (q, *J* = 6.9 Hz, 2H, CH_2CH_3), 3.95 (s, 4H, CH_2CO), 4.59 (d, *J* = 5.5 Hz, 2H, CH_2N), 7.03 – 7.09 (m, 1H, H_{Ar}), 7.15 – 7.23 (m, 1H, H_{Ar}), 7.23 – 7.28 (m, 1H, H_{Ar}), 7.29 – 7.34 (m, 1H, H_{Ar}), 7.46 – 7.35 (m, 5H, H_{Ar}), 8.27 (s, 1H, NH), 12.52 (s, 2H, COOH) ppm.

IR: 2930 (w), 1718 (m), 1594 (m), 1572 (m), 1535 (m), *ν*(CO) 1488 (s); 1453 (m), 1422 (s), 1374 (m), 1358 (m), 1310 (m), 1243 (s), 1138 (m), 1122 (m), 1095 (m), 1076 (m), 1036 (w), 968 (m), 833 (m), 776 (s), 695 (s), 599 (m), 566 (m), 528 (m) cm^{-1}.

[ReO(L^{1EtEt})]

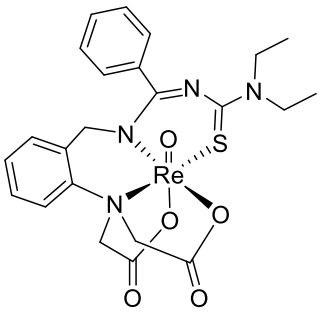

$NaReO_4$ (27 mg, 0.1 mmol) was dissolved in 3 mL of a hot acetone/EtOH (1:1) mixture and solid H_3L^{1EtEt} (46 mg, 0.1 mmol) was added. The mixture was heated to 60 °C with stirring until a clear, slightly yellow solution was obtained. $SnCl_2 \cdot 2\ H_2O$ (46 mg, 0.2 mmol) was added as a solid in one portion to this warm solution. The obtained brown mixture was stirred for 10 min and then filtered. The resulting purple solution was evaporated, the residue was redissolved in MeCN (2 mL) and filtered. $CHCl_3$ (1 mL) and CH_2Cl_2 (1 mL) were added and the resulting mixture was stored in the refrigerator for crystallization. Yield 23 % (15 mg). The product was identical with the previously published complex [ReO(L^{1EtEt})].[87]

^{1}H NMR ($CDCl_3$): δ = 1.28 – 1.20 (m, 6H, CH_3), 3.85 – 3.68 (m, 2H, CH_2CH_3), 4.00 (s, 2H, CH_2), 4.49 – 4.41 (m, 2H, CH_2CH_3), 4.83 – 4.75 (m, 2H, CH_2), 5.12 – 5.04 (m, 2H, CH_2), 5.68 – 5.59 (m, 2H, CH_2), 6.98 – 6.91 (m, 1H, H_{Ar}), 7.21 – 7.13 (m, 1H, H_{Ar}), 7.49 – 7.25 (m, 7H, H_{Ar}) ppm.

^{13}C NMR ($CDCl_3$): δ = 13.07 (CH_3), 47.04 ($\underline{C}H_2CH_3$), 47.67 ($\underline{C}H_2CH_3$), 64.89 (NCH_2CO), 65.54 ($N\underline{C}H_2$), 67.62 ($N\underline{C}H_2CO$), 118.67 (C_{Ar}), 128.44 (C_{Ar}), 128.64 (C_{Ar}), 129.13 (C_{Ar}), 130.31 (C_{Ar}), 131.05 (C_{Ar}), 131.21 (C_{Ar}), 133.10 (C_{Ar}), 137.00 (C_{Ar}), 153.65 (C_{Ar}), 170.96 (C=N), 174.28 (C=O), 174.80 (C=S), 184.11 (C=O) ppm.

ESI+ MS (m/z): 679.101 (calc. 679.0995) $[M+Na]^+$, 695.074 (calc. 695.0735) $[M+K]^+$.

[Re(NPh)(L^{1EtEt})]

H_3L^{1EtEt} (91 mg, 0.2 mmol), $[Re(NPh)Cl_3(PPh_3)_2]$ (181 mg, 0.2 mmol) and three drops of NEt_3 were dissolved in 5 mL $CHCl_3$ and heated on reflux for 30 min. The solvent was evaporated and the residue was dissolved in a minimum amount of CH_2Cl_2. The product was separated by column chromatography (silica column: CH_2Cl_2 → CH_2Cl_2/MeOH 100:1 → CH_2Cl_2/MeOH 50:1) and crystallised from MeOH/$CHCl_3$ in the refrigerator giving light-purple crystals. Yield 40 % (58 mg).

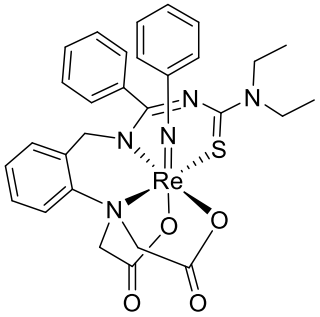

^{1}H NMR ($CDCl_3$): δ = 1.23 (t, *J* = 7.2 Hz, 3H), 1.31 (t, *J* = 7.1 Hz, 3), 3.72 – 3.62 (m, 1H), 3.84 – 3.72 (m, 1H), 4.10 – 3.90 (m, 3H), 4.25 – 4.10 (m, 1H), 4.37 (d, *J* = 14.0 Hz, 1H), 4.55 (d, *J* = 15.4 Hz, 1H), 5.11 (d, *J* = 14.0 Hz, 1H), 5.53 (d, *J* = 15.4 Hz, 1H), 6.35 (d, *J* = 7.8 Hz, 2H), 7.04 – 6.95 (m, 2H), 7.51 – 7.38 (m, 1H), 7.15 – 7.08 (m, 1H), 7.37 – 7.21 (m, 9H) ppm.

^{13}C NMR ($CDCl_3$): δ = 13.16 (CH_3), 13.47 (CH_3), 45.99 ($\underline{C}H_2CH_3$), 47.10 ($\underline{C}H_2CH_3$), 64.25 ($N\underline{C}H_2CO$), 66.35 ($N\underline{C}H_2$), 68.45 ($N\underline{C}H_2CO$), 118.54 (C_{Ar}), 120.51 (C_{Ar}), 128.09 (C_{Ar}), 128.18 (C_{Ar}), 128.59 (C_{Ar}), 128.98 (C_{Ar}), 129.37 (C_{Ar}), 129.69 (C_{Ar}), 130.33 (C_{Ar}), 132.81 (C_{Ar}), 133.16 (C_{Ar}), 138.92 (C_{Ar}), 154.58 (C_{Ar}), 156.56 (C_{Ar}), 170.10 (C=N), 175.41 (C=O), 175.82 (C=S), 183.24 (C=O) ppm.

IR: 2964 (w), 1687 (m), 1494 (m), 1422 (m), 1348 (m), 1302 (m), 1252 (m), 1225 (m), 1203 (w), 1171 (w), 1139 (w), 1120 (w), 1120 (w), 1068 (w), 1042 (w), 1025 (m), 972 (w), 939 (w), 909 (s), 862 (m), 803 (w) 762 (s), 742 (w), 721 (m), 704 (m), 683 (s), 645 (w), 624 (w), 589 (w), 570 (m), 563 (m), 546 (m) cm^{-1}.

ESI+ MS (m/z): 770.1176 (calc. 770.2559) $[M+K]^+$.

Anal. Calcd for $C_{29}H_30N_5O_4ReS$: C, 47.66; H, 4.14; N, 9.58; S, 4.39 %. Found: C, 47.36; H, 4.56; N, 9.24; S, 4.23 %.

[Re(NPhF)(L^{1EtEt})]

H_3L^{1EtEt} (46 mg, 0.1 mmol) and [Re(NPhF)Cl_3(PPh_3)$_2$] (93 mg, 0.1 mmol) were heated on reflux in 5 mL $CHCl_3$ for 10 h. The solvent was evaporated, the residue was redissolved in CH_2Cl_2 and filtered. This product was separated by column chromatography (silica column: CH_2Cl_2 → CH_2Cl_2/MeOH 100:1 → CH_2Cl_2/MeOH 50:1). It was crystallised from MeOH/$CHCl_3$ in the refrigerator giving purple crystals. Yield 30 % (22 mg).

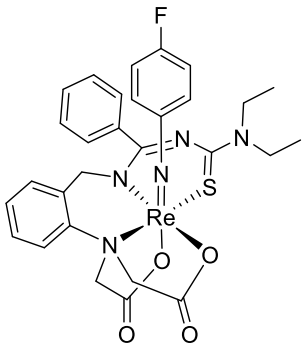

^{1}H NMR ($CDCl_3$): δ = 1.25 (t, *J* = 7.1 Hz, 3H, CH_3), 1.33 (t, *J* = 7.1 Hz, 3H, CH_3), 3.75 – 3.61 (m, 1H, CH_2), 3.87 – 3.70 (m, 1H, CH_2), 4.12 – 3.91 (m, 3H, CH_2), 4.28 – 4.12 (m, 1H, CH_2), 4.35 (d, *J* = 13.9 Hz, 1H, CH_2), 4.55 (d, *J* = 15.4 Hz, 1H, CH_2), 5.11 (d, *J* = 13.9 Hz, 1H, CH_2), 5.55 (d, *J* = 15.4 Hz, 1H, CH_2), 6.39 – 6.32 (m, 2H, H_{Ar}), 6.73 – 6.66 (m, 2H, H_{Ar}), 7.16 – 7.10 (m, 1H, H_{Ar}), 7.37 – 7.23 (m, 4H, H_{Ar}), 7.55 – 7.39 (m, 4H, H_{Ar}) ppm.

^{13}C NMR ($CDCl_3$): *δ* = 13.21 (CH_3), 13.54 (CH_3), 46.12 ($\underline{C}H_2CH_3$), 47.24 ($\underline{C}H_2CH_3$), 64.32 (N$\underline{C}H_2$CO), 66.43 (NCH_2), 68.48 (N$\underline{C}H_2$CO), 116.76 (d, *J* = 23.65 Hz, C_{Ar}), 118.57 (C_{Ar}), 122.56 (d, *J* = 8.92 Hz, C_{Ar}), 128.26 (C_{Ar}), 128.70 (C_{Ar}), 129.04 (C_{Ar}), 129.76 (C_{Ar}), 130.48 (C_{Ar}), 132.92 (C_{Ar}), 133.33 (C_{Ar}), 138.92 (C_{Ar}), 153.42 (C_{Ar}), 154.70 (C_{Ar}), 159.63 (C_{Ar}), 162.16 (C_{Ar}), 170.17 (C=N), 175.29 (C=O), 175.90 (C=S), 183.09 (C=O) ppm.

^{19}F NMR ($CDCl_3$): δ = -107.3 (m) ppm.

IR: 3062 (w), 2970 (w), 2931 (w), 2870 (w), 1688 (s), 1585 (m), *ν*(CO) 1490 (s), *ν*(CO) 1423 (m), 1348 (m), 1348 (m), 1303 (m), 1253 (m), 1225 (m), 1172 (w), 1140 (m), 1120 (w), 1074 (w), 1043 (w), 1025 (w), 1009 (w), 973 (w), 910 (s), 863 (m), 839 (m), 804 (m), 788 (m), 774 (m), 742 (w), 722 (m), 705 (m), 687 (m), 673 (w), 645 (w), 625 (w), 594 (w), 569 (w), 556 (w), 543 (w), 528 (m) cm^{-1}.

ESI+ MS (m/z): 772.136 (calc. 772.1374) $[M+Na]^+$, 788.111 (calc. 788.1113) $[M+K]^+$.

Anal. Calcd for for $C_{29}H_{29}FN_5O_4ReS$: C, 46.51; H, 3.90; N, 9.35; S, 4.28 %. Found: C, 45.84; H, 4.16; N, 9.08; S, 4.34 %.

5.8 Synthesis and Reactions of the "C-Terminus" $KH_3L^{2RR'}$ Ligands

The syntheses of $KH_3L^{2RR'}$ have been described before and were repeated with slight changes.[92]

KH_3L^{2EtEt}

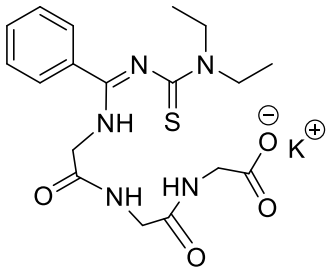

Triglycine (1.14 g, 6 mmol) and KOH (660 mg) were dissolved in dry EtOH (40 mL). Solid diethylcarbamothioylbenzimidoyl chloride (1.52 g, 6 mmol) was added. The pale-yellow reaction mixture was stirred at room temperature for 7 h. The obtained KCl was filtered off and the volume of the solution was reduced to about 5 mL. This solution was added dropwise to rigorously stirred Et_2O. The obtained precipitate was filtered off, washed with Et_2O and dried. The dry product is a pale-yellow solid. Yield 70 % (1.6 g).

^{1}H NMR (d_6-DMSO): δ = 1.14 – 1.02 (m, 6H, CH_3), 3.42 – 3.34 (m, 2H, CH_2), 3.51 (q, *J* = 7.0 Hz, 2H), 3.78 – 3.69 (m, 4H, CH_2), 3.90 (d, *J* = 5.7 Hz, 2H, CH_2), 7.46 – 7.32 (m, 5H, H_{Ar}), 7.62 (t, *J* = 4.9 Hz, 1H, NH), 8.37 (t_{br}, *J* = 5.9 Hz, 1H, NH), 8.48 (t, *J* = 5.8 Hz, 1H, NH) ppm.

^{13}C NMR (d_6-DMSO): δ = 11.85 (CH_3), 12.85 (CH_3), 42.33 ($\underline{C}H_2CH_3$), 43.46 ($\underline{C}H_2CH_3$), 44.04 (CH_2), 44.92 (CH_2), 45.40 (CH_2), 127.88 (C_{Ar}), 127.95 (C_{Ar}), 130.02 (C_{Ar}), 133.65 (C_{Ar}), 156.89 (C=N), 168.00 (C=O) 169.40 (C=O), 171.16 (C=O), 188.57 (C=S) ppm.

IR: 3270 (w), 3061 (w), 2973 (w), 2930 (w), 1648 (m), *v*(CO) 1594 (s), *v*(CO) 1526 (s), *v*(CO) 1484 (s), 1419 (m), 1386 (m), 1386 (m), 1310 (m), 1238 (s), 1128 (m), 1094 (w), 1076 (w), 1049 (w), 1026 (m), 992 (w), 915 (w), 886 (m), 812 (w), 776 (m), 693 (s), 591 (s) cm^{-1}.

ESI- MS (m/z): 406.1473 (calc. 406.1554) $[M]^-$.

Anal. Calcd for for $C_{18}H_{24}N_5O_4SK$: C, 48.52; H, 5.43; N, 15.72; S, 7.20 %. Found: C, 44.67; H, 6.12; N, 14.07; S, 8.26 %. Deviations in the analytical data are due to an impurity, which could not be separated.

KH_3L^{2MePh}

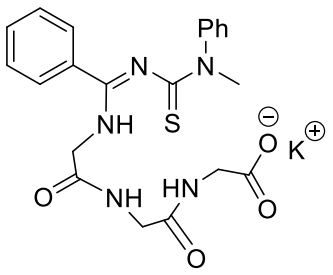

Triglycine (1.14 g, 6 mmol) and KOH (660 mg) were dissolved in dry EtOH (40 mL). Solid methylphenylcarbamothioylbenzimidoyl chloride (1.73 g, 6 mmol) was added. The pale-yellow reaction mixture was stirred at room temperature for 8 h. The obtained KCl was filtered off and the volume of the solution was reduced to about 5 mL. This solution was added dropwise to rigorously stirred Et_2O. The obtained precipitate was filtered off, washed with Et_2O and dried. The dry product is a yellow solid. Yield 48 % (1.37 g).

^{1}H NMR (d_6-DMSO): 3.44 (m, 2H, CH_2), 3.48 (s, 3H, CH_2), 3.71 (s, 3H, CH_3, *overlapped with a water signal), 3.87 (s, 2H, CH_2), 7.46 (m, 5H, H_{Ar}), 7.63 (t, J = 4.65 Hz, 1H, NH), 8.38 (s, 2H, NH) ppm.

^{13}C NMR (d_6-DMSO): 42.46 (CH_2), 43.57 (CH_2), 44.84 (CH_2), 126.54 (C_{Ar}), 128.12 (C_{Ar}), 128.20 (C_{Ar}), 128.68 (C_{Ar}), 130.40 (C_{Ar}), 133.44 (C_{Ar}), 157.40 (C=N), 168.24 (C=O), 169.24 (C=O), 171.75 (C=O) ppm. Carbon atom of the methyl group and quaternary C=S not visible.

IR: 3280 (w), 2973 (w), 2931 (w), 1650 (m), *v*(CO) 1593 (s), *v*(CO) 1529 (s), *v*(CO) 1489 (s), 1420 (m), 1385 (m), 1310 (m), 1240 (s), 1129 (m), 1095 (m), 1076 (m), 1026 (m), 992 (w), 915 (w), 887 (w), 777 (m), 694 (s), 582 (m) cm^{-1}.

ESI- MS (m/z): 440.1351 (calc. 440.1398) [M]$^-$.

Anal. Calcd for for $C_{21}H_{22}N_5O_4SK$: C, 52.59; H, 4.62; N, 14.60; S, 6.68 %. Found: C, 52.75; H, 5.18; N, 14.60; S, 8.22 %.

KH_3L^{2PhPh}

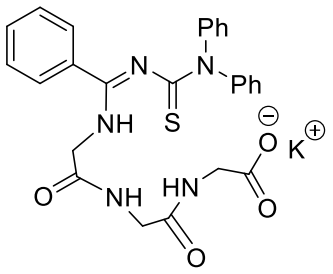

Triglycine (567 mg g, 3 mmol) and KOH (330 mg) were dissolved in dry EtOH (20 mL). Solid diphenylcarbamothioylbenzimidoyl chloride (1.05 g, 3 mmol) was added. The yellow reaction mixture was stirred at room temperature for 8 h. The obtained KCl was filtered off and the volume of the solution was reduced to about 5 mL. This solution was added dropwise to rigorously stirred Et_2O. The obtained precipitate was filtered off, washed with Et_2O and dried. The dry product is a yellow-orange solid. Yield 42 % (337 mg).

^{1}H NMR (d_6-DMSO): δ = 3.67 (d, *J* = 5.7 Hz, 2H, CH_2), 3.72 (s, 2H, CH_2), 3.88 (s, 2H, CH_2), 7.64 – 7.15 (m, 15H, H_{Ar}), 8.44 (t, *J* = 5.55 Hz, 1H, NH), 8.54 (s, 2H, NH) ppm.

^{13}C NMR (d_6-DMSO): δ = 42.58 (CH_2), 44.32 (CH_2), 45.69 (CH_2), 126.27 (C_{Ar}), 128.11 (C_{Ar}), 128.20 (C_{Ar}), 128.33 (C_{Ar}), 128.76 (C_{Ar}), 129.15 (C_{Ar}), 129.40 (C_{Ar}), 130.45 (C_{Ar}), 146.21 (C=N), 168.40 (C=O), 168.56 (C=O), 169.45 (C=O) ppm. Quaternary carbon atom C=S not visible.

IR: 3266 (w), 3059 (w), 1650 (m), *v*(CO) 1589 (s), *v*(CO) 1528 (s), *v*(CO) 1489 (s), 1382 (s), 1279 (s), 1150 (m), 1073 (m), 1025 (m), 1002 (m), 907 (m), 873 (m), 779 (m), 752 (m), 691 (s), 621 (m), 581 (m), 561 (m) cm^{-1}.

ESI- MS (m/z): 502.1553 (calc. 502.1554) [M]$^-$.

[ReO(HL^{2EtEt})]

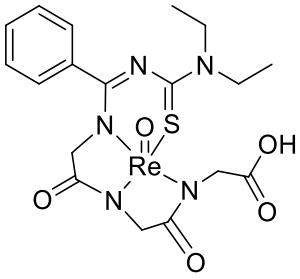

KH_3L^{2EtEt} (44 mg, 0.1 mmol) and $(NBu_4)[ReOCl_4]$ (59 mg, 0.1 mmol) were dissolved in 5 mL $CHCl_3$ and heated on reflux for 30 min. The reaction mixture was cooled to room temperature and filtered. The solvent was evaporated and the residue was redissolved in acetone and overlayered with *n*-hexane. Orange-red blocks suitable for X-ray analysis were obtained after storing the sample in a refrigerator for several weeks. Yield: 12 % (8 mg).

^{1}H NMR (d_6-DMSO): δ = 1.21 (t, J = 1.7 Hz, 3H, CH_3), 1.32 (t, J = 7.1 Hz, 3H, CH_3), 4.08 – 3.76 (m, 4H, CH_2), 4.19 (d, J = 18.5 Hz, 1H, CH_2), 4.41 – 4.33 (m, 2H, CH_2), 4.78 (d, J = 17.4 Hz, 1H, CH_2), 4.89 (d, J = 17.3 Hz, 1H, CH_2), 4.93 (d, J = 17.3 Hz, 1H, CH_2), 7.63 – 7.51 (m, 5H, H_{Ar}), 12.94 (s, 1H, COOH) ppm.

^{13}C NMR (d_6-DMSO): δ = 13.10 (CH_3), 13.30 (CH_3), 46.87 ($\underline{C}H_2CH_3$), 47.58 ($\underline{C}H_2CH_3$), 52.34 (CH_2), 55.27 (CH_2), 62.69 (CH_2), 128.69 (C_{Ar}), 129.16 (C_{Ar}), 131.03 (C_{Ar}), 136.78 (C_{Ar}), 157.93 (C=N), 167.17 (C=O), 170.17 (C=O), 171.93 (C=O), 190.49 (C=S) ppm.

ESI- MS (m/z): 606.0800 (calc. 606.0826) $[M]^-$.

The compound was not analysed by elemental analysis because it could not be dried completely after the NMR measurements in d_6-DMSO.

[ReO(HL^{2MePh})]

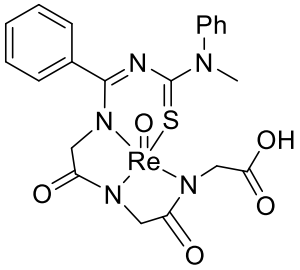

KH_3L^{2MePh} (200 mg, 0.47 mmol) and $(NBu_4)[ReOCl_4]$ (278 mg, 0.47 mmol) were dissolved in 5 mL $CHCl_3$ and heated on reflux for 30 min. The reaction mixture was cooled to room temperature and filtered. Crystals suitable for X-ray analysis were obtained from the MeOH/$CHCl_3$ mixture after weeks by slow evaporation. Yield 10 % (29 mg).

^{1}H NMR (d_6-DMSO): δ = 3.72 (s, 3H, CH_3), 4.15 (d, ^2J = 18.5 Hz, 1H, CH_2), 4.33 (d, ^2J = 18.5 Hz, 1H, CH_2), 4.37 (d, ^2J = 17.3 Hz, 1H, CH_2), 4.45 (d, ^2J = 17.4, 1H, CH_2), 4.63 (d, ^2J = 17.3 Hz, 1H, CH_2), 4.95 (d, ^2J = 17.4 Hz, 1H, CH_2), 7.58 (m, 10H, H_{Ar}) ppm.

^{13}C NMR (d_6-DMSO): δ = 43.27 (CH_3), 52.29 (CH_2), 54.66 (CH_2), 62.82 (CH_2), 127.29 (C_{Ar}), 127.29 (C_{Ar}), 128.80 (C_{Ar}), 128.80 (C_{Ar}), 129.23 (C_{Ar}), 130.09 (C_{Ar}), 130.73 (C_{Ar}), 131.59 (C_{Ar}), 143.99 (C=N), 171.60 (C=O), 186.02 (C=O), 190.17 (C=S) ppm. Signals was determined via HMQC and HMBC experiments. Quaternary carbon atoms are not all visible.

IR: *v*(CO) 1739 (m), *v*(CO) 1667 (s), *v*(CO) 1612 (m), 1477 (s), *v*(CO) 1453 (w), 1434 (w), 1400 (w), 1379 (m), 1364 (s), 1306 (w), 1262 (w), 1233 (m), 1137 (w), 1127 (m), 1070 (w), 1054 (w), 1026 (w), 995 (w), 984 (s), 936 (w), 902 (w), 867 (w), 853 (w), 818 (w), 788 (m), 769 (m), 757 (w), 732 (w), 697 (s), 682 (m), 657 (m), 626 (w), 602 (w), 562 (m) cm^{-1}.

ESI- MS (m/z): 640.0623 (calc. 640.0670) $[M]^-$.

Anal. Calcd for $C_{21}H_{20}N_5O_5ReS$: C, 39.37; H, 3.15; N, 10.93; S, 5.00 %. Found: C, 39.27; H, 3.42; N, 10.54; S, 6.97 %.

[ReO(HL^{2PhPh})]

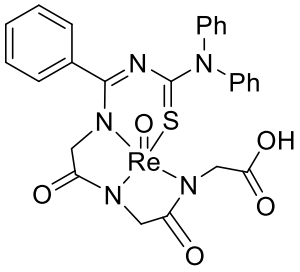

KH_3L^{2PhPh} (111 mg, 0.2 mmol) and $(NBu_4)[ReOCl_4]$ (118 mg, 0.2 mmol) were dissolved in 5 mL $CHCl_3$ and heated on reflux for 30 min. The obtained red-brown mixture was cooled to room temperature and filtered. The solvent was evaporated under reduced pressure and the residue was redissolved in acetone. After slow evaporation of the solvent in the refrigerator, orange-yellow needles suitable for X-Ray analysis were formed. They were filtered off and dried under vacuum. Yield: 37 % (52 mg).

^{1}H NMR (d_6-DMSO): δ = 4.18 (d, ^2J = 18.5 Hz, 1H, CH_2), 4.37 (d, ^2J = 18.5, 1H, CH_2), 4.39 (d, ^2J = 17.3 Hz, 1H, CH_2), 4.42 (d, ^2J = 17.5 Hz, 1H, CH_2), 4.82 (d, ^2J = 17.3 Hz, 1H, CH_2), 5.08 (d, ^2J = 17.5, 1H, CH_2), 7.26-7.64 (m, 15H, H_{Ar}), 12.32 (s, 1H, COOH) ppm.

^{13}C NMR (d_6-DMSO): δ = 51.90 (CH_2), 55.60 (CH_2), 61.98 (CH_2), 126.92 (C_{Ar}), 128.19 (C_{Ar}), 128.49 (C_{Ar}), 129.10 (C_{Ar}), 129.17 (C_{Ar}), 130.00 (C_{Ar}), 131.25 (C_{Ar}), 134.89 (C_{Ar}), 169.76 (C=O), 171.02 (C=O), 185.13 (C=O), 189.91 (C=S) ppm. Quaternary carbon atoms are not all visible.

IR: *v*(CO) 1714 (m), *v*(CO) 1666 (m), *v*(CO) 1634 (m), 1511 (m), 1484 (m), 1462 (m), 1394 (m), 1357 (m), 1297 (m), 1264 (m), 1220 (m), 1181 (w), 1150 (w), 1110 (w), 1073 (w), 1051 (w), 1022 (w), 991 (s), 948 (w), 882 (m), 853 (w), 821 (w), 758 (w), 761 (s), 738 (w), 700 (s), 673 (m), 643 (w), 629 (w), 611 (m), 581 (w), 559 (w) cm^{-1}.

ESI- MS (m/z): 702.0825 (calc. 702.0826) $[M]^-$.

Anal. Calcd for $C_{26}H_{22}N_5O_5ReS$: C, 44.44; H, 3.16; N, 9.97; S, 4.56 %. Found: C, 41.64; H, 3.49; N, 9.28; S, 4.22 %.

[^{99m}TcO(HL^{2EtEt})]

KH_3L^{2EtEt} (240 µg), $SnCl_2 \cdot 2\ H_2O$ (100 µg), 50 MBq of Na[$^{99m}TcO_4$] in 0.5 mL saline solution and EtOH (100 µL) were kept at 45 °C for 30 min. After cooling to room temperature, the reaction mixture was neutralized with a PBS buffer (0.3 mL). The reaction mixture was analysed by HPLC. The retention time of 21.75 min for the radio trace is similar to the UV trace of the rhenium compound [ReO(HL^{2EtEt})] (21.39 min).

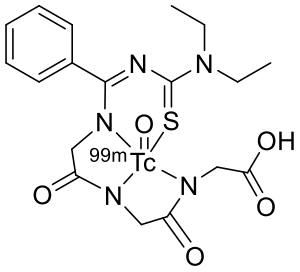

Radiochemical purity: 91 %.

[^{99m}TcO(HL^{2MePh})]

KH_3L^{2MePh} (230 µg), $SnCl_2 \cdot 2\ H_2O$ (100 µg) and 50 MBq of Na[$^{99m}TcO_4$] in 1.7 mL saline solution were kept at 80 °C for 15 min. After cooling to room temperature, the reaction mixture was neutralized with a PBS buffer (0.1 mL). The reaction mixture was analysed by HPLC. The retention time of 21.95 min for the radio trace (main component) is close to the UV trace of the rhenium compound [ReO(HL^{2MePh})] (21.56 min).

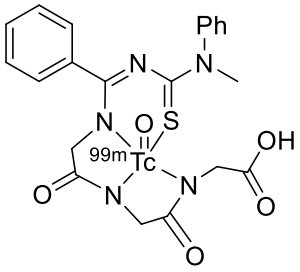

Radiochemical purity: 67 %.

5.9 Synthesis and Reactions of H_3P^{EtEt} and H_3P^{MePh}

General Procedures

Fmoc deprotection: The resin was soaked in DMF for 30 min in a syringe with a frit under gentle agitation. The fmoc protection group was cleaved with 3 mL of a solution of 20 % piperidine in DMF three times for 10 min under gentle agitation. Afterwards, the resin was washed three times with 8 mL DMF.

Coupling reaction: The new building block (Fmoc-L-2NaI-OH, N-Fmoc-traneamix, KH_3L^{2EtEt} or KH_3L^{2MePh}) (0.3 mmol) was prereacted with HBTU (0.294 mmol, 111 mg), diisopropylethyl amine (DIPEA) (0.6 mmol, 105 µL) in 3 mL DMF for 2 min under vigorous stirring. The reaction mixture was added to the fmoc deprotected resin and left for 1 h at room temperature under gentle agitation. This procedure was done twice for each new building block (double coupling).

Capping reaction: A solution of 10 % acetanhydride and 10 % DIPEA in 3 mL DMF was added after the coupling reaction under gentle agitation. This procedure was done three times for 8 min. Finally, the resin was washed three times with 8 mL of DMF.

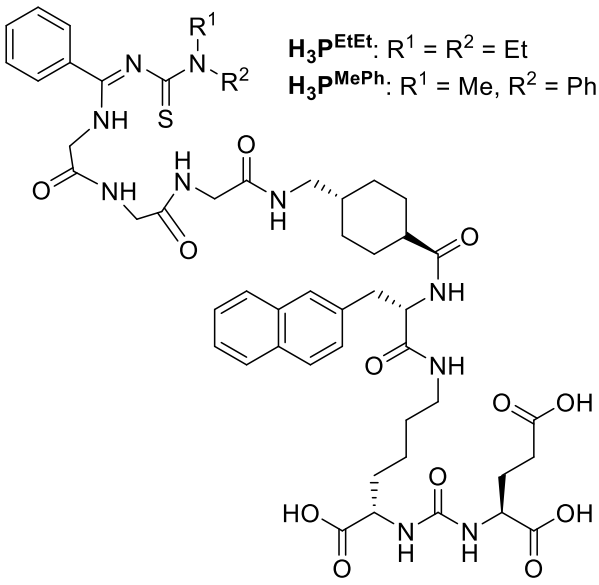

Di-*tert*-butyl-(R)-2-isocyanatopentanedioate was generated *in situ* by a dropwise addition of bis(*tert*-butyl)-L-glutamate hydrochloride (0.6 mmol, 178 mg) and diisopropylethyl amine (DIPEA) (1.7 mmol, 0.3 mL) in 40 mL CH_2Cl_2 to an ice-cold solution of trisphosgene (59 mg, 0.2 mmol) in 2 mL CH_2Cl_2 over 2 h. The obtained solution was stirred for 1 h at room temperature. The fmoc deprotected Lys(Mtt)-Wang resin (0.1 mmol, 175 mg) was added in one portion and the mixture was stirred under gentle stirring at room temperature overnight. The resin-bonded Glu-urea-Lys(Mtt) was filtered off. The Mtt group was cleaved overnight with a 1 % solution of TFA and MeOH in CH_2Cl_2 under gentle agitation. The next three building blocks (Fmoc-L-2Nal-OH, N-Fmoc-traneamix, KH_3L^{2EtEt}, KH_3L^{2MePh}) were coupled as described above (see coupling reaction). After the first coupling reaction, a capping reaction was done (see general procedure). The final peptide was cleaved from the resin by the addition of 2 mL of trifluoroacetic acid (TFA), H_2O and triisopropylsilane (TIPS) (95:2.5:2.5) (2 h under gentle agitation). The resin was washed with CH_2Cl_2 and the solvent was reduced under a stream of N_2 until a volume of about 1 mL. The peptide was precipitated with ice-cold Et_2O, centrifuged and redissvoled in a mixture of EtOH and H_2O + 0.1% TFA solution. The crude product was lyophilized giving a colourless powder. Both products were purified by preparative HPLC (see Analytical Methods) obtaining 132 mg for H_3P^{EtEt} and 6 mg for H_3P^{MePh}. The compounds were analysed by ESI MS or UPLC MS. The retention times on the analytical HPLC were determined.

Preparative HPLC of H_3P^{EtEt}

Method 1	0-5 min	isocratic 5 % MeCN; 95 % H_2O + 0.1 % TFA, 10 mL/min
	5-15 min	gradient 5 to 70 % MeCN; 95 to 30 % H_2O + 0.1 % TFA, 20 mL/min
Method 2	0-15 min	isocratic 30 % MeCN; 70 % H_2O; 0.5 M AcOH; 20 mL/min

Preparative HPLC of H_3P^{MePh}

Method	0-3 min	isocratic 40 % MeCN; 60 % H_2O + 0.1 % TFA, 40 mL/min
	3-23 min	gradient 40 to 100 % MeCN; 60 to 0 % H_2O + 0.1 % TFA, 40 mL/min
	23-38 min	isocratic 100 % MeCN, 40 mL/min

H_3P^{EtEt}: HPLC MS (m/z): 1045.4809 (calc. 1045.4817) $[M+H]^+$.

Retention time: 20.88 min

H_3P^{MePh}: UPLC MS: 1079.53 (calc. 1079.4661) $[M+H]^+$.

Retention time: 20.98 min

Anal. Calcd for $C_{51}H_{68}N_{10}O_{12}S$: C, 58.61; N, 13.40; H, 6.56, S, 3.07 %. Found: C, 55.73; H, 6.71; N, 12.72; S, 2.73 %.

[ReO(P^{EtEt})] and [ReO(P^{MePh})]

H_3P^{EtEt} (642 µg, 0.61 µmol) or H_3P^{MePh} (2.5 mg, 2.3 µmol) were dissolved in 1 mL EtOH/$CHCl_3$ (1:2). $(NBu_4)[ReOCl_4]$ (442 µg, 0.61 µmol) dissolved in 0.5 mL $CHCl_3$ was added dropwise to a stirred solution of the peptide. The reaction mixture was heated on reflux for 30 min and analysed by UPLC MS. The retention times on the analytical HPLC were determined.

[ReO(P^{EtEt})]**:** UPLC MS (m/z): 1245.46 (calc. 1245.41) $[M+H]^+$.

Retention time: 22.06 and 22.28 min

[ReO(P^{MePh})]: UPLC MS (m/z): 1279.46 (calc. 1279.39) $[M+H]^+$.

Retention time: 22.08 and 22.52 min

Optimized complex formation of H_3P^{EtEt} with ^{99m}Tc:

H_3P^{EtEt} (123 µg) was weighted in a vial and 100 µL of EtOH, 100 µg of $SnCl_2 \cdot 2\ H_2O$ freshly dissolved in 100 µL water and $Na[^{99m}TcO_4]$ (50 MBq in 1.7 mL saline) were added. The mixture was stirred at 80 °C for 15 min and cooled to room temperature. The reaction mixture was neutralized with a PSB buffer in saline solution (0.1 mL). The progress of the complex formation was analysed by HPLC (UV and a radio detector). The product was purified using a C18 filter (Chromafix). The filter was washed with 1 mL water. The ^{99m}Tc complex was obtained by eluting the filter with 1 mL EtOH. After evaporation of the organic phase, the product was redissolved in 0.1 mL PBS buffer and analysed by HPLC (UV and a radio detector).

Radiochemical yield: 25 % (not decay-corrected).

Radiochemical purity: 98 %.

Preparation of [^{99m}TcO(P^{EtEt})] for *in vivo* Experiments

H_3P^{EtEt} (2 mg) was weighted in a vial and 100 µL of EtOH, 100 µg of $SnCl_2 \cdot 2\ H_2O$ freshly dissolved in 100 µL water and Na[$^{99m}TcO_4$] (886 MBq in 1.6 mL saline) were added. The mixture was stirred at 80 °C for 15 min and cooled to room temperature. The product was purified using a C18 filter (Chromafix). The filter was washed with 1 mL water. The ^{99m}Tc complex was obtained by eluting the filter with 3 mL EtOH. After evaporation of the organic phase, the product was redissolved in 0.1 mL PBS buffer. The pH was adjusted to 6 with NaOH. The product was analysed by HPLC (UV and a radio detector).

Radiochemical yield: 19 % (not decay-corrected).
Radiochemical purity: 79 %.

5.10 Synthesis and Reactions of the "N-Terminus Ligand" H_3L^{3EtEt}

$H_3L^{3EtEtBoc}$

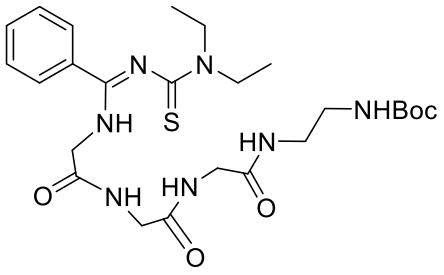

KH_3L^{2EtEt} (223 mg, 0.5 mmol) was dissolved in warm, dry THF. HBTU (101 mg, 0.75 mmol) and HOBt (284 mg, 0.75 mmol) were added to the mixture and stirred for 20 min to give a clear solution. Mono-Boc-protected ethylene diamine (0.08 mL, 0.5 mmol) was added and the reaction mixture was heated on reflux for 7 h. The colour of the solution turned orange-red after about 4 h. After completion of the reaction, a colourless precipitate was filtered off. Evaporation of the THF gave a red oil, which was dissolved in a small amount of CH_2Cl_2 and filtered. The product was separated by chromatography on a silica column (CH_2Cl_2 → CH_2Cl_2/MeOH 100:1 → 12:1). $H_3L^{3EtEtBoc}$ was obtained in the fourth fraction of this chromatography. If the product is still not pure, the chromatography can be repeated on a silica column (EtOAC → EtOAC/MeOH 10:1). The product was obtained as a fluffy, slightly orange powder after evaporation of the solvents using a rotary evaporator. Yield 31 % (85 mg).

^{1}H NMR ($CDCl_3$): δ = 1.06 – 1.16 (m, 6H, CH_3), 1.32 (s, 9H, CCH_3), 3.09 (s, 2H, CH_2), 3.16 (s, 2H, CH_2), 3.45 – 3.59 (m, 2H, CH_2), 3.71 – 3.82 (m, 4H, CH_2), 3.85 (s, 2H, CH_2), 4.05 (s, 2H, CH_2), 5.79 (s, 1H, NH), 7.25 – 7.47 (m, 5H, H_{Ar}), 7.72 (s, 1H, NH), 8.21 (s, 1H, NH) ppm.

^{13}C NMR ($CDCl_3$): δ = 12.01 (CH_3), 13.00 (CH_3), 28.45 (C(<u>C</u>H_3)$_3$), 40.04 (CH_2), 41.18 (CH_2), 43.01 (CH_2), 43.79 (CH_2), 45.00 (CH_2), 45.87 (CH_2), 46.56 (CH_2), 79.39 (<u>C</u>(CH_3)$_3$), 127.82 (C_{Ar}), 128.57 (C_{Ar}), 131.04 (C_{Ar}), 132.90 (C_{Ar}), 156.54 (C=N), 170.14 (C=O), 170.28 (C=O), 171.66 (C=O), 188.76 (C=O), 193.42 (C=S) ppm.

ESI+ MS (m/z): 550.2814 (calc. 550.2821) $[M+H]^+$, 572.2646 (calc. 572.2631) $[M+Na]^+$, 588.2377 (calc. 588.2370) $[M+K]^+$.

Anal. Calcd for $C_{25}H_{39}N_7O_5S$: C, 54.63; H, 7.15; N, 17.84; S, 5.83 %. Found: C, 51.13; H, 7.06; N, 16.68; S, 5.03 %.

{H_4L^{3EtEt}}(CF_3COO) and {H_4L^{3EtEt}}Cl

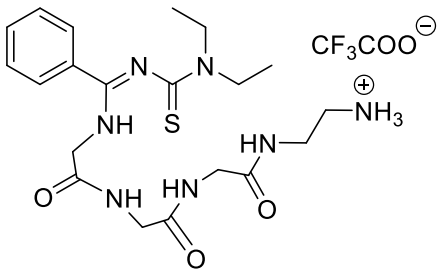

{H_4L^{3EtEt}}(CF_3COO): $H_3L^{3EtEtBoc}$ (30 mg, 0.05 mmol) was dissolved in 4 mL CH_2Cl_2 and placed in an ice-bath. TFA (0.2 mL) was added slowly. The reaction mixture was stirred for 30 min. The progress of the reaction was checked by TLC. The solvent and the excess of TFA were evaporated and the product was dried in vacuum.

{H_4L^{3EtEt}}(CF_3COO): $H_3L^{3EtEtBoc}$ (30 mg, 0.05 mmol) was dissolved in TFA (2 mL) and placed in an ice-bath. The reaction was stirred for 30 min. The progress of the reaction was checked by TLC. The excess of TFA was evaporated and the product was dried in vacuum.

{H_4L^{3EtEt}}Cl: $H_3L^{3EtEtBoc}$ (30 mg, 0.05 mmol) was added to an ice-cold solution of 4 M HCl (1 mL) in dioxane (3 mL). The progress of the reaction was checked by TLC. After 30 min the solvent was removed under reduced pressure.

In all three cases, the product was dried in vacuum giving a pale-orange oil in quantitative yields.

^{1}H NMR (d_4-MeOD): δ = 1.18 – 0.98 (m, 6H, CH_3), 2.93 (t, *J* = 5.7 Hz, 2H, CH_2), 3.35 (t, *J* = 5.7 Hz, 2H, CH_2), 3.52 (q, *J* = 7 Hz, 2H, CH_2), 3.71 (q, *J* = 7.0 Hz, 2H, CH_2), 3.76 (s, 2H, CH_2), 3.81 (s, 2H, CH_2), 3.97 (s, 2H, CH_2), 7.47 – 7.23 (m, 5H, H_{Ar}) ppm.

^{19}F NMR (d_4-MeOD): δ = - 77.4 (CF_3COO^-) ppm. (for {H_4L^{3EtEt}}(CF_3COO))

ESI- MS (m/z): 448.2146 (calc. 448.2131) $[M-2H]^-$.

[ReO($L^{3EtEtBoc}$)]

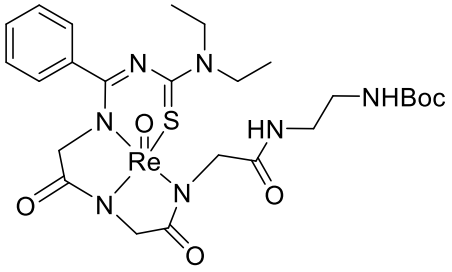

$(NBu_4)[ReOCl_4]$ (20 mg, 0.034 mmol) dissolved in 4 mL MeOH was added to ethylene glycol (1 mL). 1 M NaOH (0.5 mL) solution was added dropwise until the colour of the solution turned first blue and then dark blue to violet. The mixture was stirred for 10 min at room temperature and then $H_3L^{3EtEtBoc}$ (19.6 mg, 0.034 mmol) dissolved in 1 mL MeOH was added. The solution was stirred for additional 4 h at room temperature. During this time, the solution turned green-brown. The reaction mixture was extracted three times with water and chloroform. The organic phases were combined, dried over $MgSO_4$ and filtered. The product was separated by column chromatography (silica column, CH_2Cl_2 → CH_2Cl_2/MeOH 12:1). The product was dried in vacuum giving an orange-red oil. Yield 27 % (7 mg).

^{1}H NMR ($CDCl_3$): δ = 1.22 – 1.29 (m, 6H, CH_3), 1.39 (s, 9H, CCH_3), 3.11 – 3.26 (m, 4H, CH_2), 3.76 – 4.02 (m, 4H, CH_2), 4.36 – 4.82 (m, 5H, CH_2), 4.99 (t, J = 5.6 Hz, 1H, NH), 5.32 (d, J = 16.7 Hz, 1H, CH_2), 6.49 (t, J = 5.1 Hz, 1H, NH), 7.57 – 7.37 (m, 5H, H_{Ar}) ppm.

^{13}C NMR ($CDCl_3$): δ = 13.06 (CH_3), 13.22 (CH_3), 28.53 (C($\underline{C}H_3$)$_3$), 40.51 (CH_2), 46.91 (CH_2), 47.77 (CH_2), 52.72 (CH_2), 56.86 (CH_2), 59.21 (CH_2), 63.28 (CH_2), 100.16 ($\underline{C}(CH_3)_3$), 127.81 (C_{Ar}), 129.21 (C_{Ar}), 131.21 (C_{Ar}), 136.55 (C_{Ar}), 167.70 (C=O), 170.64 (C=O), 170.99 (C=O), 186.28 (C=O), 191.73 (C=S) ppm. *One carbon atom (C=N) is not visible.

ESI+ MS (m/z): 772.1909 (calc. 772.1897) $[M+Na]^+$.

Retention time: 22.20 min

[ReO(L^{3EtEt})]

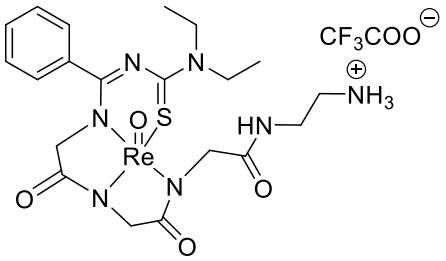

[ReO($L^{3EtEtBoc}$)] (7 mg, 0.01 mmol) from the previous reaction was dissolved in CH_2Cl_2 and placed in an ice-bath. TFA (0.5 mL) was added dropwise. The progress of the reaction was checked by TLC. The solvents were evaporated under reduced pressure and the product was dried in vacuum giving a pale orange-red product in a quantitative yield.

^{1}H NMR ($CDCl_3$): δ = 1.25 (t, J = 7.1 Hz, 3H, CH_3), 1.35 (t, J = 7.4 Hz, 3H, CH_3), 3.46 – 3.06 (m, 3H, CH_2), 3.83 – 3.58 (m, 2H, CH_2), 4.08 – 3.84 (m, 3H, CH_2), 4.56 – 4.20 (m, 3H, CH_2), 4.85 – 4.68 (m, 2H, CH_2), 5.06 – 4.92 (d, J = 17.2 Hz, 1H, CH_2), 7.55 – 7.37 (m, 4H, H_{Ar}), 7.97 (s, 1H, NH), 8.34 (s, 3H, NH) ppm.

^{19}F NMR ($CDCl_3$): δ = - 75.8 (s) ppm.

IR: 3313 (w), 2930 (w), *ν*(CO) 1655 (s), *ν*(CO) 1511 (s), *ν*(CO) 1417 (m), 1354 (s), 1294 (m), 1249 (m), 1166 (m), 1146 (m), 1097 (m), 1073 (m), 1043 (w), 1018 (m), 988 (s), 909 (m), 877 (m), 826 (m), 776 (m), 704 (m), 689 (m), 673 (m), 608 (m), 582 (m), 546 (m), 532 (m) cm^{-1}.

[^{99m}TcO($L^{3EtEtBoc}$)]

$H_3L^{3EtEtBoc}$ (2 mg) was mixed with 35 MBq Na[$^{99m}TcO_4$] in 0.7 mL saline solution and 280 µg $SnCl_2 \cdot 2\ H_2O$ in 280 µL water and kept at 75 °C for 30 min. The pH of the reaction mixture was 3. The solution was neutralized with NaOH solution. The product was analysed by HPLC.

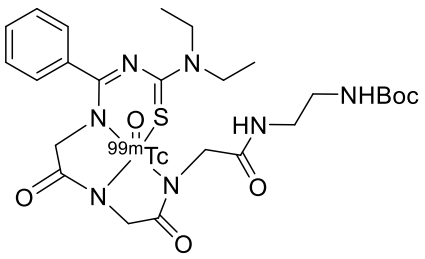

Radiochemical purity: 75 %.
Retention time: 21.10 min.

Synthesis of a ^{99m}Tc complex with the "Bisphosphonate ligand"

The bisphosphonate ligand (250 µg), 6 mg of a kit containing 34 mg tartaric acid, 48 mg sodium tartrate dihydrate, 80 mg $SnCl_2 \cdot 2\ H_2O$ and 1684 mg lactose monohydrate and 256 MBq Na[$^{99m}TcO_4$] in 1 mL saline solution were kept at 95 °C for 90 min. The pH was adjusted to pH = 7.

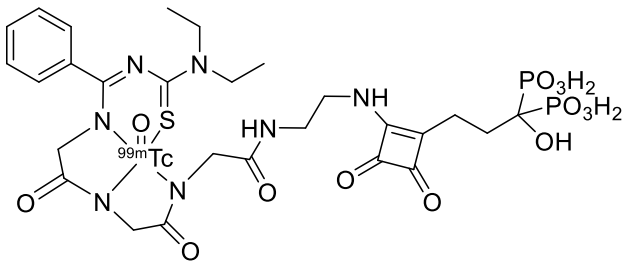

The product was analysed by TLC in H_2O and a Mini GITA. Radiochemical purity: 64 %.

6 Summary

This thesis describes the synthesis and characterisation of metal complexes with the so-called “Kläui ligand”, as well as with tetra- and pentadentate thiourea ligands. The focus is set to their potential as tracers for nuclear medical applications. Different metals like technetium, rhenium, gallium, indium and lutetium were used keeping in mind the importance of ^{99m}Tc and ^{68}Ga in diagnostics and ^{111}In and ^{177}Lu for radiation therapy.

The organic ligands of Scheme 6.1 were used in this thesis. Carboxylic and amino groups were introduced for possible bioconjugation. The functional groups for bioconjugation are highlighted.

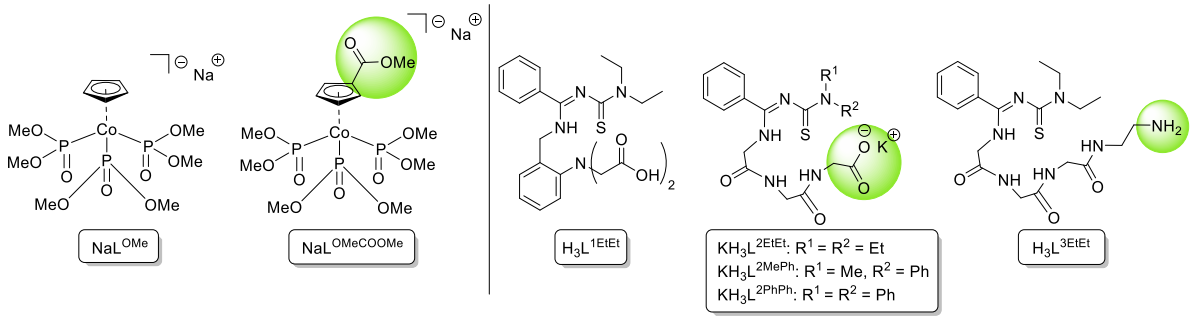

Scheme 6.1. Ligands used in this thesis. The functional groups for bioconjugation are highlighted.

The tripodal “Kläui ligand” NaL^{OMe} is able to coordinate to technetium in seven different oxidation states of the metal (Scheme 6.2). The octahedral coordination spheres of the Tc atoms are completed by nitrido, oxido, nitrosyl, chlorido or triphenylphosphine ligands giving in all cases neutral complexes. The complexes are air- and water-stable, which recommends them for nuclear medical applications. The complexes are fully characterised by NMR or EPR, IR spectroscopy and their molecular structures have been determined. The arrangement and bonding situation of the “Kläui ligand” is almost not influenced by the technetium site. Bond length modifications are only obtained for the two nitrido complexes, where a significant *trans* influence was observed.

Besides the coordination chemistry of technetium with NaL^{OMe}, also some rhenium complexes with this ligand were synthesised (Scheme 6.3). This comprises compounds with the $\{Re^{I}(CO)_3\}^+$, $\{Re^{V}OCl_2\}^+$, $\{Re^{V}NCl(PPh_3)\}^+$, $\{Re^{VI}NCl_2\}^+$ and $\{Re^{VII}O_3\}^+$ core. The obtained neutral, air- and water-stable complexes were fully characterised and exhibit the same structural features as their technetium analogues. The obtained series of ^{99}Tc and Re complexes provides a good fundament for ^{99m}Tc reactions. Restrictions in the synthesis of a defined technetium oxidation state or core structure do not longer play a crucial role in the preparation of suitable bioconjugates.

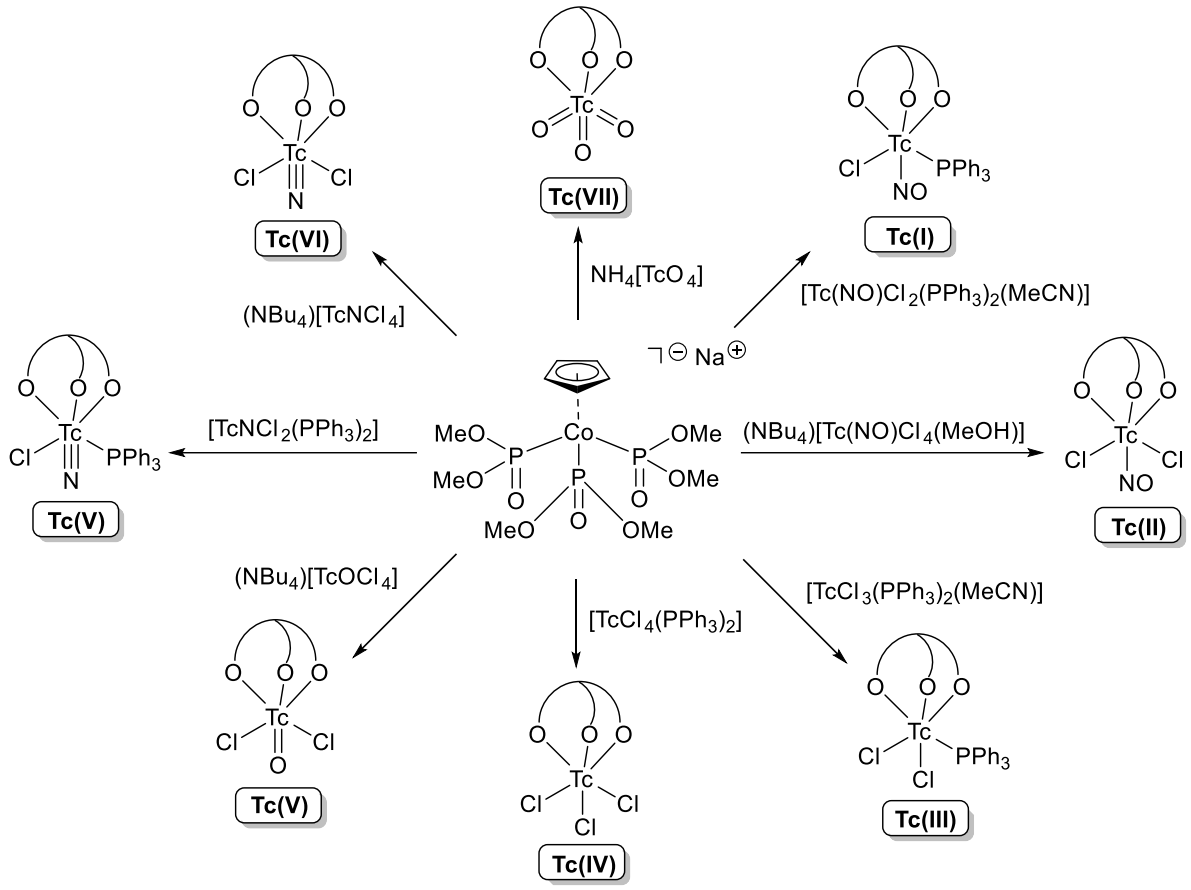

Scheme 6.2. Overview of the synthesised technetium complexes with NaL^{OMe}.[54]

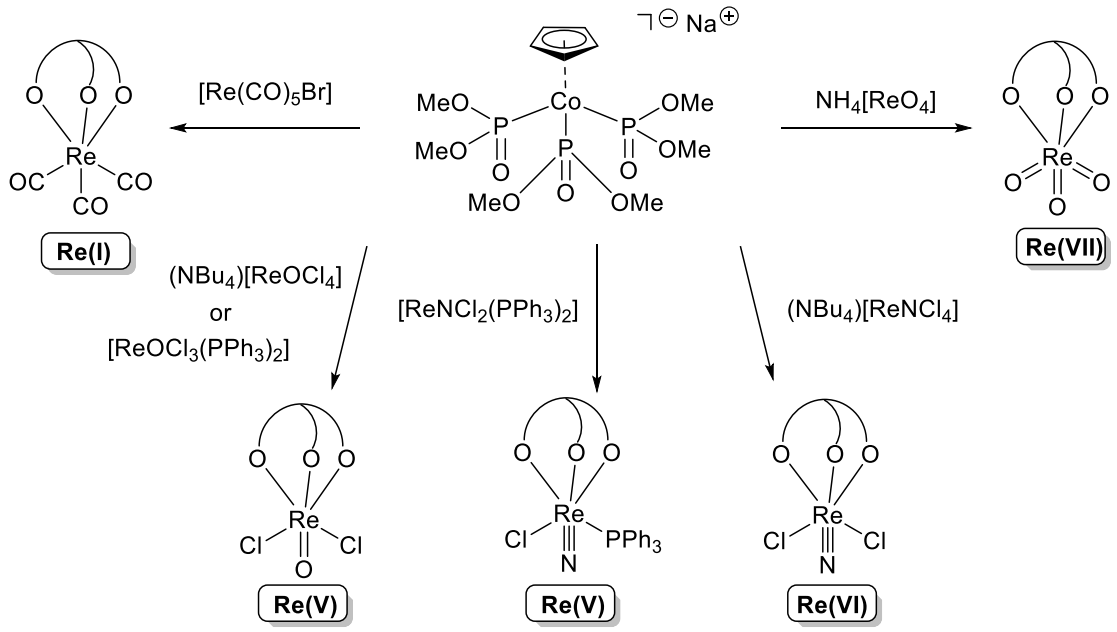

Scheme 6.3. Overview of the synthesised rhenium complexes with NaL^{OMe}.

In addition, $[Ga(L^{OMe})_2]NO_3$, $[In(L^{OMe})_2]NO_3$ and $[Lu(L^{OMe})_2(NO_3)]$ were synthesised from the corresponding metal nitrates and two equivalents of NaL^{OMe} (Scheme 6.4). The molecular structure of the positively charged complexes with Ga^{3+} and In^{3+} ions show an octahedral arrangement of the donor atoms while the Lu^{3+} ion establishes a neutral complex with the coordination number 8.

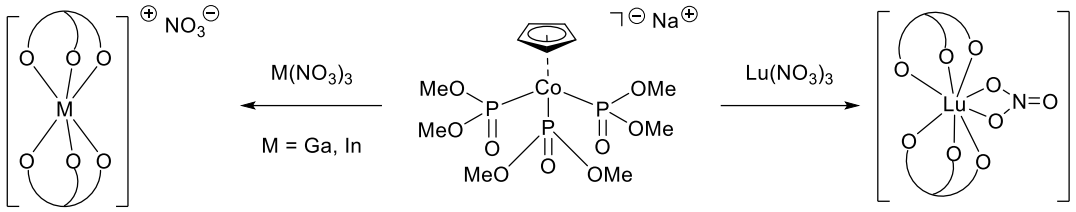

Scheme 6.4. Synthesis of the $[Ga(L^{OMe})_2]NO_3$, $[In(L^{OMe})_2]NO_3$ and $[Lu(L^{OMe})_2(NO_3)]$ complexes.

Modifications of the Cp ring may provide a position for possible bioconjugation. The formation of a complex of the composition $[Tc^{VII}O_3(L^{OMeCOOMe})]$ was proofed by ^{99}Tc NMR spectroscopy.

Tetra- and pentadentate thiourea ligands were synthesised in multi-step syntheses and coordinated to the $\{ReO\}^{3+}$, $\{Re(NPh)\}^{3+}$ and $\{Re(NPhF)\}^{3+}$ cores. The resulting neutral complexes with the pentadentate ligand $\{L^{1EtEt}\}^{3-}$ are shown in Scheme 6.5. For a potential use in nuclear medicine, it is favourable to start from a $Na[^{99m}TcO_4]$. Hence, $[ReO(L^{1EtEt})]$ was synthesised from $Na[ReO_4]$ using $SnCl_2 \cdot 2\,H_2O$ as a reducing agent. $[Re(NPhR)(L^{1EtEt})]$ (R = H, F) complexes were obtained from $[Re(NPhR)Cl_3(PPh_3)_2]$ precursors and H_3L^{1EtEt} in boiling chloroform in the presence of NEt_3.

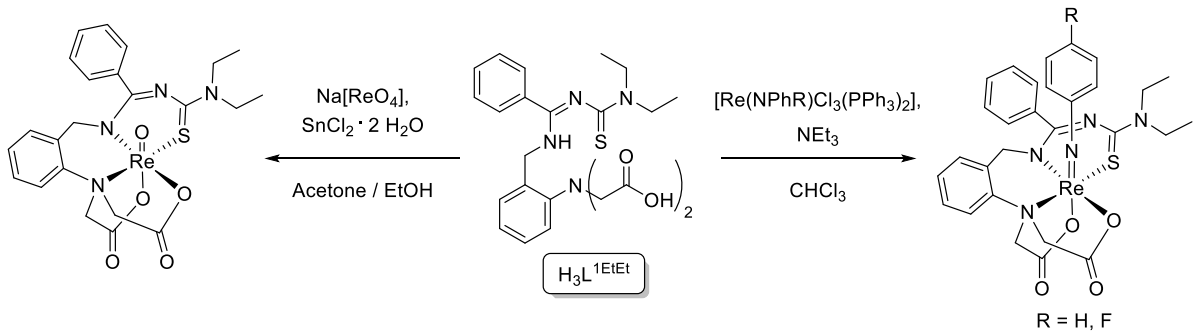

Scheme 6.5. Synthesis of $[ReO(L^{1EtEt})]$, $[Re(NPh)(L^{1EtEt})]$ and $[Re(NPhF)(L^{1EtEt})]$.

Oxidorhenium(V) complexes with the ligands KH_3L^{2EtEt}, KH_3L^{2MePh} and KH_3L^{2PhPh}, which contain an additional carboxylic group, were synthesised starting from $(NBu_4)[ReOCl_4]$ in boiling chloroform (Scheme 6.6). The coordination of the ligands to rhenium occurs *via* a SN_3 donor set leaving the

terminal carboxylic group available for further couplings. The substituents at the nitrogen atoms have no influence on the coordination mode. KH_3L^{2EtEt} and KH_3L^{2MePh} were also reacted with $Na[^{99m}TcO_4]$ and $SnCl_2 \cdot 2\,H_2O$ as a reducing agent. The resulting $[^{99m}TcO(HL^{2EtEt})]$ complex was obtained with a radiochemical purity of 91 %.

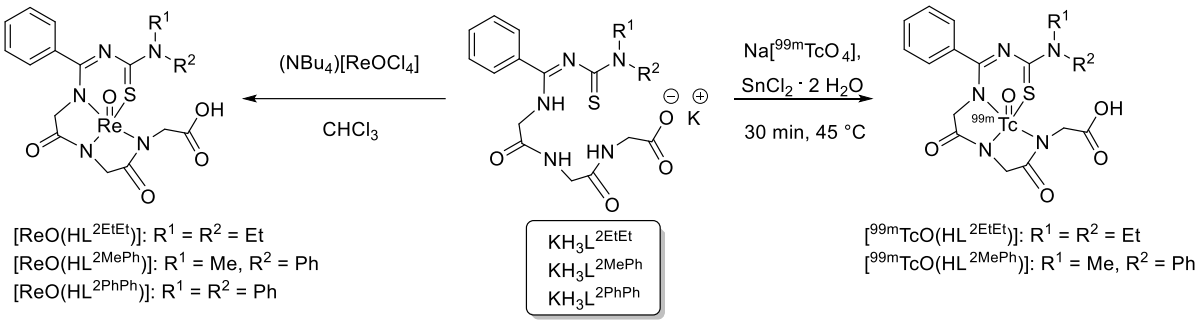

Scheme 6.6. Synthesis of $[ReO(HL^{2RR'})]$ and $[^{99m}TcO(HL^{2RR'})]$ complexes.

The terminal carboxylic groups of the tetradentate ligands KH_3L^{2EtEt} and KH_3L^{2MePh} were used for the bioconjugation of a synthesised prostate-specific membrane-antigen derivative. The idea for a potential ^{99m}Tc-based tracer was taken from the already established ^{68}Ga-PSMA-617 tracer. The resulting conjugates H_3P^{EtEt} and H_3P^{MePh} were synthesised in a multi-step synthesis on a Fmoc-Lys(Mtt)-Wang resin. Both conjugates were purified by preparative HPLC and analysed by ESI MS. After reactions with $(NBu_4)[ReOCl_4]$, also ^{99m}Tc experiments were performed (Scheme 6.7). $[^{99m}TcO(P^{EtEt})]$ was obtained in a radiochemical purity of 98 % after 15 min at 80 °C and was stable in a PBS buffer at room temperature under air over 3 h.

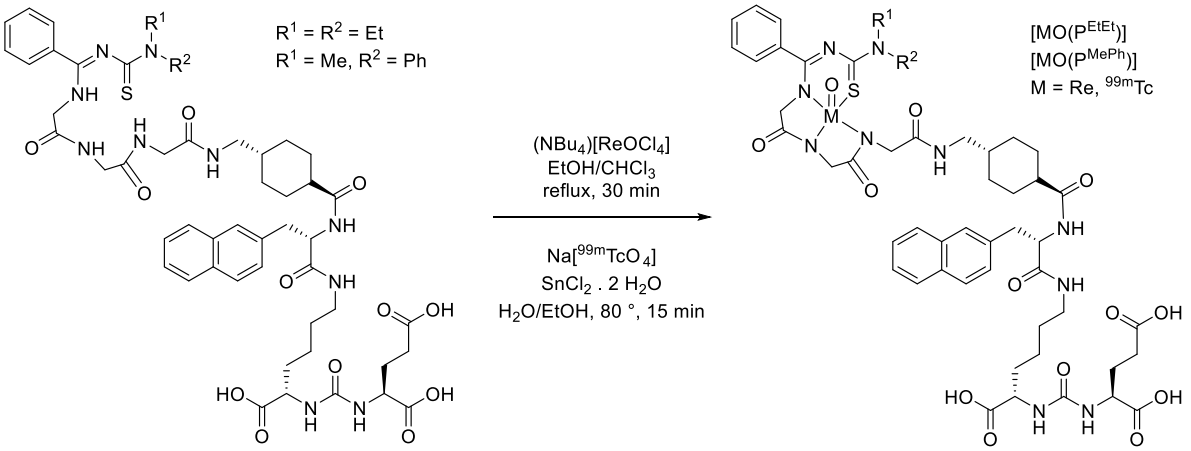

Scheme 6.7. Synthesis of $[ReO(P^{RR'})]$ and $[^{99m}TcO(P^{RR'})]$ complexes.

In vivo experiments with $[^{99m}TcO(P^{EtEt})]$ show the typical behaviour of a lipophilic compound. SPECT/CT scans exhibit that most of the compound was excreted through the liver into the intestines. High

uptake was obtained in the kidney and gall bladder. No tumor uptake was observed during the scan. However, no pertechnetate is released from the chelator demonstrating the *in vivo* stability of the ^{99m}Tc complex with the thiourea ligand $\{L^{2EtEt}\}^{3-}$.

KH_3L^{2EtEt} was elongated by a Boc-protected ethylene diamine forming after deprotection $\{H_4L^{3EtEt}\}(CF_3COO)$ and provides a free N-terminus for bioconjugation. After the reaction with $(NBu_4)[ReOCl_4]$ in MeOH *via* the intermediate ethylene glycol rhenium complex, the Boc-protected ligand was also labelled with ^{99m}Tc (Scheme 6.8). A radiochemical purity of 75 % after 30 min at 75 °C was reached.

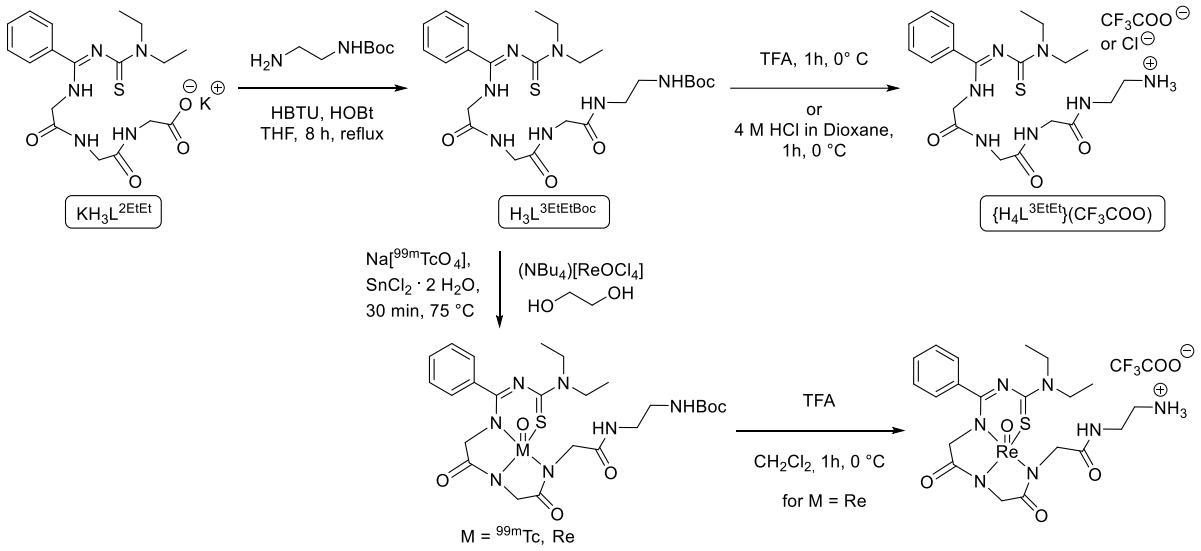

Scheme 6.8. Synthesis of $\{H_4L^{3EtEt}\}(CF_3COO)$ and its rhenium and ^{99m}Tc complexes.

The ligand was coupled *via* the N-terminus to a bisphosphonate residue and reacted with $Na[^{99m}TcO_4]$ in the presence of a kit, which includes tartaric acid, sodium tartrate dihydrate, $SnCl_2 \cdot 2\ H_2O$ and lactose monohydrate (Scheme 6.9). A radiochemical purity of 64 % was reached determined by TLC in H_2O under harsh reaction conditions.

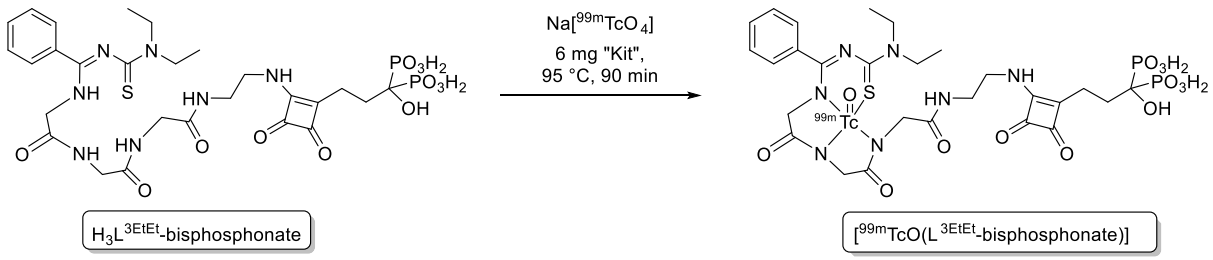

Scheme 6.9. Synthesis of $[^{99m}TcO(L^{3EtEt}$-bisphosphonate)] complex.

Zusammenfassung

Die Doktorarbeit beschreibt die Synthesen und Charakterisierung von Metallkomplexen mit dem sogenannten „Kläui Liganden“, sowie mit vier- und fünfzähnigen Thioharnstoff Derivaten. Der Fokus der Arbeit ist auf potenzielle Anwendungen der Metallkomplexe in der Nuklearmedizin ausgerichtet. Nuklide verschiedener Metalle wie Technetium, Rhenium, Gallium, Indium und Lutetium werden hier in der Diagnostik (^{99m}Tc und ^{68}Ga) und in der Radiotherapie (^{111}In und ^{177}Lu) verwendet.

Die organischen Liganden aus Schema 6.1 wurden in der vorliegenden Arbeit verwendet. Dabei wurden Carbonsäuren und Aminogruppen für eine potenzielle Biokonjugation in die Ligandsysteme eingeführt. Diese funktionellen Gruppen sind farblich hervorgehoben.

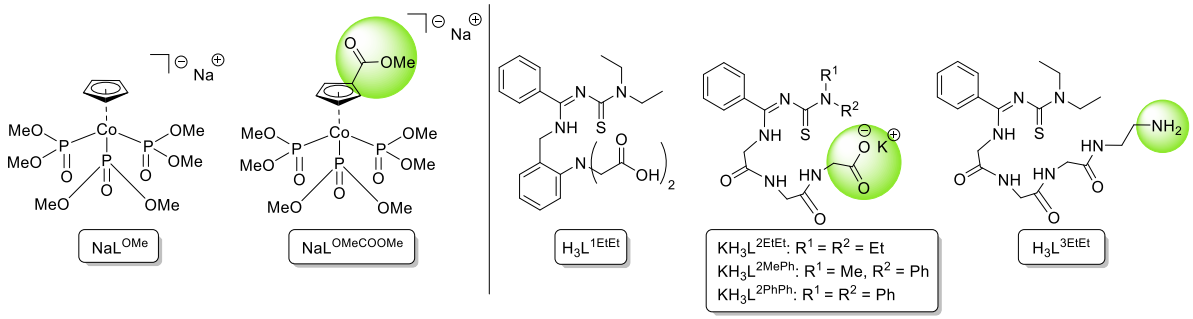

Schema 6.1. Liganden, die in der Doktorarbeit verwendet worden sind. Die funktionellen Gruppen für eine Biokonjugation sind farblich hervorgehoben.

Der tripodale „Kläui Ligand“ NaL^{OMe} koordiniert Technetium in sieben verschiedenen Oxidationsstufen des Metalls (Schema 6.2). Die oktaedrische Koordinationssphäre von Technetium wurde mit Nitrido-, Oxido-, Nitrosyl-, Chlorido- oder Triphenylphosphan-Liganden vervollständigt. In allen Fällen entstanden neutrale Komplexe. Die Komplexe sind luft- und wasserstabil, was für nuklearmedizinische Anwendungen Voraussetzung ist. Die erhaltenen Komplexe sind vollständig mit Hilfe von NMR- oder EPR- und IR-Spektroskopie charakterisiert und ihre Strukturen wurden kristallographisch bestimmt. Die Bindungssituation im „Kläui Ligand“ ist dabei nahezu unbeeinflusst von der restlichen Koordinationsumgebung oder der Oxidationsstufe. Modifikationen der Bindungslängen wurden nur für die Nitrido-Komplexe erhalten, wobei ein signifikanter *trans*-Einfluss der „N^{3-}“-Liganden beobachtet werden konnte.

Neben den Technetiumkomplexen mit NaL^{OMe} wurden auch Rheniumkomplexe mit diesem Liganden synthetisiert (Schema 6.3). Dies beinhaltet die Struktureinheiten $\{Re^{I}(CO)_3\}^+$, $\{Re^{V}OCl_2\}^+$, $\{Re^{V}NCl(PPh_3)\}^+$, $\{Re^{VI}NCl_2\}^+$ und $\{Re^{VII}O_3\}^+$. Die erhaltenen neutralen, luft- und wasserstabilen Komplexe wurden vollständig charakterisiert und weisen die gleichen Strukturmerkmale wie die entsprechenden Technetiumkomplexe auf. Die Reihe von ^{99}Tc- und Re-Komplexen bietet eine gute

Grundlage für Reaktionen mit dem metastabilen ^{99m}Tc. Einschränkungen bezüglich der Oxidationsstufe spielen keine bedeutende Rolle mehr in der Synthese von geeigneten Biokonjugaten.

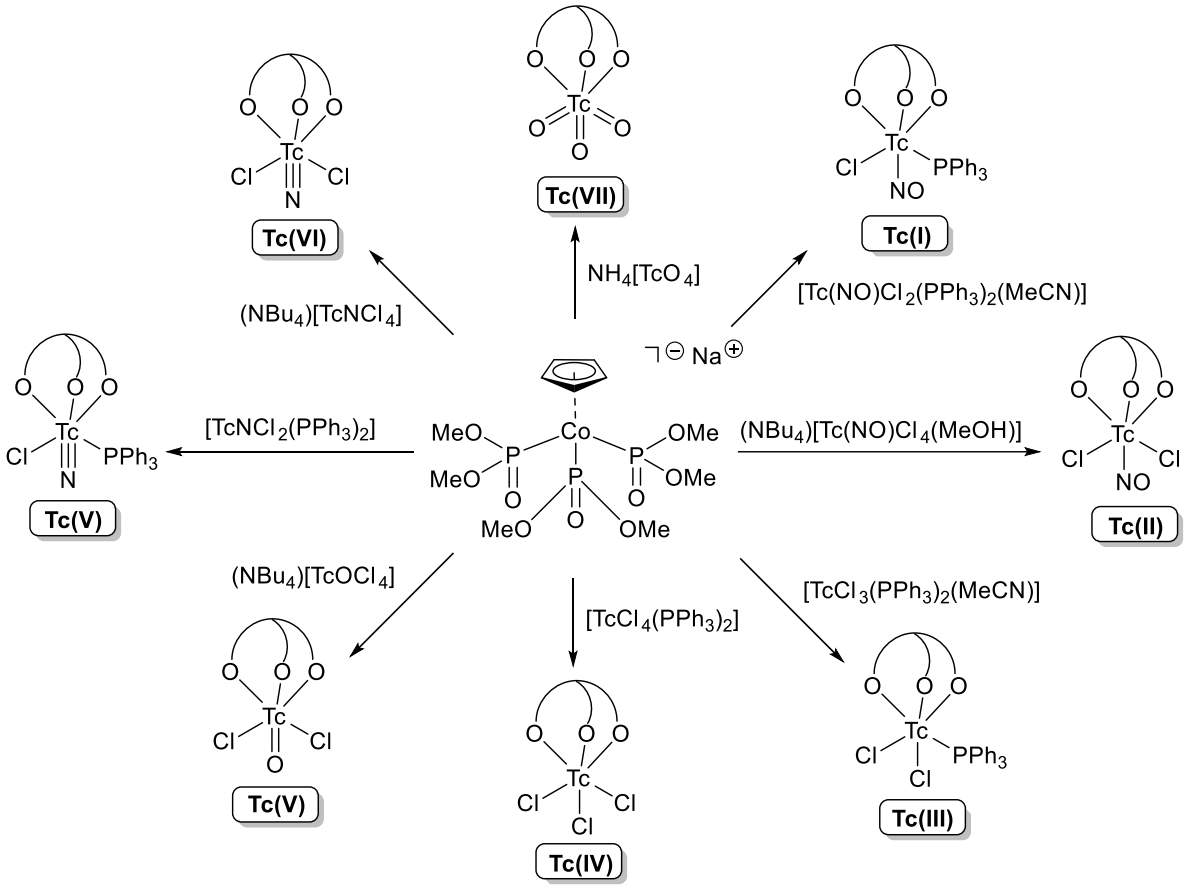

Schema 6.2. Übersicht über die synthetisierten Technetiumkomplexe mit NaL^{OMe}.[54]

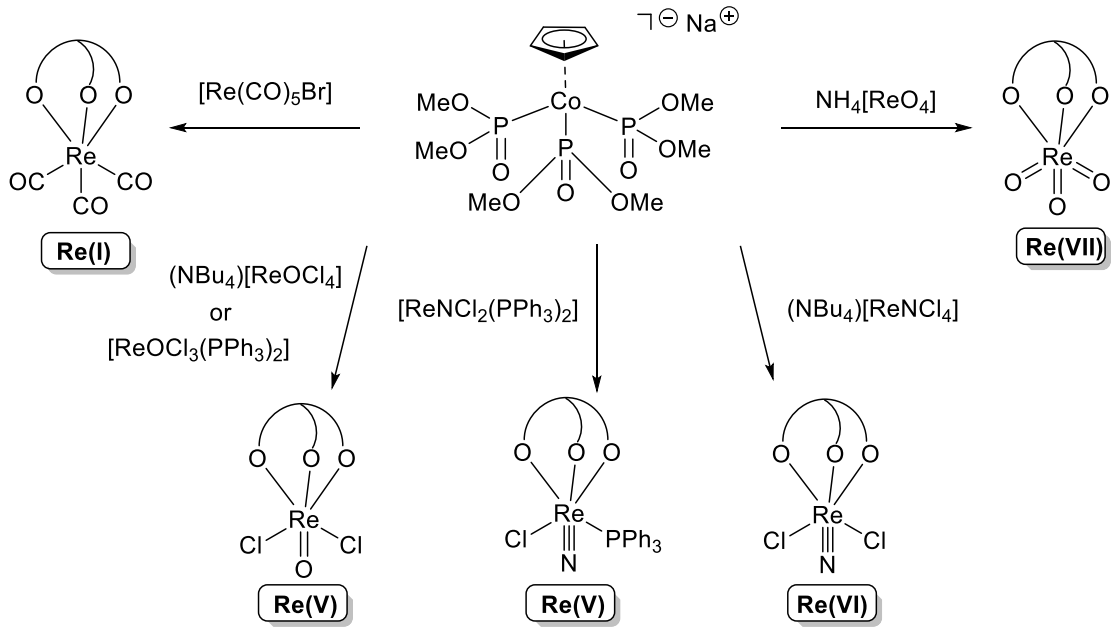

Schema 6.3. Übersicht über die synthetisierten Rheniumkomplexe mit NaL^{OMe}.

Des weiteren wurden die Komplexe $[Ga(L^{OMe})_2]NO_3$, $[In(L^{OMe})_2]NO_3$ und $[Lu(L^{OMe})_2(NO_3)]$ ausgehend von den entsprechenden Metallnitraten und zwei Äquivalenten NaL^{OMe} synthetisiert. Die positiv geladenen Ga^{3+} und In^{3+} Komplexe zeigen eine oktaedrische Anordnung der Donoratome, während Lu^{3+} einen neutralen Komplex mit einer Koordinationszahl von 8 bildet.

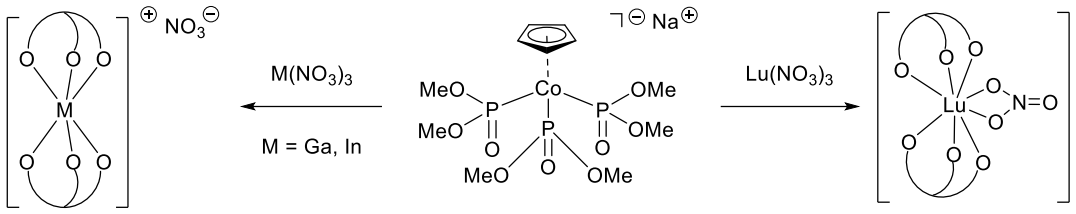

Schema 6.4. Synthesen von $[Ga(L^{OMe})_2]NO_3$, $[In(L^{OMe})_2]NO_3$ und $[Lu(L^{OMe})_2(NO_3)]$.

Modifikationen am Cp-Ring von NaL^{OMe} bieten eine Möglichkeit für eine Biokonjugation. $[Tc^{VII}O_3(L^{OMeCOOMe})]$ wurde synthetisiert und mit Hilfe von ^{99}Tc NMR-Spektroskopie charakterisiert.

Vier- und fünfzähnige Thioharnstoff-Liganden wurden in mehrstufigen Synthesen hergestellt und zu entsprechenden $\{ReO\}^{3+}$-, $\{Re(NPh)\}^{3+}$- und $\{Re(NPhF)\}^{3+}$-Komplexen umgesetzt. Die entstanden, neutralen Komplexe mit dem fünfzähnigen Liganden $\{L^{1EtEt}\}^{3-}$ sind in Schema 6.5 dargestellt. Für eine potenzielle Anwendung in der Nuklearmedizin ist eine Reaktion ausgehend von $Na[^{99m}TcO]$ unumgänglich. Deshalb wurde $[ReO(L^{1EtEt})]$ ausgehend von $Na[ReO_4]$ mit Hilfe des Reduktionsmittels $SnCl_2 \cdot 2\ H_2O$ durchgeführt. Die $[Re(NPhR)](L^{1EtEt})]$ Komplexe (R = H, R) wurden aus Reaktionen von $[Re(NPhR)Cl_3(PPh_3)_2]$ und H_3L^{1EtEt} in siedendem Chloroform in Anwesenheit von NEt_3 isoliert.

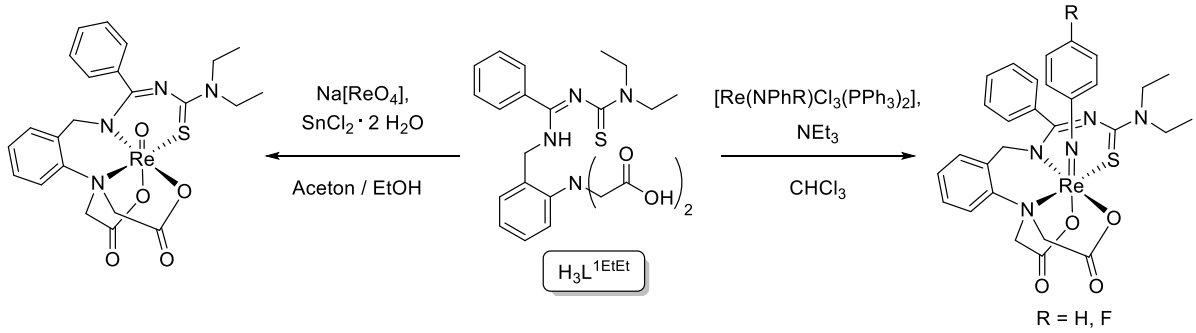

Schema 6.5. Synthese von $[ReO(L^{1EtEt})]$, $[Re(NPh)(L^{1EtEt})]$ und $[Re(NPhF)(L^{1EtEt})]$.

Oxidorhenium(V)-Komplexe mit den Liganden KH_3L^{2EtEt}, KH_3L^{2MePh} and KH_3L^{2PhPh}, die über eine zusätzliche Carbonylgruppe verfügen, wurden ausgehend von $(NBu_4)[ReOCl_4]$ in siedenden Chloroform synthetisiert (Schema 6.6). Die Koordination von Rhenium erfolgt über die SN_3-Donoratomen, sodass die Carbonsäure für eine Biokonjugation verfügbar bleibt. KH_3L^{2EtEt} und KH_3L^{2MePh} wurden mit

$Na[^{99m}TcO_4]$ und $SnCl_2 \cdot 2\ H_2O$ umgesetzt. Der Komplex $[^{99m}TcO(L^{2EtEt})]$ wurde mit einer radiochemischen Reinheit von 91 % erhalten.

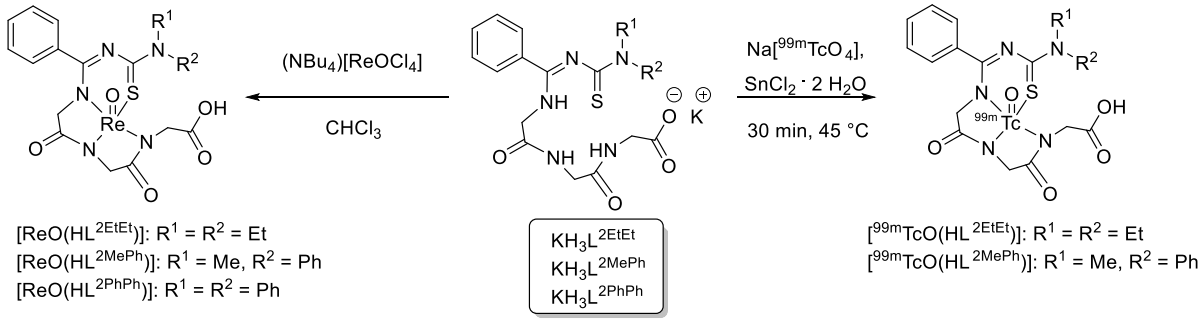

Schema 6.6. Synthese von $[ReO(HL^{2RR'})]$- und $[^{99m}TcO(HL^{2RR'})]$-Komplexen.

Die freie Carbonsäure der Liganden KH_3L^{2EtEt} und KH_3L^{2MePh} wurden zur Biokonjugation eines prostataspezifischen Membran-Antigen-Derivats verwendet. Die Grundidee dieses potenziellen ^{99m}Tc-Tracers basiert auf dem bereits etablierten ^{68}Ga-PSMA-61-Derivat. Die Konjugate H_3P^{EtEt} und H_3P^{MePh} wurden in einer mehrstufigen Synthese ausgehend von einem Fmoc-Lys(Mtt)-Wang-Harz erhalten. Die beiden Konjugate wurden mittels präparativer HPLC aufgereinigt und per ESI MS analysiert. Neben Reaktionen mit $(NBu_4)[ReOCl_4]$ wurden auch ^{99m}Tc Versuche durchgeführt (Schema 6.7). $[^{99m}TcO(P^{EtEt})]$ wurde mit einer radiochemischen Reinheit von 98 % nach 15 min bei 80 °C erhalten und war über 3 h in einem PBS Puffer bei Raumtemperatur an der Luft stabil.

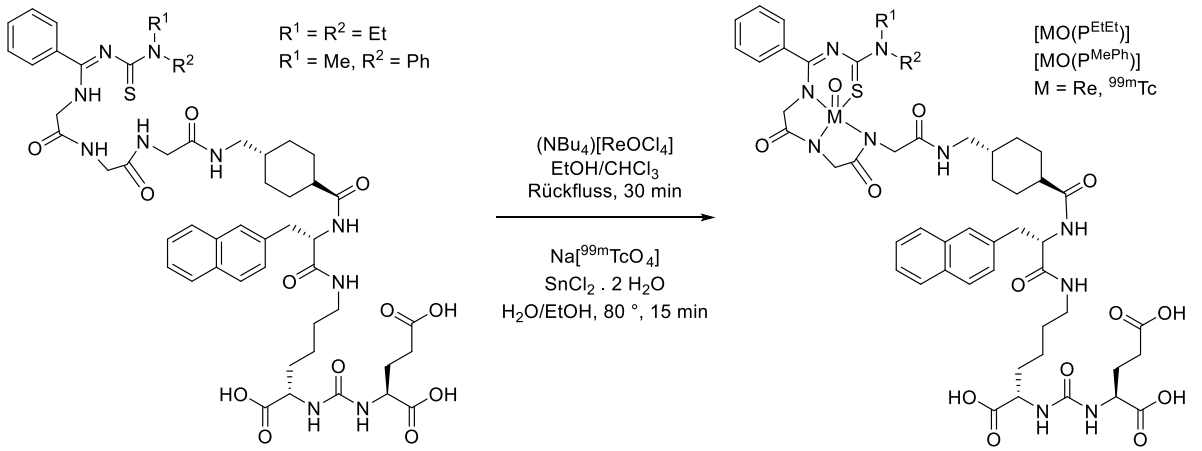

Schema 6.7. Synthese von $[ReO(P^{RR'})]$ und $[^{99m}TcO(P^{RR'})]$ Komplexen.

In vivo Experimente mit $[^{99m}TcO(P^{EtEt})]$ zeigen das typische Verhalten einer lipophilen Verbindung. SPECT/CT Scans zeigen, dass ein Großteil der Verbindung über die Leber und den Magen-Darm-Trakt

ausgeschieden wird. Eine höhe Anreicherung war in der Niere und Gallenblase zu beobachten. Es wurde keine Anreicherung im Tumor während des Scans detektiert. Da keine Rückbildung von Pertechnetat beobachten werden konnte, kann davon ausgegangen werden, dass das ^{99m}Tc-Konjugat *in vivo* stabil ist.

KH_3L^{2EtEt} wurde um eine Boc-geschützte Ethylendiamin-Einheit verlängert. Nach der Entschützung steht der freie N-Terminus für eine Biokonjugation zur Verfügung. Es wurden Reaktionen des geschützten Liganden $H_3L^{3EtEtBoc}$ mit $(NBu_4)[ReOCl_4]$ und $Na[^{99m}TcO_4]$ durchgeführt (Schema 6.8). Eine radiochemische Reinheit von 75 % wurde nach 30 min bei 75 ° für die entsprechende Reaktion mit Technetium erhalten.

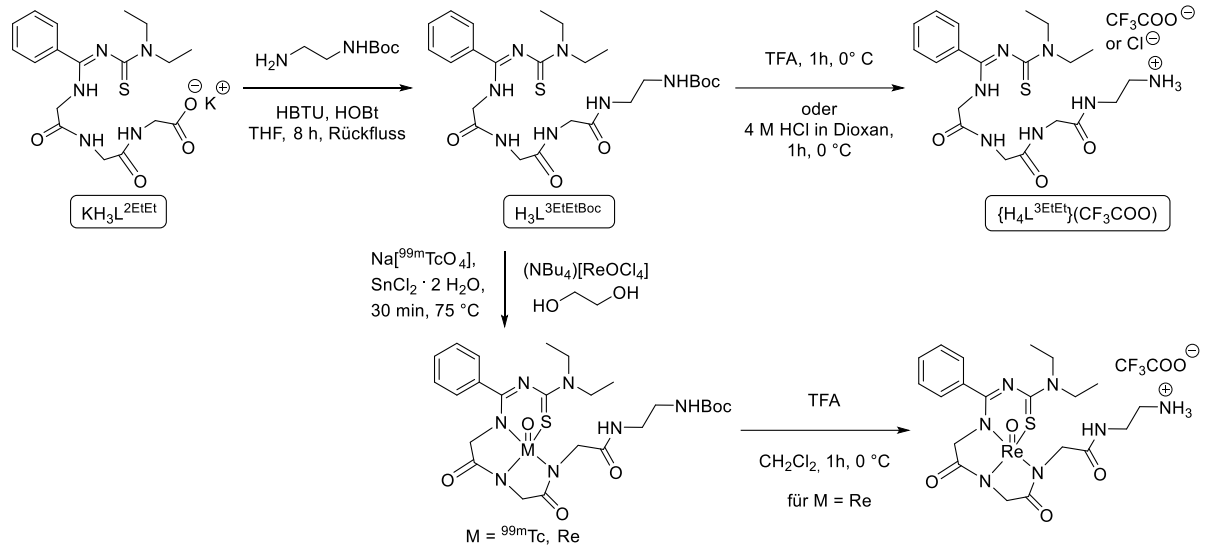

Schema 6.8. Synthese von $\{H_4L^{3EtEt}\}(CF_3COO)$ und dessen Rhenium- und ^{99m}Tc-Komplexe.

Der entschützte Ligand wurde über seinen N-Terminus an ein Bisphosphonat gekoppelt. Das Konjugat wurde mit $Na[^{99m}TcO_4]$ in Anwesenheit eines Kits, der Weinsäure, Natriumtartrat-Dihydrat, $SnCl_2 \cdot 2\ H_2O$ und Lactosemonohydrat enthielt, umgesetzt (Schema 6.9). Das Produkt entstand in einer radiochemischen Reinheit von 64 %.

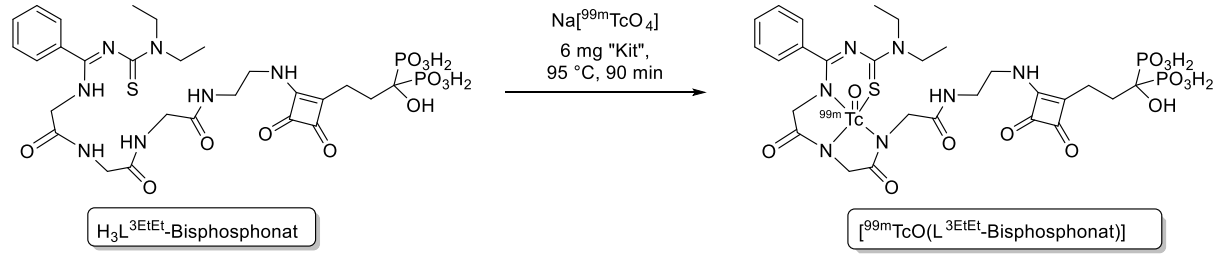

Scheme 6.9. Synthese eines $[^{99m}TcO(L^{3EtEt}$-Bisphosphonat$)]$-Komplexes.

7 References

[1] Deng, X.; Rong, J.; Wang, L.; Vasdev, N.; Zhang, L.; Josephson, L.; Liang, S. H. *Chemistry for Positron Emission Tomography: Recent Advances in (^{11})C-, (^{18})F-, (^{13})N-, and (^{15})O-Labeling Reactions, Angew. Chem. Int. Ed. Engl.* **2019**, *58*, 2580-2605.

[2] Fu, H.; Chen, Z.; Josephson, L.; Li, Z.; Liang, S. H. *Positron Emission Tomography (PET) Ligand Development for Ionotropic Glutamate Receptors: Challenges and Opportunities for Radiotracer Targeting N-Methyl-d-aspartate (NMDA), alpha-Amino-3-hydroxy-5-methyl-4-isoxazolepropionic Acid (AMPA), and Kainate Receptors, J. Med. Chem.* **2019**, *62*, 403-419.

[3] Jacobson, O.; Kiesewetter, D. O.; Chen, X. *Fluorine-18 radiochemistry, labeling strategies and synthetic routes, Bioconjug. Chem.* **2015**, *26*, 1-18.

[4] Kuntic, V.; Brboric, J.; Vujic, Z.; Uskokovic-Markovic, S. *Radioisotopes Used as Radiotracers for in vitro and in vivo Diagnostics, Asian J. Chem.* **2016**, *28*, 235-241.

[5] Bartholomä, M. D.; Louie, A. S.; Valliant, J. F.; Zubieta, J. *Technetium and gallium derived radiopharmaceuticals: comparing and contrasting the chemistry of two important radiometals for the molecular imaging era, Chem. Rev.* **2010**, *110*, 2903-2920.

[6] Papagiannopoulou, D. *Technetium-99m radiochemistry for pharmaceutical applications, J. Labelled Comp. Radiopharm.* **2017**, *60*, 502-520.

[7] Abram, U.; Alberto, R. *Technetium and rhenium: coordination chemistry and nuclear medical applications, J. Braz. Chem. Soc.* **2006**, *17*, 1486-1500.

[8] World Nuclear association. Radioisotopes in Medicine; https://www.world-nuclear.org/information-library/non-power-nuclear-applications/radioisotopes-research/radioisotopes-in-medicine.aspx (updated May 2020).

[9] Bubeck, B.; Brandau, W.; Weber, E.; Kälble, T.; Parekh, N.; Georgi, P. *Pharmacokinetics of technetium-99m-MAG3 in humans, J. Nucl. Med.* **1990**, *31*, 1285-1293.

[10] Dougall, N. J.; Bruggink, S.; Ebmeier, K. P. *Database of Abstracts of Reviews of Effects (DARE): Quality-assessed Reviews*, Centre for Reviews and Dissemination (UK) **2004**.

[11] Champailler, A.; Gremillet, E.; Decousus, M.; Kassir, A.; Voutay, M.; Healy, J. C. *Plasma transport of ^{99m}Tc-p-butyl-IDA, Eur. J. Nucl. Med.* **1985**, *10*, 437-440.

[12] https://www.who.int/news-room/fact-sheets/detail/cancer (26.11.2020).

[13] Zippel, C.; Ronski, S. C.; Bohnet-Joschko, S.; Giesel, F. L.; Kopka, K. *Current Status of PSMA-Radiotracers for Prostate Cancer: Data Analysis of Prospective Trials Listed on ClinicalTrials.gov, Pharmaceuticals (Basel)* **2020**, *13*, 1-13.

[14] Eder, M.; Schäfer, M.; Bauder-Wüst, U.; Hull, W. E.; Wangler, C.; Mier, W.; Haberkorn, U.; Eisenhut, M. *^{68}Ga-complex lipophilicity and the targeting property of a urea-based PSMA inhibitor for PET imaging, Bioconjug. Chem.* **2012**, *23*, 688-697.

[15] Benešová, M.; Bauder-Wüst, U.; Schäfer, M.; Klika, K. D.; Mier, W.; Haberkorn, U.; Kopka, K.; Eder, M. *Linker Modification Strategies To Control the Prostate-Specific Membrane Antigen (PSMA)-Targeting and Pharmacokinetic Properties of DOTA-Conjugated PSMA Inhibitors, J. Med. Chem.* **2016**, *59*, 1761-1775.

[16] Afshar-Oromieh, A.; Hetzheim, H.; Kratochwil, C.; Benešová, M.; Eder, M.; Neels, O. C.; Eisenhut, M.; Kubler, W.; Holland-Letz, T.; Giesel, F. L.; Mier, W.; Kopka, K.; Haberkorn, U. *The Theranostic PSMA Ligand PSMA-617 in the Diagnosis of Prostate Cancer by PET/CT: Biodistribution in Humans, Radiation Dosimetry, and First Evaluation of Tumor Lesions, J. Nucl. Med.* **2015**, *56*, 1697-1705.

[17] Benešová, M.; Schäfer, M.; Bauder-Wüst, U.; Afshar-Oromieh, A.; Kratochwil, C.; Mier, W.; Haberkorn, U.; Kopka, K.; Eder, M. *Preclinical Evaluation of a Tailor-Made DOTA-Conjugated PSMA Inhibitor with Optimized Linker Moiety for Imaging and Endoradiotherapy of Prostate Cancer, J. Nucl. Med.* **2015**, *56*, 914-920.

[18] Wester, D. W.; Coveney, J. R.; Nosco, D. L.; Robbins, M. S.; Dean, R. T. *Synthesis, characterization and myocardial uptake of cationic bis(arene)technetium(I) complexes, J. Med. Chem.* **1991**, *34*, 3284-3290.

[19] Benz, M.; Braband, H.; Schmutz, P.; Halter, J.; Alberto, R. *From Tc(VII) to Tc(I); facile syntheses of bis-arene complexes $[^{99(m)}Tc(arene)_2]^+$ from pertechnetate, Chem. Sci.* **2015**, *6*, 165-169.

[20] Meola, G.; Braband, H.; Jordi, S.; Fox, T.; Blacque, O.; Spingler, B.; Alberto, R. *Structure and reactivities of rhenium and technetium bis-arene sandwich complexes $[M(\eta^6\text{-arene})_2]^+$, Dalton Trans.* **2017**, *46*, 14631-14637.

[21] Hernández-Valdés, D.; Meola, G.; Braband, H.; Spingler, B.; Alberto, R. *Direct Synthesis of Non-Alkyl Functionalized Bis-Arene Complexes of Rhenium and $^{99(m)}$Technetium, Organometallics* **2018**, *37*, 2910-2916.

[22] Nadeem, Q.; Meola, G.; Braband, H.; Bolliger, R.; Blacque, O.; Hernandez-Valdes, D.; Alberto, R. *To Sandwich Technetium: Highly Functionalized Bis-Arene Complexes $[^{(99m)}Tc(\eta^6\text{-arene})_2]^+$ Directly from Water and $[^{(99m)}TcO_4]^-$, Angew. Chem. Int. Ed. Engl.* **2020**, *59*, 1197-1200.

[23] Alberto, R.; Schibli, R.; Egli, A.; Abram, U.; Abram, S.; Kaden, T. A.; August Schubiger, P. *Steps towards $[(C_5Me_5)TcO_3]$: Novel synthesis of $[(C_5Me_5)Tc(CO)_3]$ from $[\{Tc(\mu_3\text{–}OH)(CO)_3\}_4]$ and oxidation of $[(C_5Me_5)M(CO)_3]$ (M = Tc, Re) with Br_2, Polyhedron* **1998**, *17*, 1133-1140.

[24] Bernard, J.; Ortner, K.; Spingler, B.; Pietzsch, H. J.; Alberto, R. *Aqueous synthesis of derivatized cyclopentadienyl complexes of technetium and rhenium directed toward radiopharmaceutical application, Inorg. Chem.* **2003**, *42*, 1014-1022.

[25] Zobi, F.; Spingler, B.; Alberto, R. *Syntheses, Structures and Reactivities of $[CpTc(CO)_3X]^+$ and $[CpRe(CO)_3X]^+$, Eur. J. Inorg. Chem.* **2008**, *2008*, 4205-4214.

[26] Wald, J.; Alberto, R.; Ortner, K.; Candreia, L. *Aqueous One-Pot Synthesis of Derivatized Cyclopentadienyl-Tricarbonyl Complexes of ^{99m}Tc with an In Situ CO Source: Application to a Serotonergic Receptor Ligand, Angew. Chem. Int. Ed.* **2001**, *40*, 3062-3066.

[27] Peindy N'Dongo, H. W.; Liu, Y.; Can, D.; Schmutz, P.; Spingler, B.; Alberto, R. *Aqueous syntheses of [(Cp-R)M(CO)$_3$] type complexes (Cp = cyclopentadienyl, M = Mn, ^{99m}Tc, Re) with bioactive functionalities, J. Organomet. Chem.* **2009**, *694*, 981-987.

[28] Morais, G. R.; Paulo, A.; Santos, I. *Organometallic Complexes for SPECT Imaging and/or Radionuclide Therapy, Organometallics* **2012**, *31*, 5693-5714.

[29] Frei, A.; Spingler, B.; Alberto, R. *Multifunctional Cyclopentadienes as a Scaffold for Combinatorial Bioorganometallics in $[(\eta^5\text{-}C_5H_2R_1R_2R_3)M(CO)_3]$ (M = Re, $^{(99m)}Tc$) Piano-Stool Complexes, Chem. Eur. J.* **2018**, *24*, 10156 –10164.

[30] Masi, S.; Top, S.; Boubekeur, L.; Jaouen, G.; Mundwiler, S.; Spingler, B.; Alberto, R. *Direct Synthesis of Tricarbonyl(cyclopentadienyl)rhenium and Tricarbonyl(cyclopentadienyl)-technetium Units from Ferrocenyl Moieties− Preparation of 17α-Ethynylestradiol Derivatives Bearing a Tricarbonyl(cyclopentadienyl)technetium Group, Eur. J. Inorg. Chem.* **2004**, *2004*, 2013-2017.

[31] Ackermann, J.; Hagenbach, A.; Abram, U. *$\{Tc(NO)(Cp)(PPh_3)\}^+$ - a novel technetium(I) core, Chem. Commun.* **2016**, *52*, 10285-10288.

[32] Ackermann, J.; Abdulkader, A.; Scholtysik, C.; Jungfer, M. R.; Hagenbach, A.; Abram, U. *$[Tc^I(NO)X(Cp)(PPh_3)]$ Complexes ($X^- = I^-, I_3^-, SCN^-, CF_3SO_3^-$, or CF_3COO^-) and Their Reactions, Organometallics* **2019**, *38*, 4471-4478.

[33] *Alberto, R. Technetium in Comprehensive Coordination Chemistry II; McCleverty, J. A., Mayer, T. J., Eds.; Elsevier: Amsterdam, The Netherlands, **2003**, 5, 127−268, and references cited therein*.

[34] *Sattelberger, A. P.; Scott, B. L.; Poineau, F. Technetium Organometallics in Comprehensive Organometallic Chemistry III; Mingos, D. M. P., Crabtree, R. H., Eds.; Elsevier: **2007**; 833−854, and references cited therein*.

[35] Joachim, J. E.; Apostolidis, C.; Kanellakopulos, B.; Maier, R.; Ziegler, M. L. *Synthese, Charakterisierung und Untersuchung der Verbindungen Hydrotris(1-pyrazolyl)borato-technetium(VII)- trioxid und Hydrotris (3,5-dimethyl-1-pyrazolyl)borato-technetium(VII)trioxid,*

LX. Mitteilung / Synthesis, Characterization and Investigation of Hydrotris(1-pyrazolyl)borato-technetium(VII) Trioxide and Hydrotris(3,5-dimethyl-1-pyrazolyl)borato-technetium(VII) Trioxide, Z. Naturforsch. B **1993**, *48*, 227-229.

[36] Braband, H.; Abram, U. *Technetium complexes with triazacyclononane, Inorg. Chem.* **2006**, *45*, 6589-6591.

[37] Braband, H.; Tooyama, Y.; Fox, T.; Alberto, R., *Syntheses of high-valent fac-[$^{99m}TcO_3$]$^+$ complexes and [3+2] cycloadditions with alkenes in water as a direct labelling strategy,* **2009**, *15*, 633-638.

[38] Braband, H.; Tooyama, Y.; Fox, T.; Simms, R.; Forbes, J.; Valliant, J. F.; Alberto, R. *Fac-[TcO_3(tacn)]$^+$: a versatile precursor for the labelling of pharmacophores, amino acids and carbohydrates through a new ligand-centred labelling strategy,* **2011**, *17*, 12967-12974.

[39] Braband, H.; Imstepf, S.; Benz, M.; Spingler, B.; Alberto, R. *Combining bifunctional chelator with (3+2)-cycloaddition approaches: synthesis of dual-function technetium complexes, Inorg. Chem.* **2012**, *51*, 4051-4057.

[40] Wuillemin, M. A.; Stuber, W. T.; Fox, T.; Reber, M. J.; Brühwiler, D.; Alberto, R.; Braband, H. *A novel ^{99m}Tc labelling strategy for the development of silica based particles for medical applications,* **2014**, *43*, 4260-4263.

[41] Dyckhoff, B.; Schulte, H.-J.; Englert, U.; Spaniol, T. P.; Kläui, W.; Schubiger, P. A. *Rhenium-Komplexe von Sauerstoffchelatliganden: Ein Weg zu neuen Radiopharmaka?, Z. Anorg. Allg. Chem.* **1992**, *614*, 131-141.

[42] Thomas, J. A.; Davison, A. *Technetium complexes of tripodal oxygen donor ligands, Inorg. Chem.* **1992**, *31*, 1976-1978.

[43] Kramer, D. J.; Davison, A.; Jones, A. G. *Structural models for [$M(CO)_3(H_2O)_3$]$^+$ (M = Tc, Re): fully aqueous synthesis of technetium and rhenium tricarbonyl complexes of tripodal oxygen donor ligands, Inorg. Chim. Acta* **2001**, *312*, 215-220.

[44] Banbery, H. J.; Hussain, W.; Evans, I. G.; Hamor, T. A.; Jones, C. J.; McCleverty, J. A.; Schulte, H.-J.; Engles, B.; Kläui, W. *The syntheses of high oxidation state metal complexes containing the tripodal ligand [(η^5-C_5H_5)Co{$P(OMe)_2(=O)$}$_3$]$^-$ and the X-ray crystal structure of [(η^5-C_5H_5)Co{$P(OMe)_2(=O)$}$_3$$ReO_3$], Polyhedron* **1990**, *9*, 2549-2551.

[45] Al-Harbi, A.; Sattler, W.; Sattler, A.; Parkin, G. *Synthesis and structural characterization of tris(2-oxo-1-tert-butylimidazolyl) and tris(2-oxo-1-methylbenzimidazolyl) hydroborato complexes: a new class of tripodal oxygen donor ligand, Chem. Commun.* **2011**, *47*, 3123-3125.

[46] Leung, W.-H.; Chan, E. Y. Y.; Lai, T. C. Y.; Wong, W.-T. *Synthesis and reactivity of nitrido-rhenium and -osmium complexes with an oxygen tripod ligand, J. Chem. Soc., Dalton Trans.* **2000**, 51-56.

[47] So, Y. M.; Chiu, W. H.; Cheung, W. M.; Ng, H. Y.; Lee, H. K.; Sung, H. H.; Williams, I. D.; Leung, W.-H. *Heterobimetallic rhenium nitrido complexes containing the Kläui tripodal ligand $[Co(\eta^5\text{-}C_5H_5)\{P(O)(OEt)_2\}_3]^-$, Dalton Trans.* **2015**, *44*, 5479-5487.

[48] Navon, G.; Kläui, W. *Cobalt-59 NMR of a cobalt(III) spin-crossover compound, Inorg. Chem.* **1984**, *23*, 2722-2725.

[49] Kläui, W.; Müller, A.; Eberspach, W.; Boese, R.; Goldberg, I. *Crystal structure and coordination chemistry of the pentane-soluble sodium salt of an oxygen tripod ligand, J. Am. Chem. Soc.* **1987**, *109*, 164-169.

[50] Kläui, W. *The Coordination Chemistry and Organometallic Chemistry of Tridentate Oxygen Ligands with π-Donor Properties, Angew. Chem. Int. Ed. Engl.* **1990**, *29*, 627-637.

[51] Leung, W.; Zhang, Q.; Yi, X. *Recent developments in the coordination and organometallic chemistry of Kläui oxygen tripodal ligands, Coord. Chem. Rev.* **2007**, *251*, 2266-2279.

[52] Kiplinger, J. L.; Scott, B. L.; Burns, C. J. *Actinide complexes with the Kläui tripodal oxygen ligand – crystal structure of $[\{\eta^4\text{-}C_5H_5(CH_2C(CH_3)_3)\}Co\{P(O)(OC_2H_5)_2\}_3]_2U$, Inorg. Chim. Acta* **2005**, *358*, 2813-2816.

[53] Davidson, K. A.; Kilpin, K. J.; Lloyd, N. C.; Nicholson, B. K. *A six-coordinate aryl-germanium complex formed by the Kläui ligand, J. Organomet. Chem.* **2007**, *692*, 1871-1874.

[54] Grunwald, A. C. ; Scholtysik, C.; Hagenbach, A.; Abram, U. *One Ligand, One Metal, Seven Oxidation States: Stable Technetium Complexes with the "Klaui Ligand", Inorg. Chem.* **2020**, *59*, 9396-9405.

[55] Sawallisch, T.; Abdulkader, A.; Abram, U. Unpublished results.

[56] Nicholson, T.; Chun, E.; Mahmood, A.; Müller, P.; Davison, A.; Jones, A. G. *Synthesis, spectroscopy and structural analysis of Technetium and Rhenium nitrosyl complexes, Commun. Inorg. Synth. **2015**, 3,* 31−39 and references cited therein.

[57] Nicholson, T.; Müller, P.; Davison, A.; Jones, A. G. *The synthesis and characterization of a cationic technetium nitrosyl complex: The X-ray crystal structure of $[TcCl(NO)(DPPE)_2](PF_6)\cdot CH_2Cl_2$, Inorg. Chim. Acta* **2006**, *359*, 1296-1298.

[58] Balasekaran, S. M.; Spandl, J.; Hagenbach, A.; Köhler, K.; Drees, M.; Abram, U. *Fluoridonitrosyl Complexes of Technetium(I) and Technetium(II). Synthesis, Characterization, Reactions, and DFT calculations, Inorg. Chem.,* **2014**, *53*, 5117-5128.

[59] Ackermann, J.; Hagenbach, A.; Abram, U. *Nitrosyltechnetium complexes with (2-aminomethylphenyl) diphenylphosphine, Inorg. Chim. Acta* **2014**, *419*, 59-65.

[60] Ackermann, J.; Noufele, C. N.; Hagenbach, A.; Abram, U. *Nitrosyltechnetium(I) Complexes with 2-(Diphenylphosphanyl)aniline, Z. Anorg. Allg. Chem.* **2019**, *645*, 8-13.

[61] Balasekaran, S.; Hagenbach, A.; Drees, M.; Abram, U. *[$Tc^{II}(NO)(trifluoroacetate)_4F]^{2-}$–synthesis and reactions, Dalton Trans.* **2017**, *46*, 13544-13552.

[62] Kirmse, R.; Lorenz, B.; Schmidt, K. *EPR on trichloro-nitrosyl-bis(dimethylphenylphosphine)-technetium(II) $TcCl_3(NO)(PMe_2Ph)_2$, Polyhedron* **1983**, *2*, 935-939.

[63] Wendlandt, D.; Bauche, J.; Luc, P. *Hyperfine structure in Tc^{I}: experiment and theory, J. Phys. B: Atom. Mol. Phys.* **1977**, *10*, 1989-2002.

[64] Abram, U.; Lorenz, B.; Kaden, L.; Scheller, D. *Nitrido complexes of technetium with tertiary phosphines and arsines, Polyhedron* **1988**, *7*, 285-289.

[65] Abram, U.; Abram, S.; Spies, H.; Kirmse, R.; Stach, J.; Köhler, K. *Zum Ligandenaustausch an $TcNX_4^-$Komplexen (X = Cl, Br), Z. Anorg. Allg. Chem.* **1987**, *544*, 167-180.

[66] Baldas, J.; Boas, J. F.; Bonnyman, J.; Williams, G. A. *Studies of technetium complexes. Part 6. The preparation, characterisation, and electron spin resonance spectra of salts of tetrachloro- and tetrabromo-nitridotechnetate(VI): crystal structure of tetraphenylarsonium tetrachloronitridotechnetate(VI), J. Chem. Soc., Dalton Trans.* **1984**, *1*, 2395-2400.

[67] Köhler, K.; Kirmse, R.; Abram, U. *Determination of Equilibrium Constants for Ligand Exchange Reactions of $(TcNX_4)^-$ (X: Cl, Br) by Means of EPR, Z. Anorg. Allg. Chem.* **1991**, *600*, 83-87.

[68] Baldas, J.; Boas, J. F.; Williams, G. A. *EPR studies of technetium complexes in frozen solution, J. Appl. Magn. Reson.* **1996**, *11*, 499-508.

[69] Baldas, J.; Boas, J. F.; Bonnyman, J. *Preparation and Properties of Nitridotechnetic(VI) Acid. I. Observation of the E.S.R.-Spectrum of the $[TcNF_4]^-$ Anion in Hydrofluoric Acid Solution, Aust. J. Chem.* **1989**, *42*.

[70] Balasekaran, S. M.; Hagenbach, A.; Abram, U. *Tetrafluoridonitridotechnetate(VI)–Reactions and Structures, Z. Anorg. Allg. Chem.* **2018**, *644*, 1158-1163.

[71] Abram, U.; Schmidt-Brücken, B.; Hagenbach, A.; Hecht, M.; Kirmse, R.; Voigt, A. *Reactions of Rhenium and Technetium Nitrido Complexes with ER_3 Fragments (E = B, Ga, Al, C, P; R = H, Alkyl, Aryl), Z. Anorg. Allg. Chem.* **2003**, *629*, 838-852.

[72] Hagenbach, A.; Abram, U. *Reactions of Nitridotechnetium(V) Complexes with Boranes, Z. Anorg. Allg. Chem.* **2005**, *631*, 2303-2305.

[73] Baldas, J.; Colmanet, S. F.; Ivanov, Z.; Williams, G. A. *Preparation and structure of $[\{Tc^{V}N(thiourea)\}_4(edta)_2] \cdot 6H_2O$: the first example of a cyclic nitrido-bridged tetrameric technetium complex, J. Chem. Soc., Chem. Commun.* **1994**, 2153-2154.

[74] Hagenbach, A.; Abram, U. *$[Tc(NBCl_2Ph)Cl_2(Me_2PhP)_3]$ und $[Tc(NBH_3)Cl_2(Me_2PhP)_3]$ - die ersten Technetium-Komplexe mit Nitridobrücken zwischen Technetium und Bor, Z. Anorg. Allg. Chem.* **2002**, *628*, 31-33.

[75] Thomas, J. A.; Davison, A. *High oxidation state technetium and rhenium complexes of hydrotris(1-pyrazolyl)borate, Inorg. Chim. Acta* **1991**, *190*, 231-235.

[76] Oehlke, E.; Alberto, R.; Abram, U. *Synthesis, characterization, and structures of R_3EOTcO_3 complexes (E= C, Si, Ge, Sn, Pb) and related compounds, Inorg. Chem.* **2010**, *49*, 3525-3530.

[77] Tooyama, Y.; Braband, H.; Spingler, B.; Abram, U.; Alberto, R. *High-Valent Technetium Complexes with the $[^{99}TcO_3]^+$ Core from in Situ Prepared Mixed Anhydrides of $[^{99}TcO_4]^-$ and Their Reactivities, Inorg. Chem.* **2008**, *47*, 257-264.

[78] Pearlstein, R. M.; Davison, A. *Alkene—glycol interconversion with technetium and rhenium oxo complexes, Polyhedron* **1988**, *7*, 1981-1989.

[79] Mikhalev, V. A. *^{99}Tc NMR Spectroscopy. Radiochemistry* ***2005***, *47*, 319−333.

[80] Harris, R. K. *NMR and the Periodic Table;* London Academic: **1978**.

[81] Kläui, W.; Okuda, J.; Scotti, M.; Valderrama, M. *Synthesis and characterization of manganese and rhenium tricarbonyl complexes with (O,O,O)-donor ligands, J. Organomet. Chem.* **1985**, *280*, C26-C30.

[82] Reger, D. L.; Ding, Y.; Rheingold, A. L.; Ostrander, R. L. *Reactions of $\{(C_5H_5)Co[P(O)(OC_2H_5)_2]_3\}^-$ with MCl_3 and $M(CH_3)Cl_2$ (M = Ga, In). Crystal and molecular structure of $[\{(C_5H_5)Co[P(O)(OC_2H_5)_2]_3\}_2Ga]Ga(CH_3)Cl_3$, Polyhedron* **1994**, *13*, 3053-3058.

[83] Englert, U.; Ganter, B.; Wagner, T.; Kläui, W. *Reversible Topotactic Hydration and Dehydration of an Europium Complex, Z. Anorg. Allg. Chem.* **1998**, *624*, 970-974.

[84] Hu, J. Y.; Ning, Y.; Meng, Y. S.; Zhang, J.; Wu, Z. Y.; Gao, S.; Zhang, J. L. *Highly near-IR emissive ytterbium(III) complexes with unprecedented quantum yields, Chem. Sci.* **2017**, *8*, 2702-2709.

[85] Ahrens, L. H. *The use of ionization potentials Part 1. Ionic radii of the elements, Geochimica et Cosmochimica Acta* **1952**, *2*, 155-169.

[86] Shannon, R. D. *Revised effective ionic radii and systematic studies of interatomic distances in halides and chalcogenides, Acta Crystallogr., Sect. A* **1976**, *32*, 751–767.

[87] Nguyen, H. H.; Pham, C. T.; Abram, U. *Rhenium and Technetium Complexes with Pentadentate Thiocarbamoylbenzamidines: Steps toward Bioconjugation, Inorg. Chem.* **2015**, *54*, 5949-5959.

[88] Nguyen, H. H.; Pham, C. T.; Abram, U. *Re^VO and Re^VNPh complexes with pentadentate benzamidines – Synthesis, structural characterization and DFT evaluation of isomeric complexes, Polyhedron* **2015**, *99*, 216-222.

[89] Hung Huy Nguyen, Doctoral Thesis, Freie Universität Berlin, **2009**.

[90] Scholtysik, C.; Njiki Noufele, C.; Hagenbach, A.; Abram, U. *Complexes of Technetium(V) and Rhenium(V) with beta-Diketonates, Inorg. Chem.* **2019**, *58*, 5241-5252.

[91] Clemens Scholtysik, Doctoral Thesis, Freie Universität Berlin, **2017**.

[92] Gomez, J. D. C.; Hagenbach, A.; Gerling-Driessen, U. I. M.; Koksch, B.; Beindorff, N.; Brenner, W.; Abram, U. *Thiourea derivatives as chelating agents for bioconjugation of rhenium and technetium, Dalton Trans.* **2017**, *46*, 14602-14611.

[93] Mayer, J. M. *Metal-oxygen multiple bond lengths: a statistical study, Inorg. Chem.* **1988**, *27*, 3899-3903.

[94] Szonyi, G.; Bowers, P.; Allwright, S.; Ellis, G.; Wiseman, J.; Cooper, R.; Hales, I. *A comparative study of ^{99m}Tc and ^{131}I in thyroid scanning, Eur. J. Nucl. Med.* **1982**, *7*, 444-446.

[95] Beindorff, N.; Bartelheimer, A.; Huang, K.; Lukas, M.; Lange, C.; Huang, E. L.; Aschenbach, J. R.; Eary, J. F.; Steffen, I. G.; Brenner, W. *Normal Values of Thyroid Uptake of ^{99m}Technetium Pertechnetate SPECT in Mice with Respect to Age, Sex, and Circadian Rhythm, Nuklearmedizin* **2018**, *57*, 181-189.

[96] WinEPR SimFonia, Bruker Instruments, Inc.: Billerica, MA USA, **1995**.

[97] PerkinElmer Informatics Inc., ChemDraw Professional, Version 18.11.10.535.

[98] Sheldrick, G. M.; SADABS, University of Göttingen, Germany, **2014**.

[99] Coppens, P.; The evaluation of absorption and extinction in single crystal structure analysis. In 'Crystallographic Computing', ed. Ahmed, R. F.; Hall, R. S and Huber, P. C.; Munksgaard, **1979**, 1255-1270.

[100] Sheldrick, G. M. *Acta Crystallogr., Sect. A* **2008**, *64*, 112-122.

[101] Sheldrick, G. M. *Acta Crystallogr., Sect. C* **2015**, *71*, 3-8.

[102] Farrugia, L. J. *WinGX. suite for small-molecule single-crystal crystallography, J. Appl. Crystallogr.* **1999**, *32*, 837-838.

[103] Diamond - Crystal and Molecular Structure Visualization Crystal Impact, Version 4.2.2, Dr. H. Putz & Dr. K. Brandenburg GbR, Bonn (Germany).

[104] Cason, C. Persistance of Vision Raytacer (TM) for Windows Version 3.6.

[105] Farrugia, L. J. *ORTEP-3 for Windows - a version of ORTEP-III with a Graphical User Interface (GUI), J. Appl. Crystallogr.* **1997**, *30*, 565-565.

[106] Copyright Scientific Software, Agilent Technologies, CA, USA, Version 3.3.2 SP2.

[107] Elysia Raytest; GINA Star TLC^{TM}, Windows Radiochromatographie for miniGita & miniGita Single/Dual, Version 6.3.

[108] Pearlstein, R. M.; Davis, W. M.; Jones, A. G.; Davison, A. *Preparation and characterization of (acetonitrile)trichlorobis(triphenylphosphine)technetium and its reactions with small π-accepting ligands, Inorg. Chem.* **1989**, *28*, 3332-3334.

[109] Mazzi, U.; de Paoli, G.; Di Bernardo, P.; Magon, L. *Complexes of technetium(IV) and (III) with tertiary phosphines, J. Inorg. Nucl. Chem.* **1976**, *38*, 721-725.

[110] Alberto, R.; Schibli, R.; Egli, A.; Schubiger, P. A.; Herrmann, W. A.; Artus, G.; Abram, U.; Kaden, T. A. *Metal carbonyl syntheses XXII. Low-pressure carbonylation of $[MOCl_4]^-$ and $[MO_4]^-$. The technetium (I) and rhenium (I) complexes $[NEt_4]_2[MCl_3(CO)_3]$, J. Organomet. Chem.* **1995**, *492*, 217-224.

[111] Baldas, J.; Bonnyman, J.; Williams, G. A. *Studies of technetium complexes. 9. Use of the tetrachloronitridotechnetate(VI) anion for the preparation of nitrido complexes of technetium. Crystal structure of bis(8-quinolinethiolato)nitridotechnetium(V), Inorg. Chem.* **1986**, *25*, 150-153.

[112] Angelici, R. J. *Inorganic Syntheses: Reagents for Transition Metal Complex and Organometallic Syntheses, Vol. 28*, John Wiley & Sons, Inc, **1990**.

[113] Chatt, J.; Falk, C. D.; Leigh, G. J.; Paske, R. J. *Nitrido-complexes of rhenium which contain tertiary phosphines, and attempts to prepare their osmium analogues, J. Chem. Soc. A* **1969**, 2288-2293.

[114] Abram, U.; Braun, M.; Abram, S.; Kirmse, R.; Voigt, A. *$[NBu_4][ReNCl_4]$: Facile synthesis, structure, electron paramagnetic resonance spectroscopy and reactions, J. Chem. Soc., Dalton Trans.* **1998**, 231-238.

[115] Johnson, N.; Lock, C.; Wilkinson, G. *Amine, phosphine, arsine, and stibine complexes of rhenium-(III),-(IV), and-(V), J. Chem. Soc.* **1964**, 1054-1066.

[116] Chatt, J.; Rowe, G. A. *Complex Compounds of Tertiary Phosphines and a Tertiary Arsine with Rhenium(V), Rhenium(III) and Rhenium(II), J. Chem. Soc.* **1962**, 4019-4033.

[117] Scholtysik, C.; Jungfer, M. R.; Hagenbach, A.; Abram, U. *Reactions of $[ReOCl_3(PPh_3)_2]$ with 4-Fluoroaniline, Z. Anorg. Allg. Chem.* **2018**, *644*, 1451-1455.

[118] Beyer, L.; Widera, R. *N-(amino-thiocarbonyl)-benzimidchloride, Tetrahedron Lett.* **1982**, *23*, 1881-1882.

[119] Hart, W. P.; Shihua, D.; Rausch, M. D. *The formation and reactions of (η^5-carboxycyclopenta-dienyl)dicarbonylcobalt, J. Organomet. Chem.* **1985**, *282*, 111-121.

[120] Moreno, C.; Macazaga, M. J.; Delgado, S. *Reactions of $(\eta^5\text{-}C_5H_4CO_2CH_3)Co(CO)I_2$ with polydentate phosphines, J. Organomet. Chem.* **1990**, *397*, 93-99.

8 Crystallographic Appendix

Table 8.1. Crystal data and structure refinement for [$Tc^{I}(NO)Cl(PPh_3)(L^{OMe})$].

Empirical formula	$C_{29}H_{38}ClCoNO_{10}P_4Tc$	
Formula weight	876.86	
Temperature	100(2) K	
Wavelength	0.71073 Å	
Crystal system	Monoclinic	
Space group	$P2_1/c$	
Unit cell dimensions	a = 21.9056(2) Å	α = 90°
	b = 10.3707(8) Å	β = 97.041(2)°
	c = 15.2883(1) Å	γ = 90°
Volume	3446.9(5) $Å^3$	
Z	4	
Density (calculated)	1.690 g/cm^3	
Absorption coefficient	1.201 mm^{-1}	
F(000)	1784	
Crystal size	0.60 x 0.20 x 0.15 mm^3	
Theta range for data collection	2.176 to 27.174°	
Index ranges	-28<=h<=28, -13<=k<=13, -19<=l<=19	
Reflections collected	137645	
Independent reflections	7639 [R(int) = 0.0269]	
Completeness to theta = 25.242°	99.7 %	
Absorption correction	Semi-empirical from equivalents	
Max. and min. transmission	0.7456 and 0.6353	
Refinement method	Full-matrix least-squares on F^2	
Data / restraints / parameters	7639 / 0 / 428	
Goodness-of-fit on F^2	1.100	
Final R indices [I>2sigma(I)]	R1 = 0.0237, wR2 = 0.0592	
R indices (all data)	R1 = 0.0243, wR2 = 0.0596	
Largest diff. peak and hole	0.444 and -0.797 e · $Å^{-3}$	
Diffractometer	Bruker Venture D8	

Table 8.2. Atomic coordinates (x 10^4) and equivalent isotropic displacement parameters ($Å^2$ x 10^3) for [Tc^I(NO)Cl(PPh_3)(L^{OMe})].

	x	y	z	U(eq)
Tc(1)	2575(1)	5(1)	2272(1)	7(1)
Co(1)	940(1)	183(1)	3248(1)	9(1)
C(1)	367(1)	-793(2)	4010(1)	22(1)
C(2)	46(1)	-549(2)	3162(1)	18(1)
C(3)	25(1)	795(2)	3033(1)	20(1)
C(4)	338(1)	1392(2)	3798(1)	24(1)
C(5)	542(1)	398(2)	4402(1)	25(1)
P(1)	1327(1)	-1497(1)	2687(1)	9(1)
O(1)	1160(1)	-2826(1)	3145(1)	16(1)
O(2)	951(1)	-1723(1)	1733(1)	14(1)
O(3)	2015(1)	-1527(1)	2639(1)	11(1)
C(6)	1566(1)	-3394(2)	3845(1)	23(1)
C(7)	1188(1)	-2649(2)	1154(1)	20(1)
P(2)	1196(1)	1359(1)	2188(1)	10(1)
O(4)	638(1)	1686(1)	1432(1)	19(1)
O(5)	1316(1)	2782(1)	2573(1)	15(1)
O(6)	1721(1)	898(1)	1714(1)	12(1)
C(8)	505(2)	903(3)	689(2)	53(1)
C(9)	1593(1)	3718(2)	2039(1)	21(1)
P(3)	1822(1)	612(1)	3982(1)	9(1)
O(7)	1768(1)	1842(1)	4598(1)	15(1)
O(8)	1952(1)	-516(1)	4693(1)	13(1)
O(9)	2375(1)	813(1)	3488(1)	11(1)
C(10)	2168(1)	2946(2)	4612(1)	21(1)
C(11)	2488(1)	-416(2)	5350(1)	17(1)
P(4)	3484(1)	-1033(1)	2893(1)	9(1)
C(12)	3378(1)	-2755(2)	3044(1)	12(1)
C(13)	3440(1)	-3577(2)	2334(1)	15(1)
C(14)	3342(1)	-4891(2)	2407(1)	17(1)
C(15)	3185(1)	-5406(2)	3186(1)	18(1)
C(16)	3118(1)	-4598(2)	3890(1)	19(1)
C(17)	3204(1)	-3276(2)	3818(1)	16(1)
C(18)	4144(1)	-1013(2)	2258(1)	14(1)
C(19)	4146(1)	-251(2)	1517(1)	26(1)

C(20)	4668(1)	-207(3)	1071(2)	36(1)
C(21)	5180(1)	-950(3)	1360(1)	35(1)
C(22)	5174(1)	-1742(2)	2087(1)	28(1)
C(23)	4660(1)	-1767(2)	2540(1)	20(1)
C(24)	3816(1)	-409(2)	3966(1)	14(1)
C(25)	3738(1)	904(2)	4126(1)	19(1)
C(26)	3962(1)	1436(2)	4939(1)	28(1)
C(27)	4265(1)	668(3)	5592(1)	34(1)
C(28)	4359(1)	-629(3)	5434(1)	32(1)
C(29)	4140(1)	-1168(2)	4621(1)	22(1)
Cl(1A)	3060(1)	1938(1)	1921(1)	15(1)
N(1A)	2673(2)	-803(4)	1325(3)	21(1)
O(10A)	2715(2)	-1429(4)	656(2)	21(1)
Cl(1B)	2599(1)	-1040(1)	901(1)	15(1)
N(1B)	3004(1)	1303(4)	2003(2)	21(1)
O(10B)	3272(2)	2211(3)	1772(2)	21(1)

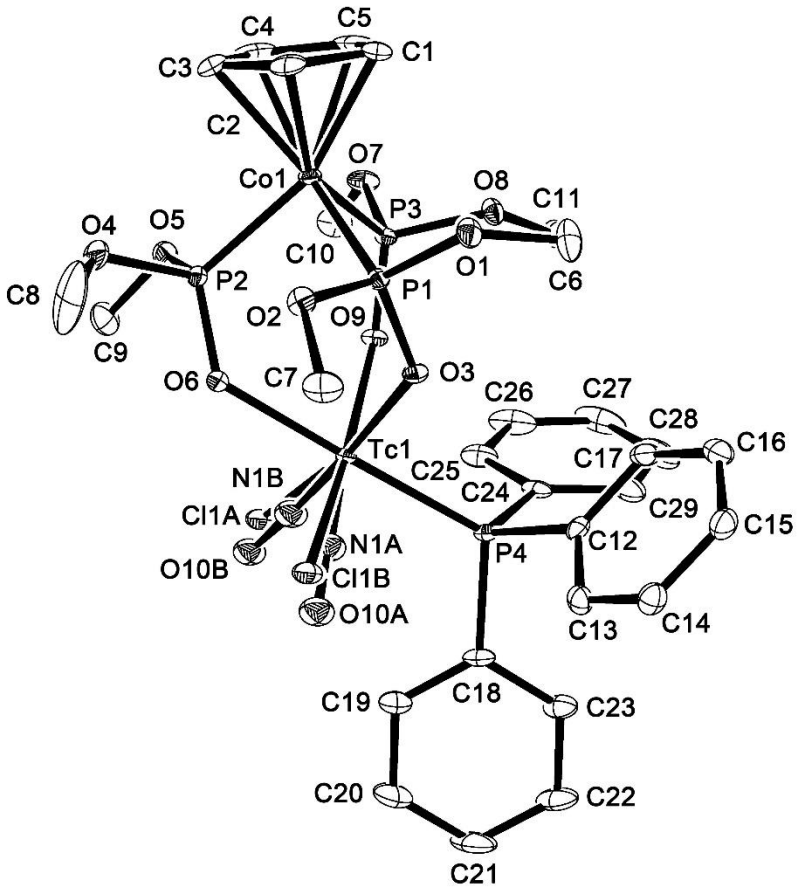

Figure 8.1. Ellipsoid representation of $[Tc^{I}(NO)Cl(PPh_3)(L^{OMe})]$. Thermal ellipsoids are at 50 % of probability. The hydrogen atoms have been omitted for clarity.

Table 8.3. Crystal data and structure refinement for $[Tc^{II}(NO)Cl_2(L^{OMe})]$.

Empirical formula	$C_{11}H_{23}Cl_2Co\ O_{10}P_3Tc$	
Formula weight	650.04	
Temperature	100(2) K	
Wavelength	0.71073 Å	
Crystal system	Triclinic	
Space group	$P\bar{1}$	
Unit cell dimensions	a = 8.4189(2) Å	α = 77.771(9)°
	b = 10.0117(2) Å	β = 74.031(5)°
	c = 14.636(3) Å	γ = 68.276(4)°
Volume	1093.4(3) $Å^3$	
Z	2	
Density (calculated)	1.974 g/cm^3	
Absorption coefficient	1.903 mm^{-1}	
F(000)	650	
Crystal size	0.180 x 0.070 x 0.020 mm^3	
Theta range for data collection	2.491 to 27.180°	
Index ranges	-10<=h<=10, -12<=k<=12, -18<=l<=18	
Reflections collected	18975	
Independent reflections	4836 [R(int) = 0.0411]	
Completeness to theta = 25.242°	99.9 %	
Absorption correction	Semi-empirical from equivalents	
Max. and min. transmission	0.7455 and 0.6636	
Refinement method	Full-matrix least-squares on F^2	
Data / restraints / parameters	4836 / 0 / 262	
Goodness-of-fit on F^2	1.047	
Final R indices [I>2sigma(I)]	R1 = 0.0420, wR2 = 0.0931	
R indices (all data)	R1 = 0.0531, wR2 = 0.0979	
Largest diff. peak and hole	1.685 and -1.420 e · $Å^{-3}$	
Diffractometer	Bruker Venture D8	

Table 8.4. Atomic coordinates (x 10^4) and equivalent isotropic displacement parameters ($Å^2$ x 10^3) for $[Tc^{II}(NO)Cl_2(L^{OMe})]$.

	x	y	z	U(eq)
Tc(1)	5784(1)	4818(1)	2175(1)	11(1)
Co(1)	9022(1)	803(1)	2736(1)	11(1)
C(1)	9421(6)	-1381(5)	2714(4)	21(1)
C(2)	9287(6)	-1122(5)	3654(3)	20(1)
C(3)	10665(6)	-607(5)	3622(3)	20(1)
C(4)	11616(6)	-520(5)	2672(3)	20(1)
C(5)	10847(6)	-1002(5)	2107(3)	21(1)
P(1)	6576(1)	1317(1)	2322(1)	12(1)
O(1)	7012(4)	613(3)	1367(2)	17(1)
O(2)	5316(4)	502(3)	3031(2)	17(1)
O(3)	5420(4)	2899(3)	2176(2)	16(1)
C(6)	5622(7)	625(6)	961(4)	25(1)
C(7)	3793(6)	1261(5)	3706(3)	22(1)
P(2)	7835(1)	2359(1)	3751(1)	11(1)
O(4)	6644(4)	1701(3)	4638(2)	17(1)
O(5)	9222(4)	2543(3)	4225(2)	17(1)
O(6)	6747(4)	3873(3)	3404(2)	17(1)
C(8)	5483(6)	2627(5)	5370(3)	23(1)
C(9)	9397(6)	3928(5)	4222(4)	24(1)
P(3)	9725(1)	2464(1)	1675(1)	13(1)
O(7)	11088(4)	2902(4)	2007(2)	23(1)
O(8)	10855(4)	1898(4)	682(2)	26(1)
O(9)	8268(4)	3852(3)	1420(2)	16(1)
C(10)	11524(7)	4189(6)	1509(4)	31(1)
C(11)	10131(9)	2063(8)	-101(4)	51(2)
N(1)	4955(6)	5639(5)	1110(4)	35(1)
Cl(1)	3017(2)	5576(1)	3205(1)	31(1)
O(10)	4226(6)	6406(5)	549(3)	48(1)
Cl(2)	6488(2)	6851(1)	2250(1)	29(1)

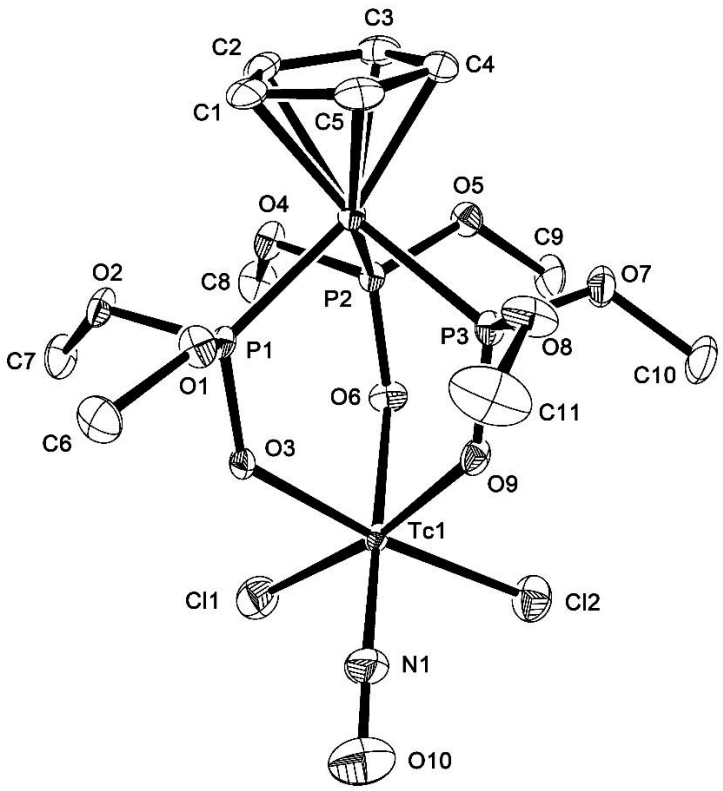

Figure 8.2. Ellipsoid representation of $[Tc^{II}(NO)Cl_2(L^{OMe})]$. Thermal ellipsoids are at 50 % of probability. The hydrogen atoms have been omitted for clarity.

Table 8.5. Crystal data and structure refinement for $[Tc^{III}Cl_2(PPh_3)(L^{OMe})]$.

Empirical formula	$C_{29}H_{38}Cl_2CoO_9P_4Tc$	
Formula weight	882.30	
Temperature	100(2) K	
Wavelength	1.54178 Å	
Crystal system	Monoclinic	
Space group	$P2_1/c$	
Unit cell dimensions	a = 21.9832(7) Å	α = 90°
	b = 10.3195(3) Å	β = 97.127(2)°
	c = 15.2169(5) Å	γ = 90°
Volume	3425.37(2) $Å^3$	
Z	4	
Density (calculated)	1.711 g/cm^3	
Absorption coefficient	10.716 mm^{-1}	
F(000)	1792	
Crystal size	0.08 x 0.02 x 0.005 mm^3	
Theta range for data collection	2.025 to 74.686°	
Index ranges	-27<=h<=25, -12<=k<=12, -19<=l<=18	
Reflections collected	69432	
Independent reflections	6973 [R(int) = 0.0970]	
Completeness to theta = 67.679°	100.0 %	
Absorption correction	Semi-empirical from equivalents	
Max. and min. transmission	0.7538 and 0.3998	
Refinement method	Full-matrix least-squares on F^2	
Data / restraints / parameters	6973 / 0 / 415	
Goodness-of-fit on F^2	1.039	
Final R indices [I>2sigma(I)]	R1 = 0.0535, wR2 = 0.1059	
R indices (all data)	R1 = 0.0730, wR2 = 0.1149	
Largest diff. peak and hole	1.073 and -0.954 e · $Å^{-3}$	
Diffractometer	Bruker Venture D8	

Table 8.6. Atomic coordinates (x 10^4) and equivalent isotropic displacement parameters ($Å^2$ x 10^3) for $[Tc^{III}Cl_2(PPh_3)(L^{OMe})]$.

	x	y	z	U(eq)
Tc(1)	2556(1)	5016(1)	2279(1)	12(1)
Co(1)	941(1)	4844(1)	3246(1)	15(1)
C(1)	340(3)	3639(6)	3798(4)	32(1)
C(2)	30(2)	4226(6)	3035(4)	26(1)
C(3)	51(2)	5562(6)	3161(4)	26(1)
C(4)	365(3)	5843(6)	4002(4)	31(1)
C(5)	541(2)	4642(7)	4398(4)	34(2)
P(1)	1820(1)	4398(1)	3985(1)	15(1)
O(1)	1957(2)	5526(4)	4702(2)	20(1)
O(2)	1768(2)	3162(4)	4597(2)	22(1)
O(3)	2373(1)	4195(3)	3484(2)	14(1)
C(6)	2492(2)	5421(6)	5359(3)	22(1)
C(7)	2167(3)	2052(5)	4613(4)	26(1)
P(2)	1191(1)	3671(1)	2178(1)	18(1)
O(4)	1306(2)	2237(4)	2562(2)	24(1)
O(5)	637(2)	3370(4)	1414(2)	33(1)
O(6)	1721(2)	4136(3)	1709(2)	18(1)
C(8)	1579(3)	1290(6)	2030(4)	29(1)
C(9)	543(4)	4090(8)	640(6)	76(3)
P(3)	1327(1)	6536(1)	2688(1)	16(1)
O(7)	949(2)	6757(4)	1725(2)	20(1)
O(8)	1165(2)	7867(4)	3145(2)	24(1)
O(9)	2009(2)	6576(3)	2634(2)	14(1)
C(10)	1180(3)	7685(6)	1143(4)	27(1)
C(11)	1568(3)	8435(6)	3851(4)	30(1)
P(4)	3494(1)	6041(1)	2888(1)	14(1)
C(12)	3820(2)	5402(5)	3973(3)	17(1)
C(13)	4146(2)	6166(6)	4626(3)	27(1)
C(14)	4364(3)	5615(8)	5441(4)	38(2)
C(15)	4261(3)	4331(8)	5600(4)	39(2)
C(16)	3960(3)	3552(7)	4952(4)	33(1)
C(17)	3737(2)	4093(6)	4135(4)	23(1)
C(18)	4153(2)	6012(5)	2252(3)	18(1)
C(19)	4658(2)	6811(6)	2527(4)	28(1)

C(20)	5175(3)	6785(7)	2081(4)	35(2)
C(21)	5190(3)	5969(8)	1372(4)	41(2)
C(22)	4686(3)	5208(8)	1085(5)	47(2)
C(23)	4169(3)	5240(6)	1523(4)	31(1)
C(24)	3383(2)	7765(5)	3046(3)	19(1)
C(25)	3211(2)	8278(5)	3829(3)	21(1)
C(26)	3118(3)	9604(5)	3907(4)	26(1)
C(27)	3176(2)	10426(5)	3207(4)	24(1)
C(28)	3343(2)	9920(5)	2427(3)	21(1)
C(29)	3448(2)	8611(5)	2347(3)	21(1)
Cl(1)	3063(1)	3133(1)	1911(1)	30(1)
Cl(2)	2633(1)	6056(1)	931(1)	26(1)

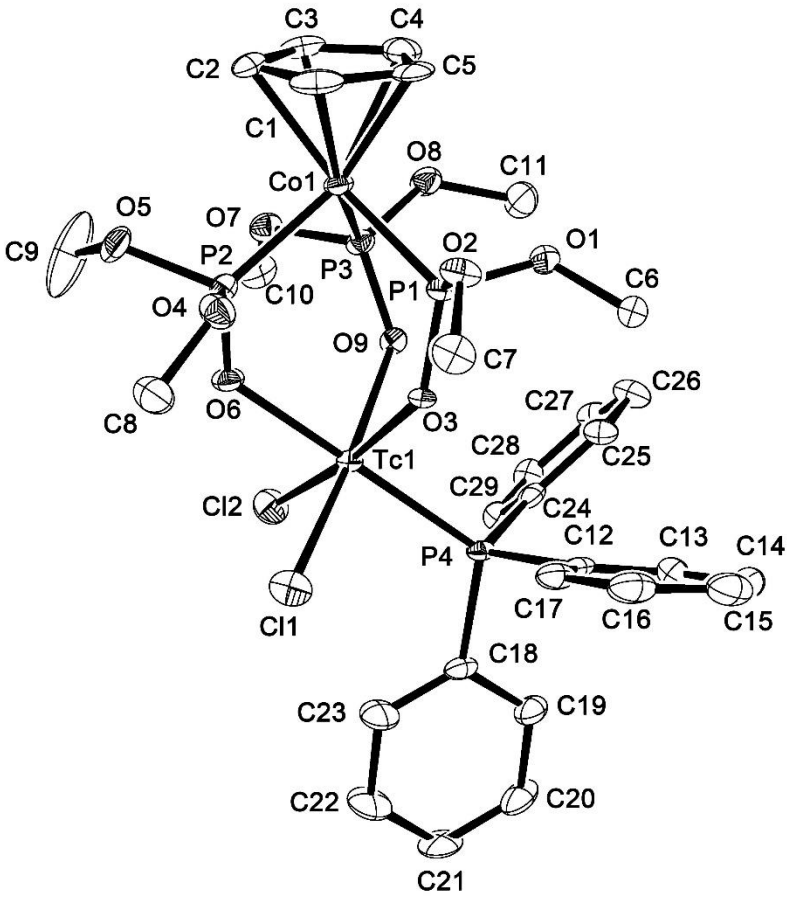

Figure 8.3. Ellipsoid representation of $[Tc^{III}Cl_2(PPh_3)(L^{OMe})]$. Thermal ellipsoids are at 50 % of probability. The hydrogen atoms have been omitted for clarity.

Table 8.7. Crystal data and structure refinement for $[Tc^{IV}Cl_3(L^{OMe})]$.

Empirical formula	$C_{11}H_{23}Cl_3CoO_9P_3Tc$	
Formula weight	655.48	
Temperature	100(2) K	
Wavelength	0.71073 Å	
Crystal system	Triclinic	
Space group	$P\bar{1}$	
Unit cell dimensions	a = 8.7716(7) Å	α = 89.429(3)°
	b = 15.2457(1) Å	β = 79.971(3)°
	c = 16.7984(1) Å	γ = 86.526(3)°
Volume	2208.0(3) $Å^3$	
Z	4	
Density (calculated)	1.972 g/cm^3	
Absorption coefficient	1.998 mm^{-1}	
F(000)	1308	
Crystal size	0.130 x 0.130 x 0.110 mm^3	
Theta range for data collection	2.362 to 26.432°	
Index ranges	-10<=h<=10, -19<=k<=19, -20<=l<=21	
Reflections collected	59822	
Independent reflections	9044 [R(int) = 0.0518]	
Completeness to theta = 25.242°	100.0 %	
Absorption correction	Semi-empirical from equivalents	
Max. and min. transmission	0.7454 and 0.6650	
Refinement method	Full-matrix least-squares on F^2	
Data / restraints / parameters	9044 / 0 / 499	
Goodness-of-fit on F^2	1.027	
Final R indices [I>2sigma(I)]	R1 = 0.0252, wR2 = 0.0537	
R indices (all data)	R1 = 0.0356, wR2 = 0.0574	
Largest diff. peak and hole	0.504 and -0.565 e $\cdot$ $Å^{-3}$	
Diffractometer	Bruker Venture D8	

Table 8.8. Atomic coordinates (x 10^4) and equivalent isotropic displacement parameters ($Å^2$ x 10^3) for $[Tc^{IV}Cl_3(L^{OMe})]$.

	x	y	z	U(eq)
Tc(1)	340(1)	1543(1)	2070(1)	7(1)
Co(1)	2341(1)	3218(1)	466(1)	8(1)
C(1)	2113(3)	3962(2)	-561(2)	18(1)
C(2)	3461(3)	3396(2)	-724(2)	16(1)
C(3)	4440(3)	3608(2)	-171(2)	16(1)
C(4)	3688(3)	4297(2)	334(2)	18(1)
C(5)	2237(4)	4518(2)	92(2)	19(1)
P(1)	-19(1)	2833(1)	560(1)	8(1)
O(1)	-1092(2)	3676(1)	894(1)	12(1)
O(2)	-634(2)	2673(1)	-259(1)	14(1)
O(3)	-493(2)	2032(1)	1088(1)	9(1)
C(6)	-2713(3)	3578(2)	1225(2)	17(1)
C(7)	-501(4)	1818(2)	-645(2)	19(1)
P(2)	3138(1)	1863(1)	571(1)	9(1)
O(4)	2818(2)	1382(1)	-211(1)	15(1)
O(5)	4963(2)	1670(1)	517(1)	16(1)
O(6)	2418(2)	1365(1)	1326(1)	10(1)
C(8)	2864(4)	436(2)	-254(2)	23(1)
C(9)	5633(3)	1457(2)	1234(2)	17(1)
P(3)	2015(1)	3380(1)	1758(1)	7(1)
O(7)	3676(2)	3238(1)	2009(1)	11(1)
O(8)	1509(2)	4346(1)	2088(1)	12(1)
O(9)	873(2)	2787(1)	2271(1)	9(1)
C(10)	3813(3)	3269(2)	2860(2)	18(1)
C(11)	-96(3)	4649(2)	2361(2)	19(1)
Cl(1)	1547(1)	1081(1)	3127(1)	13(1)
Cl(2)	-2056(1)	1835(1)	2869(1)	13(1)
Cl(3)	-259(1)	142(1)	1766(1)	14(1)
Tc(2)	6208(1)	6708(1)	3263(1)	6(1)
Co(2)	2300(1)	8061(1)	4072(1)	7(1)
C(12)	184(3)	8010(2)	4855(2)	16(1)
C(13)	-74(3)	8181(2)	4055(2)	16(1)
C(14)	615(3)	8983(2)	3802(2)	13(1)
C(15)	1306(3)	9295(2)	4436(2)	13(1)

C(16)	1048(3)	8685(2)	5089(2)	15(1)
P(4)	2919(1)	6776(1)	4496(1)	7(1)
O(10)	3150(2)	6886(1)	5402(1)	11(1)
O(11)	1583(2)	6104(1)	4570(1)	12(1)
O(12)	4359(2)	6279(1)	4016(1)	9(1)
C(17)	3552(4)	6116(2)	5858(2)	22(1)
C(18)	1741(3)	5294(2)	4115(2)	14(1)
P(5)	3027(1)	7631(1)	2840(1)	7(1)
O(13)	1995(2)	6859(1)	2667(1)	11(1)
O(14)	2699(2)	8303(1)	2151(1)	11(1)
O(15)	4748(2)	7321(1)	2593(1)	8(1)
C(19)	2325(3)	6431(2)	1883(2)	15(1)
C(20)	3678(3)	9012(2)	1880(2)	19(1)
P(6)	4578(1)	8495(1)	4120(1)	8(1)
O(16)	4881(2)	9297(1)	3517(1)	13(1)
O(17)	4744(2)	8925(1)	4955(1)	16(1)
O(18)	5969(2)	7816(1)	3930(1)	10(1)
C(21)	6430(3)	9625(2)	3324(2)	24(1)
C(22)	5576(4)	8502(2)	5532(2)	22(1)
Cl(4)	8253(1)	7247(1)	2368(1)	13(1)
Cl(5)	7839(1)	6119(1)	4098(1)	13(1)
Cl(6)	6219(1)	5417(1)	2533(1)	12(1)

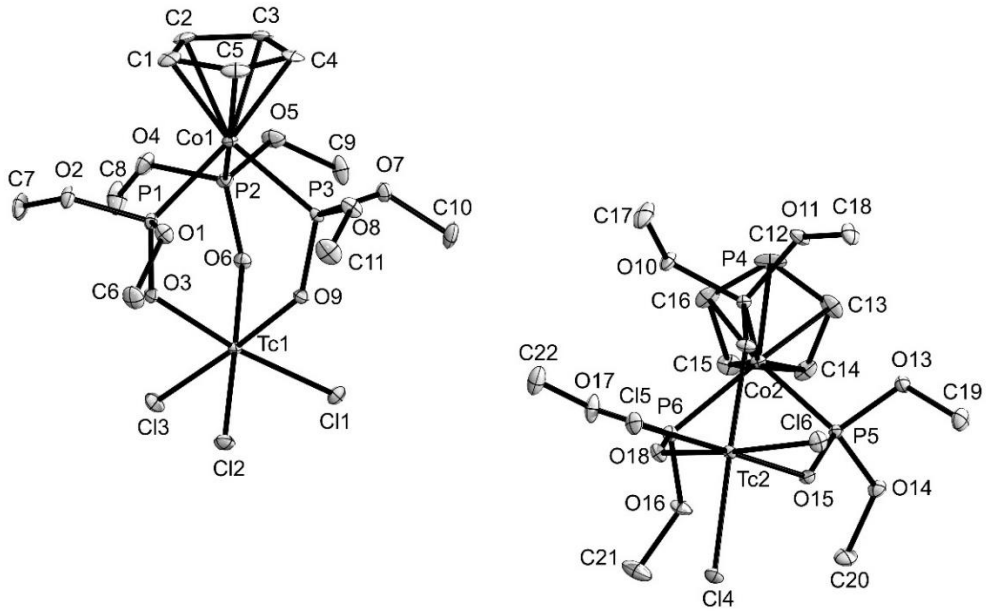

Figure 8.4. Ellipsoid representation of $[Tc^{IV}Cl_3(L^{OMe})]$. Thermal ellipsoids are at 50 % of probability. The hydrogen atoms have been omitted for clarity.

Table 8.9. Crystal data and structure refinement for $[Tc^{V}OCl_2(L^{OMe})]$.

Empirical formula	$C_{11}H_{23}Cl_2CoO_{10}P_3Tc$	
Formula weight	636.03	
Temperature	100(2) K	
Wavelength	0.71073 Å	
Crystal system	Monoclinic	
Space group	Pn	
Unit cell dimensions	a = 9.9609(5) Å	α = 90°
	b = 9.8786(5) Å	β = 95.632(2)°
	c = 10.7903(5) Å	γ = 90°
Volume	1056.64(9) $Å^3$	
Z	2	
Density (calculated)	1.999 g/cm^3	
Absorption coefficient	1.965 mm^{-1}	
F(000)	636	
Crystal size	0.200 x 0.110 x 0.100 mm^3	
Theta range for data collection	2.656 to 27.164°	
Index ranges	-12<=h<=12, -12<=k<=12, -13<=l<=13	
Reflections collected	26759	
Independent reflections	4468 [R(int) = 0.0203]	
Completeness to theta = 25.242°	99.8 %	
Absorption correction	Semi-empirical from equivalents	
Max. and min. transmission	0.7455 and 0.6748	
Refinement method	Full-matrix least-squares on F^2	
Data / restraints / parameters	4468 / 2 / 254	
Goodness-of-fit on F^2	1.100	
Final R indices [I>2sigma(I)]	R1 = 0.0156, wR2 = 0.0413	
R indices (all data)	R1 = 0.0158, wR2 = 0.0414	
Absolute structure parameter	0.025(12)	
Largest diff. peak and hole	0.408 and -0.534 e $\cdot$ $Å^{-3}$	
Diffractometer	Bruker Venture D8	

Table 8.10. Atomic coordinates (x 10^4) and equivalent isotropic displacement parameters ($Å^2$ x 10^3) for [$Tc^{V}OCl_2(L^{OMe})$].

	x	y	z	U(eq)
Tc(1)	4045(1)	7987(1)	3130(1)	5(1)
Co(1)	5744(1)	7342(1)	6609(1)	6(1)
C(1)	6425(4)	8337(4)	8252(3)	17(1)
C(2)	7513(3)	7670(3)	7773(3)	14(1)
C(3)	7209(3)	6255(3)	7683(3)	14(1)
C(4)	5940(4)	6058(3)	8136(3)	16(1)
C(5)	5442(4)	7336(4)	8483(3)	19(1)
P(1)	6739(1)	8168(1)	5097(1)	6(1)
O(1)	6967(2)	9726(2)	5400(2)	10(1)
O(2)	8262(2)	7680(2)	5058(2)	11(1)
O(3)	6085(2)	7968(2)	3763(2)	8(1)
C(6)	7704(4)	10568(3)	4609(3)	18(1)
C(7)	8637(3)	6528(3)	4338(3)	14(1)
P(2)	4915(1)	5770(1)	5390(1)	6(1)
O(4)	6144(2)	4898(2)	5001(2)	10(1)
O(5)	4053(2)	4630(2)	5992(2)	11(1)
O(6)	4043(2)	6255(2)	4222(2)	8(1)
C(8)	5913(4)	3785(4)	4144(4)	21(1)
C(9)	2620(3)	4739(3)	6038(3)	14(1)
P(3)	4001(1)	8589(1)	6117(1)	6(1)
O(7)	2726(2)	7845(2)	6612(2)	12(1)
O(8)	4123(2)	9978(2)	6849(2)	13(1)
O(9)	3613(2)	8945(2)	4745(2)	8(1)
C(10)	1369(3)	8251(4)	6180(3)	17(1)
C(11)	3469(4)	11218(3)	6424(3)	18(1)
Cl(1)	1750(1)	7606(1)	2650(1)	11(1)
Cl(2)	4507(1)	6542(1)	1500(1)	11(1)
O(10)	4200(2)	9433(2)	2405(2)	12(1)

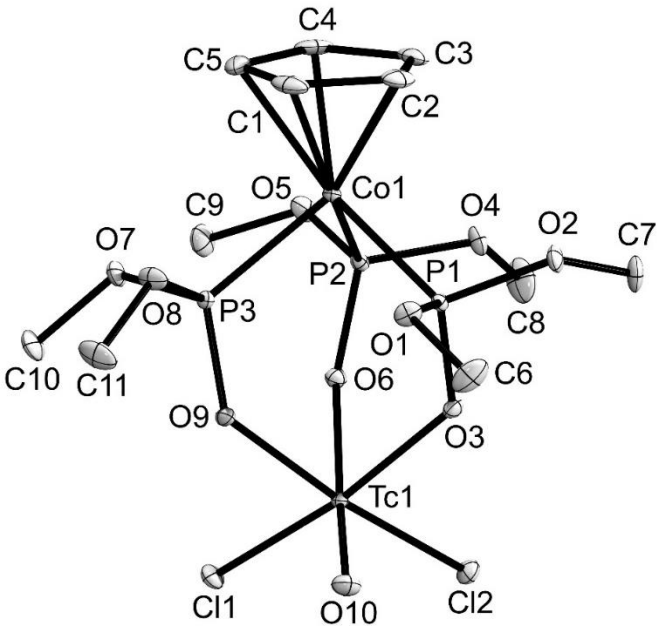

Figure 8.5. Ellipsoid representation of $[Tc^{V}OCl_2(L^{OMe})]$. Thermal ellipsoids are at 50 % of probability. The hydrogen atoms have been omitted for clarity.

Table 8.11. Crystal data and structure refinement for $[Tc^{V}NCl(PPh_3)(L^{OMe})]$.

Empirical formula	$C_{29}H_{38}ClCoNO_9P_4Tc$	
Formula weight	860.86	
Temperature	100(2) K	
Wavelength	0.71073 Å	
Crystal system	Monoclinic	
Space group	$P2_1/c$	
Unit cell dimensions	a = 21.9876(1) Å	α = 90°
	b = 10.1840(4) Å	β = 96.494(2)°
	c = 15.1748(7) Å	γ = 90°
Volume	3376.2(3) $Å^3$	
Z	4	
Density (calculated)	1.694 g/cm^3	
Absorption coefficient	1.222 mm^{-1}	
F(000)	1752	
Crystal size	0.800 x 0.300 x 0.200 mm^3	
Theta range for data collection	2.206 to 27.974°	
Index ranges	-28<=h<=28, -13<=k<=13, -20<=l<=20	
Reflections collected	68322	
Independent reflections	8082 [R(int) = 0.1099]	
Absorption correction	Semi-empirical from equivalents	
Max. and min. transmission	0.7456 and 0.5921	
Completeness to theta = 25.242°	100.0 %	
Refinement method	Full-matrix least-squares on F^2	
Data / restraints / parameters	8082 / 0 / 425	
Goodness-of-fit on F^2	1.048	
Final R indices [I>2sigma(I)]	R1 = 0.0364, wR2 = 0.0683	
R indices (all data)	R1 = 0.0770, wR2 = 0.0732	
Largest diff. peak and hole	0.437 and -0.681 $e \cdot Å^{-3}$	
Diffractometer	Bruker Venture D8	

Table 8.12. Atomic coordinates (x 10^4) and equivalent isotropic displacement parameters ($Å^2$ x 10^3) for $[Tc^{V}NCl(PPh_3)(L^{OMe})]$.

	x	y	z	U(eq)
Co(1)	9053(1)	4873(1)	6738(1)	12(1)
C(1)	9643(1)	5875(3)	6005(2)	23(1)
C(2)	9463(1)	4674(3)	5586(2)	27(1)
C(3)	9653(1)	3645(2)	6178(2)	24(1)
C(4)	9959(1)	4220(2)	6956(2)	22(1)
C(5)	9949(1)	5579(2)	6850(2)	21(1)
P(1)	8179(1)	4477(1)	5986(1)	12(1)
O(1)	8239(1)	3254(2)	5338(1)	19(1)
O(2)	8061(1)	5652(2)	5289(1)	16(1)
O(3)	7625(1)	4259(2)	6471(1)	15(1)
C(6)	7852(1)	2119(2)	5328(2)	26(1)
C(7)	7524(1)	5584(2)	4639(2)	20(1)
P(2)	8664(1)	6578(1)	7311(1)	13(1)
O(4)	8842(1)	7929(2)	6859(1)	22(1)
O(5)	9041(1)	6775(2)	8270(1)	17(1)
O(6)	7983(1)	6611(1)	7368(1)	14(1)
C(8)	8441(1)	8549(2)	6182(2)	27(1)
C(9)	8795(1)	7665(2)	8878(2)	24(1)
P(3)	8781(1)	3680(1)	7798(1)	13(1)
O(7)	9325(1)	3357(2)	8566(1)	22(1)
O(8)	8666(1)	2231(2)	7415(1)	18(1)
O(9)	8250(1)	4136(1)	8276(1)	15(1)
C(10)	9449(2)	4130(3)	9324(2)	57(1)
C(11)	8401(1)	1274(2)	7969(2)	24(1)
P(4)	6493(1)	6063(1)	7104(1)	18(1)
C(12)	6176(1)	5422(2)	6027(2)	20(1)
C(13)	5839(1)	6184(3)	5380(2)	29(1)
C(14)	5628(1)	5642(4)	4566(2)	42(1)
C(15)	5741(1)	4344(4)	4393(2)	49(1)
C(16)	6052(1)	3563(3)	5031(2)	41(1)
C(17)	6271(1)	4098(3)	5844(2)	29(1)
C(18)	6616(1)	7806(2)	6937(2)	22(1)
C(19)	6566(1)	8667(3)	7640(2)	27(1)
C(20)	6684(1)	9990(3)	7548(2)	32(1)

C(21)	6846(1)	10477(3)	6763(2)	31(1)
C(22)	6898(1)	9639(3)	6059(2)	31(1)
C(23)	6791(1)	8303(2)	6147(2)	26(1)
C(24)	5832(1)	6037(3)	7740(2)	23(1)
C(25)	5806(1)	5165(3)	8438(2)	39(1)
C(26)	5284(1)	5104(4)	8874(2)	48(1)
C(27)	4791(1)	5909(4)	8625(2)	43(1)
C(28)	4813(1)	6793(3)	7944(2)	36(1)
C(29)	5329(1)	6849(3)	7499(2)	27(1)
Tc(1A)	7378(1)	4792(1)	7689(1)	10(1)
Cl(1A)	7327(1)	5899(2)	9056(1)	18(1)
N(1A)	6953(2)	3505(5)	7821(3)	19(1)
Tc(1B)	7422(1)	5181(1)	7880(1)	10(1)
Cl(1B)	6928(1)	3146(1)	8133(1)	18(1)
N(1B)	7297(3)	5990(7)	8770(4)	19(1)

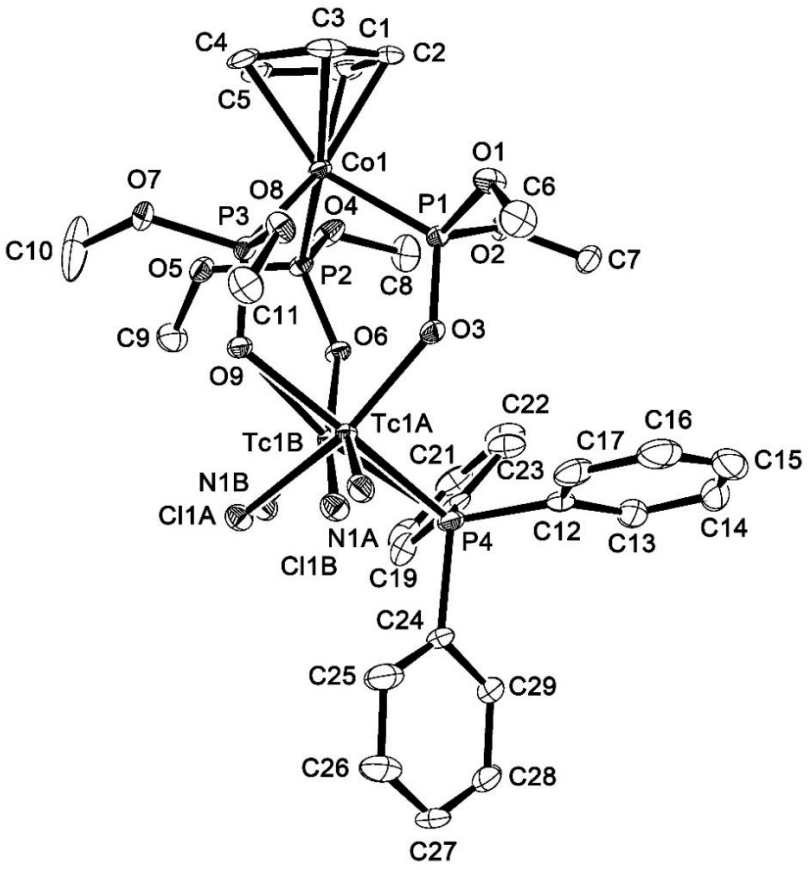

Figure 8.6. Ellipsoid representation of [$Tc^{V}NCl(PPh_3)(L^{OMe})$]. Thermal ellipsoids are at 50 % of probability. The hydrogen atoms have been omitted for clarity.

Table 8.13. Crystal data and structure refinement for $[Tc^{VI}NCl_2(L^{OMe})]$.

Empirical formula	$C_{11}H_{23}Cl_2CoNO_9P_3Tc$	
Formula weight	634.04	
Temperature	100(2) K	
Wavelength	0.71073 Å	
Crystal system	Monoclinic	
Space group	$P2_1/n$	
Unit cell dimensions	a = 9.6181(1) Å	α = 90°
	b = 14.8087(2) Å	β = 101.308(4)°
	c = 15.2790(2) Å	γ = 90°
Volume	2134.0(4) $Å^3$	
Z	4	
Density (calculated)	1.974 g/cm^3	
Absorption coefficient	1.944 mm^{-1}	
F(000)	1268	
Crystal size	0.270 x 0.090 x 0.050 mm^3	
Theta range for data collection	2.315 to 27.250°	
Index ranges	-12<=h<=12, -19<=k<=19, -19<=l<=19	
Reflections collected	59158	
Independent reflections	4752 [R(int) = 0.0578]	
Completeness to theta = 25.242°	100.0 %	
Absorption correction	Semi-empirical from equivalents	
Max. and min. transmission	0.7455 and 0.5956	
Refinement method	Full-matrix least-squares on F^2	
Data / restraints / parameters	4752 / 0 / 253	
Goodness-of-fit on F^2	1.057	
Final R indices [I>2sigma(I)]	R1 = 0.0253, wR2 = 0.0620	
R indices (all data)	R1 = 0.0311, wR2 = 0.0643	
Largest diff. peak and hole	0.619 and -0.709 e $\cdot$ $Å^{-3}$	
Diffractometer	Bruker Venture D8	

Table 8.14. Atomic coordinates (x 10^4) and equivalent isotropic displacement parameters ($Å^2$ x 10^3) for $[Tc^{VI}NCl_2(L^{OMe})]$.

	x	y	z	U(eq)
Tc(1)	3574(1)	2991(1)	8615(1)	9(1)
Co(1)	5866(1)	3192(1)	6634(1)	10(1)
C(1)	7088(3)	2431(2)	5918(2)	24(1)
C(2)	7940(3)	3098(2)	6415(2)	24(1)
C(3)	7347(3)	3951(2)	6138(2)	24(1)
C(4)	6149(3)	3804(2)	5451(2)	24(1)
C(5)	5972(3)	2866(2)	5322(2)	23(1)
P(1)	4367(1)	2145(1)	6761(1)	10(1)
O(1)	3132(2)	2076(2)	5905(1)	25(1)
O(2)	5146(2)	1192(1)	6786(1)	20(1)
O(3)	3641(2)	2156(1)	7567(1)	13(1)
C(6)	1657(3)	2099(3)	5914(2)	44(1)
C(7)	4373(3)	381(2)	6922(2)	29(1)
P(2)	6707(1)	3206(1)	8048(1)	10(1)
O(4)	7843(2)	2430(1)	8368(1)	20(1)
O(5)	7659(2)	4082(1)	8266(1)	18(1)
O(6)	5686(2)	3172(1)	8701(1)	15(1)
C(8)	7489(4)	1617(2)	8777(2)	33(1)
C(9)	8301(3)	4296(2)	9184(2)	26(1)
P(3)	4285(1)	4194(1)	6783(1)	11(1)
O(7)	4899(2)	5202(1)	6834(1)	23(1)
O(8)	3189(2)	4248(1)	5847(1)	21(1)
O(9)	3487(2)	4059(1)	7527(1)	15(1)
C(10)	5288(5)	5677(2)	7669(2)	46(1)
C(11)	1880(3)	4737(2)	5807(2)	34(1)
N(1)	3712(2)	2178(1)	9355(1)	15(1)
Cl(1)	3591(1)	4193(1)	9592(1)	17(1)
Cl(2)	1111(1)	3016(1)	8221(1)	17(1)

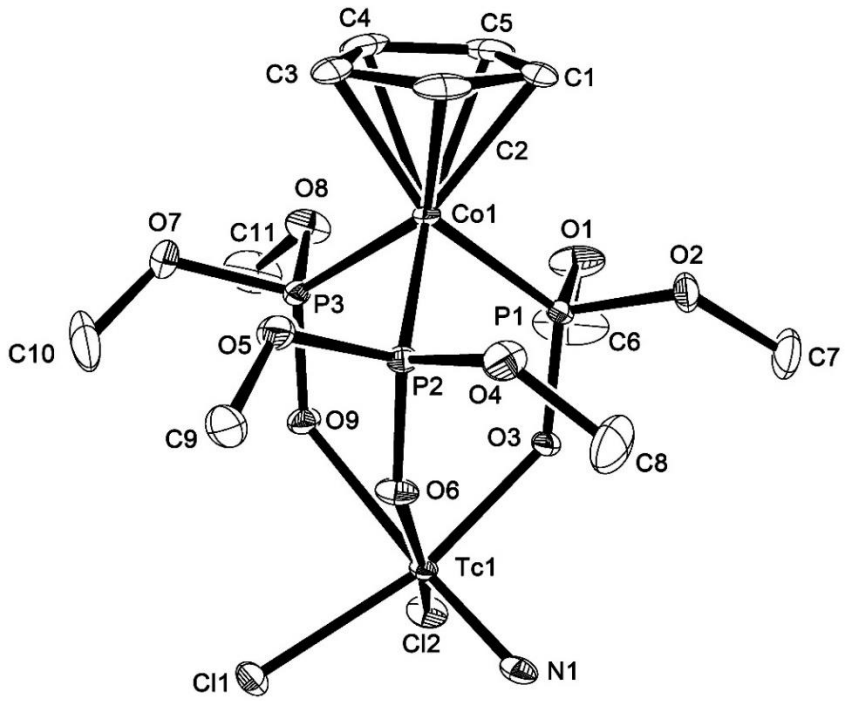

Figure 8.7. Ellipsoid representation of $[Tc^{VI}NCl_2(L^{OMe})]$. Thermal ellipsoids are at 50 % of probability. The hydrogen atoms have been omitted for clarity.

Table 8.15. Crystal data and structure refinement for $[Tc^{VII}O_3(L^{OMe})]$.

Empirical formula	$C_{11}H_{23}CoO_{12}P_3Tc$	
Formula weight	597.13	
Temperature	100(2) K	
Wavelength	0.71073 Å	
Crystal system	Triclinic	
Space group	$P\bar{1}$	
Unit cell dimensions	a = 8.3038(1) Å	α = 90.486(5)°
	b = 8.8035(1) Å	β = 102.845(5)°
	c = 14.762(2) Å	γ = 108.777(5)°
Volume	992.4(3) $Å^3$	
Z	2	
Density (calculated)	1.998 g/cm^3	
Absorption coefficient	1.832 mm^{-1}	
F(000)	600	
Crystal size	0.420 x 0.270 x 0.040 mm^3	
Theta range for data collection	2.453 to 27.966°	
Index ranges	-10<=h<=10, -11<=k<=11, -19<=l<=19	
Reflections collected	37463	
Independent reflections	4759 [R(int) = 0.0669]	
Completeness to theta = 25.242°	100.0 %	
Absorption correction	Semi-empirical from equivalents	
Max. and min. transmission	0.7456 and 0.5811	
Refinement method	Full-matrix least-squares on F^2	
Data / restraints / parameters	4759 / 0 / 253	
Goodness-of-fit on F^2	1.084	
Final R indices [I>2sigma(I)]	R1 = 0.0293, wR2 = 0.0659	
R indices (all data)	R1 = 0.0420, wR2 = 0.0697	
Largest diff. peak and hole	0.841 and -0.720 e $\cdot$ $Å^{-3}$	
Diffractometer	Bruker Venture D8	

Table 8.16. Atomic coordinates (x 10^4) and equivalent isotropic displacement parameters ($Å^2$ x 10^3) for $[Tc^{VII}O_3(L^{OMe})]$.

	x	y	z	U(eq)
Tc(1)	3252(1)	4647(1)	2239(1)	7(1)
Co(1)	7010(1)	9272(1)	2739(1)	6(1)
C(1)	8391(4)	11244(3)	2126(2)	13(1)
C(2)	9582(3)	10673(3)	2758(2)	14(1)
C(3)	9272(4)	10781(3)	3651(2)	15(1)
C(4)	7879(4)	11410(3)	3580(2)	16(1)
C(5)	7350(4)	11712(3)	2640(2)	16(1)
P(1)	6829(1)	7422(1)	1718(1)	7(1)
O(1)	6509(2)	7968(2)	683(1)	14(1)
O(2)	8709(2)	7231(2)	1847(1)	12(1)
O(3)	5521(2)	5748(2)	1708(1)	9(1)
C(6)	4871(4)	7304(4)	2(2)	19(1)
C(7)	8828(4)	5916(3)	1287(2)	17(1)
P(2)	6677(1)	7519(1)	3745(1)	7(1)
O(4)	8383(2)	6996(2)	4088(1)	13(1)
O(5)	6628(2)	8386(2)	4688(1)	11(1)
O(6)	5093(2)	5999(2)	3498(1)	9(1)
C(8)	8378(4)	5400(3)	3869(2)	19(1)
C(9)	6192(4)	7385(3)	5436(2)	15(1)
P(3)	4216(1)	8743(1)	2292(1)	7(1)
O(7)	3390(2)	9429(2)	3017(1)	12(1)
O(8)	3875(2)	9768(2)	1433(1)	12(1)
O(9)	3083(2)	6996(2)	2013(1)	10(1)
C(10)	2582(4)	8417(3)	3671(2)	16(1)
C(11)	2119(4)	9689(4)	970(2)	24(1)
O(10)	4070(2)	3130(2)	2516(1)	12(1)
O(11)	1715(2)	4382(2)	2868(1)	13(1)
O(12)	2047(2)	4065(2)	1127(1)	14(1)

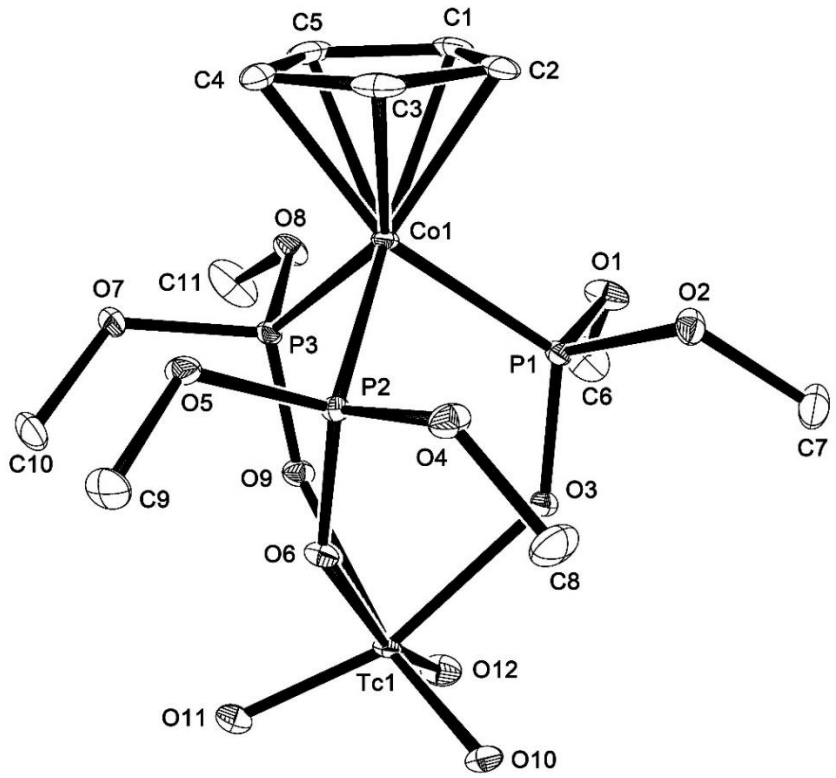

Figure 8.8. Ellipsoid representation of $[Tc^{VII}O_3(L^{OMe})]$. Thermal ellipsoids are at 50 % of probability. The hydrogen atoms have been omitted for clarity.

Table 8.17. Crystal data and structure refinement for [$Tc^{V}O$(glycolate)(L^{OMe})].

Empirical formula	$C_{13}H_{27}CoO_{12}P_3Tc$	
Formula weight	625.18	
Temperature	273(2) K	
Wavelength	0.71073 Å	
Crystal system	Monoclinic	
Space group	Pn	
Unit cell dimensions	a = 9.3029(2) Å	α = 90°
	b = 10.161(2) Å	β = 93.10(3)°
	c = 11.878(2) Å	γ = 90°
Volume	1121.2(4) $Å^3$	
Z	2	
Density (calculated)	1.852 g/cm^3	
Absorption coefficient	1.626 mm^{-1}	
F(000)	632	
Crystal size	0.540 x 0.383 x 0.210 mm^3	
Theta range for data collection	3.491 to 27.001°.	
Index ranges	-11<=h<=11, -12<=k<=12, -13<=l<=15	
Reflections collected	7087	
Independent reflections	4267 [R(int) = 0.0261]	
Completeness to theta = 25.242°	98.5 %	
Absorption correction	Integration	
Max. and min. transmission	0.6622 and 0.4886	
Refinement method	Full-matrix least-squares on F^2	
Data / restraints / parameters	4267 / 825 / 380	
Goodness-of-fit on F^2	1.019	
Final R indices [I>2sigma(I)]	R1 = 0.0427, wR2 = 0.1076	
R indices (all data)	R1 = 0.0446, wR2 = 0.1091	
Absolute structure parameter	0.00(3)	
Largest diff. peak and hole	0.708 and -1.287 e $\cdot$ $Å^{-3}$	
Diffractometer	STOE IPDS II T	

Table 8.18. Atomic coordinates (x 10^4) and equivalent isotropic displacement parameters ($Å^2$ x 10^3) for [$Tc^{V}O$(glycolate)(L^{OMe})].

	x	y	z	U(eq)
Tc(01)	3444(1)	7762(1)	3760(1)	56(1)
Co(1)	5607(1)	7392(1)	6832(1)	38(1)
C(1)	6268(12)	6079(11)	8097(8)	69(2)
C(2)	5324(12)	6976(12)	8509(8)	69(2)
C(3)	5923(12)	8228(11)	8441(8)	68(2)
C(4)	7240(11)	8106(11)	7925(8)	68(2)
C(5)	7454(10)	6762(11)	7739(8)	67(2)
C(6)	4230(20)	11454(15)	6568(14)	117(5)
C(7)	7098(16)	10071(14)	4368(11)	99(4)
C(8)	8777(13)	6467(17)	4450(12)	98(4)
C(9)	5441(17)	4129(13)	4562(11)	93(4)
C(10)	2028(15)	4599(14)	6599(13)	101(4)
C(11)	1172(12)	8484(15)	6572(13)	99(4)
C(12)	4481(12)	8333(11)	1665(8)	71(2)
C(13)	3665(15)	7126(11)	1530(9)	79(3)
P(1)	5233(7)	9300(5)	6000(5)	54(2)
P(2)	6213(6)	6586(5)	5315(4)	49(1)
P(3)	3410(5)	6862(6)	6455(5)	47(1)
P(1A)	6641(3)	7749(3)	5271(3)	45(1)
P(2A)	4394(5)	5798(4)	5951(3)	60(1)
P(3A)	3969(4)	8755(4)	6306(3)	56(1)
O(1)	4880(30)	10330(20)	6810(20)	73(5)
O(2)	6630(20)	9960(20)	5620(20)	85(5)
O(3)	4217(19)	9297(16)	4943(13)	51(3)
O(4)	8210(20)	7360(20)	5160(20)	72(5)
O(5)	6130(20)	5021(19)	5315(17)	68(4)
O(6)	5580(20)	7090(20)	4220(15)	47(4)
O(7)	3080(20)	5530(20)	7020(20)	60(4)
O(8)	2310(20)	7630(20)	7100(20)	80(5)
O(9)	2884(16)	6716(18)	5237(12)	52(3)
O(1A)	7182(16)	9228(13)	5259(10)	78(3)
O(2A)	7951(13)	6688(15)	5323(11)	66(3)
O(3A)	5778(12)	7457(12)	4184(10)	42(3)
O(4A)	5430(20)	4660(13)	5643(14)	92(4)

O(5A)	3450(20)	5039(17)	6789(16)	93(5)
O(6A)	3451(13)	6102(12)	4895(9)	63(3)
O(7A)	2541(15)	8350(30)	6894(14)	102(5)
O(8A)	4200(20)	10146(17)	6913(15)	90(4)
O(9A)	3653(12)	9074(12)	5097(8)	54(2)
O(10)	1713(8)	7994(14)	3706(8)	121(3)
O(11)	4142(7)	8932(6)	2717(5)	56(1)
O(12)	3647(11)	6500(7)	2610(6)	90(2)

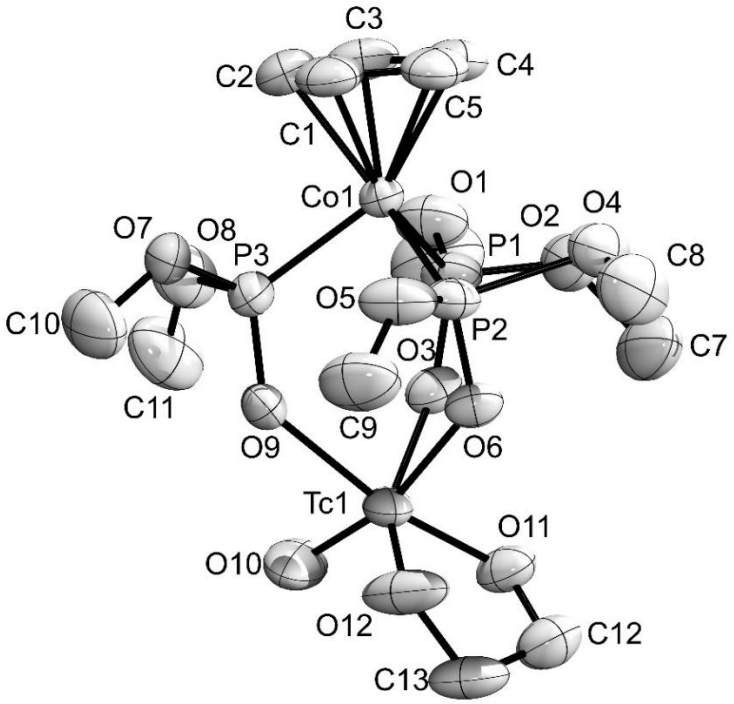

Figure 8.9. Ellipsoid representation of [$Tc^{V}O$(glycolate)(L^{OMe})]. Thermal ellipsoids are at 50 % of probability. The hydrogen atoms have been omitted for clarity.

Table 8.19. Crystal data and structure refinement for [$ReOCl_2(L^{OMe})$].

Empirical formula	$C_{11}H_{23}Cl_2CoO_{10}P_3Re$	
Formula weight	724.23	
Temperature	100(2) K	
Wavelength	0.71073 Å	
Crystal system	Monoclinic	
Space group	Pn	
Unit cell dimensions	a = 9.9693(7) Å	α = 90°
	b = 9.8630(7) Å	β = 95.261(2)°
	c = 10.8122(8) Å	γ = 90°
Volume	1058.65(1) $Å^3$	
Z	2	
Density (calculated)	2.272 g/cm^3	
Absorption coefficient	7.021 mm^{-1}	
F(000)	700	
Crystal size	0.27 x 0.19 x 0.15 mm^3	
Theta range for data collection	2.660 to 27.174°	
Index ranges	-12<=h<=12, -12<=k<=12, -13<=l<=13	
Reflections collected	44224	
Independent reflections	4626 [R(int) = 0.0550]	
Completeness to theta = 25.242°	99.9 %	
Absorption correction	Semi-empirical from equivalents	
Max. and min. transmission	0.7455 and 0.5011	
Refinement method	Full-matrix least-squares on F^2	
Data / restraints / parameters	4626 / 2 / 248	
Goodness-of-fit on F^2	1.142	
Final R indices [I>2sigma(I)]	R1 = 0.0200, wR2 = 0.0496	
R indices (all data)	R1 = 0.0200, wR2 = 0.0496	
Absolute structure parameter	0.107(7)	
Largest diff. peak and hole	0.967 and -1.508 e $\cdot$ $Å^{-3}$	
Diffractometer	Bruker Venture D8	

Table 8.20. Atomic coordinates (x 10^4) and equivalent isotropic displacement parameters ($Å^2$ x 10^3) for [$ReOCl_2(L^{OMe})$].

	x	y	z	U(eq)
Re(1)	2525(1)	2004(1)	2510(1)	6(1)
Co(1)	841(1)	2662(1)	-966(1)	6(1)
Cl(1)	4824(2)	2376(2)	2972(2)	12(1)
Cl(2)	2054(2)	3465(2)	4131(2)	12(1)
C(1)	-639(7)	3725(7)	-2024(7)	13(1)
C(2)	-925(7)	2320(8)	-2133(6)	15(1)
C(3)	189(8)	1677(8)	-2619(7)	19(2)
C(4)	1141(8)	2694(9)	-2838(6)	19(2)
C(5)	622(8)	3973(8)	-2477(7)	17(2)
P(1)	-161(2)	1825(2)	542(2)	7(1)
O(1)	-1684(5)	2305(5)	584(5)	12(1)
O(2)	-372(5)	268(5)	241(4)	11(1)
O(3)	483(6)	2031(5)	1862(5)	10(1)
C(6)	-2064(7)	3458(7)	1296(7)	16(1)
C(7)	-1132(9)	-583(7)	1014(7)	19(2)
P(2)	2580(2)	1415(2)	-483(2)	7(1)
O(4)	2475(5)	25(5)	-1207(5)	15(1)
O(5)	3855(5)	2169(5)	-966(5)	12(1)
O(6)	2950(5)	1054(5)	883(4)	10(1)
C(8)	3107(8)	-1230(7)	-779(7)	20(2)
C(9)	5214(7)	1737(8)	-556(7)	17(1)
P(3)	1666(2)	4232(2)	252(2)	7(1)
O(7)	2532(5)	5372(5)	-342(5)	12(1)
O(8)	442(5)	5103(5)	648(5)	14(1)
O(9)	2532(5)	3742(5)	1421(4)	9(1)
C(10)	3964(7)	5274(7)	-389(7)	15(1)
C(11)	682(7)	6219(7)	1499(8)	14(1)
O(10)	2358(5)	530(5)	3243(4)	13(1)

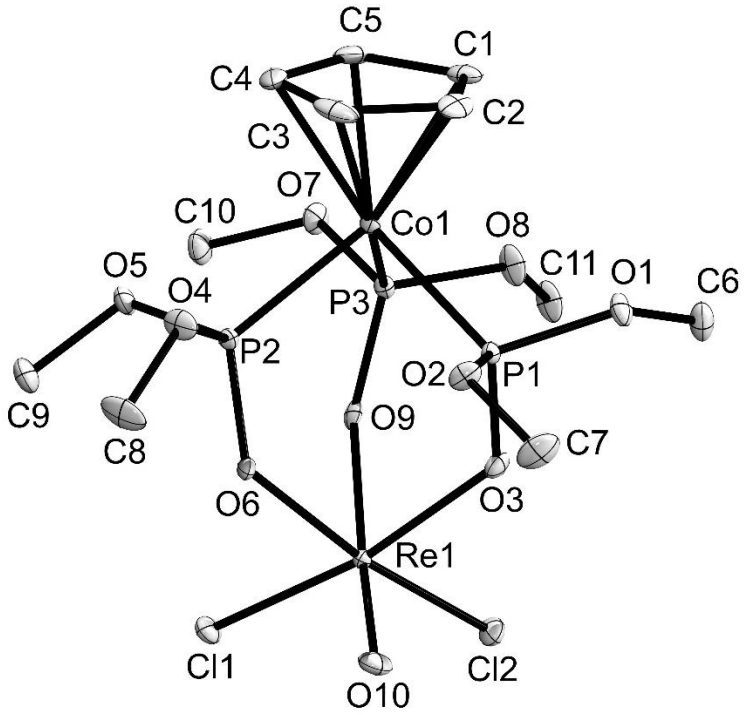

Figure 8.10. Ellipsoid representation of [$ReOCl_2(L^{OMe})$]. Thermal ellipsoids are at 50 % of probability. The hydrogen atoms have been omitted for clarity.

Table 8.21. Crystal data and structure refinement for [ReNCl(PPh_3)(L^{OMe})].

Empirical formula	$C_{29}H_{38}ClCoNO_9P_4Re$	
Formula weight	949.06	
Temperature	100(2) K	
Wavelength	0.71073 Å	
Crystal system	Monoclinic	
Space group	$P2_1/c$	
Unit cell dimensions	a = 21.9974(2) Å	α = 90°
	b = 10.1889(1) Å	β = 96.611(3)°
	c = 15.1694(1) Å	γ = 90°
Volume	3377.3(5) $Å^3$	
Z	4	
Density (calculated)	1.867 g/cm^3	
Absorption coefficient	4.394 mm^{-1}	
F(000)	1880	
Crystal size	0.450 x 0.350 x 0.070 mm^3	
Theta range for data collection	2.413 to 27.159°	
Index ranges	-28<=h<=28, -13<=k<=11, -19<=l<=19	
Reflections collected	41761	
Independent reflections	7469 [R(int) = 0.0519]	
Completeness to theta = 25.242°	99.9 %	
Absorption correction	Semi-empirical from equivalents	
Max. and min. transmission	0.7455 and 0.3313	
Refinement method	Full-matrix least-squares on F^2	
Data / restraints / parameters	7469 / 0 / 425	
Goodness-of-fit on F^2	1.217	
Final R indices [I>2sigma(I)]	R1 = 0.0419, wR2 = 0.0944	
R indices (all data)	R1 = 0.0462, wR2 = 0.0961	
Largest diff. peak and hole	1.443 and -2.140 e $\cdot$ $Å^{-3}$	
Diffractometer	Bruker Venture D8	

Table 8.22. Atomic coordinates (x 10^4) and equivalent isotropic displacement parameters ($Å^2$ x 10^3) for [ReNCl(PPh_3)(L^{OMe})].

	x	y	z	U(eq)
Co(1)	9056(1)	4892(1)	6744(1)	12(1)
C(1)	9959(2)	4237(5)	6963(3)	22(1)
C(2)	9950(2)	5600(5)	6863(3)	22(1)
C(3)	9644(2)	5905(5)	6007(3)	22(1)
C(4)	9467(2)	4708(6)	5587(3)	27(1)
C(5)	9655(2)	3670(5)	6181(4)	25(1)
P(1)	8786(1)	3696(1)	7799(1)	14(1)
O(1)	8677(2)	2242(3)	7427(2)	20(1)
O(2)	9326(2)	3404(4)	8578(3)	35(1)
O(3)	8248(1)	4146(3)	8267(2)	16(1)
C(6)	8408(2)	1286(5)	7972(3)	24(1)
C(7)	9408(3)	4099(6)	9360(4)	35(1)
P(2)	8666(1)	6586(1)	7319(1)	12(1)
O(4)	9041(1)	6790(3)	8282(2)	17(1)
O(5)	8835(2)	7950(3)	6871(2)	21(1)
O(6)	7981(1)	6605(3)	7379(2)	13(1)
C(8)	8796(2)	7675(5)	8894(3)	23(1)
C(9)	8431(3)	8561(5)	6192(3)	27(1)
P(3)	8183(1)	4486(1)	5994(1)	13(1)
O(7)	8057(1)	5664(3)	5298(2)	15(1)
O(8)	8238(2)	3255(3)	5352(2)	20(1)
O(9)	7632(1)	4261(3)	6488(2)	15(1)
C(10)	7519(2)	5593(5)	4646(3)	19(1)
C(11)	7838(3)	2134(5)	5334(4)	29(1)
P(4)	6499(1)	6054(1)	7111(1)	19(1)
C(12)	6177(2)	5416(5)	6029(3)	22(1)
C(13)	5842(2)	6184(6)	5387(3)	29(1)
C(14)	5628(3)	5646(8)	4574(4)	39(2)
C(15)	5735(3)	4341(8)	4394(4)	47(2)
C(16)	6048(3)	3559(7)	5030(5)	43(2)
C(17)	6269(2)	4088(6)	5854(4)	29(1)
C(18)	6614(2)	7804(5)	6943(3)	22(1)
C(19)	6567(2)	8659(6)	7652(4)	27(1)
C(20)	6679(2)	9988(6)	7565(4)	31(1)

C(21)	6838(2)	10489(6)	6779(4)	31(1)
C(22)	6887(3)	9645(6)	6067(4)	32(1)
C(23)	6783(2)	8310(5)	6156(4)	26(1)
C(24)	5836(2)	6020(6)	7752(3)	23(1)
C(25)	5816(3)	5131(7)	8430(4)	37(1)
C(26)	5283(3)	5063(7)	8875(4)	42(2)
C(27)	4796(2)	5876(7)	8632(4)	37(2)
C(28)	4817(2)	6766(7)	7949(4)	34(1)
C(29)	5336(2)	6842(6)	7500(3)	26(1)
ReA	7372(1)	4819(2)	7681(1)	10(1)
NA	6941(5)	3532(11)	7822(9)	23(2)
ClA	7353(3)	5899(6)	9073(3)	16(1)
ReB	7423(1)	5182(2)	7890(1)	10(1)
NB	7297(11)	5990(20)	8778(11)	23(4)
ClB	6957(2)	3130(4)	8139(2)	19(1)

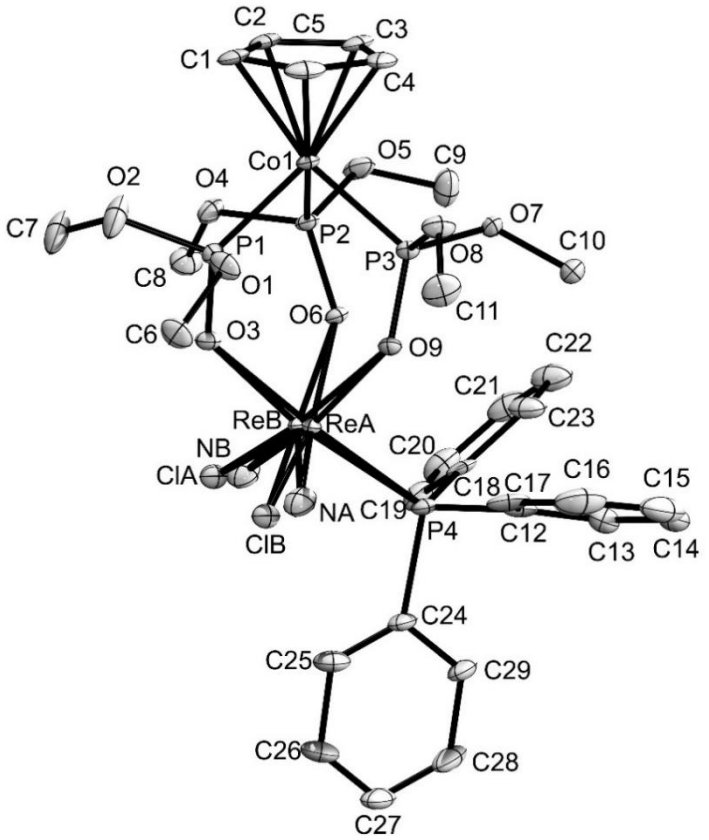

Figure 8.11. Ellipsoid representation of [ReNCl(PPh_3)(L^{OMe})]. Thermal ellipsoids are at 50 % of probability. The hydrogen atoms have been omitted for clarity.

Table 8.23. Crystal data and structure refinement for $[ReNCl_2(L^{OMe})]$.

Empirical formula	$C_{11}H_{23}Cl_2CoNO_9P_3Re$	
Formula weight	722.24	
Temperature	100(2) K	
Wavelength	0.71073 Å	
Crystal system	Monoclinic	
Space group	$P2_1/n$	
Unit cell dimensions	a = 9.5954(1) Å	α = 90°
	b = 14.8050(1) Å	β = 101.163(4)°
	c = 15.3205(1) Å	γ = 90°
Volume	2135.3(3) $Å^3$	
Z	4	
Density (calculated)	2.247 g/cm^3	
Absorption coefficient	6.959 mm^{-1}	
F(000)	1396	
Crystal size	0.48 x 0.14 x 0.08 mm^3	
Theta range for data collection	2.320 to 27.160°	
Index ranges	-12<=h<=12, -18<=k<=18, -19<=l<=19	
Reflections collected	27847	
Independent reflections	4719 [R(int) = 0.0376]	
Completeness to theta = 25.242°	100.0 %	
Absorption correction	Semi-empirical from equivalents	
Max. and min. transmission	0.3330 and 0.1367	
Refinement method	Full-matrix least-squares on F^2	
Data / restraints / parameters	4719 / 3 / 263	
Goodness-of-fit on F^2	1.145	
Final R indices [I>2sigma(I)]	R1 = 0.0268, wR2 = 0.0626	
R indices (all data)	R1 = 0.0286, wR2 = 0.0634	
Largest diff. peak and hole	1.353 and -1.799 e $\cdot$ $Å^{-3}$	
Diffractometer	Bruker Venture D8	

Table 8.24. Atomic coordinates (x 10^4) and equivalent isotropic displacement parameters ($Å^2$ x 10^3) for [$ReNCl_2(L^{OMe})$].

	x	y	z	U(eq)
Re(1A)	6774(6)	6896(3)	1549(3)	9(1)
Re(1B)	6446(1)	7025(1)	1414(1)	9(1)
Co(1)	4151(1)	6813(1)	3399(1)	11(1)
C(1)	2071(5)	6886(4)	3609(3)	27(1)
C(2)	2899(6)	7571(3)	4094(3)	30(1)
C(3)	4013(6)	7154(4)	4699(3)	30(1)
C(4)	3880(5)	6219(4)	4589(3)	26(1)
C(5)	2682(5)	6048(3)	3904(3)	25(1)
P(1)	5642(1)	7866(1)	3269(1)	12(1)
O(1)	4839(4)	8813(2)	3205(2)	24(1)
O(2)	6853(4)	7963(3)	4123(2)	31(1)
O(3)	6397(3)	7836(2)	2474(2)	14(1)
C(6)	5599(6)	9628(3)	3040(4)	35(1)
C(7)	8346(6)	7938(5)	4137(4)	41(2)
P(2)	5747(1)	5817(1)	3250(1)	13(1)
O(4)	6855(4)	5779(2)	4174(2)	26(1)
O(5)	5133(4)	4809(2)	3196(2)	27(1)
O(6)	6532(3)	5952(2)	2499(2)	16(1)
C(8)	8190(6)	5313(4)	4225(3)	37(1)
C(9)	4841(10)	4311(4)	2381(5)	61(2)
P(3)	3317(1)	6792(1)	1993(1)	12(1)
O(7)	2375(4)	5907(2)	1769(2)	23(1)
O(8)	2171(3)	7562(2)	1658(2)	26(1)
O(9)	4348(3)	6831(2)	1347(2)	16(1)
C(10)	1772(6)	5678(4)	856(3)	33(1)
C(11)	2506(7)	8368(4)	1240(4)	40(1)
Cl(1)	8913(1)	6979(1)	1812(1)	21(1)
N(1A)	6680(60)	6050(20)	840(30)	18(1)
Cl(2A)	6290(20)	8099(11)	631(13)	15(1)
N(1B)	6316(6)	7831(3)	683(4)	18(1)
Cl(2B)	6420(1)	5810(1)	449(1)	15(1)

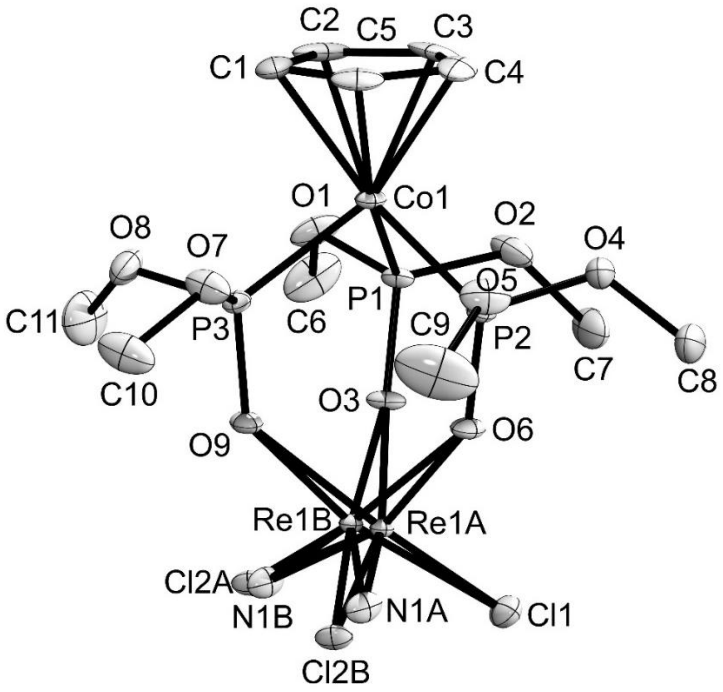

Figure 8.12. Ellipsoid representation of [$ReNCl_2(L^{OMe})$]. Thermal ellipsoids are at 50 % of probability. The hydrogen atoms have been omitted for clarity.

Table 8.25. Crystal data and structure refinement for $[Ga(L^{OMe})_2]NO_3$.

Empirical formula	$C_{22}H_{46}Co_2GaNO_{21}P_6$	
Formula weight	1034.00	
Temperature	293(2) K	
Wavelength	0.71073 Å	
Crystal system	Monoclinic	
Space group	P 2_1/n	
Unit cell dimensions	a = 10.1147(6) Å	α = 90°
	b = 10.4711(4) Å	β = 91.277(5)°
	c = 18.8867(1) Å	γ = 90°
Volume	1999.83(2) $Å^3$	
Z	2	
Density (calculated)	1.717 g/cm^3	
Absorption coefficient	1.807 mm^{-1}	
F(000)	1056	
Crystal size	0.520 x 0.330 x 0.220 mm^3	
Theta range for data collection	3.508 to 27.057°.	
Index ranges	-12<=h<=12, -13<=k<=13, -24<=l<=19	
Reflections collected	15645	
Independent reflections	4359 [R(int) = 0.0433]	
Completeness to theta = 25.242°	99.7 %	
Absorption correction	Integration	
Max. and min. transmission	0.4650 and 0.3272	
Refinement method	Full-matrix least-squares on F^2	
Data / restraints / parameters	4359 / 486 / 335	
Goodness-of-fit on F^2	1.027	
Final R indices [I>2sigma(I)]	R1 = 0.0352, wR2 = 0.0956	
R indices (all data)	R1 = 0.0443, wR2 = 0.0996	
Largest diff. peak and hole	0.615 and -0.431 e $\cdot$ $Å^{-3}$	
Diffractometer	STOE IPDS II T	

Table 8.26. Atomic coordinates (x 10^4) and equivalent isotropic displacement parameters ($Å^2$ x 10^3) for $[Ga(L^{OMe})_2]NO_3$.

	x	y	z	U(eq)
Ga(1)	5000	5000	5000	27(1)
Co(1)	5865(1)	4639(1)	3042(1)	32(1)
C(1)	5085(4)	4416(4)	2022(2)	61(1)
C(2)	5913(4)	5497(4)	2044(2)	64(1)
C(3)	7183(4)	5109(4)	2251(2)	59(1)
C(4)	7158(3)	3761(3)	2359(2)	52(1)
C(5)	5864(3)	3356(3)	2202(2)	52(1)
P(1)	4529(1)	6049(1)	3450(1)	36(1)
O(1)	3071(2)	5811(4)	3159(1)	79(1)
O(2)	4868(3)	7400(2)	3108(1)	65(1)
O(3)	4484(2)	6214(2)	4248(1)	36(1)
C(6)	1927(4)	5823(6)	3542(3)	94(2)
C(7)	4323(6)	8550(4)	3334(3)	95(2)
P(2)	7248(1)	5072(1)	3890(1)	41(1)
O(4A)	8050(12)	6249(10)	3821(3)	52(2)
O(4B)	7484(11)	6701(9)	3802(3)	41(2)
O(5A)	8405(5)	3918(8)	3786(2)	46(2)
O(5B)	8703(5)	4712(10)	3845(3)	47(2)
O(6)	6798(2)	4889(2)	4645(1)	35(1)
C(8A)	8040(20)	7370(20)	4324(12)	96(6)
C(8B)	8013(12)	7340(20)	4365(10)	51(3)
C(9A)	9372(16)	3720(17)	4363(8)	60(3)
C(9B)	9140(20)	3590(19)	4163(10)	69(4)
P(3)	4932(1)	3195(1)	3674(1)	42(1)
O(7A)	6219(19)	2133(10)	3830(6)	60(3)
O(8A)	3990(20)	2340(20)	3303(7)	61(4)
O(9)	4453(2)	3559(2)	4401(1)	36(1)
C(10A)	6100(30)	1240(20)	4441(12)	97(7)
C(11A)	2730(30)	2090(30)	3503(15)	85(9)
O(7B)	5632(11)	1899(6)	3710(4)	44(2)
O(8B)	3563(8)	2788(8)	3209(3)	45(2)
C(10B)	6298(15)	1446(13)	4334(6)	56(2)
C(11B)	2636(15)	1887(17)	3521(10)	64(3)
N(1)	5710(7)	5281(7)	9733(3)	79(2)

O(10)	5350(9)	4207(8)	9523(5)	98(2)
O(11)	6587(6)	5894(8)	9396(3)	97(2)
O(12)	5258(12)	5725(10)	10292(6)	120(4)

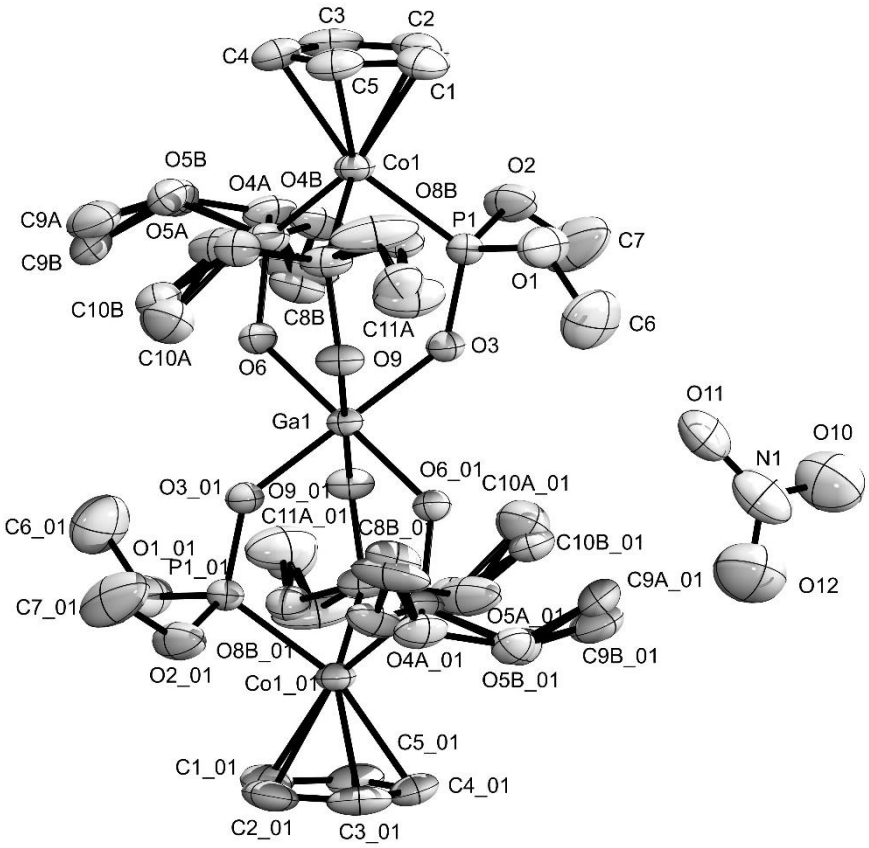

Figure 8.13. Ellipsoid representation of $[Ga(L^{OMe})_2]NO_3$. Thermal ellipsoids are at 50 % of probability. The hydrogen atoms have been omitted for clarity.

Table 8.27. Crystal data and structure refinement for $[In(L^{OMe})_2]NO_3 \cdot 1.5\ H_2O$.

Empirical formula	$C_{22}H_{49}Co_2InNO_{22.5}P_6$	
Formula weight	1106.12	
Temperature	100(2) K	
Wavelength	0.71073 Å	
Crystal system	Triclinic	
Space group	$P\bar{1}$	
Unit cell dimensions	a = 9.656(2) Å	α = 106.038(8)°
	b = 12.357(3) Å	β = 97.505(9)°
	c = 17.966(5) Å	γ = 96.798(1)°
Volume	2015.6(9) $Å^3$	
Z	2	
Density (calculated)	1.823 g/cm^3	
Absorption coefficient	1.701 mm^{-1}	
F(000)	1122	
Crystal size	0.330 x 0.270 x 0.200 mm^3	
Theta range for data collection	2.280 to 27.284°	
Index ranges	-12<=h<=12, -15<=k<=15, -23<=l<=23	
Reflections collected	76405	
Independent reflections	8948 [R(int) = 0.0414]	
Completeness to theta = 25.242°	99.9 %	
Absorption correction	Semi-empirical from equivalents	
Max. and min. transmission	0.7455 and 0.6637	
Refinement method	Full-matrix least-squares on F^2	
Data / restraints / parameters	8948 / 3 / 519	
Goodness-of-fit on F^2	1.094	
Final R indices [I>2sigma(I)]	R1 = 0.0188, wR2 = 0.0464	
R indices (all data)	R1 = 0.0233, wR2 = 0.0476	
Largest diff. peak and hole	0.403 and -0.664 e $\cdot$ $Å^{-3}$	
Diffractometer	Bruker Venture D8	

Table 8.28. Atomic coordinates (x 10^4) and equivalent isotropic displacement parameters ($Å^2$ x 10^3) for $[In(L^{OMe})_2]NO_3 \cdot 1.5\ H_2O$.

	x	y	z	U(eq)
In(1)	0	0	5000	6(1)
In(2)	0	5000	0	7(1)
Co(2)	-2018(1)	1884(1)	-288(1)	7(1)
Co(1)	-1857(1)	-3025(1)	4994(1)	8(1)
C(1)	-1772(2)	-4758(1)	4728(1)	18(1)
C(2)	-2988(2)	-4577(2)	4269(1)	19(1)
C(3)	-3842(2)	-4036(2)	4784(1)	19(1)
C(4)	-3167(2)	-3867(1)	5566(1)	18(1)
C(5)	-1897(2)	-4331(2)	5523(1)	18(1)
P(1)	-117(1)	-2010(1)	5900(1)	8(1)
O(1)	-690(1)	-1787(1)	6714(1)	15(1)
O(2)	1123(1)	-2723(1)	6041(1)	12(1)
O(3)	600(1)	-880(1)	5833(1)	11(1)
C(6)	235(2)	-1078(2)	7418(1)	25(1)
C(7)	2568(2)	-2390(2)	5959(1)	22(1)
P(2)	-623(1)	-2766(1)	4115(1)	8(1)
O(4)	755(1)	-3333(1)	4240(1)	14(1)
O(5)	-1252(1)	-3505(1)	3231(1)	14(1)
O(6)	-207(1)	-1551(1)	4086(1)	10(1)
C(8)	1857(2)	-3262(2)	3773(1)	23(1)
C(9)	-2309(2)	-3137(2)	2754(1)	23(1)
P(3)	-2965(1)	-1600(1)	4997(1)	9(1)
O(7)	-4002(1)	-1932(1)	4177(1)	14(1)
O(8)	-4119(1)	-1462(1)	5571(1)	13(1)
O(9)	-2126(1)	-411(1)	5153(1)	11(1)
C(10)	-4763(2)	-1079(2)	3978(1)	24(1)
C(11)	-3669(2)	-968(2)	6406(1)	16(1)
C(12)	-2823(2)	296(1)	-1103(1)	14(1)
C(13)	-3943(2)	802(1)	-796(1)	14(1)
C(14)	-3699(2)	990(1)	31(1)	17(1)
C(15)	-2431(2)	581(1)	224(1)	17(1)
C(16)	-1874(2)	160(1)	-472(1)	15(1)
P(4)	-750(1)	2942(1)	807(1)	8(1)
O(10)	345(1)	2238(1)	1133(1)	14(1)

O(11)	-1759(1)	3162(1)	1458(1)	16(1)
O(12)	90(1)	4085(1)	846(1)	12(1)
C(17)	1809(2)	2724(2)	1447(1)	34(1)
C(18)	-1164(2)	3940(2)	2233(1)	27(1)
P(5)	-3007(1)	3261(1)	-542(1)	8(1)
O(13)	-4533(1)	3319(1)	-286(1)	12(1)
O(14)	-3439(1)	2903(1)	-1468(1)	12(1)
O(15)	-2217(1)	4483(1)	-246(1)	11(1)
C(19)	-4644(2)	3935(2)	511(1)	21(1)
C(20)	-3814(2)	3741(2)	-1853(1)	24(1)
P(6)	-270(1)	2241(1)	-879(1)	7(1)
O(16)	-466(1)	1482(1)	-1774(1)	13(1)
O(17)	1035(1)	1753(1)	-526(1)	13(1)
O(18)	198(1)	3470(1)	-867(1)	10(1)
C(21)	-1100(2)	1866(2)	-2404(1)	19(1)
C(22)	2392(2)	1965(2)	-770(1)	23(1)
N(1)	4597(2)	4062(1)	2718(1)	17(1)
O(19)	3845(2)	4762(1)	3010(1)	25(1)
O(20)	5497(2)	4313(1)	2329(1)	31(1)
O(21)	4461(2)	3083(1)	2822(1)	23(1)
O(23)	3585(3)	228(2)	7530(2)	27(1)
O(24)	3944(2)	8334(1)	8084(1)	29(1)

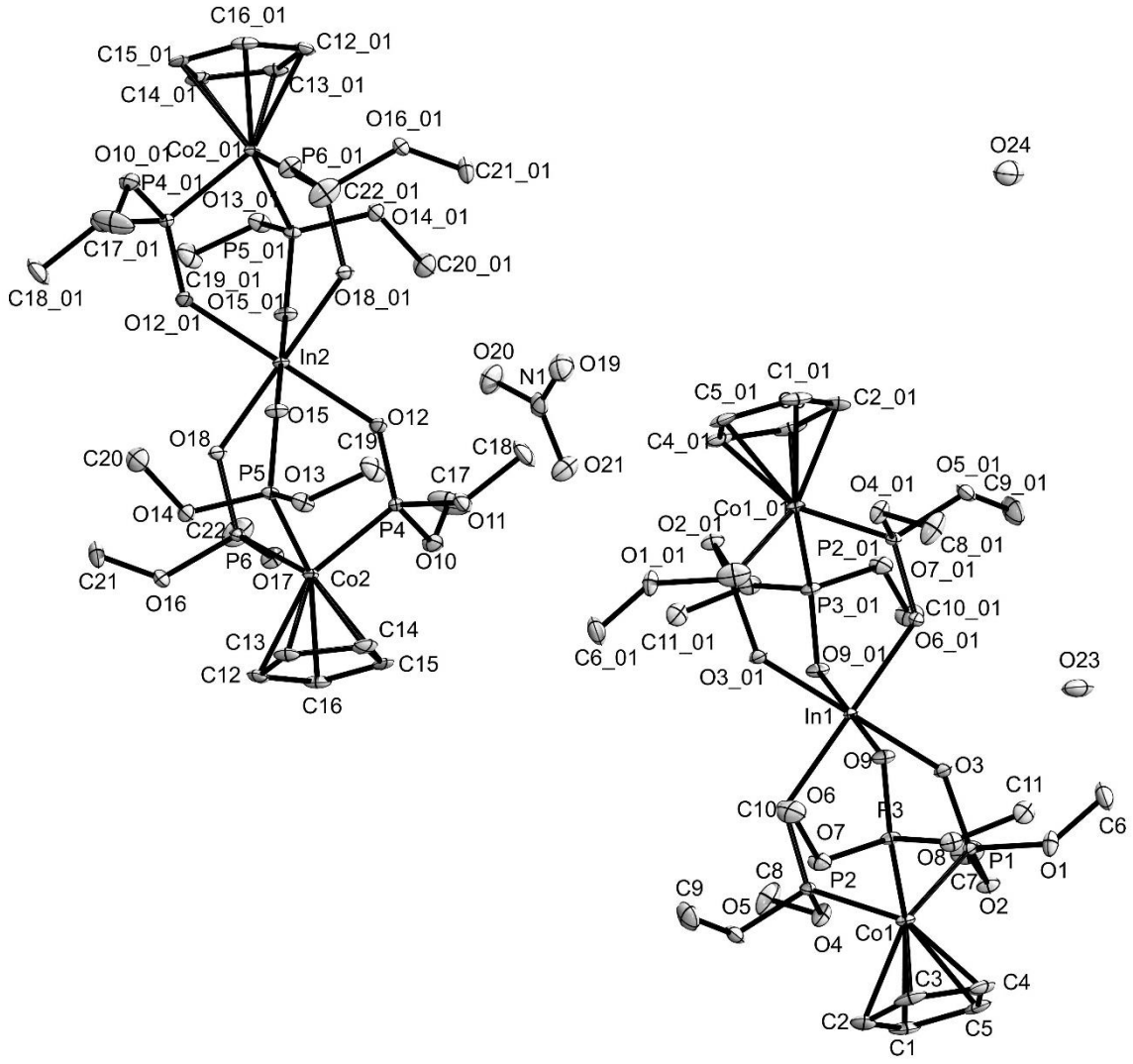

Figure 8.14. Ellipsoid representation of $[In(L^{OMe})_2]NO_3 \cdot 1.5\ H_2O$. Thermal ellipsoids are at 50 % of probability. The hydrogen atoms have been omitted for clarity.

Table 8.29. Crystal data and structure refinement for $[Lu(L^{OMe})_2(NO_3)] \cdot 0.5$ THF.

Empirical formula	$C_{24}H_{50}Co_2LuNO_{21.5}P_6$	
Formula weight	1175.30	
Temperature	240(2) K	
Wavelength	0.71073 Å	
Crystal system	Monoclinic	
Space group	P2/n	
Unit cell dimensions	a = 12.7983(6) Å	α = 90°
	b = 11.5683(5) Å	β = 93.520(4)°
	c = 18.0468(8) Å	γ = 90°
Volume	2666.9(2) $Å^3$	
Z	2	
Density (calculated)	1.464 g/cm^3	
Absorption coefficient	2.693 mm^{-1}	
F(000)	1176	
Crystal size	0.090 x 0.073 x 0.050 mm^3	
Theta range for data collection	4.755 to 26.831°	
Index ranges	-16<=h<=16, -14<=k<=14, -22<=l<=22	
Reflections collected	16885	
Independent reflections	5625 [R(int) = 0.1225]	
Completeness to theta = 25.242°	99.1 %	
Absorption correction	Integration	
Max. and min. transmission	0.2899 and 0.1588	
Refinement method	Full-matrix least-squares on F^2	
Data / restraints / parameters	5625 / 802 / 317	
Goodness-of-fit on F^2	1.012	
Final R indices [I>2sigma(I)]	R1 = 0.0563, wR2 = 0.1607	
R indices (all data)	R1 = 0.0595, wR2 = 0.1636	
Largest diff. peak and hole	1.491 and -1.943 e $\cdot$ $Å^{-3}$	
Diffractometer	STOE IPDS II T	

Table 8.30. Atomic coordinates (x 10^4) and equivalent isotropic displacement parameters ($Å^2$ x 10^3) for $[Lu(L^{OMe})_2(NO_3)] \cdot 0.5$ THF.

	x	y	z	U(eq)
Lu(1)	7500	3117(1)	2500	31(1)
Co(1)	4861(1)	2188(1)	3677(1)	42(1)
P(1)	6296(2)	1181(2)	3702(1)	50(1)
P(1A)	6400(7)	2392(10)	4155(5)	48(2)
P(2)	5802(2)	3721(2)	3887(1)	43(1)
P(2A)	4936(8)	3728(10)	3010(6)	53(2)
P(3)	4863(2)	2402(2)	2486(1)	47(1)
P(3A)	5411(8)	1224(10)	2736(7)	60(2)
O(1)	6089(5)	-153(5)	3619(3)	50(1)
O(1A)	6824(16)	1450(20)	4699(13)	48(2)
O(2)	6702(5)	1132(5)	4531(3)	50(1)
O(2A)	6319(18)	3200(20)	4850(11)	48(2)
O(3)	7151(4)	1526(5)	3225(3)	44(1)
O(3A)	7252(16)	2830(20)	3717(9)	48(4)
O(4)	5969(5)	4015(8)	4745(3)	70(2)
O(4A)	5100(40)	5040(40)	3600(30)	53(2)
O(5)	5022(9)	4743(6)	3636(7)	61(2)
O(5A)	4010(20)	3820(30)	2417(15)	53(2)
O(6)	6835(4)	3816(5)	3551(3)	42(1)
O(6A)	5829(13)	3850(20)	2517(13)	47(4)
O(7)	3926(4)	3161(5)	2164(3)	47(1)
O(7A)	4699(17)	730(30)	2112(12)	60(2)
O(8)	4467(4)	1212(6)	2134(3)	47(1)
O(8A)	5653(19)	-44(17)	3123(15)	60(2)
O(9)	5839(4)	2790(5)	2128(3)	39(1)
O(9A)	6417(15)	1588(19)	2393(14)	49(4)
C(5)	4339(6)	1732(9)	4707(4)	60(2)
C(4)	4013(8)	892(6)	4167(6)	60(2)
C(3)	3365(7)	1451(12)	3609(4)	60(2)
C(2)	3291(6)	2636(11)	3804(6)	60(2)
C(1)	3893(8)	2810(7)	4482(6)	60(2)
C(5A)	4255(13)	909(13)	4366(11)	55(3)
C(4A)	3628(15)	972(18)	3691(10)	55(3)
C(3A)	3216(11)	2110(20)	3622(10)	55(3)

C(2A)	3589(15)	2750(13)	4256(13)	55(3)
C(1A)	4232(13)	2008(17)	4716(8)	55(3)
C(6)	6181(7)	-784(8)	2999(5)	50(1)
C(6A)	7915(19)	1140(40)	4700(20)	48(2)
C(7)	7711(6)	681(8)	4766(5)	50(1)
C(7A)	7180(30)	3920(40)	5120(30)	48(2)
C(8)	6895(9)	3959(17)	5134(8)	87(5)
C(8A)	5720(40)	6080(50)	3620(40)	53(2)
C(9)	5380(10)	5922(10)	3631(9)	75(3)
C(9A)	4270(30)	4370(40)	1718(14)	53(2)
C(10)	3993(6)	4348(7)	1954(5)	47(1)
C(10A)	4980(30)	730(40)	1350(14)	60(2)
C(11)	4511(6)	1012(8)	1356(4)	47(1)
C(11A)	6430(30)	-660(20)	2710(30)	60(2)
O(10)	7330(30)	5040(20)	1889(19)	58(7)
O(11)	6737(5)	5051(5)	2206(4)	50(1)
O(12)	7500	6688(7)	2500	79(3)
N(1)	7500	5623(7)	2500	49(2)
O(13)	9980(30)	3370(40)	5150(30)	48(6)
C(12)	11170(30)	3480(50)	5270(40)	45(5)
C(13)	11570(40)	2480(50)	5620(40)	45(5)
C(14)	10750(30)	1800(40)	5880(40)	45(5)
C(15)	9800(30)	2380(50)	5690(40)	45(5)
O(14)	11630(20)	2910(30)	5620(20)	48(6)
C(16)	10920(30)	2190(50)	6090(30)	45(5)
C(17)	9980(30)	2050(40)	5650(30)	45(5)
C(18)	9780(30)	3170(40)	5390(40)	45(5)
C(19)	10760(30)	3690(40)	5290(30)	45(5)

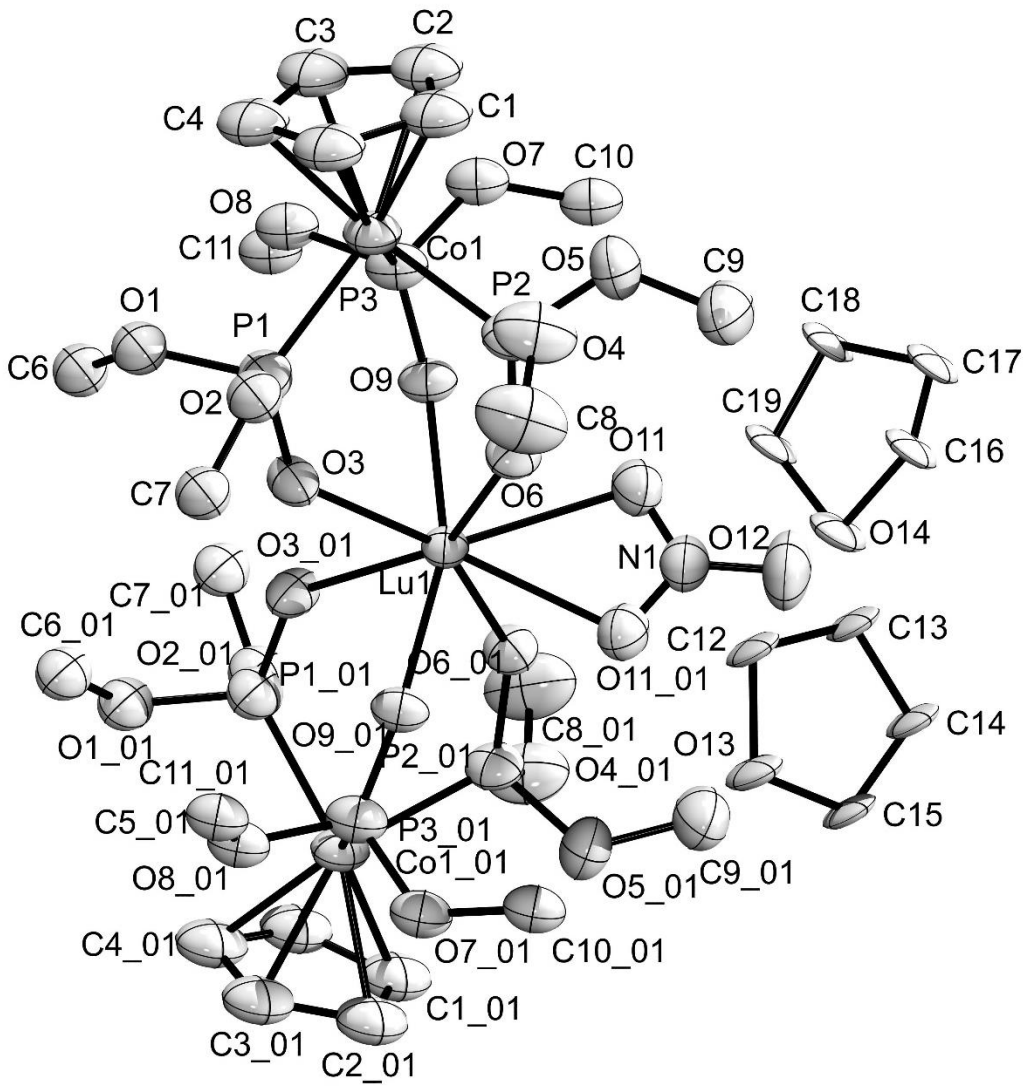

Figure 8.15. Ellipsoid plot of $[Lu(L^{OMe})_2(NO_3)] \cdot 0.5$ THF. Thermal ellipsoids are at 50 % of probability. The hydrogen atoms and the disorder have been omitted for clarity.

Table 8.31. Crystal data and structure refinement for $[Co(L^{OMeCOOMe})_2]$.

Empirical formula	$C_{26}H_{50}Co_3O_{22}P_6$	
Formula weight	1077.27	
Temperature	100(2) K	
Wavelength	0.71073 Å	
Crystal system	Triclinic	
Space group	$P\bar{1}$	
Unit cell dimensions	a = 9.4289(7) Å	α = 90.855(2)°
	b = 10.5413(7) Å	β = 109.101(2)°
	c = 11.3830(8) Å	γ = 102.313(2)°
Volume	1040.10(1) $Å^3$	
Z	1	
Density (calculated)	1.720 g/cm^3	
Absorption coefficient	1.494 mm^{-1}	
F(000)	553	
Crystal size	0.3 x 0.24 x 0.2 mm^3	
Theta range for data collection	2.349 to 27.966°	
Index ranges	-12<=h<=12, -13<=k<=12, -15<=l<=14	
Reflections collected	33931	
Independent reflections	4985 [R(int) = 0.0298]	
Completeness to theta = 25.242°	99.9 %	
Absorption correction	Semi-empirical from equivalents	
Max. and min. transmission	0.7456 and 0.5910	
Refinement method	Full-matrix least-squares on F^2	
Data / restraints / parameters	4985 / 0 / 259	
Goodness-of-fit on F^2	1.046	
Final R indices [I>2sigma(I)]	R1 = 0.0260, wR2 = 0.0677	
R indices (all data)	R1 = 0.0286, wR2 = 0.0691	
Largest diff. peak and hole	0.705 and -0.679 e $\cdot$ $Å^{-3}$	
Diffractometer	Bruker D8 Venture	

Table 8.32. Atomic coordinates (x 10^4) and equivalent isotropic displacement parameters ($Å^2$ x 10^3) for $[Co(L^{OMeCOOMe})_2]$.

	x	y	z	U(eq)
Co(1)	2349(1)	2154(1)	-2548(1)	6(1)
Co(2)	5000	5000	0	6(1)
C(1)	458(2)	1655(2)	-4214(2)	12(1)
C(2)	98(2)	1008(2)	-3233(2)	13(1)
C(3)	1159(2)	195(2)	-2776(2)	12(1)
C(4)	2178(2)	352(2)	-3460(2)	10(1)
C(5)	1753(2)	1267(2)	-4354(2)	9(1)
C(6)	2456(2)	1685(2)	-5314(2)	13(1)
C(7)	4469(3)	1493(2)	-6048(2)	31(1)
O(1)	2050(2)	2439(1)	-6065(1)	21(1)
O(2)	3583(2)	1066(1)	-5248(1)	17(1)
P(1)	2131(1)	4164(1)	-2565(1)	8(1)
O(3)	1873(2)	4528(1)	-3974(1)	15(1)
O(4)	505(2)	4236(1)	-2433(1)	17(1)
O(5)	3388(1)	5219(1)	-1698(1)	10(1)
C(8)	1802(2)	5854(2)	-4224(2)	20(1)
C(9)	411(3)	4941(3)	-1402(3)	38(1)
P(2)	2636(1)	2205(1)	-570(1)	7(1)
O(6)	937(1)	1652(1)	-508(1)	12(1)
O(7)	3463(2)	1091(1)	95(1)	13(1)
O(8)	3361(1)	3466(1)	244(1)	9(1)
C(10)	769(2)	1655(2)	712(2)	16(1)
C(11)	5082(2)	1411(2)	856(2)	15(1)
P(3)	4825(1)	2842(1)	-2121(1)	6(1)
O(9)	5493(1)	1558(1)	-2120(1)	11(1)
O(10)	5229(2)	3497(1)	-3271(1)	13(1)
O(11)	5752(1)	3697(1)	-935(1)	9(1)
C(12)	7134(2)	1753(2)	-1862(2)	25(1)
C(13)	5833(3)	4877(2)	-3238(2)	20(1)

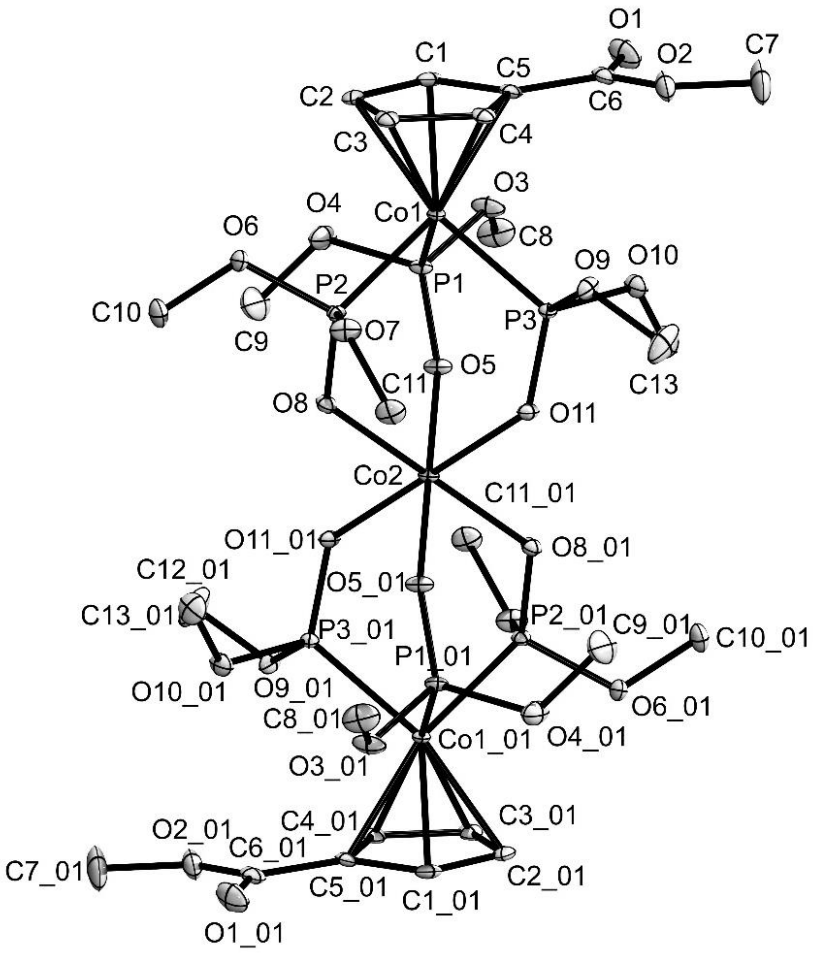

Figure 8.16. Ellipsoid plot of [Co($L^{OMeCOOMe}$)$_2$]. Thermal ellipsoids are at 50 % of probability. The hydrogen atoms have been omitted for clarity.

Table 8.33. Crystal data and structure refinement for [Re(NPhF)(L^{1EtEt})] · 0.5 CH_3OH.

Empirical formula	$C_{29.5}H_{31}FN_5O_{4.5}ReS$	
Formula weight	764.85	
Temperature	100(2) K	
Wavelength	0.71073 Å	
Crystal system	Hexagonal	
Space group	R 3 c :H	
Unit cell dimensions	a = 38.877(2) Å	α = 90°
	b = 38.877(2) Å	β = 90°
	c = 12.4429(5) Å	γ = 120°
Volume	16286.9(2) $Å^3$	
Z	18	
Density (calculated)	1.404 g/cm^3	
Absorption coefficient	3.458 mm^{-1}	
F(000)	6822	
Crystal size	0.4 x 0.2 x 0.2 mm^3	
Theta range for data collection	2.289 to 26.520°	
Index ranges	-48<=h<=48, -48<=k<=48, -14<=l<=15	
Reflections collected	161140	
Independent reflections	7355 [R(int) = 0.0828]	
Completeness to theta = 25.242°	99.8 %	
Absorption correction	Semi-empirical from equivalents	
Max. and min. transmission	0.7454 and 0.5502	
Refinement method	Full-matrix least-squares on F^2	
Data / restraints / parameters	7355 / 10 / 388	
Goodness-of-fit on F^2	1.117	
Final R indices [I>2sigma(I)]	R1 = 0.0388, wR2 = 0.0986	
R indices (all data)	R1 = 0.0483, wR2 = 0.1067	
Absolute structure parameter	-0.008(4)	
Largest diff. peak and hole	0.876 and -1.325 e · $Å^{-3}$	
Diffractometer	Bruker D8 Venture	

Table 8.34. Atomic coordinates (x 10^4) and equivalent isotropic displacement parameters ($Å^2$ x 10^3) for [Re(NPhF)(L^{1EtEt})] · 0.5 CH_3OH.

	x	y	z	U(eq)
Re(1)	3112(1)	813(1)	2458(1)	45(1)
N(1)	3581(3)	1088(2)	1927(7)	43(2)
F(1)	5139(4)	1848(4)	775(13)	132(5)
C(1)	3977(4)	1287(3)	1624(9)	48(3)
C(2)	4260(5)	1610(3)	2232(9)	55(3)
C(3)	4652(5)	1800(4)	1922(12)	72(4)
C(4)	4742(6)	1658(5)	1059(14)	81(5)
C(5)	4489(6)	1357(6)	450(13)	86(5)
C(6)	4090(5)	1165(4)	733(10)	64(4)
S(1)	2729(1)	668(1)	923(2)	52(1)
O(1)	2607(3)	481(2)	3356(6)	53(2)
O(2)	2325(3)	145(2)	4844(7)	67(3)
O(3)	3081(3)	270(2)	2373(6)	51(2)
O(4)	3360(2)	-71(2)	2998(6)	41(2)
N(2)	3352(3)	784(2)	4055(7)	48(2)
N(3)	3026(3)	1270(2)	2893(7)	48(2)
N(5)	2698(3)	1343(3)	1381(8)	53(2)
C(11)	3629(4)	1186(3)	4475(8)	54(3)
C(12)	3520(4)	1477(3)	4418(8)	53(3)
C(13)	3787(5)	1860(4)	4787(9)	64(4)
C(14)	4144(5)	1948(4)	5180(10)	74(5)
C(15)	4248(4)	1651(4)	5270(10)	63(4)
C(16)	3981(5)	1265(3)	4927(9)	62(4)
C(21)	3110(4)	1914(3)	2429(9)	44(2)
C(22)	2875(4)	2072(3)	2633(10)	53(3)
C(23)	3040(5)	2473(4)	2877(11)	65(4)
C(24)	3446(5)	2712(3)	2912(10)	61(4)
C(25)	3685(5)	2556(3)	2697(10)	55(3)
C(26)	3518(4)	2159(3)	2481(10)	54(3)
C(27)	3562(4)	550(3)	3797(9)	51(3)
C(28)	3312(4)	217(3)	3028(8)	43(3)
C(29)	3019(4)	565(3)	4845(8)	53(3)
C(30)	2614(4)	375(3)	4311(8)	52(3)
C(31)	3121(4)	1399(3)	4026(9)	58(3)

C(32)	2940(4)	1482(3)	2219(8)	44(2)
C(33)	2522(4)	980(3)	973(10)	55(3)
C(34)	1938(5)	437(4)	98(15)	88(5)
C(35)	1710(8)	152(6)	1022(19)	129(9)
N(4A)	2153(11)	846(9)	610(50)	81(5)
C(36A)	1917(10)	1041(9)	990(30)	81(5)
C(37A)	1737(10)	954(9)	2130(30)	81(5)
N(4B)	2199(10)	869(7)	420(40)	81(5)
C(37B)	2036(9)	1214(8)	-1000(30)	81(5)
C(36B)	2032(9)	1148(8)	220(30)	81(5)
O(5)	4909(8)	1768(5)	7362(19)	94(9)
C(40)	4747(15)	1963(10)	8010(30)	103(14)

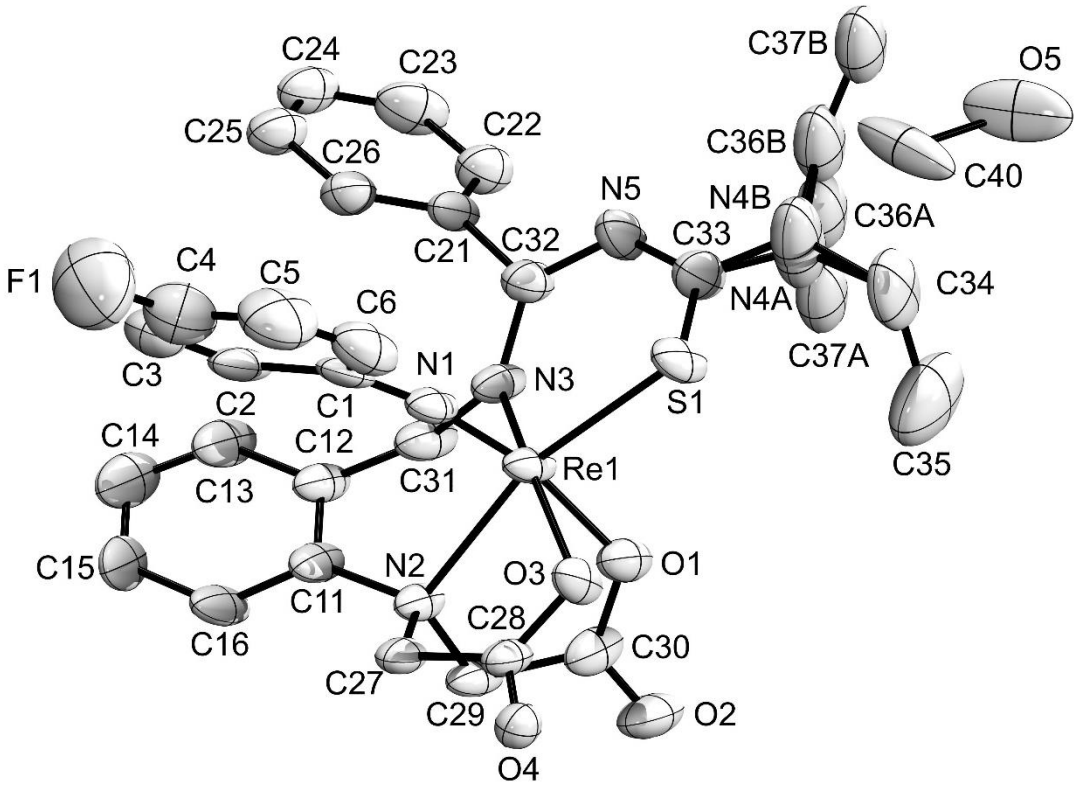

Figure 8.17. Ellipsoid plot of [Re(NPhF)(L^{1EtEt})] · 0.5 CH_3OH. Thermal ellipsoids are at 50 % of probability. The hydrogen atoms have been omitted for clarity.

Table 8.35. Crystal data and structure refinement for [Re(NPh)(L^{1EtEt})] · 0.5 CH_3OH.

Empirical formula	$C_{29.5}H_{32}N_5O_{4.5}ReS$	
Formula weight	746.86	
Temperature	293(2) K	
Wavelength	0.71073 Å	
Crystal system	Monoclinic	
Space group	P 2_1	
Unit cell dimensions	a = 12.873(3) Å	α = 90°
	b = 7.5040(2) Å	β = 96.84(3)°
	c = 15.749(3) Å	γ = 90°
Volume	1510.6(5) $Å^3$	
Z	2	
Density (calculated)	1.642 g/cm^3	
Absorption coefficient	4.136 mm^{-1}	
F(000)	742	
Crystal size	0.45 x 0.2 x 0.05 mm^3	
Theta range for data collection	3.297 to 25.991°.	
Index ranges	-15<=h<=15, -9<=k<=8, -19<=l<=19	
Reflections collected	17679	
Independent reflections	5785 [R(int) = 0.0420]	
Completeness to theta = 25.242°	99.6 %	
Absorption correction	Integration	
Max. and min. transmission	0.8238 and 0.5476	
Refinement method	Full-matrix least-squares on F^2	
Data / restraints / parameters	5785 / 13 / 310	
Goodness-of-fit on F^2	0.930	
Final R indices [I>2sigma(I)]	R1 = 0.0302, wR2 = 0.0611	
R indices (all data)	R1 = 0.0402, wR2 = 0.0626	
Absolute structure parameter	0.532(13)	
Largest diff. peak and hole	0.851 and -1.066 e · $Å^{-3}$	
Diffractometer	STOE IPDS II T	

Table 8.36. Atomic coordinates (x 10^4) and equivalent isotropic displacement parameters ($Å^2$ x 10^3) for [Re(NPh)(L^{1EtEt})] · 0.5 CH_3OH.

	x	y	z	U(eq)
Re(1)	1485(1)	-3739(1)	2641(1)	21(1)
N(1)	2723(5)	-4137(8)	2394(5)	21(2)
C(1)	3764(6)	-3920(30)	2220(6)	48(1)
C(2)	4024(8)	-4213(13)	1393(7)	48(1)
C(3)	5058(7)	-4121(14)	1263(7)	48(1)
C(4)	5849(7)	-3940(20)	1928(6)	48(1)
C(5)	5563(7)	-3489(19)	2748(7)	48(1)
C(6)	4536(6)	-3710(40)	2892(6)	48(1)
S(1)	1526(2)	-5085(3)	3960(2)	32(1)
O(1)	-33(5)	-2870(8)	2742(4)	30(2)
O(2)	-1574(5)	-1967(12)	2100(5)	52(2)
O(3)	697(5)	-5923(8)	2092(5)	32(2)
O(4)	154(6)	-7190(9)	848(5)	43(2)
N(2)	943(6)	-2631(11)	1343(6)	25(2)
N(3)	1901(6)	-1274(9)	3155(5)	24(2)
N(4)	1825(6)	-3910(30)	5546(5)	42(3)
N(5)	2505(6)	-2033(11)	4596(5)	36(2)
C(11)	1688(7)	-1284(12)	1109(6)	27(2)
C(12)	2028(7)	40(12)	1695(6)	30(2)
C(13)	2695(7)	1410(30)	1435(7)	39(3)
C(14)	2999(8)	1390(30)	627(7)	50(3)
C(15)	2651(9)	55(17)	53(8)	48(3)
C(16)	1981(8)	-1295(14)	291(7)	38(2)
C(21)	3246(10)	468(15)	4026(9)	54(1)
C(22)	3979(9)	726(13)	3445(9)	54(1)
C(23)	4771(10)	2005(14)	3623(9)	54(1)
C(24)	4799(10)	3029(16)	4374(9)	54(1)
C(25)	4095(9)	2803(15)	4918(9)	54(1)
C(26)	3304(8)	1460(20)	4763(7)	54(1)
C(27)	917(8)	-4307(11)	810(7)	29(2)
C(28)	535(9)	-5927(13)	1269(7)	29(2)
C(29)	-120(8)	-1853(14)	1308(6)	29(2)
C(30)	-632(7)	-2267(12)	2086(6)	30(2)
C(31)	1674(7)	248(11)	2557(6)	29(2)

C(32)	2494(7)	-1028(12)	3895(6)	28(2)
C(33)	1965(7)	-3510(30)	4728(6)	34(4)
C(34)	2297(14)	-2770(20)	6259(11)	94(4)
C(35)	1559(14)	-1600(30)	6623(11)	94(4)
C(36)	1214(10)	-5401(17)	5788(8)	52(3)
C(37)	55(11)	-5050(20)	5639(9)	70(4)

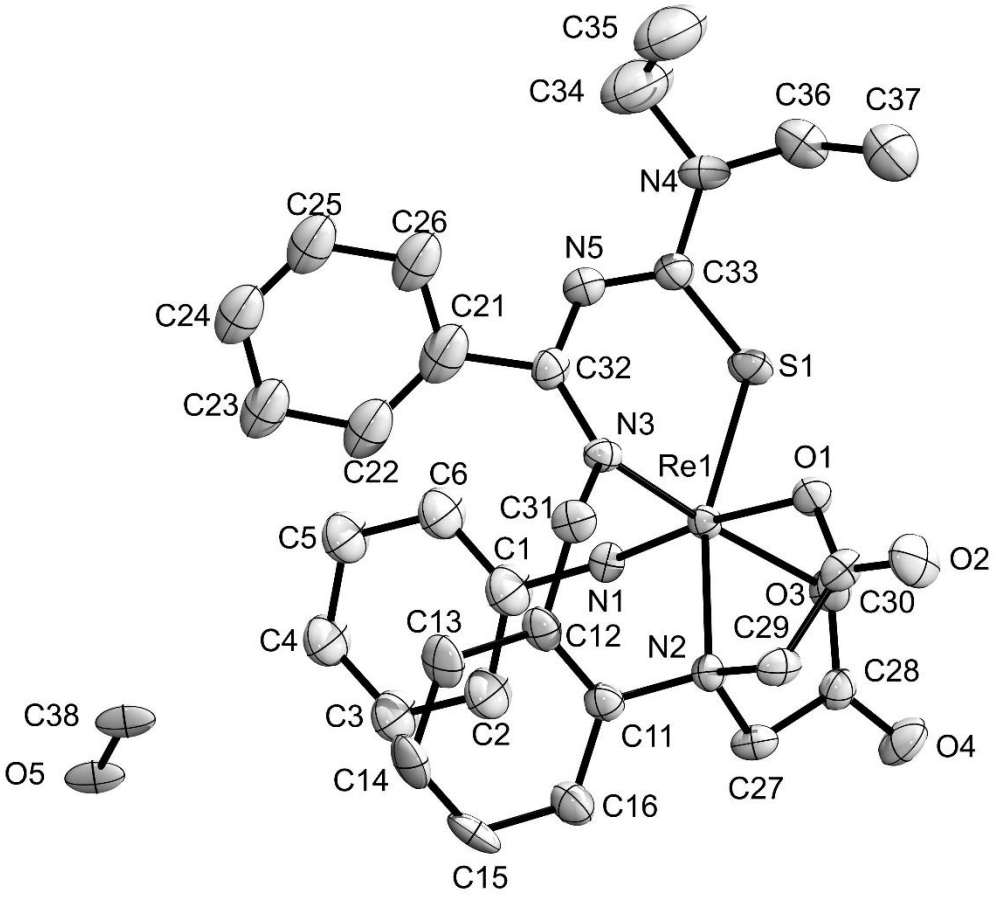

Figure 8.18. Ellipsoid plot of [Re(NPh)(L^{1EtEt})] · 0.5 CH_3OH. Thermal ellipsoids are at 50 % of probability. The hydrogen atoms have been omitted for clarity.

Table 8.37. Crystal data and structure refinement for [ReO(HL^{2EtEt})] · acetone · 0.5 H_2O.

Empirical formula	$C_{21}H_{29}N_5O_{6.5}ReS$	
Formula weight	673.75	
Temperature	100(2) K	
Wavelength	0.71073 Å	
Crystal system	Monoclinic	
Space group	$P2_1/c$	
Unit cell dimensions	a = 23.3084(2) Å	α = 90°
	b = 11.6201(8) Å	β = 91.233(3)°
	c = 19.0234(1) Å	γ = 90°
Volume	5151.2(6) $Å^3$	
Z	8	
Density (calculated)	1.738 g/cm^3	
Absorption coefficient	4.846 mm^{-1}	
F(000)	2664	
Crystal size	0.600 x 0.300 x 0.130 mm^3	
Theta range for data collection	2.223 to 27.987°	
Index ranges	-30<=h<=30, -15<=k<=15, -25<=l<=25	
Reflections collected	158954	
Independent reflections	12406 [R(int) = 0.0544]	
Completeness to theta = 25.242°	99.9 %	
Absorption correction	Semi-empirical from equivalents	
Max. and min. transmission	0.7456 and 0.4262	
Refinement method	Full-matrix least-squares on F^2	
Data / restraints / parameters	12406 / 0 / 631	
Goodness-of-fit on F^2	1.092	
Final R indices [I>2sigma(I)]	R1 = 0.0268, wR2 = 0.0598	
R indices (all data)	R1 = 0.0314, wR2 = 0.0613	
Largest diff. peak and hole	1.181 and -1.531 e · $Å^{-3}$	
Diffractometer	Bruker Venture D8	

Table 8.38. Atomic coordinates (x 10^4) and equivalent isotropic displacement parameters ($Å^2$ x 10^3) for [ReO(HL^{2EtEt})] · acetone · 0.5 H_2O.

	x	y	z	U(eq)
Re(1)	6733(1)	3504(1)	6535(1)	13(1)
S(1)	6559(1)	2591(1)	5480(1)	17(1)
O(1)	7005(1)	2556(2)	7119(1)	20(1)
O(2)	7028(1)	6780(2)	7215(1)	25(1)
O(3)	5156(1)	4405(3)	7265(2)	34(1)
O(4)	5664(2)	1753(3)	7558(2)	45(1)
O(5)	5057(1)	916(3)	6784(2)	39(1)
N(1)	6995(1)	2905(2)	4222(1)	16(1)
N(2)	7628(1)	3337(2)	5109(1)	15(1)
N(3)	7395(1)	4376(2)	6140(1)	14(1)
N(4)	6620(1)	5052(2)	6934(1)	17(1)
N(5)	5873(1)	3559(2)	6646(2)	20(1)
C(1)	7765(1)	3917(3)	5680(2)	14(1)
C(2)	8396(1)	4041(3)	5797(2)	17(1)
C(3)	8644(2)	3800(3)	6455(2)	20(1)
C(4)	9238(2)	3809(3)	6540(2)	26(1)
C(5)	9579(2)	4065(4)	5973(2)	32(1)
C(6)	9334(2)	4296(4)	5318(2)	31(1)
C(7)	8743(2)	4273(3)	5228(2)	24(1)
C(8)	7101(1)	3011(3)	4903(2)	15(1)
C(9)	7449(2)	3152(3)	3715(2)	19(1)
C(10)	7460(2)	4413(3)	3519(2)	38(1)
C(11)	6432(2)	2558(3)	3925(2)	25(1)
C(12)	6383(2)	1258(4)	3846(2)	36(1)
C(13)	7564(1)	5420(3)	6534(2)	16(1)
C(14)	7046(1)	5838(3)	6930(2)	17(1)
C(15)	6072(2)	5342(3)	7247(2)	21(1)
C(16)	5657(2)	4391(3)	7060(2)	23(1)
C(17)	5462(2)	2665(3)	6431(2)	24(1)
C(18)	5421(2)	1754(4)	7000(2)	28(1)
Re(2)	8127(1)	5173(1)	8720(1)	16(1)
S(2)	8020(1)	4395(1)	9814(1)	20(1)
O(6)	7707(1)	4482(2)	8127(1)	22(1)
O(7)	8635(1)	8247(2)	7919(2)	39(1)
O(8)	9819(1)	4527(3)	8299(2)	37(1)

O(9)	8827(1)	2457(3)	7943(1)	36(1)
O(10)	9437(1)	1528(2)	8682(2)	36(1)
N(6)	7603(1)	5117(2)	11005(2)	22(1)
N(7)	7231(1)	6117(2)	10070(1)	18(1)
N(8)	7704(1)	6602(2)	9009(1)	18(1)
N(9)	8601(1)	6373(2)	8285(2)	21(1)
N(10)	8919(1)	4449(3)	8750(2)	24(1)
C(19)	7288(1)	6709(3)	9488(2)	17(1)
C(20)	6841(1)	7613(3)	9382(2)	19(1)
C(21)	6536(2)	7719(3)	8746(2)	23(1)
C(22)	6110(2)	8550(3)	8669(2)	29(1)
C(23)	5990(2)	9280(3)	9218(2)	33(1)
C(24)	6288(2)	9180(3)	9853(2)	34(1)
C(25)	6710(2)	8340(3)	9936(2)	26(1)
C(26)	7586(2)	5296(3)	10318(2)	18(1)
C(27)	7304(2)	5878(3)	11492(2)	31(1)
C(28)	6728(2)	5378(4)	11687(2)	40(1)
C(29)	7943(2)	4185(3)	11340(2)	25(1)
C(30)	8549(2)	4563(4)	11528(2)	37(1)
C(31)	7827(2)	7615(3)	8569(2)	23(1)
C(32)	8395(2)	7452(3)	8223(2)	26(1)
C(33)	9181(2)	6106(3)	8067(2)	29(1)
C(34)	9344(2)	4957(3)	8375(2)	27(1)
C(35)	9090(2)	3334(3)	9049(2)	27(1)
C(36)	9100(2)	2419(3)	8487(2)	26(1)
O(11)	9503(1)	-192(3)	7843(2)	34(1)
O(12)	5186(2)	2246(7)	4805(2)	122(3)
C(37)	4411(2)	983(6)	4910(3)	60(2)
C(38)	4770(2)	1847(6)	4530(3)	58(2)
C(39)	4603(3)	2128(6)	3805(3)	64(2)
O(11)	9503(1)	-192(3)	7843(2)	34(1)
O(12)	5186(2)	2246(7)	4805(2)	122(3)
C(37)	4411(2)	983(6)	4910(3)	60(2)
C(38)	4770(2)	1847(6)	4530(3)	58(2)
C(39)	4603(3)	2128(6)	3805(3)	64(2)
O(13)	8290(1)	7176(3)	5326(2)	54(1)
C(40)	9227(2)	7641(7)	4979(3)	72(2)
C(41)	8785(2)	7352(4)	5497(2)	37(1)
C(42)	8988(2)	7260(4)	6243(2)	45(1)

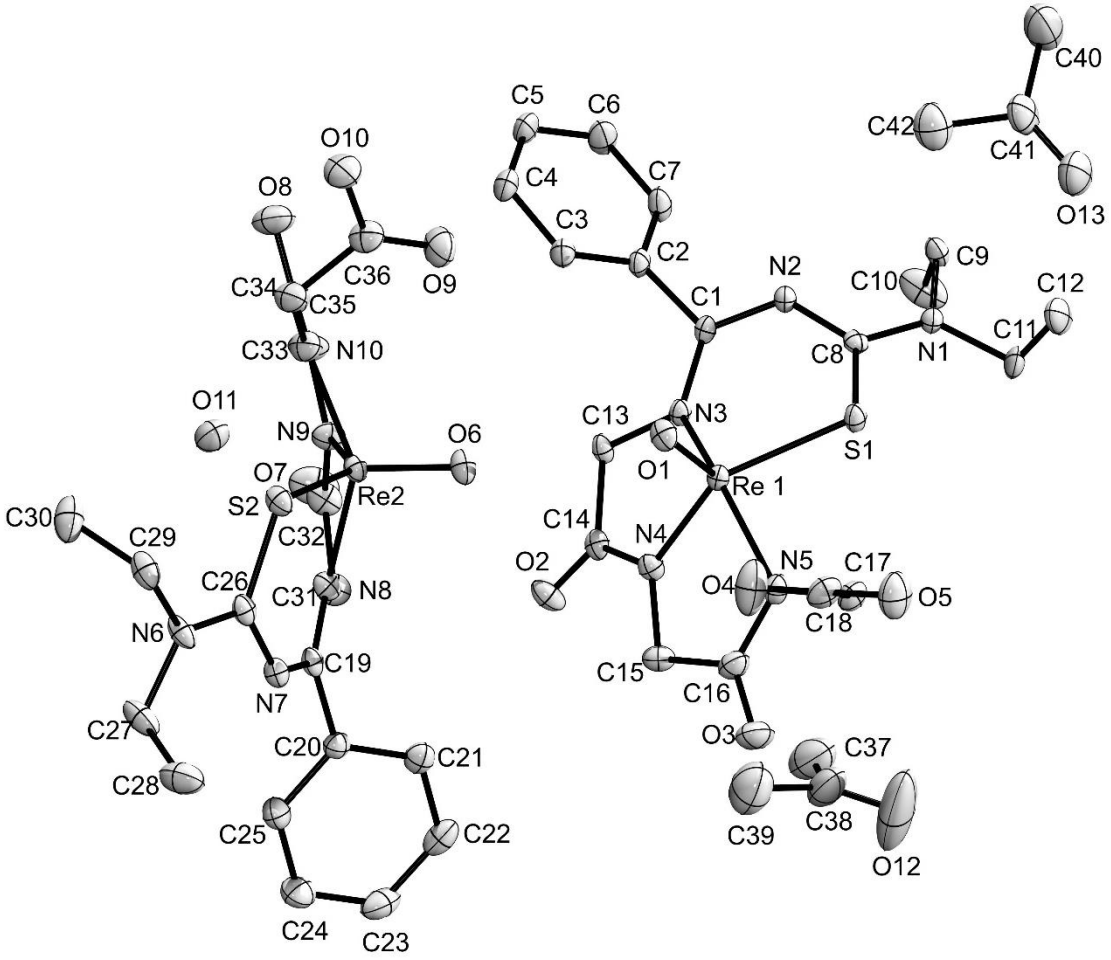

Figure 8.19. Ellipsoid plot of [ReO(HL^{2EtEt})] · acetone · 0.5 H_2O. Thermal ellipsoids are at 50 % of probability. The hydrogen atoms have been omitted for clarity.

Table 8.39. Crystal data and structure refinement for [ReO($L^{2MePh\text{-}ester}$)].

Empirical formula	$C_{22}H_{22}N_5O_5ReS$	
Formula weight	654.70	
Temperature	104(2) K	
Wavelength	0.71073 Å	
Crystal system	Monoclinic	
Space group	$P2_1/n$	
Unit cell dimensions	a = 11.2369(6) Å	α = 90°
	b = 13.4327(7) Å	β = 92.028(2)°
	c = 14.8090(8) Å	γ = 90°
Volume	2233.9(2) $Å^3$	
Z	4	
Density (calculated)	1.947 g/cm^3	
Absorption coefficient	5.579 mm^{-1}	
F(000)	1280	
Crystal size	0.600 x 0.600 x 0.130 mm^3	
Theta range for data collection	2.315 to 27.948°	
Index ranges	-13<=h<=14, -17<=k<=17, -19<=l<=19	
Reflections collected	54779	
Independent reflections	5349 [R(int) = 0.0443]	
Completeness to theta = 25.242°	100.0 %	
Absorption correction	Semi-empirical from equivalents	
Max. and min. transmission	0.2086 and 0.0605	
Refinement method	Full-matrix least-squares on F^2	
Data / restraints / parameters	5349 / 0 / 312	
Goodness-of-fit on F^2	1.044	
Final R indices [I>2sigma(I)]	R1 = 0.0265, wR2 = 0.0677	
R indices (all data)	R1 = 0.0278, wR2 = 0.0686	
Largest diff. peak and hole	2.702 and -1.231 e $\cdot$ $Å^{-3}$	
Diffractometer	Bruker Venture D8	

Table 8.40. Atomic coordinates (x 10^4) and equivalent isotropic displacement parameters ($Å^2$ x 10^3) for [ReO($L^{2MePh\text{-}ester}$)].

	x	y	z	U(eq)
Re(1)	7055(1)	4008(1)	373(1)	19(1)
S(1)	5285(1)	3825(1)	1076(1)	23(1)
O(1)	6794(2)	4472(2)	-670(2)	26(1)
O(2)	10567(2)	4396(2)	1045(2)	30(1)
O(3)	8338(3)	1160(2)	95(2)	29(1)
O(4)	6356(3)	1222(2)	1663(2)	31(1)
O(5)	4727(3)	816(2)	811(2)	35(1)
N(1)	4660(3)	4571(2)	2630(2)	22(1)
N(2)	5760(3)	5669(2)	1828(2)	22(1)
N(3)	7537(2)	5160(2)	1160(2)	21(1)
N(4)	8754(3)	3718(2)	647(2)	23(1)
N(5)	7106(2)	2510(2)	275(2)	22(1)
C(1)	6760(3)	5859(2)	1431(2)	20(1)
C(2)	7035(3)	6929(2)	1275(2)	22(1)
C(3)	7367(3)	7225(3)	412(2)	26(1)
C(4)	7579(4)	8229(3)	244(3)	33(1)
C(5)	7492(4)	8919(3)	919(3)	34(1)
C(6)	7177(4)	8631(3)	1781(3)	34(1)
C(7)	6937(3)	7633(3)	1956(3)	28(1)
C(8)	5258(3)	4775(2)	1898(2)	21(1)
C(9)	3898(3)	3705(3)	2678(2)	22(1)
C(10)	4313(3)	2864(3)	3138(2)	25(1)
C(11)	3543(3)	2065(3)	3235(2)	26(1)
C(12)	2385(4)	2109(3)	2878(2)	31(1)
C(13)	2000(4)	2948(3)	2410(3)	35(1)
C(14)	2759(3)	3757(3)	2306(3)	29(1)
C(15)	4675(3)	5249(3)	3411(2)	27(1)
C(16)	8815(3)	5403(2)	1159(2)	23(1)
C(17)	9489(3)	4460(3)	953(2)	22(1)
C(18)	9224(3)	2728(2)	492(2)	25(1)
C(19)	8189(3)	2044(2)	259(2)	24(1)
C(20)	6085(3)	1854(3)	134(2)	26(1)
C(21)	5774(3)	1276(3)	977(2)	26(1)
C(22)	4306(4)	204(3)	1538(3)	38(1)

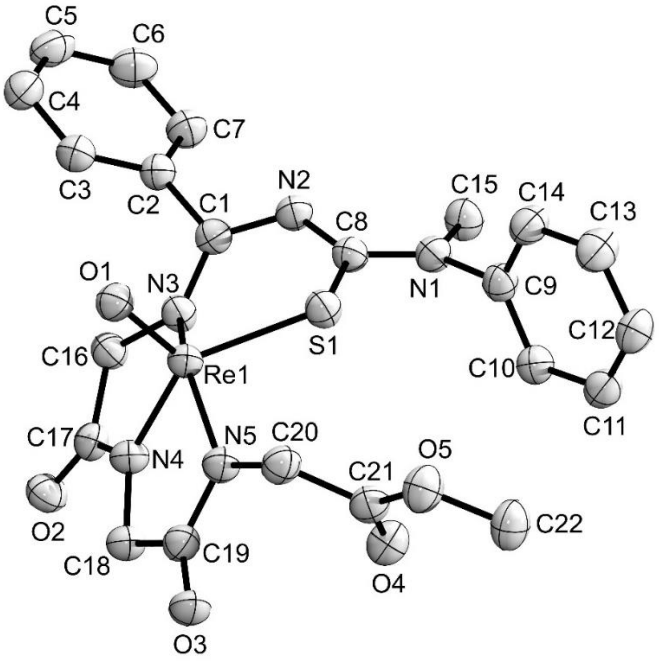

Figure 8.20. Ellipsoid plot of [ReO($L^{2MePh\text{-}ester}$)]. Thermal ellipsoids are at 50 % of probability. The hydrogen atoms have been omitted for clarity.

Table 8.41. Crystal data and structure refinement for [ReO(HL^{2PhPh})].

Empirical formula	$C_{26}H_{22}N_5O_5ReS$	
Formula weight	702.74	
Temperature	105(2) K	
Wavelength	0.71073 Å	
Crystal system	Monoclinic	
Space group	C2/c	
Unit cell dimensions	a = 42.863(3) Å	α = 90°
	b = 5.6981(4) Å	β = 127.223(2)°
	c = 26.018(2) Å	γ = 90°
Volume	5060.2(7) $Å^3$	
Z	8	
Density (calculated)	1.845 g/cm^3	
Absorption coefficient	4.933 mm^{-1}	
F(000)	2752	
Crystal size	0.34 x 0.03 x 0.02 mm^3	
Theta range for data collection	2.387 to 27.169°	
Index ranges	-54<=h<=54, -7<=k<=7, -33<=l<=33	
Reflections collected	55334	
Independent reflections	5616 [R(int) = 0.0966]	
Completeness to theta = 25.242°	99.9 %	
Absorption correction	Semi-empirical from equivalents	
Max. and min. transmission	0.7455 and 0.6285	
Refinement method	Full-matrix least-squares on F^2	
Data / restraints / parameters	5616 / 0 / 348	
Goodness-of-fit on F^2	1.062	
Final R indices [I>2sigma(I)]	R1 = 0.0303, wR2 = 0.0446	
R indices (all data)	R1 = 0.0476, wR2 = 0.0477	
Largest diff. peak and hole	1.322 and -1.144 e $\cdot$ $Å^{-3}$	
Diffractometer	Bruker Venture D8	

Table 8.42. Atomic coordinates (x 10^4) and equivalent isotropic displacement parameters ($Å^2$ x 10^3) for [ReO(HL^{2PhPh})].

	x	y	z	U(eq)
Re(1)	1547(1)	3287(1)	6070(1)	9(1)
S(1)	1032(1)	4519(2)	5064(1)	12(1)
O(1)	1728(1)	785(5)	6012(1)	16(1)
O(2)	2273(1)	6811(5)	7768(1)	20(1)
O(3)	1052(1)	1914(7)	6984(1)	36(1)
O(4)	464(1)	4928(6)	5643(1)	22(1)
O(5)	137(1)	2264(5)	4850(2)	24(1)
N(1)	944(1)	7507(5)	4213(1)	10(1)
N(2)	1590(1)	6782(6)	5028(1)	8(1)
N(3)	1891(1)	5850(5)	6128(1)	9(1)
N(4)	1794(1)	4478(6)	6947(1)	12(1)
N(5)	1155(1)	2348(6)	6221(2)	16(1)
C(1)	1900(1)	6459(6)	5642(2)	8(1)
C(2)	2284(1)	6872(7)	5771(2)	9(1)
C(3)	2574(1)	5158(7)	6097(2)	11(1)
C(4)	2929(1)	5481(7)	6203(2)	14(1)
C(5)	3001(1)	7504(7)	6002(2)	16(1)
C(6)	2715(1)	9222(7)	5682(2)	15(1)
C(7)	2354(1)	8891(6)	5556(2)	13(1)
C(8)	1218(1)	6410(6)	4774(2)	9(1)
C(9)	1035(1)	9212(6)	3912(2)	9(1)
C(10)	1298(1)	11025(6)	4265(2)	10(1)
C(11)	1368(1)	12685(6)	3960(2)	11(1)
C(12)	1178(1)	12536(7)	3298(2)	13(1)
C(13)	919(1)	10723(7)	2952(2)	14(1)
C(14)	846(1)	9054(7)	3251(2)	13(1)
C(15)	532(1)	6959(7)	3878(2)	12(1)
C(16)	376(1)	4921(7)	3518(2)	14(1)
C(17)	-14(1)	4408(7)	3220(2)	20(1)
C(18)	-242(1)	5894(8)	3282(2)	19(1)
C(19)	-86(1)	7952(8)	3635(2)	18(1)
C(20)	304(1)	8503(8)	3931(2)	14(1)
C(21)	2218(1)	6543(7)	6797(2)	11(1)
C(22)	2104(1)	6008(6)	7227(2)	12(1)

C(23)	1633(1)	3864(8)	7287(2)	23(1)
C(24)	1251(1)	2595(8)	6825(2)	24(1)
C(25)	774(1)	1280(7)	5736(2)	21(1)
C(26)	446(1)	3025(8)	5410(2)	18(1)

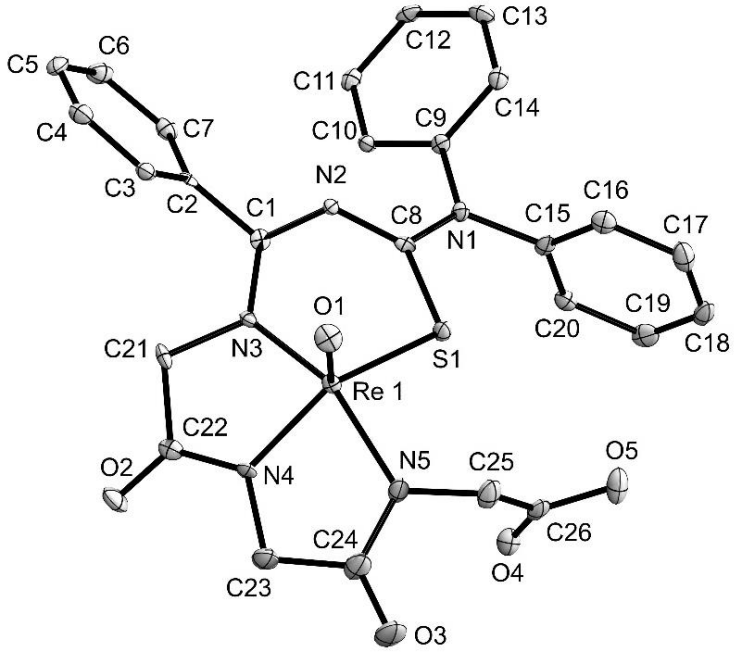

Figure 8.21. Ellipsoid plot of [ReO(HL^{2PhPh})]. Thermal ellipsoids are at 50 % of probability. The hydrogen atoms have been omitted for clarity.

9 Spectroscopic Data

Spectroscopic Data of [Tc^{I}(NO)Cl(PPh_3)(L^{OMe})]

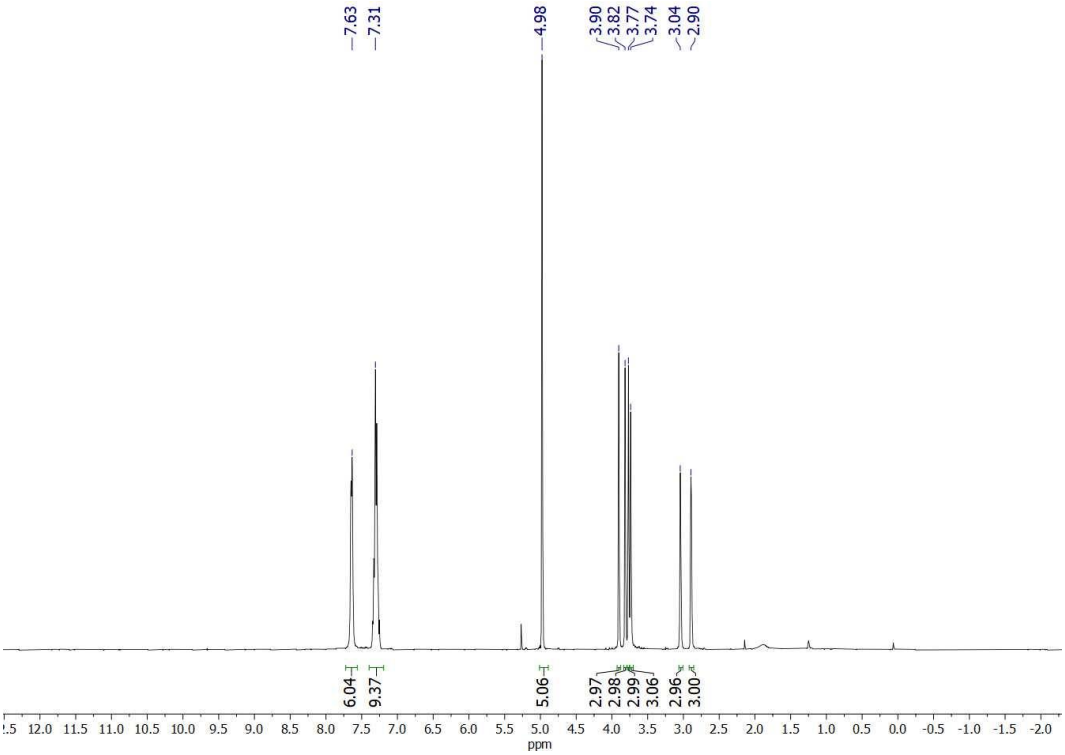

Figure 9.1. $^{1}H\{^{31}P\}$ NMR spectrum of [Tc^{I}(NO)Cl(PPh_3)(L^{OMe})] in $CDCl_3$.

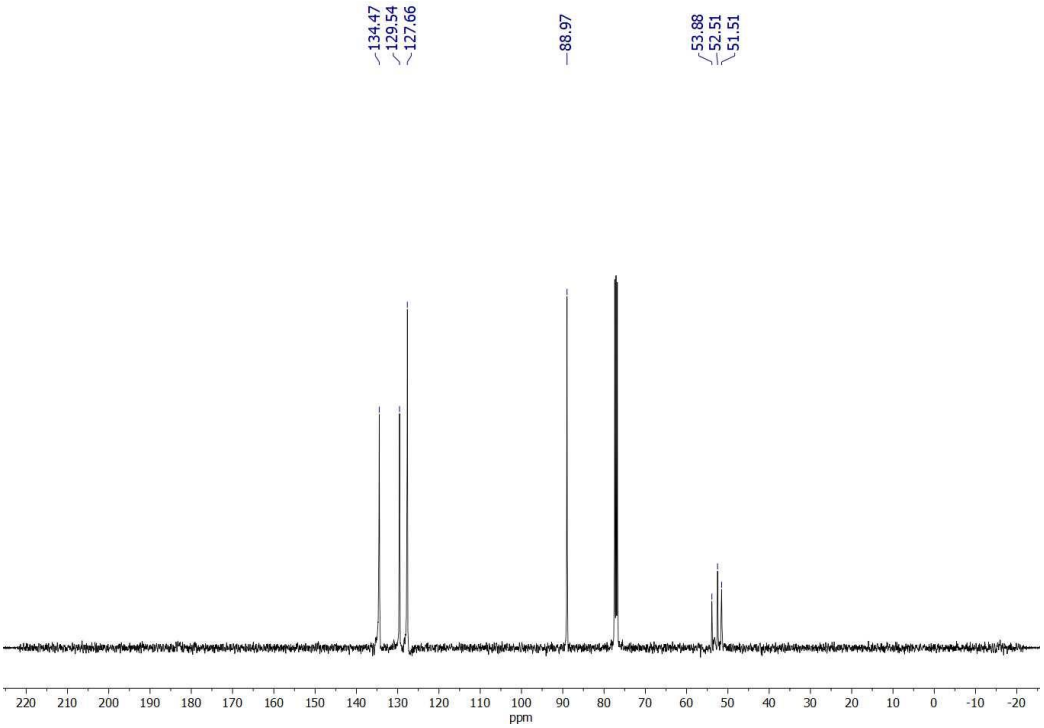

Figure 9.2. $^{13}C\{^{1}H\}$ NMR spectrum of [Tc^{I}(NO)Cl(PPh_3)(L^{OMe})] in $CDCl_3$.

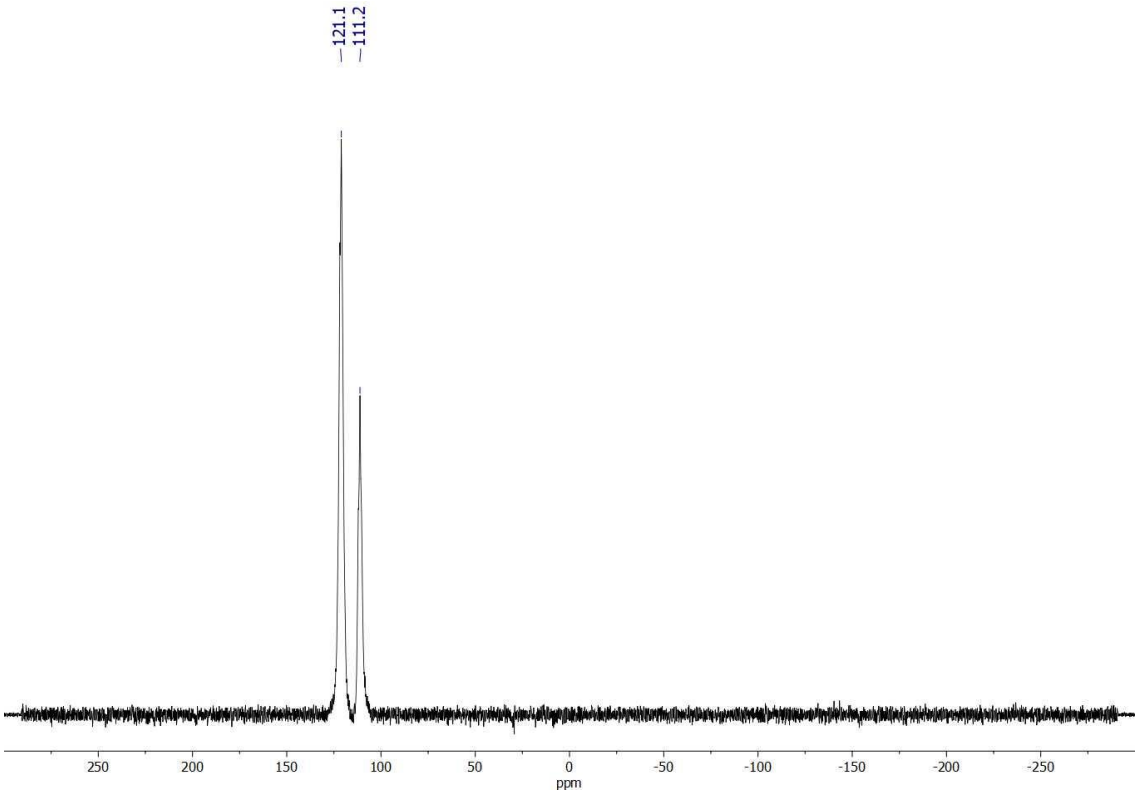

Figure 9.3. $^{31}P\{^{1}H\}$ NMR spectrum of $[Tc^{I}(NO)Cl(PPh_3)(L^{OMe})]$ in $CDCl_3$.

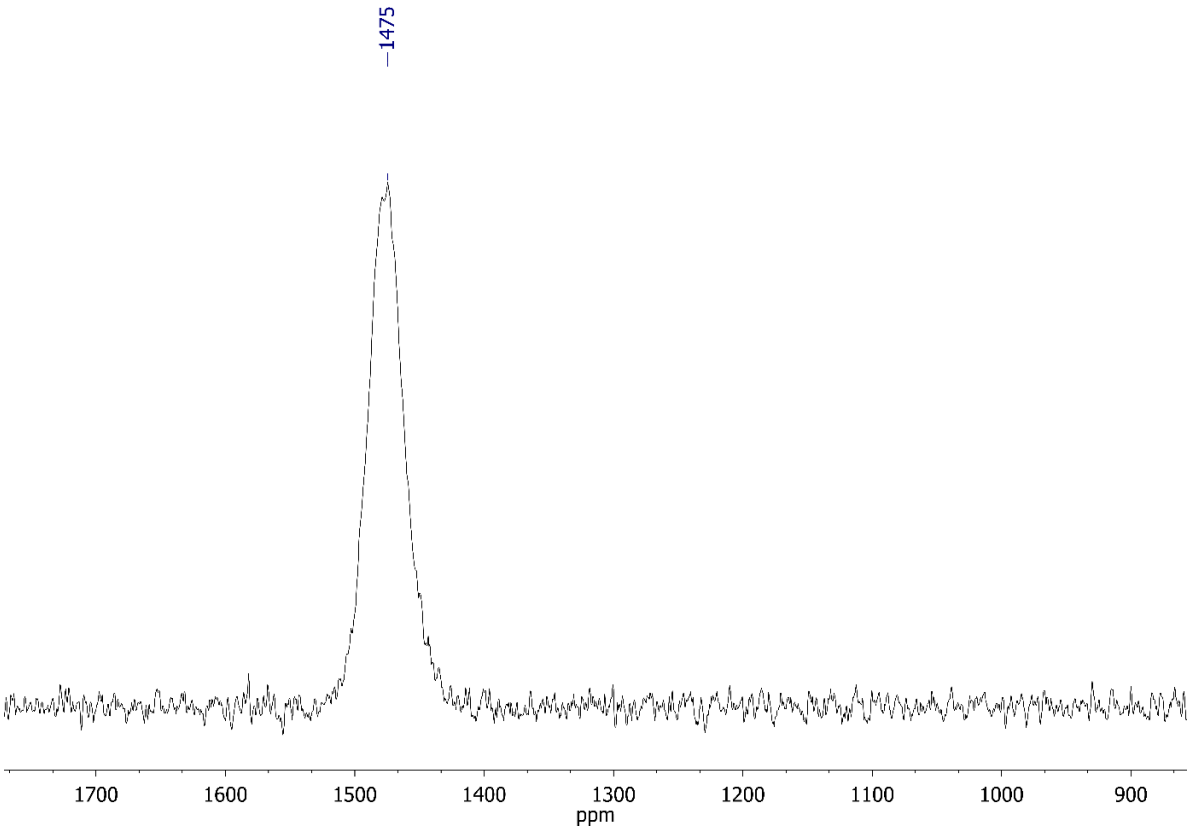

Figure 9.4. ^{99}Tc NMR spectrum of $[Tc^{I}(NO)Cl(PPh_3)(L^{OMe})]$ in $CDCl_3$.

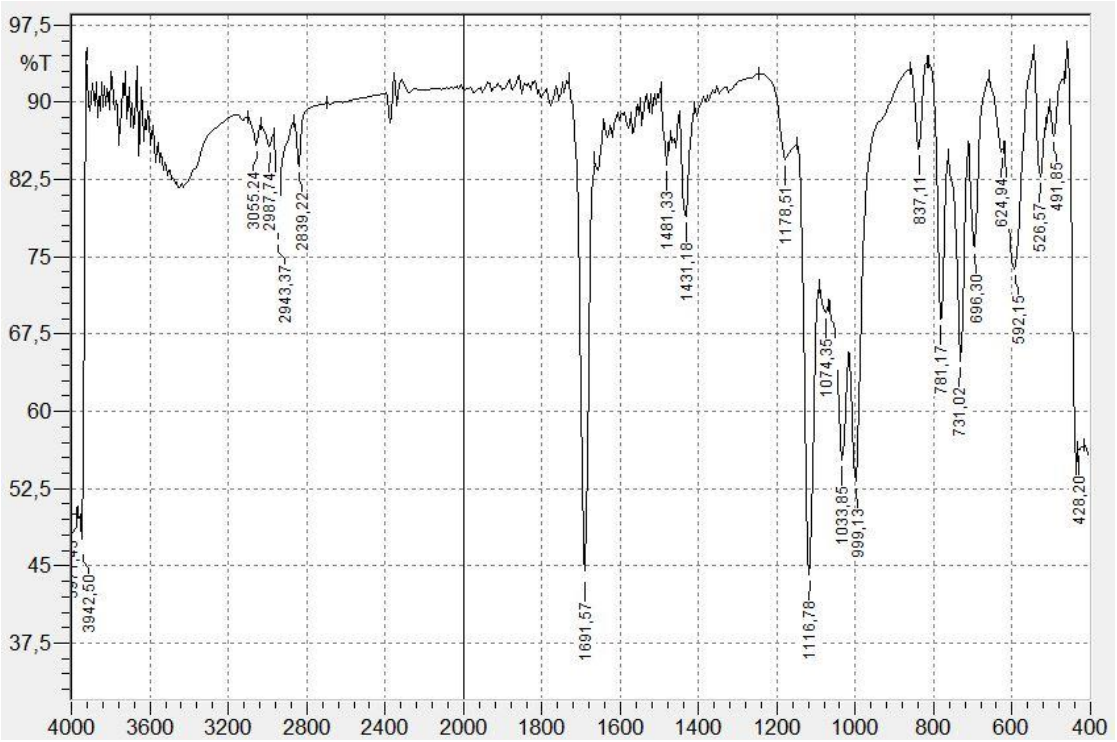

Figure 9.5. IR spectrum of [Tc^{I}(NO)Cl(PPh$_3$)(L^{OMe})].

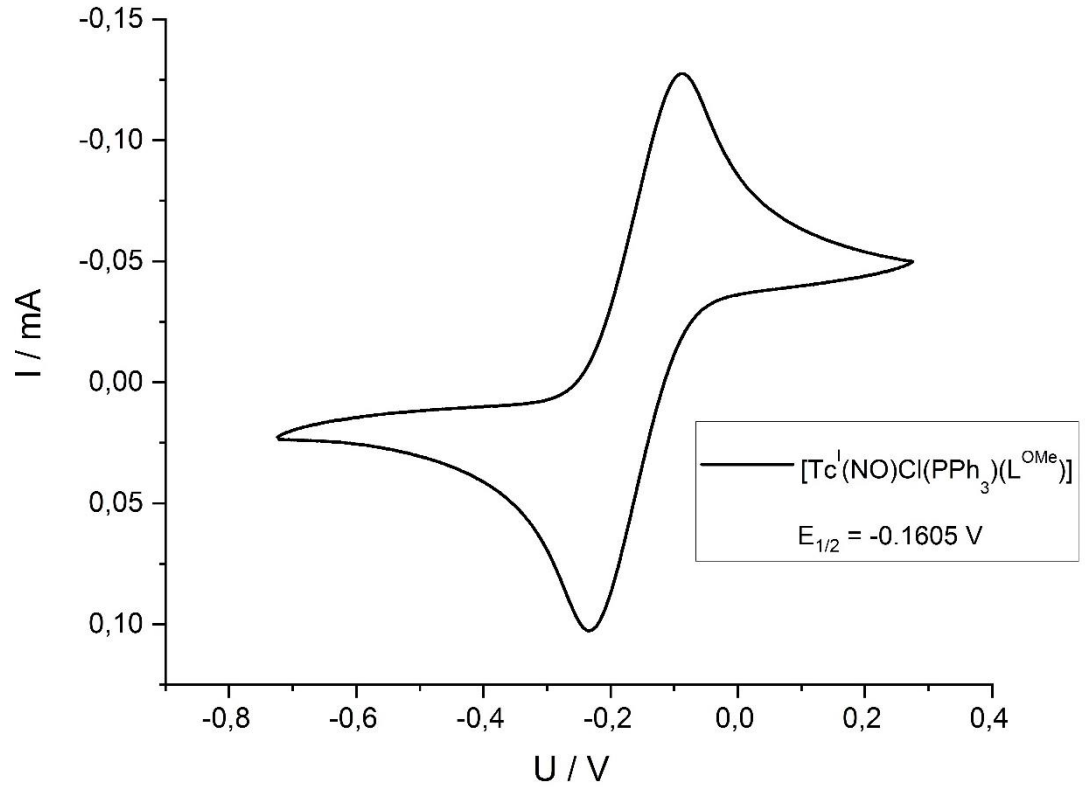

Figure 9.6. Cyclic voltammogram taken from [Tc^{I}(NO)Cl(PPh$_3$)(L^{OMe})] (0.9 mL dry CH_2Cl_2, 50 mg $(NBu_4)PF_6$, 5 mg [Tc^{I}(NO)Cl(PPh$_3$)(L^{OMe})], scan rate 500 mV/s).

Spectroscopic Data of $[Tc^{II}(NO)Cl_2(L^{OMe})]$

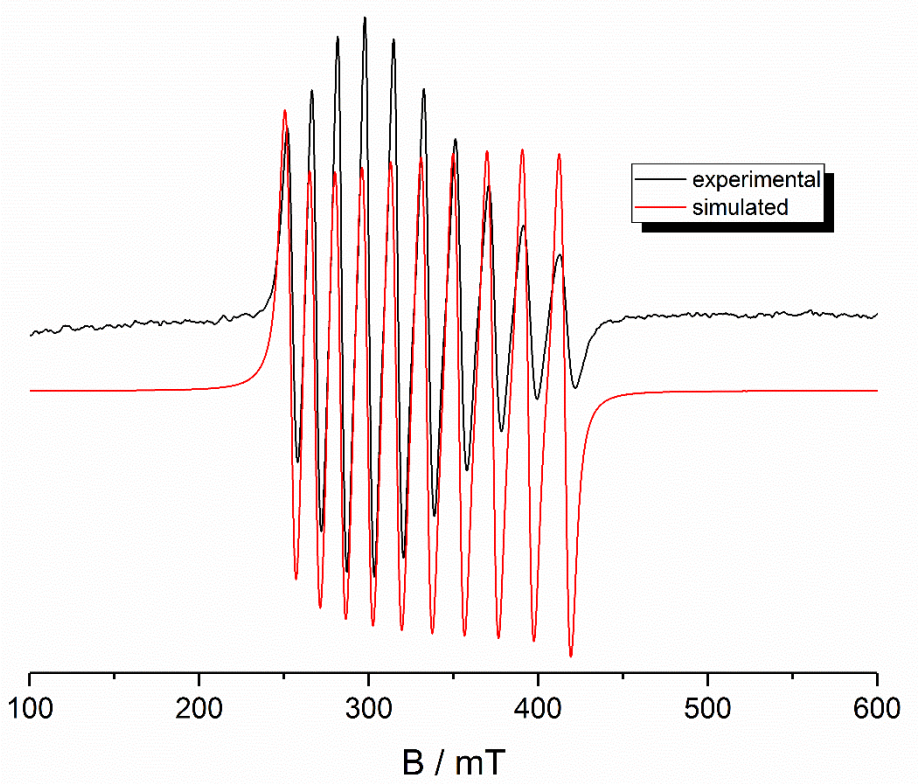

Figure 9.7. X-Band EPR spectrum of $[Tc^{II}(NO)Cl_2(L^{OMe})]$ at room temperature in CH_2Cl_2.

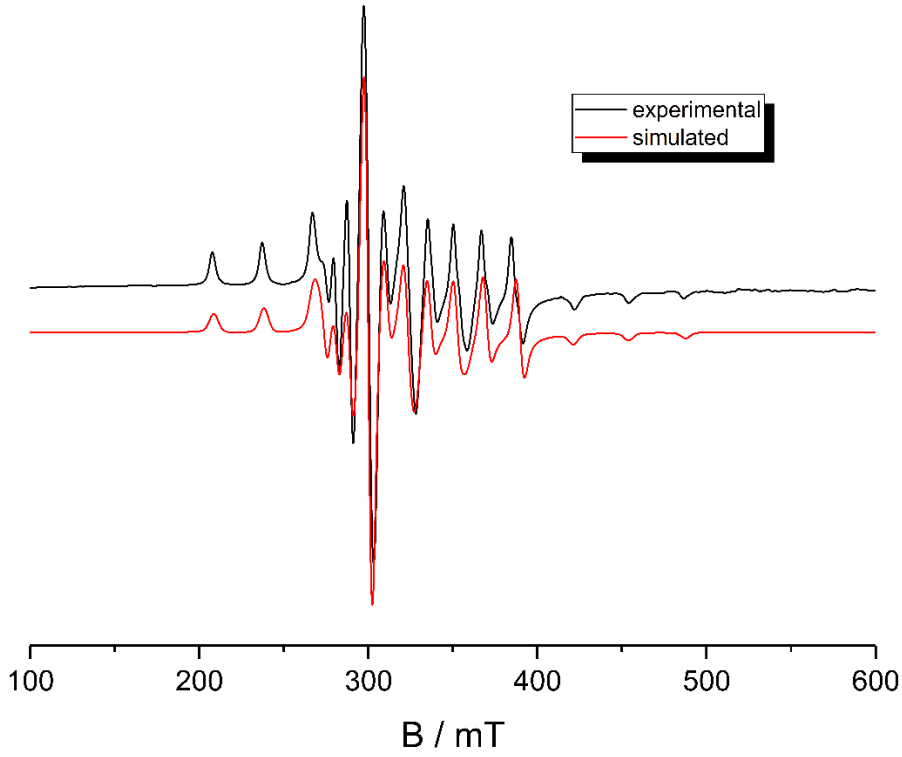

Figure 9.8. X-Band EPR spectrum of $[Tc^{II}(NO)Cl_2(L^{OMe})]$ at 77 K in CH_2Cl_2.

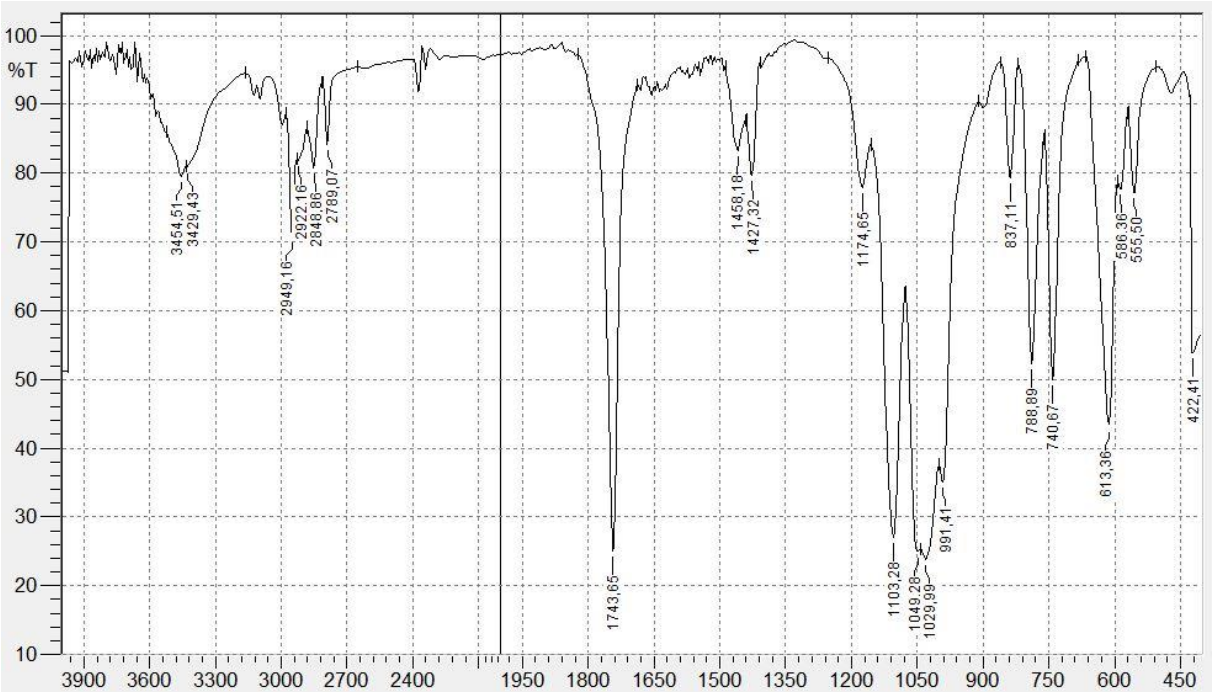

Figure 9.9. IR spectrum of $[Tc^{II}(NO)Cl_2(L^{OMe})]$.

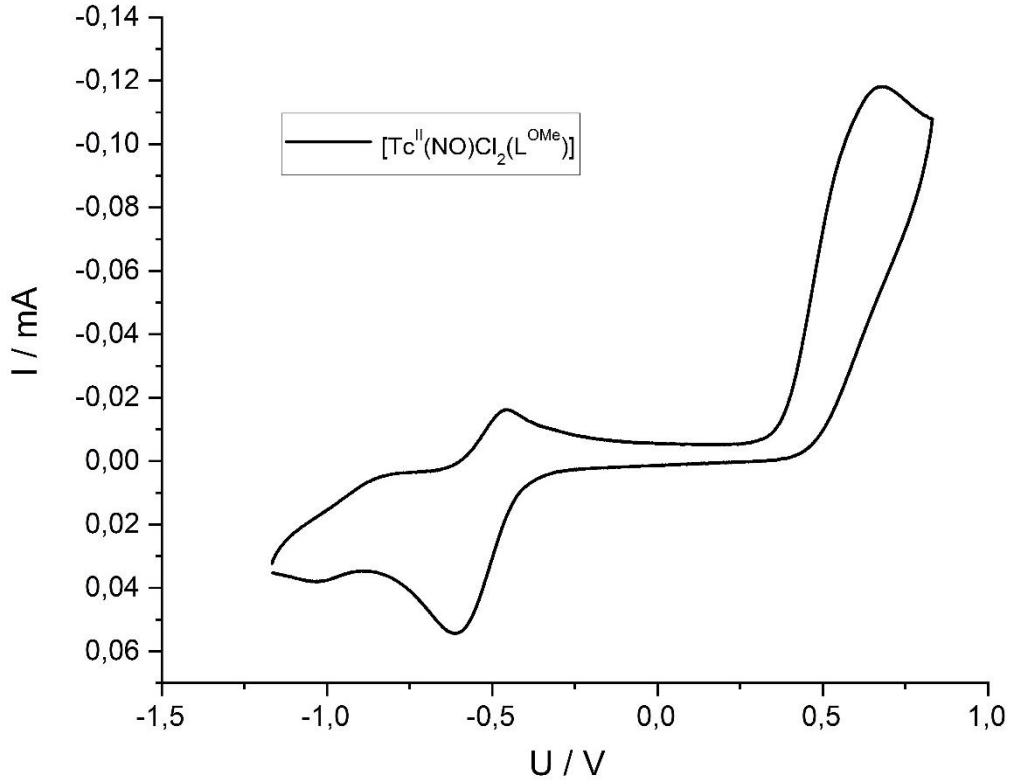

Figure 9.10. Cyclic voltammogram taken from $[Tc^{II}(NO)Cl_2(L^{OMe})]$ (0.9 mL dry CH_2Cl_2, 50 mg $(NBu_4)PF_6$, 5 mg $[Tc^{II}(NO)Cl_2(L^{OMe})]$, scan rate 1000 mV/s).

Spectroscopic Data of $[Tc^{III}Cl_2(PPh_3)(L^{OMe})]$

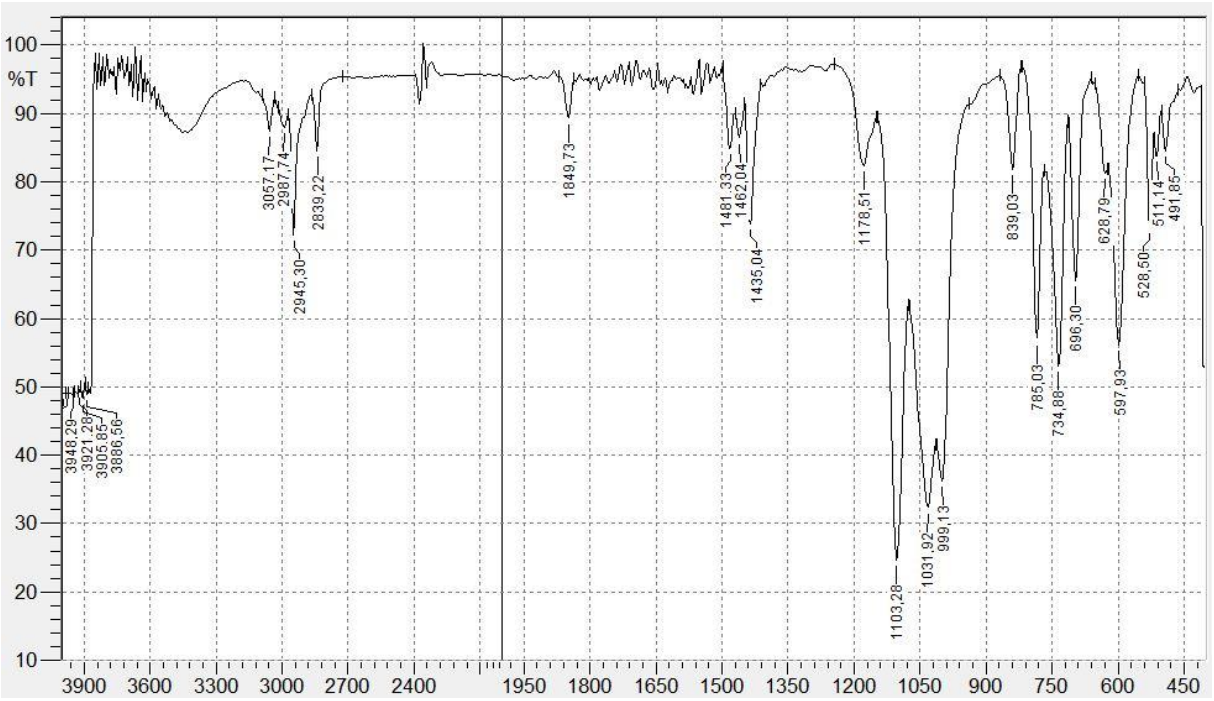

Figure 9.11. IR spectrum of $[Tc^{III}Cl_2(PPh_3)(L^{OMe})]$.

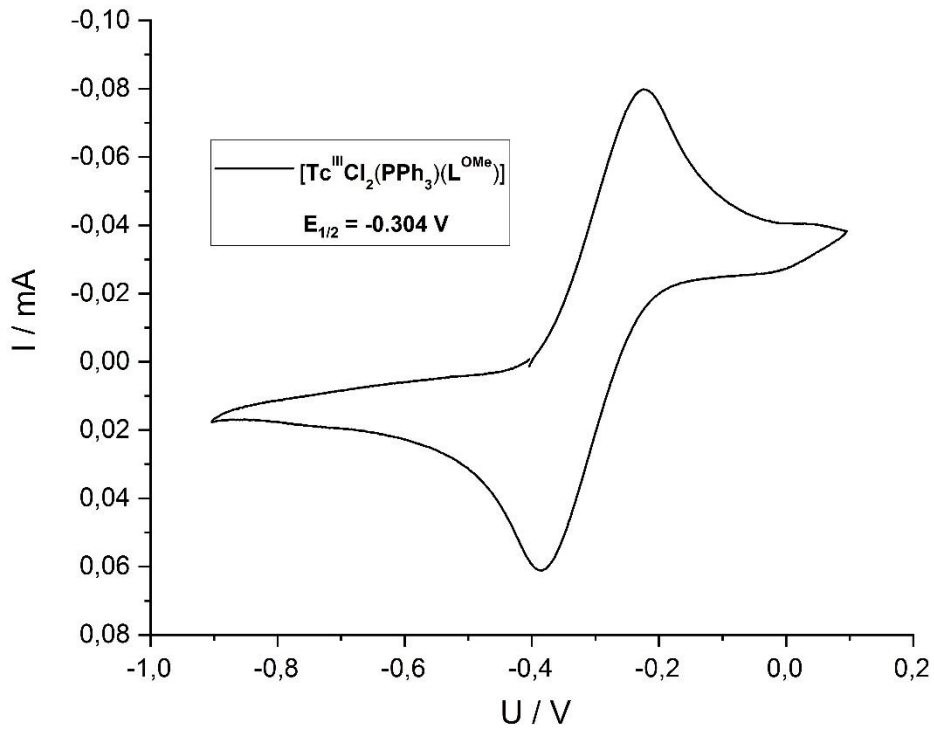

Figure 9.12. Cyclic voltammogram taken from $[Tc^{III}Cl_2(PPh_3)(L^{OMe})]$ (0.9 mL dry CH_2Cl_2, 50 mg $(NBu_4)PF_6$, 5 mg $[Tc^{III}Cl_2(PPh_3)(L^{OMe})]$, scan rate 500 mV/s).

Spectroscopic Data of $[Tc^{IV}Cl_3(L^{OMe})]$

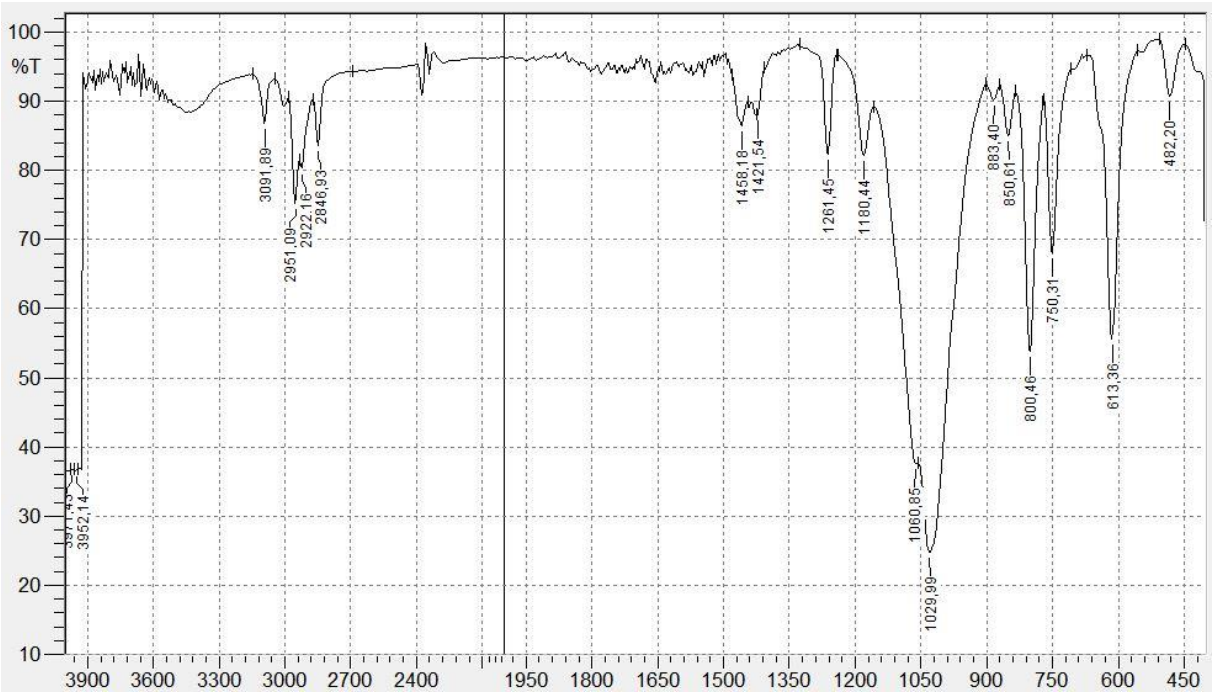

Figure 9.13. IR spectrum of $[Tc^{IV}Cl_3(L^{OMe})]$.

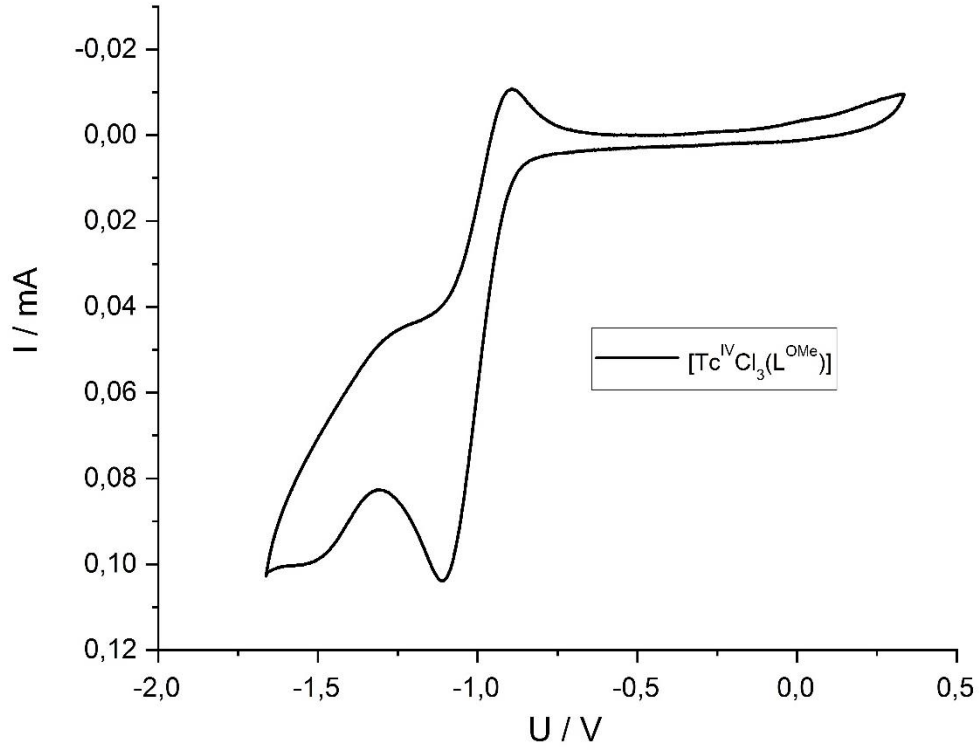

Figure 9.14. Cyclic voltammogram taken from $[Tc^{IV}Cl_3(L^{OMe})]$ (0.9 mL dry CH_2Cl_2, 50 mg $(NBu_4)PF_6$, 0.9 mL dry CH_2Cl_2, 50 mg $TBAPF_6$, 5 mg $[Tc^{IV}Cl_3(L^{OMe})]$, scan rate 500 mV/s).

Spectroscopic Data of $[Tc^{V}OCl_2(L^{OMe})]$

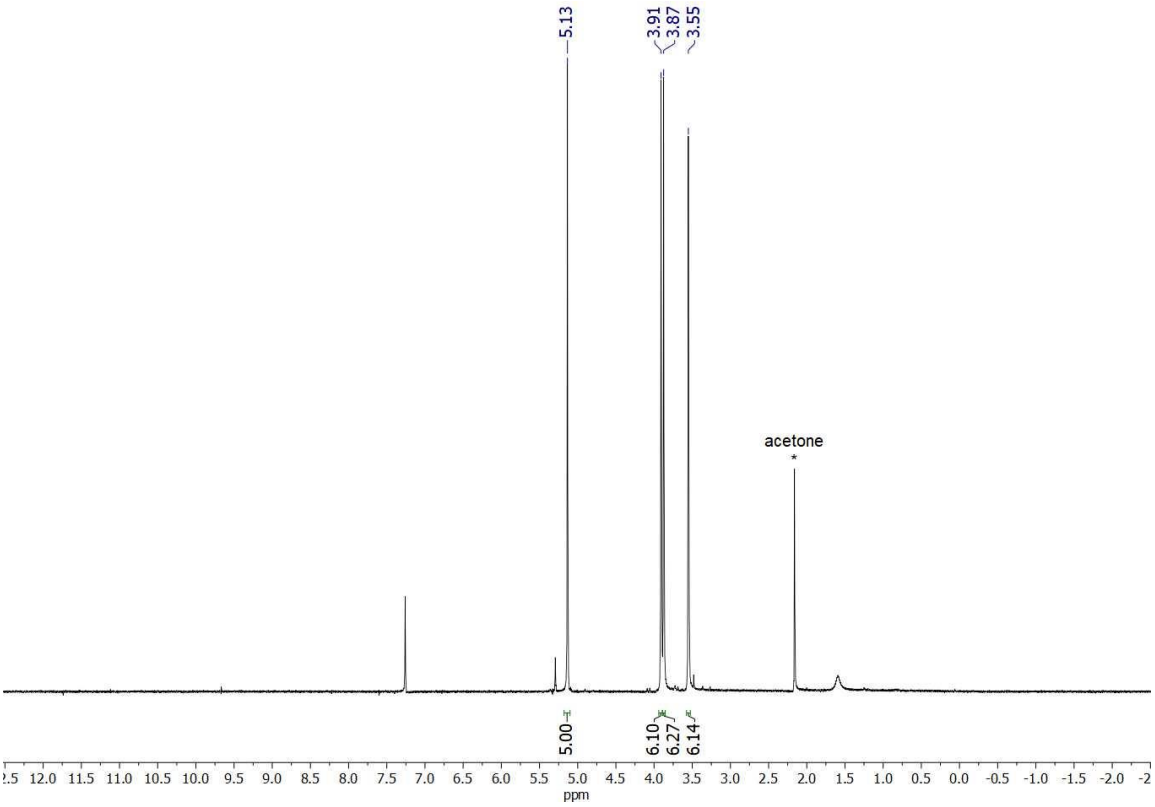

Figure 9.15. $^{1}H\{^{31}P\}$ NMR spectrum of $[Tc^{V}OCl_2(L^{OMe})]$ in $CDCl_3$.

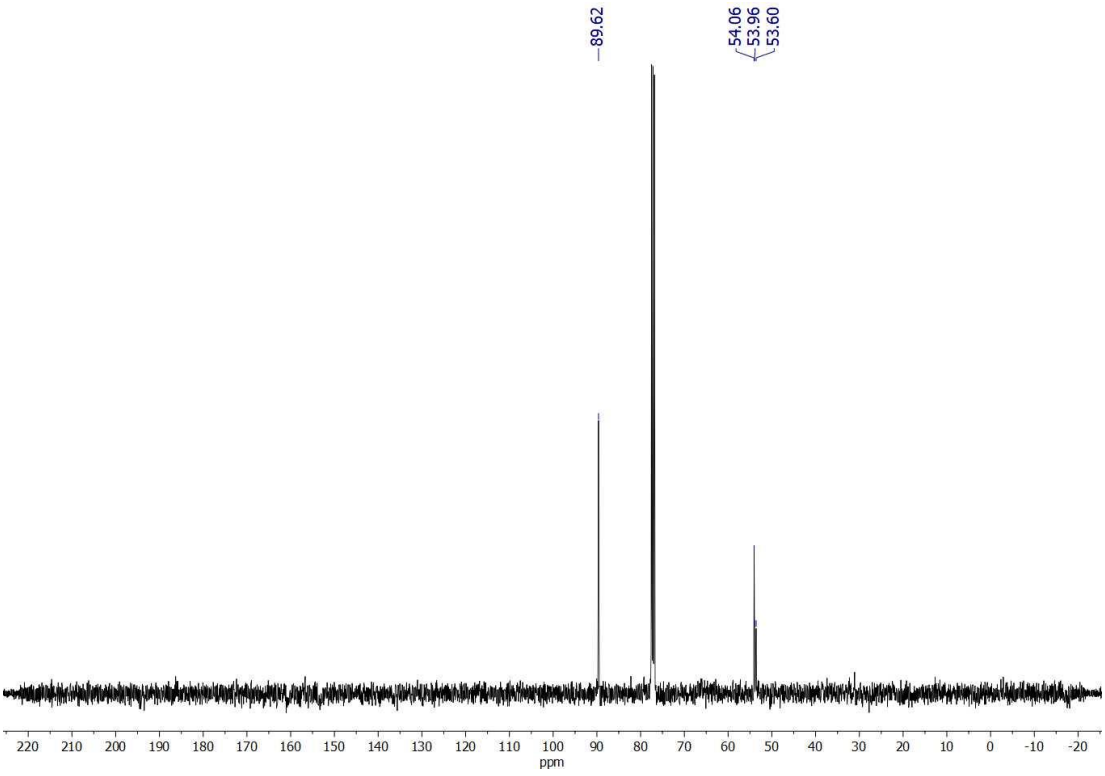

Figure 9.16. $^{13}C\{^{1}H\}$ NMR spectrum of $[Tc^{V}OCl_2(L^{OMe})]$ in $CDCl_3$.

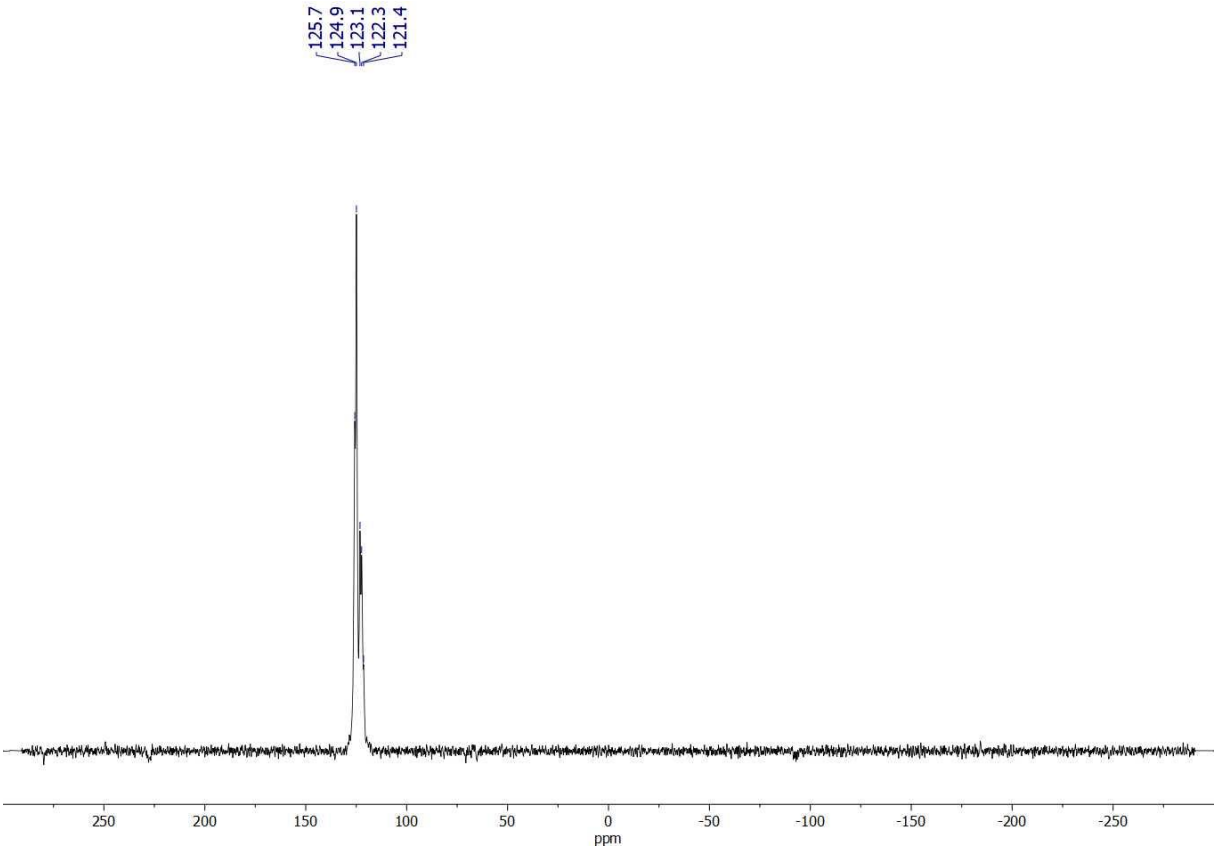

Figure 9.17. $^{31}P\{^{1}H\}$ NMR spectrum of $[Tc^{V}OCl_2(L^{OMe})]$ in $CDCl_3$.

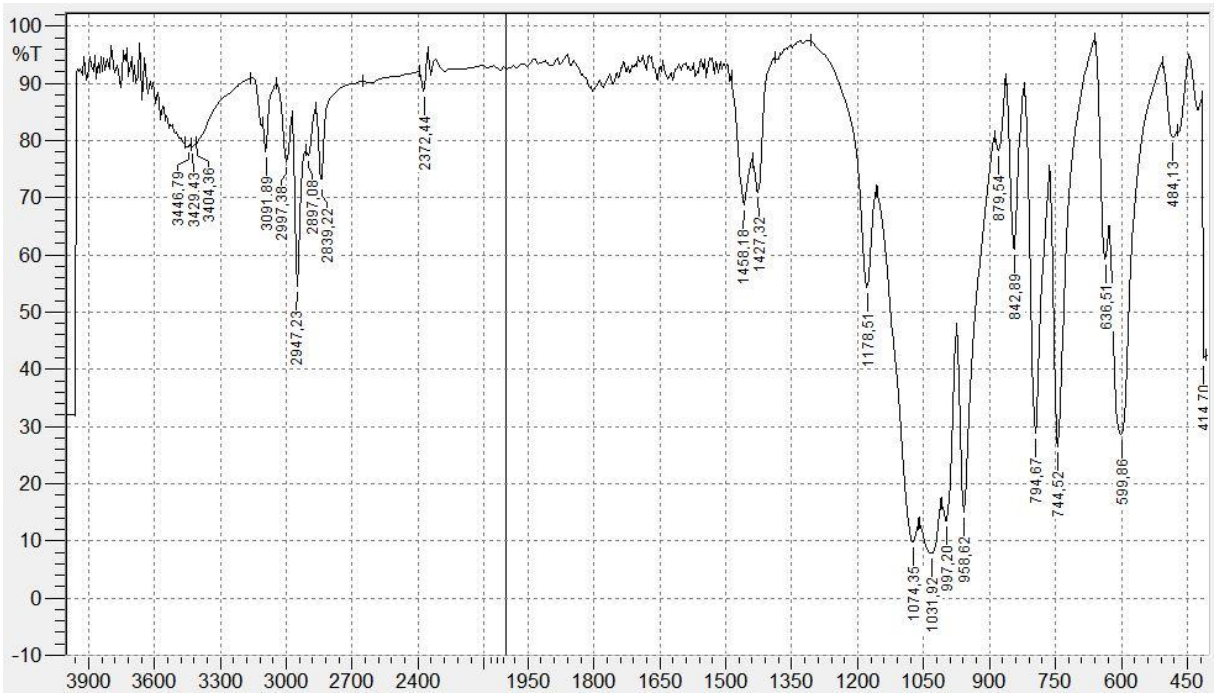

Figure 9.18. IR spectrum of $[Tc^{V}OCl_2(L^{OMe})]$.

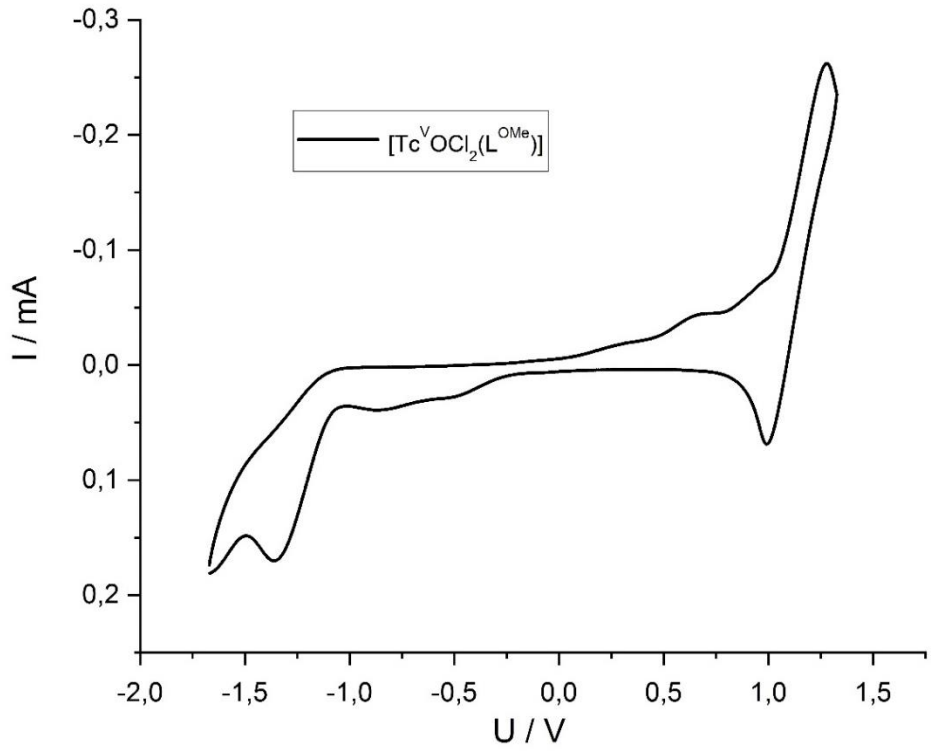

Figure 9.19. Cyclic voltammogram taken from $[Tc^{V}OCl_2(L^{OMe})]$ (0.9 mL dry CH_2Cl_2, 50 mg $(NBu_4)PF_6$, 5 mg $[Tc^{V}OCl_2(L^{OMe})]$, scan rate 500 mV/s).

Spectroscopic Data of $[Tc^{V}NCl(PPh_3)(L^{OMe})]$

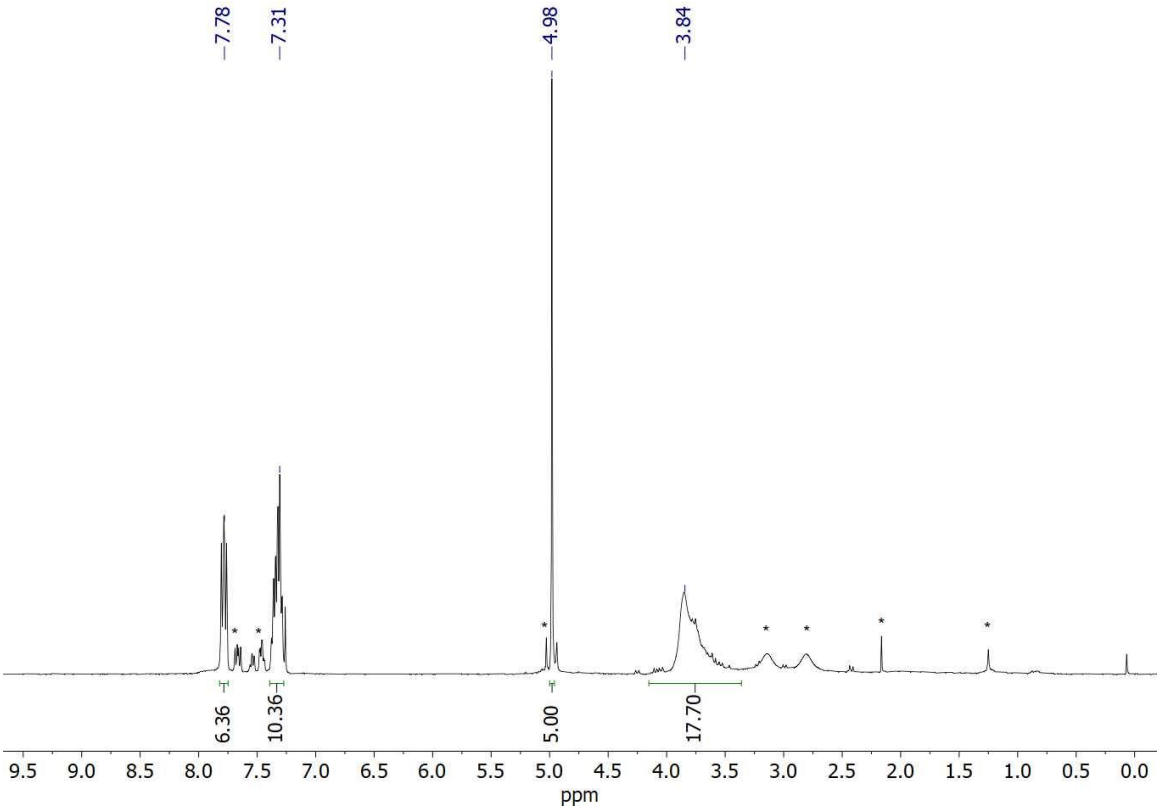

Figure 9.20. $^{1}H\{^{31}P\}$ NMR spectrum of $[Tc^{V}NCl(PPh_3)(L^{OMe})]$ in $CDCl_3$. *Side products.

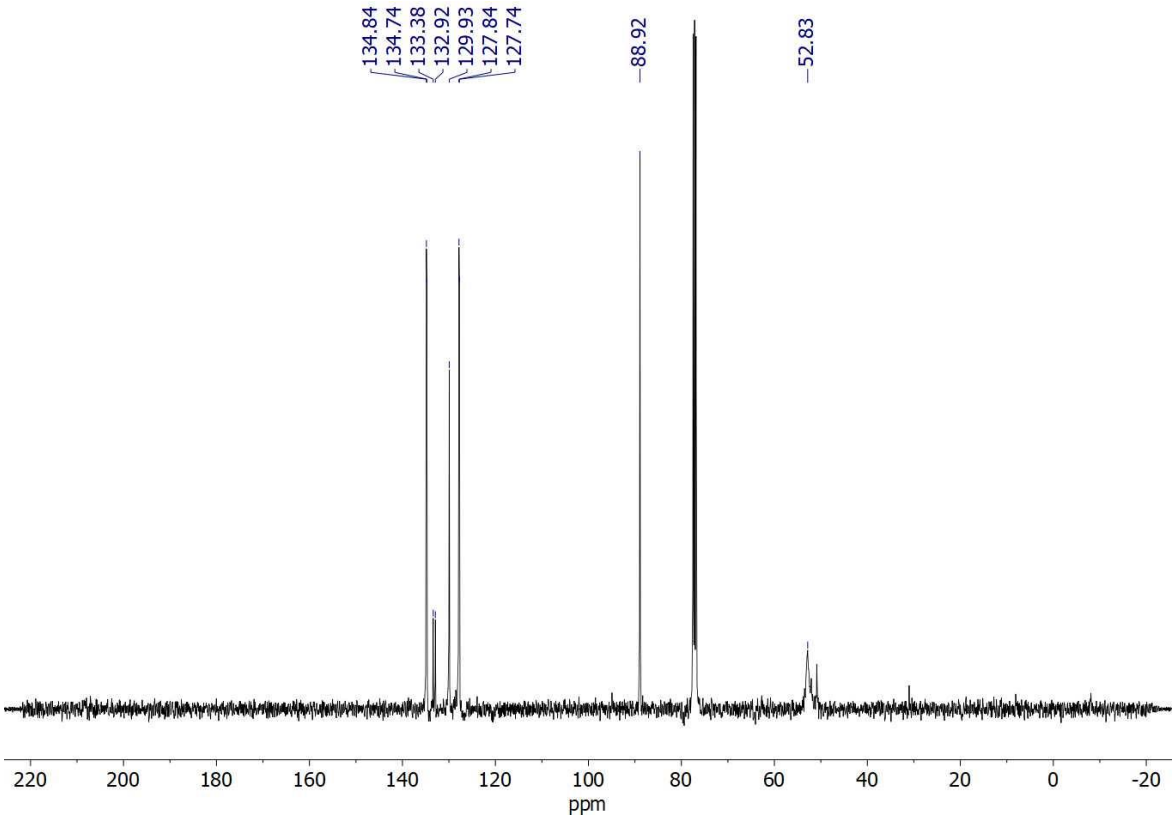

Figure 9.21. $^{13}C\{^{1}H\}$ NMR spectrum of $[Tc^{V}NCl(PPh_3)(L^{OMe})]$ in $CDCl_3$.

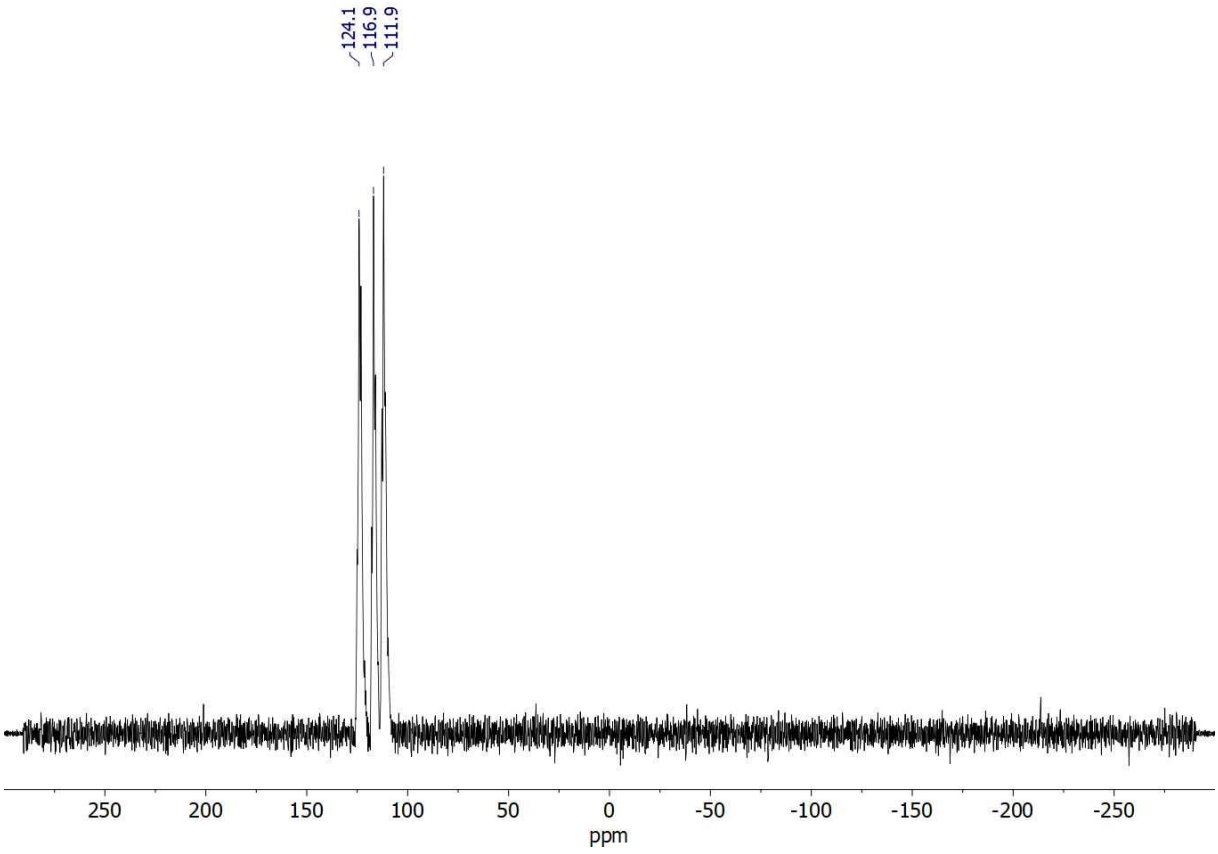

Figure 9.22. $^{31}P\{^{1}H\}$ NMR spectrum of $[Tc^{V}NCl(PPh_3)(L^{OMe})]$ in $CDCl_3$.

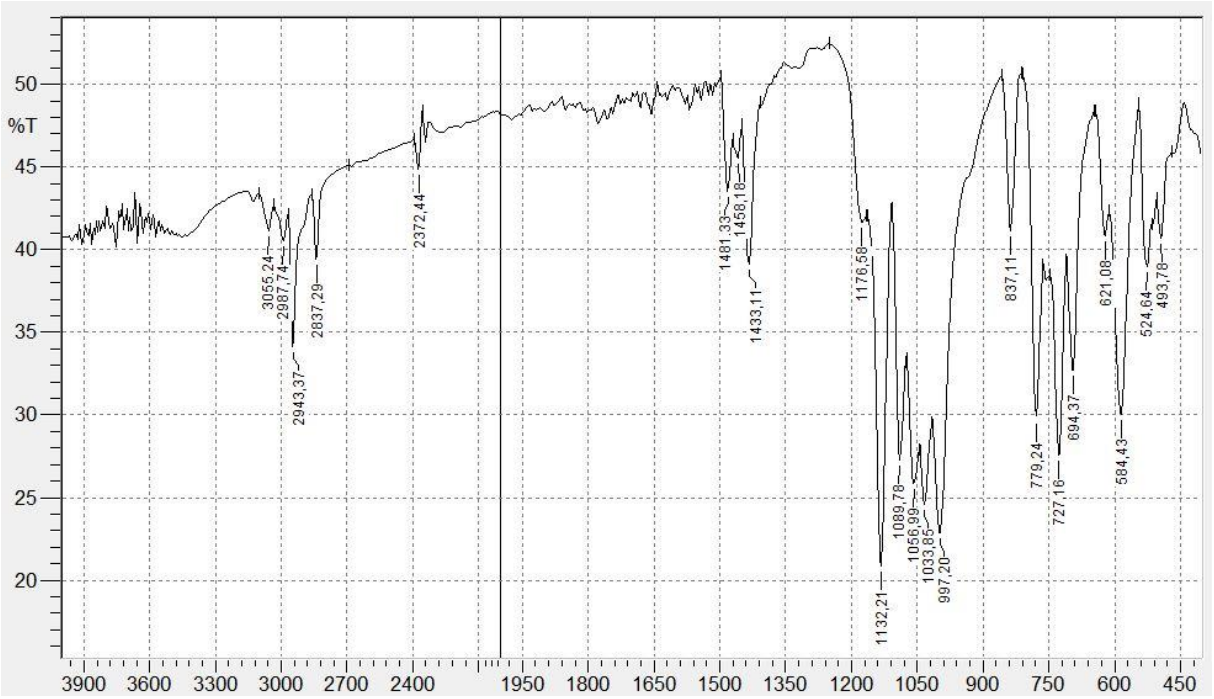

Figure 9.23. IR spectrum of $[Tc^{V}NCl(PPh_3)(L^{OMe})]$.

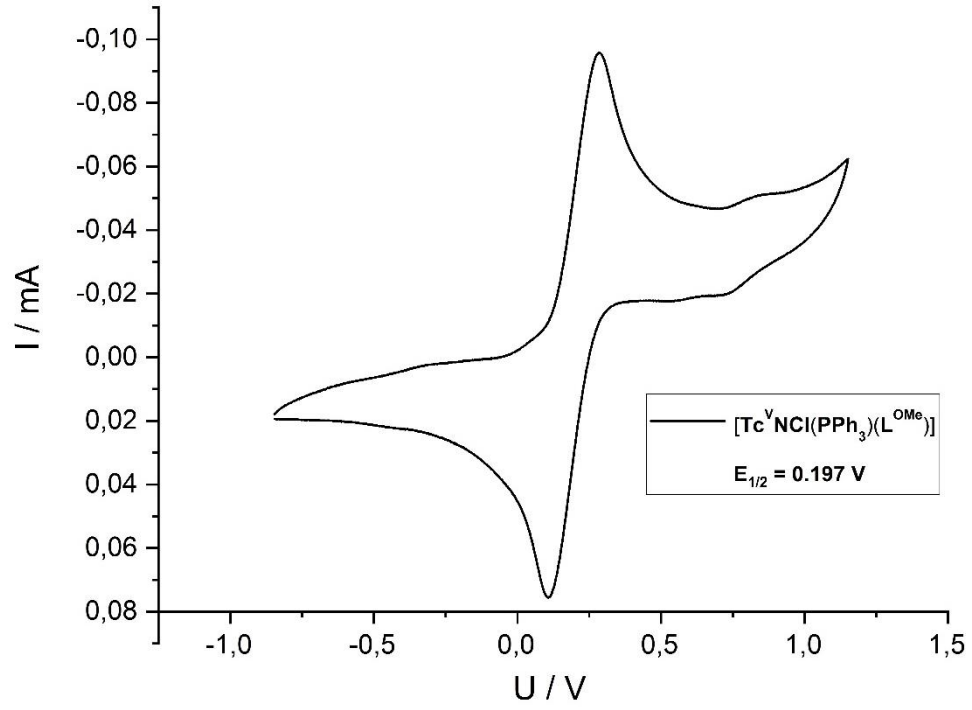

Figure 9.24. Cyclic voltammogram taken from $[Tc^{V}NCl(PPh_3)(L^{OMe})]$ (0.9 mL dry CH_2Cl_2, 50 mg $(NBu_4)PF_6$, 5 mg $[Tc^{V}NCl(PPh_3)(L^{OMe})]$, scan rate 500 mV/s).

Spectroscopic data of $[Tc^{VI}NCl_2(L^{OMe})]$

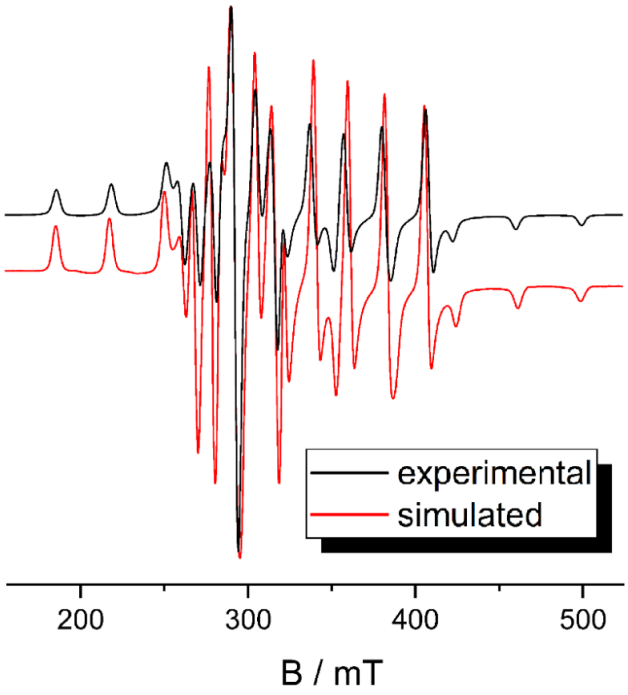

Figure 9.25. X-Band EPR spectrum of $[Tc^{VI}NCl_2(L^{OMe})]$ at 77 K in CH_2Cl_2.

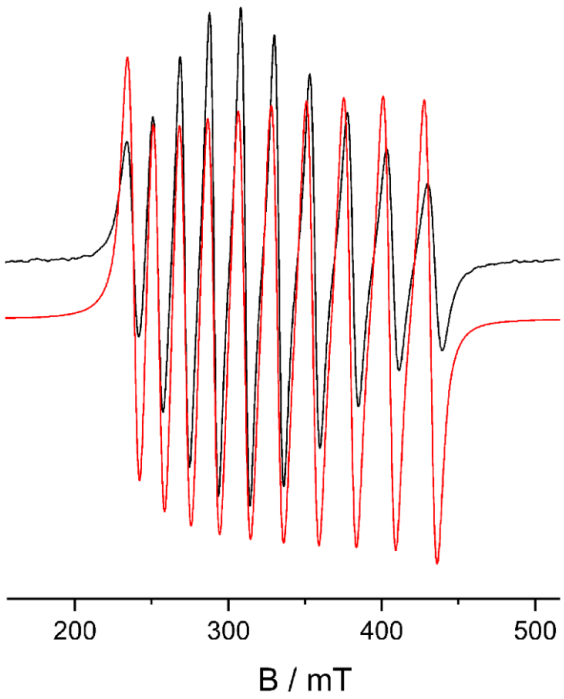

Figure 9.26. X-Band EPR spectrum of $[Tc^{VI}NCl_2(L^{OMe})]$ in CH_2Cl_2 at room temperature Black: Experimental. Red: Simulated.

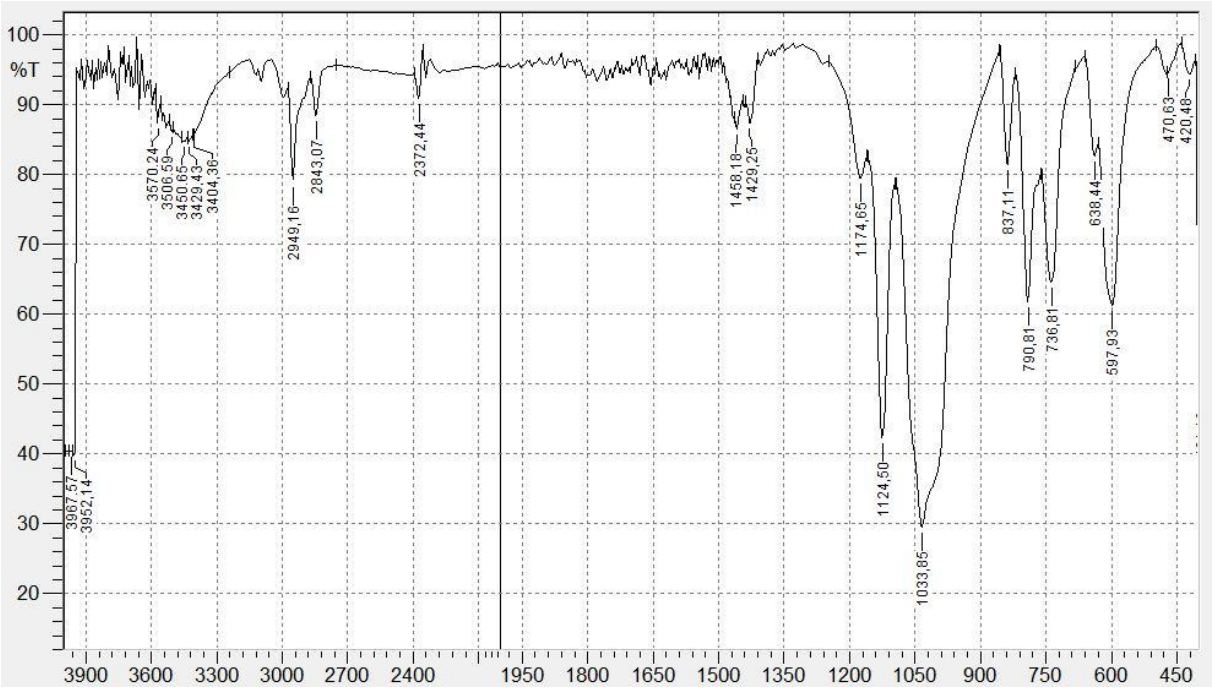

Figure 9.27. IR spectrum of $[Tc^{VI}NCl_2(L^{OMe})]$.

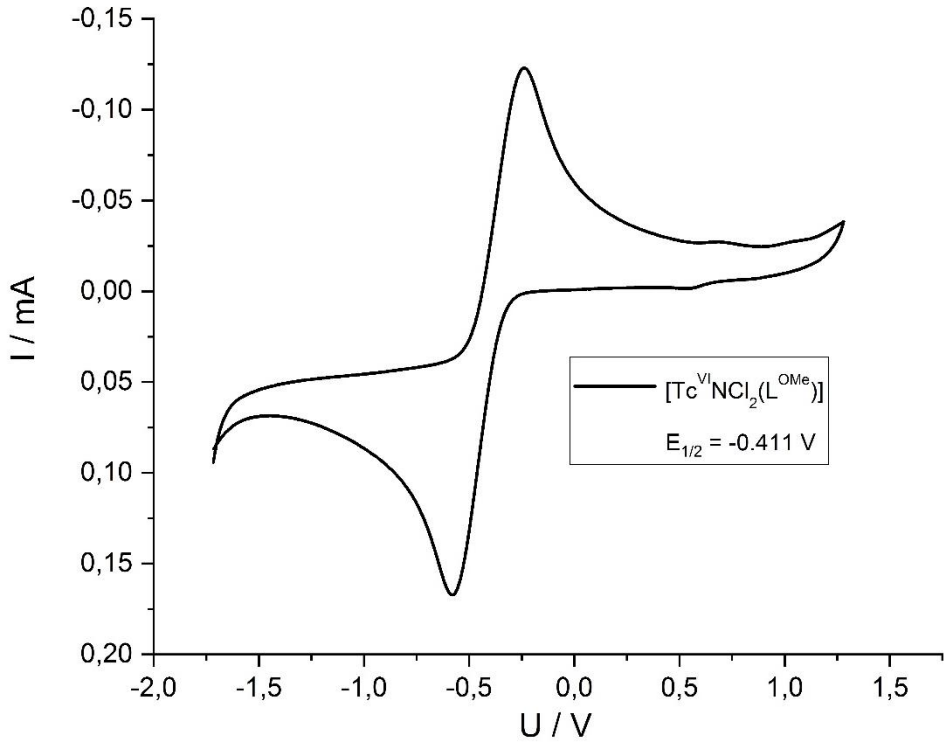

Figure 9.28. Cyclic voltammogram taken from $[Tc^{VI}NCl_2(L^{OMe})]$ (0.9 mL dry CH_2Cl_2, 50 mg $(NBu_4)PF_6$, 5 mg $[Tc^{VI}NCl_2(L^{OMe})]$, scan rate 500 mV/s).

Spectroscopic Data of $[Tc^{VII}O_3(L^{OMe})]$

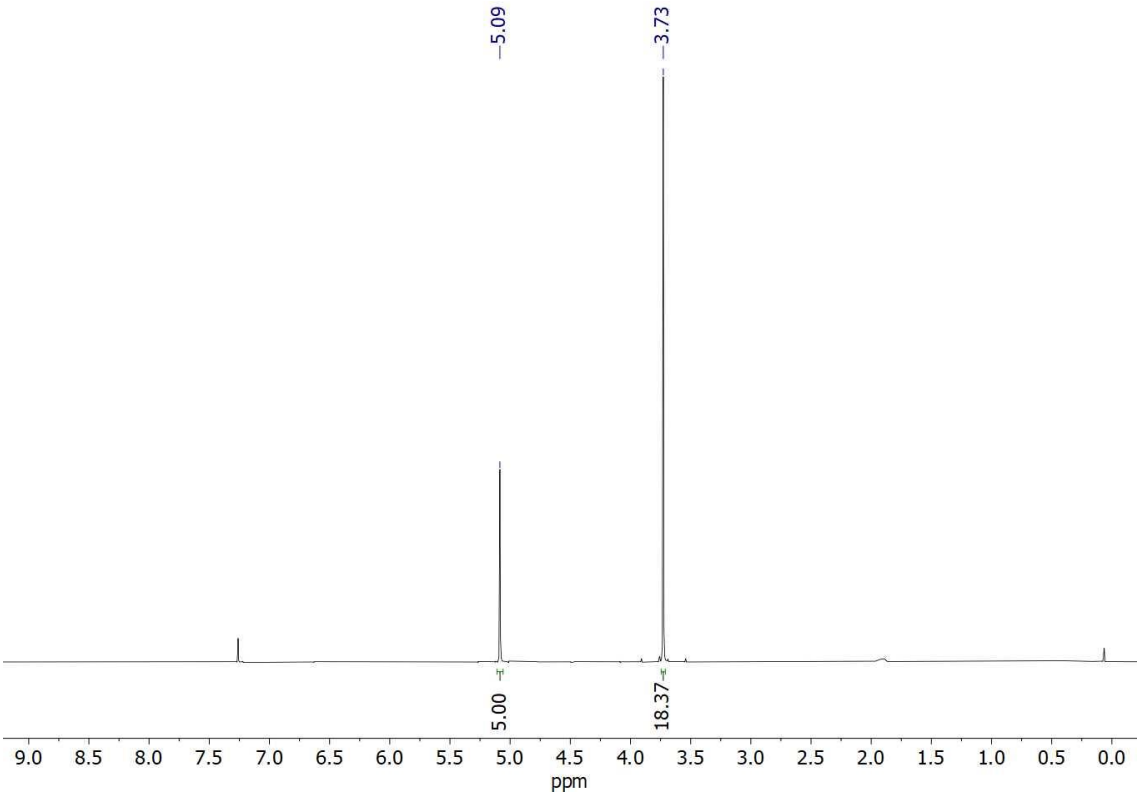

Figure 9.29. $^{1}H\{^{31}P\}$ NMR spectrum of $[Tc^{VII}O_3(L^{OMe})]$ in $CDCl_3$.

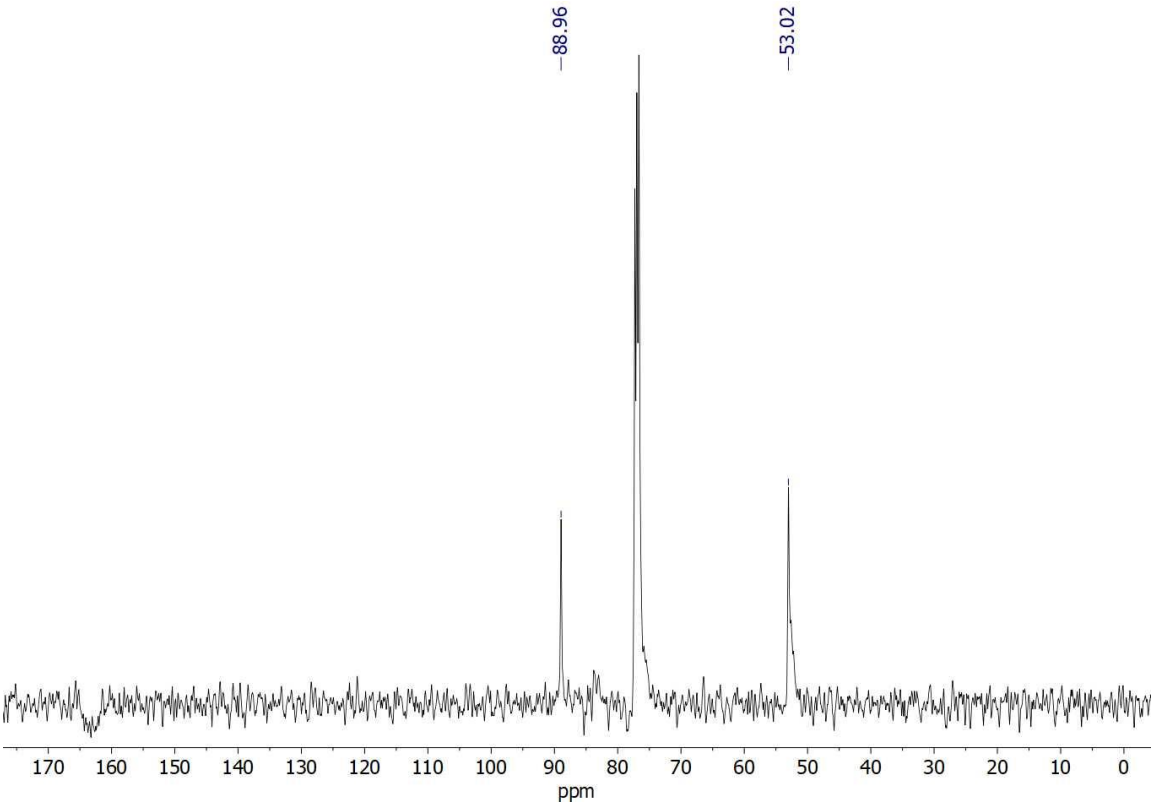

Figure 9.30. $^{13}C\{^{1}H\}$ NMR spectrum of $[Tc^{VII}O_3(L^{OMe})]$ in $CDCl_3$.

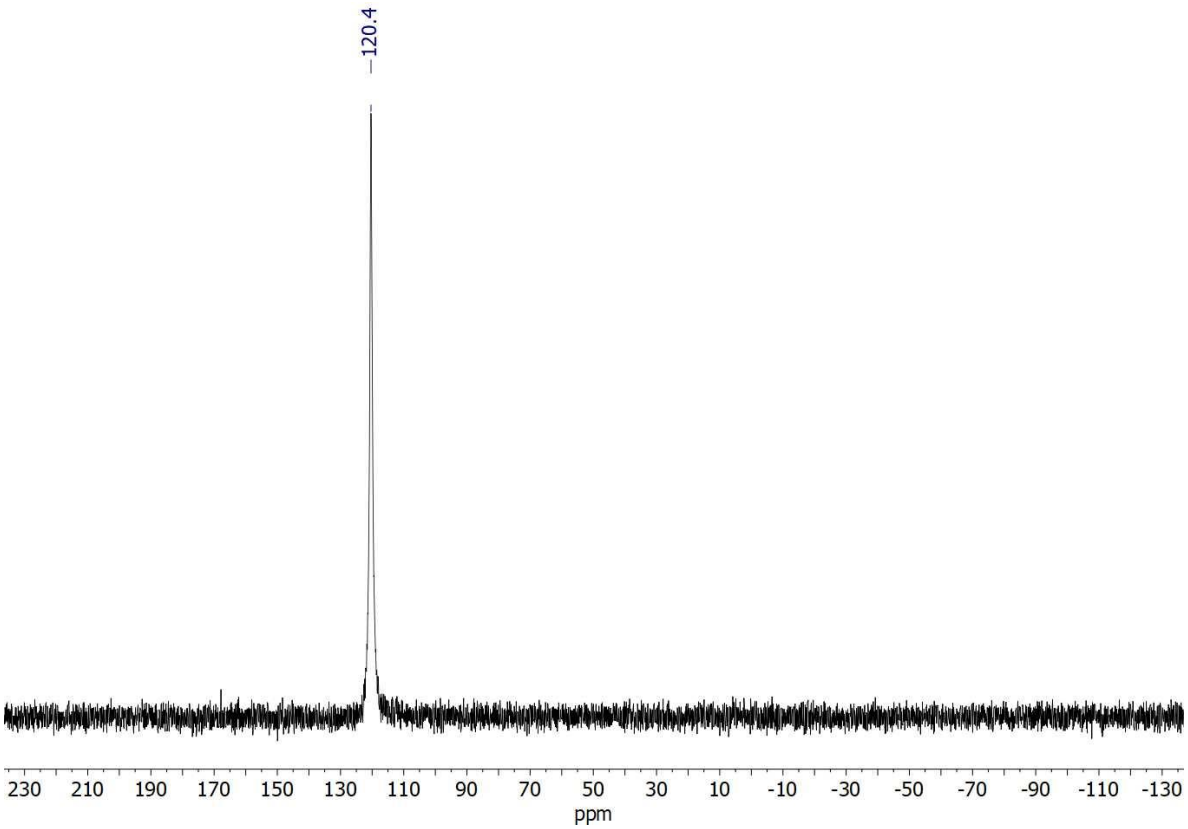

Figure 9.31. $^{31}P\{^{1}H\}$ NMR spectrum of $[Tc^{VII}O_3(L^{OMe})]$ in $CDCl_3$.

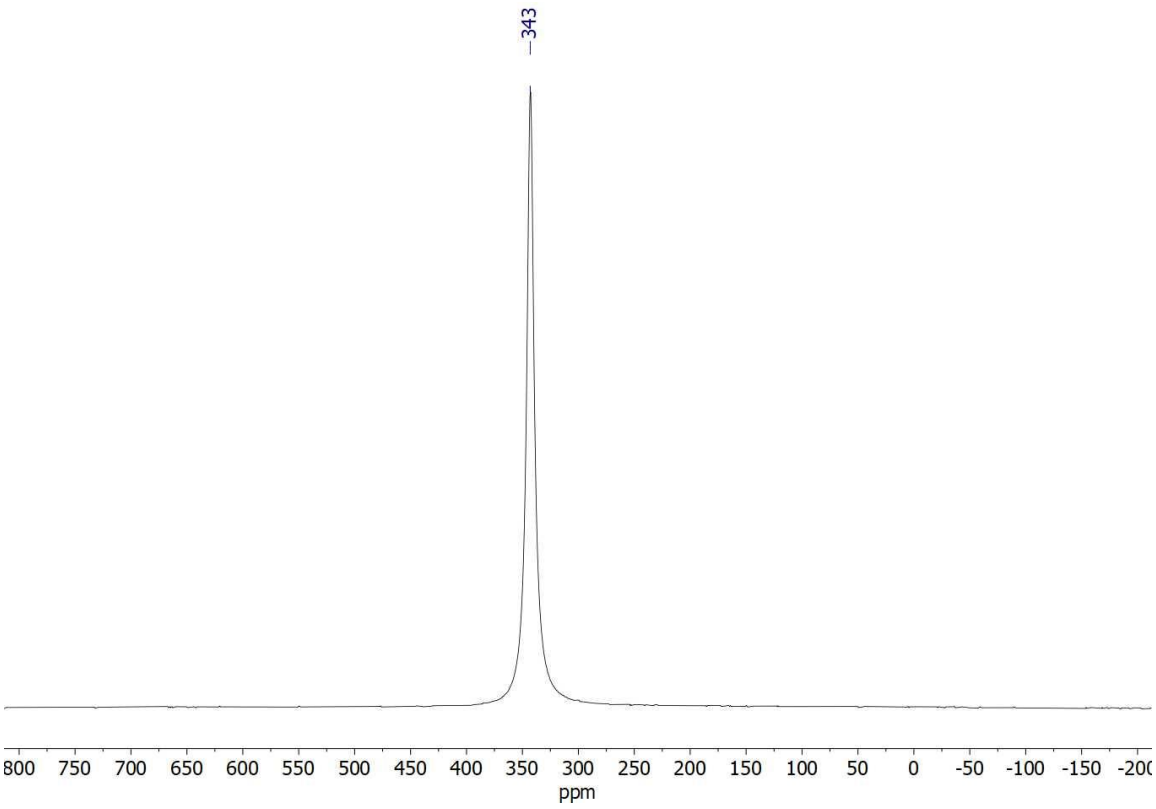

Figure 9.32. ^{99}Tc NMR spectrum of $[Tc^{VII}O_3(L^{OMe})]$ in $CDCl_3$.

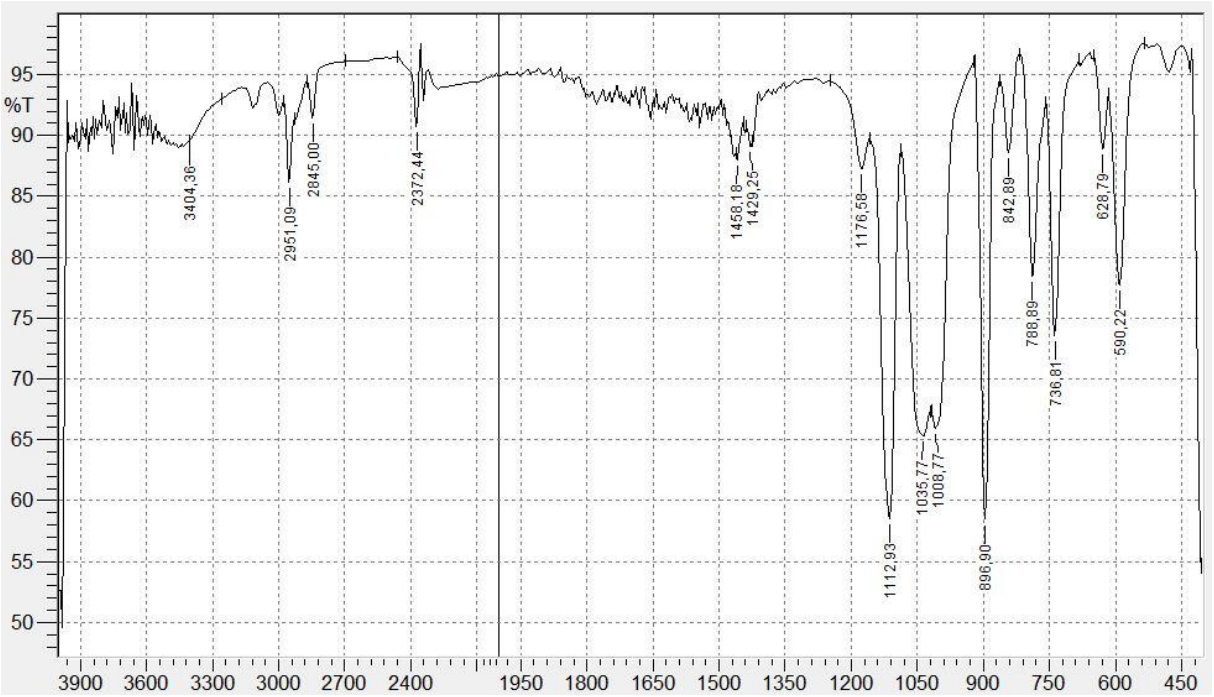

Figure 9.33. IR spectrum of $[Tc^{VII}O_3(L^{OMe})]$.

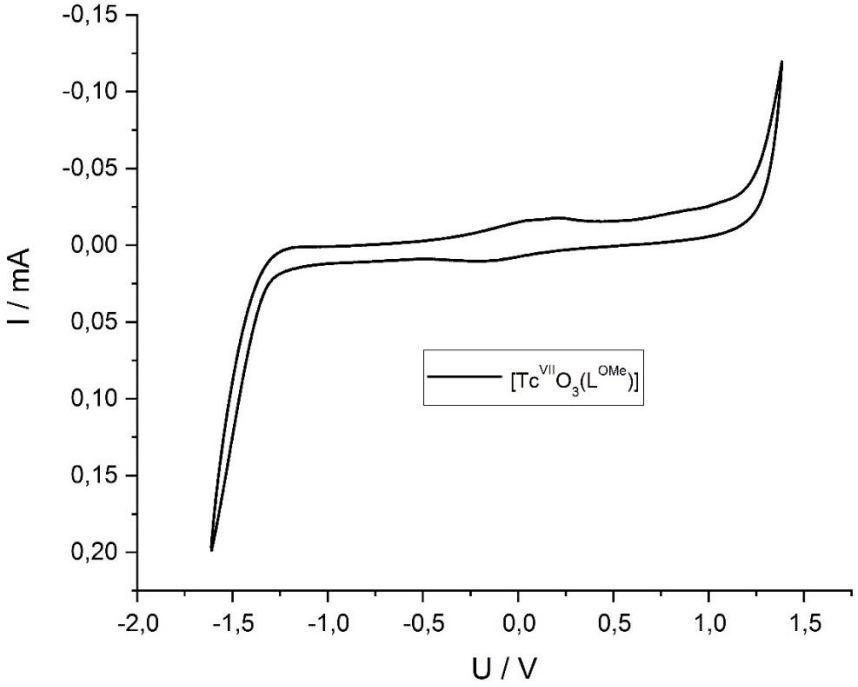

Figure 9.34. Cyclic voltammogram taken from $[Tc^{VII}O_3(L^{OMe})]$ (0.9 mL dry CH_2Cl_2, 50 mg $(NBu_4)PF_6$, 5 mg $[Tc^{VII}O_3(L^{OMe})]$, scan rate 500 mV/s).

Spectroscopic Data of [$Tc^{V}O$(glycolate)(L^{OMe})]

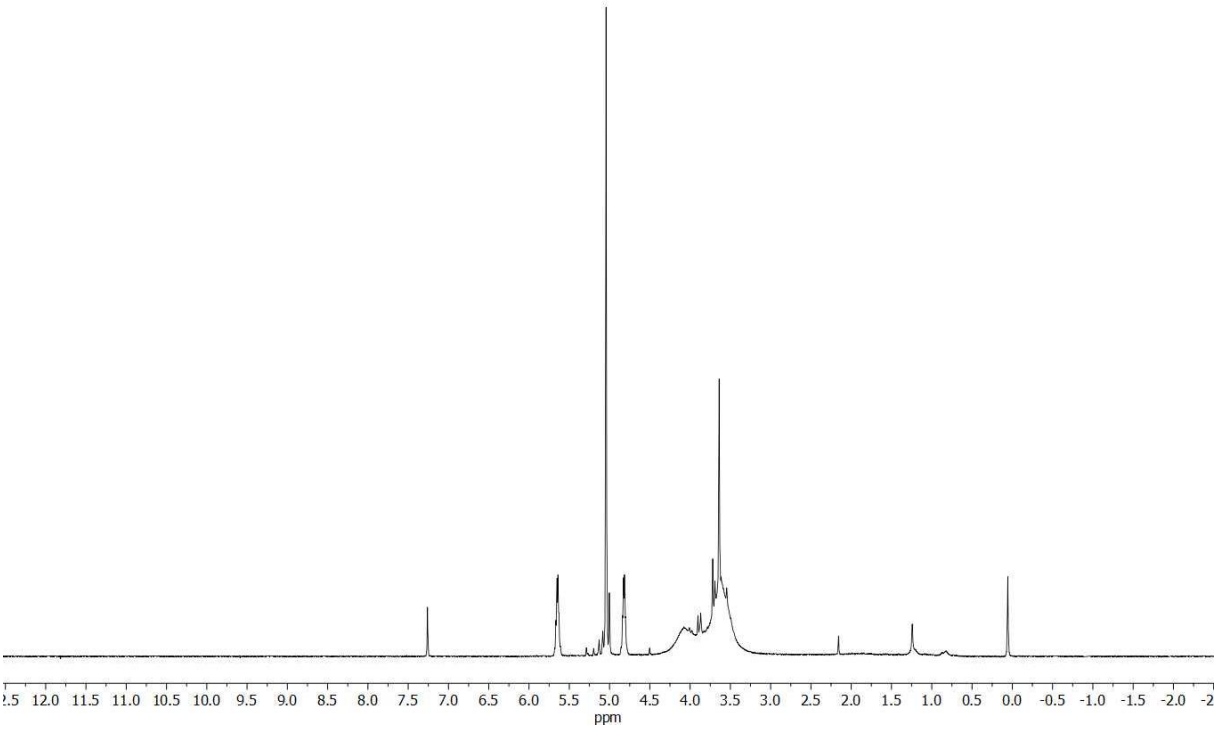

Figure 9.35. $^{1}H\{^{31}P\}$ NMR spectrum of [$Tc^{V}O$(glycolate)(L^{OMe})] in $CDCl_3$.

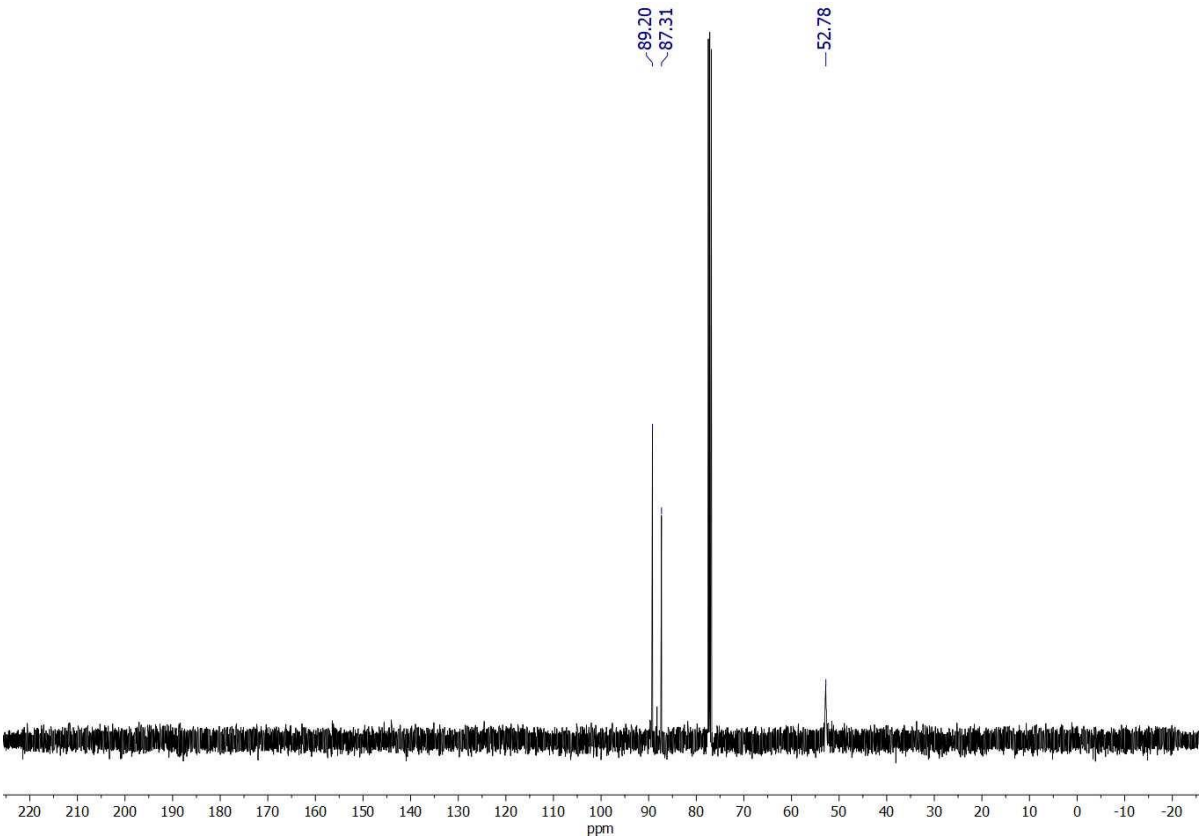

Figure 9.36. $^{13}C\{^{1}H\}$ NMR spectrum of [$Tc^{V}O$(glycolate)(L^{OMe})] in $CDCl_3$.

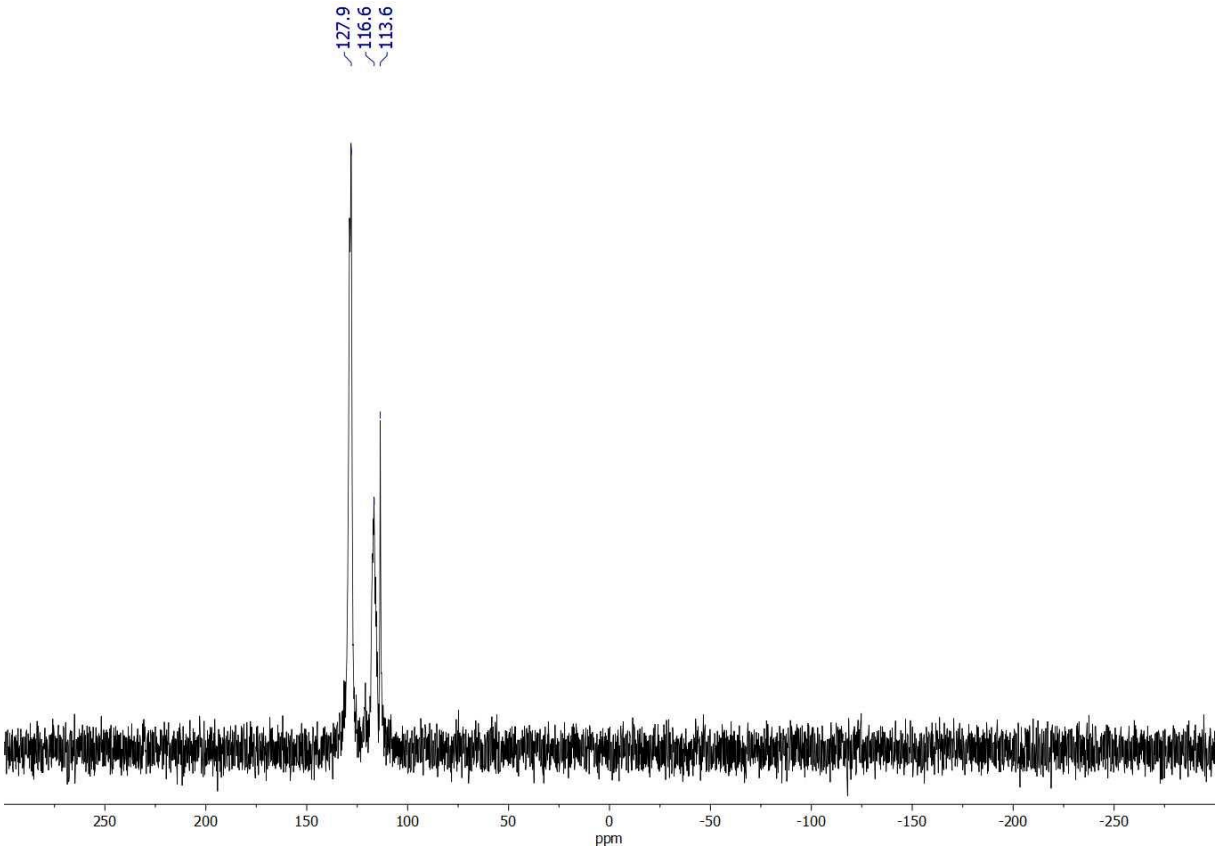

Figure 9.37. $^{31}P\{^{1}H\}$ NMR spectrum of [$Tc^{V}O$(glycolate)(L^{OMe})] in $CDCl_3$.

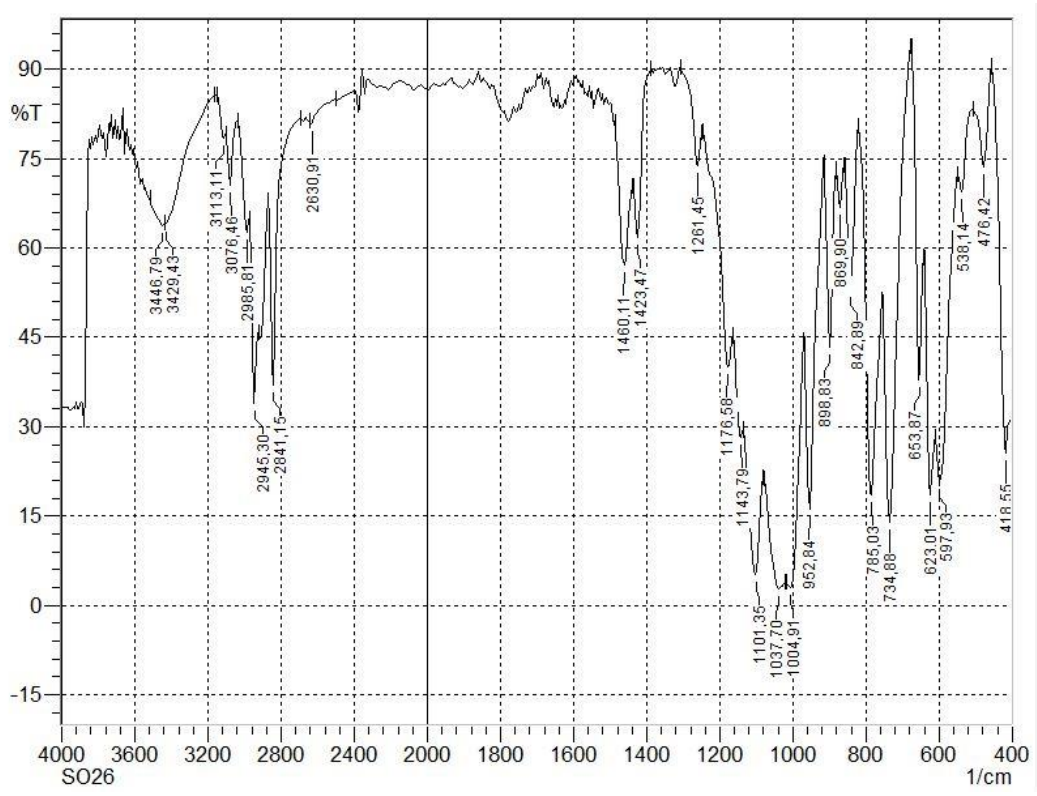

Figure 9.38. IR spectrum of [$Tc^{V}O$(glycolate)(L^{OMe})].

Spectroscopic Data of $[Re^{I}(CO)_3(L^{OMe})]$

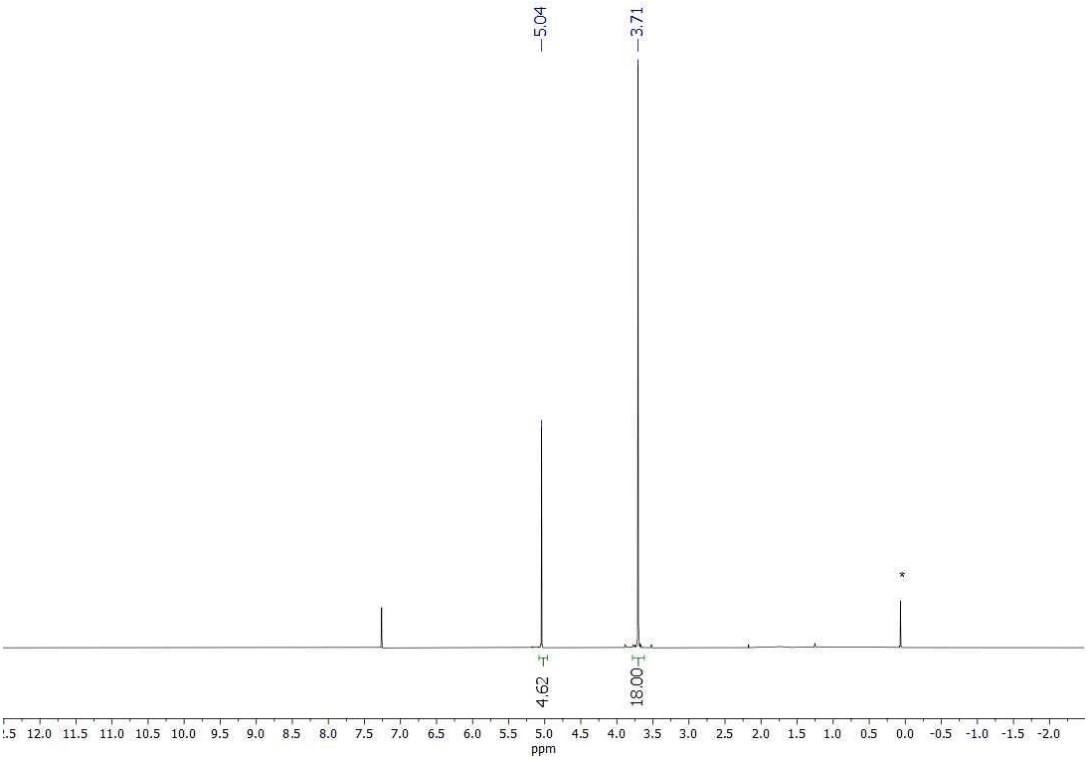

Figure 9.39. $^{1}H\{^{31}P\}$ NMR spectrum of $[Re^{I}(CO)_3(L^{OMe})]$ in $CDCl_3$.

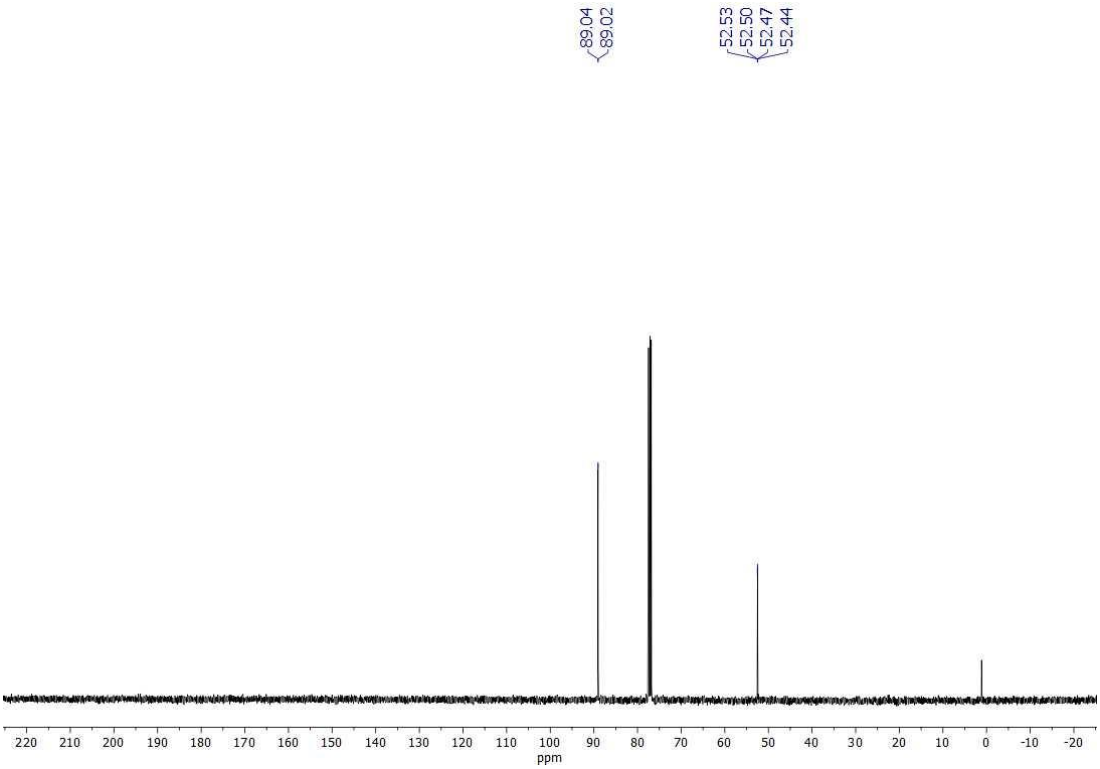

Figure 9.40. $^{13}C\{^{1}H\}$ NMR spectrum of $[Re^{I}(CO)_3(L^{OMe})]$ in $CDCl_3$.

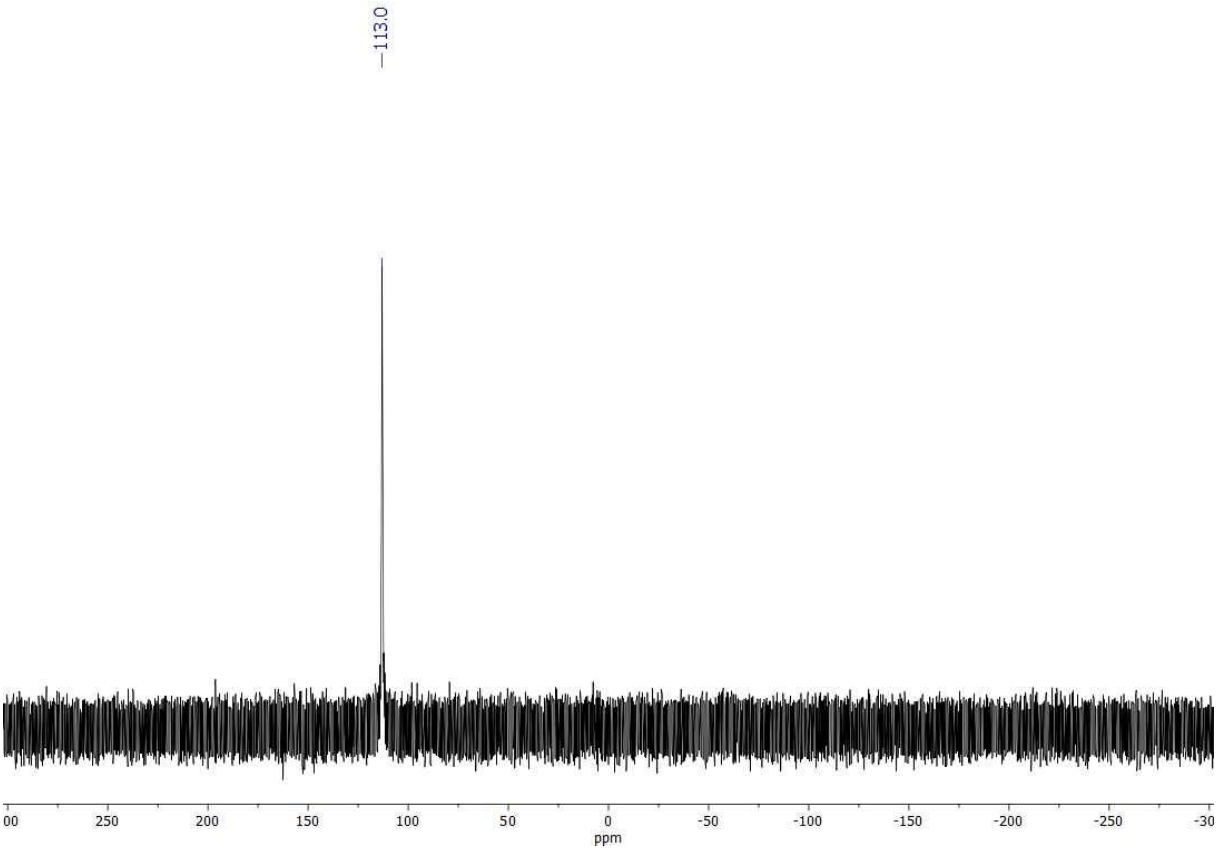

Figure 9.41. $^{31}P\{^{1}H\}$ NMR spectrum of $[Re^{I}(CO)_3(L^{OMe})]$ in $CDCl_3$.

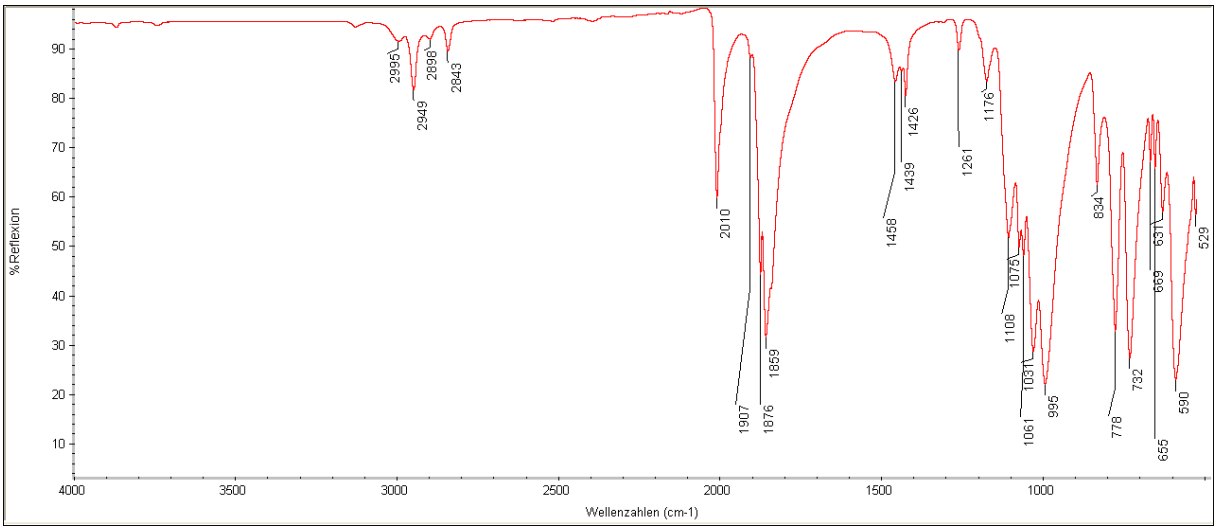

Figure 9.42. IR spectrum of $[Re^{I}(CO)_3(L^{OMe})]$.

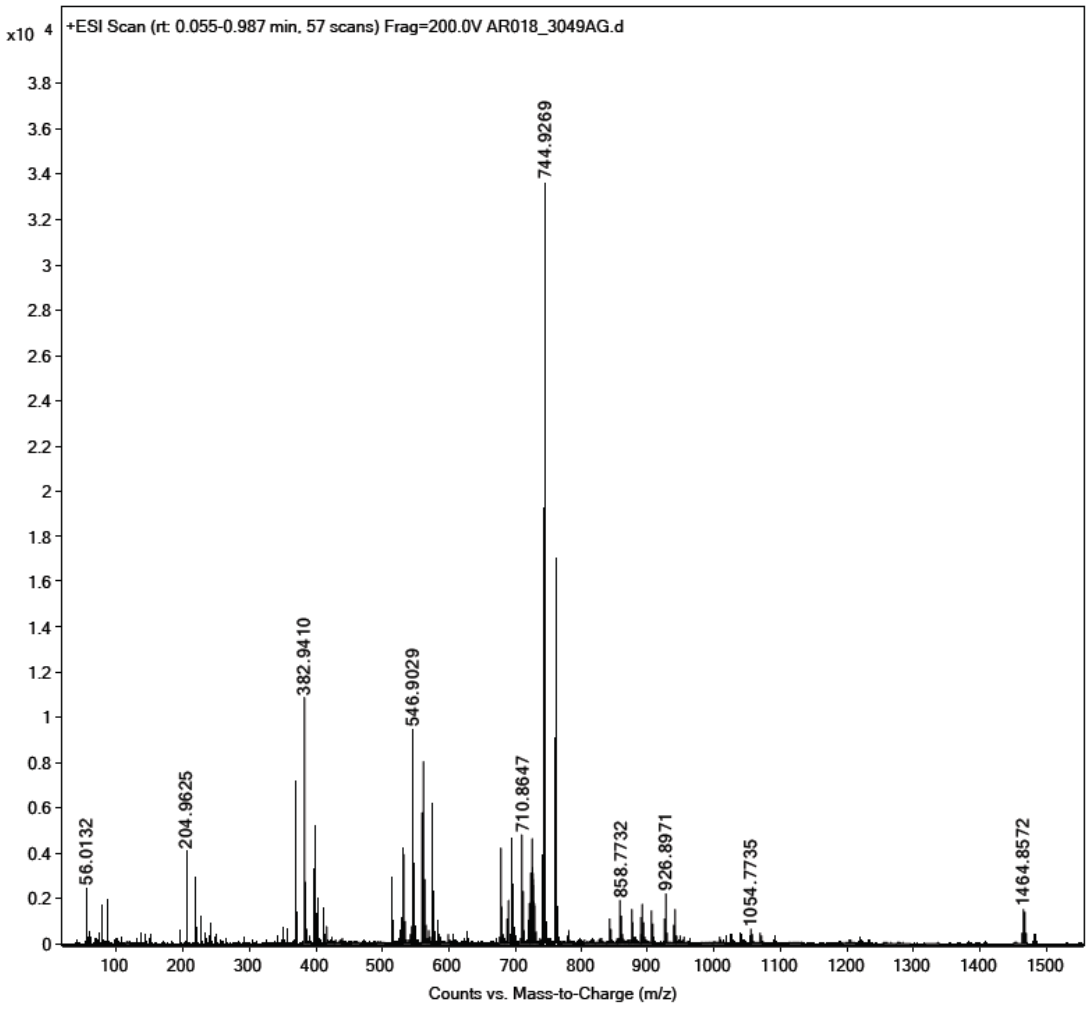

Figure 9.43. ESI+ MS spectrum of $[Re^{I}(CO)_3(L^{OMe})]$.

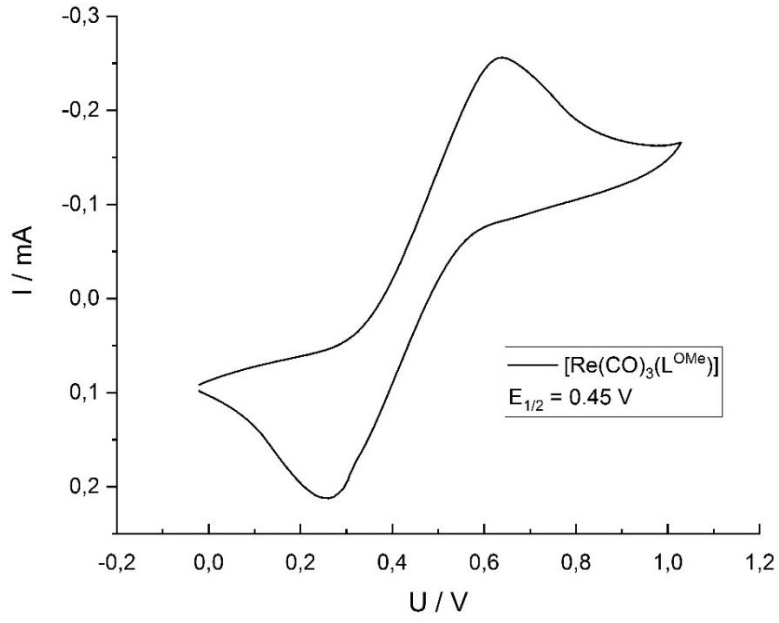

Figure 9.44. Cyclic voltammogram taken from $[Re^{I}(CO)_3(L^{OMe})]$ (0.9 mL dry CH_2Cl_2, 50 mg $(NBu_4)PF_6$, 7 mg $[Re^{I}(CO)_3(L^{OMe})]$, scan rate 500 mV/s).

Spectroscopic Data of $[Re^{V}OCl_2(L^{OMe})]$

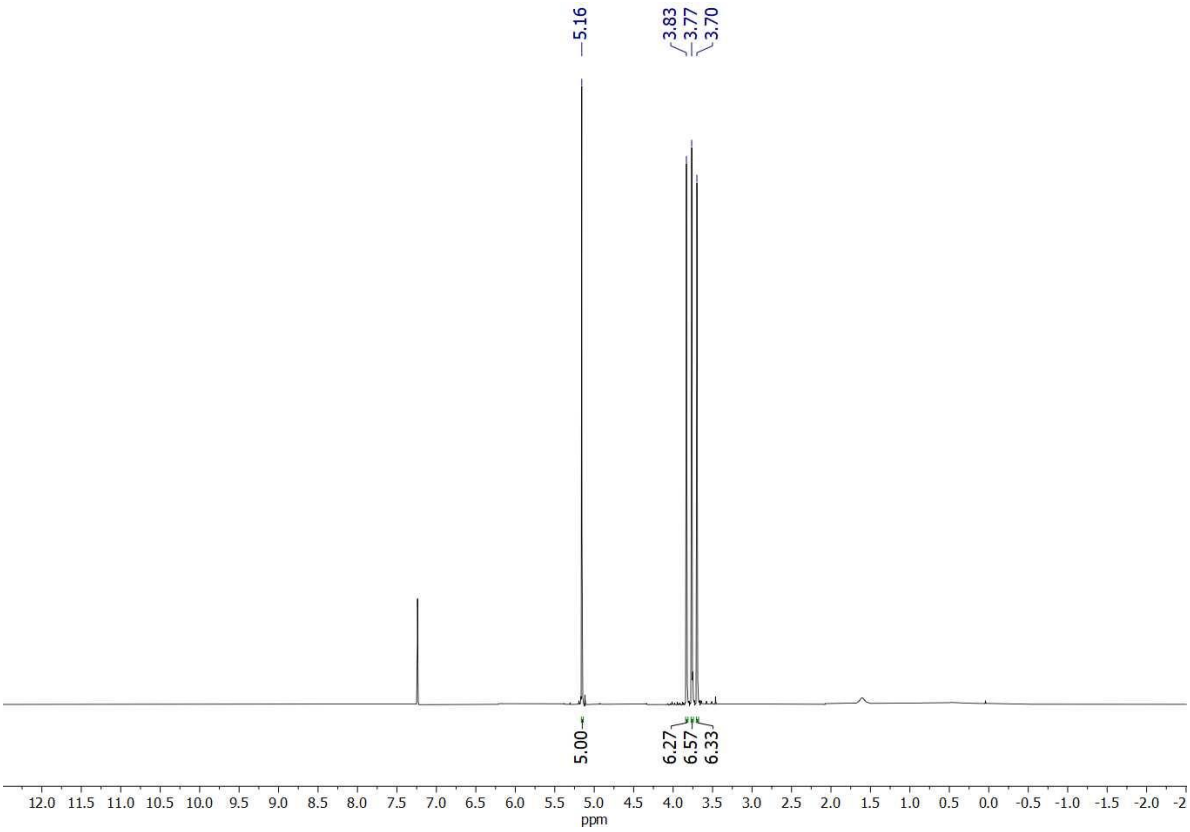

Figure 9.45. $^{1}H\{^{31}P\}$ NMR spectrum of $[Re^{V}OCl_2(L^{OMe})]$ in $CDCl_3$.

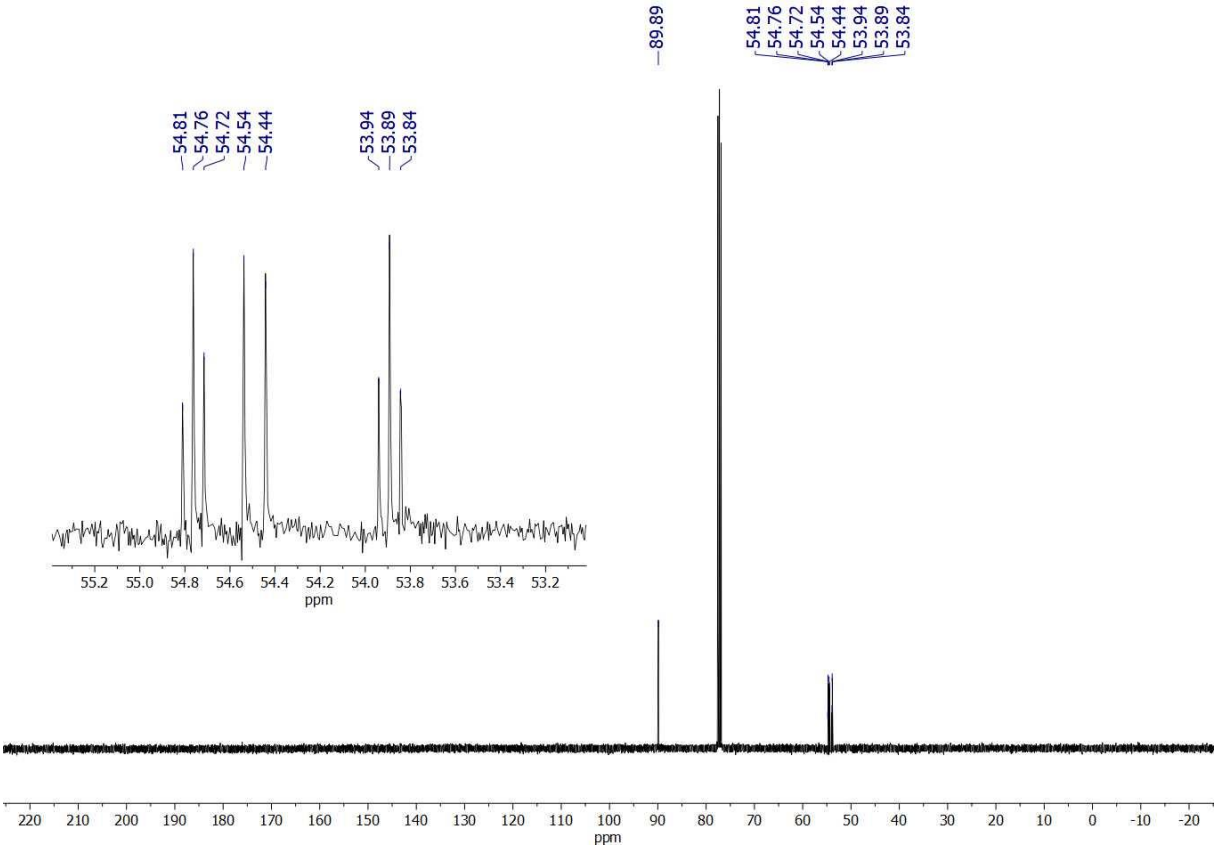

Figure 9.46. $^{13}C\{^{1}H\}$ NMR spectrum of $[Re^{V}OCl_2(L^{OMe})]$ in $CDCl_3$.

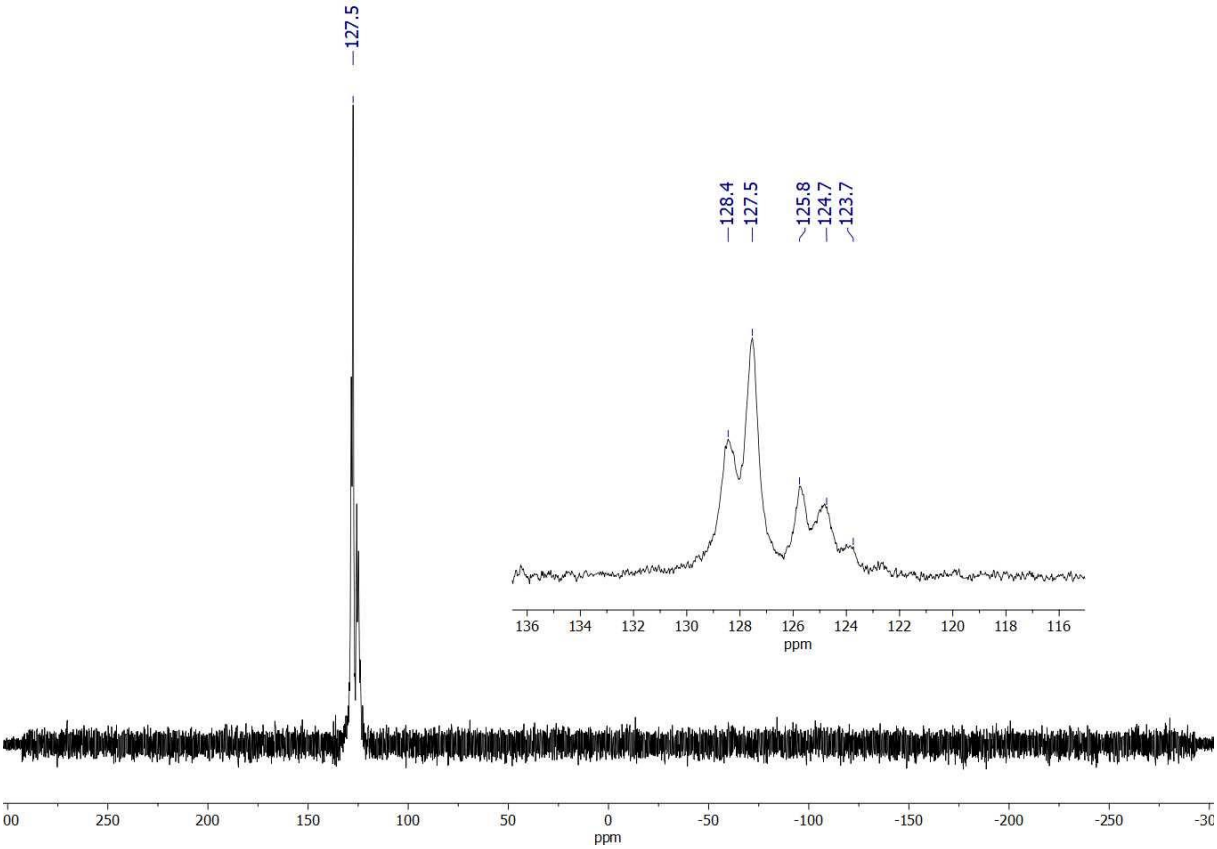

Figure 9.47. $^{31}P\{^{1}H\}$ NMR spectrum of $[Re^{V}OCl_2(L^{OMe})]$ in $CDCl_3$.

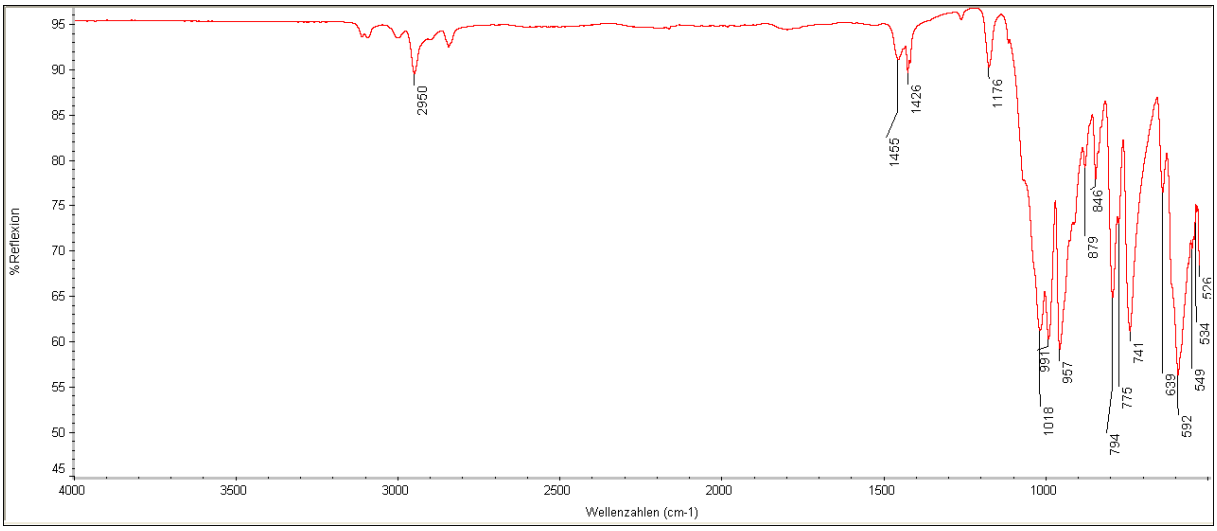

Figure 9.48. IR spectrum of $[Re^{V}OCl_2(L^{OMe})]$.

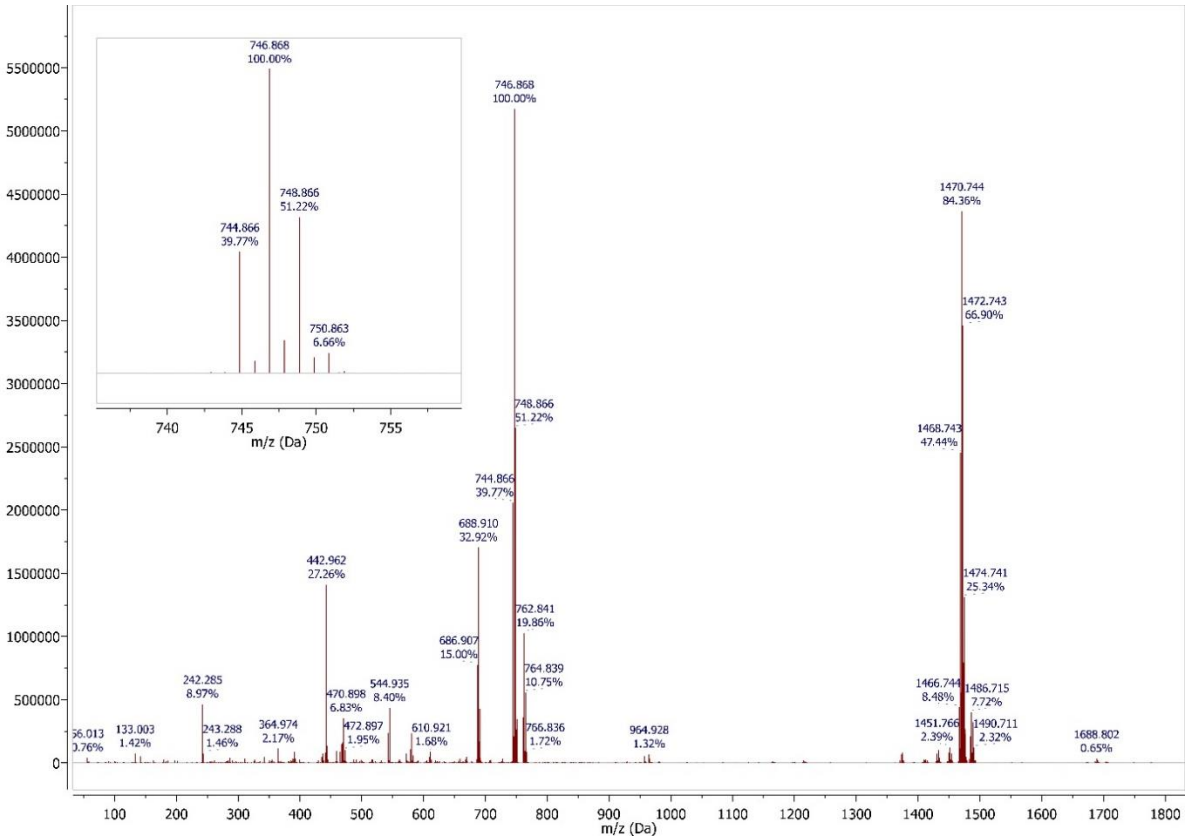

Figure 9.49. ESI+ MS spectrum of [$Re^{V}OCl_2(L^{OMe})$].

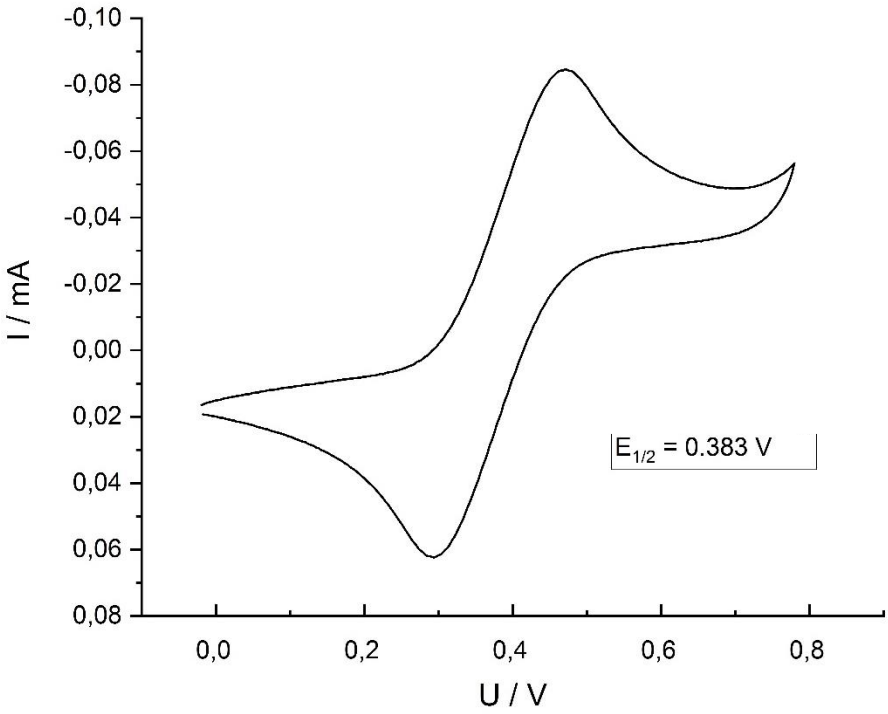

Figure 9.50. Cyclic voltammogram taken from [$Re^{V}OCl_2(L^{OMe})$] (0.9 mL dry CH_2Cl_2, 50 mg $(NBu_4)PF_6$, 7 mg [$Re^{V}OCl_2(L^{OMe})$], scan rate 500 mV/s).

Spectroscopic Data of [$Re^{V}NCl(PPh_3)(L^{OMe})$]

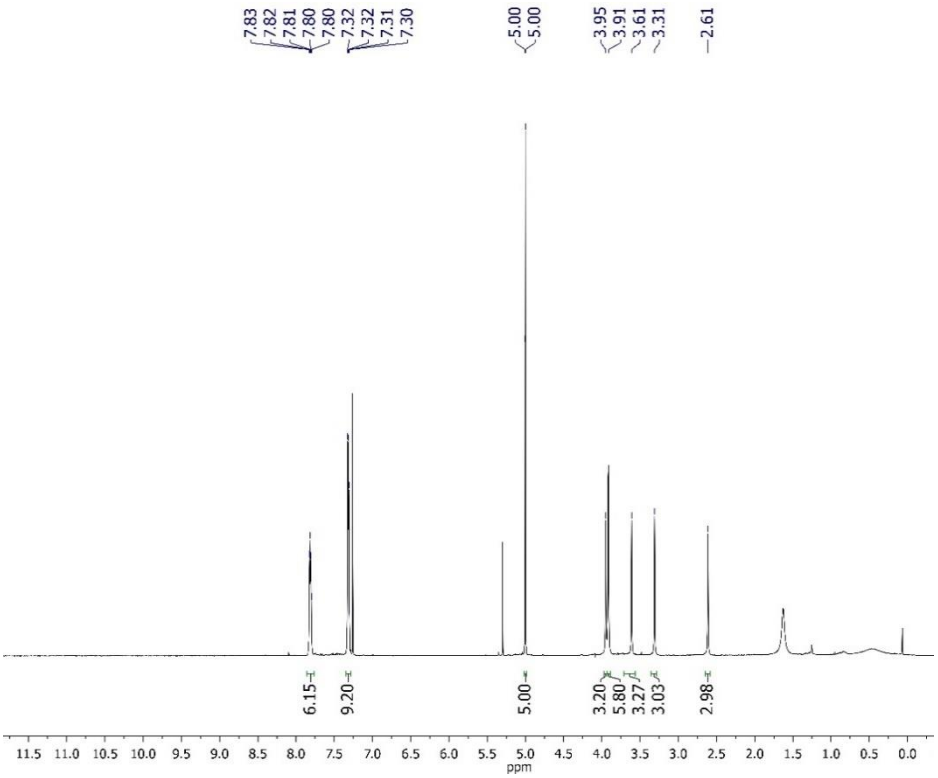

Figure 9.51. $^{1}H\{^{31}P\}$ NMR spectrum of [$Re^{V}NCl(PPh_3)(L^{OMe})$] in $CDCl_3$.

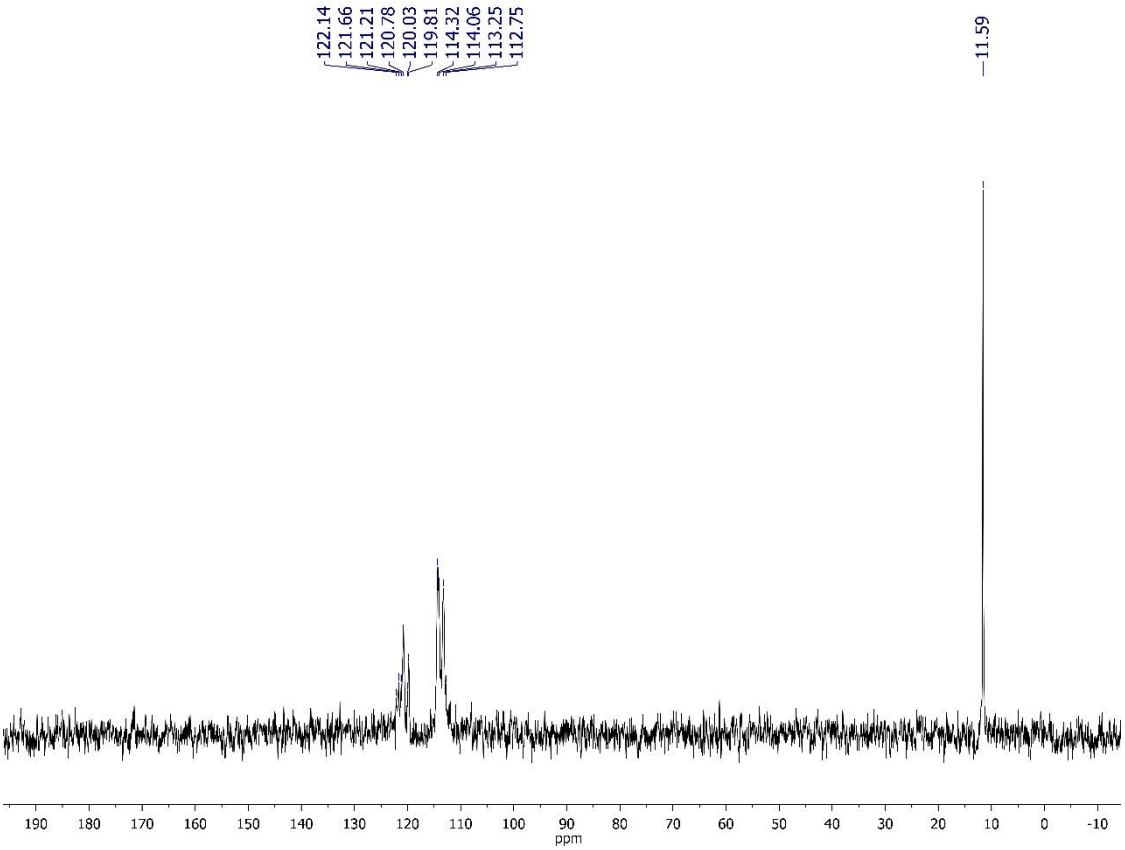

Figure 9.52. $^{31}P\{^{1}H\}$ NMR spectrum of [$Re^{V}NCl(PPh_3)(L^{OMe})$] in $CDCl_3$.

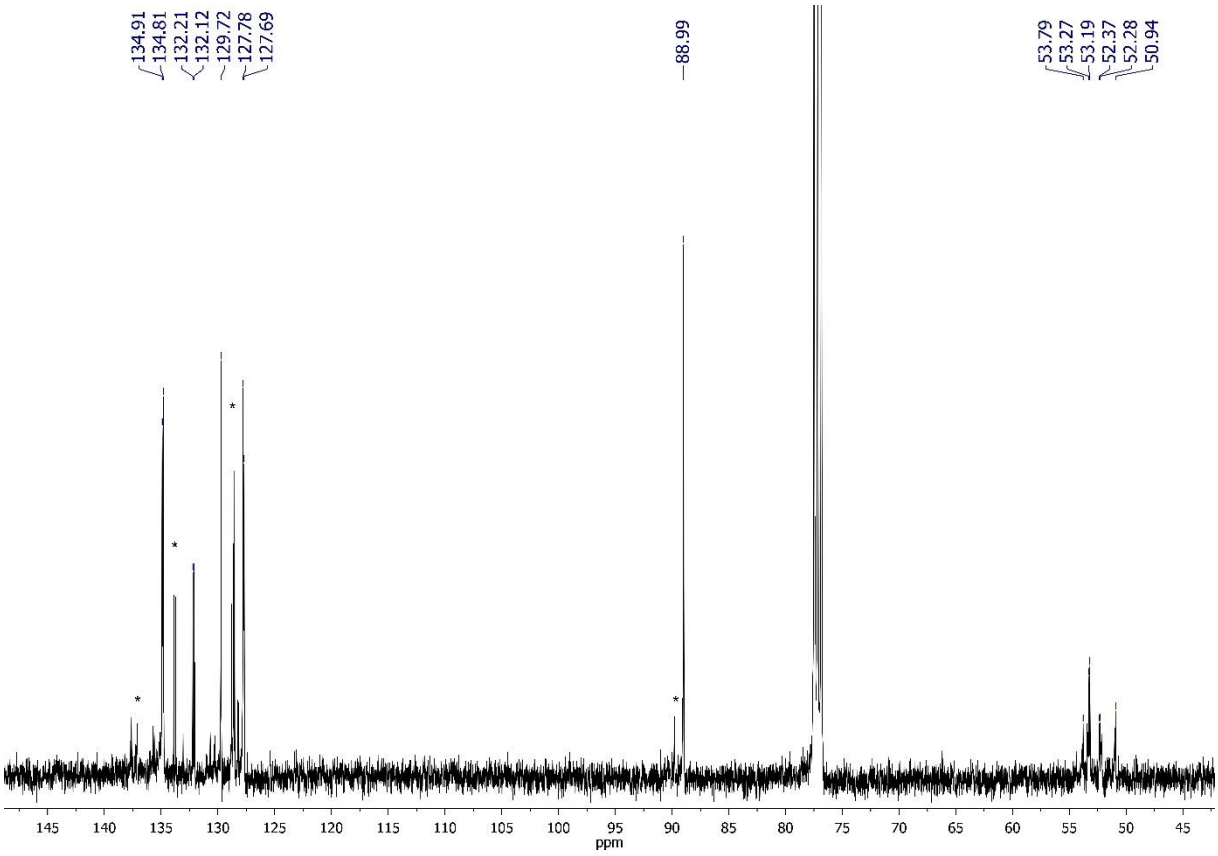

Figure 9.53. $^{13}C\{^{1}H\}$ NMR spectrum of $[Re^{V}NCl(PPh_3)(L^{OMe})]$ in $CDCl_3$. * Side products.

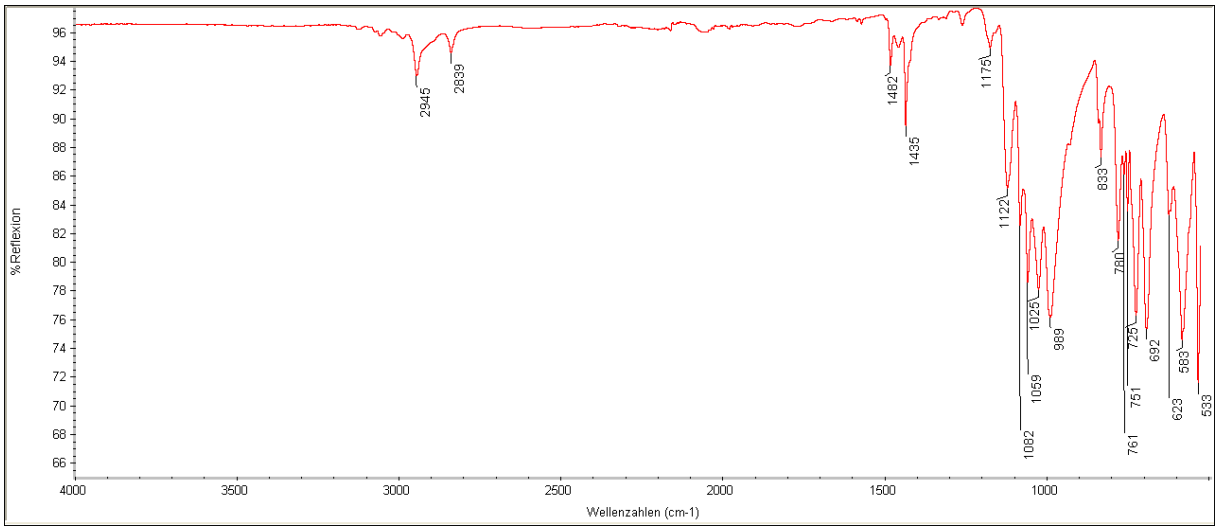

Figure 9.54. IR spectrum of $[Re^{V}NCl(PPh_3)(L^{OMe})]$.

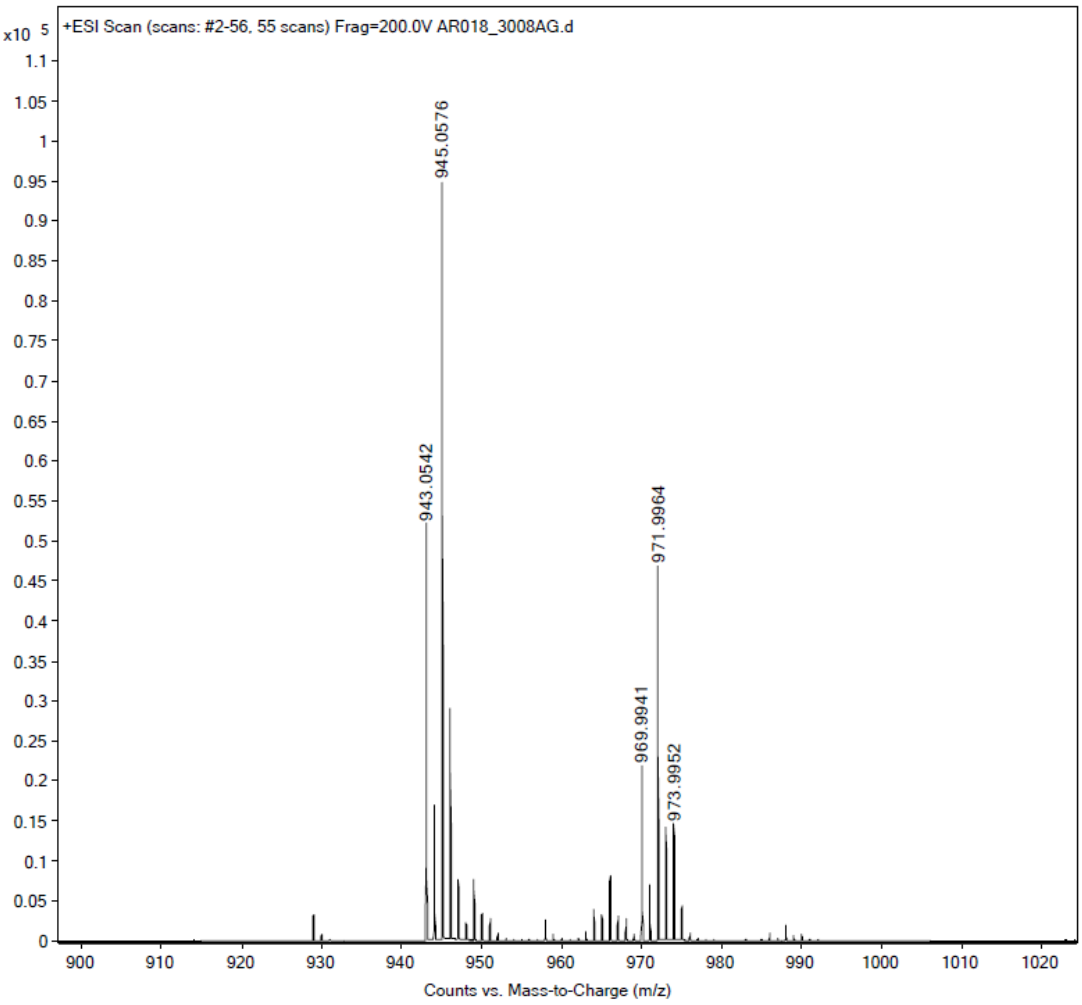

Figure 9.55. ESI+ MS spectrum of [$Re^{V}NCl(PPh_3)(L^{OMe})$].

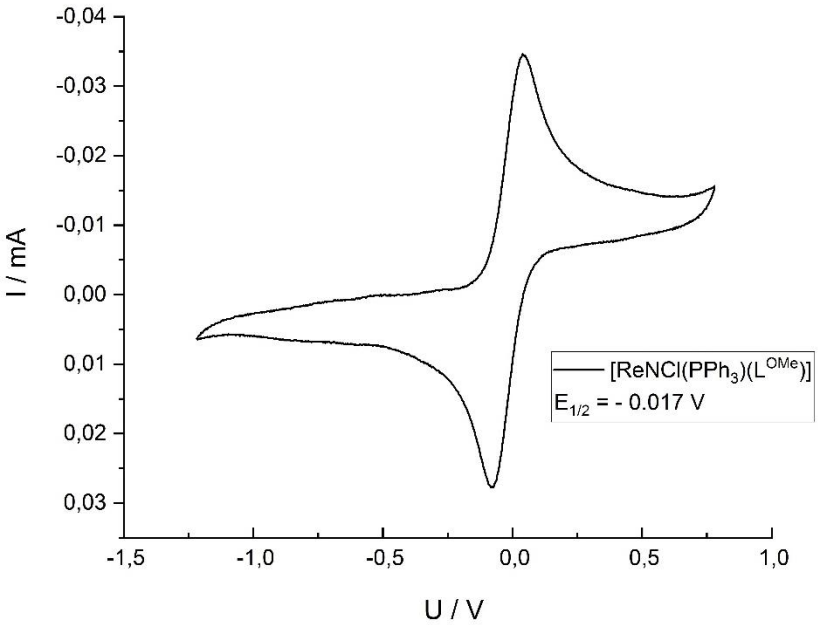

Figure 9.56. Cyclic voltammogram taken from [$Re^{V}NCl(PPh_3)(L^{OMe})$] (0.9 mL dry CH_2Cl_2, 50 mg $(NBu_4)PF_6$, 2 mg [$Re^{V}NCl(PPh_3)(L^{OMe})$], scan rate 500 mV/s).

Spectroscopic Data of $[Re^{V}NCl_2(L^{OMe})]$

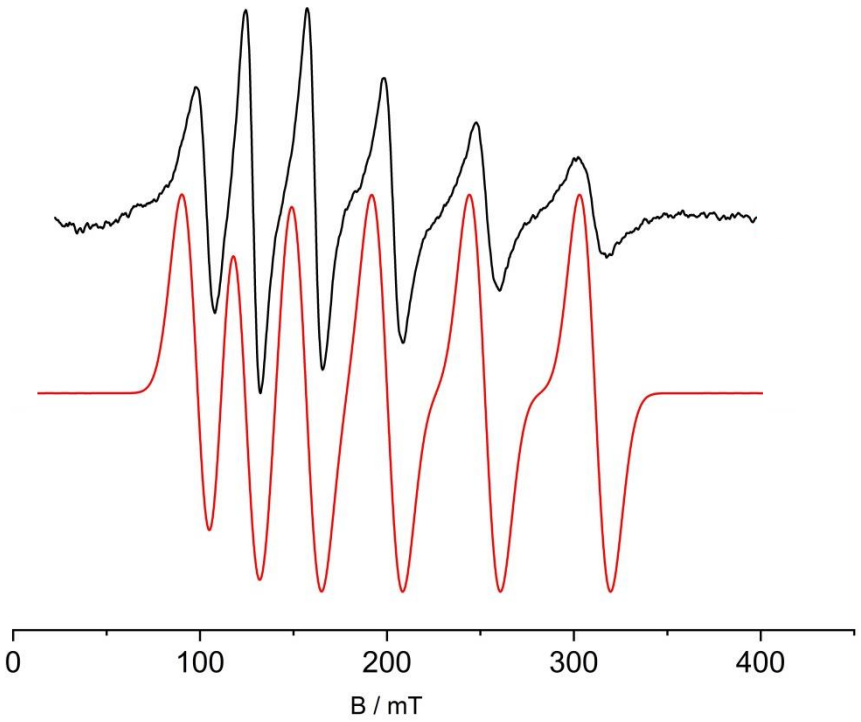

Figure 9.57. X-Band EPR spectrum of $[Re^{V}NCl_2(L^{OMe})]$ at room temperature. Black: Experimental. Red: Simulated.

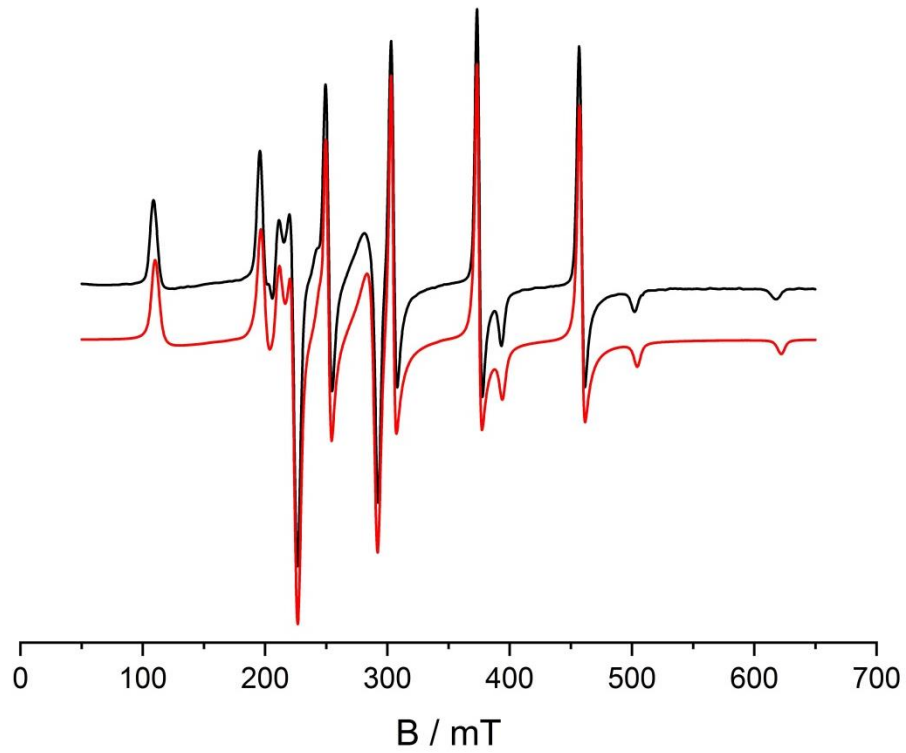

Figure 9.58. X-Band EPR spectrum of $[Re^{V}NCl_2(L^{OMe})]$ at 77 K. Black: Experimental. Red: Simulated.

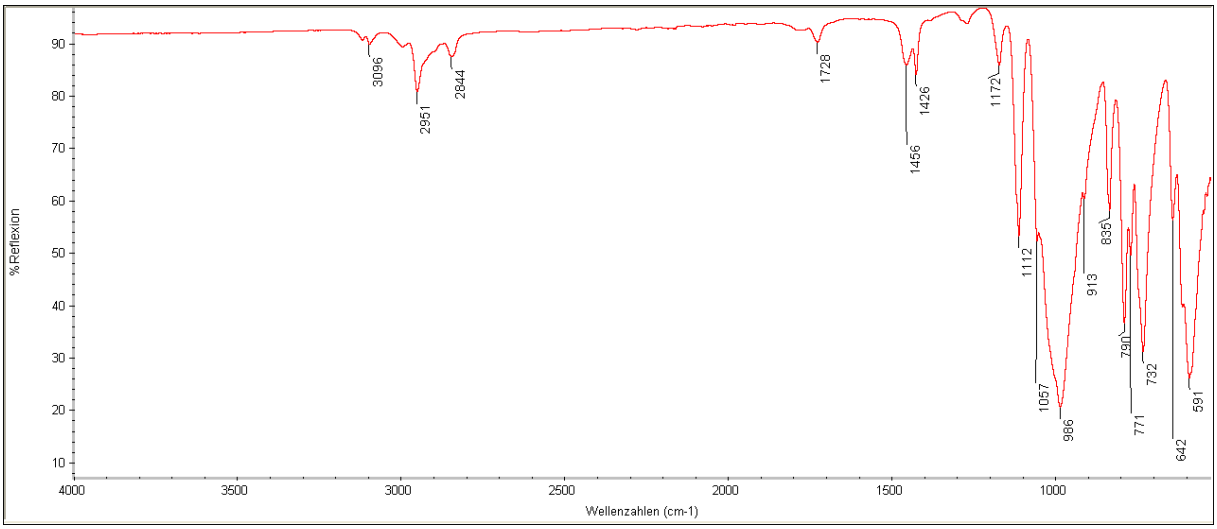

Figure 9.59. IR spectrum of $[Re^{V}NCl_2(L^{OMe})]$.

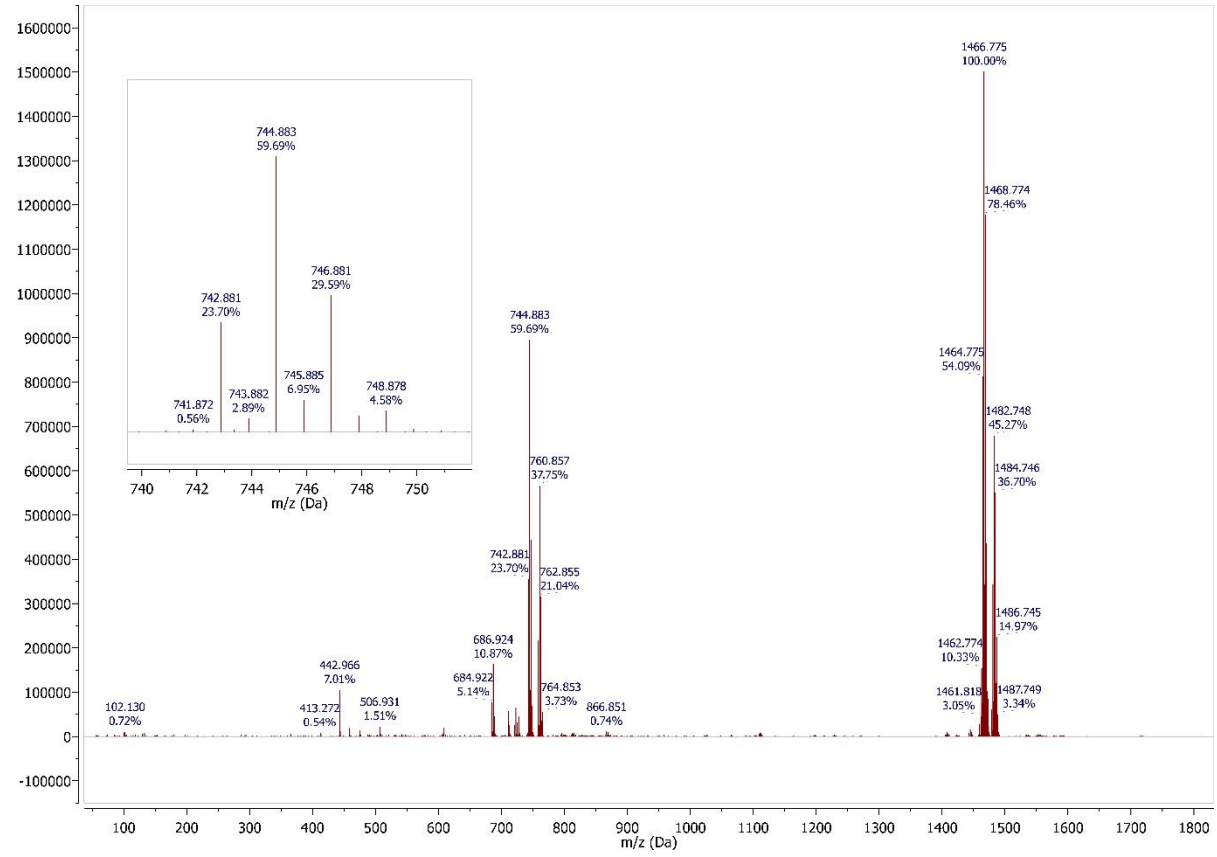

Figure 9.60. ESI+ MS spectrum of $[Re^{V}NCl_2(L^{OMe})]$.

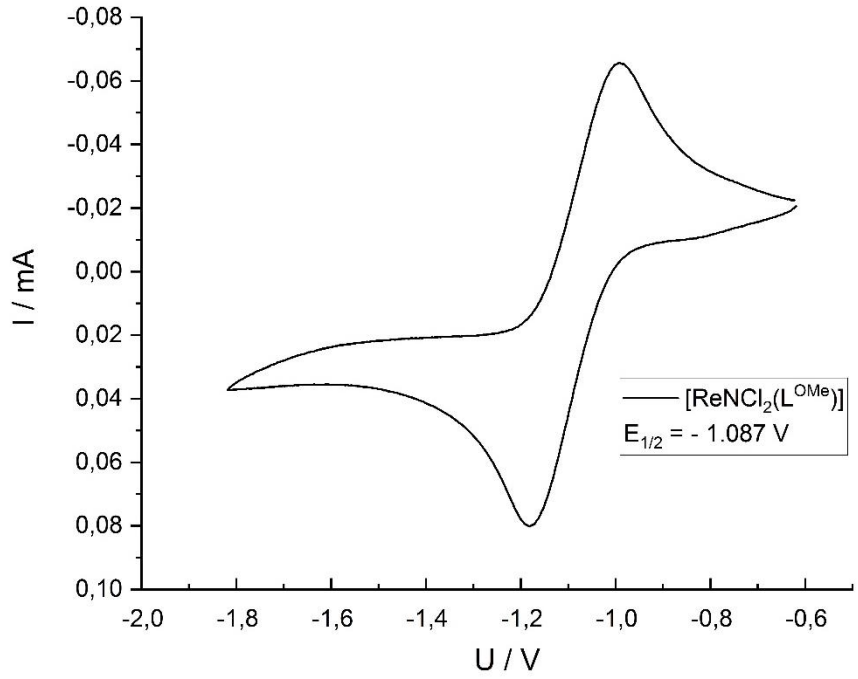

Figure 9.61. Cyclic voltammogram taken from $[Re^{V}NCl_2(L^{OMe})]$ (0.9 mL dry CH_2Cl_2, 50 mg $(NBu_4)PF_6$, 2 mg $[Re^{V}NCl_2(L^{OMe})]$, scan rate 500 mV/s).

Spectroscopic Data of $[Re^{V}O_3(L^{OMe})]$

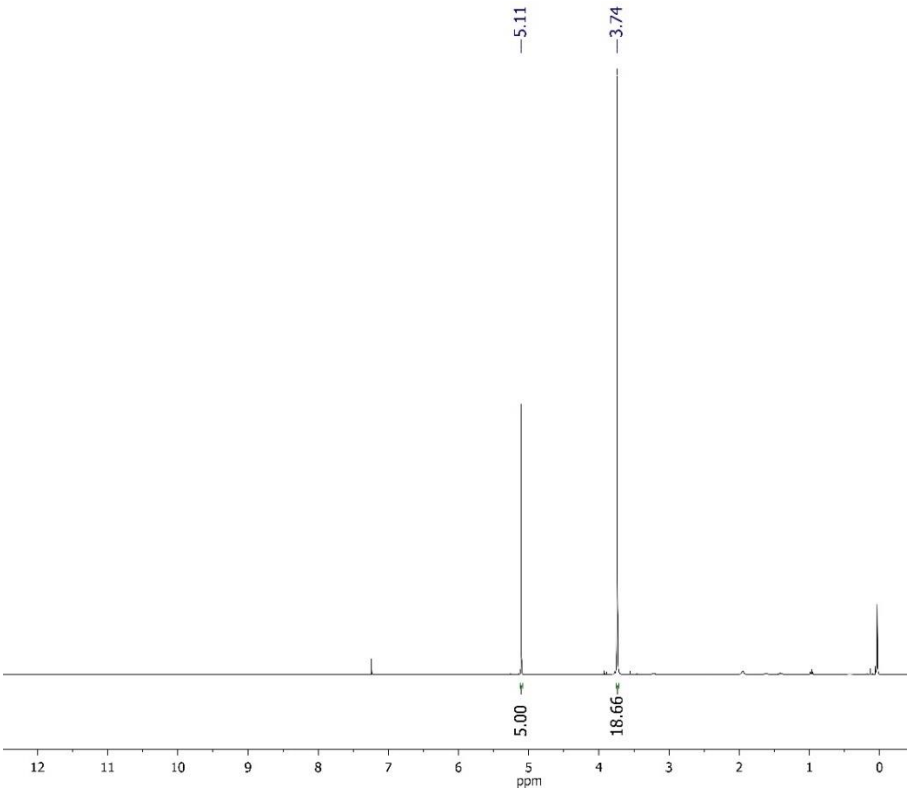

Figure 9.62. $^{1}H\{^{31}P\}$ NMR spectrum of $[Re^{V}O_3(L^{OMe})]$ in $CDCl_3$.

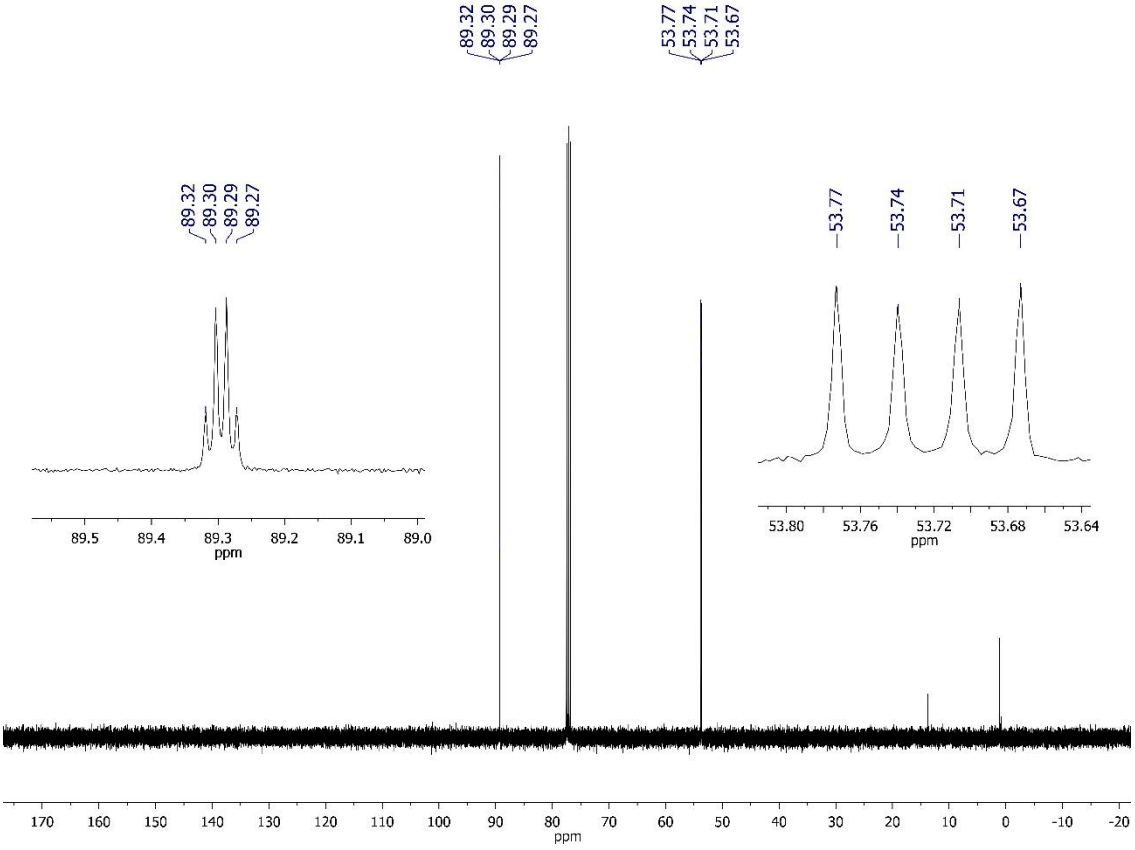

Figure 9.63. $^{13}C\{^{1}H\}$ NMR spectrum of $[Re^{V}O_3(L^{OMe})]$ in $CDCl_3$.

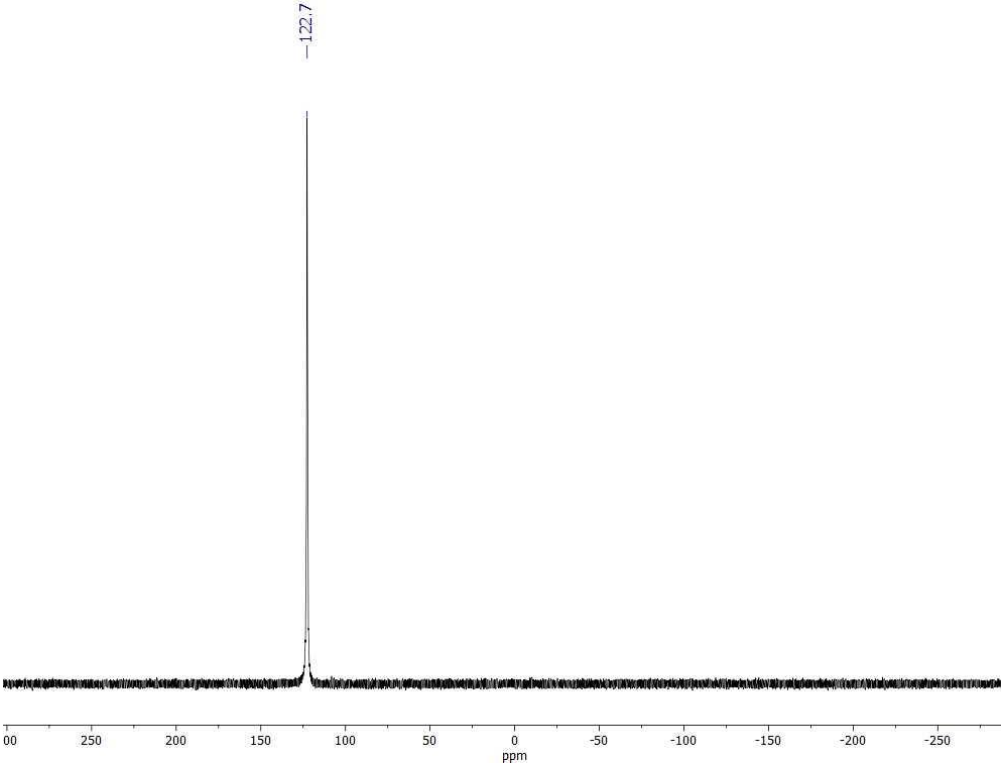

Figure 9.64. $^{31}P\{^{1}H\}$ NMR spectrum of $[Re^{V}O_3(L^{OMe})]$ in $CDCl_3$.

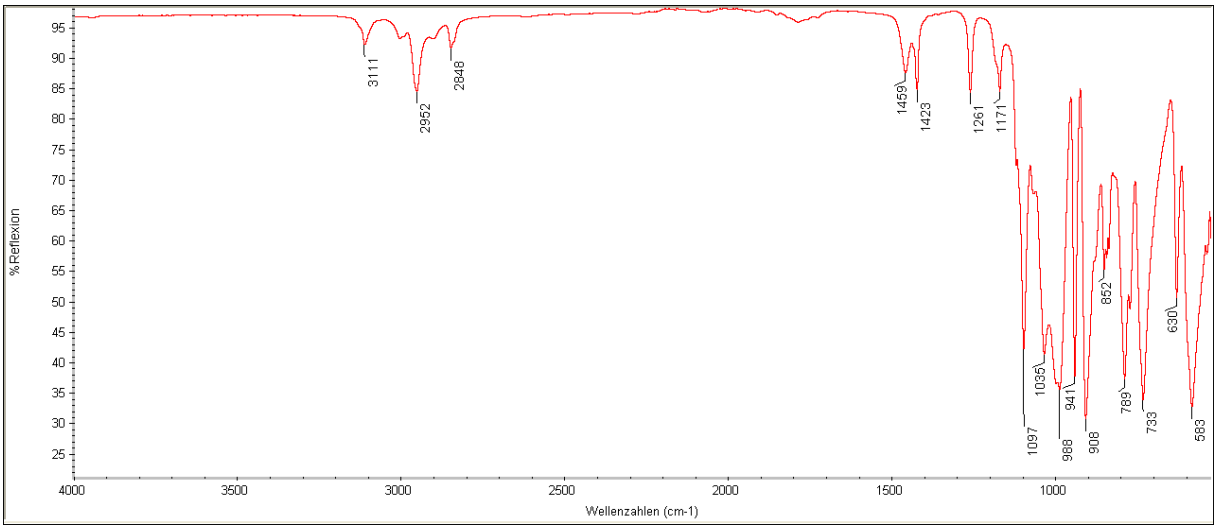

Figure 9.65. IR spectrum of [$Re^{V}O_3(L^{OMe})$].

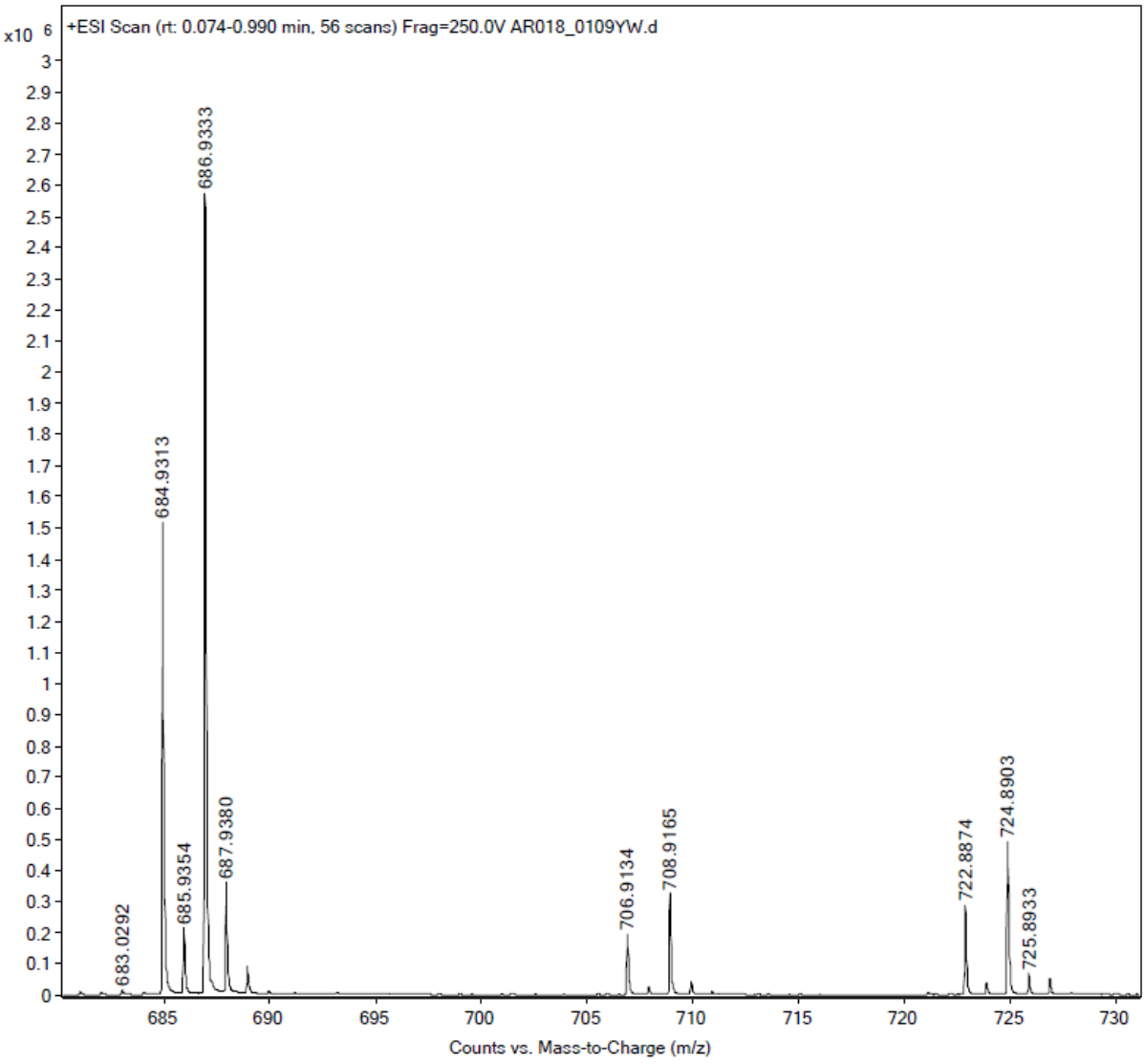

Figure 9.66. ESI+ MS spectrum of [$Re^{V}O_3(L^{OMe})$].

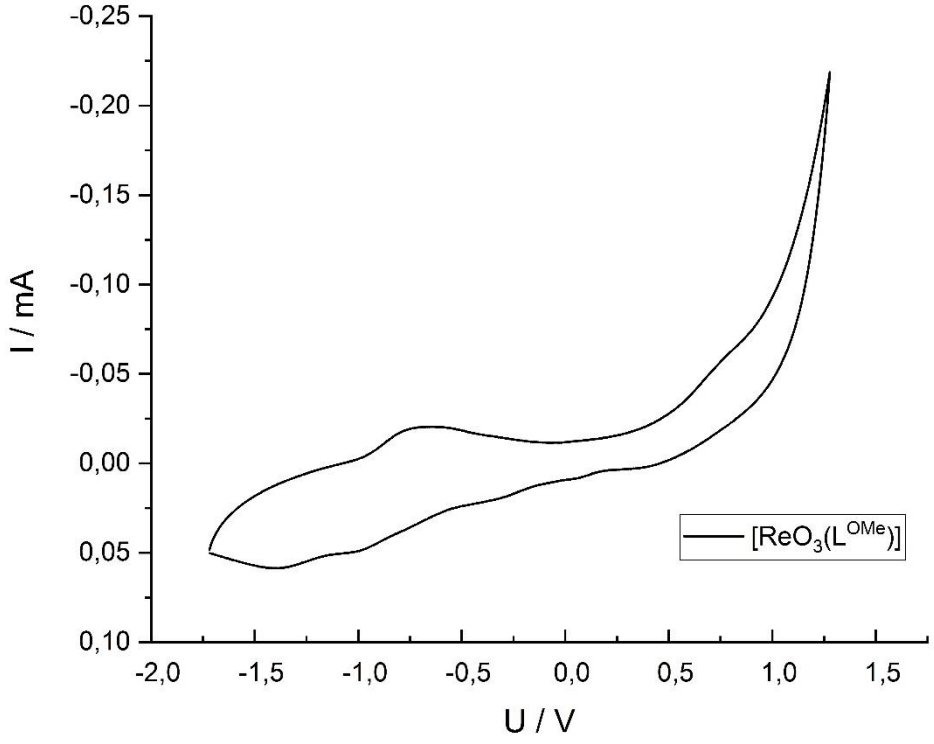

Figure 9.67. Cyclic voltammogram taken from $[Re^{V}O_3(L^{OMe})]$ (0.9 mL dry CH_2Cl_2, 50 mg $(NBu_4)PF_6$, 2 mg $[Re^{V}O_3(L^{OMe})]$, scan rate 500 mV/s).

Spectroscopic Data of $[Ga(L^{OMe})_2]NO_3$

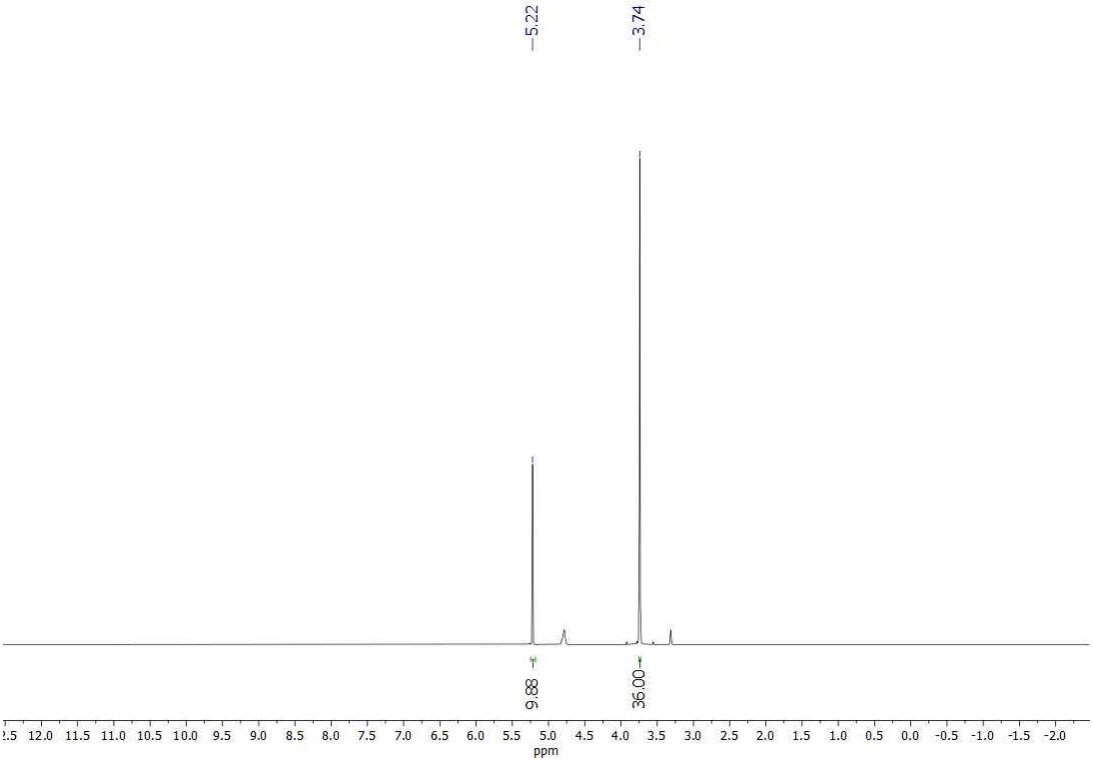

Figure 9.68. $^{1}H\{^{31}P\}$ NMR spectrum of $[Ga(L^{OMe})_2]NO_3$ in d_4-MeOD.

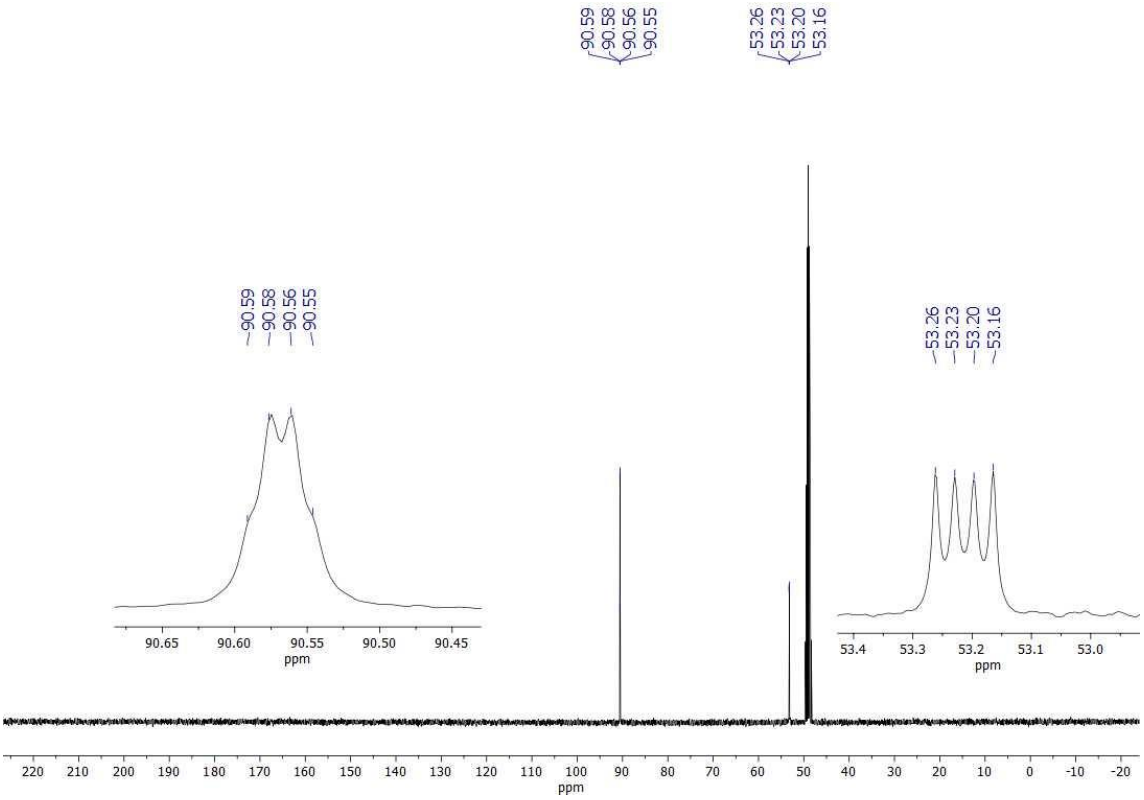

Figure 9.69. $^{13}C\{^{1}H\}$ NMR spectrum of $[Ga(L^{OMe})_2]NO_3$ in d_4-MeOD.

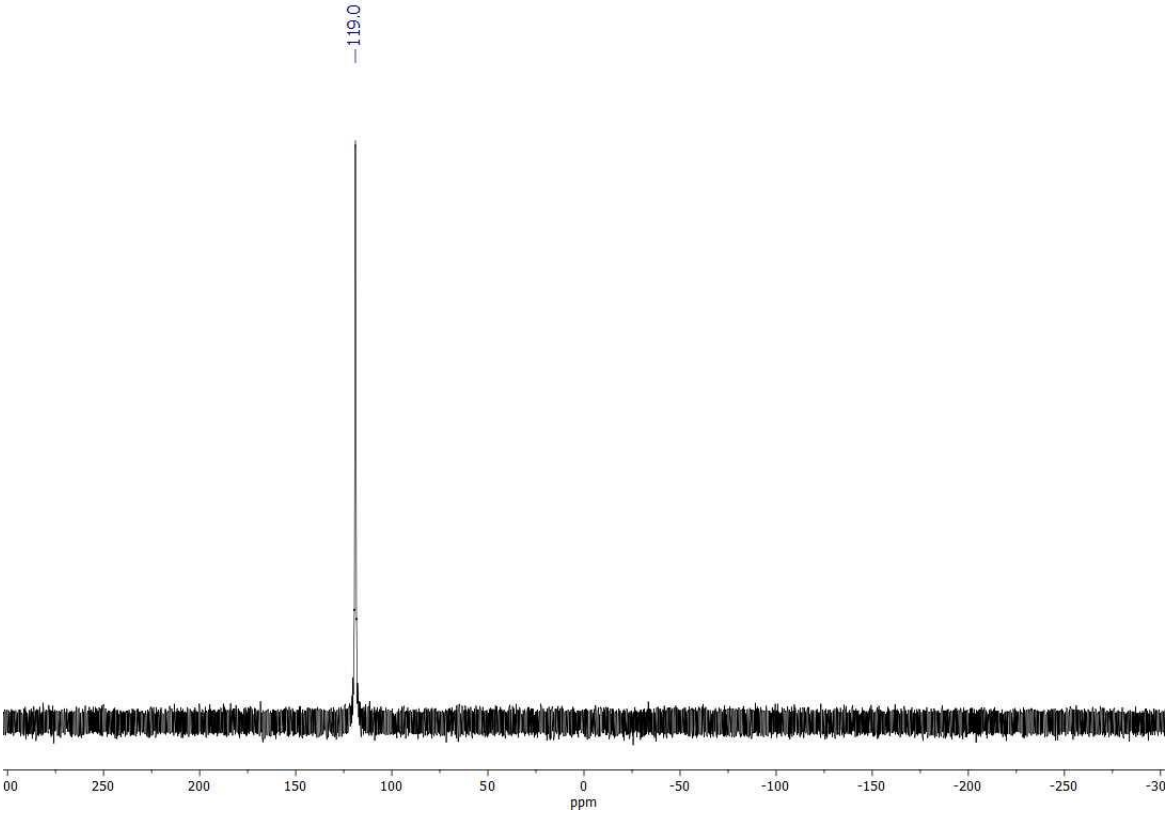

Figure 9.70. $^{31}P\{^{1}H\}$ NMR spectrum of $[Ga(L^{OMe})_2]NO_3$ in d_4-MeOD.

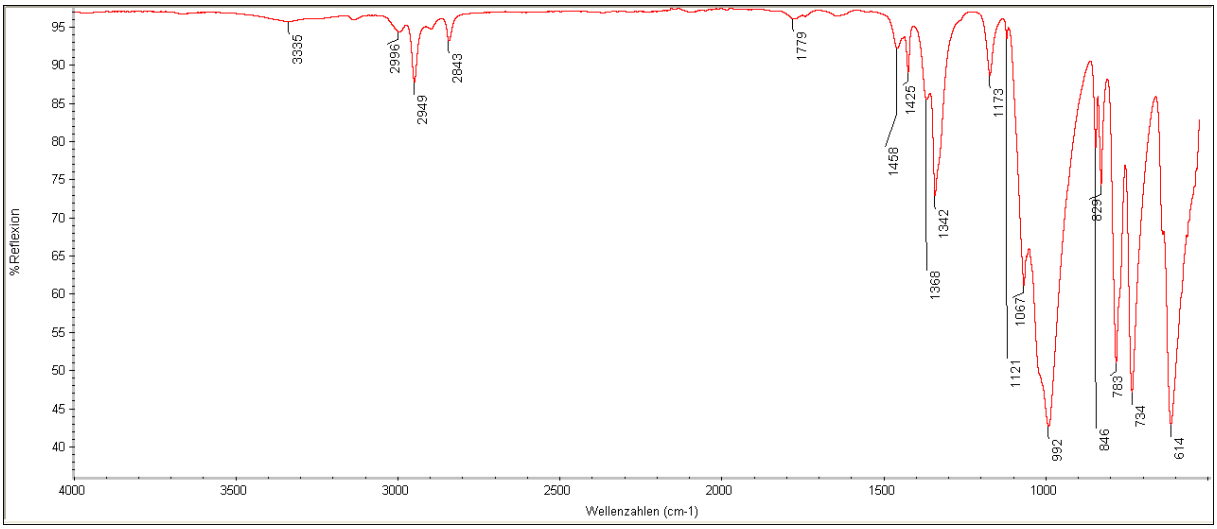

Figure 9.71. IR spectrum of $[Ga(L^{OMe})_2]NO_3$.

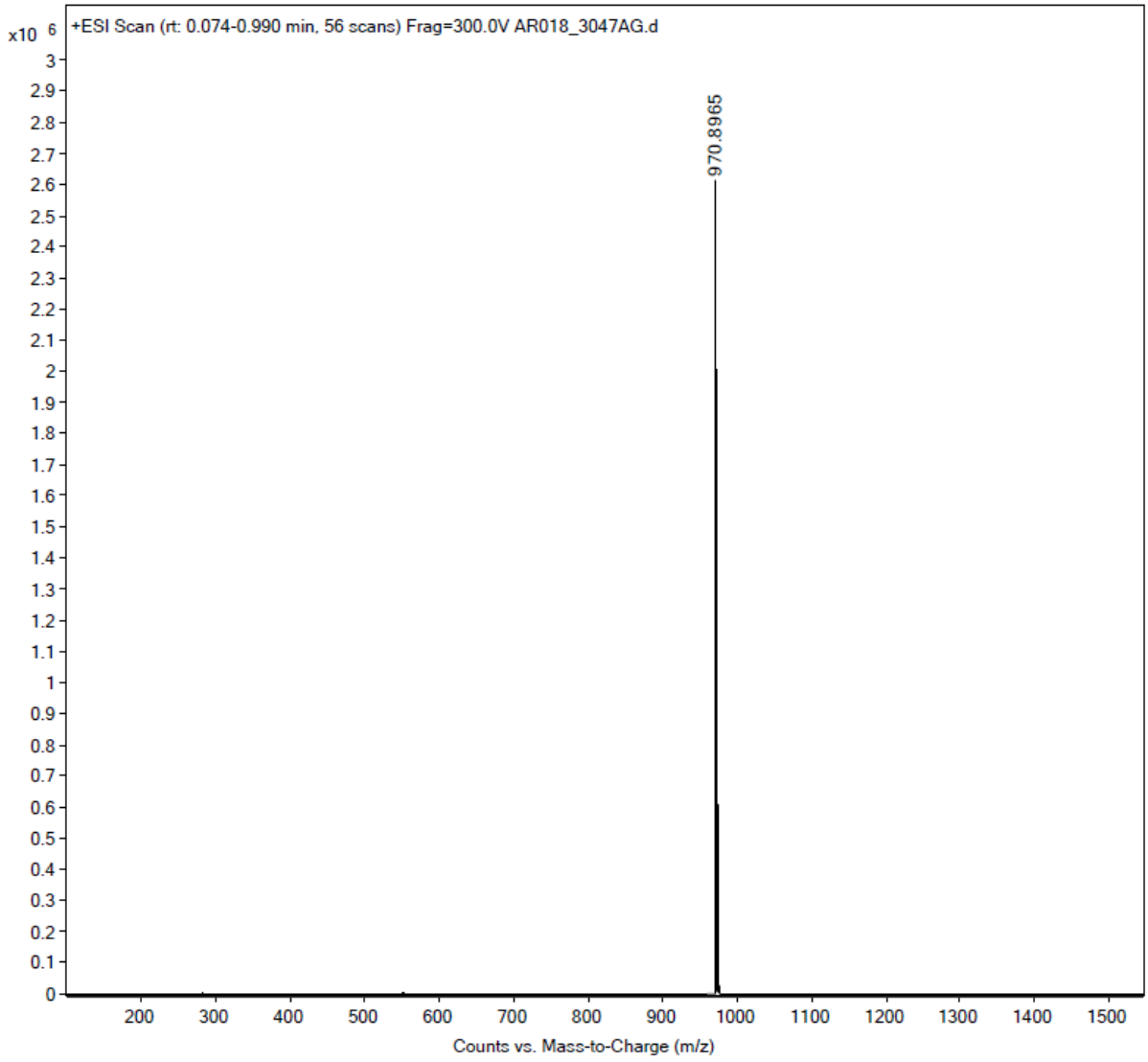

Figure 9.72. ESI+ MS spectrum of $[Ga(L^{OMe})_2]NO_3$.

Spectroscopic Data of $[In(L^{OMe})_2]NO_3$

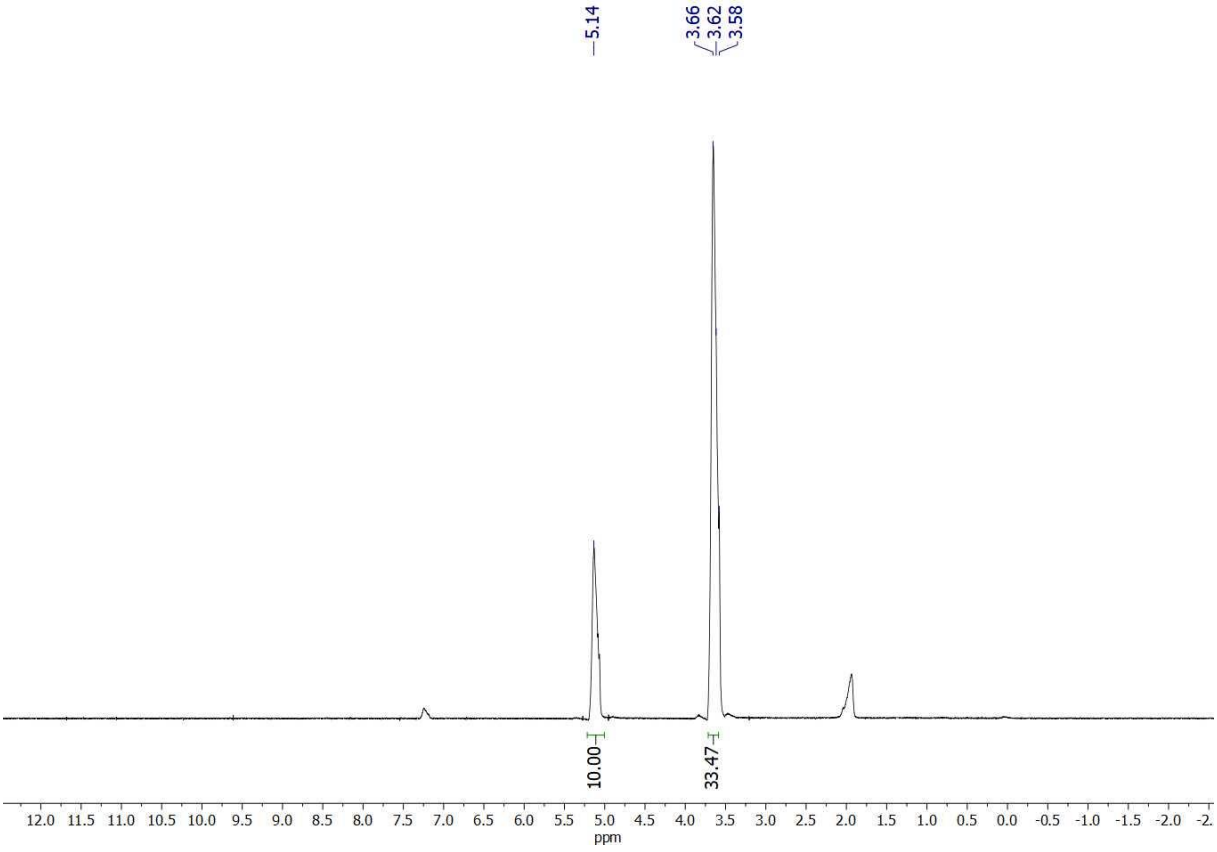

Figure 9.73. $^{1}H\{^{31}P\}$ NMR spectrum of $[In(L^{OMe})_2]NO_3$ in $CDCl_3$.

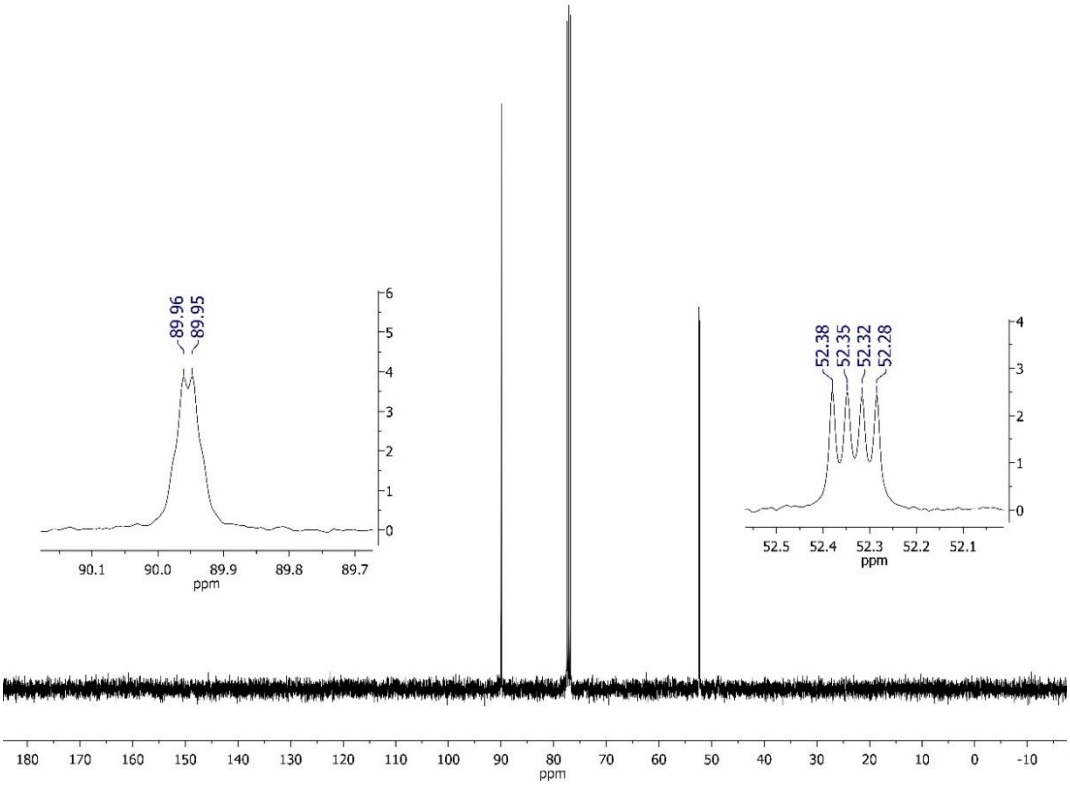

Figure 9.74. $^{13}C\{^{1}H\}$ NMR spectrum of $[In(L^{OMe})_2]NO_3$ in $CDCl_3$.

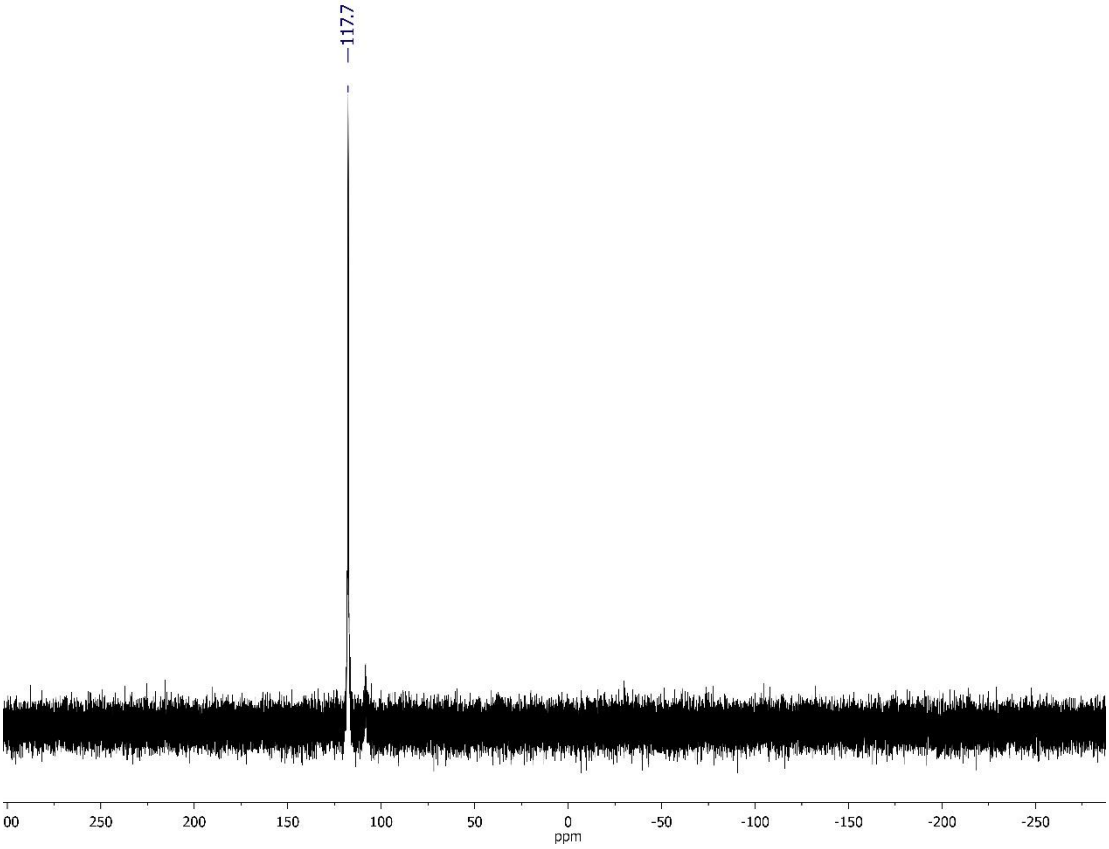

Figure 9.75. $^{31}P\{^{1}H\}$ NMR spectrum of $[In(L^{OMe})_2]NO_3$ in $CDCl_3$.

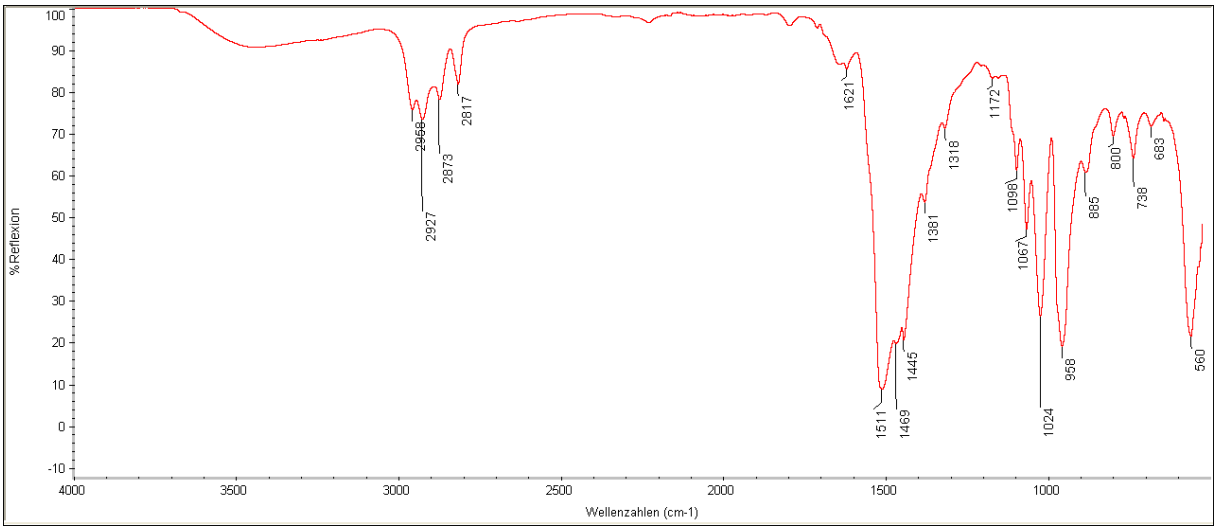

Figure 9.76. IR spectrum of $[In(L^{OMe})_2]NO_3$.

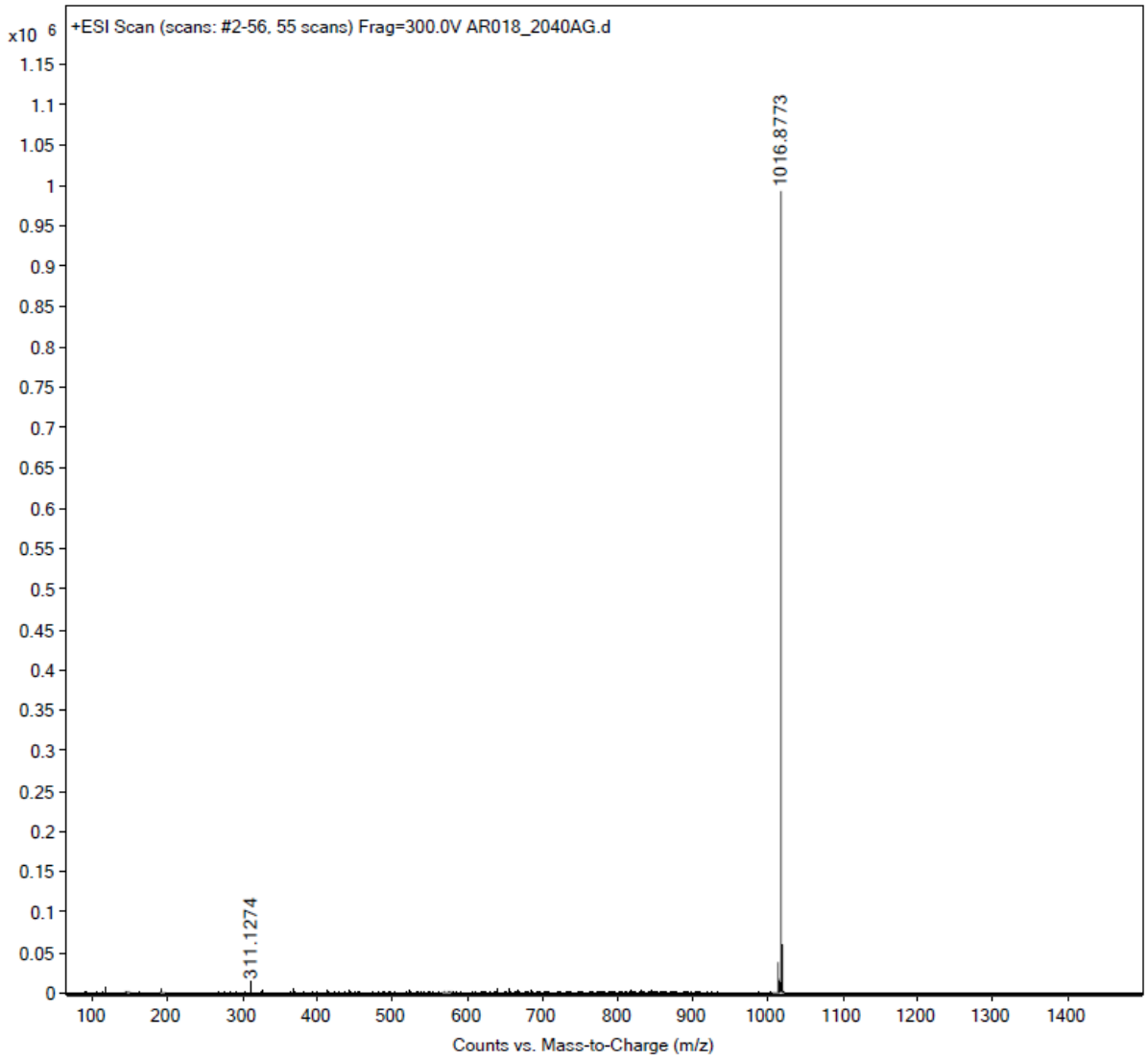

Figure 9.77. ESI+ MS spectrum of $[In(L^{OMe})_2]NO_3$.

Spectroscopic Data of $[Lu(L^{OMe})_2(NO_3)]$

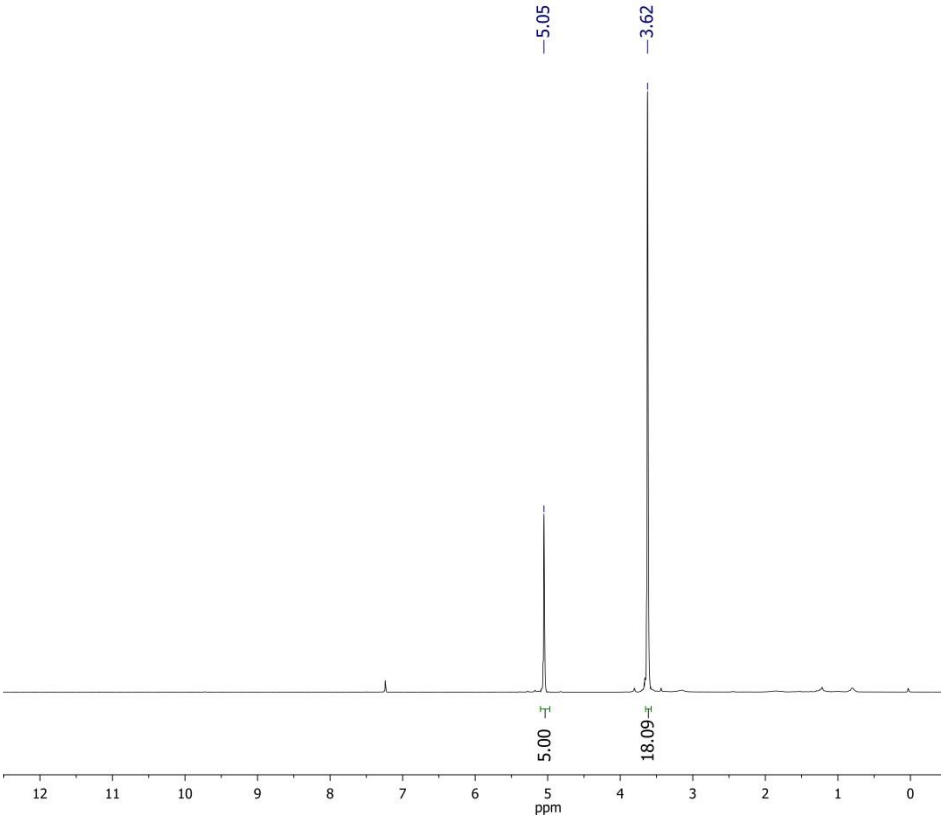

Figure 9.78. $^{1}H\{^{31}P\}$ NMR spectrum of $[Lu(L^{OMe})_2(NO_3)]$ in $CDCl_3$.

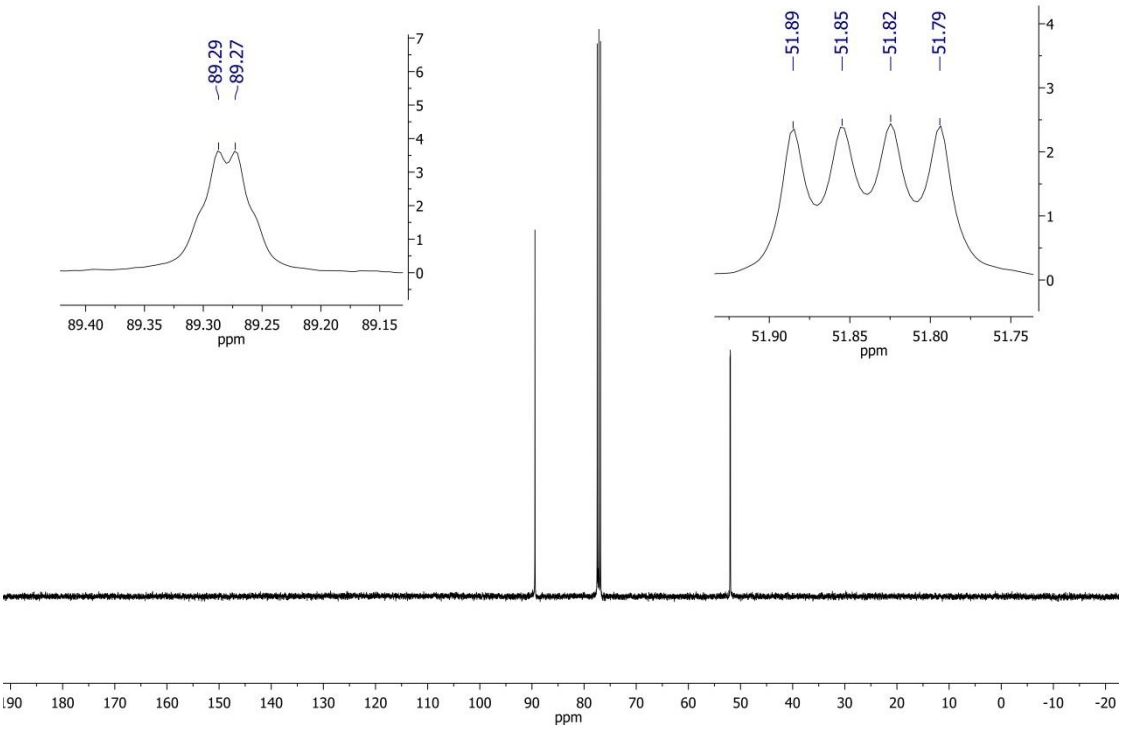

Figure 9.79. $^{13}C\{^{1}H\}$ NMR spectrum of $[Lu(L^{OMe})_2(NO_3)]$ in $CDCl_3$.

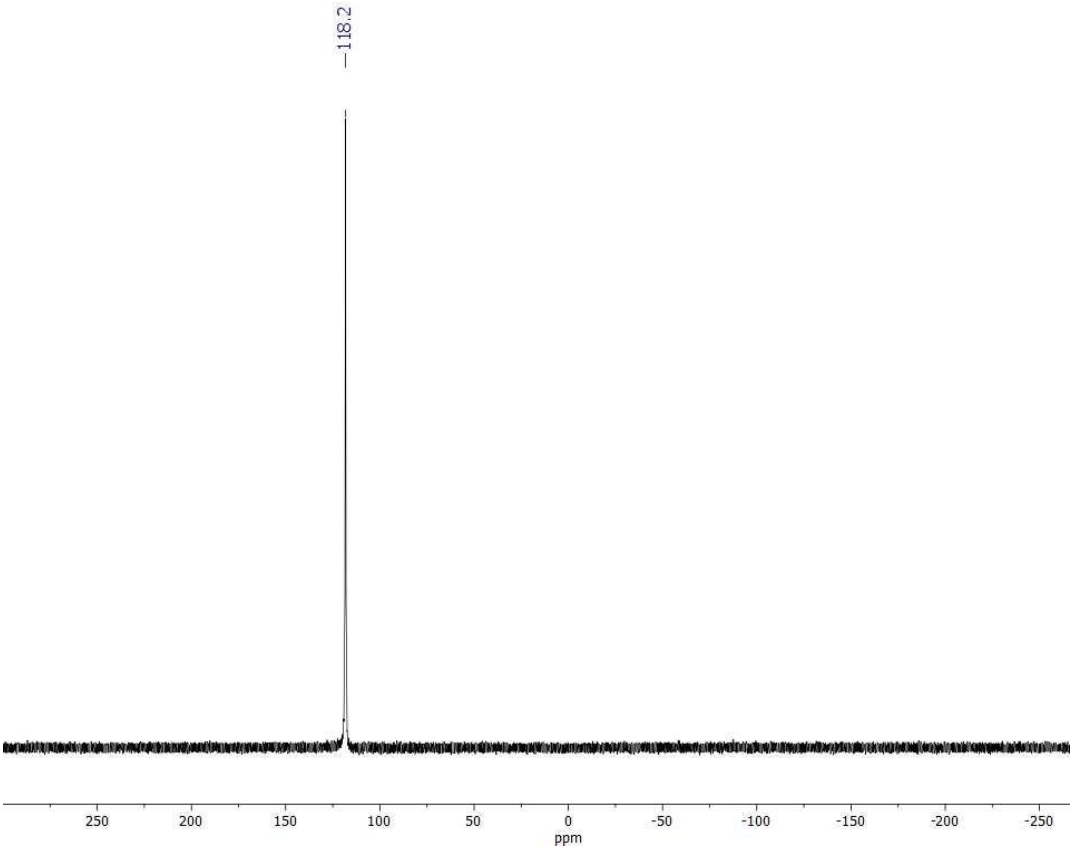

Figure 9.80. $^{31}P\{^{1}H\}$ NMR spectrum of $[Lu(L^{OMe})_2(NO_3)]$ in $CDCl_3$.

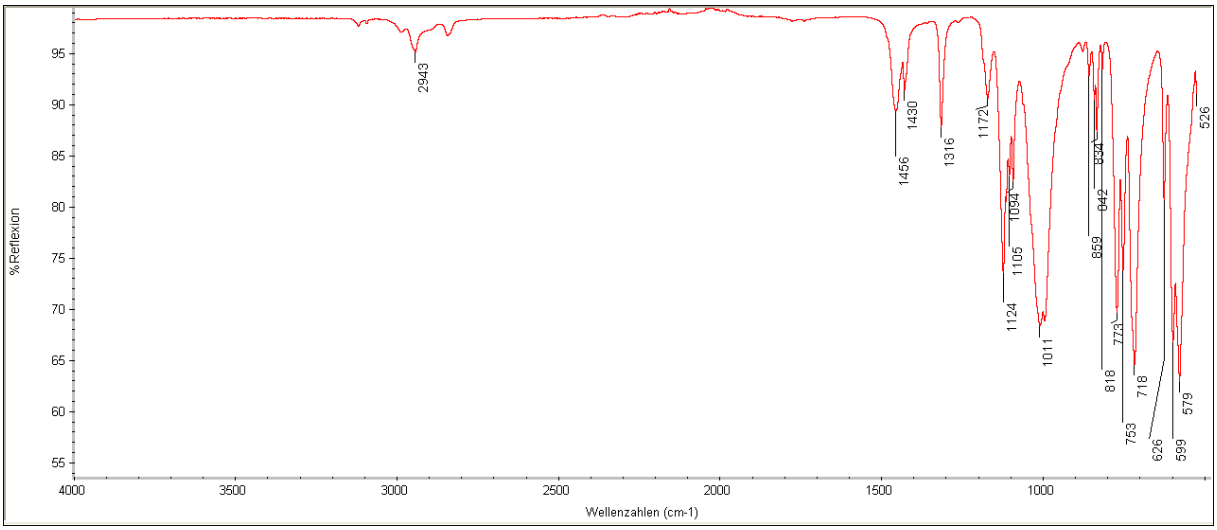

Figure 9.81. IR spectrum of $[Lu(L^{OMe})_2(NO_3)]$.

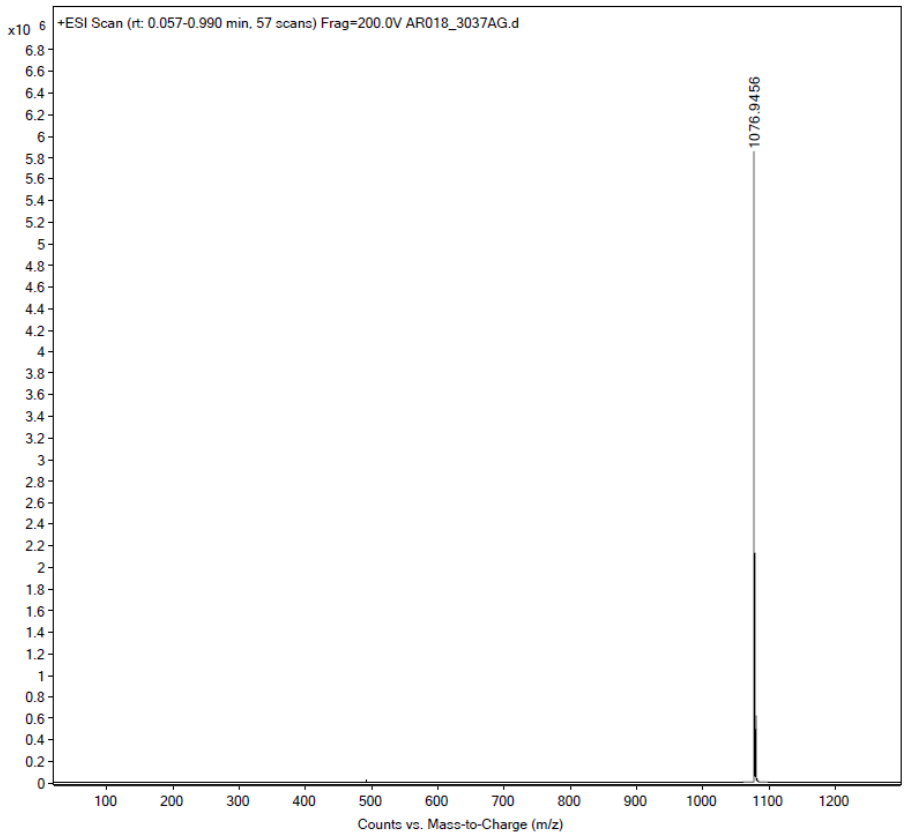

Figure 9.82. ESI+ MS spectrum of $[Lu(L^{OMe})_2(NO_3)]$.

Spectroscopic Data of $Na(Cp^{COOMe})$

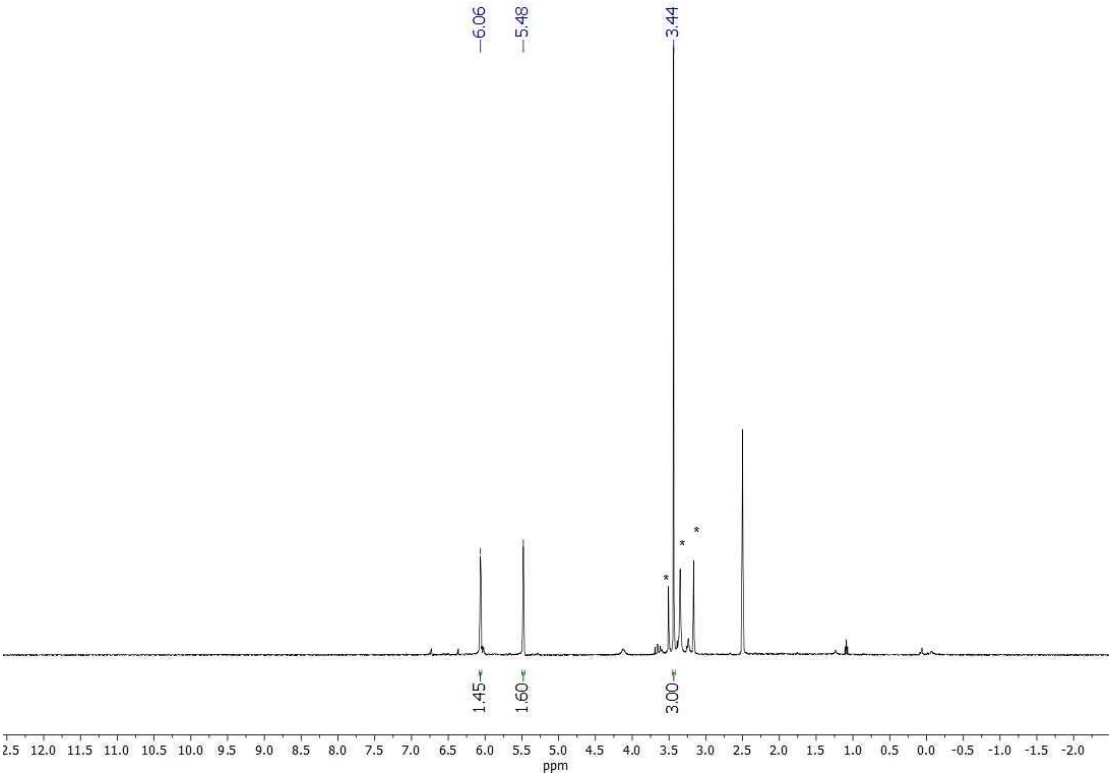

Figure 9.83. ^1H NMR spectrum of $Na(Cp^{COOMe})$ in d_6-DMSO. *Side products.

Spectroscopic Data of [Co(Cp^{COOMe})(CO)$_2$]

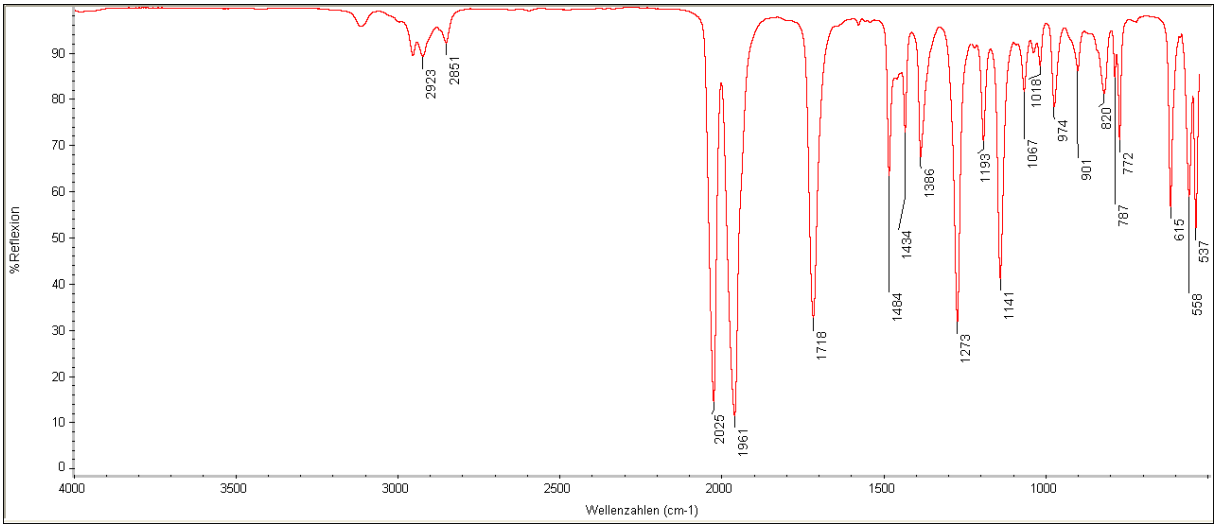

Figure 9.84. IR spectrum of [Co(Cp^{COOMe})(CO)$_2$].

Spectroscopic Data of [Co(Cp^{COOMe})(CO)I$_2$]

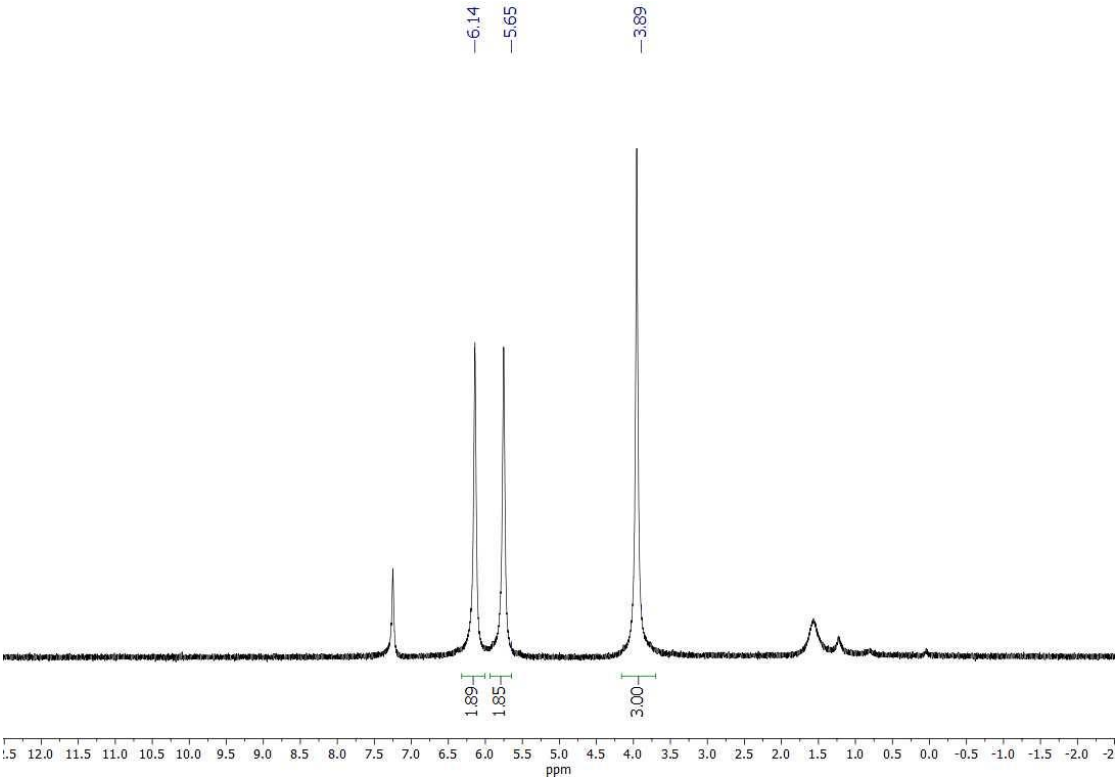

Figure 9.85. ^{1}H NMR spectrum of [Co(Cp^{COOMe})(CO)I$_2$] in CDCl$_3$.

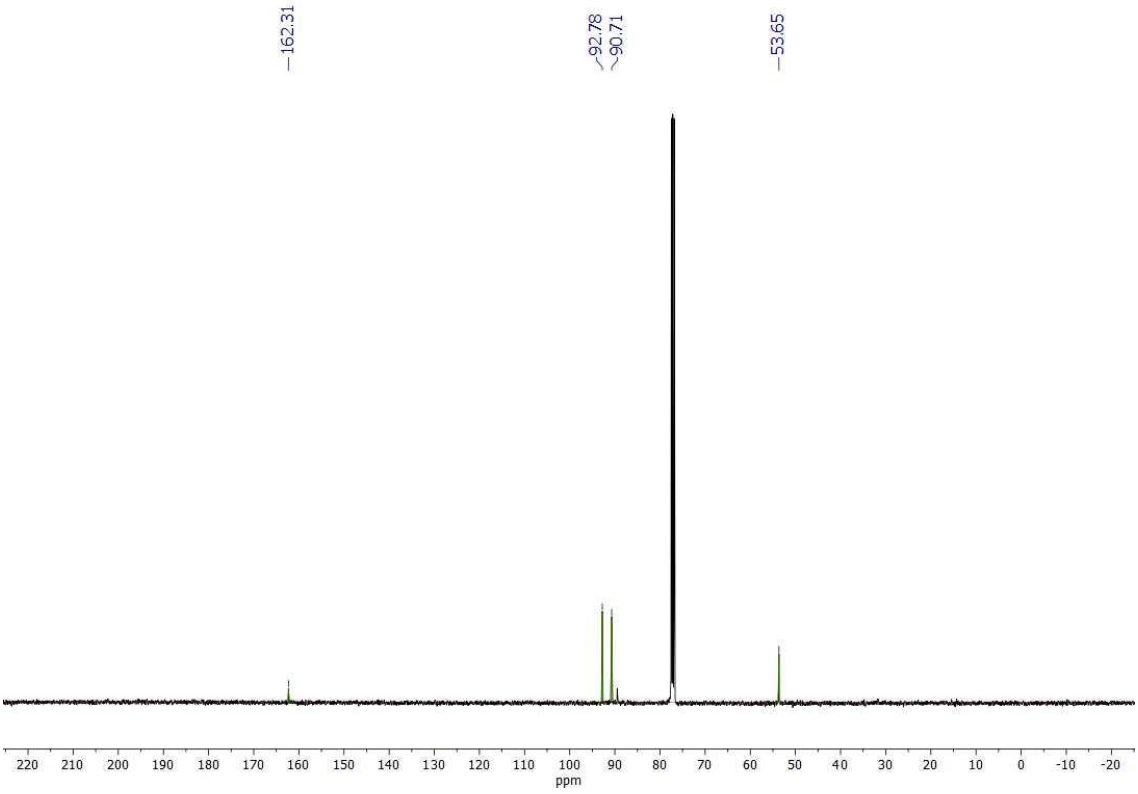

Figure 9.86. $^{13}C\{^{1}H\}$ NMR spectrum of $[Co(Cp^{COOMe})(CO)I_2]$ in $CDCl_3$.

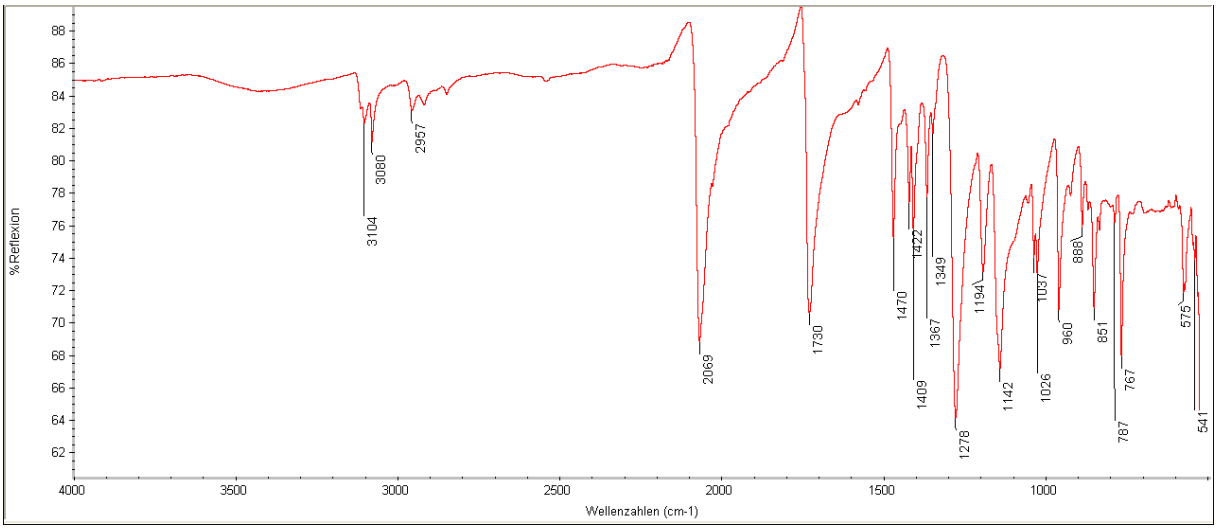

Figure 9.87. IR spectrum of $[Co(Cp^{COOMe})(CO)I_2]$.

Spectroscopic Data of $NaL^{OMeCOOMe}$

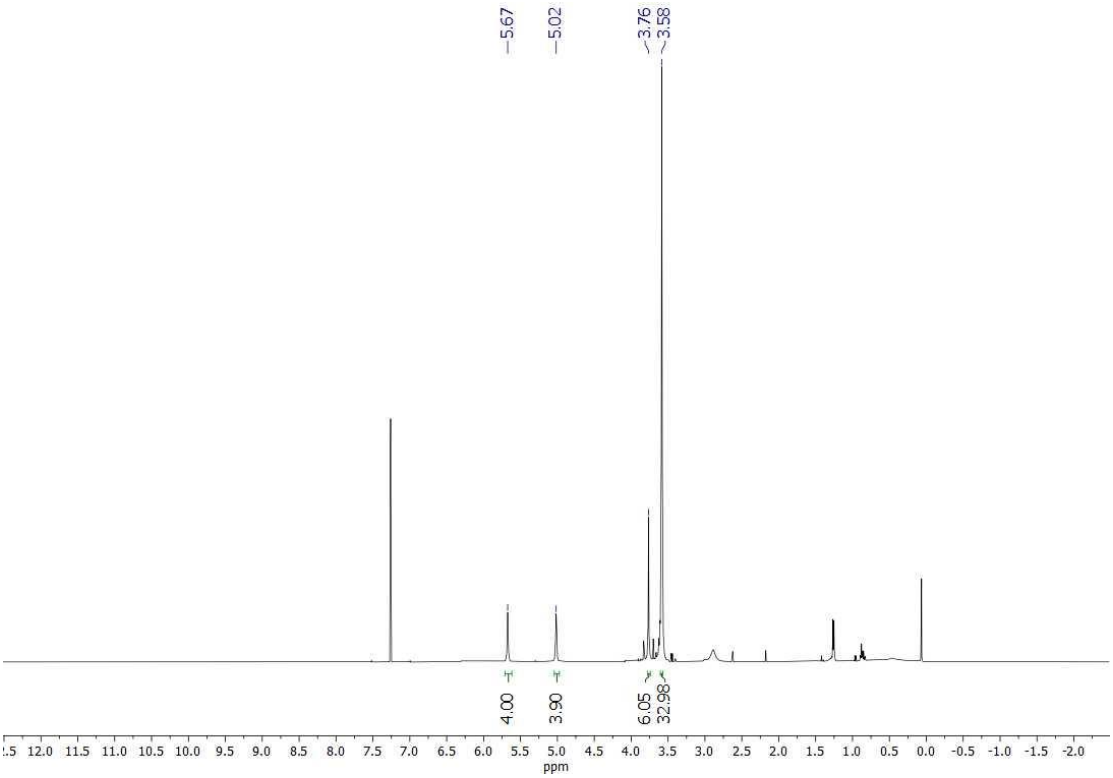

Figure 9.88. $^{1}H\{^{31}P\}$ NMR spectrum of $NaL^{OMeCOOMe}$ in $CDCl_3$.

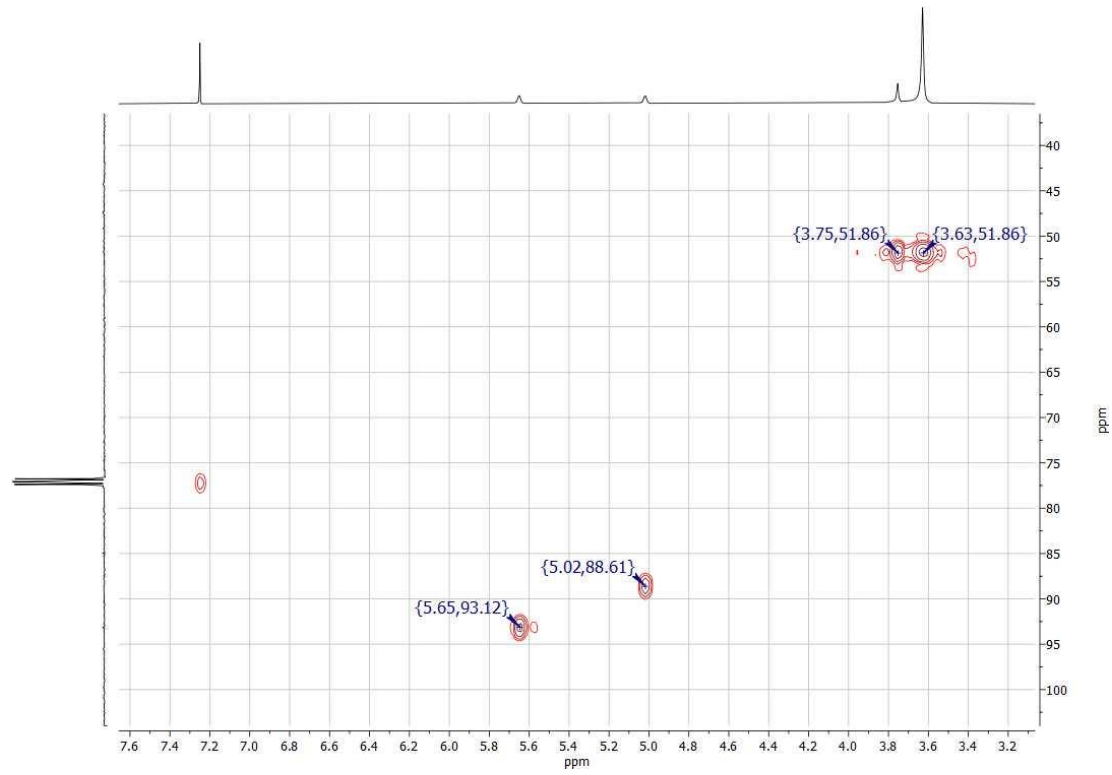

Figure 9.89. ^{1}H, ^{13}C HMQC 2D spectrum of $NaL^{OMeCOOMe}$ in $CDCl_3$.

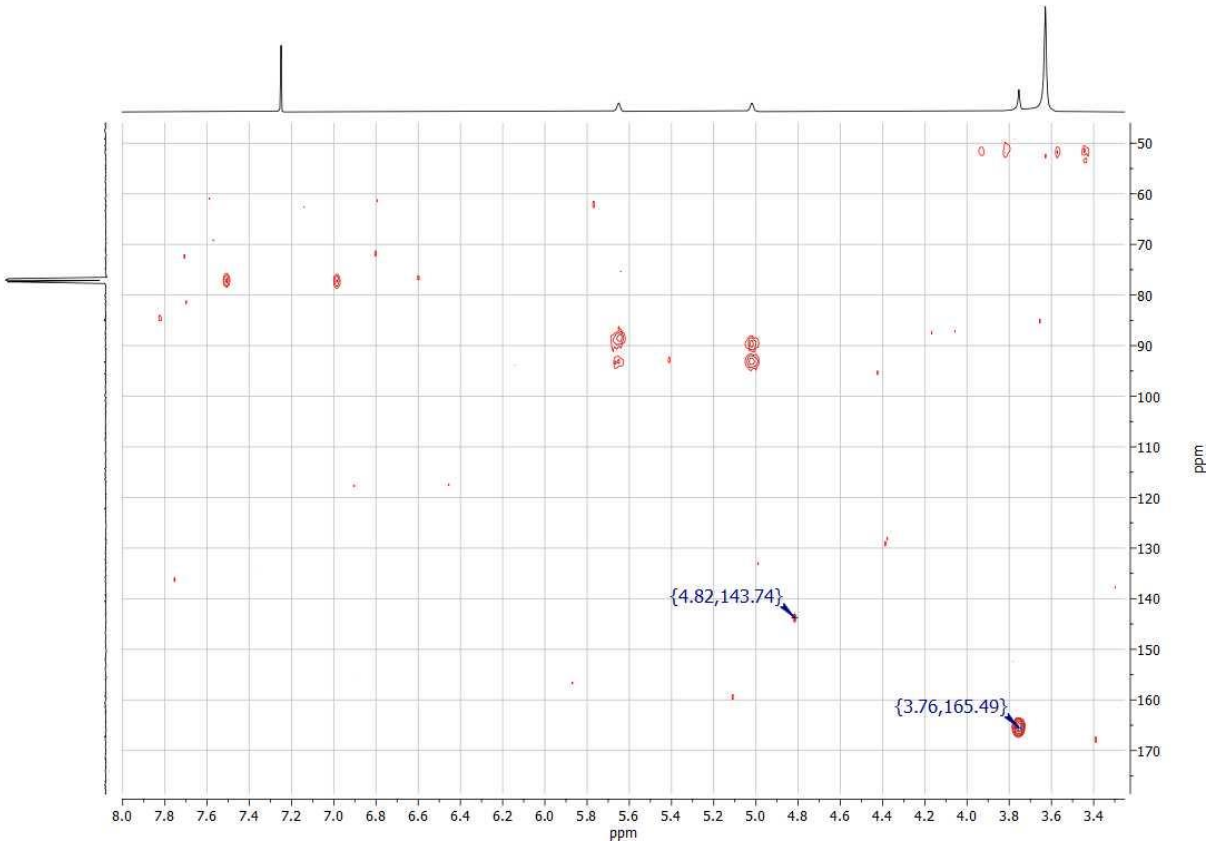

Figure 9.90. ^{1}H, ^{13}C HMBC 2D spectrum of $NaL^{OMeCOOMe}$ in $CDCl_3$.

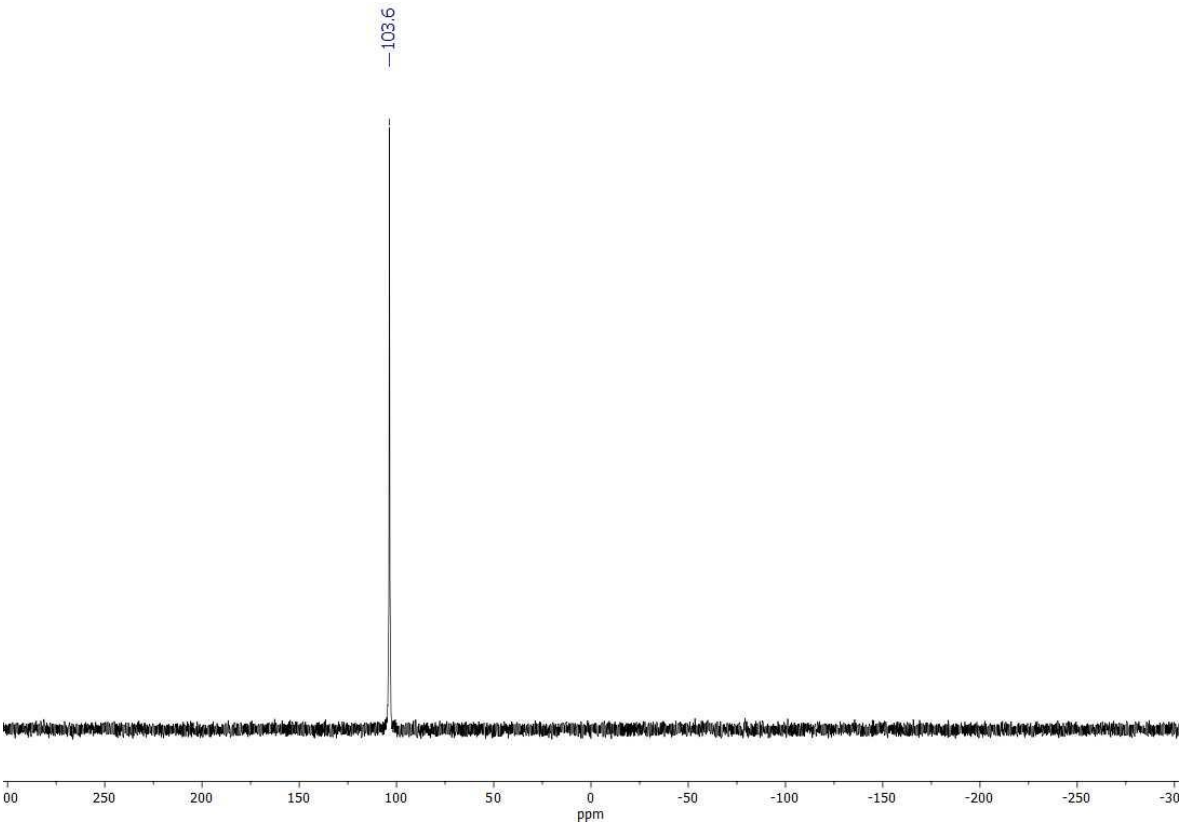

Figure 9.91. $^{31}P\{^{1}H\}$ NMR spectrum of $NaL^{OMeCOOMe}$ in $CDCl_3$.

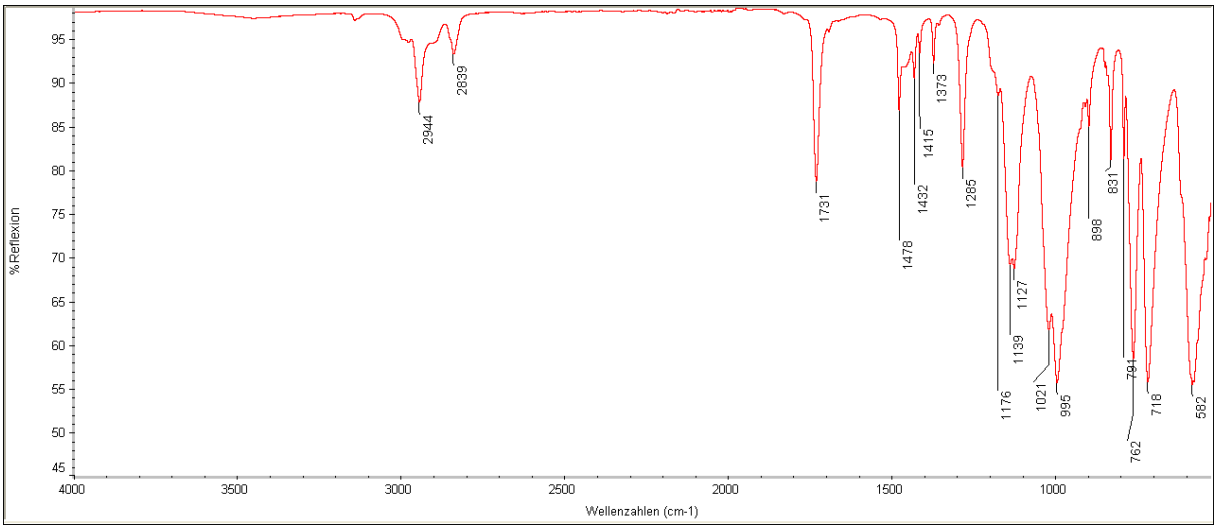

Figure 9.92. IR spectrum of $NaL^{OMeCOOMe}$.

Spectroscopic Data of $[Tc^{VII}O_3(L^{OMeCOOMe})]$

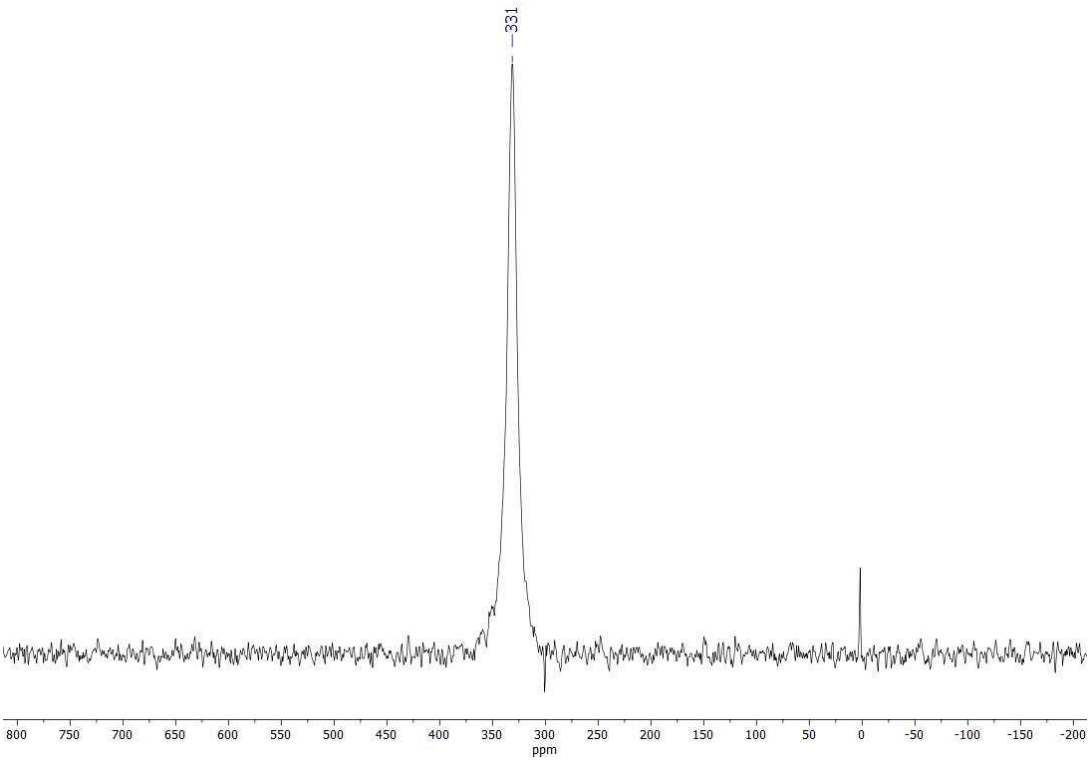

Figure 9.93. ^{99}Tc NMR spectrum of $[Tc^{VII}O_3(L^{OMeCOOMe})]$ in MeOH.

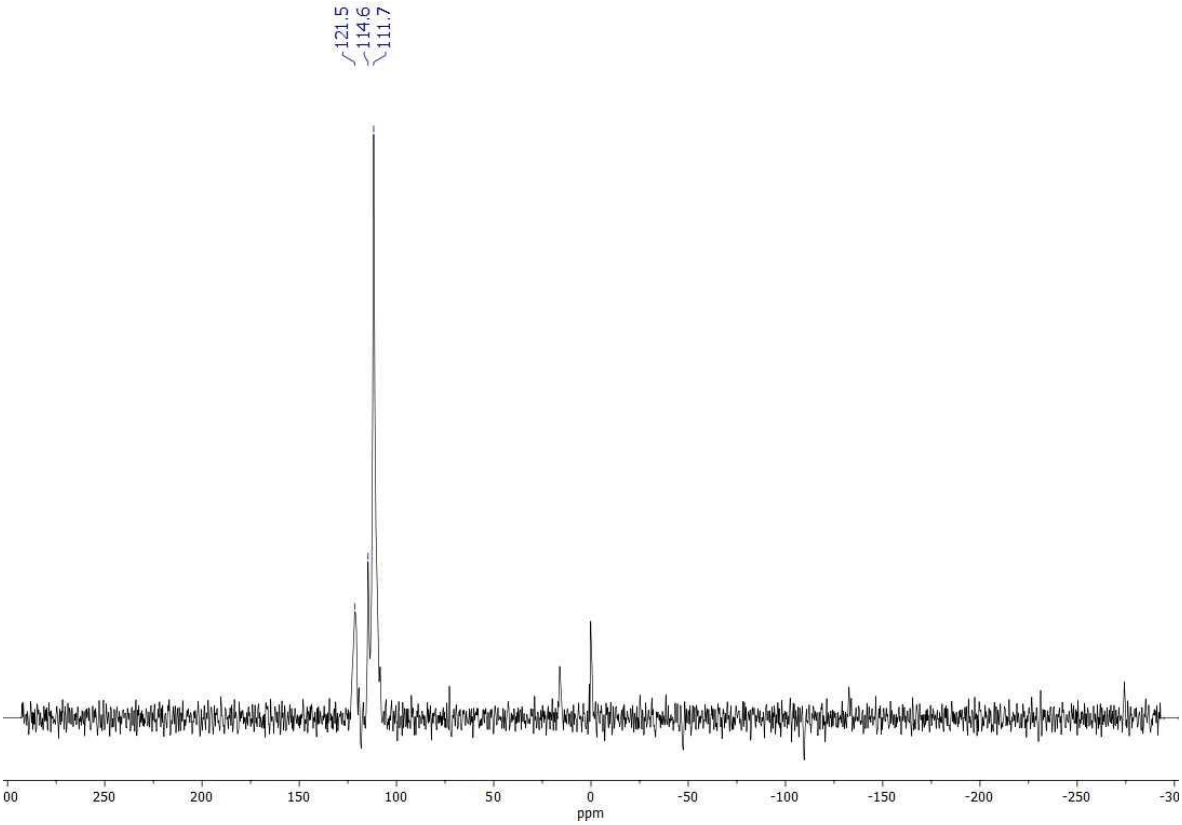

Figure 9.94. $^{31}P\{^{1}H\}$ NMR spectrum of $[Tc^{VII}O_3(L^{OMeCOOMe})]$ in MeOH.

Spectroscopic Data of **2**

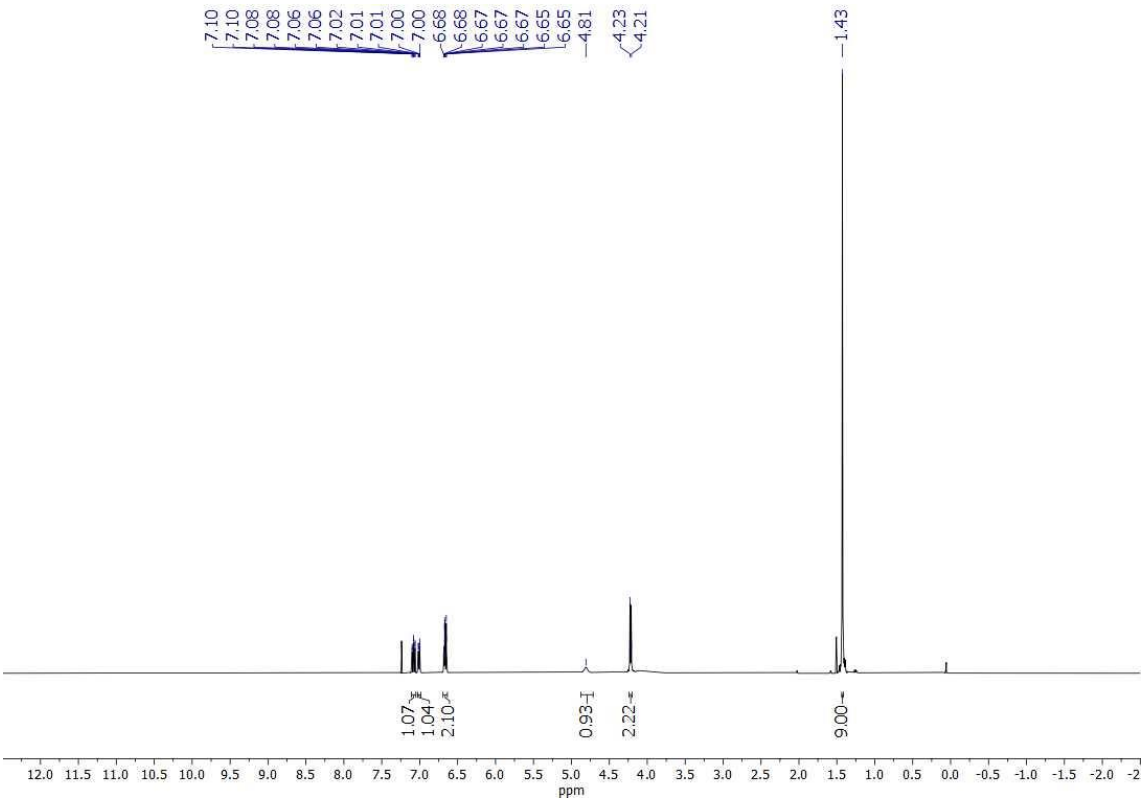

Figure 9.95. ^{1}H NMR spectrum of **2** in $CDCl_3$.

Spectroscopic Data of **3**

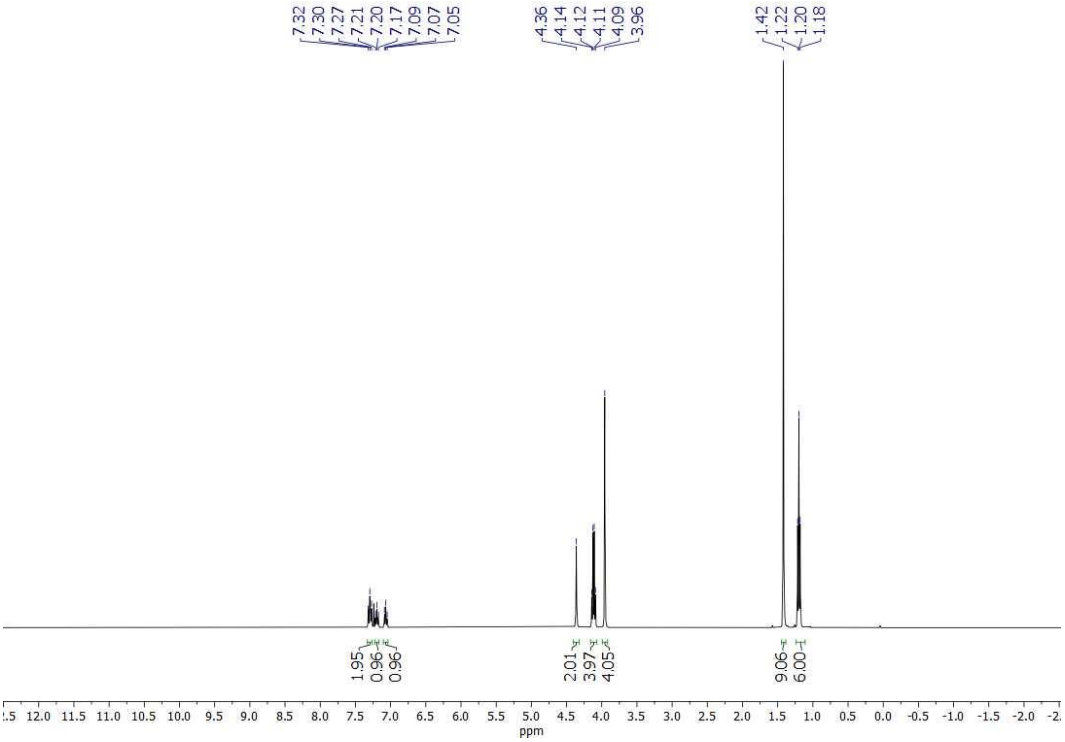

Figure 9.96. ^{1}H NMR spectrum of **3** in $CDCl_3$.

Spectroscopic Data of **4**

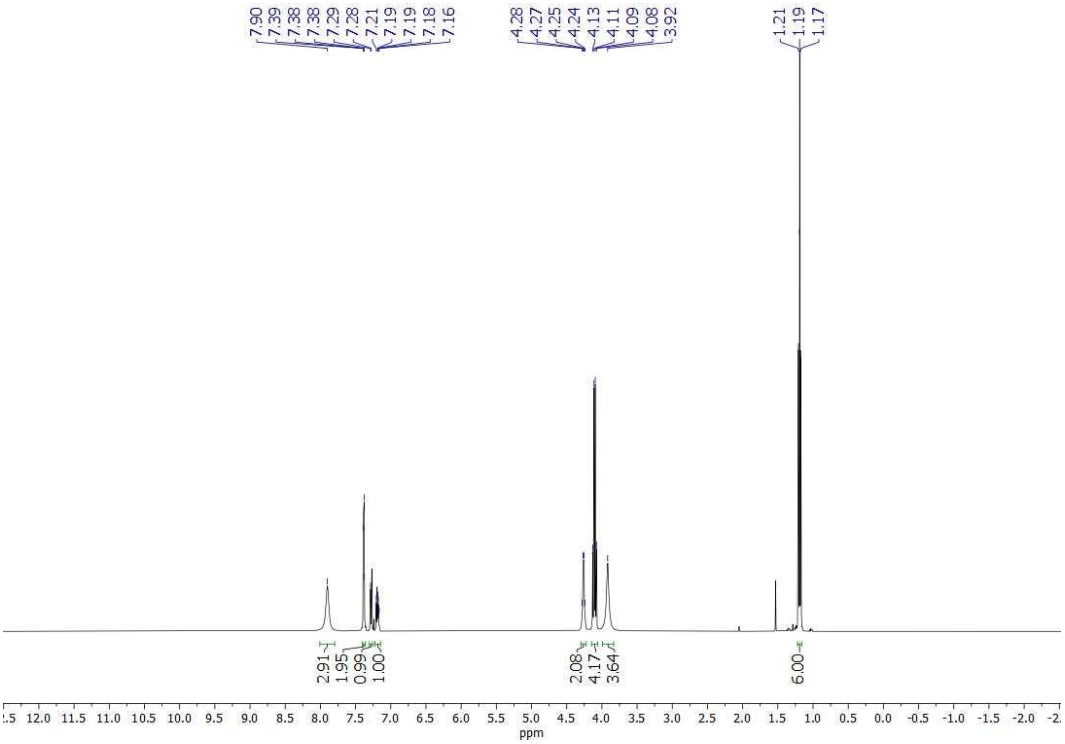

Figure 9.97. ^{1}H NMR spectrum of **4** in $CDCl_3$.

Spectroscopic Data of **5**

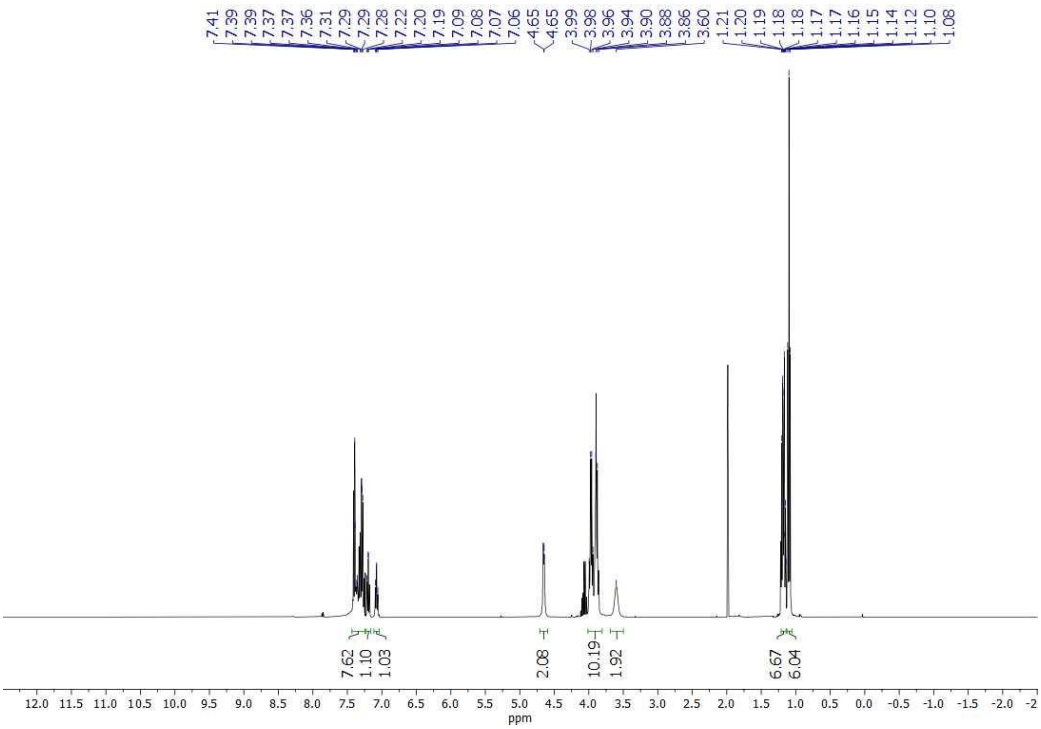

Figure 9.98. ^{1}H NMR spectrum of **5** in $CDCl_3$.

Spectroscopic Data of H_3L^{1EtEt}

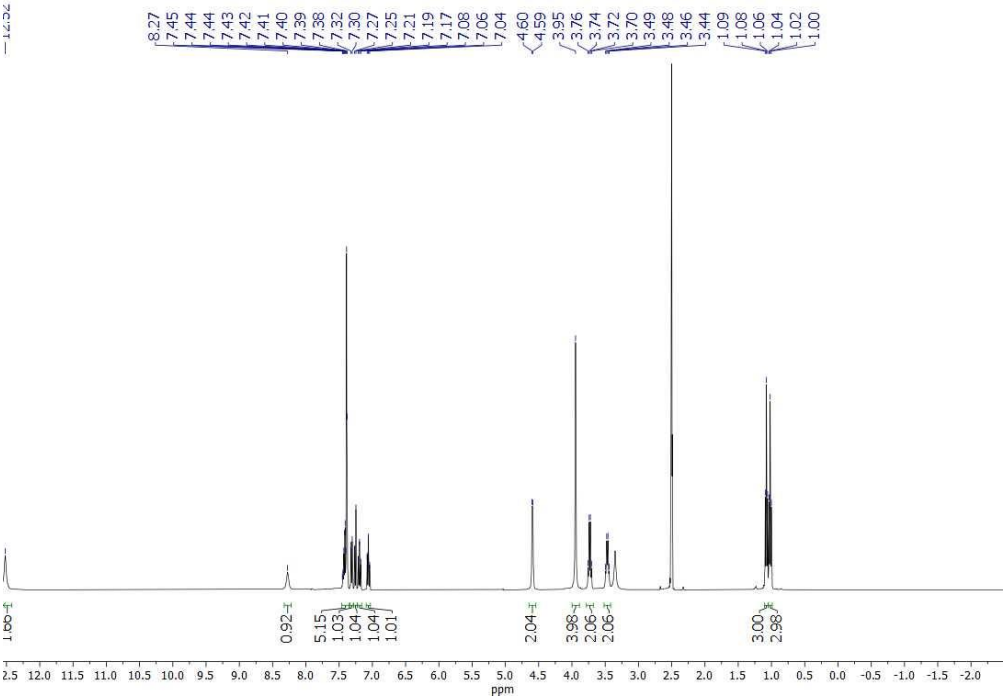

Figure 9.99. ^{1}H NMR spectrum of H_3L^{1EtEt} in d_6-DMSO.

Spectroscopic Data of [$Re^{V}O(L^{1EtEt})$]

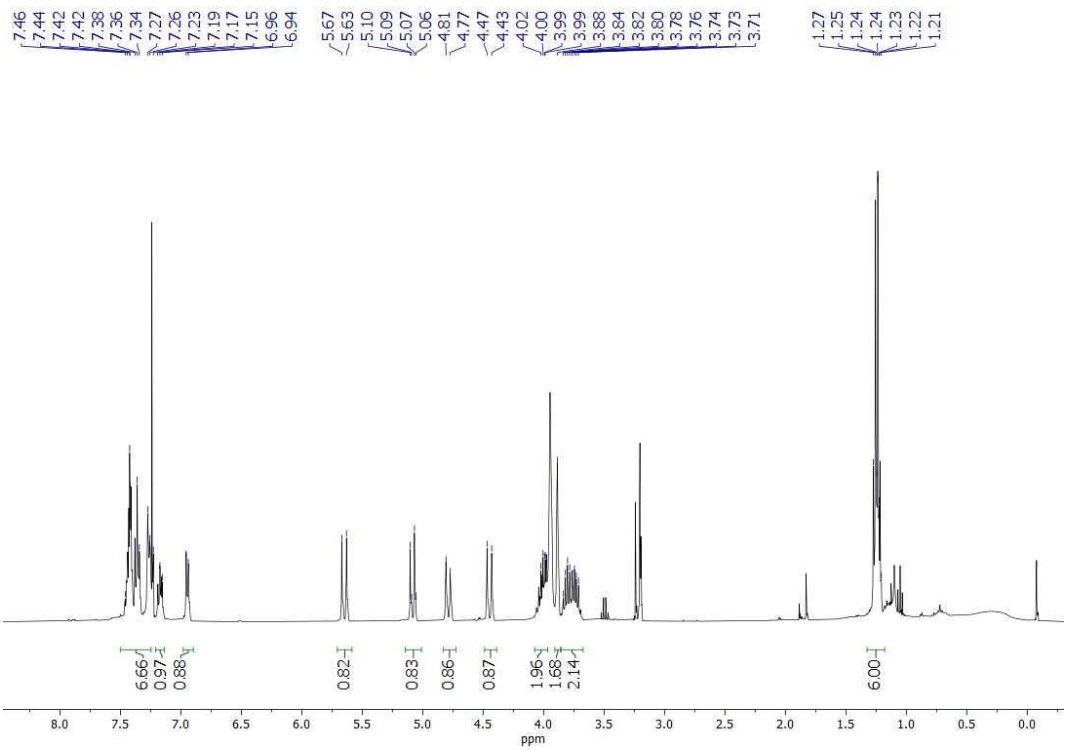

Figure 9.100. ^{1}H NMR spectrum of [$Re^{V}O(L^{1EtEt})$] in $CDCl_3$.

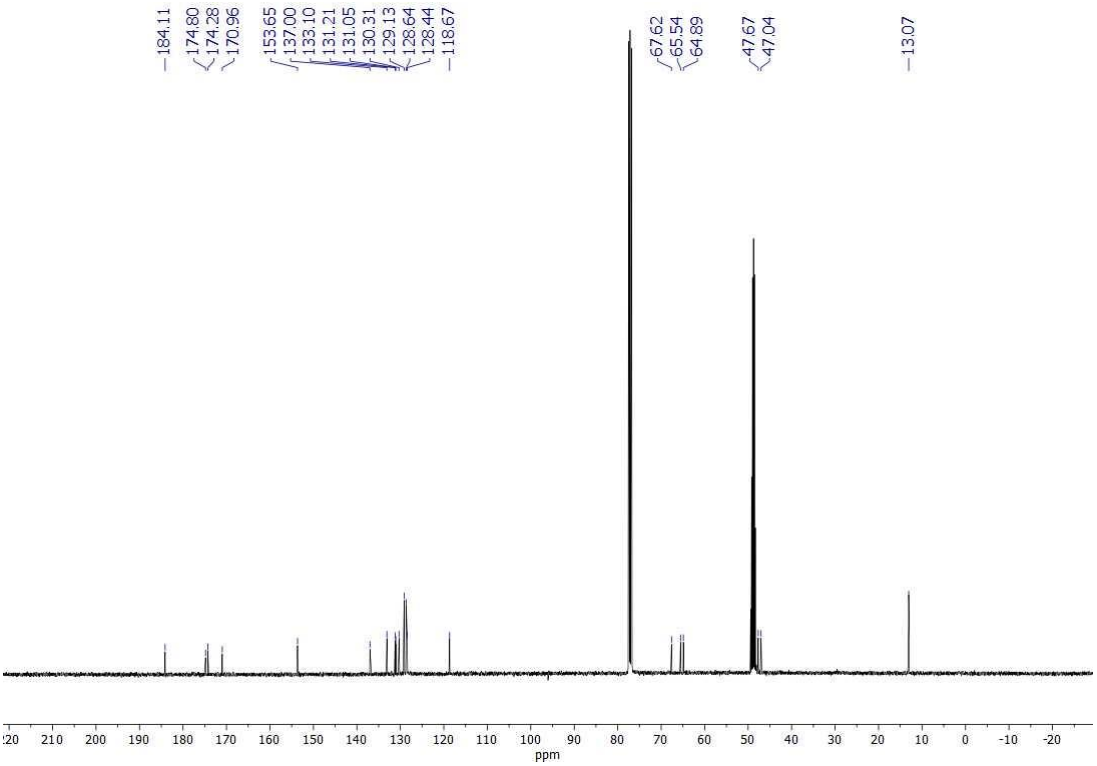

Figure 9.101. $^{13}C\{^{1}H\}$ NMR spectrum of [$Re^{V}O(L^{1EtEt})$] in $CDCl_3$.

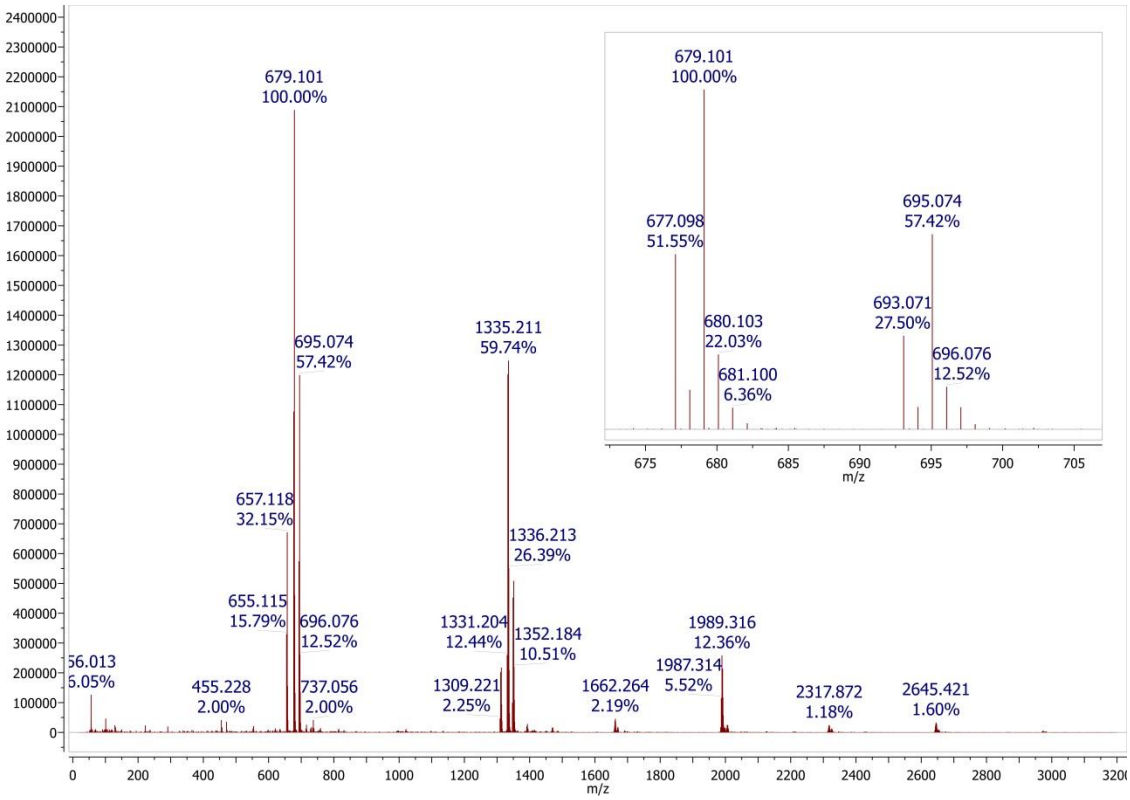

Figure 9.102. ESI+ MS spectrum of [Re^{V}O(L^{1EtEt})].

Spectroscopic Data of [Re(NPh)(L^{1EtEt})]

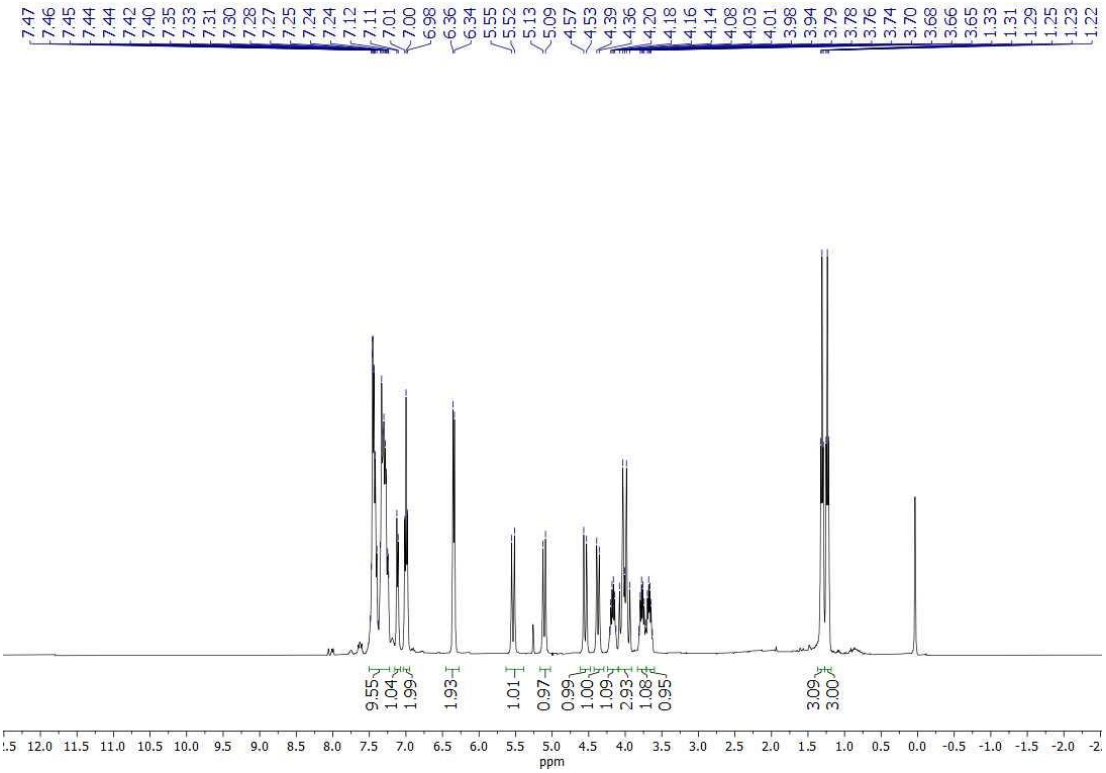

Figure 9.103. ^{1}H NMR spectrum of [Re(NPh)(L^{1EtEt})] in $CDCl_3$.

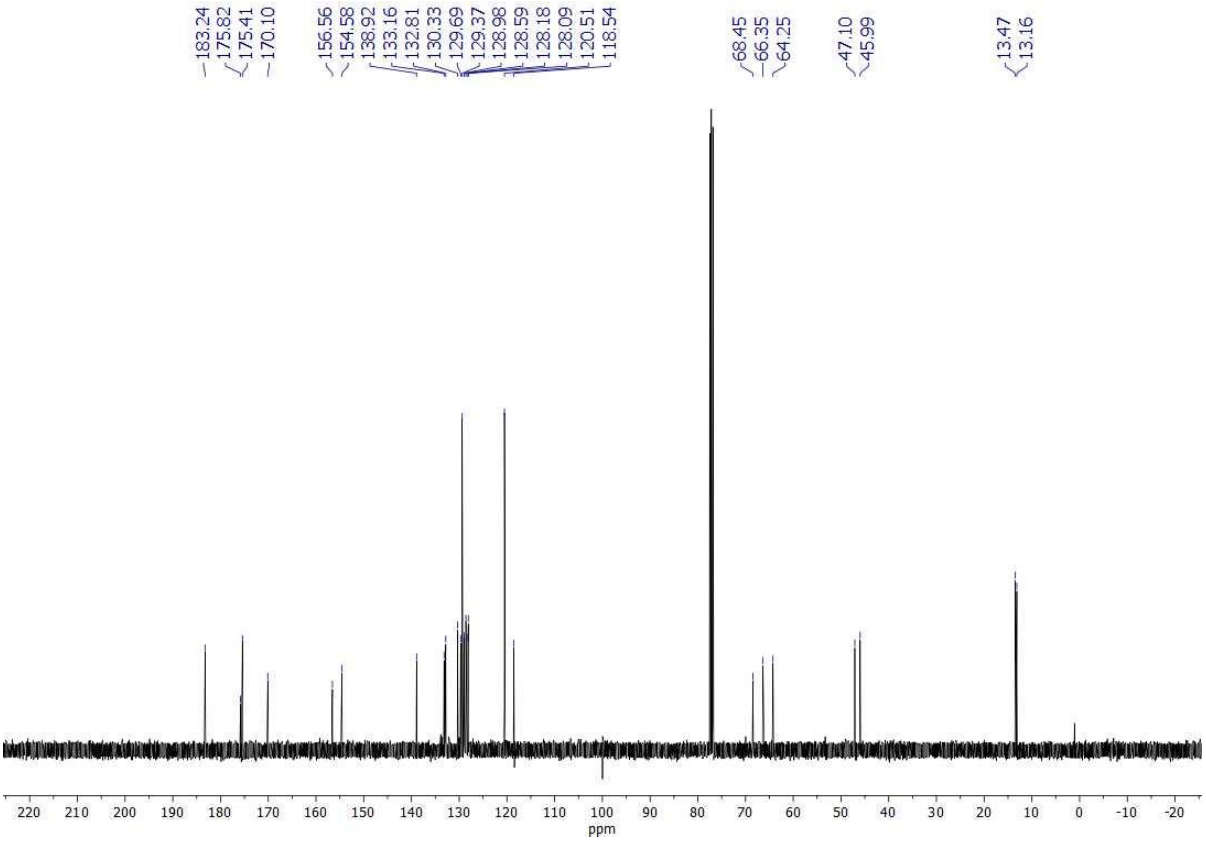

Figure 9.104. $^{13}C\{^{1}H\}$ NMR spectrum of [Re(NPh)(L^{1EtEt})] in $CDCl_3$.

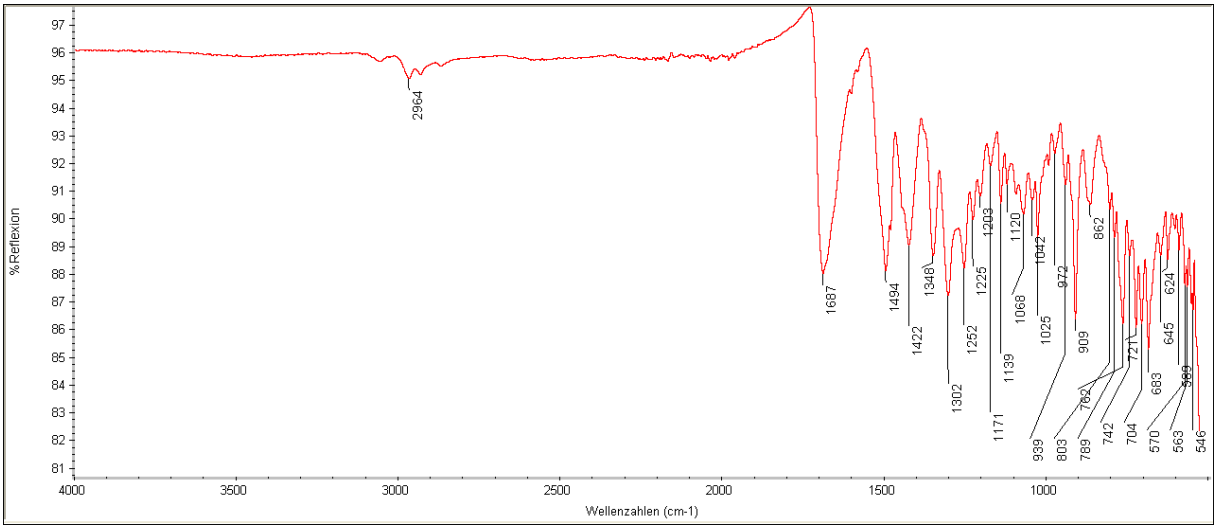

Figure 9.105. IR spectrum of [Re(NPh)(L^{1EtEt})].

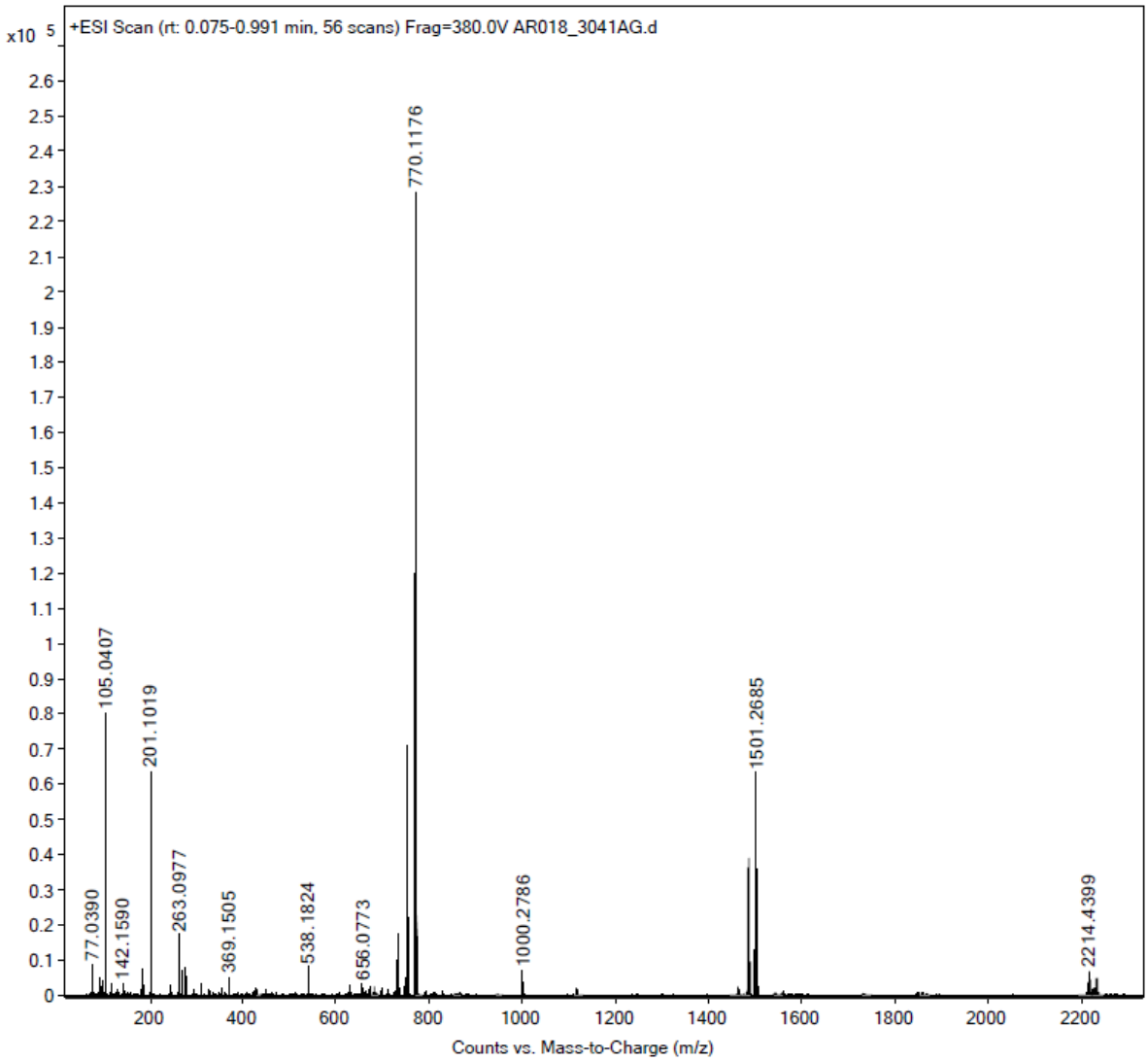

Figure 9.106. ESI+ MS spectrum of [Re(NPh)(L^{1EtEt})].

Spectroscopic Data of [Re(NPhF)(L^{1EtEt})]

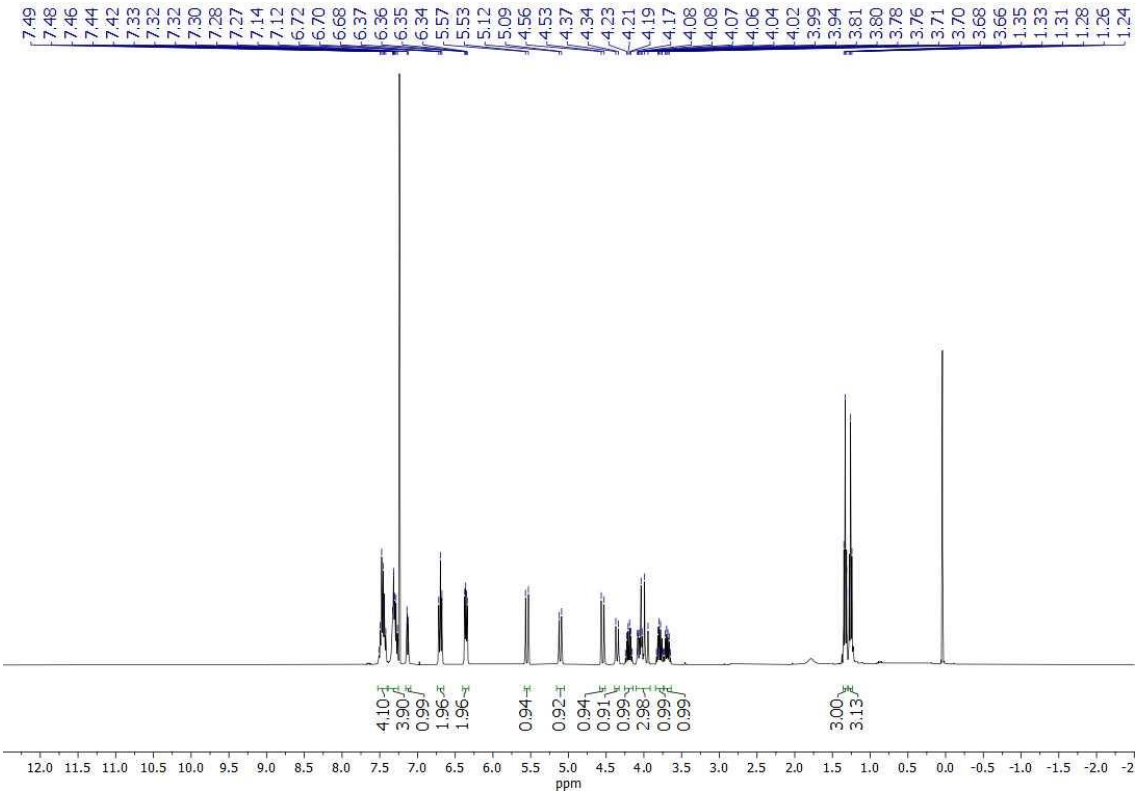

Figure 9.107. ^{1}H NMR spectrum of [Re(NPhF)(L^{1EtEt})] in $CDCl_3$.

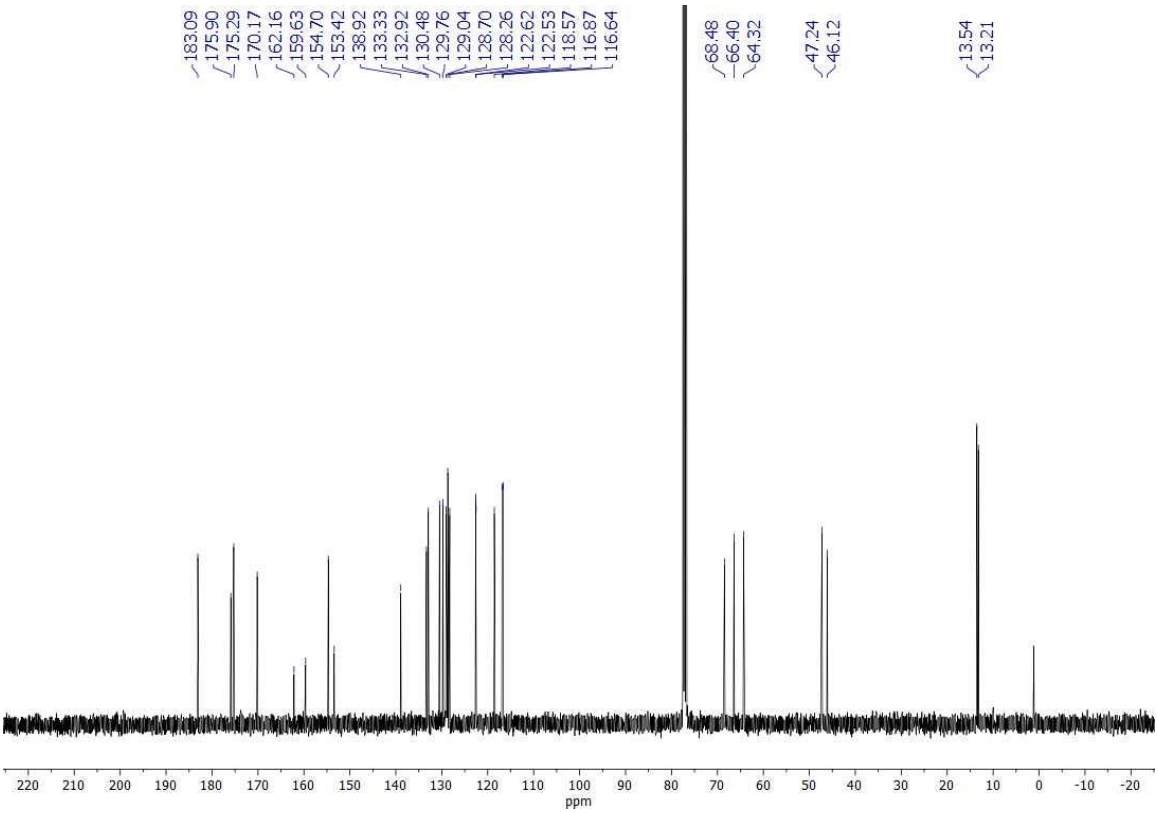

Figure 9.108. $^{13}C\{^{1}H\}$ NMR spectrum of [Re(NPhF)(L^{1EtEt})] in $CDCl_3$.

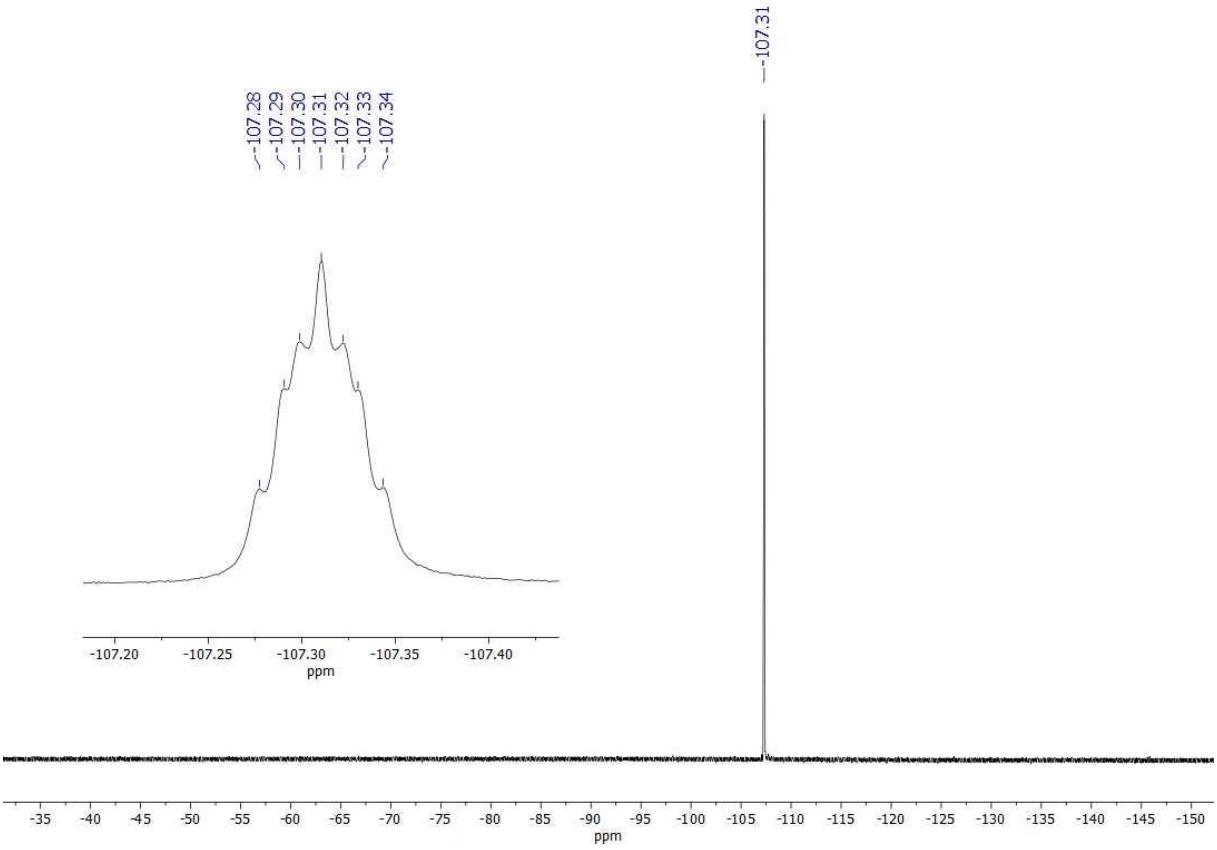

Figure 9.109. ^{19}F NMR spectrum of [Re(NPhF)(L^{1EtEt})] in $CDCl_3$.

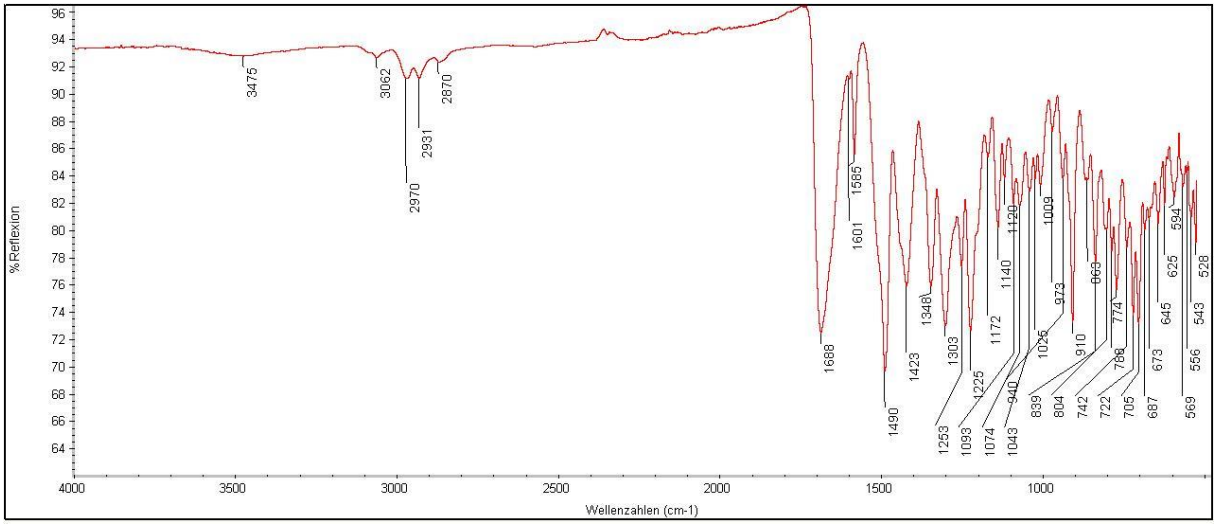

Figure 9.110. IR spectrum of [Re(NPhF)(L^{1EtEt})].

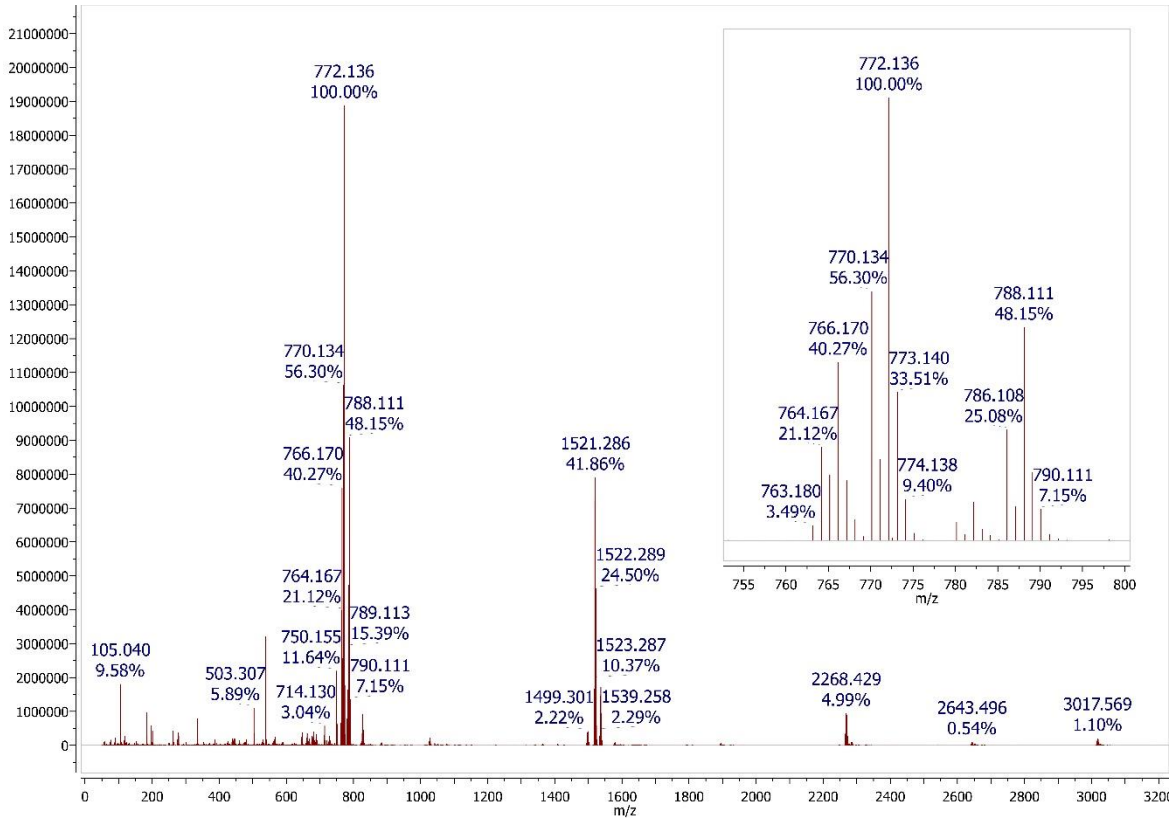

Figure 9.111. ESI+ MS spectrum of [Re(NPhF)(L^{1EtEt})].

Spectroscopic Data of KH_3L^{2EtEt}

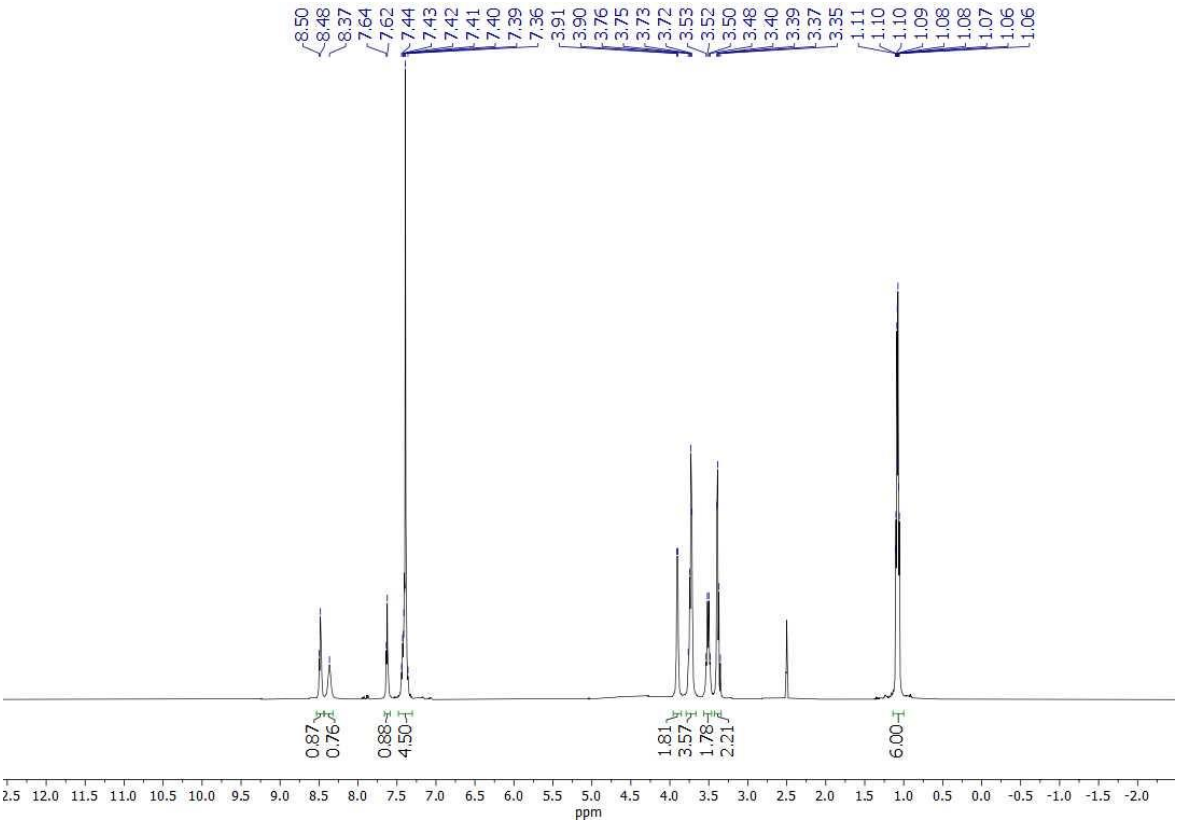

Figure 9.112. ^1H NMR spectrum of KH_3L^{2EtEt} in d_6-DMSO.

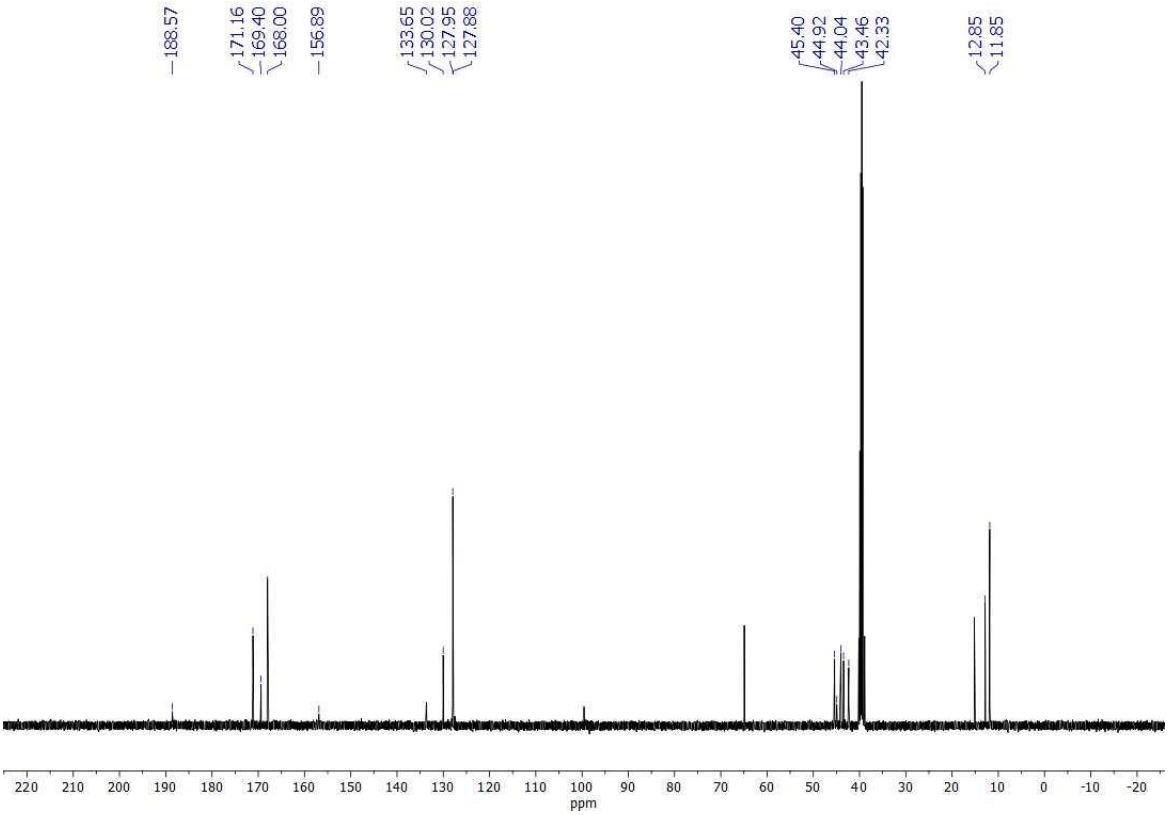

Figure 9.113. $^{13}C\{^{1}H\}$ NMR spectrum of KH_3L^{2EtEt} in d_6-DMSO.

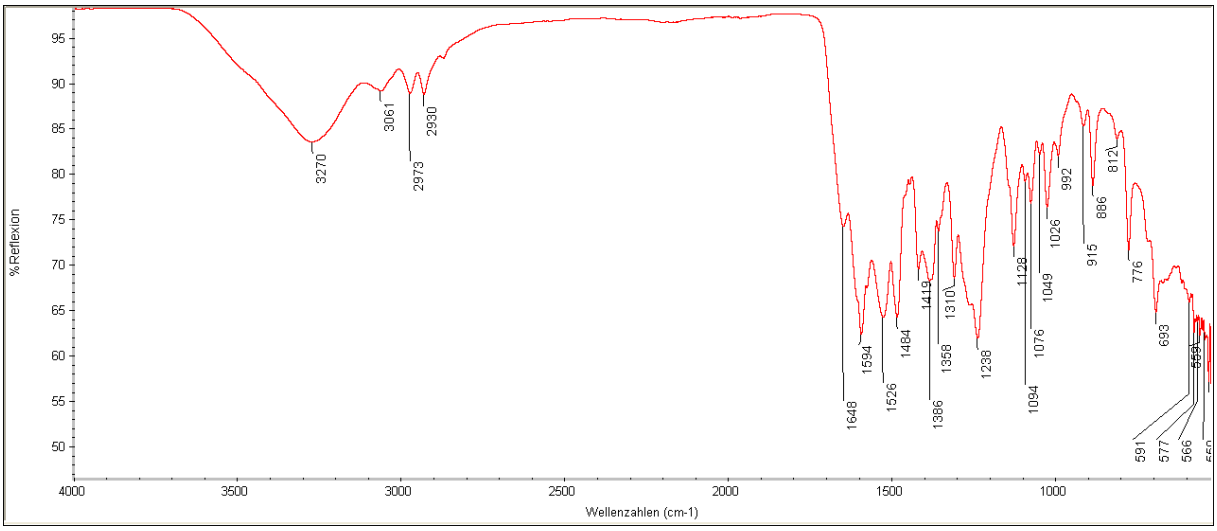

Figure 9.114. IR spectrum of KH_3L^{2EtEt}.

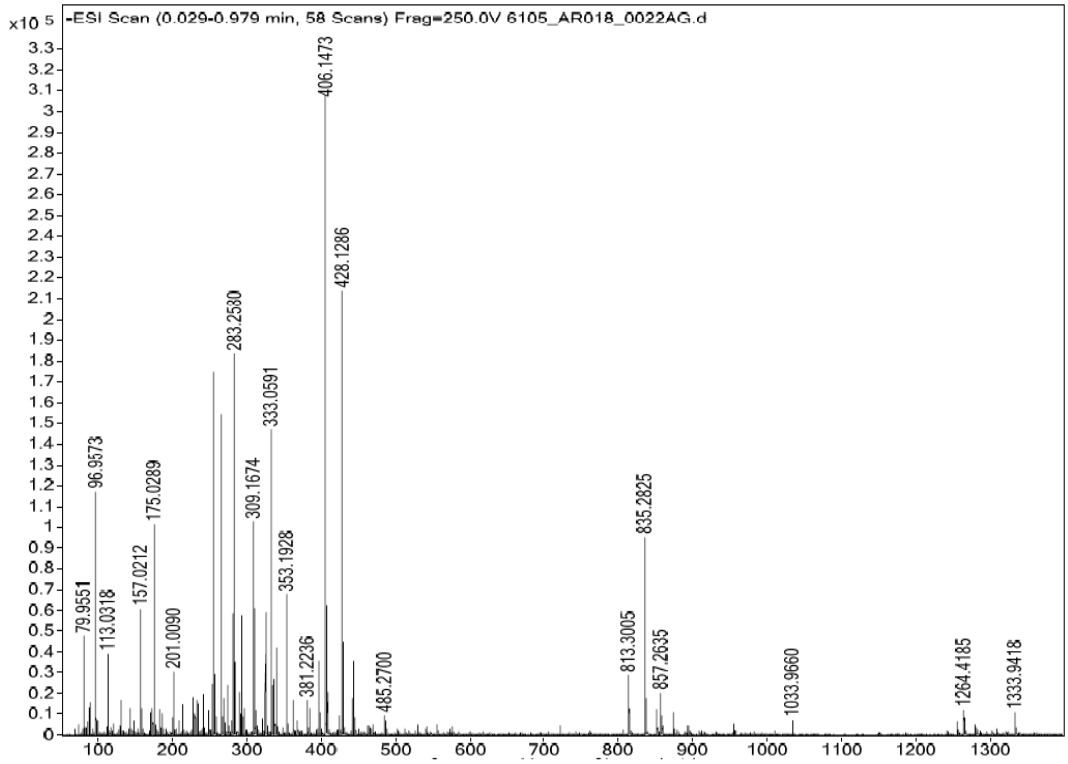

Figure 9.115. ESI- MS spectrum of KH_3L^{2EtEt}.

Spectroscopic Data of KH_3L^{2MePh}

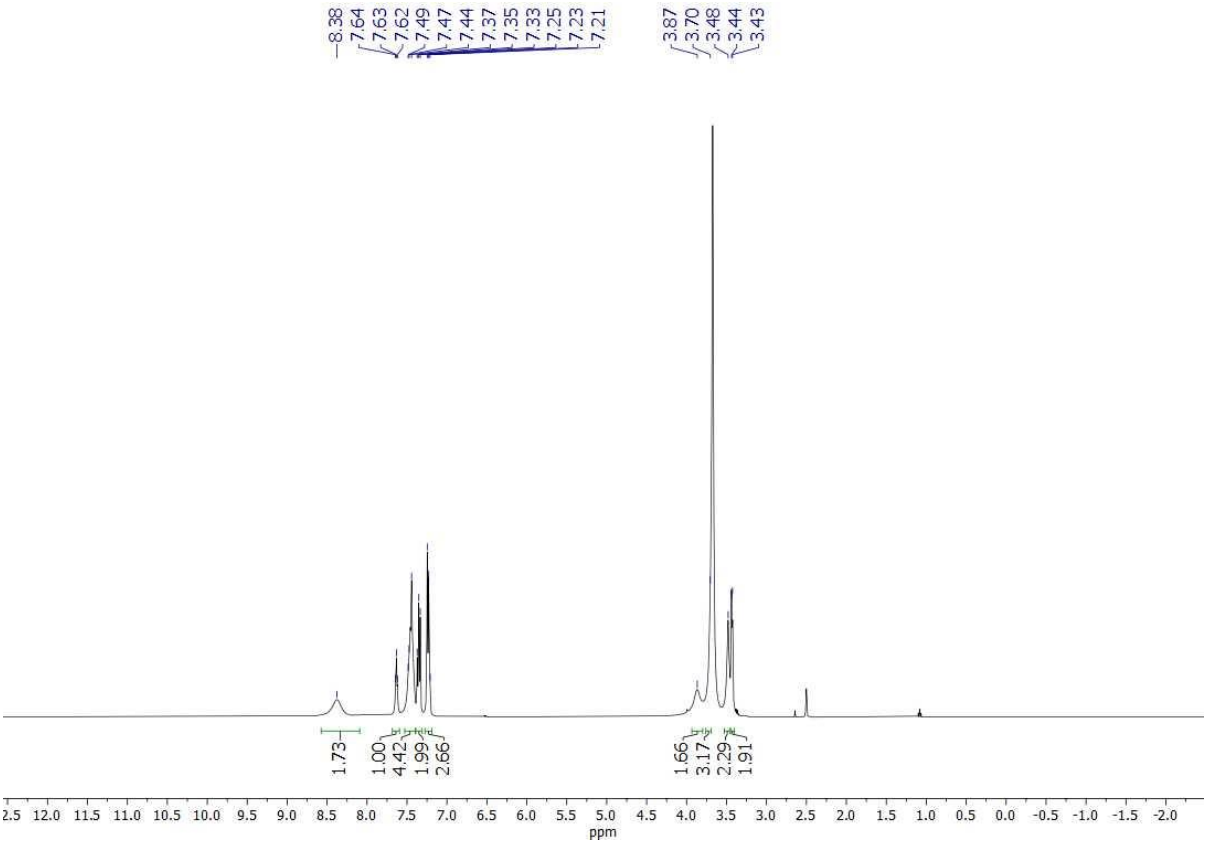

Figure 9.116. ^1H NMR spectrum of KH_3L^{2MePh} in d_6-DMSO.

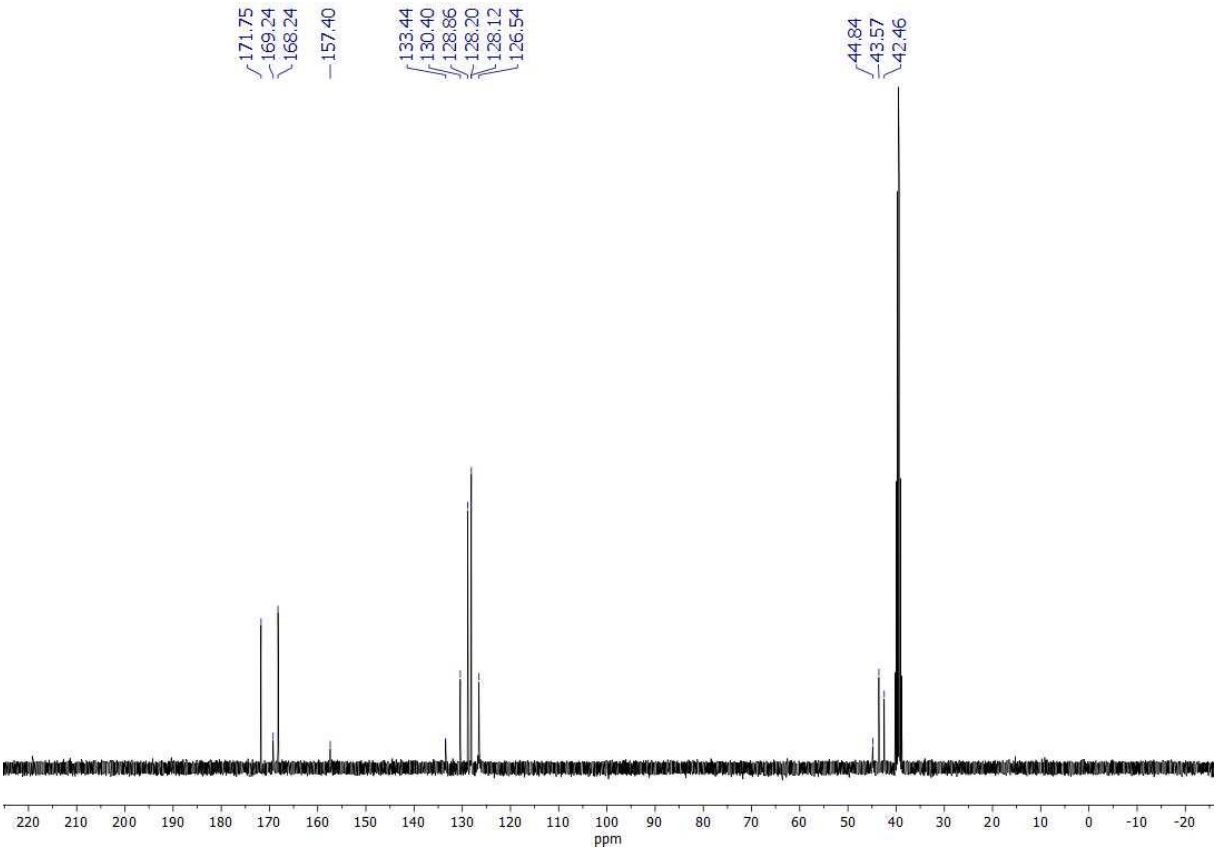

Figure 9.117. $^{13}C\{^{1}H\}$ spectrum NMR of KH_3L^{2MePh} in d_6-DMSO.

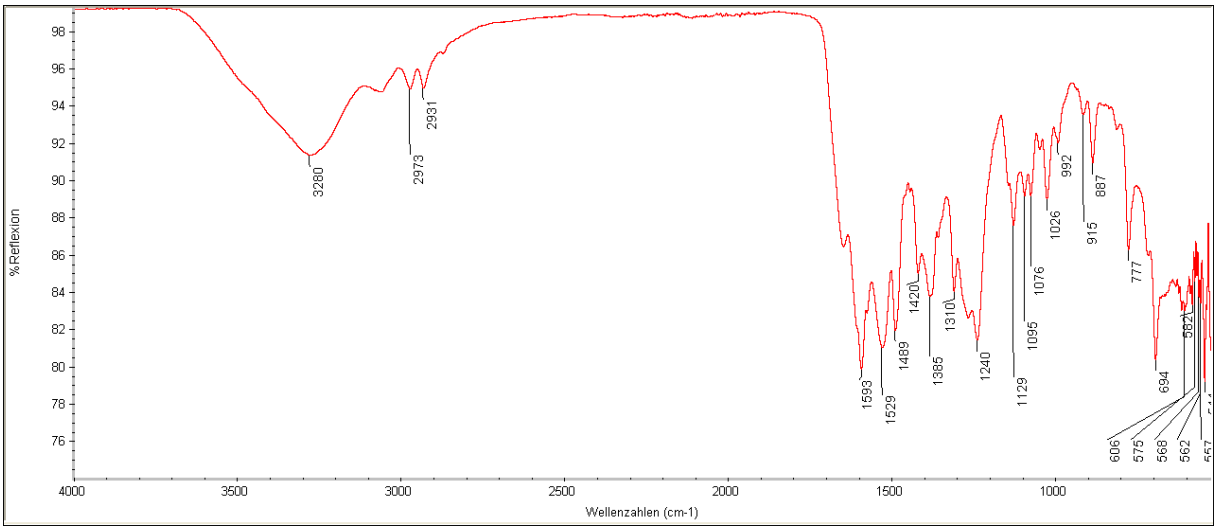

Figure 9.118. IR spectrum of KH_3L^{2MePh}.

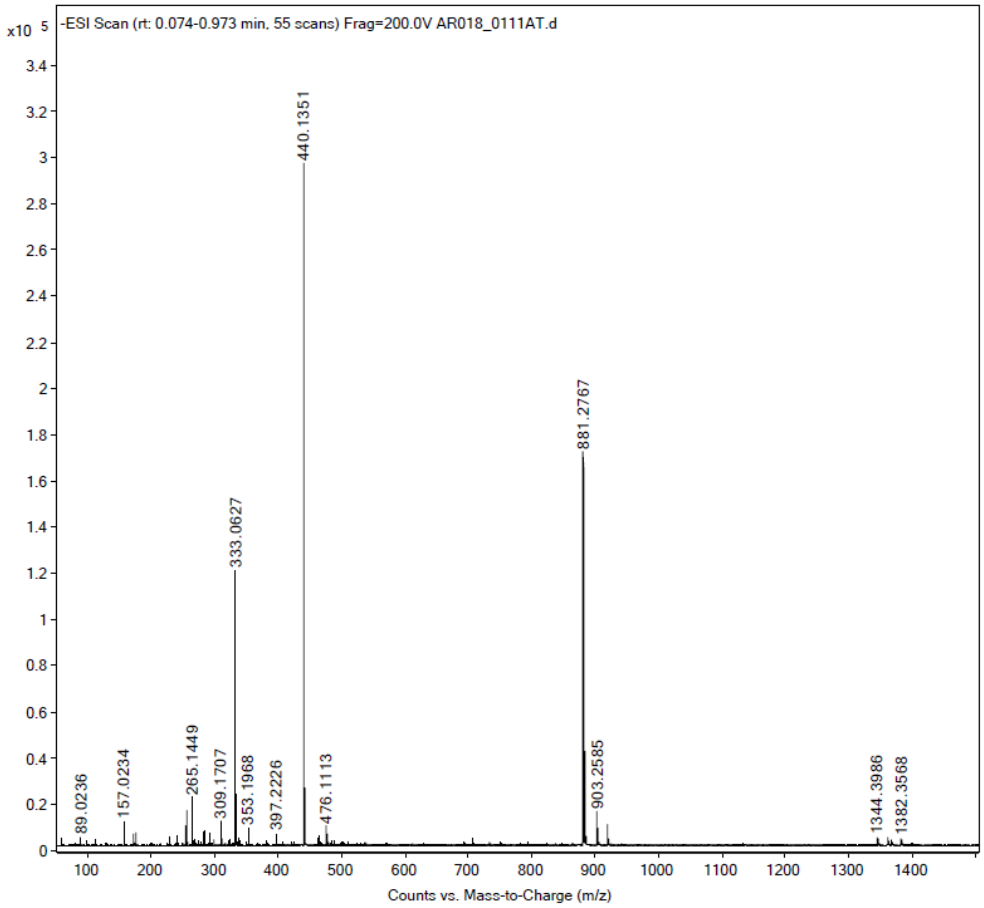

Figure 9.119. ESI- MS spectrum of KH_3L^{2MePh}.

Spectroscopic Data of KH_3L^{2PhPh}

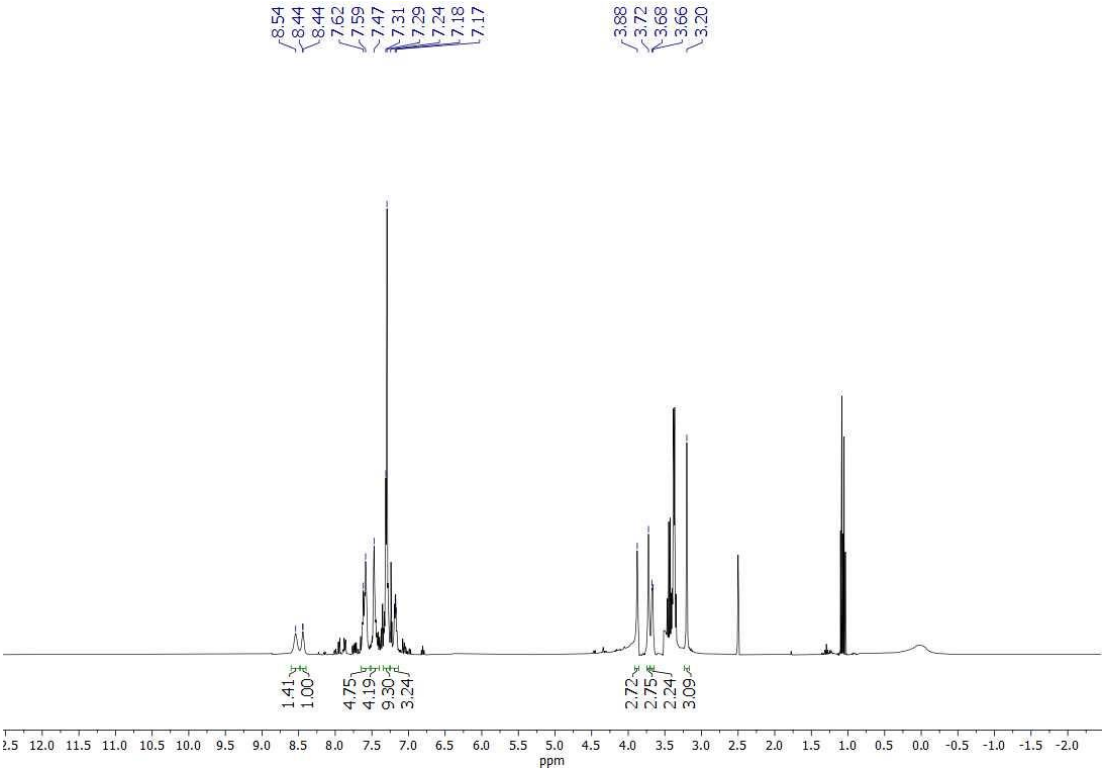

Figure 9.120. ^1H NMR spectrum of KH_3L^{2PhPh} in d_6-DMSO.

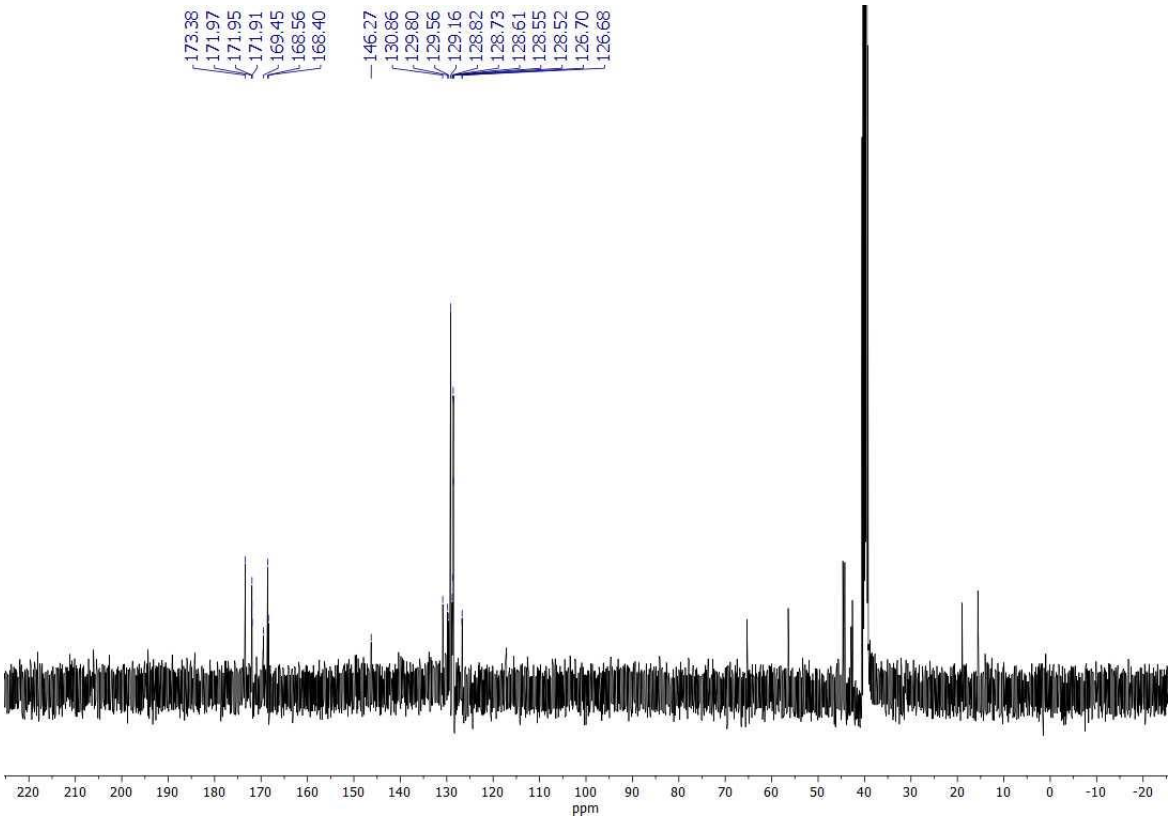

Figure 9.121. $^{13}C\{^{1}H\}$ NMR spectrum of KH_3L^{2PhPh} in d_6-DMSO.

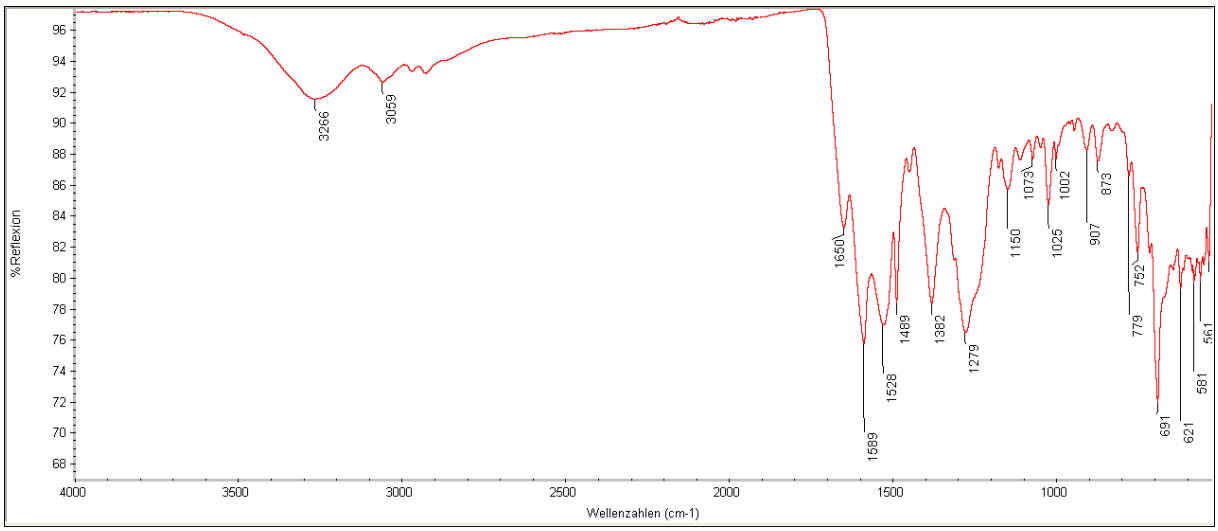

Figure 9.122. IR spectrum of KH_3L^{2PhPh}.

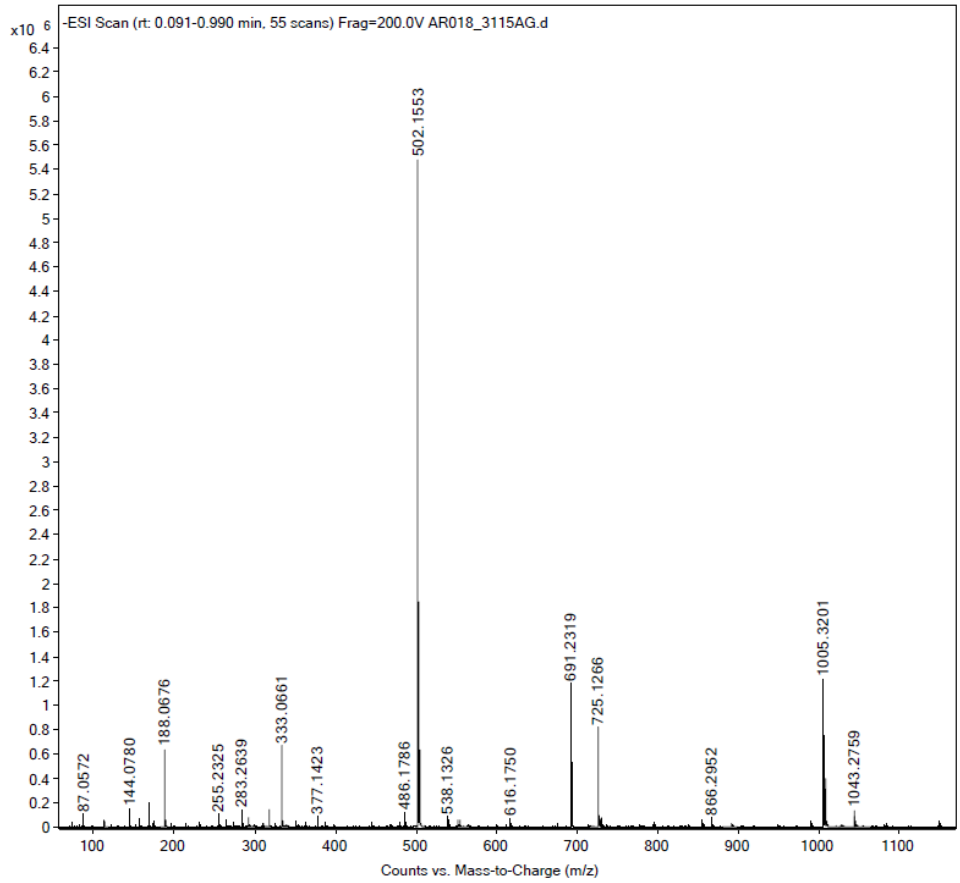

Figure 9.123. ESI- MS spectrum of KH_3L^{2PhPh}.

Spectroscopic Data of $[Re^{V}O(HL^{2EtEt})]$

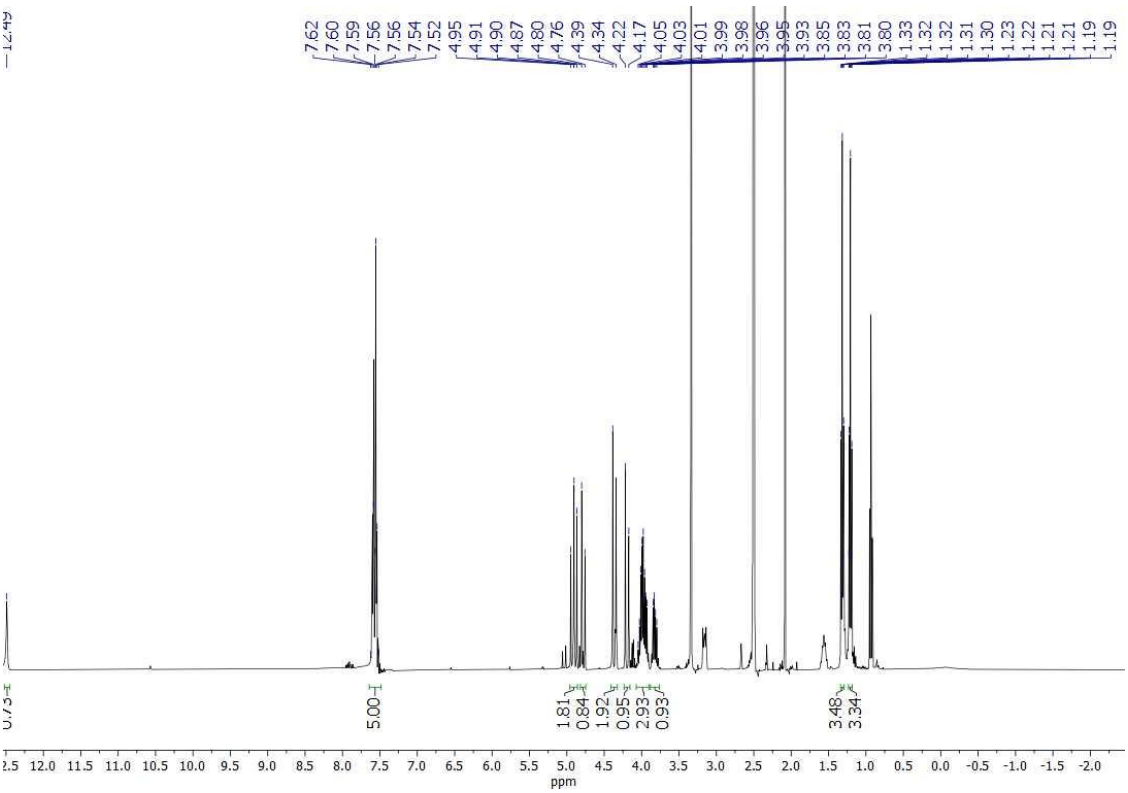

Figure 9.124. ^{1}H NMR spectrum of $[Re^{V}O(HL^{2EtEt})]$ in d_6-DMSO.

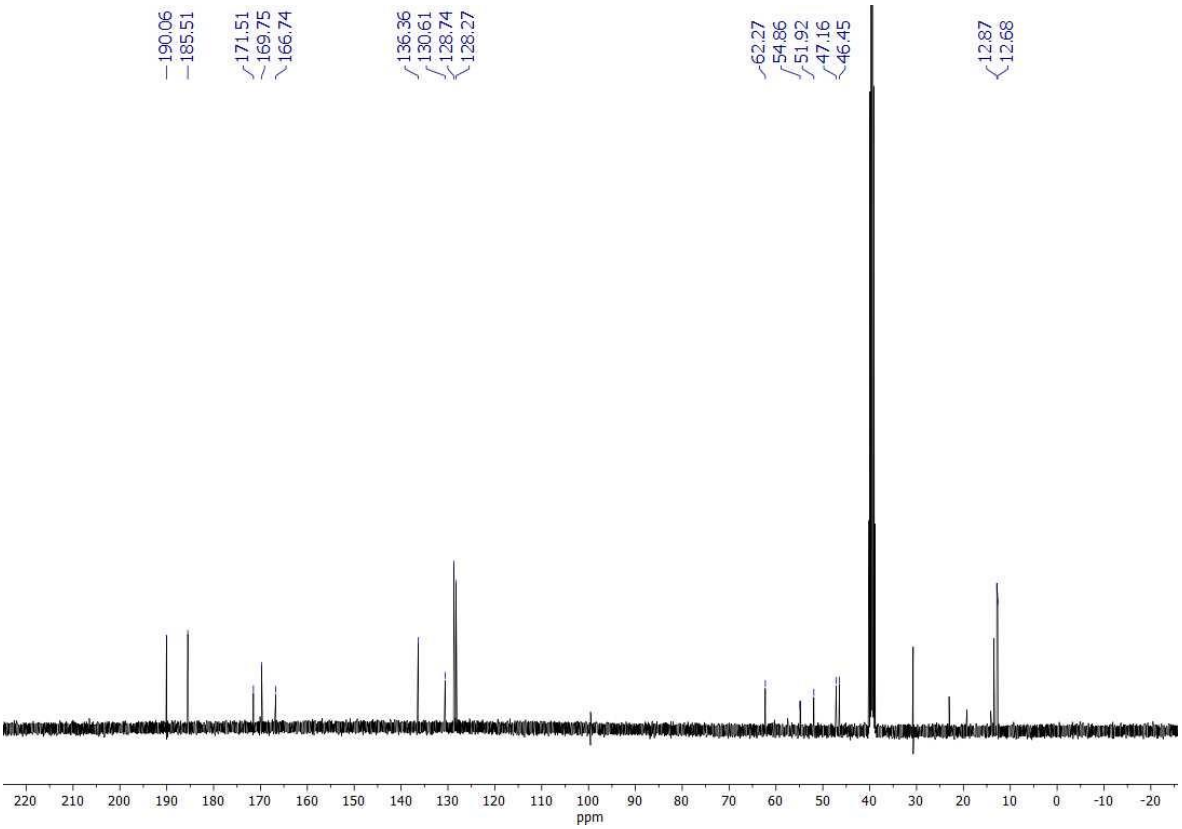

Figure 9.125. $^{13}C\{^{1}H\}$ NMR spectrum of [$Re^{V}O(HL^{2EtEt})$] in d_6-DMSO.

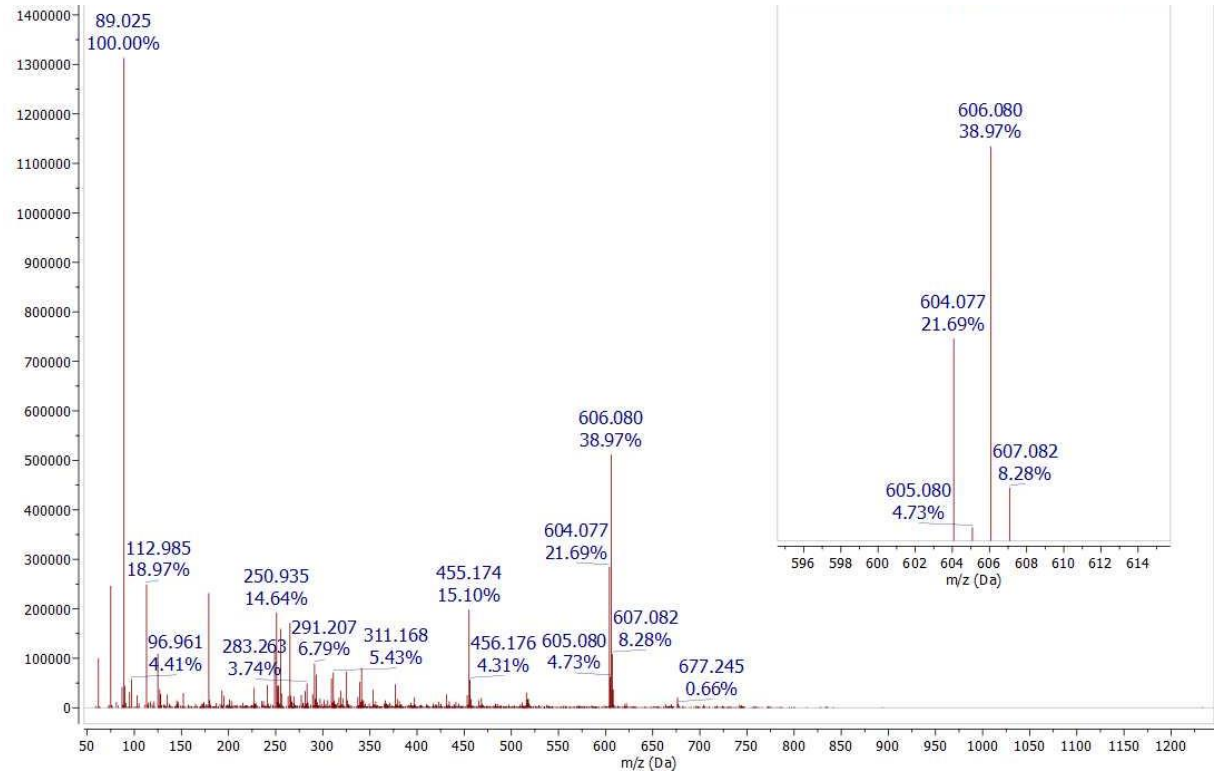

Figure 9.126. ESI- MS spectrum of [$Re^{V}O(HL^{2EtEt})$].

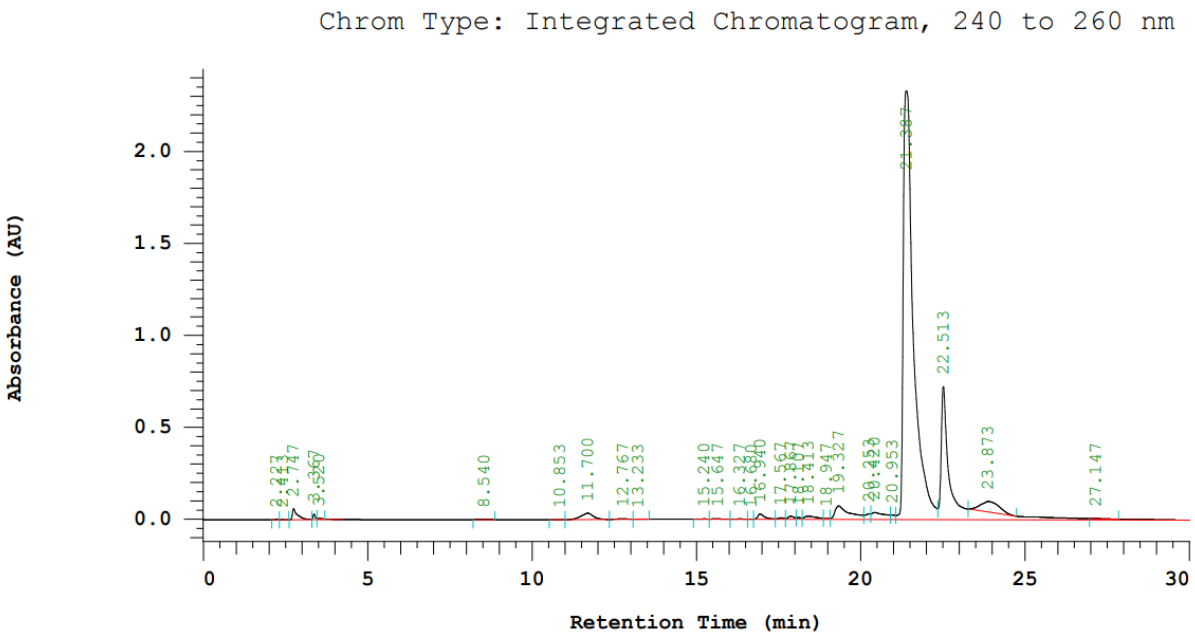

Figure 9.127. UV trace (HPLC) of [ReO(HL^{2EtEt})].

Spectroscopic Data of [Re^{V}O(HL^{2MePh})]

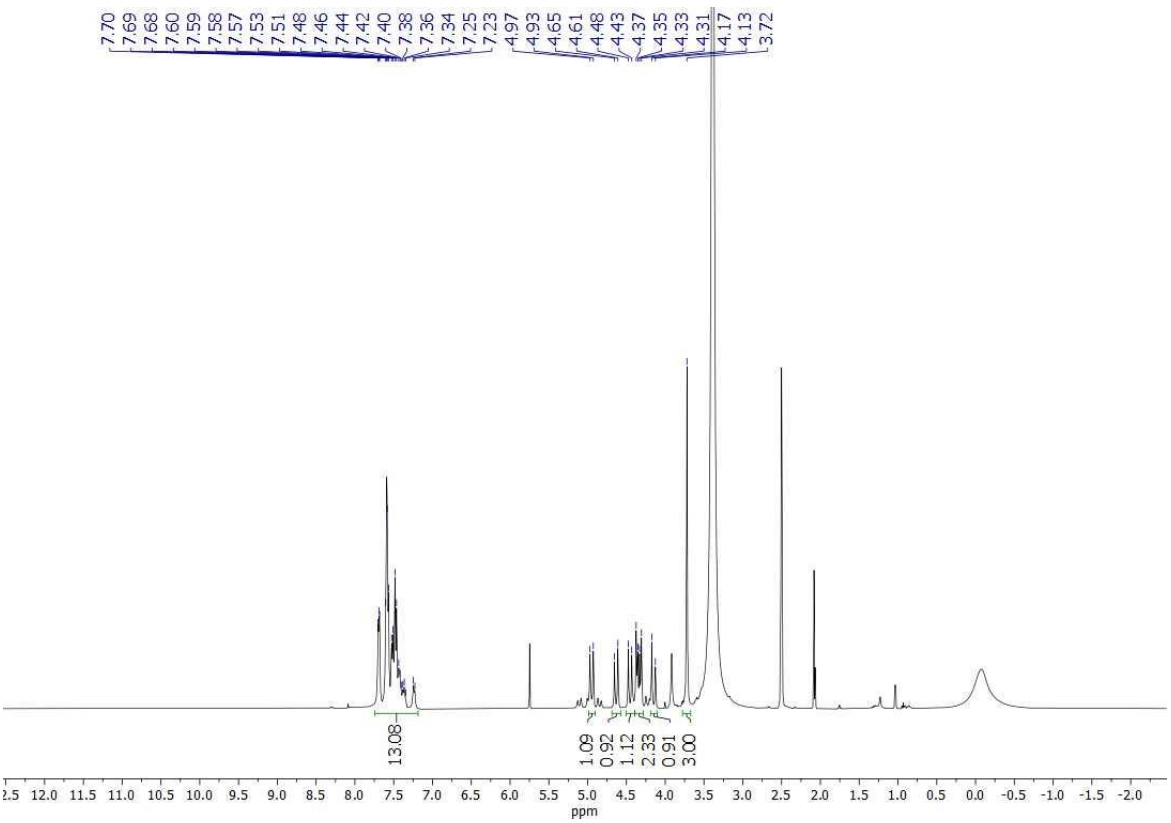

Figure 9.128. ^{1}H NMR spectrum of [Re^{V}O(HL^{2MePh})] in d_6-DMSO.

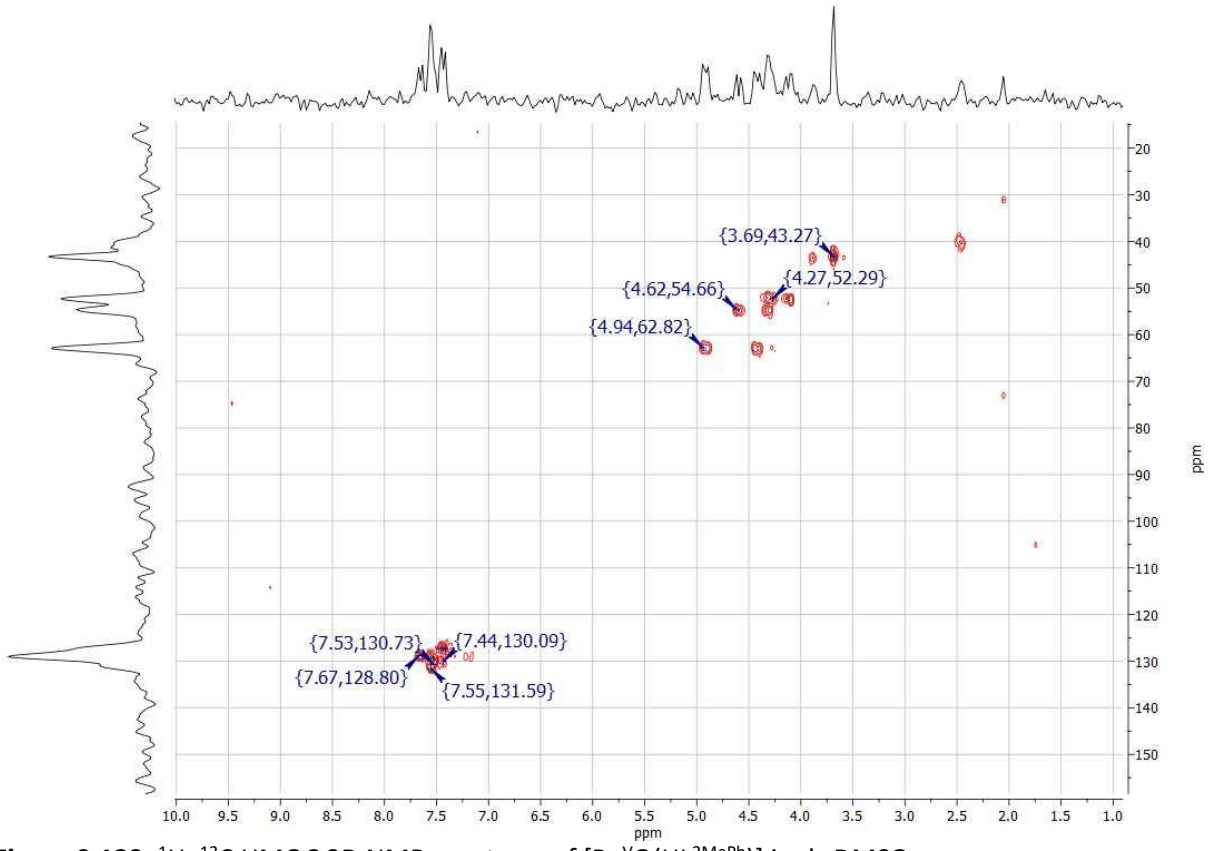

Figure 9.129. ^{1}H, ^{13}C HMQC 2D NMR spectrum of [$Re^{V}O(HL^{2MePh})$] in d_6-DMSO.

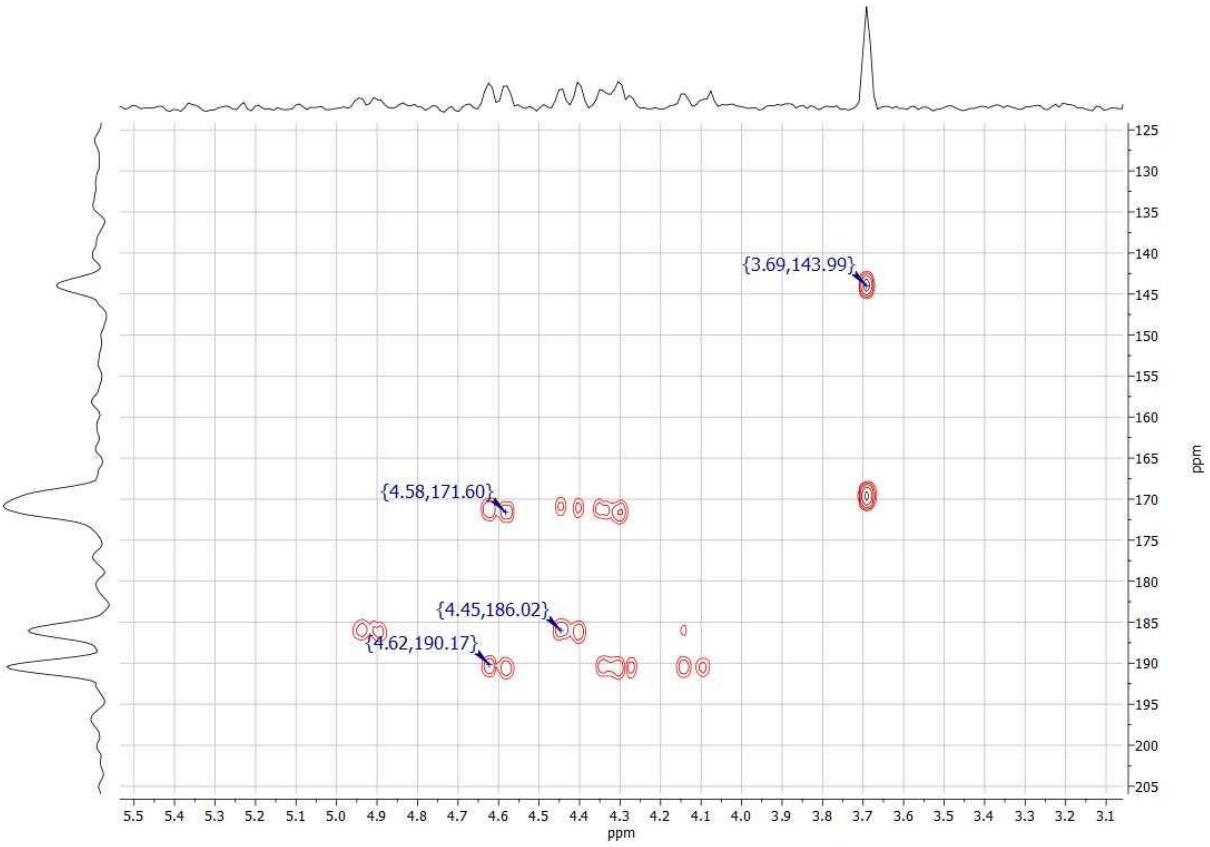

Figure 9.130. ^{1}H, ^{13}C HMBC 2D NMR spectrum of [$Re^{V}O(HL^{2MePh})$] in d_6-DMSO.

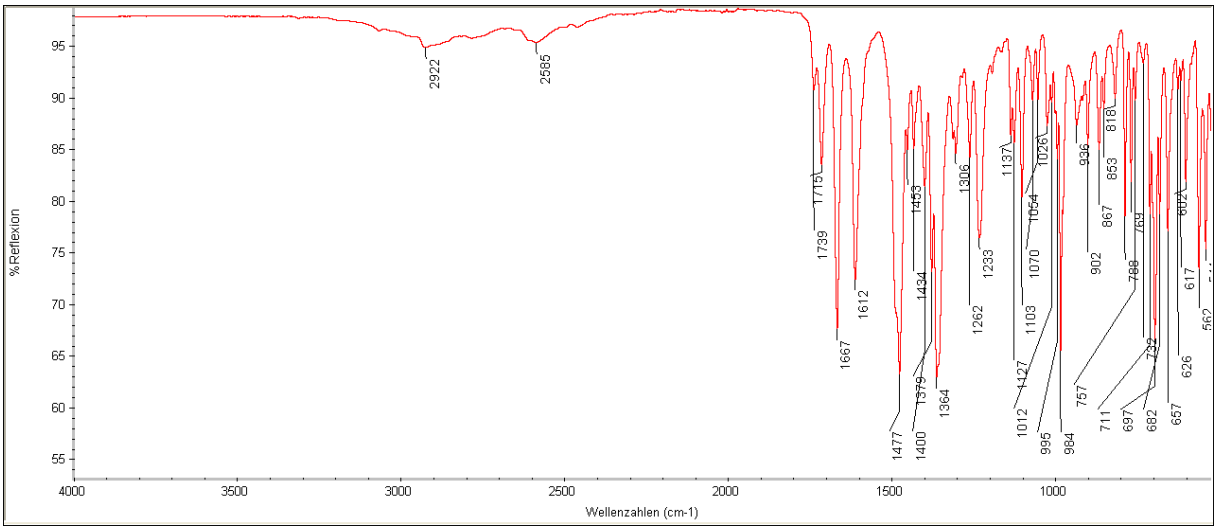

Figure 9.131. IR spectrum of [$Re^{V}O(HL^{2MePh})$].

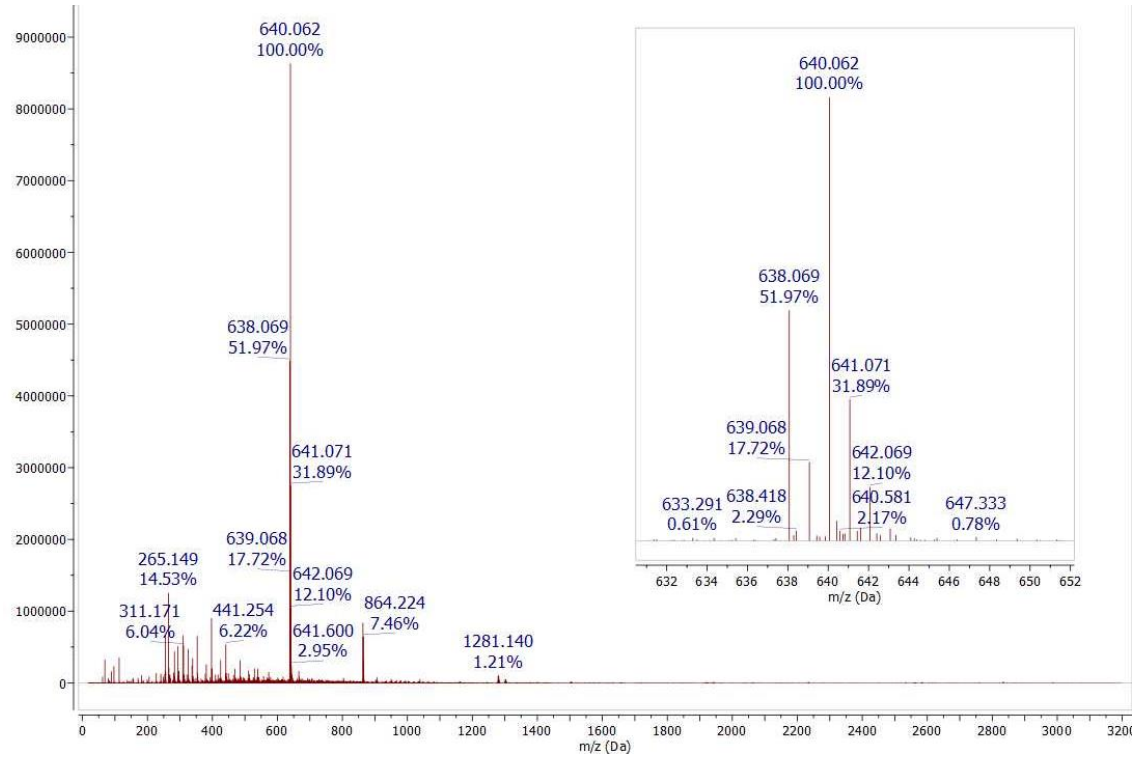

Figure 9.132. ESI- MS spectrum of [$Re^{V}O(HL^{2MePh})$].

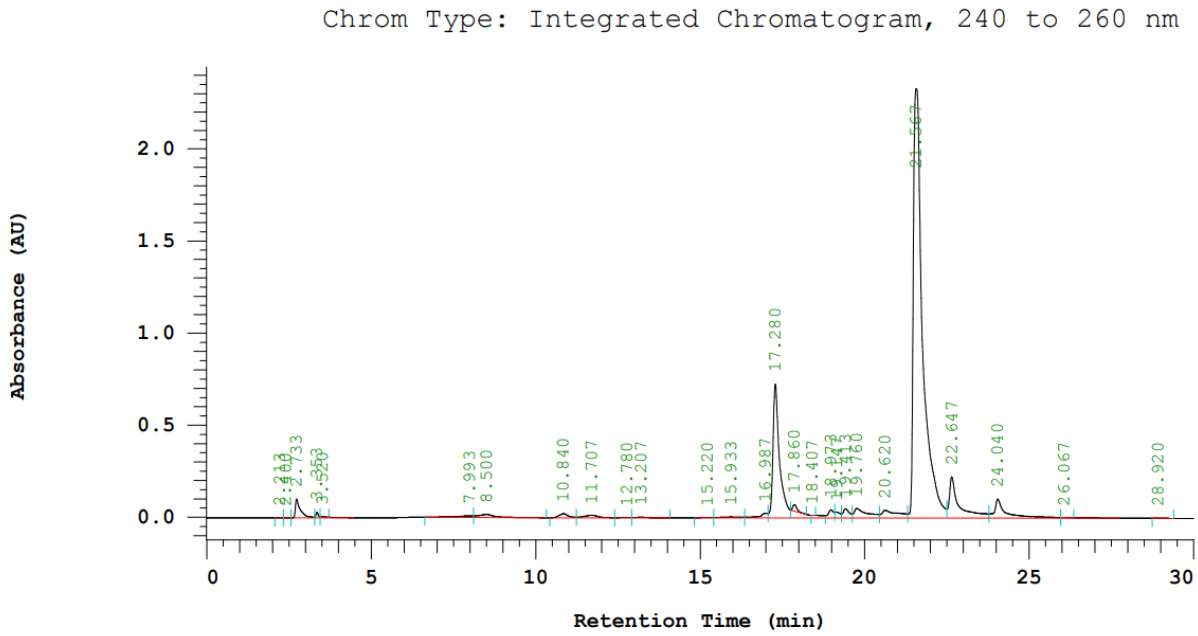

Figure 9.133. UV trace (HPLC) of [ReO(HL^{2MePh})].

Spectroscopic Data of [Re^{V}O(HL^{2PhPh})]

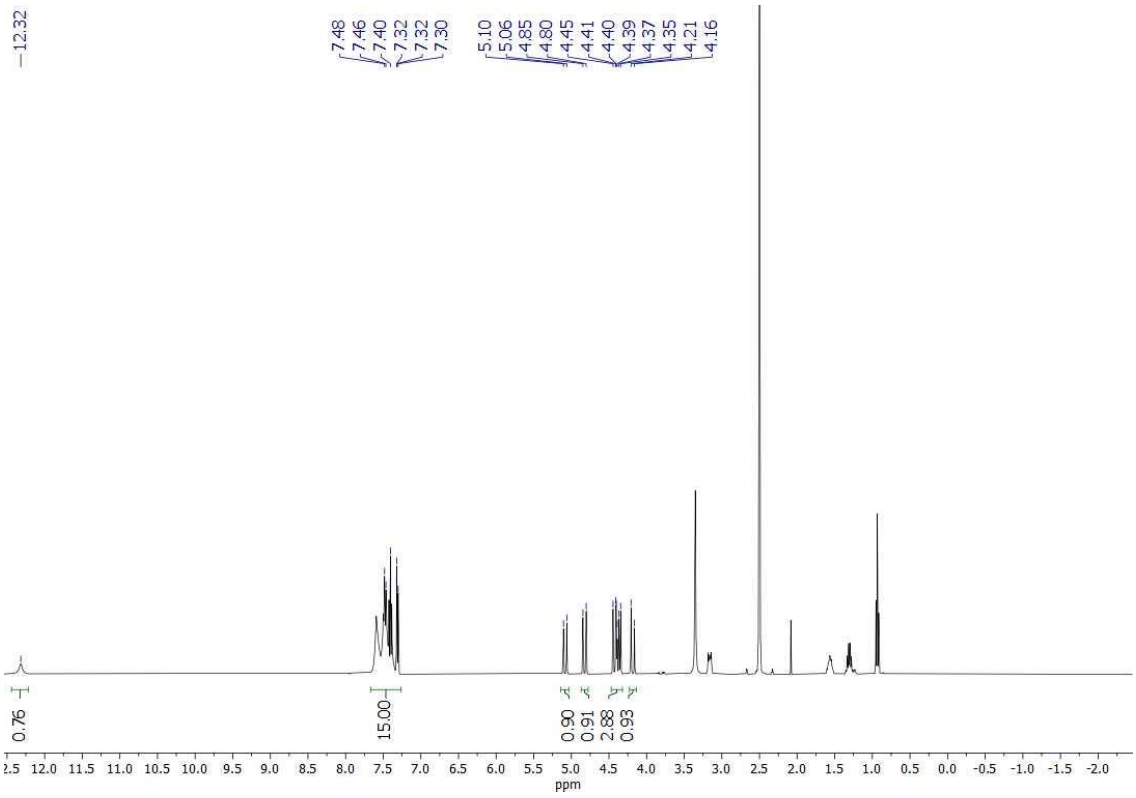

Figure 9.134. ^{1}H NMR spectrum of [Re^{V}O(HL^{2PhPh})] in d_6-DMSO.

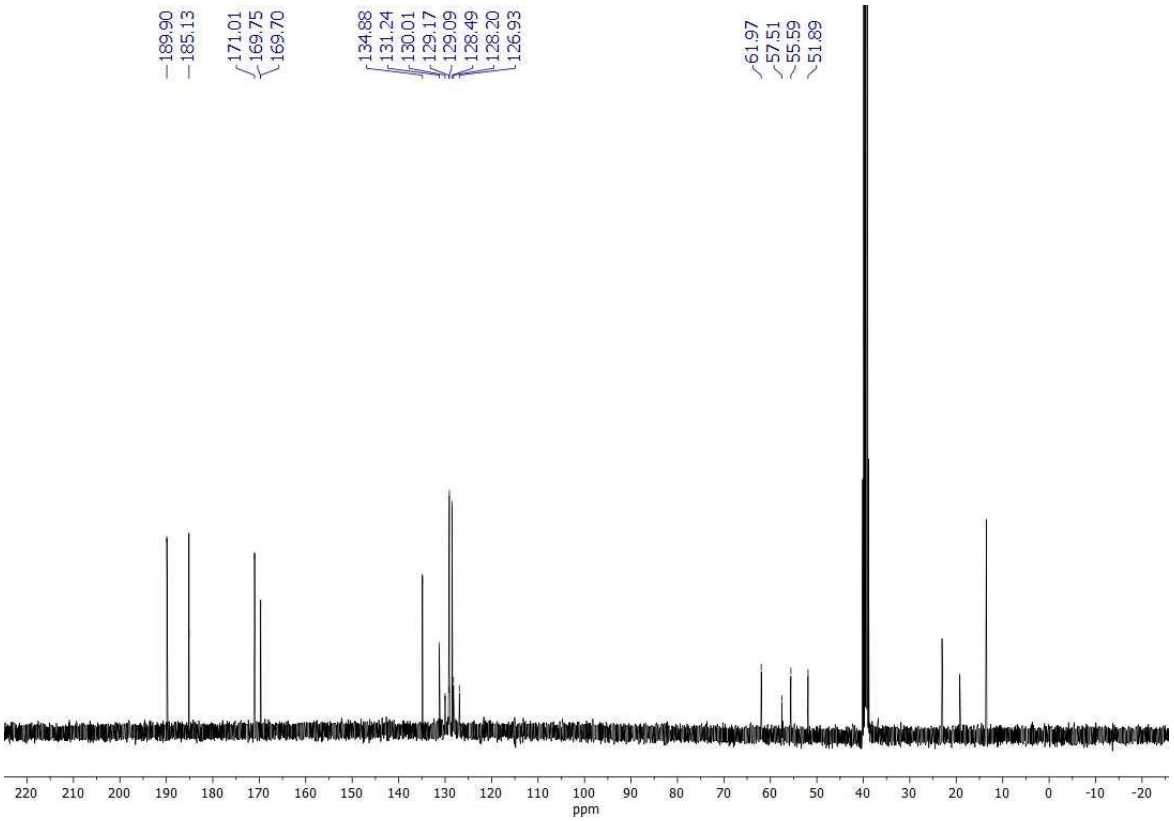

Figure 9.135. $^{13}C\{^{1}H\}$ NMR spectrum of [$Re^{V}O(L^{2PhPh})$] in d_6-DMSO.

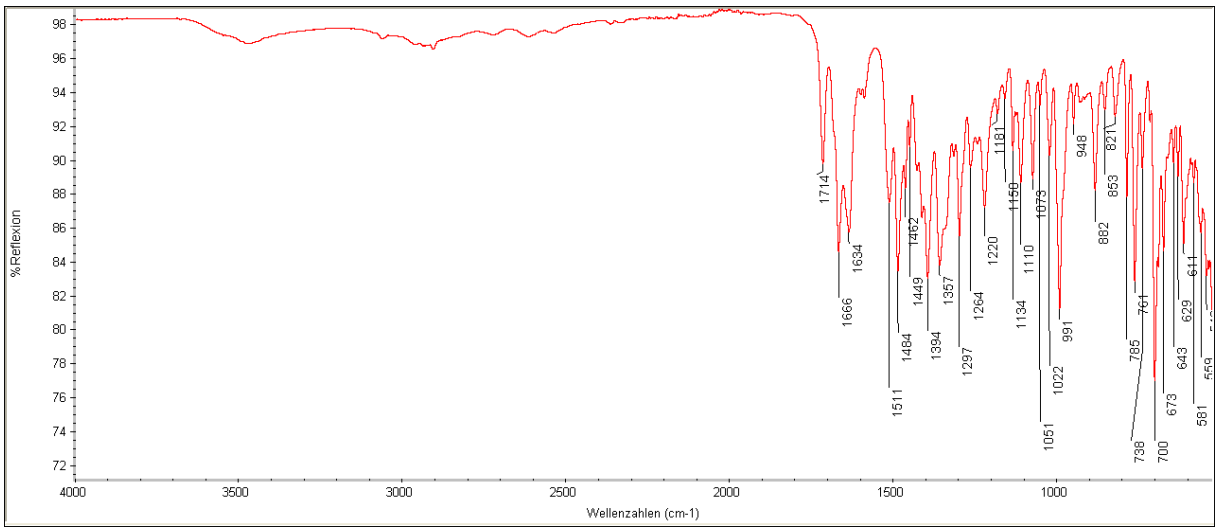

Figure 9.136. IR spectrum of [$Re^{V}O(HL^{2PhPh})$].

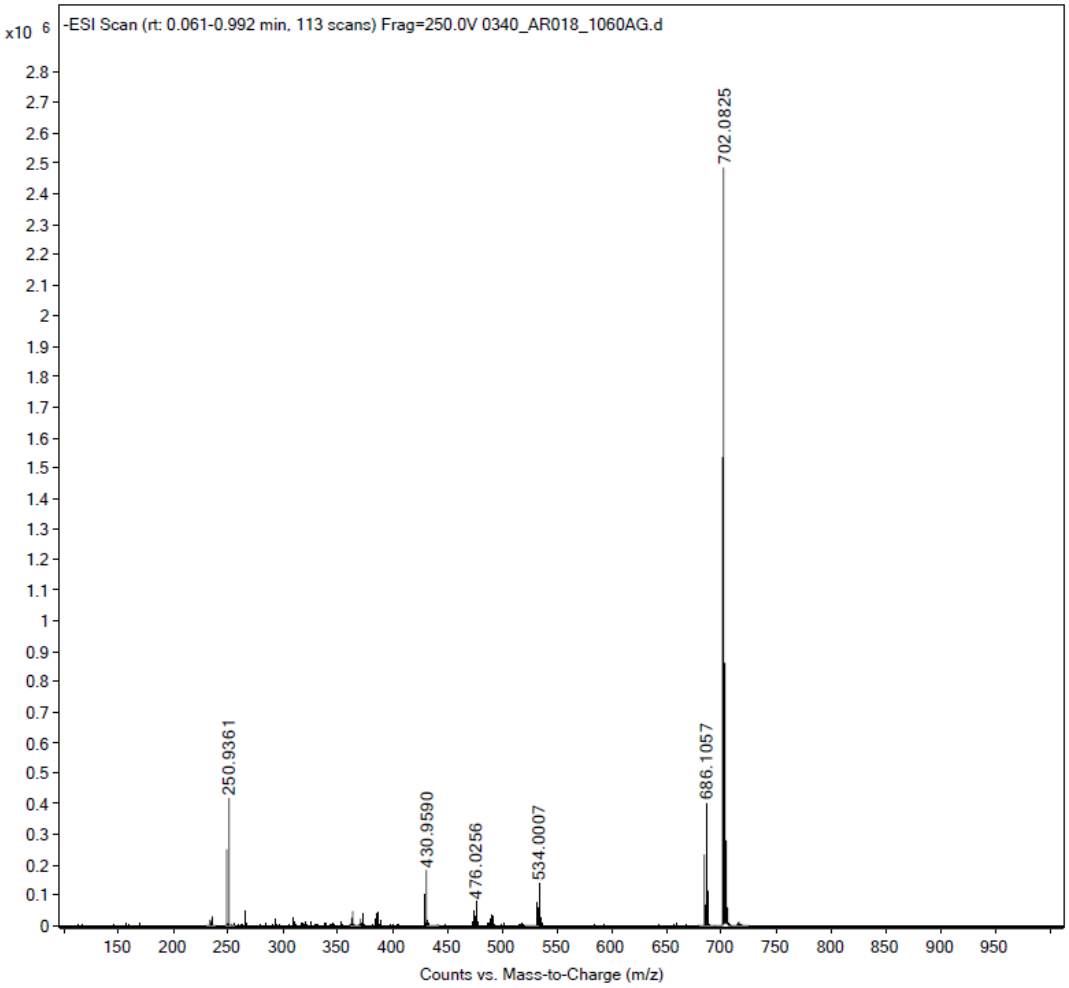

Figure 9.137. ESI- MS spectrum of [$Re^{V}O(HL^{2PhPh})$].

Spectroscopic Data of [$^{99m}Tc^{V}O(HL^{2EtEt})$]

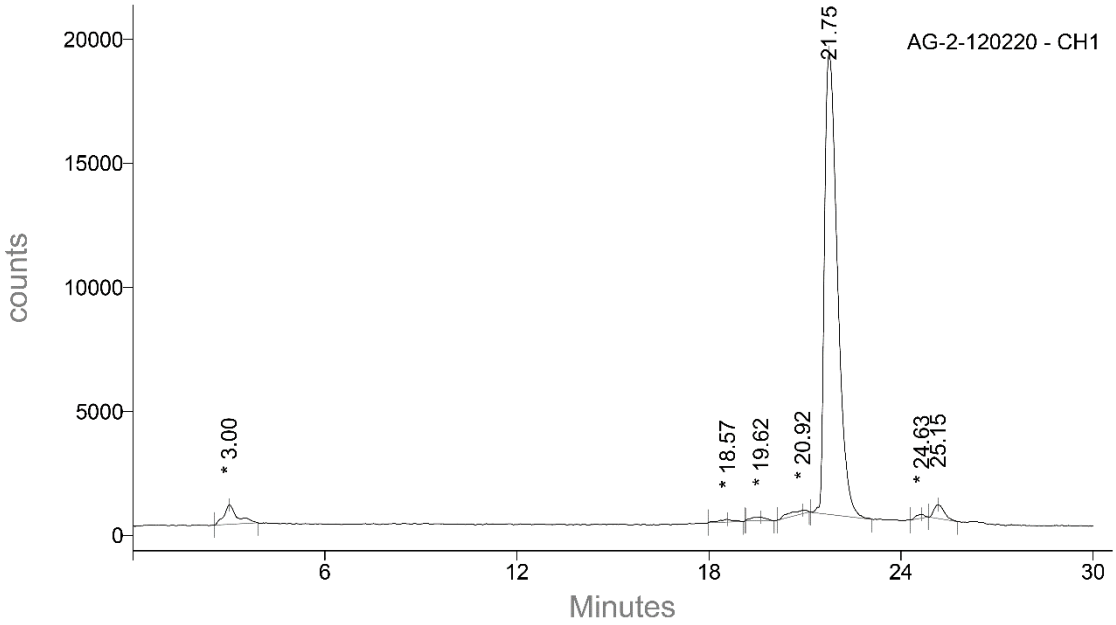

Figure 9.138. Radio trace of [$^{99m}Tc^{V}O(HL^{2EtEt})$].

Spectroscopic Data of [$^{99m}Tc^{V}O(HL^{2MePh})$]

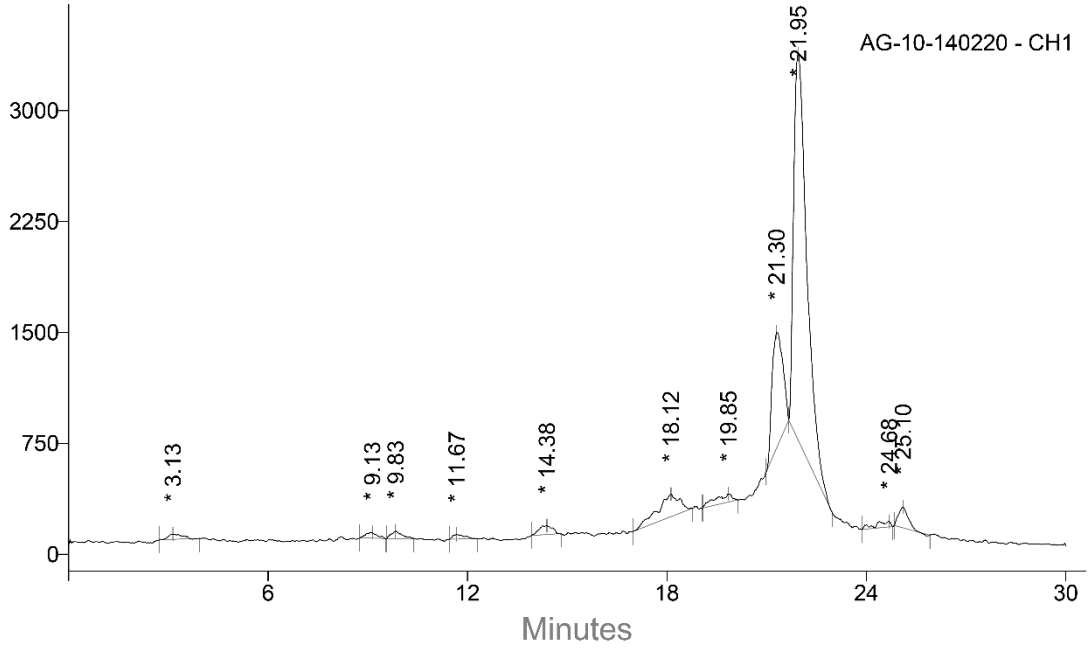

Figure 9.139. Radio trace of [$^{99m}Tc^{V}O(HL^{2MePh})$].

Spectroscopic Data of H_3P^{EtEt} and H_3P^{MePh}

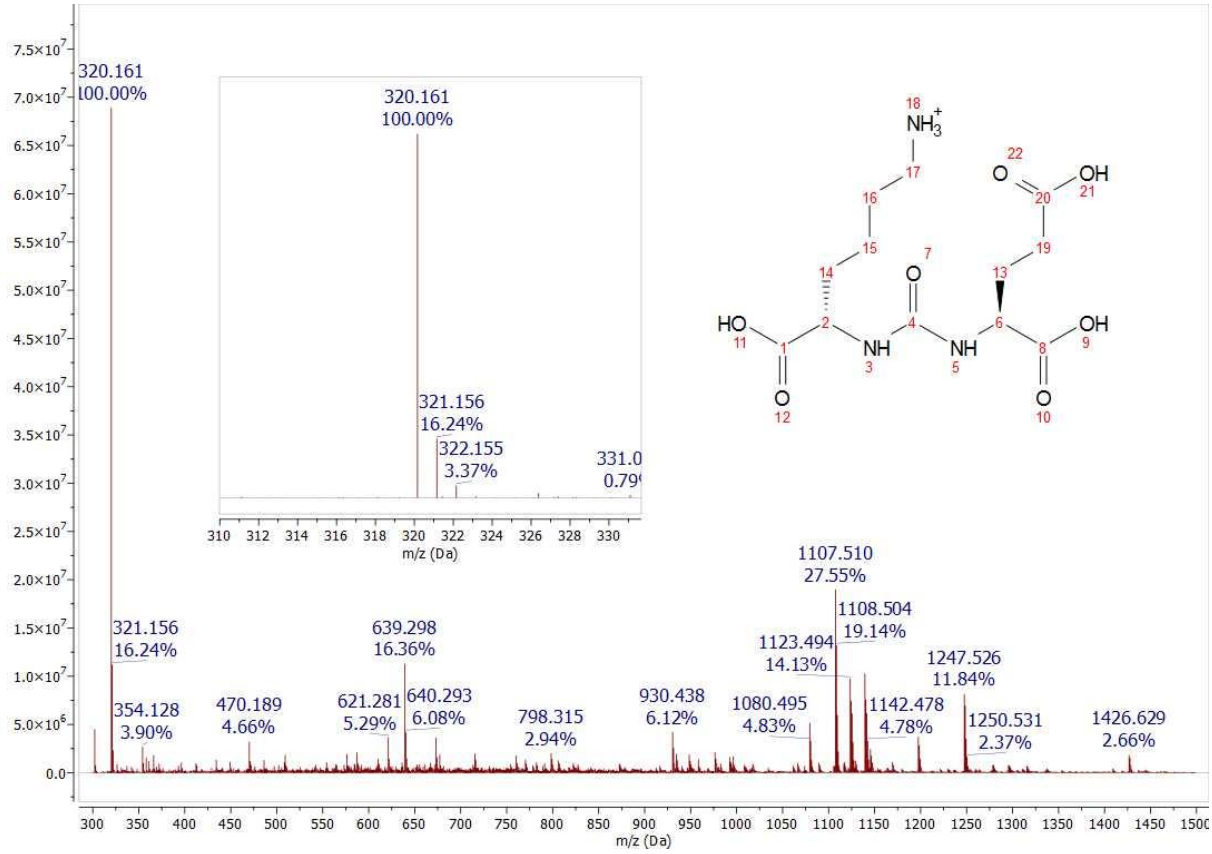

Figure 9.140. ESI+ MS spectrum of $C_{12}H_{22}N_3O_7^+$.

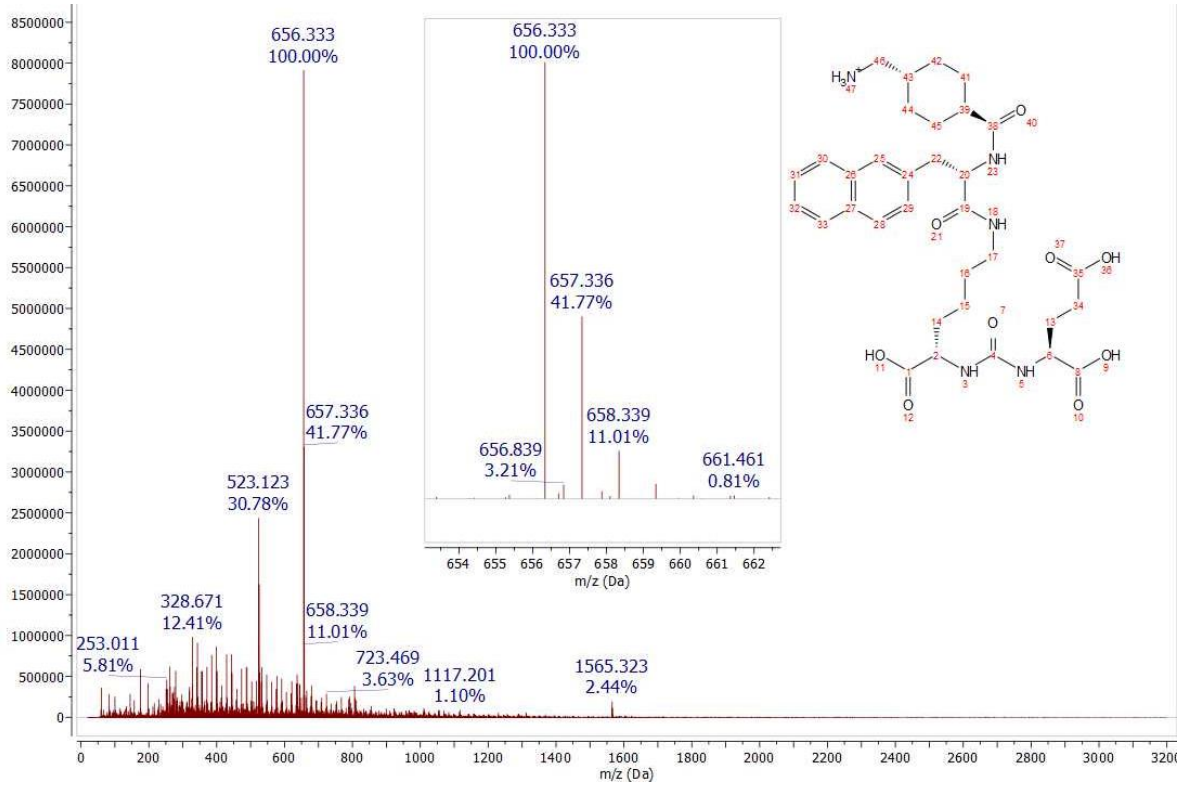

Figure 9.141. ESI+ MS spectrum of $C_{33}H_{46}N_5O_9^+$.

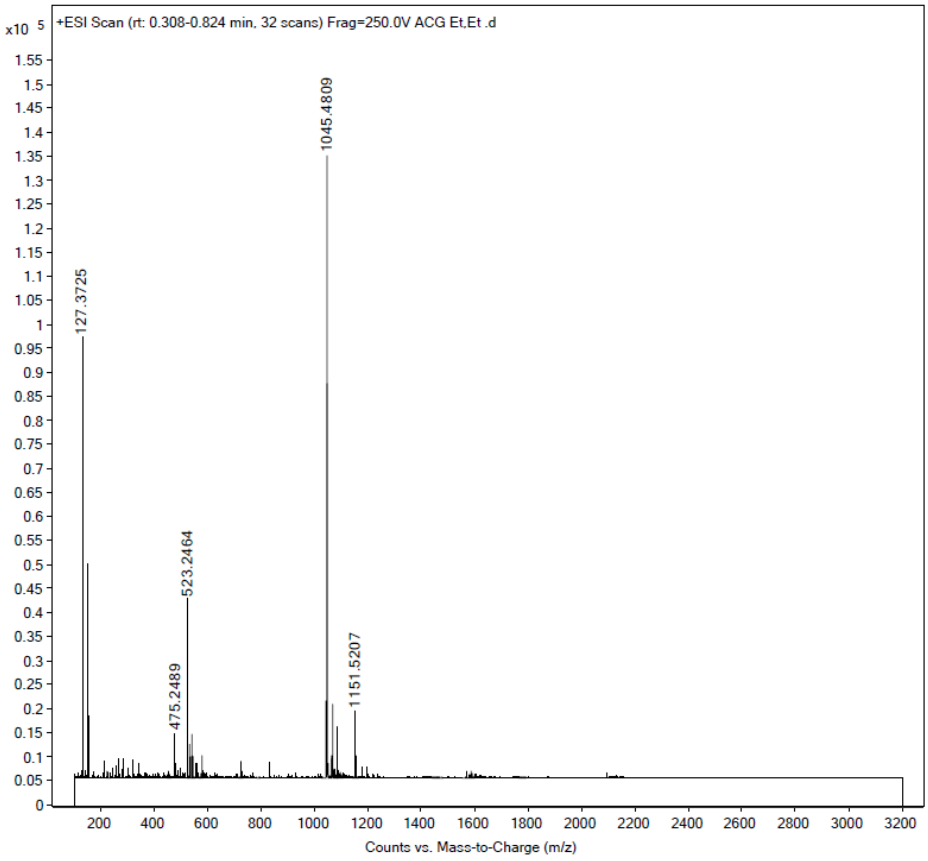

Figure 9.142. ESI+ MS spectrum of H_3P^{EtEt}.

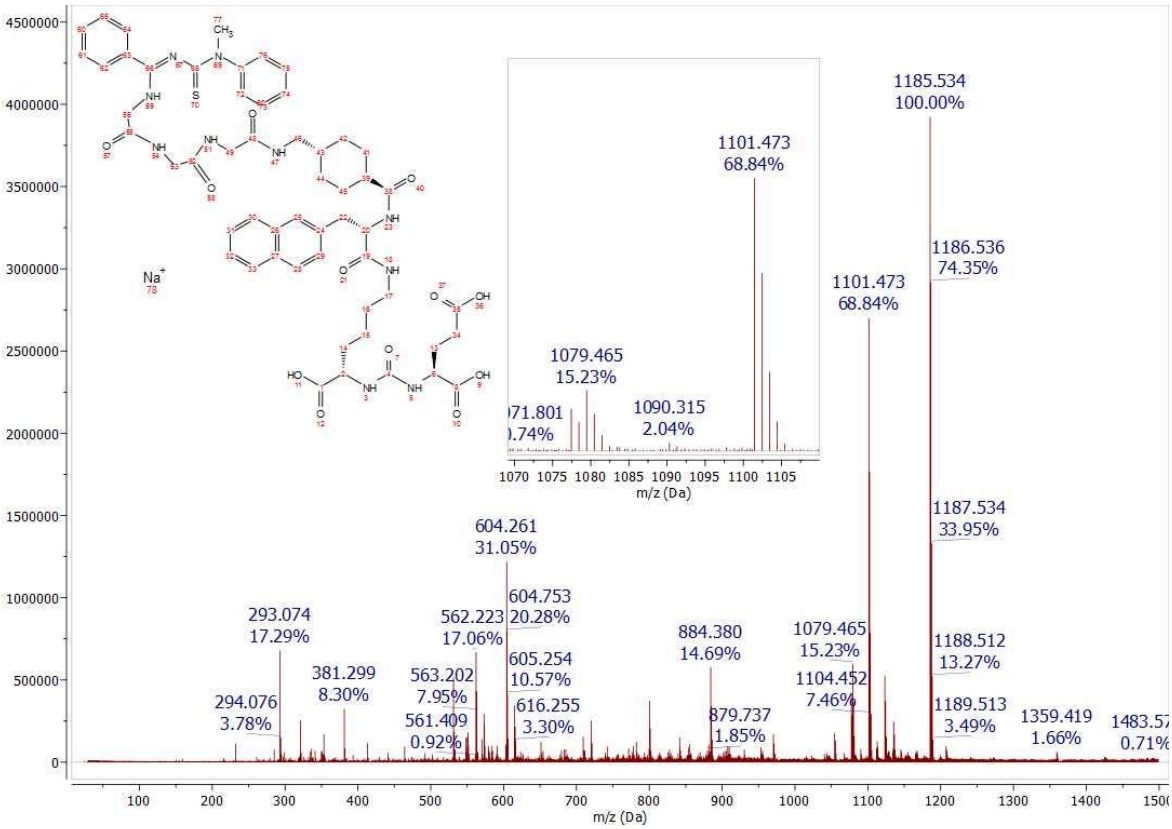

Figure 9.143. ESI+ MS spectrum of H_3P^{MePh}.

Spectroscopic Data of [$Re^{V}O(P^{EtEt})$]

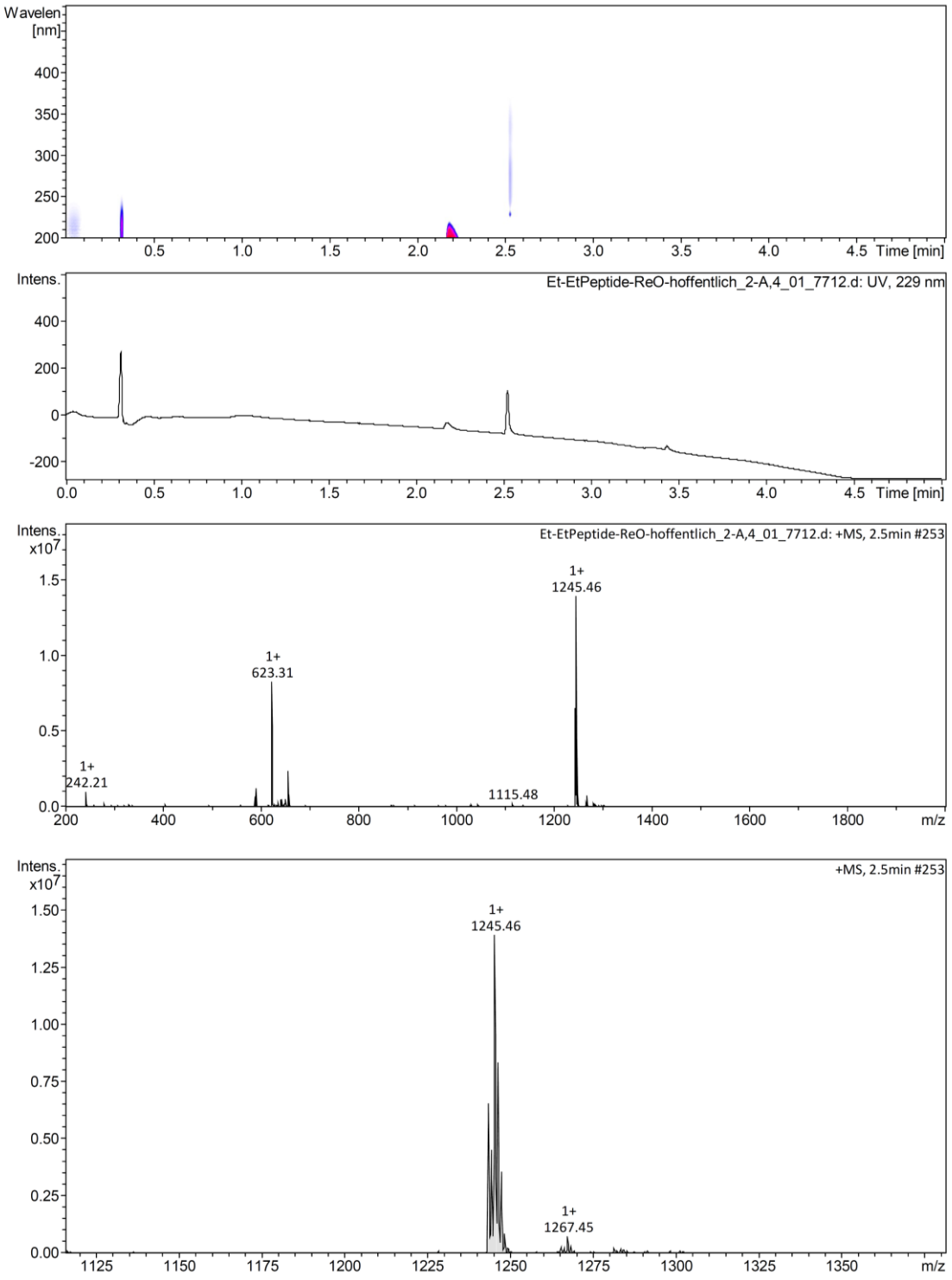

Figure 9.144. UPLC MS spectrum of [$Re^{V}O(P^{EtEt})$].

Spectroscopic Data of [$Re^{V}O(P^{MePh})$]

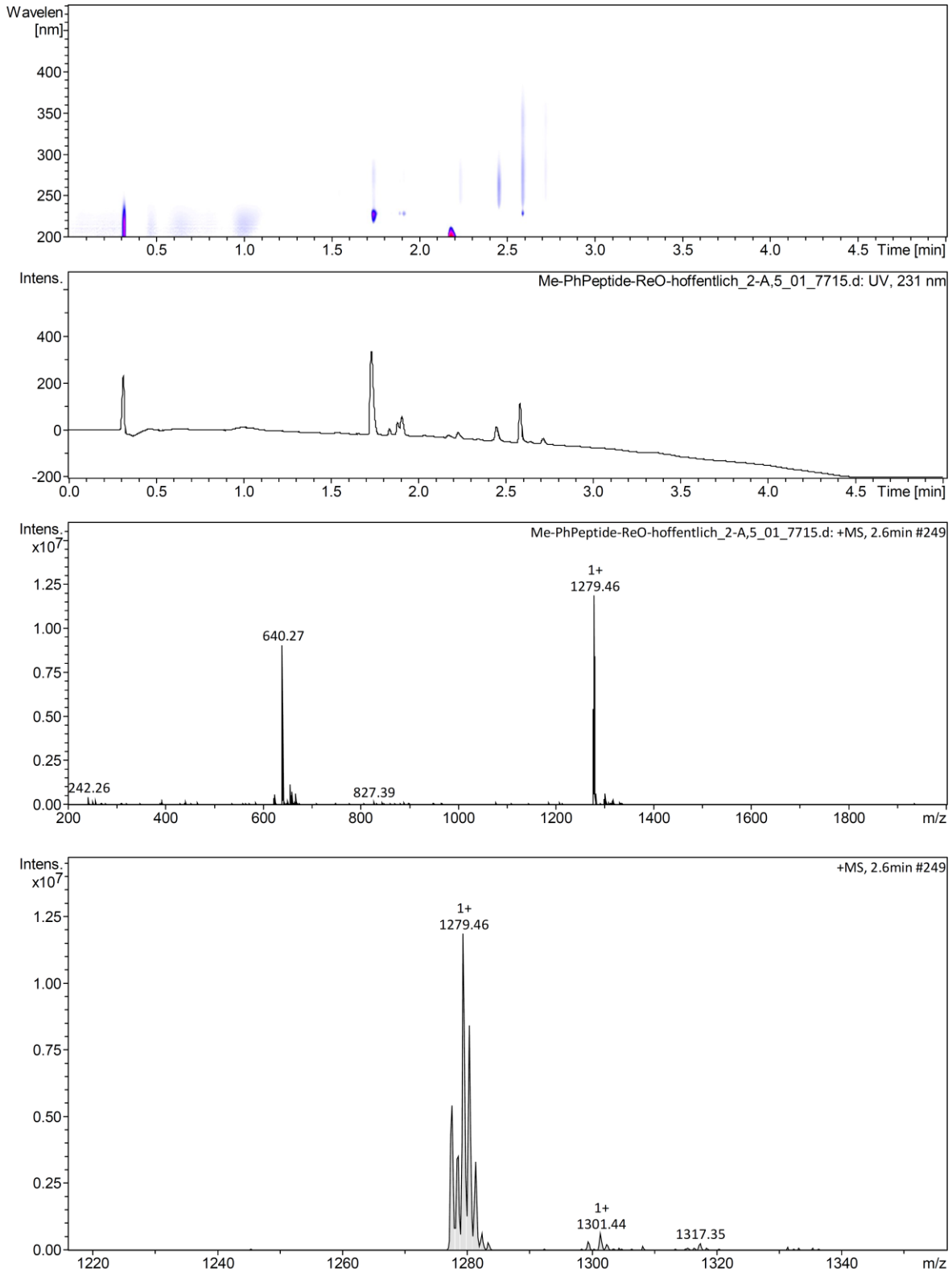

Figure 9.145. UPLC MS spectrum of [$Re^{V}O(P^{MePh})$].

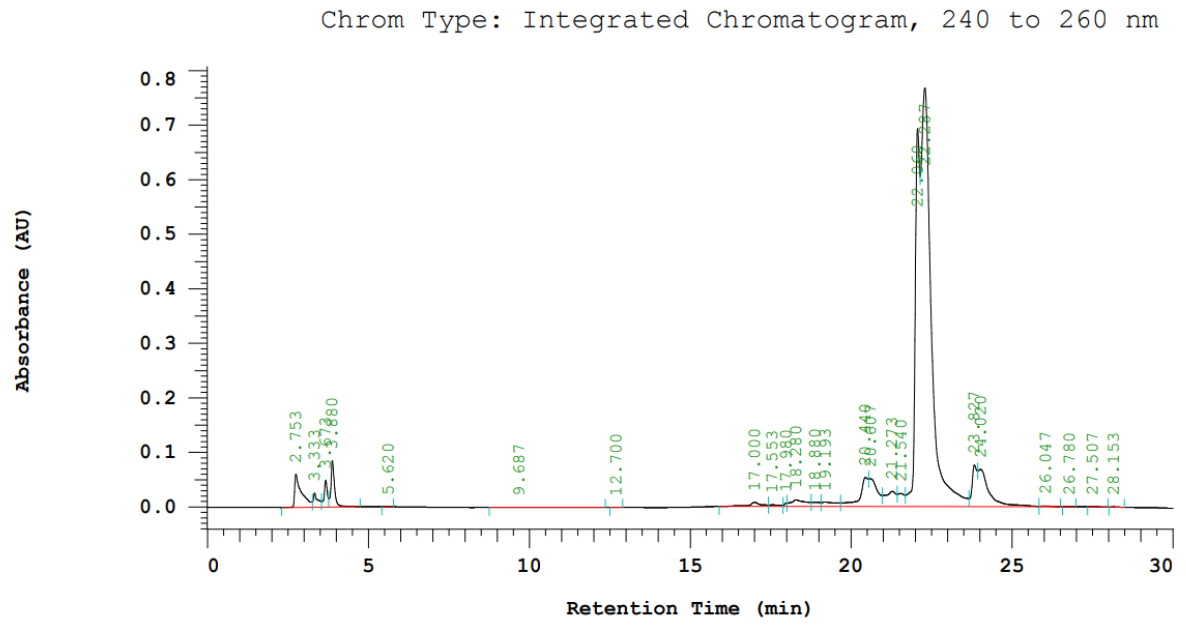

Figure 9.146. UV trace (HPLC) of [$Re^{V}O(P^{EtEt})$].

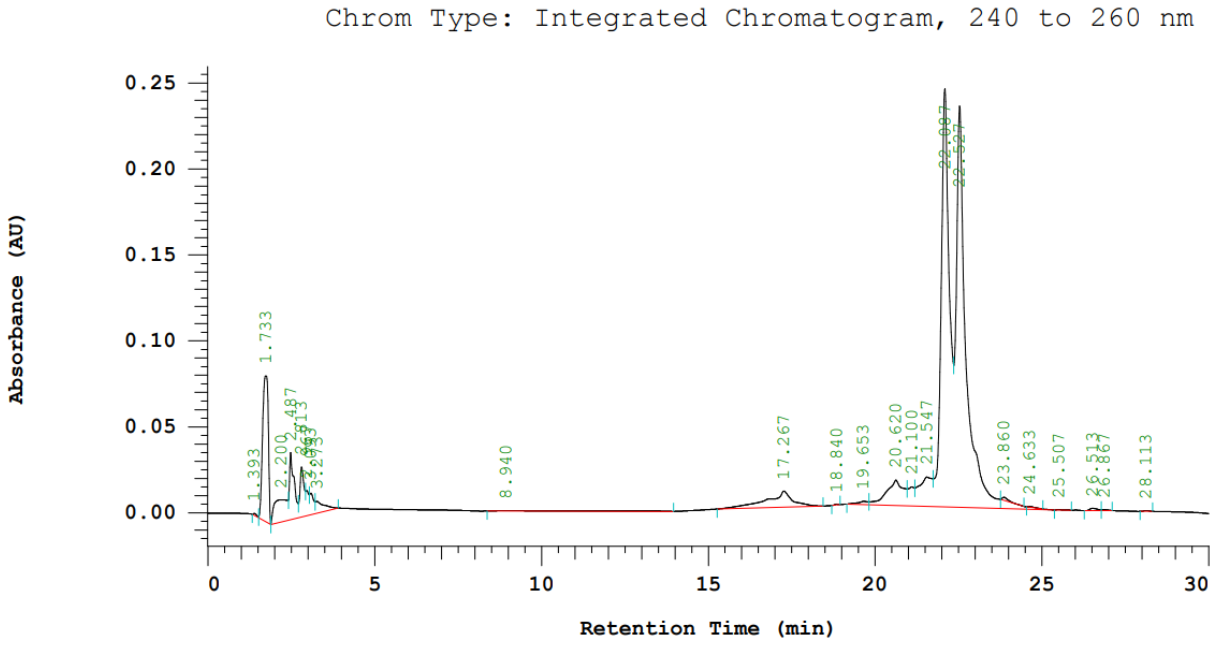

Figure 9.147. UV trace (HPLC) of [$Re^{V}O(P^{MePh})$].

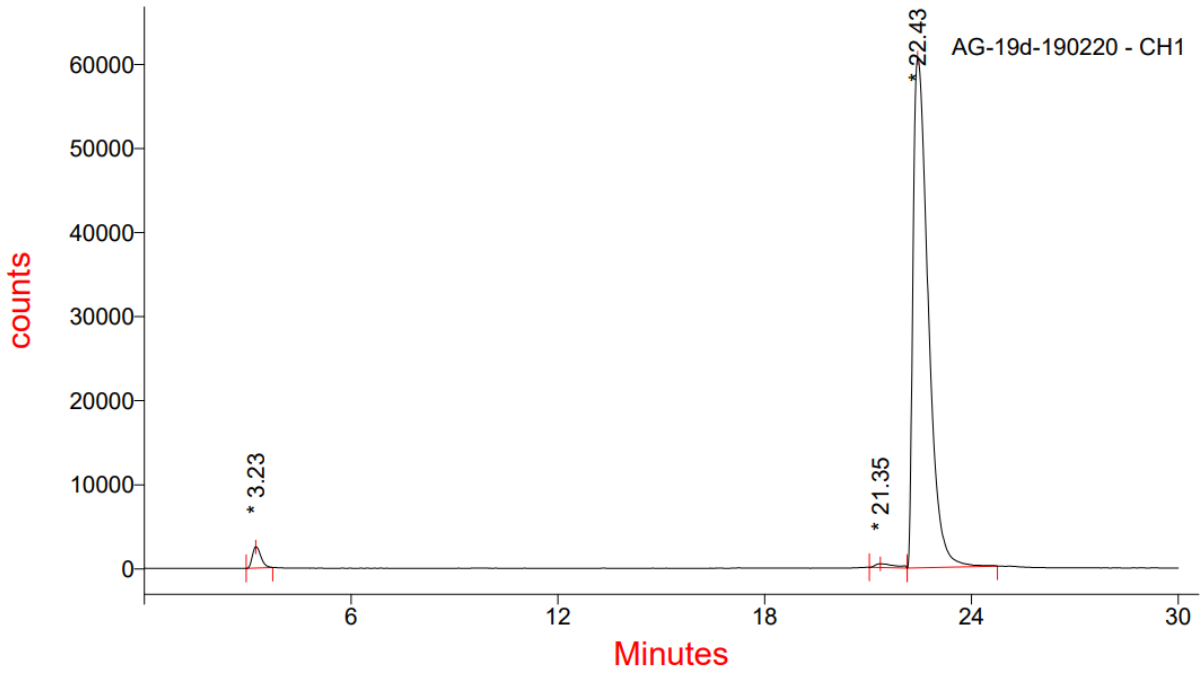

Figure 9.148. Radio trace of [$^{99m}Tc^{V}O(P^{EtEt})$] after 2 h. Stability test in PBS buffer.

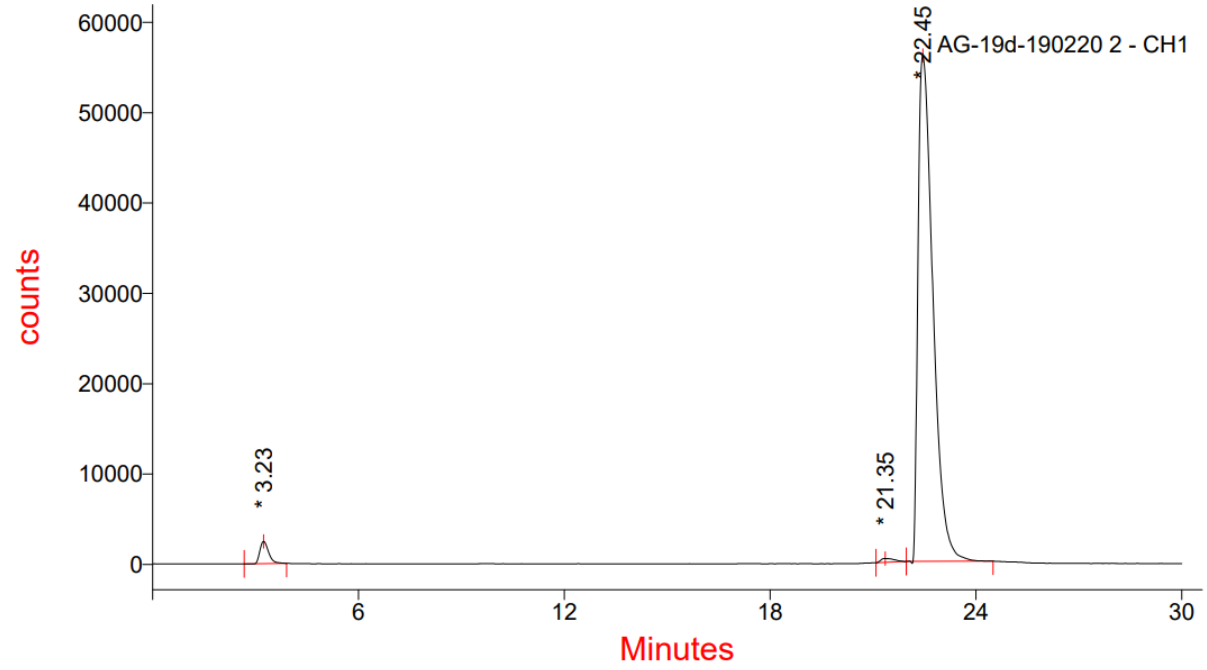

Figure 9.149. Radio trace of [$^{99m}Tc^{V}O(P^{EtEt})$] after 2.5 h. Stability test in PBS buffer.

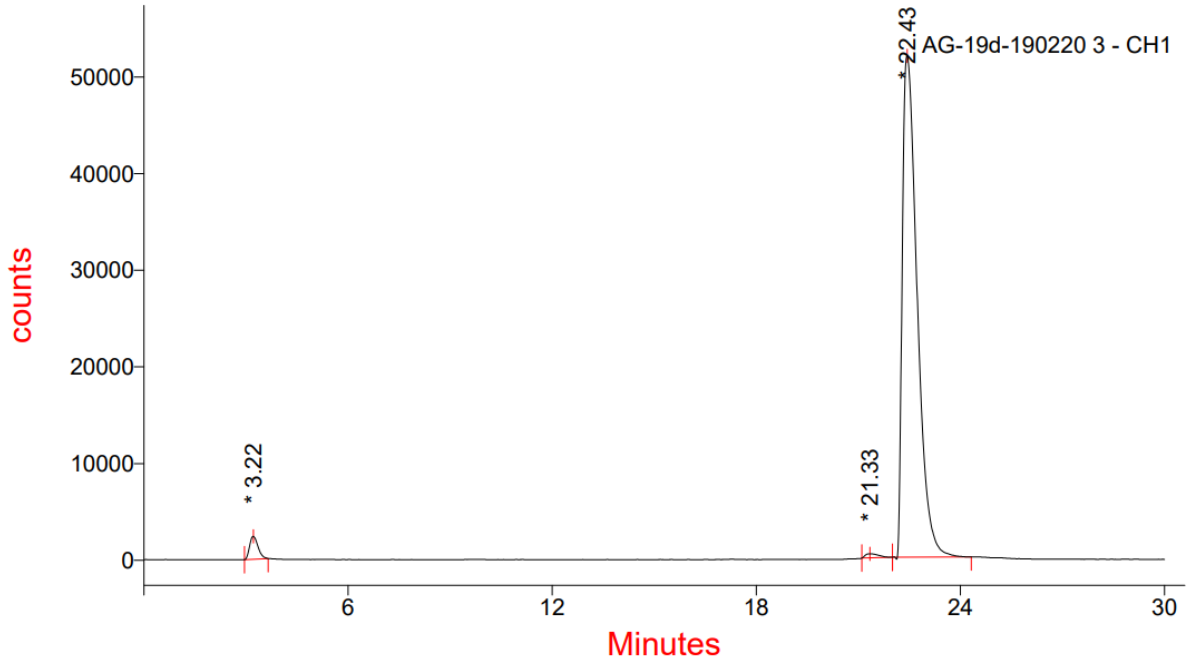

Figure 9.150. Radio trace of [$^{99m}Tc^{V}O(P^{EtEt})$] after 3 h. Stability test in PBS buffer.

Spectroscopic Data of $H_3L^{3EtEtBoc}$

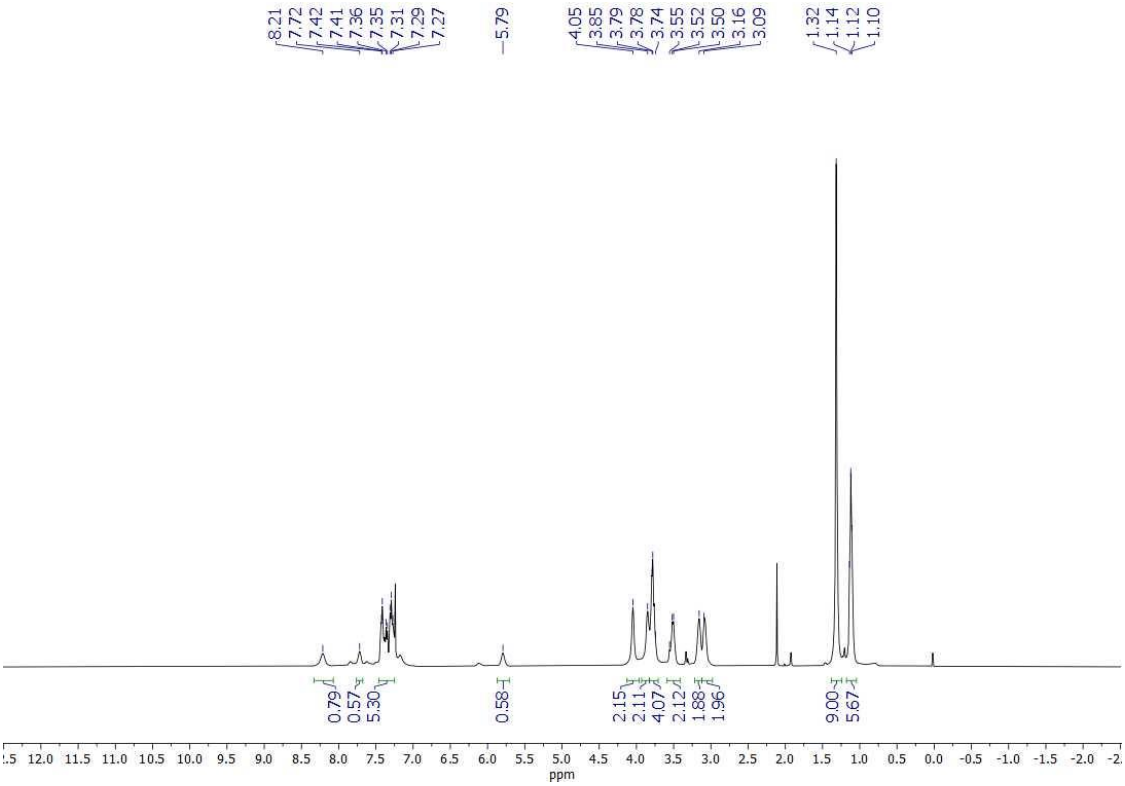

Figure 9.151. ^{1}H NMR spectrum of $H_3L^{3EtEtBoc}$ in $CDCl_3$.

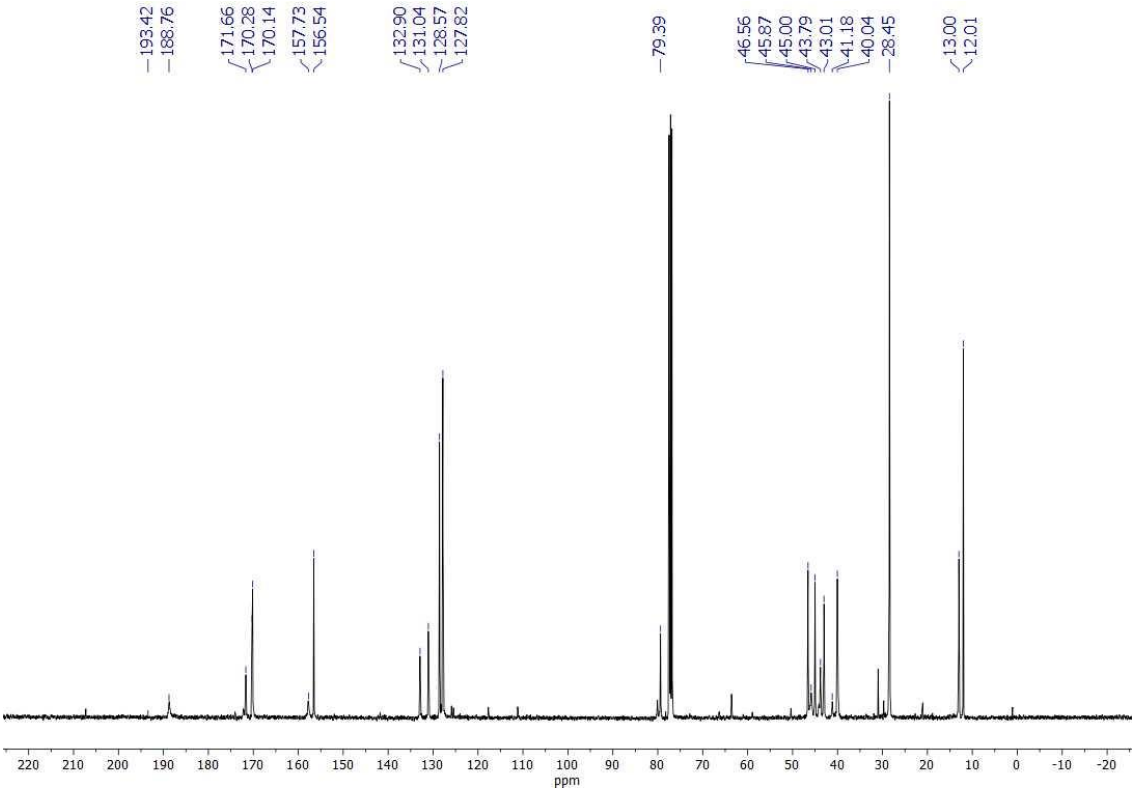

Figure 9.152. $^{13}C\{^{1}H\}$ NMR spectrum of $H_3L^{3EtEtBoc}$ in $CDCl_3$.

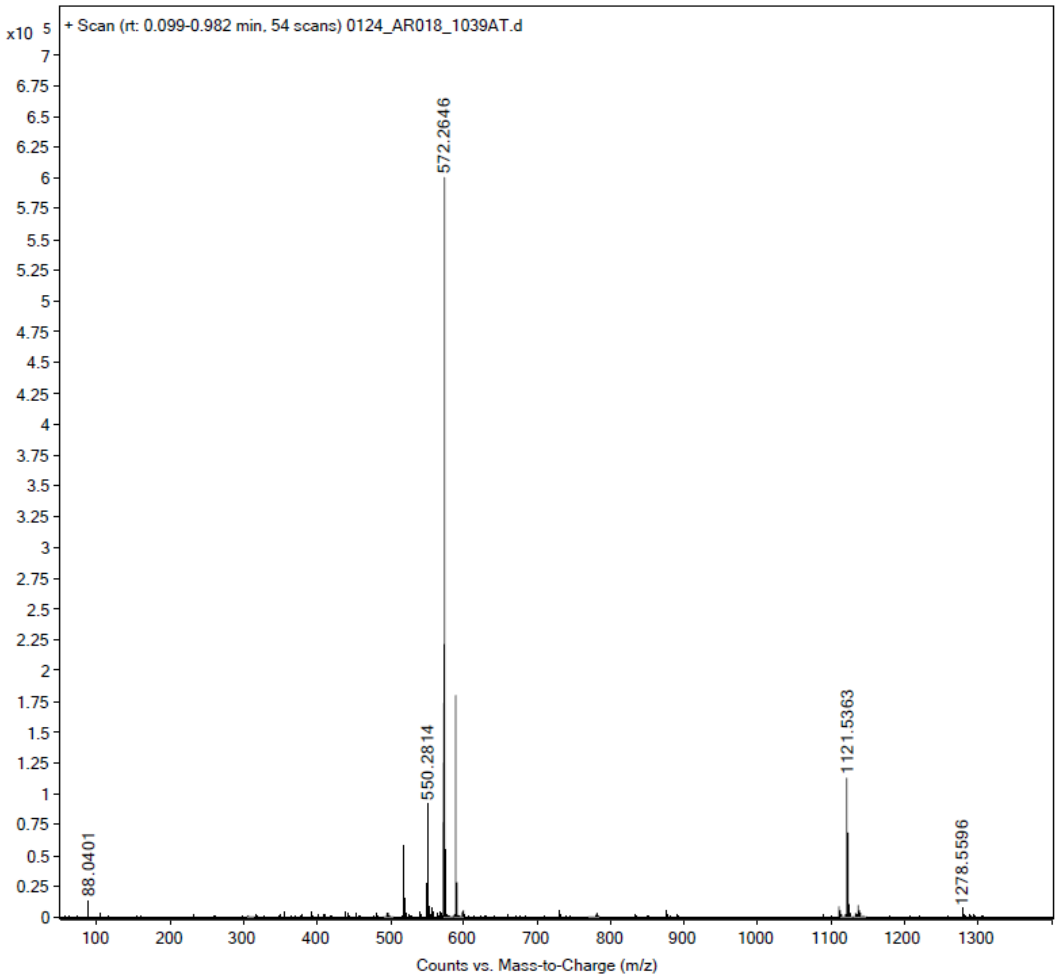

Figure 9.153. ESI+ MS spectrum of $H_3L^{3EtEtBoc}$.

Spectroscopic Data of H_3L^{3EtEt}

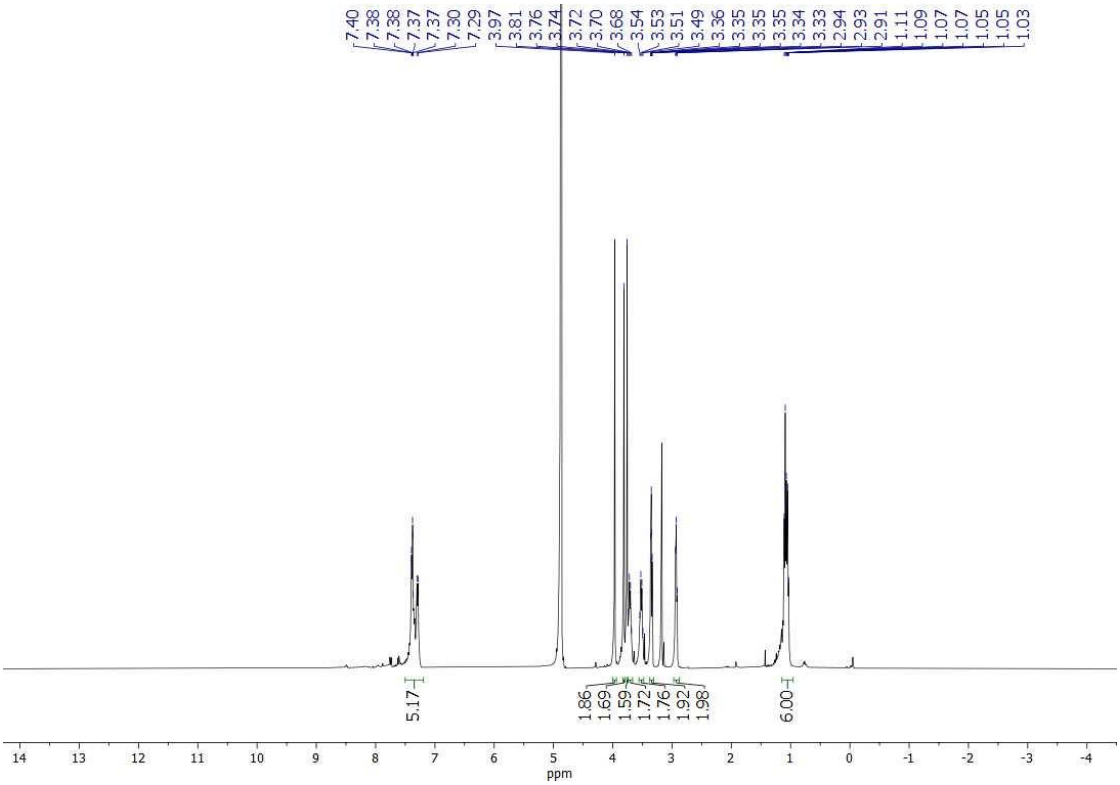

Figure 9.154. ^{1}H NMR spectrum of H_3L^{3EtEt}.

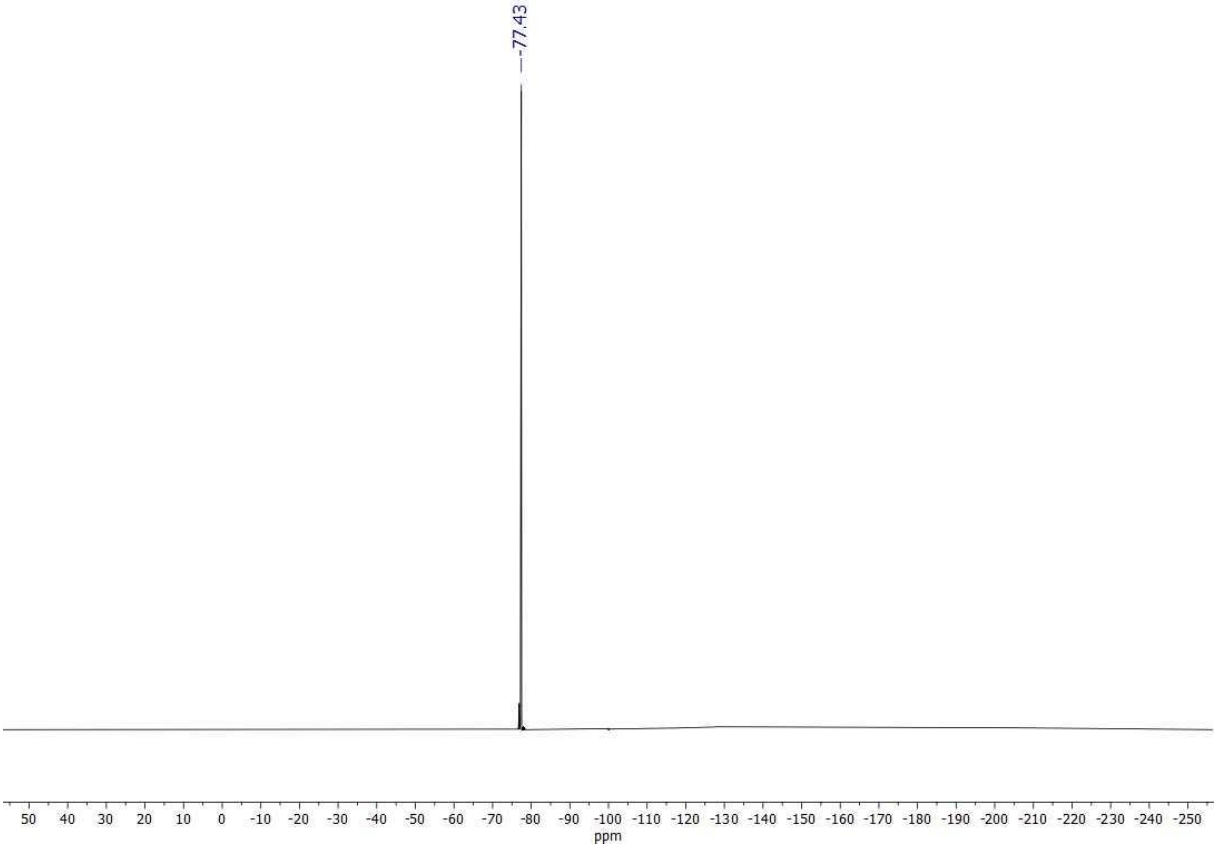

Figure 9.155. ^{19}F NMR spectrum of H_3L^{3EtEt} in $CDCl_3$.

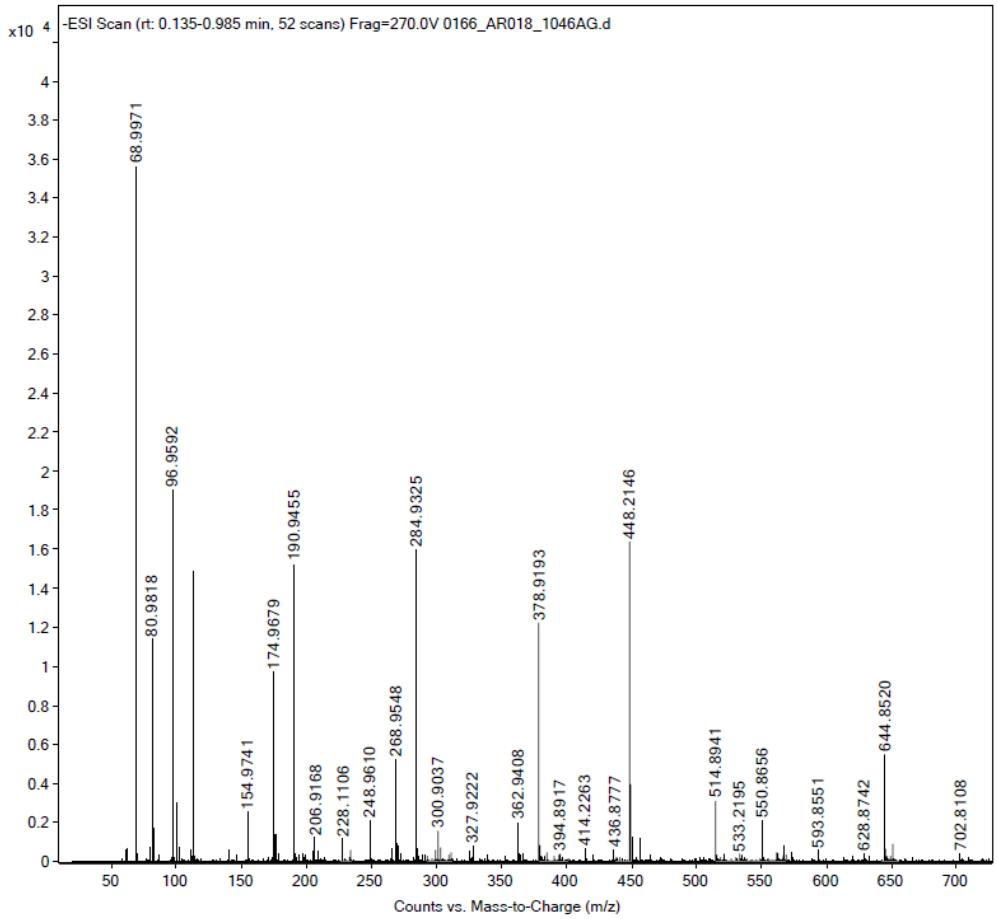

Figure 9.156. ESI- MS spectrum of H_3L^{3EtEt}.

Spectroscopic Data of [$Re^{V}O(L^{3EtEtBoc})$]

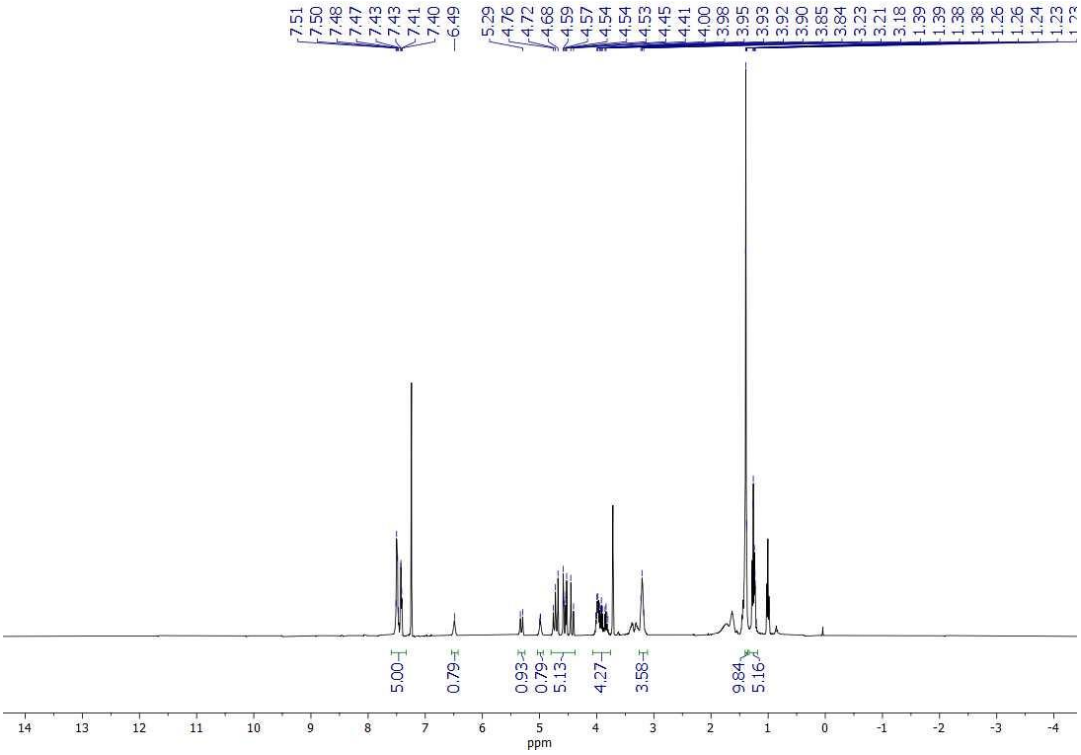

Figure 9.157. ^{1}H NMR spectrum of [$Re^{V}O(L^{3EtEtBoc})$] in $CDCl_3$.

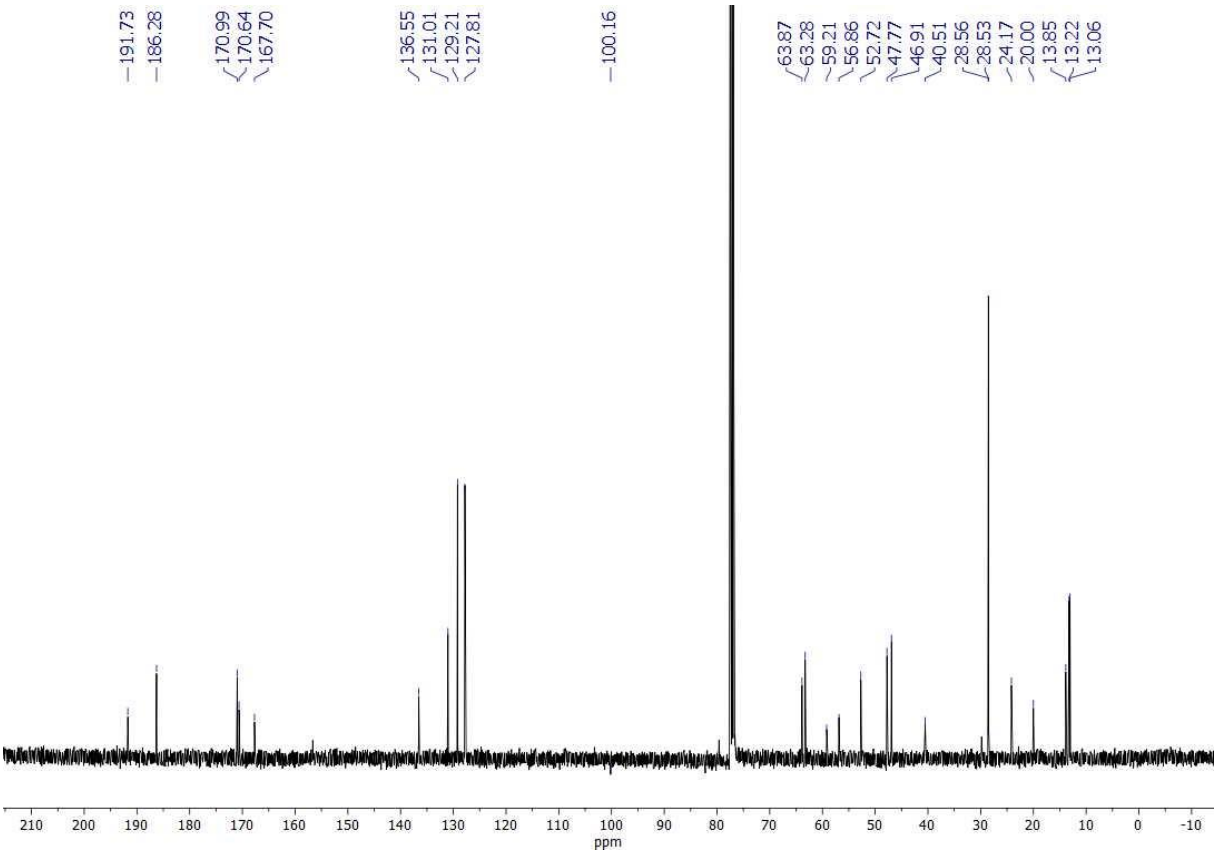

Figure 9.158. $^{13}C\{^{1}H\}$ NMR spectrum of [$Re^{V}O(L^{3EtEtBoc})$].

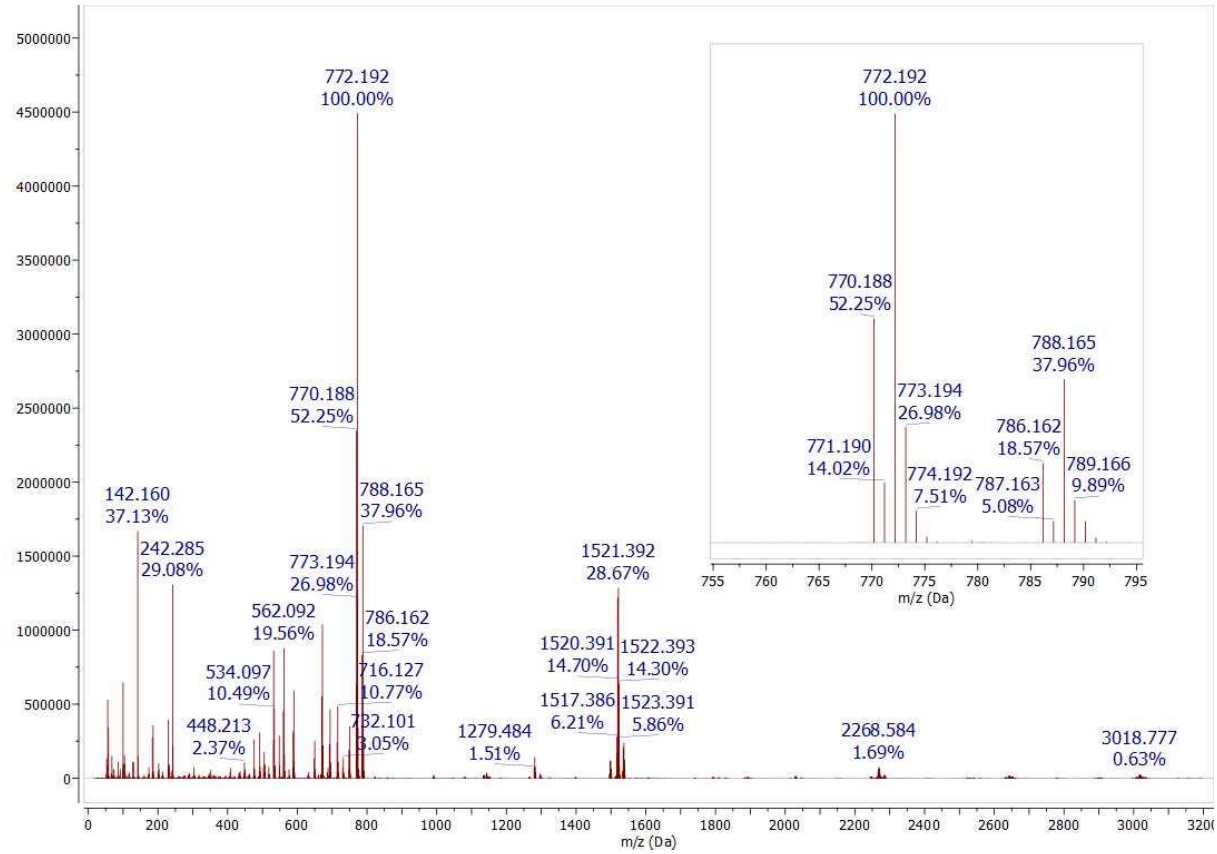

Figure 9.159. ESI+ MS spectrum of [$Re^{V}O(L^{3EtEtBoc})$].

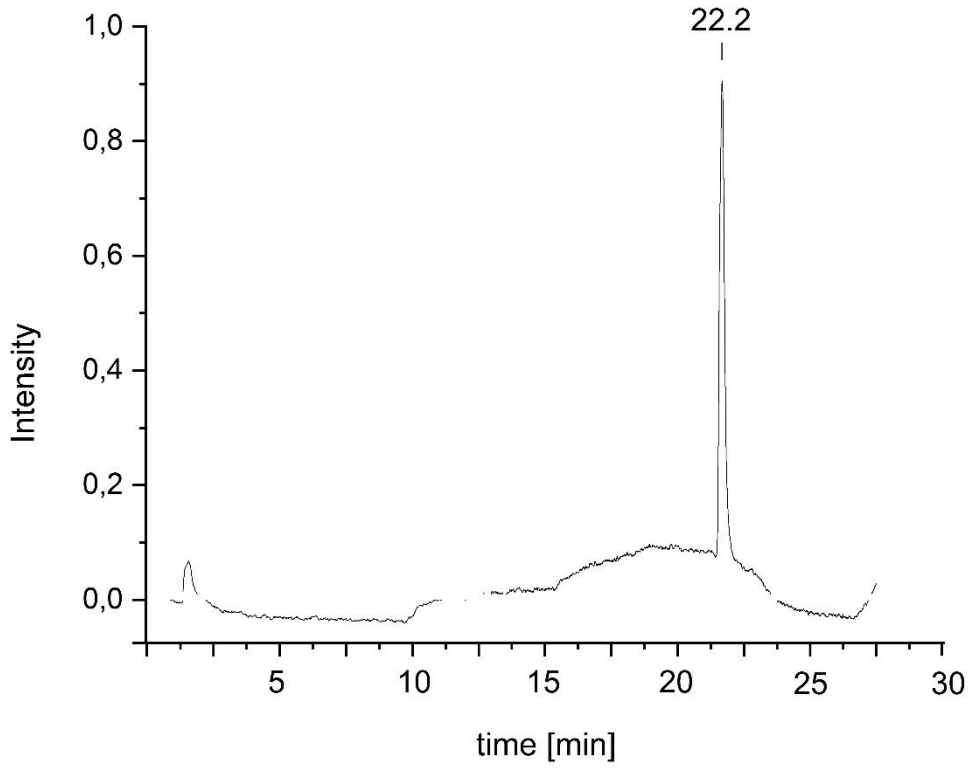

Figure 9.160. UV trace (HPLC) of [$Re^{V}O(L^{3EtEtBoc})$].

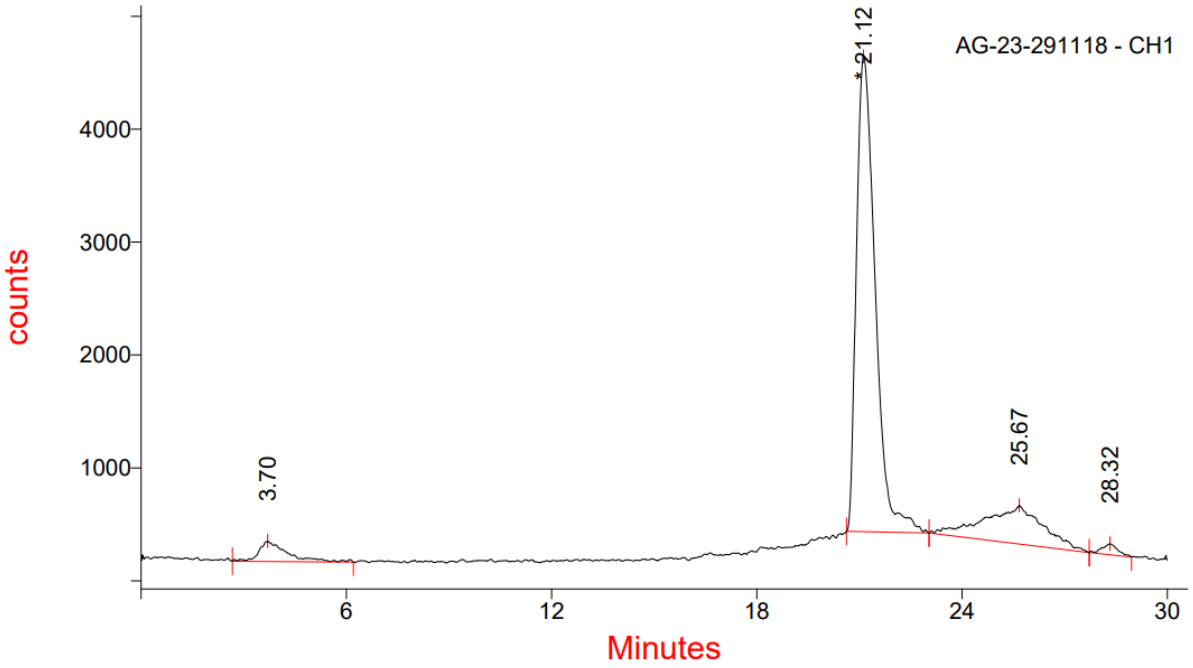

Figure 9.161. Radio trace (HPLC) of [$^{99m}Tc^{V}O(L^{3EtEtBoc})$].

Spectroscopic Data of [$Re^{V}O(L^{3EtEt})$]

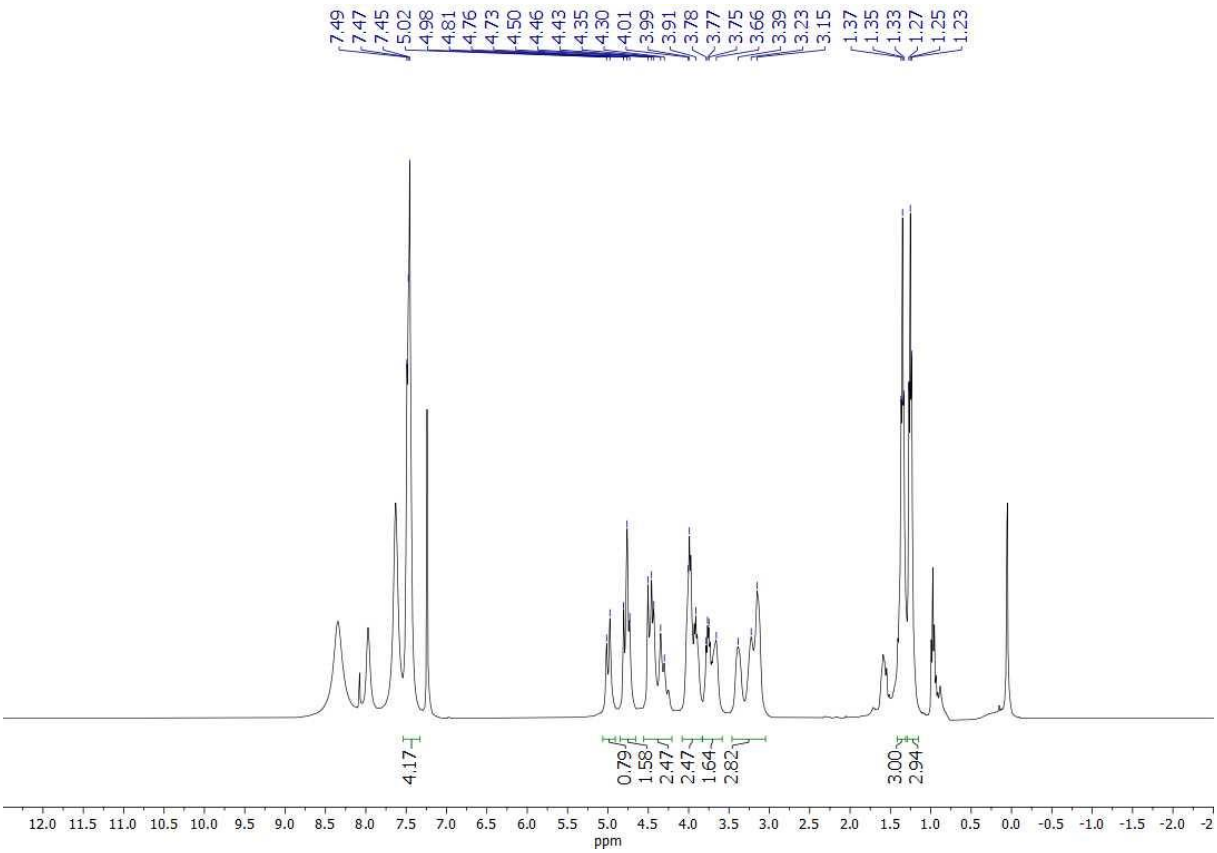

Figure 9.162. ^{1}H NMR spectrum of [$Re^{V}O(L^{3EtEt})$] in $CDCl_3$.

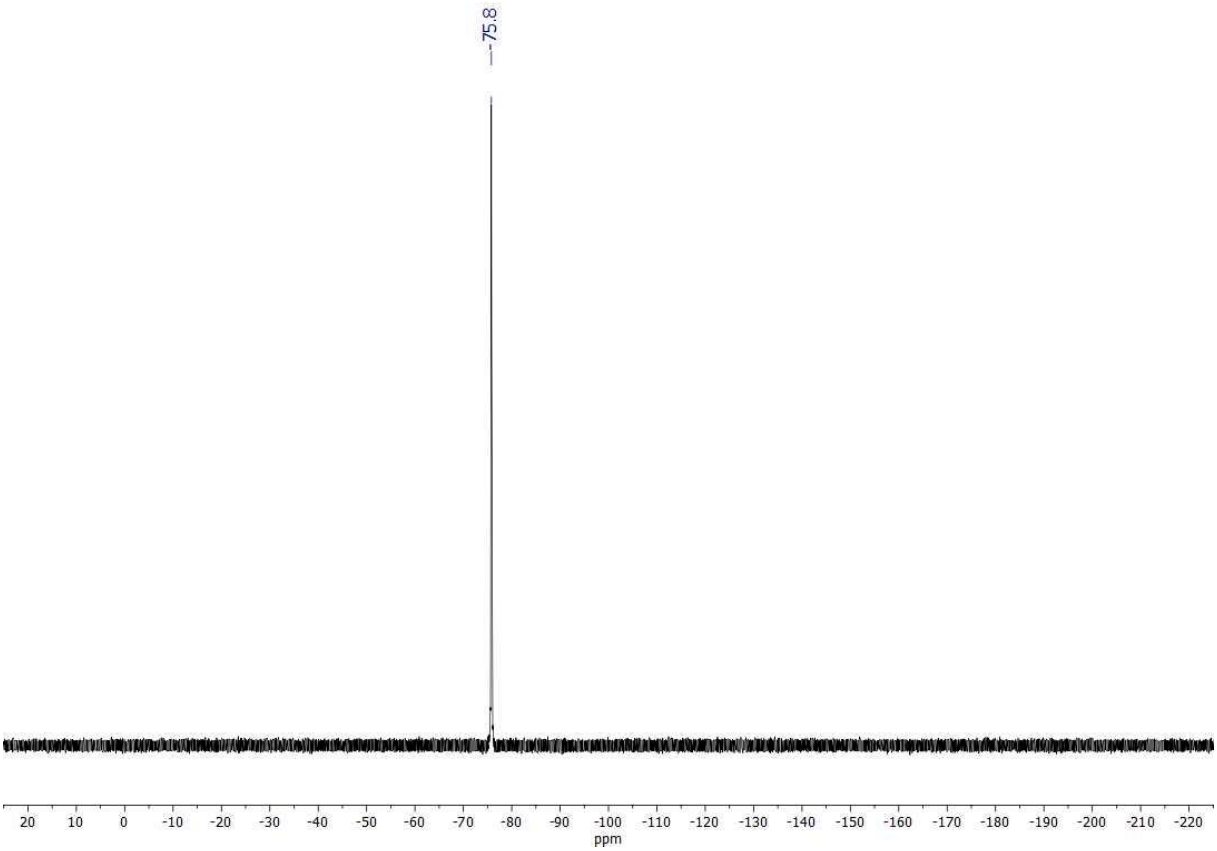

Figure 9.163. ^{19}F NMR spectrum of [$Re^{V}O(L^{3EtEt})$] in $CDCl_3$.

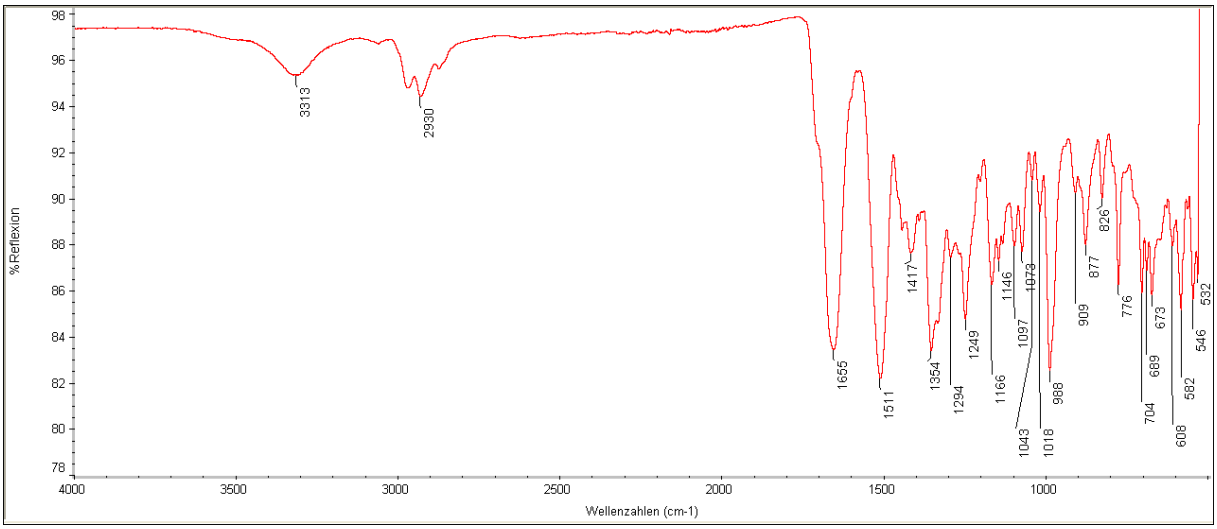

Figure 9.164. IR spectrum of [$Re^{V}O(L^{3EtEt})$].

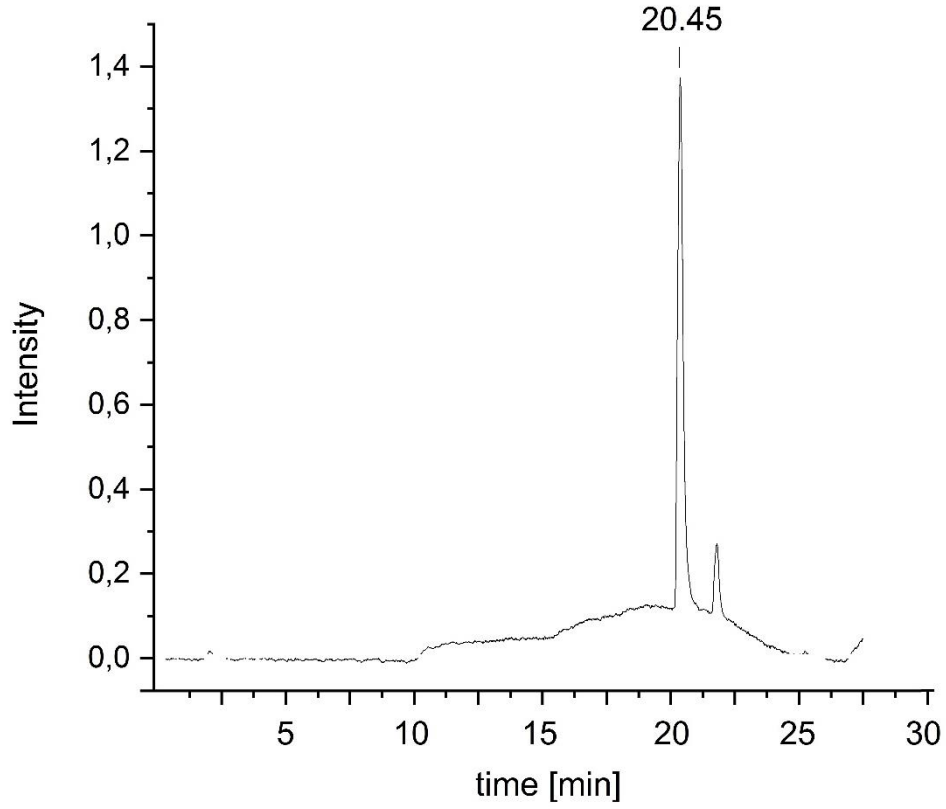

Figure 9.165. UV trace (HPLC) of [$Re^{V}O(L^{3EtEt})$].